NEUROINFLAMMATORY AND OXIDATIVE/NITROSATIVE PATHWAYS IN NEUROPSYCHIATRIC AND NEUROLOGICAL DISEASES AND THEIR POSSIBLE NEUROPHARMACOLOGICAL REGULATION, VOLUME I

EDITED BY: Javier R. Caso, Marta P. Pereira and Borja Garcia-Bueno
PUBLISHED IN: Frontiers in Pharmacology

frontiers Research Topics

ISSN 1664-8714
ISBN 978-2-83250-371-3
DOI 10.3389/978-2-83250-371-3

About Frontiers

Frontiers is more than just an open-access publisher of scholarly articles: it is a pioneering approach to the world of academia, radically improving the way scholarly research is managed. The grand vision of Frontiers is a world where all people have an equal opportunity to seek, share and generate knowledge. Frontiers provides immediate and permanent online open access to all its publications, but this alone is not enough to realize our grand goals.

Frontiers Journal Series

The Frontiers Journal Series is a multi-tier and interdisciplinary set of open-access, online journals, promising a paradigm shift from the current review, selection and dissemination processes in academic publishing. All Frontiers journals are driven by researchers for researchers; therefore, they constitute a service to the scholarly community. At the same time, the Frontiers Journal Series operates on a revolutionary invention, the tiered publishing system, initially addressing specific communities of scholars, and gradually climbing up to broader public understanding, thus serving the interests of the lay society, too.

Dedication to Quality

Each Frontiers article is a landmark of the highest quality, thanks to genuinely collaborative interactions between authors and review editors, who include some of the world's best academicians. Research must be certified by peers before entering a stream of knowledge that may eventually reach the public - and shape society; therefore, Frontiers only applies the most rigorous and unbiased reviews.
Frontiers revolutionizes research publishing by freely delivering the most outstanding research, evaluated with no bias from both the academic and social point of view. By applying the most advanced information technologies, Frontiers is catapulting scholarly publishing into a new generation.

What are Frontiers Research Topics?

Frontiers Research Topics are very popular trademarks of the Frontiers Journals Series: they are collections of at least ten articles, all centered on a particular subject. With their unique mix of varied contributions from Original Research to Review Articles, Frontiers Research Topics unify the most influential researchers, the latest key findings and historical advances in a hot research area! Find out more on how to host your own Frontiers Research Topic or contribute to one as an author by contacting the Frontiers Editorial Office: frontiersin.org/about/contact

NEUROINFLAMMATORY AND OXIDATIVE/NITROSATIVE PATHWAYS IN NEUROPSYCHIATRIC AND NEUROLOGICAL DISEASES AND THEIR POSSIBLE NEUROPHARMACOLOGICAL REGULATION, VOLUME I

Topic Editors:
Javier R. Caso, Universidad Complutense de Madrid, Spain
Marta P. Pereira, Spanish National Research Council (CSIC), Spain
Borja Garcia-Bueno, Universidad Complutense de Madrid, Spain

Citation: Caso, J. R., Pereira, M. P., Garcia-Bueno, B., eds. (2022). Neuroinflammatory and Oxidative/Nitrosative Pathways in Neuropsychiatric and Neurological Diseases and Their Possible Neuropharmacological Regulation, Volume I. Lausanne: Frontiers Media SA. doi: 10.3389/978-2-83250-371-3

Table of Contents

frontiers | Frontiers in Pharmacology

TYPE Editorial
PUBLISHED 16 September 2022
DOI 10.3389/fphar.2022.1033281

OPEN ACCESS

EDITED AND REVIEWED BY
Nicholas M. Barnes,
University of Birmingham,
United Kingdom

*CORRESPONDENCE
Javier R. Caso,
jrcaso@med.ucm.es

SPECIALTY SECTION
This article was submitted to Neuropharmacology, a section of the journal Frontiers in Pharmacology

RECEIVED 31 August 2022
ACCEPTED 06 September 2022
PUBLISHED 16 September 2022

CITATION
Pereira MP, García-Bueno B and Caso JR (2022), Editorial: Neuroinflammatory and oxidative/nitrosative pathways in neuropsychiatric and neurological diseases and their possible neuropharmacological regulation, volume I.
Front. Pharmacol. 13:1033281.
doi: 10.3389/fphar.2022.1033281

Editorial: Neuroinflammatory and oxidative/nitrosative pathways in neuropsychiatric and neurological diseases and their possible neuropharmacological regulation, volume I

Marta P. Pereira[1,2], Borja García-Bueno[3,4] and Javier R. Caso[3,4]*

[1]Departamento de Biología Molecular, Centro de Biología Molecular "Severo Ochoa" (UAM-CSIC), Madrid, Spain, [2]Instituto Universitario de Biología Molecular, IUBM, Universidad Autónoma de Madrid, Madrid, Spain, [3]Departamento de Farmacología y Toxicología, Facultad de Medicina, Universidad Complutense de Madrid (UCM), Instituto de Investigación Sanitaria Hospital 12 de Octubre (Imas12), Instituto Universitario de Investigación en Neuroquímica (IUIN-UCM), Madrid, Spain, [4]Centro de Investigación Biomédica en Red de Salud Mental, Instituto de Salud Carlos III (CIBERSAM, ISCIII), Madrid, Spain

KEYWORDS

neuropsychiatric diseases, neurological diseases, neuroinflammation, oxidative/nitrosative stress, neuropharmacology

Editorial on the Research Topic
Neuroinflammatory and oxidative/nitrosative pathways in neuropsychiatric and neurological diseases and their possible neuropharmacological regulation, volume I

There is a crucial necessity to identify new pathophysiological pathways and therapeutic targets for neurological and neuropsychiatric diseases, as they are rising as leading causes of death, disability, and overall disease burden (Murray et al., 2012). Bearing in mind the potential role of neuroinflammation and the subsequent oxidative/nitrosative damage in these illnesses (Caldwell et al., 2020) the development of new drugs based in the modulation of the immune response is a necessary approach for future therapeutic interventions that deserves further consideration from the standpoint of the neuropharmacology. Thus, the goal of this Research Topic is to offer a view of the current developments in the neuroimmune pharmacology realm for the neurological and neuropsychiatric diseases.

This Research Topic offers an overview of the neuroinflammatory and oxidative/nitrosative pathways in neuropsychiatric and neurological diseases through 11 articles written by 80 authors. This assemblage comprises one mini review, one opinion article, one brief research report, and eight original research papers.

Leite et al. reviewed the role of ouabain, a cardiac steroid known to modify certain immune responses, as a modulator of the neutrophilic neuroinflammation. The authors highlight the reduction of the proinflammatory enzymes activation, and the lower levels of the interleukin (IL)-1 caused by ouabain in the CNS. Authors concluded that ouabain and its receptor (NKA) might be of interest for developing new strategies in the fight against diseases with a neuroinflammatory component.

In an opinion article, Coppens et al. bring to mind that microglia- or astrocyte-derived tryptophan catabolites (TRYCAT) have neuromodulatory effects on the NMDA receptor. Hence, this opinion piece hypothesizes that TRYCAT might link immune responses to clinical symptomatology in psychotic and mood disorders. Additionally, authors discuss the impact of sample heterogeneity, methodological consistency, and validity on study data, putting forward conceptual and methodological advices for future research as well as suggestions for appropriate yet to come research possibilities.

Caso et al. aimed to study immune factors and related risk paths in adult female patients with eating disorders (ED) as well as to find psychological factors prompting the inflammatory response. An important feature of this article is the naïve nature of the sample, meaning that none of the patients was taking medication at the time of assessment. Patients shown higher proinflammatory and oxidative/nitrosative stress parameters than healthy controls. Besides, correlations between impulsiveness and depressive symptomatology and some inflammatory parameters were also identified. Overall, the main conclusion reached was that inflammatory factors could be considered as potential therapeutic targets in ED.

Fu et al. looked into valproic acid-resistant epilepsy, a condition in which most patients present an inflammatory response and local hypoxia. This study identified that the hypoxia-inducible factor (HIF)-1α (a critical effector parameter of hypoxia and inflammation) was overexpressed in mice with valproic acid-resistant epilepsy and regulated the expression of some proinflammatory mediators through the induction of the polarization of microglia from the M2 phenotype to M1 phenotype. Authors were also able to conclude that miR-221-3p/HIF-1α is a vital component in pathogenesis of valproic acid-resistant epilepsy, representing a potential therapeutic antiseizure target.

A classical model for the study of neuroinflammation is the injection of bacterial lipopolysaccharide (LPS) (Zhao et al., 2019). Building in this model, Piovan et al. investigated the effect of pre- and post-treatment with an extract of spirulina in an *in vitro* model of LPS-induced microglia activation, observing a downregulation of important LPS-induced proinflammatory factors and an upregulation of antioxidant mechanisms, showing that the extract of spirulina can be useful in the control of microglia activation and neuroinflammatory processes.

Neuropathic pain (NP) is a chronic condition that can be caused by nervous system damage and studies have shown that inflammation and oxidative stress are important processes in the pathological process of this kind of pain (Costigan et al., 2009). Yang et al. assessed the variations in reactive oxygen species levels, lipid peroxidation, and antioxidant systems in different rodent models of pain and the effects of higenamine (a plant-based alkaloid with anti-inflammatory and antioxidant effects) on these parameters. Higenamine improved the oxidative stress and the inflammation induced by the pain models, warranting further research as a potential drug for the treatment of NP.

Parkinson's disease (PD) is the second most frequent neurodegenerative disease in the world and the most common movement disorder for which there is presently no cure. For that reason, more tools for its study are required. In this sense, cell replacement therapy is a potential treatment for PD. Nelke et al. characterized and transplanted a line of human neural stem cells in middle-aged Parkinsonian mice. Their cell replacement therapy approach prevented motor and non-motor impairments.

Jin et al. studied the effects of metformin, a drug employed in the treatment of type 2 diabetes with previously described anti-inflammatory effects, in a mouse model of early brain injury after subarachnoid hemorrhage. Metformin was neuroprotective by modulating the production of proinflammatory factors induced by the inflammasome NLRP3 and the activation of microglia.

Deng et al. have studied the roles of pyroptosis-related genes in major depressive disorder, as pyroptosis has been found as an inflammatory form of programmed cell death. Authors were able to split depression cases into two distinct pyroptosis subtypes with dissimilar immune and biological traits. Their results indicate that pyroptosis may perform a valuable part in depression providing new insights into its diagnosis and pathophysiology.

Garcia-Partida et al. investigated the actions of mangiferin (a polyphenolic compound abundant in the leaves of *Mangifera indica* that has strong antiinflammatory and antioxidant qualities) comparing them with the actions of risperidone (an antipsychotic drug) in a rat model of schizophrenia. Their article included behavioral and neuroimaging studies and the measurement of oxidative/inflammatory and antioxidant mediators. Authors suggest that mangiferin might be a possible therapeutic or preventive add-on strategy to improve the clinical expression of schizophrenia in adulthood.

Finally, Montes et al. employed rats and post-mortem human frontal cortex and cerebellum to study the effects of the combination of chronic alcohol consumption and thiamine deficiency on the innate immune system and their specific contribution to the pathogenesis of Wernicke's encephalopathy (WE). Their findings offer data, both in the animal model and the human postmortem brain, of the upregulation of the TLR4/MyD88 proinflammatory pathway in WE related to alcohol consumption.

In conclusion, this Research Topic confirms once again the importance of neuroinflammation and oxidative stress as key players in the etiology of neurological and neuropsychiatric diseases. The effects of these players, not only at the biochemical but also at a behavioral level, support the efforts in the search of new modulatory drugs, as they are crucial targets for the development of new pharmacological therapies.

Author contributions

All authors listed have made a substantial, direct, and intellectual contribution to the work and approved it for publication.

Acknowledgments

We would like to thank all authors for their highly valuable contribution. Also, we would like to acknowledge the work of reviewers whose constructive input contributed to improving the quality of the articles.

Conflict of interest

The authors declare that the research was conducted in the absence of any commercial or financial relationships that could be construed as a potential conflict of interest.

Publisher's note

References

Caldwell, L. J., Subramaniam, S., MacKenzie, G., and Shah, D. K. (2020). Maximising the potential of neuroimmunology. *Brain Behav. Immun.* 87, 189–192. doi:10.1016/j.bbi.2020.03.010

Costigan, M., Scholz, J., and Woolf, C. J. (2009). Neuropathic pain: A maladaptive response of the nervous system to damage. *Annu. Rev. Neurosci.* 32, 1–32. doi:10.1146/annurev.neuro.051508.135531

Murray, C. J. L., Vos, T., Lozano, R., Naghavi, M., Flaxman, A. D., Michaud, C., et al. (2012). Disability-adjusted life years (DALYs) for 291 diseases and injuries in 21 regions, 1990–2010: A systematic analysis for the global burden of disease study 2010. *Lancet* 380, 2197–2223. doi:10.1016/S0140-6736(12)61689-4

Zhao, J., Bi, W., Xiao, S., Lan, X., Cheng, X., Zhang, J., et al. (2019). Neuroinflammation induced by lipopolysaccharide causes cognitive impairment in mice. *Sci. Rep.* 9, 5790. doi:10.1038/s41598-019-42286-8

frontiers in Pharmacology

ORIGINAL RESEARCH
published: 23 August 2021
doi: 10.3389/fphar.2021.714556

MicroRNA-221-3p Suppresses the Microglia Activation and Seizures by Inhibiting of HIF-1α in Valproic Acid-Resistant Epilepsy

Meng Fu[1†], Yiqing Zhu[1†], Junqi Zhang[1†], Wei Wu[1], Yunxia Sun[2], Xuemei Zhang[3], Jie Tao[4]* and Zhiping Li[1]**

[1]Department of Clinical Pharmacy, Children's Hospital of Fudan University, National Children's Medical Center, Shanghai, China, [2]Academy of Chinese Medical Sciences, Zhejiang Chinese Medical University, Hangzhou, China, [3]Department of Pharmacology, School of Pharmacy, Fudan University, Shanghai, China, [4]Central Laboratory, Putuo Hospital, Shanghai University of Traditional Chinese Medicine, Shanghai, China

One-third of patients with epilepsy suffer from drug-resistant epilepsy (DRE). Valproic acid (VPA) is a classic anticonvulsant drug, and its resistance is a crucial predictor of DRE, but the pathogenesis remain unknown. Most patients with VPA-resistant epilepsy appear distinct inflammatory response and local hypoxia. Hypoxia-inducible factor (HIF)-1α is an essential effector molecule of hypoxia and inflammation, and may exert therefore a significant effect on the development of VPA-resistant epilepsy. We systematically assess the significance of HIF-1α on children and mice with VPA-resistant epilepsy, and investigated the micro (mi) RNAs that regulate HIF-1α expression. We established models of VPA-sensitive epilepsy and VPA-resistant epilepsy in mice, and confirmed that they had significant differences in epileptic behavior and electroencephalography data. Through proteomics analysis, we identified that HIF-1α was overexpressed in mice with VPA-resistant epilepsy, and regulated the expression of interleukin-1β and tumor necrosis factor-α. Increased expression of HIF-1α led to the increase of microglia and induced their polarization from the M2 phenotype to M1 phenotype, which triggered the release of proinflammatory mediators. Bioinformatics analysis of public databases demonstrated that miR-221-3p was reduced in VPA-resistant epilepsy, and negatively regulated HIF-1α expression. Intervention using miR-221-3p mimics reduced HIF-1α expression markedly and suppressed the activation of microglia and the release of inflammatory mediators, which relieved epileptic seizures of VPA-resistant epilepsy. These observations reveal miR-221-3p/HIF-1α as essential component in pathogenesis of VPA-resistant epilepsy which represent therapeutic antiseizure targets.

Keywords: valproic acid-resistant epilepsy, microRNA-221-3p, hypoxia-inducible factor-1α, microglia, neuroinflammation

OPEN ACCESS

Edited by:
Marta P. Pereira, Severo Ochoa Molecular Biology Center (CSIC-UAM), Spain

Reviewed by:
Harshini Sarojini, University of Louisville, United States
Jyotirmoy Banerjee, All India Institute of Medical Sciences, India

****Correspondence:***
Xuemei Zhang
xuemzhang@fudan.edu.cn
Jie Tao
jietao_putuo@foxmail.com
Zhiping Li
zpli@fudan.edu.cn

†These authors share first authorship

Specialty section:
This article was submitted to Neuropharmacology, a section of the journal Frontiers in Pharmacology

Received: *25 May 2021*
Accepted: *10 August 2021*
Published: *23 August 2021*

Citation:
Fu M, Zhu Y, Zhang J, Wu W, Sun Y, Zhang X, Tao J and Li Z (2021) MicroRNA-221-3p Suppresses the Microglia Activation and Seizures by Inhibiting of HIF-1α in Valproic Acid-Resistant Epilepsy. Front. Pharmacol. 12:714556. doi: 10.3389/fphar.2021.714556

INTRODUCTION

Epilepsy is a chronic brain condition caused by sudden abnormal discharge from brain neurons. Epilepsy affects >70 million people worldwide (Thijs et al., 2019). Treatments of epilepsy include medication, surgery and ketogenic diet, among which medication is the main approach (Kanner et al., 2018). Anti-epileptic drugs (AEDs) could inhibit 60–70% seizures. However, 30–40% of patients with drug-resistant epilepsy (DRE) cannot control seizures effectively through AEDs (Kalilani et al., 2018). Valproic acid (VPA) is a classic AEDs (Chen et al., 2018). Clinical evidence suggests that VPA resistance is a vital predictor of DRE (Gesche et al., 2017), but the mechanism of VPA-resistant epilepsy remained largely elusive. Patients fail to attain a seizure-free lifestyle, which increases the risk of psychosocial dysfunction, injuries, and premature death (Löscher et al., 2020).

Numerous studies have strongly supported the role of inflammation in DRE pathophysiology (Weidner et al., 2018; Fu et al., 2020; Ouédraogo et al., 2021). Multifarious inflammatory molecules and signaling pathways have been shown to influence the outcome of experimental models and patients with DRE (Weidner et al., 2018).

Microglia are the resident immune cells in the brain. Microglia are universally involved in the response to diverse forms of insults and diseases in the central nervous system (CNS) (Patel et al., 2019). Studies have shown that microglia are activated in the brain of patients with DRE (Devinsky et al., 2013). Pioneering studies have indicated that proinflammatory factors such as interleukin (IL)-1β, tumor necrosis factor (TNF)-α, High mobility group box (HMGB)1, cyclooxygenase (COX)-2, and prostaglandin (PG)E2 have increased significantly in the epileptic foci and blood of patients with DRE (Rana and Musto, 2018). Simultaneously, expression of interleukin-1 receptor (ILR)1, and toll-like receptors (TLRs) increase correspondingly, resulting in activation of inflammation-related signaling pathways such as IL-1β/ILR1, HMGB1/TLR4 (Strauss and Elisevich, 2016). Previously, we found that expression of IL-1β, chemokine (C-C motif) ligand (CCL)3, TNF-α, HMGB1 and other inflammatory mediators was increased greatly in the blood samples of children with VPA-resistant epilepsy (Wang and Li, 2019; Fu et al., 2020). These data suggested that neuroinflammation may play a crucial part in the pathologic mechanism of VPA-resistant epilepsy.

Moreover, DRE patients are characterized by local hypoxia in the brain, which is caused by rapid consumption of oxygen and vasoconstriction due to repeated seizures (Bateman et al., 2008). Hypoxia-inducible factor (HIF)-1 is an endogenous transcription factor that contributes to the cellular response to hypoxia. HIF-1 is a heterodimer that consists of constitutively expressed HIF-1β and HIF-1α subunits (Balamurugan, 2016). If oxygen is available, HIF-1α is degraded by oxygen-dependent prolyl hydroxylation. If the oxygen concentration drops, a stable HIF-1 complex is formed, which activates the transcription of several genes encoding proteins involved in angiogenesis, glucose metabolism, and cell proliferation/survival (Semenza, 2003; 2014). Notably, HIF-1α induces the transcription of inflammation-related proteins such as T-cell immunoglobulin and mucin-domain containing-3 and vascular endothelial growth factor in various diseases. Studies have shown that HIF-1α is involved in microglia activation in patients with Alzheimer's disease (Baik et al., 2019). However, the contribution of HIF-1α in VPA-resistant epilepsy remain unknown.

MicroRNAs (miRNAs) are a class of endogenous noncoding single-stranded RNA molecules of size 22–25 nt (Lu and Rothenberg, 2018). MiRNAs are major players in posttranscriptional gene regulation in diverse biological processes (Fabian and Sonenberg, 2012). Multifarious specific miRNAs exist in different brain regions and different types of brain cells (O'Carroll and Schaefer, 2013). Various reports have suggested miRNAs to be functional regulators of epileptogenesis (Henshall et al., 2016). Different miRNAs, including miR-132 (Korotkov et al., 2020), miR-34a (Organista-Juárez et al., 2019), and miR-146a (Aronica et al., 2010) appear to be actively involved in DRE pathogenesis. As noted above, miRNAs may play crucial roles in the regulation of inflammation in patients with VPA-resistant epilepsy.

In this study, we assess the significance of HIF-1α in VPA-resistant epilepsy. We sought to identify the miRNA that regulates HIF-1α expression in a mouse model and in patients with VPA-resistant epilepsy.

METHODS

Patients Samples

The present study recruited 24 children suffering from epilepsy (0–18 years) from the Children's Hospital of Fudan University. Sixteen cases were resistant to antiepileptic drugs, including VPA (**Supplementary Table S1**), and eight cases were sensitive to VPA (**Supplementary Table S2**). The diagnosis of DRE was based on criteria published by the International League Against Epilepsy (ILAE) criteria (Kwan et al., 2010). Briefly, children with DRE failed to be free of seizures after ≥2 tolerated regimens of antiepileptic drugs, including VPA. For children with drug-sensitive epilepsy, seizures disappeared after using VPA for ≥6 months, and there are no epileptiform discharges in the electroencephalogram (EEG) after treatments. The exclusion criteria were patients with: 1) severe adverse reactions to drugs; 2) poor compliance with use of antiepileptic drugs; 3) unreliable record of seizure frequency; 4) history of pseudo-seizures; 5) drug abuse; 6) malignant diseases (e.g., brain tumors, metastasis); 7) hepatic or renal failure. The study protocol was approved by the Ethics Committee of the Children's Hospital of Fudan University (Shanghai, China). Written informed consent was obtained from all patients and healthy controls included in our study.

Approximately 2 ml of peripheral blood was collected from each enrolled individual. Then, the plasma samples were obtained by centrifugation and stored at −80°C. Hemolytic plasma samples were excluded.

Animals

C57BL/6 male mice were used for the study (n = 98). All mice were social housed under standardized conditions of light,

temperature and humidity, environmental enrichment, and had access to food and water ad libitum. All possible efforts were made to minimize animal suffering and the number of animals used. This study was carried out in accordance with the principles of the Basel Declaration. The protocol was approved by the Institutional Ethics Committee of Children's Hospital of Fudan University.

Creation of a Kainic Acid-Induced Model of Chronic Epilepsy

A KA-induced temporal lobe epilepsy (TLE) model was created in mice, as described previously. Briefly, all mice were fed for 1 week to adapt to the environment, and then were assigned randomly into an epilepsy group or control group. Seizures were induced by administration of KA (3 mg/ml, 0.2 ml/mouse, i.p.) dissolved in physiologic (0.9%) saline. Mice in the control group were given an equal amount of 0.9% saline. All mice were monitored for 1 h after KA injection to evaluate seizures using the Racine Scale (Racine, 1972). Status epilepticus (SE) was defined as an epileptic seizure of grade three or greater lasting longer than 30 min. Seizures were terminated at 1 h after onset with the use of sodium pentobarbital, if necessary.

Pharmacological Assessment

Four weeks after KA treatment, the epileptic behavior of mice was scored. Twelve epileptic mice were selected as the model group, and the number of seizures was not significantly different from that of other mice. The remaining mice were given VPA (150 mg/kg, p.o.; Sanofi, Paris, France) twice-daily for 4 weeks. Studies have shown that this dose is an efficacious therapeutic dose of VPA for epileptic mice. Mice in the control group and model group was given solvent of VPA. After the final administration, mice were housed individually and their epileptic behavior and EEG data recorded. The latter was carried out according to the stereoelectroencephalography approach in which intracerebral multiple contact electrodes (AP: −2.2 ± 0.1 mm, ML: +0.8 ± 0.1 mm, DV: −1.4 ± 0.1 mm) were employed (Bartolomei et al., 2012). Seizures were characterized by synchronized high-voltage amplitude oscillations. EEG data and behavior data were reviewed by two trained experimenters blinded to the experimental conditions to identify motor seizures. Finally, of the mice given VPA, 12 mice with the best treatment effect were placed in VPA-sensitive group and 12 mice with the worst treatment effect were placed in the VPA-resistant group.

Tissue Preparation

Mice were decapitated with isoflurane for proteomics analysis, western blotting, and real-time reverse transcription-quantitative polymerase chain reaction (RT-qPCR). Brain tissues were removed rapidly and placed in ice-cold phosphate-buffered saline (PBS). The dissected hippocampus was snap-frozen in liquid nitrogen and stored at −80°C. For histology, mice were anesthetized and underwent perfusion with 50 ml of saline, followed by 80 ml of 4% paraformaldehyde. Brains were removed and fixed in 4% paraformaldehyde overnight at 4°C. After sequential dehydration with 20 and 30% sucrose for 48 h, coronal sections of thickness 10 μm were cut using a freezing microtome and then attached to slides. These hippocampal sections were stored at 4°C for Nissl staining and immunofluorescence staining.

Proteomics Analysis

Total protein was extracted from the hippocampus of mice in the VPA-resistant epilepsy group and VPA-sensitive epilepsy group using SDT lysis buffers. The protein concentration was measured by a bicinchoninic acid (BCA) kit (Beyotime Institute of Biotechnology, Shanghai, China). Then, supernatant proteins were digested in trypsin, as described previously. The filter-aided sample preparation method was used for sample purification, chemical derivatization, and enzymatic digestion. After protein digestion, peptides were labeled according to the operation instructions of the Tandem Mass Tag kit (Thermo Fisher Scientific, Waltham, MA, United States). Labeled peptides from each group were mixed equally and then fractionated using the High pH Reversed-Phase Peptide Fractionation kit (Thermo Fisher Scientific). Each sample was desalted and passed into a trap column for gradient elution. Each eluted peptide sample was dried by vacuum centrifugation for high-performance liquid chromatography (HPLC). Each fractionation sample was separated by the Easy nLC 1,200 system (Thermo Fisher Scientific) at a nanoliter flow rate. Eluent A contained 0.1% (v/v) formic acid in water. Eluent B contained 84% acetonitrile and 0.1% formic acid in water. Mass spectrometry data were acquired with a Q-Exactive mass spectrometer (Thermo Fisher Scientific). With respect to parameters: the scanning range of the precursor ion was mass/charge (m/z) 300–1800; full scans were acquired at a resolution of 70,000 at m/z 200; dynamic exclusion was set at 60.0 s; the target for automatic gain control was 1e6; the maximum IT was 50 ms. Twenty fragment maps were collected after each full scan to obtain the m/z of peptides and peptide fragments; the type of MS2 activation was HCD; the isolation window was m/z 2; tandem mass spectrometry scans were acquired at a resolution of 35,000 at m/z 200; normalized collision energy was 30 eV; underfill was 0.1%.

Gene Ontology and Kyoto Encyclopedia of Genes and Genomes

Annotation of the proteome was undertaken based on the Gene Ontology (GO) database (http://geneontology.org/) using Blast2GO, which comprises four steps: blast, mapping, annotation, and annotation augmentation. Proteins were classified by GO annotation based on three categories: biological process (BP), cellular component (CC), and molecular function (MF). Enrichment of signaling pathways was identified based on the Kyoto Encyclopedia of Genes and Genomes (KEGG) database (www.genome.jp/kegg/pathway.html/) using the KEGG Automatic Annotation.

Construction and Analysis Protein-Protein Interaction Network

The Search Tool for the Retrieval of Interacting Genes/Proteins (STRING; http://string-db.org/) database was used to analyze the

interaction of hub genes and to construct a PPI network (Szklarczyk et al., 2015). The latter was visualized by Cytoscape (http://cytoscape.org/) (Su et al., 2014) and the MCODE plugin was used to select the hub clustered subnetworks of highly intraconnected nodes with the default parameters (degree cut-off ≥ 2, node score cut-off ≥ 0.2, K-core ≥ 2, and maximum depth = 100).

Western Blotting

Western blotting was employed to verify the results of proteomics analysis. Samples of hippocampal tissues were homogenized and centrifuged. The protein concentration was determined by the BCA protein assay kit (Beyotime Institute of Biotechnology) and adjusted to 2 μg/μl. Proteins (8 μl) were separated by sodium dodecyl sulfate–polyacrylamide gel electrophoresis using 10% gels, and then transferred to polyvinylidene difluoride (PVDF) membranes. The latter were blocked with 5% nonfat milk in PBS for 1 h. Next, the blocked PVDF membranes were incubated with antibodies (all purchased from Abcam, Cambridge, United Kingdom) against HIF-1α (1:200 dilution), anti-IL-1β (1:1,000), anti-TNF-α (1:1,000), anti-cluster of differentiation (CD)86 (1:1,000), and CD206 (1:1,000) overnight at 4 °C. After washing with Tween-20 and Tris-buffered saline (TBST), PVDF membranes were incubated with a horseradish peroxidase-conjugated secondary antibody (1:1,000; Abcam). β-actin (1: 1,000; Abcam) was used as an internal control. Gray values were measured using ImageJ (National Institutes of Health, Bethesda, MD, United States). The relative expression of samples in different duplications were standardized by a same sample of control group.

Nissl Staining

For observation of hippocampal neurons, Nissl staining was undertaken according to a method described previously. Briefly, the brain sections were washed with deionized water for 2 min, and then immersed in 1% toluidine blue (Yeasen, Beijing, China) at 37°C for 10 min. After rinsed in deionized water, slices were dehydrated in graded ethanol solutions. Slices were cover-slipped with neutral balsam.

Immunofluorescence Staining

We wished to detect the number of neurons (using NeuN) and microglia (using ionized calcium-binding adaptor molecule (Iba)-1) and whether there was co-labeling of microglia and HIF-1α in the hippocampal tissue of mice with VPA-resistant epilepsy. Hence, immunofluorescence was undertaken using previously described methods with slight adjustment (Han et al., 2018). Briefly, frozen sections were permeabilized with 1% Triton X-100 and blocked with PBS containing 5% bovine serum albumin. Without washing, sections were incubated overnight with primary antibodies against NeuN, Iba-1, and HIF-1α. Following further washing, sections were incubated with goat anti-rabbit antibody conjugated with Alexa Fluor 594 (for NeuN or Iba-1) and goat anti-mouse antibody conjugated with Alexa Fluor 488 (for HIF-1α) for 1 h at 37 °C. Then, sections were rinsed in deionized water, and mounted with Vectashield™ with 4',6-diamidino-2-phenylindole. Fluorescence images were captured using a Virtual/Digital Slice Microscope (Olympus, Tokyo, Japan). Cells with a distinct nucleus were counted by a pathologist who was blinded to the grouping of our study.

Enzyme-Linked Immunosorbent Assay

Expression of IL-1β and TNF-α in plasma from children with VPA-resistant epilepsy or VPA-sensitive epilepsy was quantified by ELISA kits (Shanghai Enzyme-linked Biotechnology, Shanghai, China) according to manufacturer instructions.

Bioinformatics Analysis

Profiling of hippocampal miRNA of two independent datasets was re-analyzed. Profile 1 was the GSE99455 dataset from Gene Expression Omnibus (www.ncbi.nlm.nih.gov/geo/query/acc.cgi?acc=GSE99455). Profile 2 was from the **Supplementary Material** of as study published by Kan and colleagues (https://link.springer.com/article/10.1007/s00018-012-0992-7) (Kan et al., 2012). Profile 1 included 16 patients with DRE and eight post mortem controls. Profile 2 included 20 DRE patients and 10 post mortem controls. Analyses of differential expression were undertaken using "DESeq2" in R (R Institute of Statistical Computing, Vienna, Austria) and adjusted $p < 0.05$ and |log2-fold change (FC)| >1.5 were the cutoff thresholds. The overlapping miRNA dataset was obtained by taking the intersection of the differentially expressed miRNA sets of Profile 1 and Profile 2. Subsequently, the miRNAs that regulate HIF-1α expression were searched for through the online database starbase (http://starbase.sysu.edu.cn/), which were verified in samples from children with VPA-resistant epilepsy or VPA-sensitive epilepsy. Simultaneously, the binding sites of miRNA and HIF-1α were detected using a luciferase reporter assay.

Real-Time PCR Analysis

Expression of miRNAs, inducible nitric oxide synthase (iNOS), CD86, arginine (Arg)1 and CD206 in the hippocampus was detected using RT-qPCR. Total RNA extracted from the hippocampus was reverse-transcribed into complimentary-DNA using a FastQuant RT kit (Tiangen, Beijing, China). Primers were synthesized by Sangon Biotechnology (Shanghai, China). RT-qPCR was done in triplicate in a minimum of three independent experiments according to the instructions of the PCR kit (Tiangen). Relative gene expression was calculated by the $2^{-\Delta\Delta CT}$ method.

Luciferase Reporter Assay

The predicted binding site of the miRNA in the target gene was verified using a luciferase reporter gene assay carried out in human embryonic kidney (HEK)-293T cells. Cells were placed in 24-well plates. The confluence reached 60–70% after 24 h of incubation. HIF-1A-3′-untranslated region (UTR) wild type (wt) and HIF-1A-3′-UTR mutant reporter plasmids were constructed in advance. Then, miRNA mimics and a mimic negative control (NC) were co-transfected with the luciferase reporter vector into HEK-293 T cells. The luciferase activity was analysed by dual luciferase assay system (Promega, Fitchburg, WI, United States).

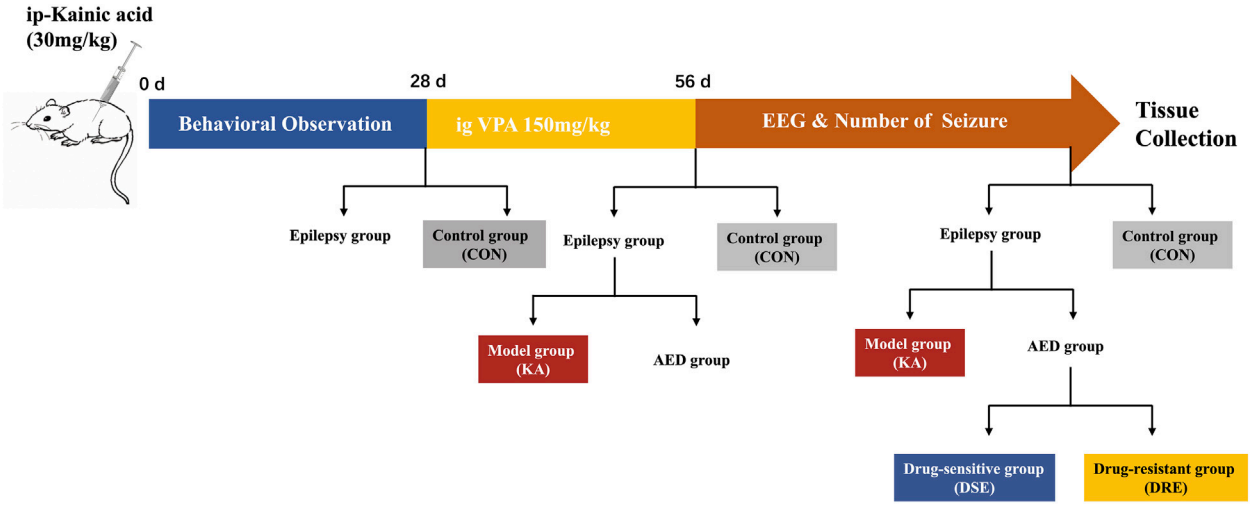

FIGURE 1 | Schematic showing the creation of a VPA-resistant epilepsy model in mice. Step 1: Sixty mice with temporal lobe epilepsy were established by intraperitoneal administration of KA. Step 2: twenty epilepsy mice were assigned into epilepsy model, and 48 epilepsy mice were treated with VPA for 4 weeks. Step 3: After administration, the mice were divided into VPA-sensitive group and VPA-resistant group according to their epileptic behavior and EEG data.

Statistical Analyses

Statistical analyses were carried out using SPSS 20.0 (IBM, Armonk, NY, United States). Data are the mean ± standard deviation (SD). The differences between two or among more groups were assessed via two-sided unpaired Student's t-test (two groups) or one-way ANOVA followed by Fisher's least significant difference post hoc test (multiple groups). $p < 0.05$ was considered significant. Analyses were undertaken in a blinded manner.

RESULTS

Behavior and Electroencephalogram in Mice With VPA-Resistant Epilepsy

Ninety-eight mice were used in this study (**Figure 1**): 12 mice were in the control group (CON), and 86 mice were given KA to induce TLE. Twelve of 86 mice died after SE; 14 of 86 were excluded because SE did not appear 2 h after KA injection. Thus, we obtained 60 epilepsy mice, of which 12 mice were assigned to the KA-induced epilepsy model (KA) and 48 mice were given VPA. After VPA administration, 12/48 mice with the best treatment effect were assigned to the VPA-sensitive group (DSE), and 12/48 mice with the worst treatment effect were assigned to the VPA-resistant group (DRE).

The number of seizures was counted according to the Racine Scale. After SE and before VPA administration, there is no obvious difference in the number of seizures among the epilepsy model, VPA-sensitive epilepsy, and VPA-resistant epilepsy groups (**Figure 2A**). 4 weeks after VPA administration, the seizure frequency of mice with VPA-sensitive epilepsy was dramatically lower than that in the VPA-resistant epilepsy group (**Figure 2B**).

EEG data confirm that there was a difference in the seizure activity between VPA-resistant epilepsy and VPA-sensitive epilepsy (**Figure 2C**): EEG data were line with the epileptic behavior. Numerous epileptiform discharges with high-amplitude spikes and sharp waves were present in mice of epilepsy model group, which were ameliorated significantly in the VPA-sensitive epilepsy group. Notably, there were many high-amplitude rhythmic discharges in the VPA-resistant epilepsy group (**Figure 2D**).

In parallel, the power spectral density was computed for each EEG frequency band in accordance with the Welch method: delta (0–4 Hz), theta (5–8 Hz), alpha (9–12 Hz), beta (13–30 Hz) and gamma (31–100 Hz). The delta band of the model group was higher than that of the control group (**Figure 2E**). This phenomenon was reduced in the VPA-sensitive epilepsy group but not in the VPA-resistant epilepsy group. Taken together, these data demonstrated difference in seizures severity between the VPA-resistant group and VPA-sensitive group after VPA treatment.

Proteomics Analysis

The abundance of hippocampal proteins was compared between the VPA-resistant epilepsy group and VPA-sensitive epilepsy group using liquid chromatography-tandem mass spectrometry. A total of 30,738 unique peptides were identified, which corresponded to 4,924 unique proteins after searching SwissProt-Rodentia protein database and annotated at a false discovery rate of 1% for peptides. The cutoff for differential abundance of proteins was FC > 1.5 (upregulated) or < 0.67 (downregulated) and $p < 0.05$. According to these screening criteria, 29 proteins exhibited significant change in abundance between the VPA-resistant epilepsy group and VPA-sensitive epilepsy group, of which 13 were upregulated and 16 were

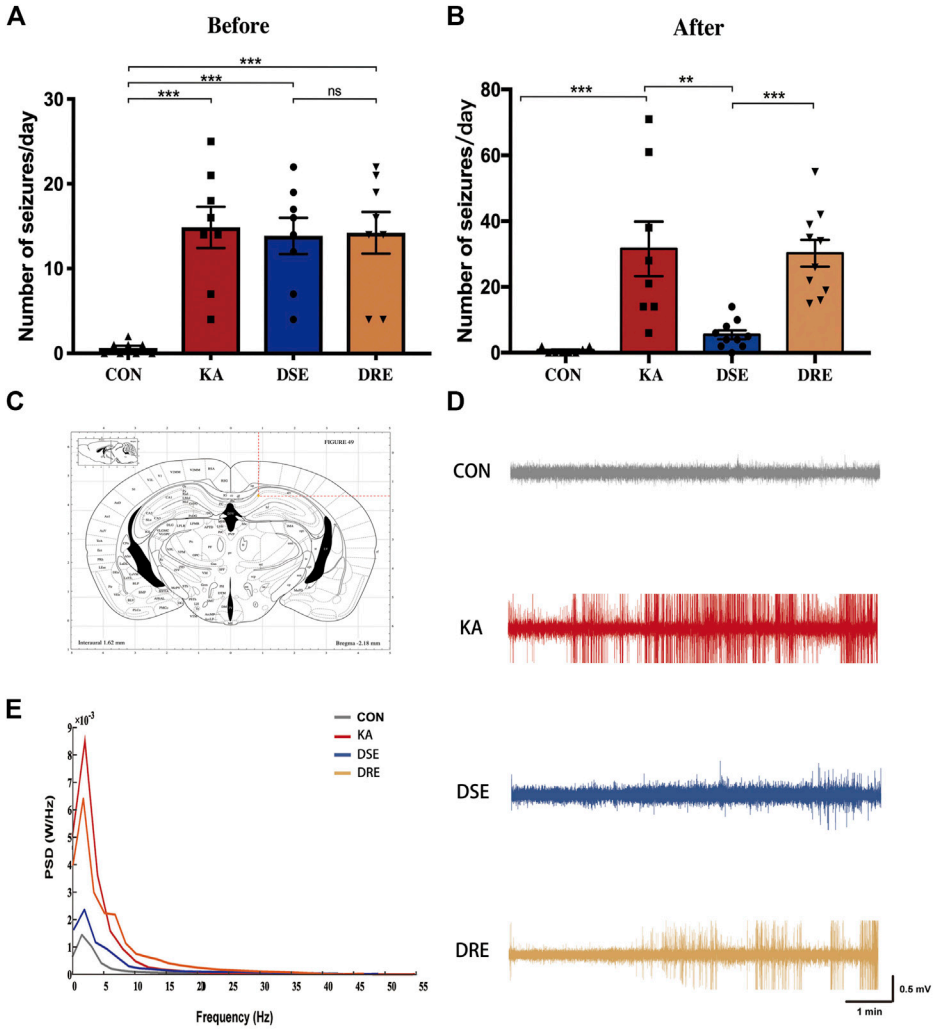

FIGURE 2 | Data of EEGs and behavior in mice with KA-induced epilepsy (n = 12). **(A)** There is no obvious difference in number of seizures in mice with VPA-sensitive epilepsy and VPA-resistant epilepsy group before VPA administration. **(B)** After VPA administration, mice with VPA-resistant displayed increased seizure severity when compared to mice with VPA-sensitive epilepsy. **(C)** Location of EEG electrodes in mouse hippocampus: AP: −2.2 ± 0.1 mm, ML: +0.8 ± 0.1 mm, DV: −1.4 ± 0.1 mm. **(D)** The field potential signal from mice in control, epilepsy model, VPA-sensitive epilepsy, and VPA-resistant epilepsy groups. **(E)** Representative EEGs showing typical epileptiform discharges in mice with VPA-resistant epilepsy. **(F)** The power spectral density of delta band of the VPA-resistant group was higher than that of the VPA-sensitive group. Values are the mean ± S.D. Unpaired t-test. $^{*}p < 0.05$, $^{**}p < 0.01$, and $^{***}p < 0.001$. ns, not significant. CON: control, KA: KA-induced epilepsy, DSE: VPA-sensitive epilepsy, and DRE: VPA-resistant epilepsy.

downregulated in the VPA-resistant epilepsy group (**Figures 3A,B**, **Supplementary Table S3**).

To obtain a more comprehensive and in-depth understanding of differentially expressed proteins (DEPs), functional annotation using the GO database and enrichment of signaling pathways using the KEGG database were carried out. These DEPs were particularly enriched in BP involving "localization", "response to stimulus", "metabolic process" and "inflammatory response". With regard to MF, the DEPs were involved in "binding", "protein binding", "ion binding" and "cytokine activity". With respect to CC, DEPs were principally enriched in "cell part", "intracellular", "intracellular part" and "organelle" (**Figure 3C**). Furthermore, the DEPs were then subjected to enrichment analysis of signaling pathways using the KEGG database: DEPs were involved in "necroptosis", "inflammation" and "cytokine–cytokine receptor interaction" (**Figure 3D**). Taken together, these results suggested that expression of inflammation-related mediators may change significantly in VPA-resistant epilepsy.

To further determine the hub DEPs between VPA-sensitive epilepsy and VPA-resistant epilepsy, a PPI network were constructed using the STRING database. To determine the module with the best connectivity, the MCODE plug-in of Cytoscape was used. Surprisingly, the top module contained HIF-1α, and IL-1β and TNF-α interacted directly with HIF-1α (**Figure 3E**). Therefore, HIF-1α, IL-1β, and TNF-α were selected as key proteins for subsequent research.

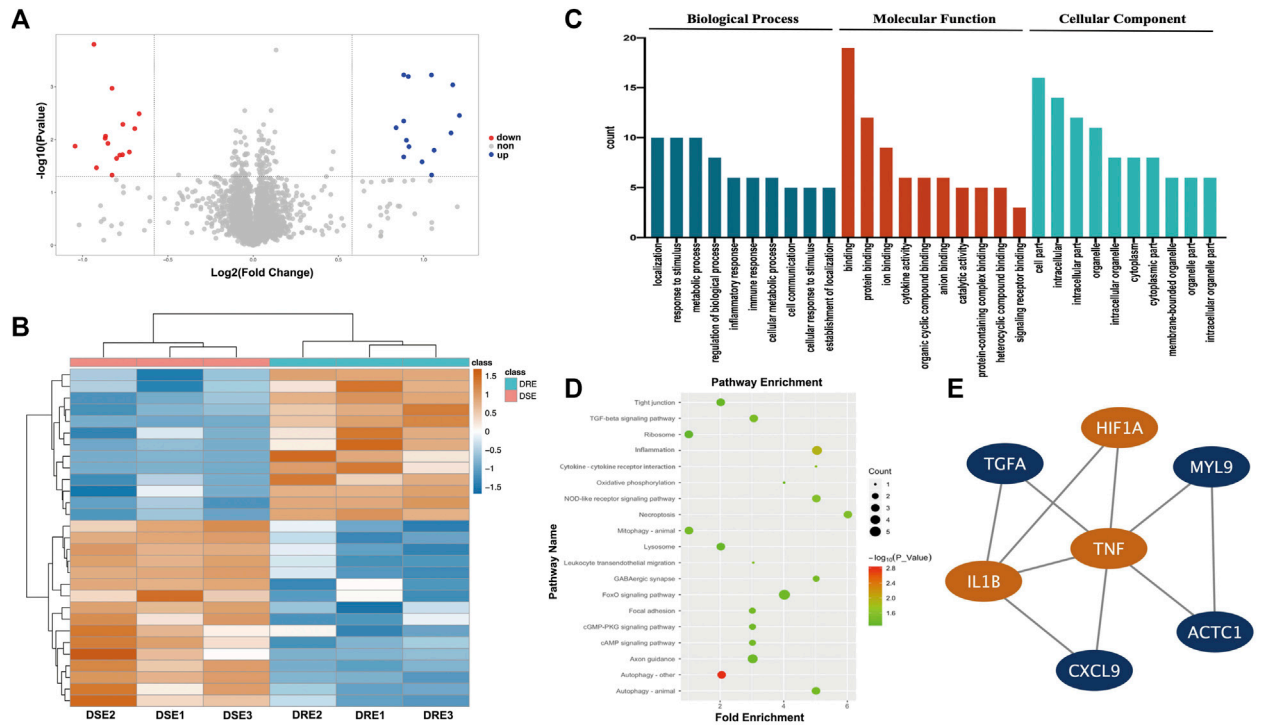

FIGURE 3 | Quantitative proteomics analysis of the hippocampus in mice. **(A)** Volcano plot of differentially expressed protein in hippocampus between VPA-resistant epilepsy and VPA-sensitive epilepsy. Red dots are down-regulated proteins. Blue dots are up-regulated proteins. **(B)** Heatmap of 29 differentially expressed protein in hippocampus between VPA-resistant epilepsy and VPA-sensitive epilepsy. **(C)** The biological process, molecular function and functional enrichment analysis of the differentially expressed proteins between the VPA-sensitive group and the VPA-resistant group through the GO database. **(D)** Differentially expressed proteins are enriched in multiple inflammation-related signaling pathways using the KEGG database. **(E)** The top 1 connectivity module contained HIF-1α, IL-1β, and TNF-α in the PPI network of differentially expressed proteins. DSE: VPA-sensitive epilepsy, DRE: VPA-resistant epilepsy.

TABLE 1 | Comparison of clinical data in patients with VPA-resistant epilepsy and VPA-sensitive epilepsy.

Variable	VPA-resistant epilepsy	VPA-sensitive epilepsy	*p* value
Sample size	16	8	NA
Age (years)	7.13 ± 3.76	8.25 ± 3.20	$p > 0.05$
F/M ration	9/7	4/4	$p > 0.05$
Course (years)	3.25 ± 1.53	3.75 ± 2.66	$p > 0.05$
Age of seizure onset (years)	3.88 ± 2.97	4.50 ± 2.07	$p > 0.05$
Seizure frequency (times/first 6 months of diagnosis)	26.69 ± 13.19	21.87 ± 16.11	$p > 0.05$
Seizure frequency (times/last 6 months)	13.68 ± 7.21	0	$p < 0.05$

F, female; M, male; NA, not applicable.

Validation of Selected Proteins

To further verify the dysregulation of these proteins, expression of IL-1β and TNF-α in blood of children with VPA-resistant epilepsy and VPA-sensitive epilepsy was measured by ELISA. HIF-1α is an unstable macromolecular substance and cannot penetrate the blood–brain barrier, so its accumulation in the brain cannot reach the blood. Therefore, we did not measure HIF-1α expression in blood samples from children. There were no obvious differences in age, sex, course, age of onset, or seizure frequency of first 6 months of diagnosis between VPA-resistant epilepsy and VPA-sensitive epilepsy (**Table 1**). The level of IL-1β and TNF-α in the VPA-resistant group was substantially higher than that in children with VPA-sensitive epilepsy (**Figures 4A,B**). Western blotting in mice hippocampal tissue was carried out, and results indicated that expression of HIF-1α, IL-1β, and TNF-α in the hippocampus of mice with VPA-resistant epilepsy was upregulated compared with that in mice with VPA-sensitive epilepsy (**Figures 4C–F**). These results were consistent with the data of proteomics analysis, and support the notion that HIF-1α, IL-1β, and TNF-α showed aberrant expression in VPA-resistant epilepsy.

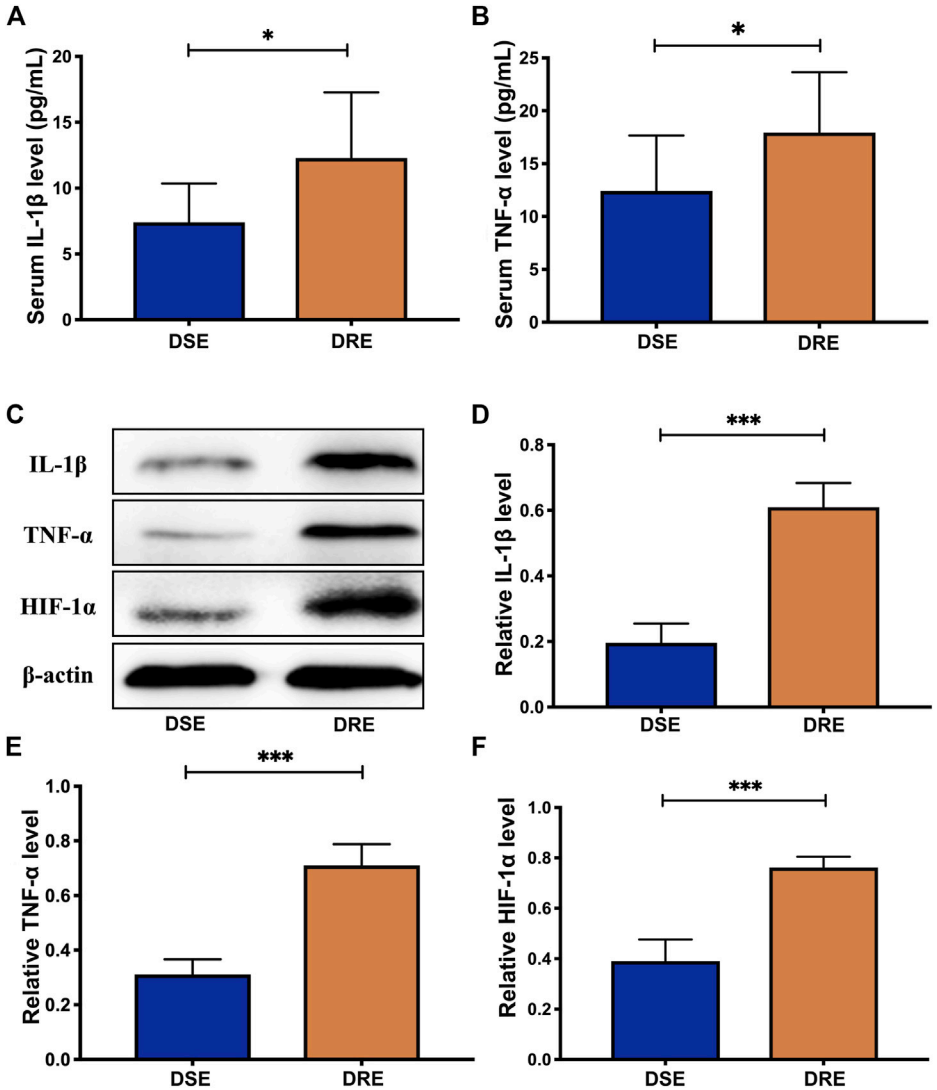

FIGURE 4 | Validation analysis of selected proteins. The level of IL-1β **(A)** and TNF-α **(B)** in the blood of children with VPA-resistant epilepsy significantly higher than that in VPA-sensitive epilepsy using ELISA analysis (DSE: $n = 8$; DRE: $n = 16$). **(C)** Representative protein bands of IL-1β, TNF-α and HIF-1α of hippocampus determined by western blotting ($n = 6$). Protein expression of IL-1β **(D)**, TNF-α **(E)** and HIF-1α **(F)** in the hippocampus of mice with VPA-resistant epilepsy greatly higher than that of mice with VPA-sensitive epilepsy ($n = 6$). Values are the mean ± S.D. Unpaired *t*-test. $^{*}p < 0.05$, $^{**}p < 0.01$, and $^{***}p < 0.001$. DSE: VPA-sensitive epilepsy and DRE: VPA-resistant epilepsy.

Increased Activation of Microglia in VPA-Resistant Epilepsy

Based on the exacerbated inflammatory response in VPA-resistant epilepsy, we examined the activated status of microglia in the hippocampus of mice brain sections by immunofluorescent staining using Iba-1. The fluorescence intensity of Iba-1-labeled microglia was significantly greater in the hippocampal CA1 and CA3 regions of mice in the VPA-resistant epilepsy group compared with that in the VPA-sensitive epilepsy group (**Figure 5A**). The number of Iba-1-positive microglia in hippocampal CA1 and CA3 regions was obviously increased in VPA-resistant epilepsy (**Figures 5B,C**).

To ascertain which microglial phenotype was activated, we measured expression of M1/M2-specific markers in the hippocampus of mice using RT-qPCR. mRNA expression of iNOS and CD86 (both markers of the M1 subtype) was increased markedly in VPA-resistant epilepsy (**Figures 5D,E**), whereas expression of Arg-1 and CD206 (both markers of the M2 subtype) was decreased significantly in VPA-resistant epilepsy compared with VPA-sensitive epilepsy (**Figures 5F,G**). The trends of protein expression of CD86 and CD206 were consistent with their mRNA expression (**Figures 5H–J**). Collectively, our data showed polarization of microglia from the M2 phenotype to the M1 phenotype in VPA-resistant epilepsy.

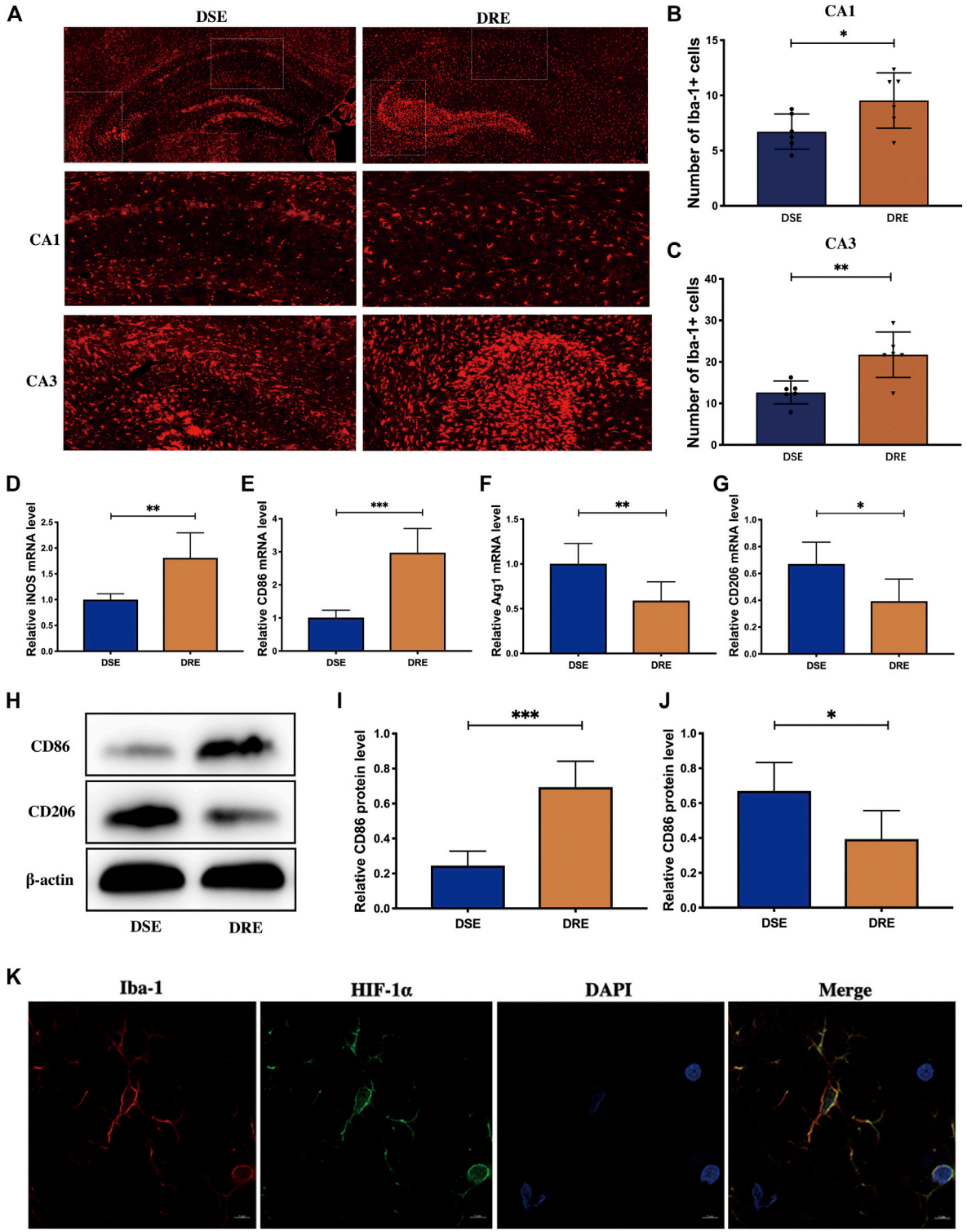

FIGURE 5 | Microglia activation in the hippocampus of mice ($n = 6$). **(A)** Representative immunohistochemistry images of Iba-1 in the hippocampus. Quantification of Iba-1-positive cells in the hippocampal CA1 **(B)** and CA3 **(C)** regions. The number of Iba-1-positive microglia in hippocampal CA1 and CA3 regions was obviously increased in VPA-resistant epilepsy. The mRNA levels of M1 subtype markers iNOS **(D)** and CD86 **(E)** are significantly increased in hippocampus of mice with VPA-resistant epilepsy. The level of M2 subtype markers Arg-1 **(F)** and CD206 **(G)** was decreased significantly in VPA-resistant epilepsy compared with VPA-sensitive epilepsy. **(H)** Representative protein bands of CD86 and CD206 of hippocampus determined by western blotting. The protein level of CD86 **(I)** was significantly decreased, and the protein level of CD208 **(J)** was significantly increased in hippocampus of VPA-resistant epilepsy mice. **(K)** Double-labeling immunofluorescence demonstrated that HIF-1α and Iba-1 co-localized in the hippocampus of mice with VPA-resistant epilepsy. Values are the mean ± S.D. Unpaired *t*-test. $^{*}p < 0.05$, $^{**}p < 0.01$, and $^{***}p < 0.001$. DSE: VPA-sensitive epilepsy and DRE: VPA-resistant epilepsy.

Multiple studies have demonstrated that HIF-1α-related signaling pathways regulate microglia activation. Given our observation, we investigated if increased expression of HIF-1α occurs in microglia by double-labeling immunofluorescence of HIF-1α and Iba-1. HIF-1α and Iba-1 co-localized in the hippocampus of mice with VPA-resistant epilepsy (**Figure 5K**). This result implied that HIF-1α may regulate inflammation by activating microglia in VPA-resistant epilepsy.

Downregulation of miR-221-3p Expression in VPA-Resistant Epilepsy

Multiple studies have shown that miRNAs are valuable biomarkers for the diagnosis and treatment of epilepsy-related diseases. Therefore, we investigated the miRNAs that regulate HIF-1α expression in patients with VPA-resistant epilepsy. Firstly, we re-analyzed two miRNA profiles of hippocampus tissue from patients with DRE published in public databases. The difference analysis of the above two miRNA profiles between DRE and control was preformed using the "DESeq2" R package. There were 71 differentially expressed miRNAs in Profile 1 (**Figure 6A**) and 135 differentially expressed miRNAs in Profile 2 (**Figure 6B**). Profile 1 and Profile 2 had 15 intersected differentially expressed miRNAs screened by a Venn diagram (**Figure 6C**). The starbase database predict that miR-374a-5p, miR-221-3p, miR-302a-5p, miR-190a-3p, miR-301a-3p, and miR-19a) had potential binding sites on and the 3′-UTR sequences of HIF-1α (**Figure 6D**).

Subsequently, expression of these six miRNAs was measured in the plasma of children with VPA-resistant/sensitive epilepsy by RT-qPCR. However, only miR-221-3p was reduced significantly in the plasma of children with VPA-resistant epilepsy compared with that in children with VPA-sensitive epilepsy (**Figure 6E**). This result was confirmed in the hippocampal tissue of VPA-resistant mice (**Figure 6F**).

The predicted binding site of miR-221-3p and HIF-1α was determined using a luciferase reporter gene assay. The luciferase activity of HIF-1α-Wt in the miR-221-3p mimic group was reduced greatly compared with that in the NC group. In HIF-1α-Mut cells, there was no obvious difference between the miR-221-3p mimic group and NC group (**Figures 6G,H**). This result illustrated that downregulated expression of miR-221-3p in VPA-resistant epilepsy may cause its negative regulatory target gene, HIF-1α, to accumulate.

MiR-221-3p Mimics/HIF-1α Inhibitor Could Attenuates Seizures and Inflammatory Response in VPA-Resistant Epilepsy

The above results indicate that down-regulated miR-221-3p and up-regulated HIF-1α may be involved in the pathogenesis of VPA-resistant epilepsy. To test this hypothesis, we surveyed the effect of miR-221-3p mimics and 2ME2 (HIF-1α inhibitor) in VPA-resistant epilepsy. First, we demonstrated that miR-221-3p mimics markedly increased miR-221-3p expression and 2ME2 evidently reduced the expression of HIF-1α in the hippocampus of mice with VPA-resistant epilepsy (**Figures 7A,B**). Subsequently, we confirmed that up-regulated miR-221-3p significantly reduce HIF-1α expression in the hippocampus of mice with VPA-resistant epilepsy, which reduced expression of IL-1β and TNF-α further (**Figure 7** B ~ E). MiR-221-3p mimics or 2ME2 could reduce the number of microglia activated in the CA1 and CA3 regions of the hippocampus in mice with VPA-resistant epilepsy (**Figures 7F–H**). Meanwhile, miR-221-3p mimics or 2ME2 could decreased the number of increased seizures in VPA-resistant epilepsy (**Figures 7I,J**). Taken together, these data showed that increasing miR-221-3p expression reduced HIF-1α expression. This action decreased expression of proinflammatory factors and the number of activated microglia and, ultimately, reduced the number of seizures in mice with VPA-resistant epilepsy (**Figure 8**).

DISCUSSION

We investigated the effect of HIF-1α in VPA-resistant epilepsy. It is a key regulator of local hypoxia and neuroinflammation, which are important clinical phenomena in VPA-resistant epilepsy. The role of HIF-1α in the mechanism of VPA-resistant epilepsy is still unclear or even controversial. We showed that downregulation of miR-221-3p expression in VPA-resistant epilepsy led to accumulation of its negative regulatory target gene: HIF-1α. These actions led to the activation of mocroglia, accompanied by upregulation of proinflammatory mediator and aggravation epileptic behavior. This is the first study to demonstrate the significance of miR-221-3p/HIF-1α in VPA-resistant epilepsy.

An increasing body of evidences suggests that inflammatory mediators are widely involved in, and sufficient for, generating epileptic seizures. Anti-inflammatory compounds, such as IRL-1 blockers and COX-2 inhibitors (Citraro et al., 2015), can significantly suppress the development of spontaneous recurrent seizures and reduce the extent of CA1 injury and sprouting of mossy fibers (Aronica et al., 2017). Previously, we showed that IL-1β, TNF-α, and other proinflammatory mediators are overexpressed in VPA-resistant epilepsy, but we did not explore the mechanisms that trigger this phenomenon.

To address this question, we established VPA-resistant mice and VPA-sensitive mice. Proteomics analysis revealed that overexpressed HIF-1α interacted with IL-1β and TNF-α in mice with VPA-resistant epilepsy, which was also confirmed by western blotting. The regulatory effect of HIF-1α on IL-1β expression has been studied in the context of sarcoidosis, infections, and cancer. Studies have shown that HIF-1 as a transcription factor be composed of HIF-1α and HIF-1β subunits, which translocate into the nucleus and bind to hypoxia-response elements to regulate the transcriptional expression of IL-1β. Studies have also shown that HIF-1α is responsible for recruiting M1 macrophages that release TNF-α in patients with heart failure (Warbrick and Rabkin, 2019). Above results evidence that upregulation of HIF-1α expression in VPA-resistant epilepsy leads to increased expression of IL-1β and TNF-α.

Prior has indicated that excessive activation of microglia in patients with epilepsy exacerbates the release of proinflammatory

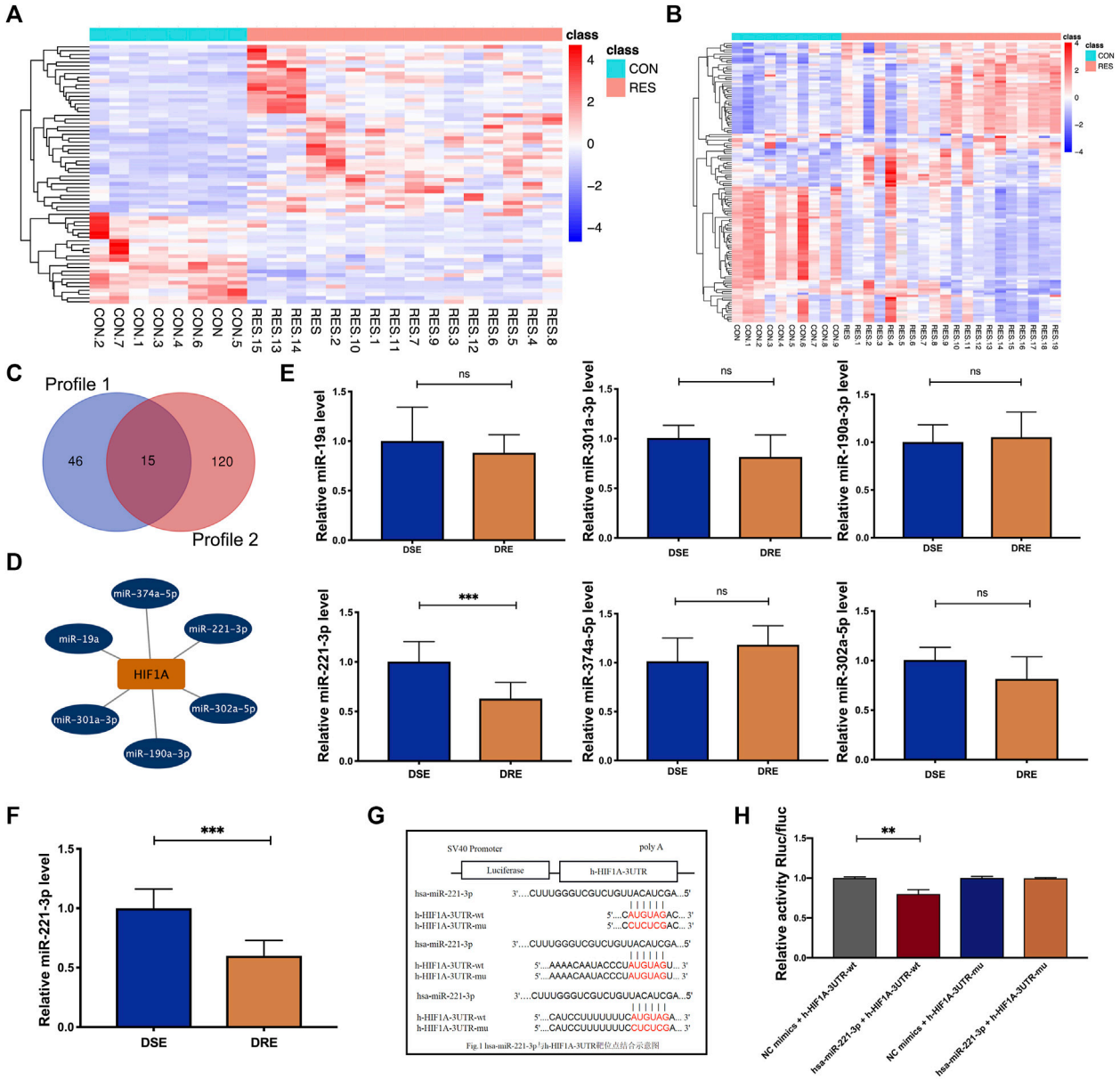

FIGURE 6 | Identification of the miRNA regulating HIF-1α expression in VAP-resistant epilepsy. **(A)** Heatmap of the 71 differentially expressed miRNAs of Profile 1. **(B)** Heatmap of the 135 differentially expressed miRNAs of Profile 2. **(C)** Profile 1 and Profile 2 had 15 intersected differentially expressed miRNAs screened by a Venn diagram. **(D)** The starbase database predicted that six differentially expressed miRNAs (miR-374a-5p, miR-221-3p, miR-302a-5p, miR-190a-3p, miR-301a-3p, and miR-19a) potentially regulate the expression of HIF-1α. **(E)** MiR-221-3p was reduced significantly in the blood of children with VPA-resistant epilepsy compared with that of children with VPA-sensitive epilepsy. There is no significant difference in miR-374a-5p, miR-302a-5p, miR-190a-3p, miR-301a-3p and miR-19a between VPA-sensitive group and VPA-resistant group (DSE: $n = 8$; DRE: n = 16). **(F)** MiR-221-3p in hippocampus of VPA-resistant group was significantly lower than that in VPA-sensitive group ($n = 6$). **(G)** The predicted binding sites of miR-221-3p in the 3′-UTR of HIF-1α was verified by luciferase reporter gene assay. **(H)** Dual luciferase reporter gene assay demonstrated that miR-221-3p could negatively regulated the expression of HIF-1α. Values are the mean ± S.D. Unpaired *t*-test. $^{*}p < 0.05$, $^{**}p < 0.01$, and $^{***}p < 0.001$. DSE: VPA-sensitive epilepsy and DRE: VPA-resistant epilepsy. NC: negative control, Wt: wild type, and Mut: mutant.

mediators (Patel et al., 2019). Activated microglia release proinflammatory cytokines, which can lead to neuronal hyperexcitability. In addition, microglia induced disruptions in neuronal circuits by impairing synaptic pruning, which leads to seizures (Schafer et al., 2016). Boer et al. found that patients with focal cortical dysplasia (a major cause of DRE) have a specific and persistent increase in the number of microglia within the dysplastic region (Boer et al., 2006). Our results indicated that the number of microglia in the CA1 and CA3 regions of the hippocampus of mice with VPA-resistant epilepsy was increased greatly, and was accompanied by microglial polarization from the M2 phenotype to the M1 phenotype. Microglial activation in the

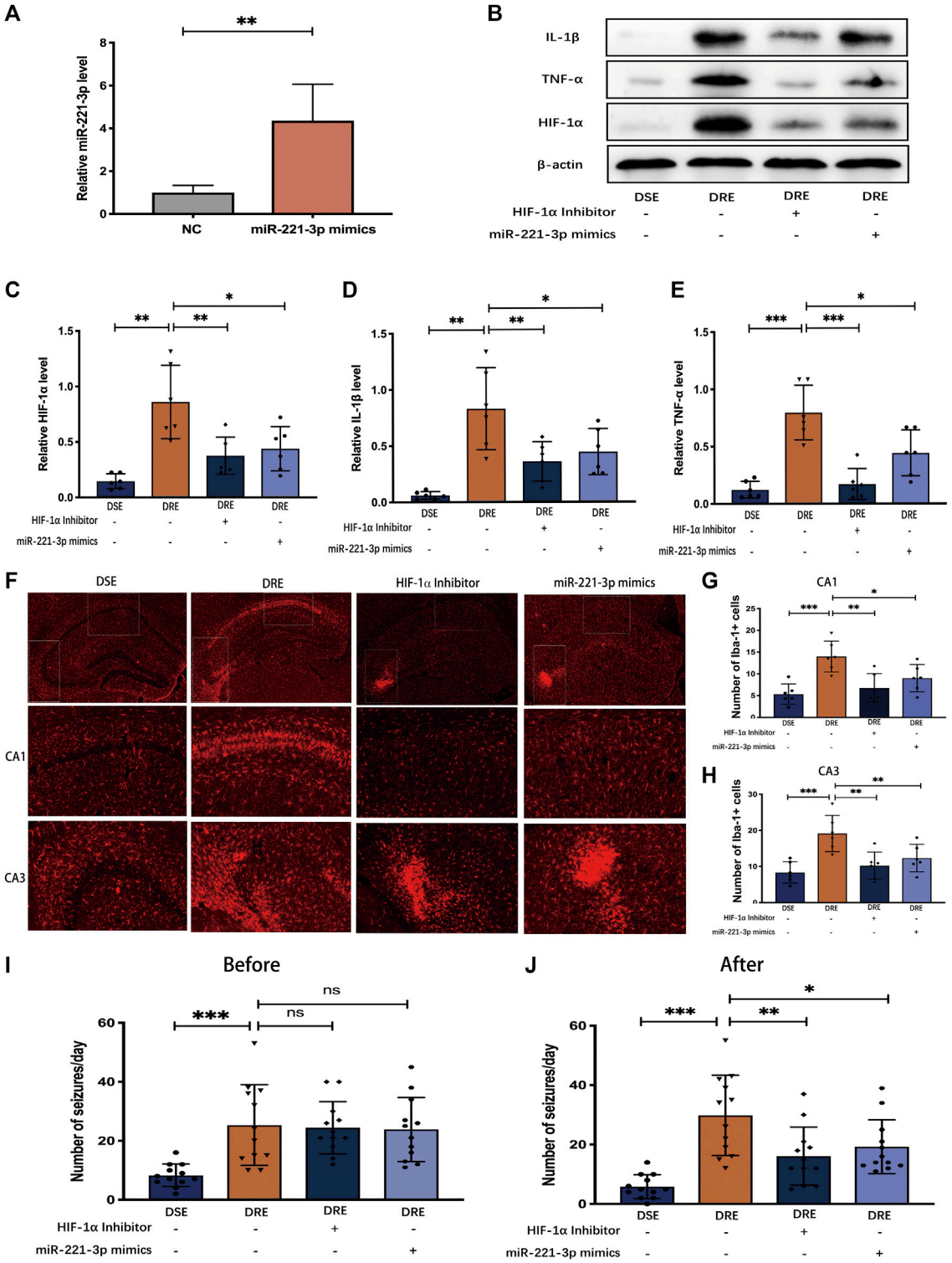

FIGURE 7 | Effect of miR-221-3p mimics and HIF-1α inhibitor in mice with VPA-resistant epilepsy ($n = 6$). **(A)** MiR-221-3p mimics effectively up-regulated the level of miR-221-3p in hippocampus by 4 times. **(B)** Representative protein bands of IL-1β, TNF-α, and HIF-1α as determined by western blotting. MiR-221-3p mimics and HIF-1α inhibitor can significantly reduce the proteins expression of IL-1β **(C)** TNF-α **(D)** and HIF-1α **(E)** in the hippocampus of mice with VPA-resistant epilepsy. **(F)** Representative immunohistochemistry images of Iba-1 in the CA1 and CA3 region of hippocampus. MiR-221-3p mimics and HIF-1α inhibitor evidently decreased the number of Iba-1-positive cells in the hippocampal CA1 **(G)** and CA3 **(H)** regions. **(I)** Before intervention with miR-221-3p mimics and HIF-1α inhibitor, there were no obvious difference in the number of seizures between the VPA-resistant group with the miR-221-3p mimics or HIF-1α inhibitor group. **(J)** MiR-221-3p mimics and HIF-1α inhibitor inhibited the seizure of VPA-resistant epilepsy. Values are the mean ± S.D. Unpaired *t*-test. $^{*}p < 0.05$, $^{**}p < 0.01$, and $^{***}p < 0.001$. DSE: VPA-sensitive epilepsy and DRE: VPA-resistant epilepsy.

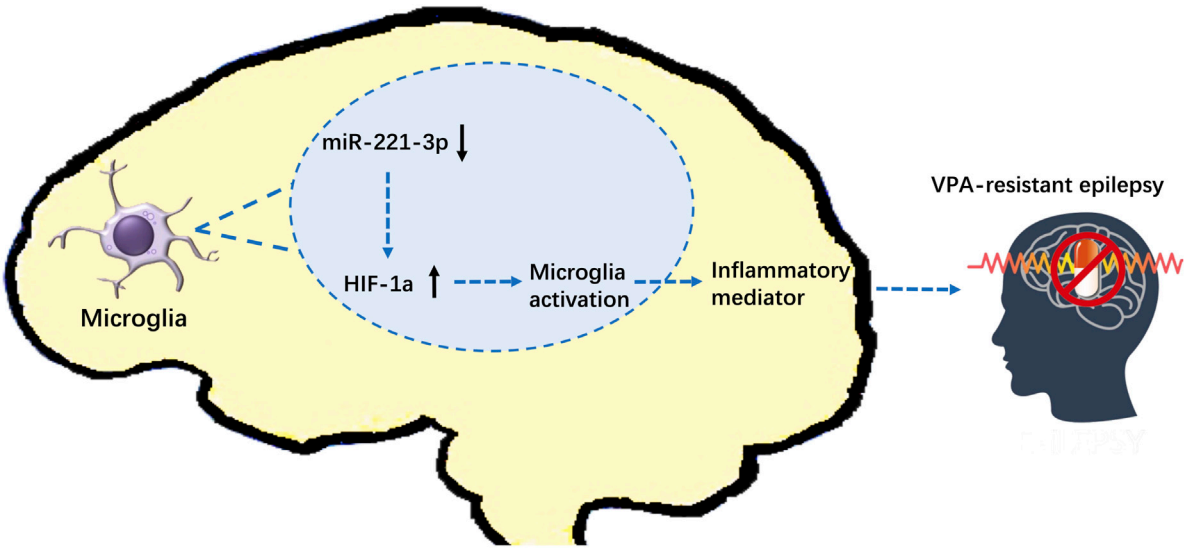

FIGURE 8 | Effect of miR-221-3p/HIF-1α on VPA-resistant epilepsy (schematic). MiR-221-3p is downregulated in VPA-resistant epilepsy, which leads to the increase of its target gene: HIF-1α. Increased expression of HIF-1α activates microglia to release proinflammatory mediators, which exacerbates seizures of VPA-resistant epilepsy.

CNS is heterogeneous, and is categorized by the M1 phenotype (pro-inflammation) and M2 phenotype (anti-inflammation) (Lan et al., 2017). The dynamic changes of microglia from the M2 subtype to M1 subtype is a hallmark of the inflammatory response of the CNS (Qiu et al., 2020). Studies have shown that HIF-1α related signaling pathways regulate microglia activation in Alzheimer's disease (Baik et al., 2019). Han et al. indicated that HIF-1α deficient glial reduced neutrophil migration and infarct, which suppressed the release of IL-1β and CXCL1. Therefore, we explored the localization of HIF-1α and microglia. The results are consistent with this point. HIF-1α was co-localized with microglia markers. That is, The accumulation of HIF-1α in VPA-resistant epilepsy caused activation of microglia and aggravated the release of proinflammatory mediators.

Biomarkers for identification and treatment of VPA-resistant epilepsy are crucial for tailored treatment and optimal allocation of healthcare resources for this patient population (Kalilani et al., 2018). As a small molecule, most of miRNAs can penetrate the blood-brain barrier and exist stably in blood and urine. Therefore, we investigated specific miRNAs in VPA-resistant epilepsy, hoping that it can become a valuable biomarker. As we know, it is difficult to collect hippocampal tissue from children with VPA-resistant epilepsy in clinical practice. In order to efficiently find the miRNA that regulates HIF-1α in VPA-resistant epilepsy, this study firstly performed integrated bioinformatics analysis on the hippocampal tissue of patients with drug-resistant epilepsy in public databases referring to the previous method (Xu et al., 2020). Subsequently, the miRNAs that potentially regulate the expression of HIF-1α were selected. Finally, these miRNAs were screened in the blood samples of children with VPA-resistant epilepsy, and were verified in the hippocampus of VPA-resistant epilepsy mice. We identified that miR-221-3p was down-regulated markedly in VPA-resistant epilepsy, and negatively regulated the expression of the target gene: *HIF-1α*. The regulatory effect of miR-221-3p on the expression of HIF-1α is consistent with a recently published study, which demonstrated that HIF-1α was the target gene of miR-221-3p in patients with heart failure and antagomiR-221-3p increased HIF-1α expression (Li et al., 2021). Subsequently, we demonstrated that miR-221-3p mimics effectively reduce the expression of HIF-1α in the hippocampus of mice with VPA-resistant epilepsy, thereby reducing the number of microglia, inhibiting the release of proinflammatory mediators, and alleviating the number of seizures markedly.

However, our present work still has some limitations. Firstly, in clinical practice, multi-drug combination therapy is the main approach for children with epilepsy. Therefore, the children with VPA-resistant epilepsy enrolled into this study were resistant to multiple AEDs. Since multiple AEDs are involved in the neuroinflammatory process (Itoh et al., 2019; Park et al., 2020), the resistance to other AEDs may be a confounding factor in our study. In future studies, we will further investigate the significance of neuroinflammatory processes in VPA-resistant epilepsy, while considering the effect of other common antiepileptic drugs. Secondly, various inflammatory mediators such as CXCL9, CXCL3, and IL-6 have been shown to be dysregulated in patients with drug-resistant epilepsy. Since this study focused on the role of HIF-1α in VPA-resistant epilepsy, we prioritized IL-1β and TNF-α that directly interact with HIF-1α. In future study, we will pay attention to the effects of chemokines and cytokines released by activated microglia in VPA-resistant epilepsy. Thirdly, this study found the dysregulation of miR-221-3p, IL-1β, and TNF-α in VPA-resistant epilepsy, and confirmed the influence of these mediators on seizure severity. However, due to the small number of patients enrolled, we have not performed further

studies on the correlation between these mediators and clinical parameters.

CONCLUSION

We demonstrated that expression of miR-221-3p, as a potential biomarker, is downregulated in VPA-resistant epilepsy, which leads to increase in expression of its target gene: HIF-1α. Increased expression of HIF-1α activates microglia to release proinflammatory mediators, which exacerbates seizures. Our data suggest the effect of miR-221-3p/HIF-1α on VPA-resistant epilepsy. These alterations should be considered when studying the mechanisms of VPA-resistant epilepsy and designing drug treatments.

DATA AVAILABILITY STATEMENT

The datasets presented in this study can be found in online repositories. The names of the repository/repositories and accession number(s) can be found in the article/ **Supplementary Material**

ETHICS STATEMENT

The studies involving human participants were reviewed and approved by Institutional Ethics Committee of Children's Hospital of Fudan University. Written informed consent to participate in this study was provided by the participants' legal guardian/next of kin.

AUTHOR CONTRIBUTIONS

ZL, JT, XZ, and MF designed the research. MF and WW performed the data analysis work. MF, YS, YZ, and JZ conducted experiments. MF and YZ wrote and revised the manuscript. MF drew the figures. JZ was responsible for the statistical analyses. MF, YZ, and JZ are co-first author. All authors read and approved the final manuscript.

FUNDING

This study was supported by the National Natural Science Foundation of China (No. 81874325), the Shanghai Municipal Health Bureau (No. 2016ZB0305), and the Science and Technology Commission of Shanghai Municipality (No. 18DZ1910604, No.19XD1400900).

SUPPLEMENTARY MATERIAL

The Supplementary Material for this article can be found online at: https://www.frontiersin.org/articles/10.3389/fphar.2021.714556/full#supplementary-material

REFERENCES

Aronica, E., Bauer, S., Bozzi, Y., Caleo, M., Dingledine, R., Gorter, J. A., et al. (2017). Neuroinflammatory Targets and Treatments for Epilepsy Validated in Experimental Models. *Epilepsia* 58 (Suppl. 3), 27–38. doi:10.1111/epi.13783

Aronica, E., Fluiter, K., Iyer, A., Zurolo, E., Vreijling, J., van Vliet, E. A., et al. (2010). Expression Pattern of miR-146a, an Inflammation-Associated microRNA, in Experimental and Human Temporal Lobe Epilepsy. *Eur. J. Neurosci.* 31 (6), 1100–1107. doi:10.1111/j.1460-9568.2010.07122.x

Baik, S. H., Kang, S., Lee, W., Choi, H., Chung, S., Kim, J. I., et al. (2019). A Breakdown in Metabolic Reprogramming Causes Microglia Dysfunction in Alzheimer's Disease. *Cell Metab* 30 (3), 493–e6. e496. doi:10.1016/j.cmet.2019.06.005

Balamurugan, K. (2016). HIF-1 at the Crossroads of Hypoxia, Inflammation, and Cancer. *Int. J. Cancer* 138 (5), 1058–1066. doi:10.1002/ijc.29519

Bartolomei, F., Barbeau, E. J., Nguyen, T., McGonigal, A., Régis, J., Chauvel, P., et al. (2012). Rhinal-hippocampal Interactions during Déjà Vu. *Clin. Neurophysiol.* 123 (3), 489–495. doi:10.1016/j.clinph.2011.08.012

Bateman, L. M., Li, C. S., and Seyal, M. (2008). Ictal Hypoxemia in Localization-Related Epilepsy: Analysis of Incidence, Severity and Risk Factors. *Brain* 131 (Pt 12), 3239–3245. doi:10.1093/brain/awn277

Boer, K., Spliet, W. G., van Rijen, P. C., Redeker, S., Troost, D., and Aronica, E. (2006). Evidence of Activated Microglia in Focal Cortical Dysplasia. *J. Neuroimmunol* 173 (1-2), 188–195. doi:10.1016/j.jneuroim.2006.01.002

Chen, Z., Brodie, M. J., Liew, D., and Kwan, P. (2018). Treatment Outcomes in Patients with Newly Diagnosed Epilepsy Treated with Established and New Antiepileptic Drugs: A 30-Year Longitudinal Cohort Study. *JAMA Neurol.* 75 (3), 279–286. doi:10.1001/jamaneurol.2017.3949

Citraro, R., Leo, A., Marra, R., De Sarro, G., and Russo, E. (2015). Antiepileptogenic Effects of the Selective COX-2 Inhibitor Etoricoxib, on the Development of Spontaneous Absence Seizures in WAG/Rij Rats. *Brain Res. Bull.* 113, 1–7. doi:10.1016/j.brainresbull.2015.02.004

Devinsky, O., Vezzani, A., Najjar, S., De Lanerolle, N. C., and Rogawski, M. A. (2013). Glia and Epilepsy: Excitability and Inflammation. *Trends Neurosci.* 36 (3), 174–184. doi:10.1016/j.tins.2012.11.008

Fabian, M. R., and Sonenberg, N. (2012). The Mechanics of miRNA-Mediated Gene Silencing: a Look under the Hood of miRISC. *Nat. Struct. Mol. Biol.* 19 (6), 586–593. doi:10.1038/nsmb.2296

Fu, M., Tao, J., Wang, D., Zhang, Z., Wang, X., Ji, Y., et al. (2020). Downregulation of MicroRNA-34c-5p Facilitated Neuroinflammation in Drug-Resistant Epilepsy. *Brain Res.* 1749, 147130. doi:10.1016/j.brainres.2020.147130

Gesche, J., Khanevski, M., Solberg, C., and Beier, C. P. (2017). Resistance to Valproic Acid as Predictor of Treatment Resistance in Genetic Generalized Epilepsies. *Epilepsia* 58 (4), e64–e69. doi:10.1111/epi.13702

Han, C. L., Ge, M., Liu, Y. P., Zhao, X. M., Wang, K. L., Chen, N., et al. (2018). LncRNA H19 Contributes to Hippocampal Glial Cell Activation via JAK/STAT Signaling in a Rat Model of Temporal Lobe Epilepsy. *J. Neuroinflammation* 15 (1), 103. doi:10.1186/s12974-018-1139-z

Henshall, D. C., Hamer, H. M., Pasterkamp, R. J., Goldstein, D. B., Kjems, J., Prehn, J. H. M., et al. (2016). MicroRNAs in Epilepsy: Pathophysiology and Clinical Utility. *Lancet Neurol.* 15 (13), 1368–1376. doi:10.1016/s1474-4422(16)30246-0

Itoh, K., Taniguchi, R., Matsuo, T., Oguro, A., Vogel, C. F. A., Yamazaki, T., et al. (2019). Suppressive Effects of Levetiracetam on Neuroinflammation and Phagocytic Microglia: A Comparative Study of Levetiracetam, Valproate and Carbamazepine. *Neurosci. Lett.* 708, 134363. doi:10.1016/j.neulet.2019.134363

Kalilani, L., Sun, X., Pelgrims, B., Noack-Rink, M., and Villanueva, V. (2018). The Epidemiology of Drug-Resistant Epilepsy: A Systematic Review and Meta-Analysis. *Epilepsia* 59 (12), 2179–2193. doi:10.1111/epi.14596

Kan, A. A., van Erp, S., Derijck, A. A., de Wit, M., Hessel, E. V., O'Duibhir, E., et al. (2012). Genome-wide microRNA Profiling of Human Temporal Lobe Epilepsy

Identifies Modulators of the Immune Response. *Cell Mol Life Sci* 69 (18), 3127–3145. doi:10.1007/s00018-012-0992-7

Kanner, A. M., Ashman, E., Gloss, D., Harden, C., Bourgeois, B., Bautista, J. F., et al. (2018). Practice Guideline Update Summary: Efficacy and Tolerability of the New Antiepileptic Drugs II: Treatment-Resistant Epilepsy: Report of the Guideline Development, Dissemination, and Implementation Subcommittee of the American Academy of Neurology and the American Epilepsy Society. *Neurology* 91 (2), 82–90. doi:10.1212/wnl.0000000000005756

Korotkov, A., Broekaart, D. W. M., Banchaewa, L., Pustjens, B., van Scheppingen, J., Anink, J. J., et al. (2020). microRNA-132 Is Overexpressed in Glia in Temporal Lobe Epilepsy and Reduces the Expression of Pro-epileptogenic Factors in Human Cultured Astrocytes. *Glia* 68 (1), 60–75. doi:10.1002/glia.23700

Kwan, P., Arzimanoglou, A., Berg, A. T., Brodie, M. J., Allen Hauser, W., Mathern, G., et al. (2010). Definition of Drug Resistant Epilepsy: Consensus Proposal by the Ad Hoc Task Force of the ILAE Commission on Therapeutic Strategies. *Epilepsia* 51 (6), 1069–1077. doi:10.1111/j.1528-1167.2009.02397.x

Lan, X., Han, X., Li, Q., Yang, Q. W., and Wang, J. (2017). Modulators of Microglial Activation and Polarization after Intracerebral Haemorrhage. *Nat. Rev. Neurol.* 13 (7), 420–433. doi:10.1038/nrneurol.2017.69

Li, Y., Yan, C., Fan, J., Hou, Z., and Han, Y. (2021). MiR-221-3p Targets Hif-1α to Inhibit Angiogenesis in Heart Failure. *Lab. Invest.* 101 (1), 104–115. doi:10.1038/s41374-020-0450-3

Löscher, W., Potschka, H., Sisodiya, S. M., and Vezzani, A. (2020). Drug Resistance in Epilepsy: Clinical Impact, Potential Mechanisms, and New Innovative Treatment Options. *Pharmacol. Rev.* 72 (3), 606–638. doi:10.1124/pr.120.019539

Lu, T. X., and Rothenberg, M. E. (2018). MicroRNA. *J. Allergy Clin. Immunol.* 141 (4), 1202–1207. doi:10.1016/j.jaci.2017.08.034

O'Carroll, D., and Schaefer, A. (2013). General Principals of miRNA Biogenesis and Regulation in the Brain. *Neuropsychopharmacology* 38 (1), 39–54. doi:10.1038/npp.2012.87

Organista-Juárez, D., Jiménez, A., Rocha, L., Alonso-Vanegas, M., and Guevara-Guzmán, R. (2019). Differential Expression of miR-34a, 451, 1260, 1275 and 1298 in the Neocortex of Patients with Mesial Temporal Lobe Epilepsy. *Epilepsy Res.* 157, 106188. doi:10.1016/j.eplepsyres.2019.106188

Ouédraogo, O., Rébillard, R. M., Jamann, H., Mamane, V. H., Clénet, M. L., Daigneault, A., et al. (2021). Increased Frequency of Proinflammatory CD4 T Cells and Pathological Levels of Serum Neurofilament Light Chain in Adult Drug-resistant Epilepsy. *Epilepsia* 62 (1), 176–189. doi:10.1111/epi.16742

Park, C. W., Ahn, J. H., Lee, T. K., Park, Y. E., Kim, B., Lee, J. C., et al. (2020). Post-treatment with Oxcarbazepine Confers Potent Neuroprotection against Transient Global Cerebral Ischemic Injury by Activating Nrf2 Defense Pathway. *Biomed. Pharmacother.* 124, 109850. doi:10.1016/j.biopha.2020.109850

Patel, D. C., Tewari, B. P., Chaunsali, L., and Sontheimer, H. (2019). Neuron-glia Interactions in the Pathophysiology of Epilepsy. *Nat. Rev. Neurosci.* 20 (5), 282–297. doi:10.1038/s41583-019-0126-4

Qiu, Z., Lu, P., Wang, K., Zhao, X., Li, Q., Wen, J., et al. (2020). Dexmedetomidine Inhibits Neuroinflammation by Altering Microglial M1/M2 Polarization through MAPK/ERK Pathway. *Neurochem. Res.* 45 (2), 345–353. doi:10.1007/s11064-019-02922-1

Racine, R. J. (1972). Modification of Seizure Activity by Electrical Stimulation. II. Motor Seizure. *Electroencephalogr Clin. Neurophysiol.* 32 (3), 281–294. doi:10.1016/0013-4694(72)90177-0

Rana, A., and Musto, A. E. (2018). The Role of Inflammation in the Development of Epilepsy. *J. Neuroinflammation* 15 (1), 144. doi:10.1186/s12974-018-1192-7

Schafer, D. P., Heller, C. T., Gunner, G., Heller, M., Gordon, C., Hammond, T., et al. (2016). Microglia Contribute to Circuit Defects in Mecp2 Null Mice Independent of Microglia-specific Loss of Mecp2 Expression. *Elife* 5. doi:10.7554/eLife.15224

Semenza, G. L. (2014). Hypoxia-inducible Factor 1 and Cardiovascular Disease. *Annu. Rev. Physiol.* 76, 39–56. doi:10.1146/annurev-physiol-021113-170322

Semenza, G. L. (2003). Targeting HIF-1 for Cancer Therapy. *Nat. Rev. Cancer* 3 (10), 721–732. doi:10.1038/nrc1187

Strauss, K. I., and Elisevich, K. V. (2016). Brain Region and Epilepsy-Associated Differences in Inflammatory Mediator Levels in Medically Refractory Mesial Temporal Lobe Epilepsy. *J. Neuroinflammation* 13 (1), 270. doi:10.1186/s12974-016-0727-z

Su, G., Morris, J. H., Demchak, B., and Bader, G. D. (2014). Biological Network Exploration with Cytoscape 3. *Curr. Protoc. Bioinformatics* 47, 8–11. doi:10.1002/0471250953.bi0813s47

Szklarczyk, D., Franceschini, A., Wyder, S., Forslund, K., Heller, D., Huerta-Cepas, J., et al. (2015). STRING V10: Protein-Protein Interaction Networks, Integrated over the Tree of Life. *Nucleic Acids Res.* 43 (Database issue), D447–D452. doi:10.1093/nar/gku1003

Thijs, R. D., Surges, R., O'Brien, T. J., and Sander, J. W. (2019). Epilepsy in Adults. *Lancet* 393 (10172), 689–701. doi:10.1016/s0140-6736(18)32596-0

Wang, Y., and Li, Z. (2019). RNA-seq Analysis of Blood of Valproic Acid-Responsive and Non-responsive Pediatric Patients with Epilepsy. *Exp. Ther. Med.* 18 (1), 373–383. doi:10.3892/etm.2019.7538

Warbrick, I., and Rabkin, S. W. (2019). Hypoxia-inducible Factor 1-alpha (HIF-1α) as a Factor Mediating the Relationship between Obesity and Heart Failure with Preserved Ejection Fraction. *Obes. Rev.* 20 (5), 701–712. doi:10.1111/obr.12828

Weidner, L. D., Kannan, P., Mitsios, N., Kang, S. J., Hall, M. D., Theodore, W. H., et al. (2018). The Expression of Inflammatory Markers and Their Potential Influence on Efflux Transporters in Drug-Resistant Mesial Temporal Lobe Epilepsy Tissue. *Epilepsia* 59 (8), 1507–1517. doi:10.1111/epi.14505

Xu, J., Sun, M., Wang, Y., Xie, A., and Gao, J. (2020). Identification of Hub Genes of Mesio Temporal Lobe Epilepsy and Prognostic Biomarkers of Brain Low-Grade Gliomas Based on Bioinformatics Analysis. *Cell Transpl.* 29, 963689720978722. doi:10.1177/0963689720978722

Conflict of Interest: The authors declare that the research was conducted in the absence of any commercial or financial relationships that could be construed as a potential conflict of interest.

Publisher's Note: All claims expressed in this article are solely those of the authors and do not necessarily represent those of their affiliated organizations, or those of the publisher, the editors and the reviewers. Any product that may be evaluated in this article, or claim that may be made by its manufacturer, is not guaranteed or endorsed by the publisher.

frontiers in Pharmacology

ORIGINAL RESEARCH
published: 09 September 2021
doi: 10.3389/fphar.2021.724993

Pre- and Early Post-treatment With *Arthrospira platensis* (Spirulina) Extract Impedes Lipopolysaccharide-triggered Neuroinflammation in Microglia

*Anna Piovan, Jessica Battaglia, Raffaella Filippini, Vanessa Dalla Costa, Laura Facci, Carla Argentini, Andrea Pagetta, Pietro Giusti and Morena Zusso**

Department of Pharmaceutical and Pharmacological Sciences, University of Padua, Padua, Italy

OPEN ACCESS

Edited by:
Javier R. Caso, Universidad Complutense de Madrid, Spain

Reviewed by:
Ravikanth Velagapudi, Duke University, United States
Dora Pinho, Universidade do Porto, Portugal

***Correspondence:**
Morena Zusso
morena.zusso@unipd.it

Specialty section:
This article was submitted to Neuropharmacology, a section of the journal Frontiers in Pharmacology

Received: *14 June 2021*
Accepted: *25 August 2021*
Published: *09 September 2021*

Citation:
Piovan A, Battaglia J, Filippini R, Dalla Costa V, Facci L, Argentini C, Pagetta A, Giusti P and Zusso M (2021) Pre- and Early Post-treatment With Arthrospira platensis *(Spirulina) Extract Impedes Lipopolysaccharide-triggered Neuroinflammation in Microglia. Front. Pharmacol. 12:724993. doi: 10.3389/fphar.2021.724993*

Background: Uncontrolled neuroinflammation and microglia activation lead to cellular and tissue damage contributing to neurodegenerative and neurological disorders. Spirulina (*Arthrospira platensis* (Nordstedt) Gomont, or *Spirulina platensis*), a blue-green microalga, which belongs to the class of cyanobacteria, has been studied for its numerous health benefits, which include anti-inflammatory properties, among others. Furthermore, *in vivo* studies have highlighted neuroprotective effects of Spirulina from neuroinflammatory insults in different brain areas. However, the mechanisms underlying the anti-inflammatory effect of the microalga are not completely understood. In this study we examined the effect of pre- and post-treatment with an acetone extract of Spirulina (E1) in an *in vitro* model of LPS-induced microglia activation.

Methods: The effect of E1 on the release of IL-1β and TNF-α, expression of iNOS, nuclear factor erythroid 2–related factor 2 (Nrf2), and heme oxygenase-1 (HO-1), and the activation of NF-κB was investigated in primary microglia by ELISA, real-time PCR, and immunofluorescence.

Results: Pre- and early post-treatment with non-cytotoxic concentrations of E1 down-regulated the release of IL-1β and TNF-α, and the over-expression of iNOS induced by LPS. E1 also significantly blocked the LPS-induced nuclear translocation of NF-κB p65 subunit, and upregulated gene and protein levels of Nrf2, as well as gene expression of HO-1.

Conclusions: These results indicate that the extract of Spirulina can be useful in the control of microglia activation and neuroinflammatory processes. This evidence can support future *in vivo* studies to test pre- and post-treatment effects of the acetone extract from Spirulina.

Keywords: neuroinflammation, microglia, spirulina, pre-treatment, post-treatment, pro-inflammatory cytokines

INTRODUCTION

Neuroinflammation is a complex and multifactorial response of the central nervous system (CNS) directed at protecting the brain from endogenous and exogenous noxious stimuli and restoring tissue homeostasis and integrity. Although the protective purpose of the inflammatory response, a minimal unbalance in its components may result harmful and contribute to virtually every neurodegenerative/neurological disorder (Amor et al., 2014; Sochocka et al., 2017; Skaper et al., 2018). Microglia are the immunocompetent cells in the CNS that largely participate in neuroinflammatory processes (Gomez-Nicola and Perry, 2015; Colonna and Butovsky, 2017). Once activated these cells secrete pro-inflammatory cytokines, chemokines, nitric oxide, and oxygen radicals, that contribute to the development of CNS damage (Lucas et al., 2006). Microglia activation mechanisms begin with the recognition of pathogens through a limited number of pattern-recognition receptors, including Toll-like receptors (TLRs), which are involved in the initiation of innate immune response (Bsibsi et al., 2002; Kawai and Akira, 2010). Among TLR family members, TLR2, 4, and 9 are mainly implicated in neurodegenerative diseases such as Alzheimer's disease, Parkinson's disease, and amyotrophic lateral sclerosis (Fiebich et al., 2018). TLR activation initiates diverse signal transduction pathways, including the activation of the transcription factor nuclear factor (NF)-κB, which regulates the transcription of many genes involved in immunity and inflammation (Bryant et al., 2010). Therefore, microglia activation and TLRs are regarded as potential targets for therapeutic intervention in brain diseases associated with neuroinflammation (Liu et al., 2019).

In recent years, microalgae are gaining a high interest for their nutritional and therapeutic applications being important sources of food ingredients and bioactive products with numerous health benefits (Gómez-Zorita et al., 2019). Microalgae are prokaryotic or eukaryotic single-cell organisms, found in fresh water and marine systems. They produce half of the atmospheric oxygen and a variety of compounds, such as photosynthetic pigments, polyunsaturated fatty acids, vitamins, minerals, fibers, polysaccharides, enzymes, and peptides (Khan et al., 2018; Galasso et al., 2019). Among the microalgae, Spirulina (*Arthrospira platensis* (Nordstedt) Gomont, or *Spirulina platensis*) is a photosynthetic, filamentous, spiral shaped, and blue-green cyanobacterium that has a long history as dietary supplement, based on its high content of proteins (60–70% of the microalga dry weight). It also contains vitamins (in particular vitamin B12), minerals (iron, calcium, magnesium, zinc, manganese, phosphorus, and potassium), essential fatty acids (e.g., γ-linoleic acid, palmitic acid, linoleic acid, oleic acid), polysaccharides, glycolipids and sulfolipids, enzymes (e.g., superoxide dismutase), and various pigments, including phycocyanins, chlorophylls, and carotenoids (Colla et al., 2004; Niccolai et al., 2019). Recently, Spirulina has been widely studied for its numerous health benefits, which include antibacterial, antiviral, antioxidant, and anti-inflammatory properties (Remirez et al., 2002; Kulshreshtha et al., 2008; Mallikarjun Gouda et al., 2015; Wu et al., 2016; Finamore et al., 2017). Furthermore, many studies have evidenced the neuroprotective properties of Spirulina in multiple models of CNS diseases, such as Parkinson's disease, schizophrenia, ischemic brain damage and in lipopolysaccharide (LPS)-induced neuroinflammation (Strömberg et al., 2005; Chen et al., 2012; Pabon et al., 2012; Lima et al., 2017; Haider et al., 2021). However, the protective properties of Spirulina have been shown mainly after a pre-treatment (i.e., prophylactic effect), whereas its effect after inflammatory stimuli has been only partially investigated.

In the present study we examined the effects of pre- and post-treatment with an acetonic extract of the microalga Spirulina (E1) on LPS-induced microglial activation *in vitro*. Then, potential mechanisms that regulate the observed effects were also clarified. We found that pre-treatment and early post-treatment with E1 lowered microglia activation by inhibiting the release of pro-inflammatory cytokines and gene expression of inflammatory markers through mechanisms that involve NF-κB and the nuclear factor erythroid 2–related factor 2 (Nrf2).

MATERIAL AND METHODS

Reagents

Unless otherwise specified, all reagents were from Sigma-Aldrich (Milan, Italy). Tissue culture media, antibiotics, and fetal bovine serum (FBS) were obtained from Life Technologies (San Giuliano Milanese, Italy). LPS (Ultra-Pure LPS-EB from *Escherichia coli*, 0111:B4 strain) was purchased from InvivoGen (InvivoGen Europe, Toulouse, France). Dried Spirulina was purchased from a local health-food store. Primary antibodies included: mouse anti-p65 (NF-κB p65, Santa Cruz Biotechnology, Santa Cruz, CA, United States, Cat. sc-8008), mouse anti-iNOS (NOS2, Santa Cruz Biotechnology, Santa Cruz, CA, United States, Cat. sc-7271), and rabbit anti-Nrf2 (GeneTex Inc., Irvine, CA, United States, Cat. GTX103322). Alexa Fluor 488 and 555 secondary antibodies were from and Invitrogen (Milan, Italy, Cat. A11008 and A21422, respectively). Enzyme-linked immunosorbent assay (ELISA) kits were obtained from Antigenix America (Huntington Station, NY, United States). Falcon tissue culture plasticwares were purchased from BD Biosciences (SACCO srl, Cadorago (CO), Italy).

Preparation and Analysis of Spirulina Extract

Properly hydrated powder of Spirulina was ground in a mortar and extracted with acetone in an ultrasonic bath for 20 min at room temperature and then centrifuged at 4,400 rpm for 10 min at 4°C. The extraction process was repeated three times and the combined extracts were concentrated under reduced pressure in a rotary evaporator. The concentrated solution was then lyophilized. Finally, the extract was stored at 4°C until use.

Chlorophyll a, chlorophyll b, and total carotenoid content was determined as described by Yang et al. (1998). Pheophytin content was measured according to the method of Lichtenthaler (1987). One aliquot of the extract was solubilized with acetone:water (4:1) and, after appropriate dilution, the

maximum absorbance was read at 663, 646, 470, 653, and 665 nm for chlorophyll a, chlorophyll b, carotenoids, pheophytin a, and pheophytin b, respectively. The content of pigments was calculated using the following equations:

$$\text{Chlorophyll a}\,(\mu g/mL) = 12.25\,A_{663} - 2.25\,A_{646}$$

$$\text{Chlorophyll b}\,(\mu g/mL) = 20.31\,A_{646} - 2.25\,A_{663}$$

$$\text{Total carotenoids}\,(\mu g/mL) = (1000\,A_{470} - 2.27\,\text{Chlorophyll a} - 81.4\,\text{Chlorophyll b})/227$$

$$\text{Pheophytin a}\,(\mu g/mL) = 22.42\,A_{665} - 6.81\,A_{653}$$

$$\text{Pheophytin b}\,(\mu g/mL) = 40.17\,A_{653} - 18.58\,A_{665}$$

Results were expressed as mg/g of dry weight of extract.

The carotenoid analysis was performed using an Agilent 1100 HPLC Series System (Agilent, Santa Clara, CA, United States) equipped with degasser, quaternary gradient pump, column thermostat, and UV-Vis detector. A Gemini 5-µm C6-Phenyl column (250 × 4.6 mm) from Phenomenex (Torrance, CA, United States) was employed, at 40°C. Analyses were done in the isocratic mode, using acetonitrile:methanol (10:90; v/v) at a flow rate of 1 ml min^{-1}, with an injection volume of 10 µl; detection was at 280, 365, and 460 nm. Carotenoid content was expressed as β-carotene equivalents.

Cell Cultures

Animal-related procedures were performed in accordance with EU Directive (2010/63/EU) for animal experiments and those of the Italian Ministry of Health (D.L. 26/2014) and were approved by the Institutional Review Board for Animal Research (Organismo Preposto al Benessere Animale, OPBA) of the University of Padua and by the Italian Ministry of Health (protocol number 41451.N.N8P). Animals were maintained under controlled conditions (22–24°C, 50%–60% humidity), with free access to water and food on a 12 h light/dark cycle (lights on at 7:00 am). One-day-old Sprague-Dawley rat pups (CD strain) of both sexes were rapidly decapitated, minimizing suffering, discomfort, or stress. Primary microglial cells were isolated from mixed glial cell cultures prepared from the cerebral cortex, as previously described (Skaper et al., 2012). When mixed glial cultures reached confluence (typically 7 days after isolation), microglia were separated from the astroglial monolayer by shaking (200 rpm for 1 h at 37°C), re-suspended in high-glucose Dulbecco's modified eagle medium (DMEM) supplemented with 2 mM L-glutamine, 10% heat-inactivated FBS, 100 units/ml penicillin, 100 µg/ml streptomycin and 50 µg/ml gentamicin (growth medium), and plated on poly-L-lysine-coated (10 µg/ml) plastic wells at a density of 1.50×10^5 cells/cm^2. Cells were allowed to adhere for 45 min and then washed to remove non-adhering cells. Cultures obtained using the shaking procedure generated 97% microglia immunopositive to a primary polyclonal antibody against ionized calcium binding adaptor molecule 1 (Iba1, 1:800, Wako Chemicals United States Inc., Richmond, VA, United States, Cat. 019–19741), a marker for microglia cell types. Cells were maintained at 37°C in a humidified atmosphere containing 5% CO2/95% air. LPS was suspended in endotoxin-free water (InvivoGen). E1 was suspended in dimethylsulfoxide (DMSO) just before use and added to the cultures so as not to exceed 0.1% of the total volume. Control cultures contained the same concentration of DMSO.

TABLE 1 | Primers for real-time PCR used in this study.

Gene target	Primer name	Sequence (5′-3′)
INOS	iNOS For	GGGAACACCTGGGGATTTTC
	iNOS Rev	CACAGTTTGGTCTGGCGAAG
Nrf2	Nrf2 For	GGATATTCCCAGCCACGTTGA
	Nrf2 Rev	AATCAGTCATGGCCGTCTCC
HO-1	HO-1 For	GTTTCCTGTTGGCGACCGTG
	HO-1 Rev	GCCAGGCAAGATTCTCCCCT
β-actin	β-actin For	GATCAGCAAGCAGGAGTACGATGA
	β-actin Rev	GGTGTAAAACGCAGCTCAGTAACA

Cell Treatment

Cells were seeded in poly-L-lysine coated 96-well plates (50,000 cells/well) in growth medium and allowed to adhere overnight. In the pre-treatment experiments, serum-containing medium was replaced with serum-free medium 2 h before pre-treatment with E1 for 1 h, followed by stimulation with 100 ng/ml Ultra-Pure LPS-EB. In the post-treatment experiments, 2 h after serum starvation, microglia were stimulated with 100 ng/ml LPS and 2 or 4 h later cells were treated with E1. In both conditions, microglia were stimulated with LPS for 6 or 16 h for the evaluation of gene expression or cytokine release, respectively.

Cell Viability Assay

Microglial cell viability was evaluated by a colorimetric method utilizing the protein-binding dye sulforhodamine B (SRB) (Skehan et al., 1990; Piovan et al., 2021). Growth medium was replaced with serum-free medium 2 h before treatment with increasing concentrations of E1 for 16 h. After the incubation, the medium was replaced with cold 10% trichloroacetic acid, and plates were incubated for 1 h at 4°C. Following this fixation step, cells were stained with 0.4% SRB and left at room temperature for 30 min. The bound protein stain was solubilized with 10 mM Tris base. The absorbance was then measured at 570 nm in a microplate reader. Absorbance of vehicle-treated cultures was considered as 100% cell viability.

Cytokine Determination

After treatments, culture media were collected and IL-1β and TNF-α assayed using commercially available ELISA kits, according to the manufacturer's instructions. Cytokine concentrations (pg/ml) in the medium were determined by reference to standard curves obtained with known amounts of IL-1β or TNF-α and the results expressed as percentage relative to corresponding control value.

Real-Time Polymerase Chain Reaction

At the end of 6-h LPS stimulation, total RNA was extracted from cells by QIAzol (Invitrogen), according to the manufacturer's instructions. RNA integrity and quantity were determined by RNA 6000 Nano assay in an Agilent BioAnalyser (Thermo

Scientific, Milan, Italy). Reverse transcription was performed with Superscript III reverse transcriptase (Invitrogen). The real-time PCR reaction was performed as described previously (Barbierato et al., 2017). Primer sequences are listed in **Table 1**. Amounts of each gene product were calculated using linear regression analysis from standard curves, demonstrating amplification efficiencies ranging from 90 to 100%. Dissociation curves were generated for each primer pair, showing single product amplification. Data are presented as specific ratio between the gene of interest and the reference gene (β-actin).

Immunofluorescence and Image Analysis

Microglia were grown on coverslips in 24-well plates, pre-treated for 1 h with E1 before stimulation with 100 ng/ml Ultra-Pure LPS-EB for an additional 90 min for the analysis of NF-κB activation, or 16 h for the analysis of iNOS and Nrf2 expression. Cells were fixed with 4% paraformaldehyde (pH 7.4, for 15 min at room temperature) and subsequently non-specific staining was blocked by incubating with 5% normal goat serum/0.1% Triton X-100 in PBS for 1 h at room temperature. Cells were then incubated sequentially with primary (2 h) and secondary antibody (1 h) in the above blocking solution. The antibodies used were mouse anti-p65 (NF-κB p65, 1:500) primary antibody, mouse anti-iNOS (1:500), and rabbit anti-Nrf2 (1:200) followed by Alexa Fluor 488- or 555-conjugated secondary antibodies (1:1000). Cells were thoroughly washed between steps with PBS. Immunostaining control included omission of the primary antibody. Nuclei were stained with 4,6-diamidino-2-phenylindole (DAPI; 0.1 μg/ml) and coverslips were mounted on microscope slides with Fluoromount-G mounting medium (Fisher Scientific, Milan, Italy) (Zusso et al., 2017). Fluorescent images were captured with a confocal laser-scanning microscope (Zeiss LSM 800; Carl Zeiss AG, Germany) and microscope settings were kept constant for all images. For each image, three z-stacks (50 μm optical section, 1.5 μm total Z-span) were acquired with a 63x, NA 1.4, oil-immersion objective. All images were taken considering the middle of nuclei as the central plane for z-stack. ImageJ software (National Institutes of Health, Bethesda, MD, United States) was used to flatten each z-stack image into a single image, representing the sum of the contributes from each focal plane. NF-κB p65 fluorescence emission intensity of single cells was profiled using ImageJ software. To quantitatively evaluate subcellular distribution of the p65 subunit, the relative staining intensities in the nucleus and cytoplasm were monitored from five random fields for each condition from three independent experiments. Cytoplasmic and nuclear fluorescence intensities were calculated using ImageJ software and are expressed as a percentage of nuclear and cytoplasmic staining.

Statistical Analysis

All data represent the results of at least three independent experiments. Data were analyzed using GraphPad Prism Software, version 6.0 (GraphPad Software, Inc., San Diego, CA, United States). Results are expressed as mean ± SEM. Statistical analyses to determine group differences were performed either by two-sample equal variance Student's *t* test, or by one-way analysis of variance (ANOVA) followed by Sidak's *post hoc* test for multiple comparisons. A value of $p < 0.05$ was considered to indicate statistically significant differences. Additional details are provided in the figure legends, where appropriate.

RESULTS

Analysis of Spirulina Extract

HPLC UV-Vis analysis of E1 led to the identification of β-carotene, several xanthophylls, chlorophylls, and pheophytins (**Figure 1A**). **Figure 1B** shows the content of chlorophyll a, chlorophyll b, pheophytin a, pheophytin b, and total carotenoids expressed as mg/g of dry extract. β-carotene represented 53% of total carotenoids present and among xanthophylls, zeaxanthin and diadinoxanthin were the most abundant (**Figure 1C**).

Effect of Pre-treatment With Spirulina Extract on Microglia Inflammatory Response

The effect of E1 on the release of the pro-inflammatory cytokines IL-1β and TNF-α on the initiation of microglia inflammatory response was examined. Cells were serum starved for 2 h, exposed for 1 h to increasing concentrations of the extract (1–100 μg/ml), and then stimulated with 100 ng/ml LPS to induce the inflammatory response. Unstimulated cells released low amounts of IL-1β and TNF-α which remained unchanged after treatment with the highest non-cytotoxic concentration of E1 (**Figures 2A,B**, white bars). In response to LPS, the release of IL-1β and TNF-α dramatically increased (**Figures 2A,B**, dark green bars) and E1 lowered it in a concentration-dependent manner. In particular, the extract completely inhibited the cytokine release starting from the concentration of 25 μg/ml (**Figures 2A,B**, light green bars). Considering that there was no effect on cell viability after treatment with the extract alone at concentrations ranging from 1-100 μg/ml (**Figure 2C**), these results indicate that the decrease in IL-1β and TNF-α release did not result from any cytotoxic effect.

Microglial activation by LPS is also accompanied by the increased expression of iNOS and the consequent nitric oxide production (Förstermann and Sessa, 2012). Therefore, we selected the extract concentration of 100 μg/ml to explore whether E1 pre-treatment could suppress the expression of iNOS upon LPS stimulation. The endotoxin induced gene and protein over-expression of iNOS, that was completely prevented by E1 (**Figure 3**), confirming the anti-inflammatory effect of E1 pre-treatment.

Effect of Post-treatment With Spirulina Extract on Microglia Inflammatory Response

Next, we explored whether E1 could decrease LPS-induced microglia inflammatory response when added after the initiation of inflammation. To test this, treatments with E1 started 2 or 4 h after LPS stimulation. When E1 was added to

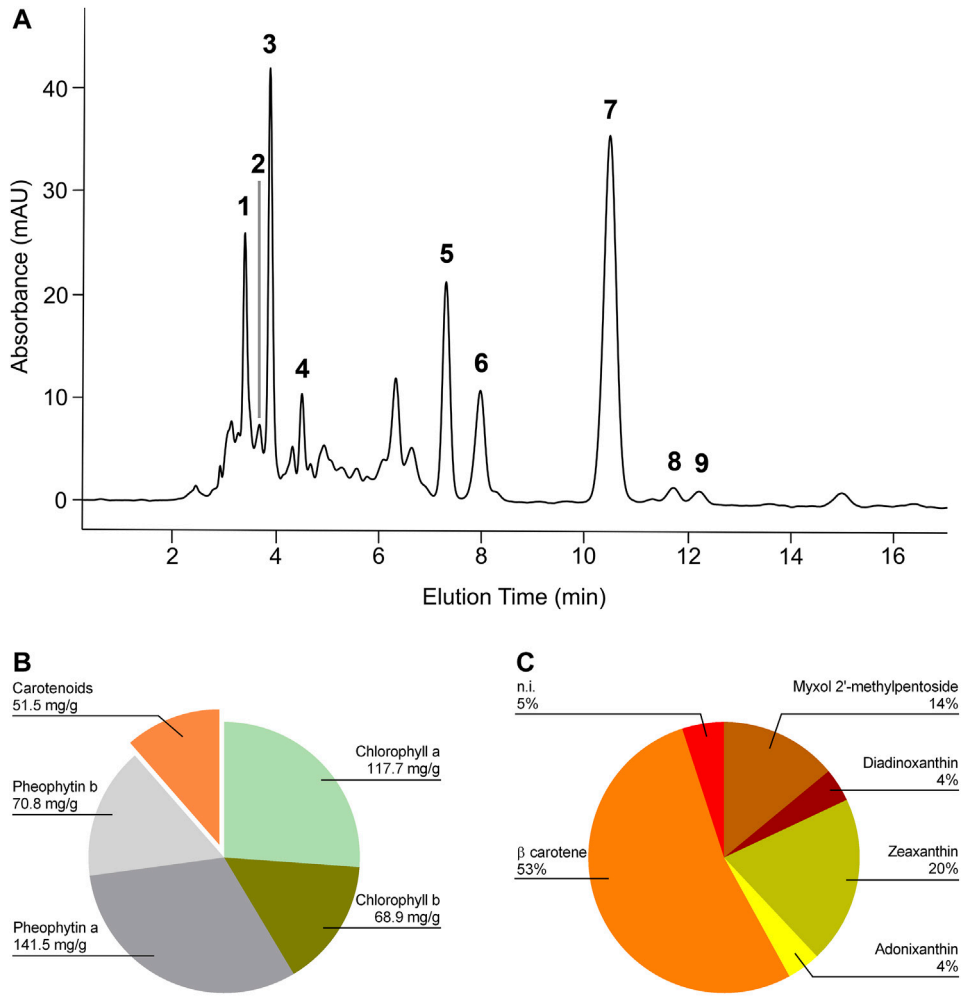

FIGURE 1 | HPLC profile of the Spirulina acetone extract and its relative composition. **(A)** Chromatogram was registered at 460 nm. Retention times: myxol 2′-methyl pentoside, 3.45 min (1); diadinoxanthin, 3.72 min (2); zeaxanthin, 3.94 min (3); adonixanthin, 4.5 min (4); unidentified xanthophylls, 3.18, 4.36, and 4.98 min; chlorophyll a, 7.35 min (5); chlorophyll b, 8.01 min (6); β carotene, 10.5 min (7); pheophytin a, 11.76 min (8); pheophytin b, 12.25 min (9). **(B)** Content of chlorophyll a, chlorophyll b, pheophytin a, pheophytin b, and total carotenoids expressed as mg/g of dry extract. **(C)** Relative carotenoid content in E1. β-carotene represented 53% of total carotenoids present.

cells 2 h after LPS, the release of both cytokines decreased only at the concentration of 100 μg/ml (**Figures 4A,B**). Differently, E1 added 4 h post-LPS stimulation did not alter IL-1β and TNF-α release (**Figures 4C,D**).

Conversely, a significant down-regulation of iNOS gene expression was found when E1 was added 2 and 4 h after stimulation with LPS. However, although statistically significant, the effect on iNOS mRNA levels tended to diminish when cells were treated with the extract longer after the initiation of inflammation (i.e., 4 h after LPS stimulation) (**Figure 4E**).

To clarify the observed effect, the kinetic of IL-1β and TNF-α release was studied and, as shown in **Table 2** and **3**, the amount of both cytokines increased over the time. In particular, 2 h after LPS stimulation, levels of IL-1β and TNF-α released into the medium were 78.7 ± 15.5 pg/ml and 195.1 ± 51.2 pg/ml, respectively. Then, the release kept increasing and 16 h after LPS stimulation the levels of IL-1β and TNF-α were 805.3 ± 99.4 pg/ml and 945.3 ± 104.8 pg/ml, respectively. E1 added to cells 2 h after LPS stimulation significantly reduced the release of both cytokines; indeed, in the period 4–16 h after LPS stimulation, the levels of IL-1β and TNF-α released were in the range between 87.6 ± 21.6 pg/ml and 250.4 ± 61.3 pg/ml and 235.8 ± 32.1 pg/ml and 389.4 ± 91.7 pg/ml, respectively.

Effect of Spirulina Extract on NF-κB Signaling in Microglia

In the attempt to define the underlying molecular mechanisms by which the extract of Spirulina modulated microglia inflammatory response, we evaluated the activation of the transcription factor NF-κB, which is required for the induction of several cytokines and inflammatory enzymes in microglia and other immune cells (Zusso et al., 2017; Tedesco et al., 2018). To measure NF-κB

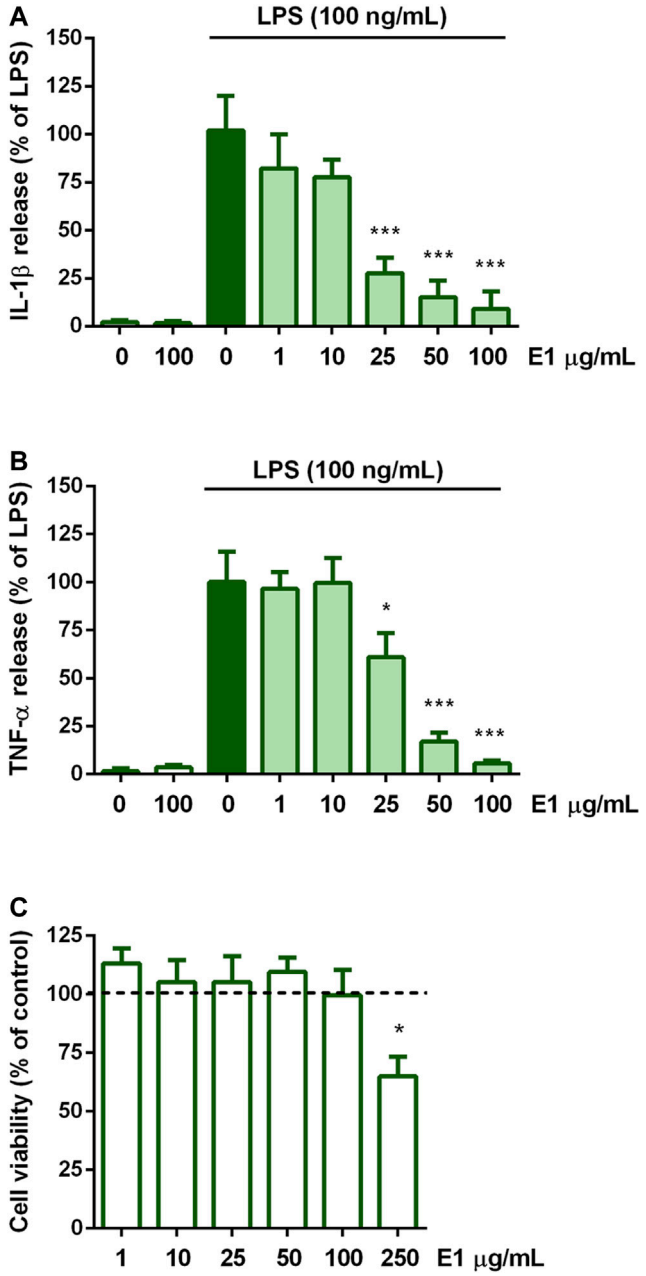

FIGURE 2 | Effect of pre-treatment with Spirulina extract on cytokine release from LPS-stimulated cortical microglia and cell viability analysis. Microglia were cultured for 24 h in 10% serum-containing medium, which was replaced with serum-free medium before pre-treatment with E1 (1–100 μg/ml) for 1 h and further stimulation with 100 ng/ml LPS for 16 h. Supernatants were collected and analyzed for **(A)** IL-1β and **(B)** TNF-α release. Results are expressed as percentage of cytokine release relative to LPS-stimulated microglia (dark green bars). Data are means ± SEM of three independent experiments. $^{*}p < 0.05$ and $^{***}p < 0.001$ versus LPS stimulation. One-way ANOVA followed by Sidak's multiple comparison test. **(C)** At the end of 16 h incubation with E1 (1–250 μg/ml), cell viability was determined by SRB assay. Results are expressed as percentage of cell viability relative to control cells (dashed line). Data are presented as means ± SEM ($n = 3$ in triplicate). $^{*}p < 0.05$ versus control cells. One-way ANOVA followed by Sidak's multiple comparison test.

activity, we monitored NF-κB p65 subunit movement from the cytoplasm to the nucleus. Under basal conditions and after E1 treatment p65 subunit was mainly distributed in the cytoplasm. As expected, LPS caused a significant translocation of the subunit to the nucleus, which was inhibited by pre-treatment with E1 (**Figure 5**).

Effect of Spirulina Extract on Nrf2 Signaling in Microglia

Nrf2 signaling is the major regulatory system able to control the expression of antioxidant and detoxification enzymes and has also a role in mitigating inflammation (Kong et al., 2011; Kobayashi et al., 2016). Thus, we next examined the possibility that Nrf2 signaling might participate in the anti-inflammatory activity of E1. Pre-treatment with the extract increased gene expression of Nrf2 (**Figure 6A**) and its nuclear translocation (**Figure 6C**), as well as mRNA levels of HO-1 (**Figure 6B**), a phase II enzyme downstream of Nrf2, both in the absence and presence of LPS, suggesting a possible involvement of this signaling in the anti-inflammatory effect of the studied extract.

DISCUSSION

The present study investigated the properties of pre- and post-treatments with an acetone extract derived from the microalga Spirulina against inflammatory response in an *in vitro* model of LPS-induced neuroinflammation. Spirulina besides being an important source of nutrients, has been widely studied for its numerous beneficial effects in *in vitro* and *in vivo* models. For instance, Spirulina possesses anti-inflammatory, antioxidant, and neuroprotective properties, that can counteract chronic neurodegenerative disorders (Simpson and Oliver, 2020). The extract used in this study showed the presence of chlorophylls, pheophytins, and carotenoids, where β-carotene and zeaxanthin were the most abundant carotenoids. The present finding is in accordance with previous studies that reported the presence of these pigments in the microalga (Jaime et al., 2005; Hynstova et al., 2018). Chlorophylls and their magnesium-free degradation products, pheophytins, are considered protective agents against many chronic diseases, being endowed with antioxidant and antimutagenic/anticarcinogenic activity (Ferruzzi and Blakeslee, 2007; Wu et al., 2010; Martel et al., 2017). Furthermore, some studies have shown that chlorophylls and pheophytins exhibited promising anti-inflammatory activities (Subramoniam et al., 2012; Li et al., 2019). Carotenoids are lipid-soluble pigments produced by plants and some microorganisms. The consumption of carotenoids has been linked with various health conditions, including the prevention of neurodegenerative diseases, such as Alzheimer's disease (Obulesu et al., 2011). Indeed, several studies have shown that carotenoids can accumulate in the CNS (Craft et al., 2004) and play a multitude of functions. The neuroprotective properties of carotenoids have been attributed to their action in the neural circuits by increasing neural efficiency or stabilizing membrane

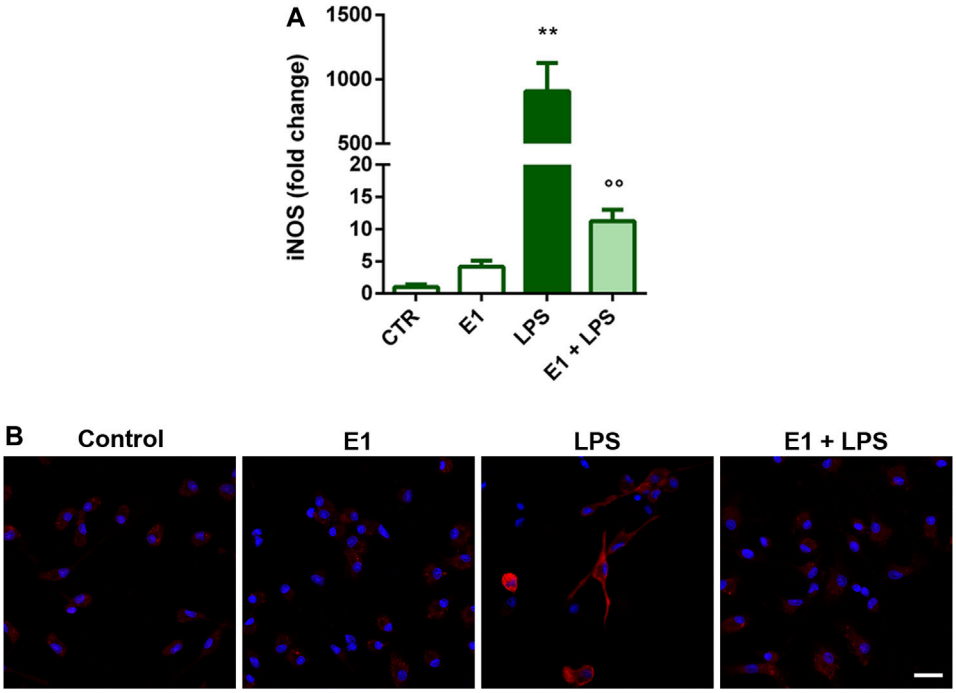

FIGURE 3 | Effect of pre-treatment with Spirulina extract on iNOS gene and protein expression in LPS-stimulated cortical microglia. Microglia were cultured for 24 h in 10% serum-containing medium, which was replaced with serum-free medium before pre-treatment with 100 µg/mL E1 followed by stimulation with 100 ng/ml LPS. **(A)** iNOS mRNA levels were quantified by real-time PCR. Data are presented as means ± SEM ($n = 3$ in triplicate). $^{**}p < 0.01$ compared to control cells; $^{\circ\circ}p < 0.01$ versus LPS stimulation. One-way ANOVA followed by Sidak's multiple comparison test. **(B)** Microglia were stained with anti-iNOS antibody (red) and nuclei with DAPI (blue). Experiments were performed three times and representative immunofluorescence images are shown. Scale bar, 20 µm.

structures (Sujak et al., 1999). Furthermore, in the brain carotenoids inhibit lipid peroxidation, reduce oxidative damage by scavenging reactive oxygen species, and are anti-neuroinflammatory agents able to suppress various inflammatory pathways (Hammond, 2015; Cho et al., 2018). These observations support the hypothesis that, due to its composition, E1 could exert anti-neuroinflammatory activities. To test this, herein we studied the effect of E1 on microglia inflammatory response. Non-cytotoxic concentrations of E1 had preventive anti-inflammatory effects on LPS-stimulated microglia. These effects were associated with the suppression of IL-1β and TNF-α release, two of the most important and earliest cytokines produced during inflammation, whose sustained and high levels have been associated with neurodegeneration (Becher et al., 2017). Additionally, pre-treatment with E1 showed a significant effect on the inflammatory signaling also by decreasing the LPS-induced over-expression of iNOS, an important regulator of inflammation. These results confirm previous studies that have suggested the use of Spirulina as a natural product to prevent inflammatory diseases, based on the anti-inflammatory effect of organic or water extracts of the microalga (Chen et al., 2012; Ku et al., 2013; Pham et al., 2017). We recently showed very similar results obtained with the use of an acetone extract from the microalga *Euglena gracilis* on the same *in vitro* model of neuroinflammation, despite some differences in the composition of the two extracts. *Euglena gracilis* extract contained diadinoxanthin as the most abundant xanthophyll, followed by zeaxanthin, whereas β-carotene represented only 8% (Piovan et al., 2021). Conversely, the most abundant carotenoid present in the Spirulina extract was β-carotene, whereas the amount of zeaxanthin resulted comparable in the two extracts. These results suggest that zeaxanthin could play an essential role in the anti-inflammatory effect of Spirulina extract and will orient future studies aimed at the direct evaluation of single isolated components of the extract.

Of particular interest, in the present study, we showed that E1 not only had a preventive anti-neuroinflammatory effect, but it was also able to reduce the release of pro-inflammatory cytokines and the expression of inflammatory markers when administered to cells early after the initiation of the inflammatory response. However, this effect was restricted to the initial stages of neuroinflammation (i.e., 2 h after LPS stimulation), when pro-inflammatory cytokines were released into the medium but their amount did not reach maximal levels (Hide et al., 2000; Sanz and Di Virgilio, 2000). Furthermore, the inhibitory effect has been observed only after treatment of microglia with a high concentration of E1 (i.e., 100 µg/ml) and it progressively declined over the time, being lost in the advanced stage of neuroinflammation (i.e., 4 h after LPS stimulation), when the release of pro-inflammatory cytokines increased. These results clearly indicate the existence of a link between the timing of

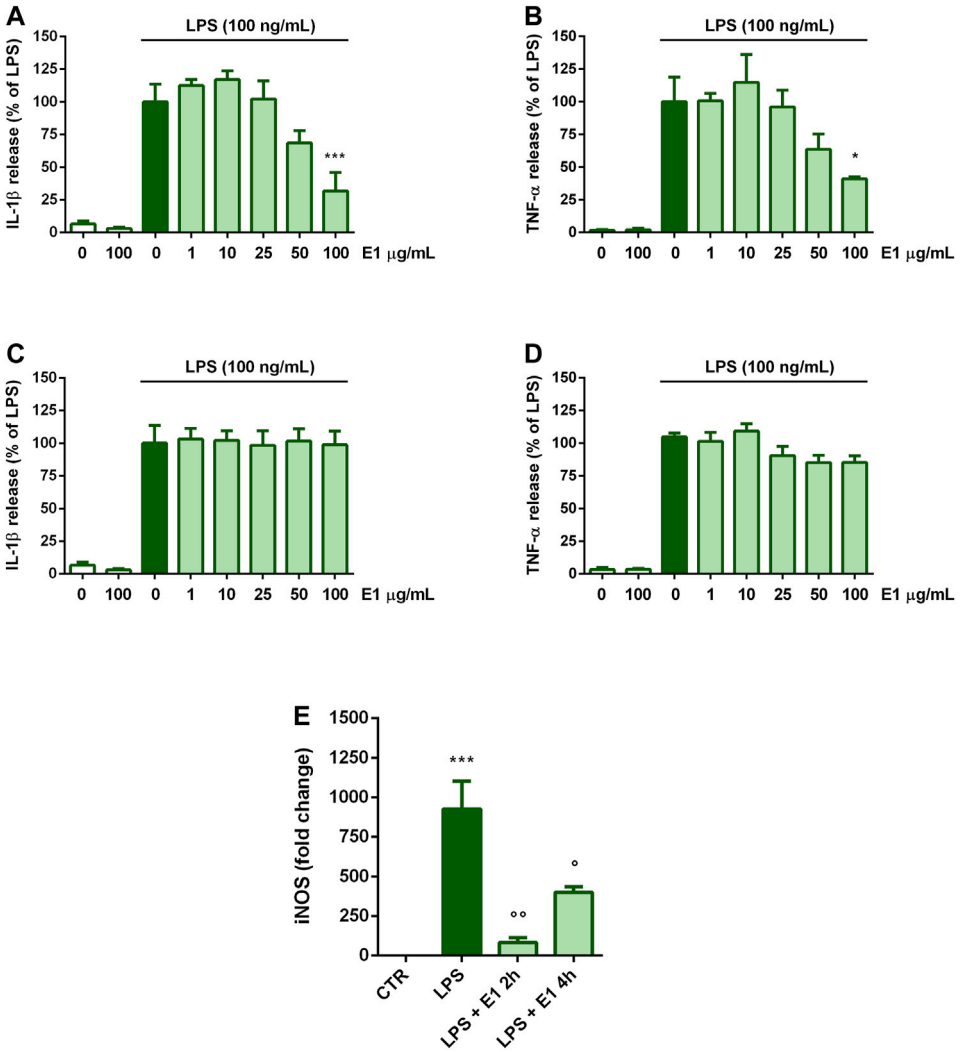

FIGURE 4 | Effect of post-treatment with Spirulina extract on cytokine release and iNOS gene expression in LPS-stimulated cortical microglia. Microglia were cultured for 24 h in 10% serum-containing medium, which was replaced with serum-free medium before stimulation with 100 ng/ml LPS. **(A,B)** Two, or **(C,D)** 4 h later cells were treated with E1 (1–100 μg/ml). Supernatants were collected and analyzed for IL-1β and TNF-α release. Results are expressed as percentage of cytokine release relative to LPS-stimulated microglia (dark green bars). Data are means ± SEM of three independent experiments. *$p < 0.05$, **$p < 0.01$, and ***$p < 0.001$ versus LPS stimulation **(E)** One or 4 h after LPS stimulation cells were treated with 100 μg/ml E1 and iNOS mRNA levels were quantified by real-time PCR. Data are presented as means ± SEM ($n = 3$ in triplicate). ***$p < 0.001$ compared to control cells; °°$p < 0.05$ and °$p < 0.01$ versus LPS stimulation. One-way ANOVA followed by Sidak's multiple comparison test.

TABLE 2 | Time course of IL-1β release (pg/ml) after LPS stimulation and effect of post-treatment with E1.

E1		Time (hours) after LPS stimulation				
2	4	0	2	4	8	16
-	-	2.4 ± 1.3	78.7 ± 15.5	257.1 ± 41.7	523.7 ± 79.7	805.3 ± 99.4
+	-	nd	nd	87.6 ± 21.6 * (–65.9 ± 11.5%)	157.6 ± 39.5 * (– 70.0 ± 13.5%)	250.4 ± 61.3 ** (– 68.9 ± 23.4%)
-	+	nd	nd	nd	487.3 ± 90.2	825.65 ± 101.32

E1 at the concentration of 100 μg/ml was added to cells 2 or 4 h after LPS stimulation (first and second column). Supernatant were collected at the indicated periods of time after LPS stimulation and analyzed for IL-1β release. Numbers in brackets denote the percentage change of IL-1β release compared to the corresponding treatment with LPS. Data are means ± SEM of three independent experiments.

*p < *0.05 and* **p < *0.01 versus the corresponding LPS stimulation. Student's* t *test. nd, not determined.*

TABLE 3 | Time course of TNF-α release (pg/ml) after LPS stimulation and effect of post-treatment with E1.

E1		Time (hours) after LPS stimulation				
2	4	0	2	4	8	16
-	-	2.4 ± 1.3	195.1 ± 51.2	489.1 ± 74.1	750.2 ± 87.7	945.3 ± 104.8
+	-	nd	nd	235.8 ± 32.1 * (–51.8 ± 17.3%)	397.2 ± 56.5 * (– 47.0 ± 23.7%)	389.4 ± 91.7 * (– 58.8 ± 18.8%)
-	+	nd	nd	nd	687.2 ± 140.9	926.5 ± 112.6

E1 at the concentration of 100 μg/ml was added to cells 2 or 4 h after LPS stimulation (first and second column). Supernatant were collected at the indicated periods of time after LPS stimulation and analyzed for TNF-α release. Numbers in brackets denote the percentage change of TNF-α release compared to the corresponding treatment with LPS. Data are means ± SEM of three independent experiments.

**p < 0.05 versus the corresponding LPS stimulation. Student's t test. nd, not determined.*

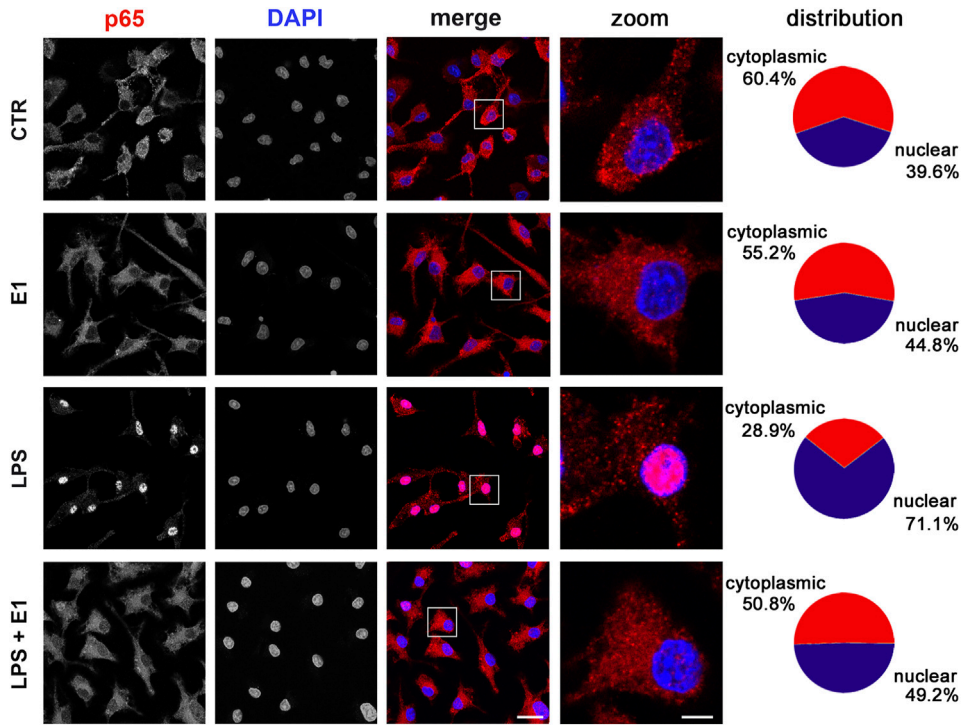

FIGURE 5 | Effect of Spirulina extract on NF-κB activation in unstimulated and LPS-stimulated microglia. Cells were cultured for 24 h in 10% serum-containing medium, which was replaced with serum-free medium before pre-treatment with 100 μg/ml E1 followed by stimulation with 100 ng/ml LPS. Cells were then processed for NF-κB p65 immunostaining (red) and nuclei were counterstained with DAPI (blue). Experiments were performed 3 times and representative confocal images showing subcellular localization of p65 are shown. Scale bars in merged and zoomed images, 10 and 2 μm, respectively. The fluorescence intensity of cytoplasmic and nuclear p65 subunit was calculated using ImageJ software and results are presented as percentage of nuclear and cytoplasmic NF-κB p65 distribution in the fifth column. Data are mean from three independent experiments.

intervention and the entity of E1 effect on microglia activation, suggesting that E1, besides being a valid preventive option, may be of potential application in the early stages of inflammatory CNS diseases.

The expression of many cytokines, chemokines, receptors, and enzymes involved in inflammatory response is dependent on NF-κB pathway activation. In fact, an excessive or inappropriate activation of NF-κB has been associated with the development of inflammatory diseases and its inhibition can decrease the disease progression (Tak and Firestein, 2001; Lawrence, 2009; Liu et al., 2017). In the inactive form, NF-κB exists in the cytoplasm associated with the inhibitory proteins IκB. Inflammation leads to IκB phosphorylation and release of the heterodimer p50/p65, that, after translocation to the nucleus, binds to κB enhancer elements of target genes and induces the transcription of pro-inflammatory genes (Liu et al., 2017). Thus, monitoring NF-κB movement from the cytoplasm to the nucleus is a common method to measure NF-κB activity. In microglia cells, NF-κB p65 nuclear translocation induced by LPS was significantly attenuated by pre-treatment with E1, suggesting that the inhibition of NF-κB activation could be one of the potential anti-inflammatory mechanisms of the

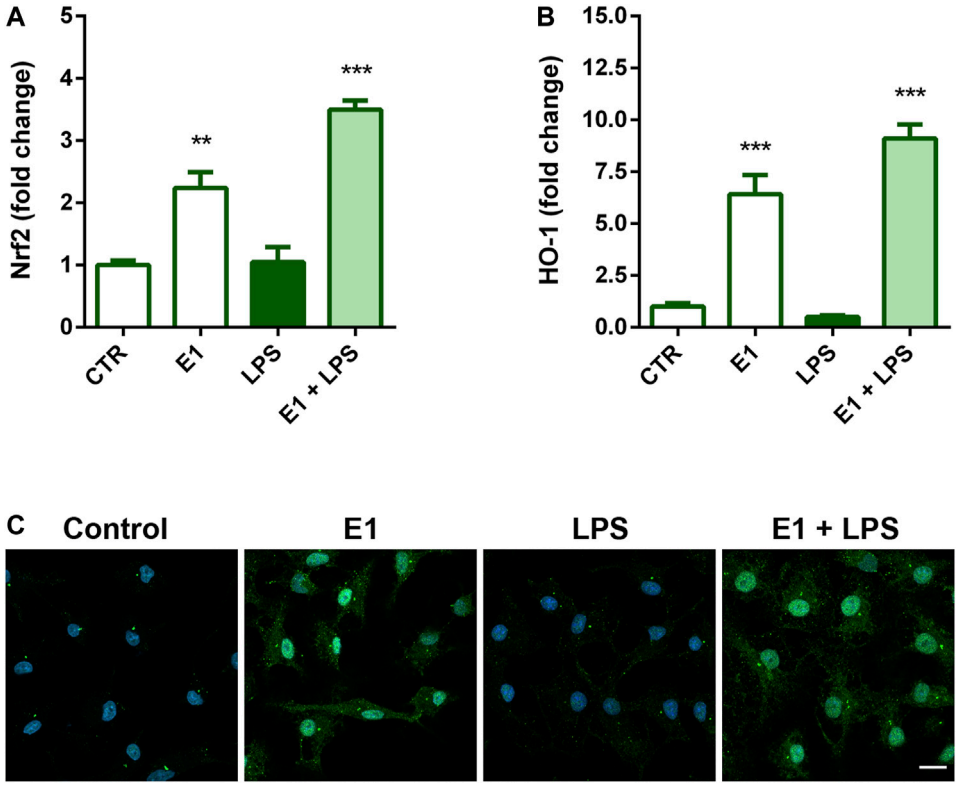

FIGURE 6 | Effect of Spirulina extract on Nrf2 signaling in unstimulated and LPS-stimulated microglia. Cells were cultured for 24 h in 10% serum-containing medium, which was replaced with serum-free medium before pre-treatment with 100 µg/ml E1 for 1 h followed by stimulation with 100 ng/ml LPS. **(A)** Nrf2 and **(B)** HO-1 mRNA levels were quantified by real-time PCR. Data are presented as means ± SEM ($n = 3$ in triplicate). $^{**}p < 0.01$ and $^{***}p < 0.001$ compared to control cells. One-way ANOVA followed by Sidak's multiple comparison test. **(C)** Microglia were stained with anti-Nrf2 antibody (green) and nuclei with DAPI (blue). Experiments were performed three times and representative immunofluorescence images are shown. Scale bar, 10 µm.

studied extract. In previous studies the anti-inflammatory effect of carotenoids has been ascribed to the inhibition of NF-κB activity, through a mechanism that involved the inhibition of DNA-binding activity of p65 (Palozza et al., 2003; Linnewiel-Hermoni et al., 2014; Li et al., 2019). Therefore, we cannot exclude the possibility that E1 components can act by directly interacting with NF-κB.

Oxidative stress, associated with increased levels of reactive species and a decrease in the antioxidant systems, has been implicated in the development and maintenance of inflammation and progression of neurodegenerative diseases. In this context, Nrf2 signaling, in addition to control intracellular redox homeostasis, has anti-inflammatory properties and has emerged as a therapeutic target in neurodegenerative conditions (Brandes and Gray, 2020). This signaling acts as an environmental sensor that allows cells to monitor for the presence of insults. Once activated, Nrf2 signaling leads the subsequent transcription of genes that are involved in antioxidant and anti-inflammatory responses. Thus, stimulation of Nrf2 appears a promising method for reducing the level of neuroinflammation and neurodegeneration. In our experimental conditions, E1 alone increased the expression of Nrf2 and that of its downstream gene HO-1, a potent anti-inflammatory target, suggesting that the induction of an antioxidant response might contribute, at least in part, to the anti-inflammatory properties of the extract components. However, more studies are necessary to verify a possible direct interaction of the extract components with Nrf2, as already showed for some carotenoids and their derivatives that can interact with Keap1, the negative regulator of Nrf2, by changing its physical properties (Kaulmann and Bohn, 2014). However, in this regard, it should be noted that, despite Nrf2 is considered a key regulator of inflammatory processes (Ahmed et al., 2017), based on the existence of a complex interaction between oxidative stress and inflammation, we recently showed that the anti-inflammatory effect of the acetone extract of *Euglena gracilis* is Nrf2 independent (Piovan et al., 2021). Similarly, the anti-inflammatory effect of E1 could be independent of the activation of Nrf2.

Taken together, our data indicate that the acetone extract from Spirulina can suppress the activation of NF-κB and induce the activation of Nrf2/HO-1, two intracellular signaling pathways that could act independently or in complementary manner. Clearly, additional studies using pathway specific inhibitors must be considered to elucidate the precise anti-inflammatory mechanism and explore other potential mechanisms. However, the results of this study represent promising evidence to support future *in vivo* studies to test the effect of pre-treatment

(i.e., prophylactic effect) and post-treatment with the acetone extract from Spirulina.

DATA AVAILABILITY STATEMENT

The original contributions presented in the study are included in the article/supplementary files, further inquiries can be directed to the corresponding author.

ETHICS STATEMENT

The animal study was reviewed and approved by the Institutional Review Board for Animal Research (Organismo Preposto al Benessere Animale, OPBA) of the University of Padua and by the Italian Ministry of Health (protocol number 41451.N.N8P).

AUTHOR CONTRIBUTIONS

API, RF, PG, and MZ designed research; JB, VDC, LF, and CA performed experiments; API, RF, APA, PG, and MZ analyzed data; API, RF, PG, and MZ wrote the paper; all authors read and approved the final version of the manuscript.

FUNDING

This study was supported by grants from the University of Padua, Italy (UNIPD-DSF-DOR founds to API, RF, and MZ).

ACKNOWLEDGMENTS

We thank Massimo Rizza for technical assistance in animal handling.

REFERENCES

Ahmed, S. M., Luo, L., Namani, A., Wang, X. J., and Tang, X. (2017). Nrf2 Signaling Pathway: Pivotal Roles in Inflammation. *Biochim. Biophys. Acta Mol. Basis Dis.* 1863, 585–597. doi:10.1016/j.bbadis.2016.11.005

Amor, S., Peferoen, L. A., Vogel, D. Y., Breur, M., van der Valk, P., Baker, D., et al. (2014). Inflammation in Neurodegenerative Diseases-Aan Update. *Immunology* 142, 151–166. doi:10.1111/imm.12233

Barbierato, M., Borri, M., Facci, L., Zusso, M., Skaper, S. D., and Giusti, P. (2017). Expression and Differential Responsiveness of Central Nervous System Glial Cell Populations to the Acute Phase Protein Serum Amyloid A. *Sci. Rep.* 7, 12158. doi:10.1038/s41598-017-12529-7

Becher, B., Spath, S., and Goverman, J. (2017). Cytokine Networks in Neuroinflammation. *Nat. Rev. Immunol.* 17, 49–59. doi:10.1038/nri.2016.123

Brandes, M. S., and Gray, N. E. (2020). NRF2 as a Therapeutic Target in Neurodegenerative Diseases. *ASN Neuro.* 12, 1759091419899782. doi:10.1177/1759091419899782

Bryant, C. E., Spring, D. R., Gangloff, M., and Gay, N. J. (2010). The Molecular Basis of the Host Response to Lipopolysaccharide. *Nat. Rev. Microbiol.* 8, 8–14. doi:10.1038/nrmicro2266

Bsibsi, M., Ravid, R., Gveric, D., and van Noort, J. M. (2002). Broad Expression of Toll-like Receptors in the Human central Nervous System. *J. Neuropathol. Exp. Neurol.* 61, 1013–1021. doi:10.1093/jnen/61.11.1013

Chen, J. C., Liu, K. S., Yang, T. J., Hwang, J. H., Chan, Y. C., and Lee, I. T. (2012). Spirulina and C-Phycocyanin Reduce Cytotoxicity and Inflammation-Related Genes Expression of Microglial Cells. *Nutr. Neurosci.* 15, 252–256. doi:10.1179/1476830512Y.0000000020

Cho, K. S., Shin, M., Kim, S., and Lee, S. B. (2018). Recent Advances in Studies on the Therapeutic Potential of Dietary Carotenoids in Neurodegenerative Diseases. *Oxid. Med. Cel Longev.* 2018, 4120458. doi:10.1155/2018/4120458

Colla, L. M., Bertolin, T. E., and Costa, J. A. (2004). Fatty Acids Profile of Spirulina Platensis Grown under Different Temperatures and Nitrogen Concentrations. *Z. Naturforsch C. J. Biosci.* 59, 55–59. doi:10.1515/znc-2004-1-212

Colonna, M., and Butovsky, O. (2017). Microglia Function in the central Nervous System during Health and Neurodegeneration. *Annu. Rev. Immunol.* 35, 441–468. doi:10.1146/annurev-immunol-051116-052358

Craft, N. E., Haitema, T. B., Garnett, K. M., Fitch, K. A., and Dorey, C. K. (2004). Carotenoid, Tocopherol, and Retinol Concentrations in Elderly Human Brain. *J. Nutr. Health Aging* 8, 156–162.

Ferruzzi, M. G., and Blakeslee, J. (2007). Digestion, Absorption, and Cancer Preventative Activity of Dietary Chlorophyll Derivatives. *Nutr. Res.* 27, 1–12. doi:10.1016/j.nutres.2006.12.003

Fiebich, B. L., Batista, C. R. A., Saliba, S. W., Yousif, N. M., and de Oliveira, A. C. P. (2018). Role of Microglia TLRs in Neurodegeneration. *Front. Cel Neurosci.* 12, 329. doi:10.3389/fncel.2018.00329

Finamore, A., Palmery, M., Bensehaila, S., and Peluso, I. (2017). Antioxidant, Immunomodulating, and Microbial-Modulating Activities of the Sustainable and Ecofriendly Spirulina. *Oxid. Med. Cel Longev.* 2017, 3247528. doi:10.1155/2017/3247528

Förstermann, U., and Sessa, W. C. (2012). Nitric Oxide Synthases: Regulation and Function. *Eur. Heart J.* 33, 829–837d. doi:10.1093/eurheartj/ehr304

Galasso, C., Gentile, A., Orefice, I., Ianora, A., Bruno, A., Noonan, D. M., et al. (2019). Microalgal Derivatives as Potential Nutraceutical and Food Supplements for Human Health: a Focus on Cancer Prevention and Interception. *Nutrients* 11, E1226. doi:10.3390/nu11061226

Gomez-Nicola, D., and Perry, V. H. (2015). Microglial Dynamics and Role in the Healthy and Diseased Brain: a Paradigm of Functional Plasticity. *Neuroscientist* 21, 169–184. doi:10.1177/1073858414530512

Gómez-Zorita, S., Trepiana, J., González-Arceo, M., Aguirre, L., Milton-Laskibar, I., González, M., et al. (2019). Anti-obesity Effects of Microalgae. *Int. J. Mol. Sci.* 21, 41. doi:10.3390/ijms21010041

Haider, S., Shahzad, S., Batool, Z., Sadir, S., Liaquat, L., Tabassum, S., et al. (2021). Spirulina Platensis Reduces the Schizophrenic-like Symptoms in Rat Model by Restoring Altered APO-E and RTN-4 Protein Expression in Prefrontal Cortex. *Life Sci.* 277, 119417. doi:10.1016/j.lfs.2021.119417

Hammond, B. R. (2015). Dietary Carotenoids and the Nervous System. *Foods* 4, 698–701. doi:10.3390/foods4040698

Hide, I., Tanaka, M., Inoue, A., Nakajima, K., Kohsaka, S., Inoue, K., et al. (2000). Extracellular ATP Triggers Tumor Necrosis Factor-Alpha Release from Rat Microglia. *J. Neurochem.* 75, 965–972. doi:10.1046/j.1471-4159.2000.0750965.x

Hynstova, V., Sterbova, D., Klejdus, B., Hedbavny, J., Huska, D., and Adam, V. (2018). Separation, Identification and Quantification of Carotenoids and Chlorophylls in Dietary Supplements Containing Chlorella Vulgaris and Spirulina Platensis Using High Performance Thin Layer Chromatography. *J. Pharm. Biomed. Anal.* 148, 108–118. doi:10.1016/j.jpba.2017.09.018

Jaime, L., Mendiola, J. A., Herrero, M., Soler-Rivas, C., Santoyo, S., Señorans, F. J., et al. (2005). Separation and Characterization of Antioxidants from *Spirulina Platensis* Microalga Combining Pressurized Liquid Extraction, TLC, and HPLC-DAD. *J. Sep. Sci.* 28, 2111–2119. doi:10.1002/jssc.200500185

Kaulmann, A., and Bohn, T. (2014). Carotenoids, Inflammation, and Oxidative Stress-Iimplications of Cellular Signaling Pathways and Relation to Chronic Disease Prevention. *Nutr. Res.* 34, 907–929. doi:10.1016/j.nutres.2014.07.010

Kawai, T., and Akira, S. (2010). The Role of Pattern-Recognition Receptors in Innate Immunity: Update on Toll-like Receptors. *Nat. Immunol.* 11, 373–384. doi:10.1038/ni.1863

Khan, M. I., Shin, J. H., and Kim, J. D. (2018). The Promising Future of Microalgae: Current Status, Challenges, and Optimization of a Sustainable and Renewable Industry for Biofuels, Feed, and Other Products. *Microb. Fact.* 17, 36. doi:10.1186/s12934-018-0879-x

Kobayashi, E. H., Suzuki, T., Funayama, R., Nagashima, T., Hayashi, M., Sekine, H., et al. (2016). Nrf2 Suppresses Macrophage Inflammatory Response by Blocking Proinflammatory Cytokine Transcription. *Nat. Commun.* 7, 11624. doi:10.1038/ncomms11624

Kong, X., Thimmulappa, R., Craciun, F., Harvey, C., Singh, A., Kombairaju, P., et al. (2011). Enhancing Nrf2 Pathway by Disruption of Keap1 in Myeloid Leukocytes Protects against Sepsis. *Am. J. Respir. Crit. Care Med.* 184, 928–938. doi:10.1164/rccm.201102-0271OC

Ku, C. S., Pham, T. X., Park, Y., Kim, B., Shin, M. S., Kang, I., et al. (2013). Edible Blue-green Algae Reduce the Production of Pro-inflammatory Cytokines by Inhibiting NF-κB Pathway in Macrophages and Splenocytes. *Biochim. Biophys. Acta* 1830, 2981–2988. doi:10.1016/j.bbagen.2013.01.018

Kulshreshtha, A., Zacharia, A. J., Jarouliya, U., Bhadauriya, P., Prasad, G. B., and Bisen, P. S. (2008). Spirulina in Health Care Management. *Curr. Pharm. Biotechnol.* 9, 400–405. doi:10.2174/138920108785915111

Lawrence, T. (2009). The Nuclear Factor NF-kappaB Pathway in Inflammation. *Cold Spring Harb. Perspect. Biol.* 1, a001651. doi:10.1101/cshperspect.a001651

Li, Y., Cui, Y., Hu, X., Liao, X., and Zhang, Y. (2019a). Chlorophyll Supplementation in Early Life Prevents Diet-Induced Obesity and Modulates Gut Microbiota in Mice. *Mol. Nutr. Food Res.* 63, e1801219. doi:10.1002/mnfr.201801219

Li, R., Hong, P., and Zheng, X. (2019b). β-Carotene Attenuates Lipopolysaccharide-Induced Inflammation via Inhibition of the NF-κB, JAK2/STAT3 and JNK/p38 MAPK Signaling Pathways in Macrophages. *Anim. Sci. J.* 90, 140–148. doi:10.1111/asj.13108

Lichtenthaler, H. K. (1987). Chlorophylls and Carotenoids: Pigments of Photosynthetic Biomembranes. *Method. Enzymol.* 148, 350–382. doi:10.1016/0076-6879(87)48036-1

Lima, F. A. V., Joventino, I. P., Joventino, F. P., de Almeida, A. C., Neves, K. R. T., do Carmo, M. R., et al. (2017). Neuroprotective Activities of Spirulina Platensis in the 6-OHDA Model of Parkinson's Disease Are Related to its Anti-inflammatory Effects. *Neurochem. Res.* 42, 3390–3400. doi:10.1007/s11064-017-2379-5

Linnewiel-Hermoni, K., Motro, Y., Miller, Y., Levy, J., and Sharoni, Y. (2014). Carotenoid Derivatives Inhibit Nuclear Factor Kappa B Activity in Bone and Cancer Cells by Targeting Key Thiol Groups. *Free Radic. Biol. Med.* 75, 105–120. doi:10.1016/j.freeradbiomed.2014.07.024

Liu, T., Zhang, L., Joo, D., and Sun, S. C. (2017). NF-κB Signaling in Inflammation. *Signal. Transduct. Target. Ther.* 2, 17023. doi:10.1038/sigtrans.2017.23

Liu, C. Y., Wang, X., Liu, C., and Zhang, H. L. (2019). Pharmacological Targeting of Microglial Activation: New Therapeutic Approach. *Front. Cel. Neurosci.* 13, 514. doi:10.3389/fncel.2019.00514

Lucas, S. M., Rothwell, N. J., and Gibson, R. M. (2006). The Role of Inflammation in CNS Injury and Disease. *Br. J. Pharmacol.* 147 (Suppl. 1), S232–S240. doi:10.1038/sj.bjp.0706400

Mallikarjun Gouda, K. G., Kavitha, M. D., and Sarada, R. (2015). Antihyperglycemic, Antioxidant and Antimicrobial Activities of the Butanol Extract from S Pirulina Platensis. *J. Food Biochem.* 39, 594–602. doi:10.1111/jfbc.12164

Martel, J., Ojcius, D. M., Chang, C. J., Lin, C. S., Lu, C. C., Ko, Y. F., et al. (2017). Anti-obesogenic and Antidiabetic Effects of Plants and Mushrooms. *Nat. Rev. Endocrinol.* 13, 149–160. doi:10.1038/nrendo.2016.142

Niccolai, A., Shannon, E., Abu-Ghannam, N., Biondi, N., Rodolfi, L., and Tredici, M. R. (2019). Lactic Acid Fermentation of *Arthrospira Platensis* (Spirulina) Biomass for Probiotic-Based Products. *J. Appl. Phycol.* 31, 1077–1083. doi:10.1007/s10811-018-1602-3

Obulesu, M., Dowlathabad, M. R., and Bramhachari, P. V. (2011). Carotenoids and Alzheimer's Disease: an Insight into Therapeutic Role of Retinoids in Animal Models. *Neurochem. Int.* 59, 535–541. doi:10.1016/j.neuint.2011.04.004

Pabon, M. M., Jernberg, J. N., Morganti, J., Contreras, J., Hudson, C. E., Klein, R. L., et al. (2012). A Spirulina-Enhanced Diet Provides Neuroprotection in an α-synuclein Model of Parkinson's Disease. *PLoS One* 7, e45256. doi:10.1371/journal.pone.0045256

Palozza, P., Serini, S., Torsello, A., Di Nicuolo, F., Piccioni, E., Ubaldi, V., et al. (2003). Beta-carotene Regulates NF-kappaB DNA-Binding Activity by a Redox Mechanism in Human Leukemia and colon Adenocarcinoma Cells. *J. Nutr.* 133, 381–388. doi:10.1093/jn/133.2.381

Pham, T. X., Park, Y. K., Bae, M., and Lee, J. Y. (2017). The Potential Role of an Endotoxin Tolerance-like Mechanism for the Anti-inflammatory Effect of Spirulina Platensis Organic Extract in Macrophages. *J. Med. Food* 20, 201–210. doi:10.1089/jmf.2016.0119

Piovan, A., Filippini, R., Corbioli, G., Costa, V. D., Giunco, E. M. V., Burbello, G., et al. (2021). Carotenoid Extract Derived from Euglena Gracilis Overcomes Lipopolysaccharide-Induced Neuroinflammation in Microglia: Role of NF-κB and Nrf2 Signaling Pathways. *Mol. Neurobiol.* 58, 3515. doi:10.1007/s12035-021-02353-6

Remirez, D., González, R., Merino, N., Rodriguez, S., and Ancheta, O. (2002). Inhibitory Effects of Spirulina in Zymosan-Induced Arthritis in Mice. *Mediators Inflamm.* 11, 75–79. doi:10.1080/09629350220131917

Sanz, J. M., and Di Virgilio, F. (2000). Kinetics and Mechanism of ATP-dependent IL-1 Beta Release from Microglial Cells. *J. Immunol.* 164, 4893–4898. doi:10.4049/jimmunol.164.9.4893

Simpson, D. S. A., and Oliver, P. L. (2020). ROS Generation in Microglia: Understanding Oxidative Stress and Inflammation in Neurodegenerative Disease. *Antioxidants (Basel)* 9, 743. doi:10.3390/antiox9080743

Skaper, S. D., Argentini, C., and Barbierato, M. (2012). Culture of Neonatal Rodent Microglia, Astrocytes, and Oligodendrocytes from Cortex and Spinal Cord. *Methods Mol. Biol.* 846, 67–77. doi:10.1007/978-1-61779-536-7_7

Skaper, S. D., Facci, L., Zusso, M., and Giusti, P. (2018). An Inflammation-Centric View of Neurological Disease: beyond the Neuron. *Front. Cel. Neurosci.* 12, 72. doi:10.3389/fncel.2018.00072

Skehan, P., Storeng, R., Scudiero, D., Monks, A., McMahon, J., Vistica, D., et al. (1990). New Colorimetric Cytotoxicity Assay for Anticancer-Drug Screening. *J. Natl. Cancer Inst.* 82, 1107–1112. doi:10.1093/jnci/82.13.1107

Sochocka, M., Diniz, B. S., and Leszek, J. (2017). Inflammatory Response in the CNS: Friend or Foe? *Mol. Neurobiol.* 54, 8071–8089. doi:10.1007/s12035-016-0297-1

Strömberg, I., Gemma, C., Vila, J., and Bickford, P. C. (2005). Blueberry- and Spirulina-Enriched Diets Enhance Striatal Dopamine Recovery and Induce a Rapid, Transient Microglia Activation after Injury of the Rat Nigrostriatal Dopamine System. *Exp. Neurol.* 196, 298–307. doi:10.1016/j.expneurol.2005.08.013

Subramoniam, A., Asha, V. V., Nair, S. A., Sasidharan, S. P., Sureshkumar, P. K., Rajendran, K. N., et al. (2012). Chlorophyll Revisited: Anti-inflammatory Activities of Chlorophyll a and Inhibition of Expression of TNF-α Gene by the Same. *Inflammation* 35, 959–966. doi:10.1007/s10753-011-9399-0

Sujak, A., Gabrielska, J., Grudziński, W., Borc, R., Mazurek, P., and Gruszecki, W. I. (1999). Lutein and Zeaxanthin as Protectors of Lipid Membranes against Oxidative Damage: the Structural Aspects. *Arch. Biochem. Biophys.* 371, 301–307. doi:10.1006/abbi.1999.1437

Tak, P. P., and Firestein, G. S. (2001). NF-kappaB: a Key Role in Inflammatory Diseases. *J. Clin. Invest.* 107, 7–11. doi:10.1172/JCI11830

Tedesco, S., Zusso, M., Facci, L., Trenti, A., Boscaro, C., Belluti, F., et al. (2018). Bisdemethoxycurcumin and its Cyclized Pyrazole Analogue Differentially Disrupt Lipopolysaccharide Signalling in Human Monocyte-Derived Macrophages. *Mediators Inflamm.* 2018, 2868702. doi:10.1155/2018/2868702

Wu, S. J., Ng, L. T., Wang, G. H., Huang, Y. J., Chen, J. L., and Sun, F. M. (2010). Chlorophyll a, an Active Anti-proliferative Compound of *Ludwigia Octovalvis*, Activates the CD95 (APO-1/CD95) System and AMPK Pathway in 3T3-L1 Cells. *Food Chem. Toxicol.* 48, 716–721. doi:10.1016/j.fct.2009.12.001

Wu, Q., Liu, L., Miron, A., Klímová, B., Wan, D., and Kuča, K. (2016). The Antioxidant, Immunomodulatory, and Anti-inflammatory Activities of Spirulina: an Overview. *Arch. Toxicol.* 90, 1817–1840. doi:10.1007/s00204-016-1744-5

Yang, C. M., Chang, K. W., Yin, M. H., and Huang, H. M. (1998). Methods for the Determination of the Chlorophylls and Their Derivatives. *Taiwania* 43, 116–122. doi:10.6165/tai.1998.43(2).116

Zusso, M., Mercanti, G., Belluti, F., Di Martino, R. M. C., Pagetta, A., Marinelli, C., et al. (2017). Phenolic 1,3-diketones Attenuate Lipopolysaccharide-Induced Inflammatory Response by an Alternative Magnesium-Mediated Mechanism. *Br. J. Pharmacol.* 174, 1090–1103. doi:10.1111/bph.13746

Conflict of Interest: The authors declare that the research was conducted in the absence of any commercial or financial relationships that could be construed as a potential conflict of interest.

frontiers in Pharmacology

ORIGINAL RESEARCH
published: 24 September 2021
doi: 10.3389/fphar.2021.716684

Higenamine Attenuates Neuropathic Pain by Inhibition of NOX2/ROS/TRP/P38 Mitogen-Activated Protein Kinase/NF-κB Signaling Pathway

*Bing Yang†, Shengsuo Ma†, Chunlan Zhang, Jianxin Sun, Di Zhang, Shiquan Chang, Yi Lin and Guoping Zhao**

School of Traditional Chinese Medicine, Jinan University, Guangzhou, China

Oxidative stress damage is known as one of the important factors that induce neuropathic pain (NP). Using antioxidant therapy usually achieves an obvious curative effect and alleviates NP. Previous pharmacological studies have shown that higenamine (Hig) performs to be antioxidant and anti-inflammatory. However, the protective effect and mechanism of Hig on NP are still unclear. This study mainly evaluated the changes in reactive oxygen species (ROS) level, lipid peroxidation, and antioxidant system composed of superoxide dismutase (SOD) and glutathione (GSH) through chronic constrict injury (CCI) model rats and t-BHP-induced Schwann cell (SC) oxidative stress model. The expressions of two inflammatory factors, tumor necrosis factor-alpha (TNF-α) and interleukin-6 (IL-6), were also assessed. The possible molecular mechanism of Hig in the treatment of NP was explored in conjunction with the expression of mitochondrial apoptosis pathway and NOX2/ROS/TRP/P38 mitogen-activated protein kinase (MAPK)/NF-κB pathway-related indicators. Hig showed substantial antioxidant and anti-inflammatory properties both *in vivo* and *in vitro*. Hig significantly reduced the upregulated levels of ROS, malondialdehyde (MDA), TNF-α, and IL-6 and increased the levels of SOD and GSH, which rebalanced the redox system and improved the survival rate of cells. In the animal behavioral test, it was also observed that Hig relieved the CCI-induced pain, indicating that Hig had a pain relief effect. Our research results suggested that Hig improved NP-induced oxidative stress injury, inflammation, and apoptosis, and this neuroprotective effect may be related to the NOX2/ROS/TRP/P38 MAPK/NF-κB signaling pathway.

Keywords: higenamine, neuropathic pain, oxidative stress, neuroinflammation, transient receptor potential, NOX2

OPEN ACCESS

Edited by:
Borja Garcia-Bueno, Universidad Complutense de Madrid, Spain

Reviewed by:
Jeseong Won, Medical University of South Carolina, United States
Sergei V. Fedorovich, Belarusian State University, Belarus

****Correspondence:***
Guoping Zhao
tguo428@jnu.edu.cn

†These authors have contributed equally to this work

Specialty section:
This article was submitted to Neuropharmacology, a section of the journal Frontiers in Pharmacology

Received: *29 May 2021*
Accepted: *02 September 2021*
Published: *24 September 2021*

Citation:
Yang B, Ma S, Zhang C, Sun J, Zhang D, Chang S, Lin Y and Zhao G (2021) Higenamine Attenuates Neuropathic Pain by Inhibition of NOX2/ROS/TRP/P38 Mitogen-Activated Protein Kinase/NF-κB Signaling Pathway. Front. Pharmacol. 12:716684. doi: 10.3389/fphar.2021.716684

INTRODUCTION

Neuropathic pain (NP) is a chronic pain condition caused by nervous system damage or disease leading to abnormal signals in the somatosensory system (Finnerup et al., 2021). NP is usually accompanied by hyperalgesia and/or allodynia manifested as burning and tingling sensations (Campbell and Meyer, 2006). At present, a variety of clinical diseases give rise to NP, mainly including metabolic or nutritional nerve changes, viral infections, and accompanying nerve damage. With the increasing incidence of metabolic diseases and the application of cancer chemotherapy, the rate of NP has risen year by year, which not only

brings a great impact on patients but also seriously increases the social and economic burden (Colloca et al., 2017). It is widely accepted that the pathophysiology of evoked pain involves peripheral and central sensitization. Alterations in ion channels and interactions between cells and molecular signaling transmission are based on the sensitization of nociceptive pathways (Campbell and Meyer, 2006; Zhang et al., 2017). Previous researches showed that oxidative stress and inflammation are also important mechanisms in inducing and maintaining NP and they are in the pathological process of NP throughout (Costigan et al., 2009; Areti et al., 2014). The products of oxidative stress and inflammation, such as reactive oxygen species (ROS), tumor necrosis factor-α (TNF-α), and interleukin-6 (IL-6), promote each other *via* specific signaling pathways, aggravate the release of these factors, cause irreversible damage to cells, and even lead to cell apoptosis. The clinical treatment of NP includes drug therapy and interventional therapy, of which drug therapy is the main one. As the common treatment drugs, antidepressants and anticonvulsants (gabapentin and pregabalin, for example) have shown only partial pain relief effect, always followed by side effects to patients (Baron et al., 2010). Therefore, the development of new therapeutic drugs is still a hot topic at present.

Higenamine (Hig) is a plant-based alkaloid with antioxidation (Guler et al., 2020), anti-inflammatory (Yang et al., 2020a), and antiapoptosis (Yang et al., 2020b) effects. Hig is mainly used to scavenge oxygen free radicals to achieve antioxidant effects (Romeo et al., 2020). Our previous study showed that Hig inhibited the production of ROS in hypothermia-induced oxidative stress and also prevented the transport of α2C-AR from the cytoplasm to the membrane in hypothermic HDMECs, which indicated that Hig may reduce the cold-induced vasoconstriction (Guan et al., 2019). Besides, Hig is one of the tetrahydroisoquinolinic derivatives and there is a report speculating that it may be provided with neuroprotective effects (Peana et al., 2019). Indeed, existing studies have shown that Hig protected brain/reimplantation (I/R) damage by inhibiting Akt and Nrf2/HO-1 signaling pathways against oxygen-glucose deprivation/reperfusion-induced injury (Zhang et al., 2019). And Hig showed the neuroprotective effect on Alzheimer's disease model rats by improving the cognitive impairment, regulating enzyme activity, and reducing cytotoxicity to inhibit oxidative stress damage (Yang et al., 2020b). Although more and more researches in recent year have proved that Hig has a good effect on many diseases, its effect and mechanism of how to act on NP are still unclear; thus, further research is needed by far.

This present study mainly explored the biological effects and potential molecular mechanisms of Hig on NP and demonstrated that Hig may regulate NP *via* NOX2/ROS/TRP/P38 mitogen-activated protein kinase (MAPK)/NF-κB signaling pathway, providing an experimental basis for the research and development of novel drugs.

MATERIALS AND METHODS

Chemical Reagent

Demethylcoclaurine hydrochloride (≥98%) was purchased from Shanghai Yuanye Bio-Technology Co., Ltd. (Shanghai, China). Tert-butyl hydroperoxide (t-BHP) was from Energy Chemical (Shanghai, China). Dulbecco's modified Eagle's medium (DMEM), Penicillin-Streptomycin solution, and 0.25% trypsin were obtained from Gibco (Grand Island, NY, United States). Fetal bovine serum (FBS) was from Double-Helix (Beijing, China). Cell Counting Kit-8 (CCK-8) was purchase from Beijing Biosynthesis Biotechnology Co., Ltd. (Beijing, China). ROS assay kit, microreduced glutathione (GSH) assay kit, and mitochondrial membrane potential (MMP) assay kit with JC-1 were from Beijing Solarbio Science & Technology Co., Ltd. (Beijing, China). Annexin V-FITC/PI apoptosis kit was obtained from Shanghai Yishan Biotechnology Co., Ltd. (Shanghai, China). Hoechst 33258/PI Apoptosis Assay Kit was from Beyotime Biotechnology (Shanghai, China). Malondialdehyde (MDA) assay kit and superoxide dismutase (SOD) assay kit were from Nanjing Jiancheng Bioengineering Institute (Nanjing, Jiangsu, China). IL-6, IL-1β, TNF-α, and ROS ELISA kit were obtained from Wuhan Meimian Biotechnology Co., Ltd. (Wuhan, Hubei, China). RNAiso Plus (Trizol) was purchased from TaKaRa (Tokyo, Japan). Evo M-MLV RT Kit with gDNA Clean for qPCR and SYBR® Green Premix Pro Taq HS qPCR Kit were from Accurate Biology (Changsha, Hunan, China). FGSuper Sensitive ECL Luminescence Reagent was purchased from Meilunbio® (Dalian, Liaoning, China). All of the primary antibodies were obtained from Cell Signaling Technology unless otherwise stated (Danvers, MA, United States).

Cell Culture

The immortal rat Schwann cell 96 (RSC96) was purchased from iCell Bioscience Inc. (Shanghai, China). RSC96 is cultivated in a complete medium made up of 90% DMEM, 10% FBS, and 1% Penicillin-Streptomycin solution in a sterile environment with 5% CO_2 and 37°C.

Cell Viability Assay

CCK-8 was used to evaluate cell viability. RSC96 was plated in a 96-well plate with a density of 5×10^3 cells/well and treated with a different drug concentration. Then 100 μL of cell culture complete medium containing 10% CCK-8 solution was added to 96-well plate and incubated for 1 h at 37°C. The absorbance values (450 nm) were detected by a microplate reader (BioTek, United States).

Cell Treatment

Hig was dissolved in dimethyl sulfoxide (DMSO). As previous research reported, t-BHP was performed to establish an oxidase stress injury model on cells (Zhao et al., 2017). RSC96 was pretreated with different concentration of Hig for 12 h and then t-BHP with a complete medium was added to each well for 2 h to assess the effect of Hig on t-BHP-exposed RSC96.

Analysis of ROS

The intracellular ROS levels were measured by fluorometry and flow cytometry using 2,7-dichlorodi-hydrofluorescein diacetate (DCFH-DA) dye. The DCFH-DA probe was mixed with FBS-free medium at 1:2,000 (1:5,000 for flow cytometry). The volume of

mixed medium to cell cultural plate was added appropriately to cover the cells and incubated for 20 min at 37°C. After that, RSC96 was washed by an FBS-free medium three times to completely remove fluorescent probes. The ROS level was observed under a fluorescence microscope (Carl Zeiss AG, Germany) and analyzed by flow cytometer (Beckman Coulter, Inc., United States).

Determinations of GSH, SOD, and MDA

The intracellular levels of GSH, SOD, and MDA contents were measured according to the manufacturer's instructions. In brief, RSC96 was washed and resuspended with PBS after administration. The same RSC96 volume of GSH extract was added three times to resuspend the cells, frozen and thawed twice in liquid nitrogen, and centrifuged to aspirate the supernatant for testing. Samples and reagents were mixed following the instructions, which were reacted at room temperature for 2 min, and the absorbance was measured at a wavelength of 412 nm. As for the extraction of SOD and MDA, ultrasonication was applied to gain cellular SOD and MDA. The absorbance of SOD and MDA was detected, respectively, at 550 and 532 nm with the microplate reader (BioTek, United States).

Hoechst 33258/PI Staining

The Hoechst 33258/PI staining of RSC96 was performed to observe the state of cell apoptosis and necrosis directly. A suitable cover glass was put into the cell plate in advance and the glass was washed gently with PBS after administration. 95% ethanol was used to fix cell for 15 min at room temperature. Then, the surface liquid was dried, and 10 μL Hoechst 33258/PI solution was added on it and mounted. The changes of the apoptotic and necrotic nucleus were observed and photographed by fluorescence microscopy (Olympus, Japan).

Flow Cytometry

Flow cytometry was used to account for the apoptosis rate of RSC96 and detect the functional condition of the mitochondrion, which were measured through Annexin V-FITC/PI staining and JC-1 staining, respectively. In brief, after administration, the cell culture medium was drawn into a prelabeled 15 ml centrifuge tube, RSC96 was washed twice with cold PBS, and PBS was drawn again into the corresponding centrifuge tube. 0.25% trypsin without EDTA digested cell for 1 min and was centrifuged at 1500 rpm for 5 min. RSC96 were resuspended in 500 μL 1× binding buffer, stained with 5 μL Annexin V-FITC and 10 μL PI solution, incubated at room temperature for 5 min in the dark environment, and immediately examined by flow cytometer (Beckman Coulter, Inc., United States). As for the detection of MMP, RSC96 were resuspended in 0.5 ml cell culture medium, mixed with 0.5 ml JC-1 staining solution, and incubated for 20 min at 37°C, 5% CO_2. After the incubation, the cells were centrifuged at 4°C and 600 g for 3 min, washed with prechilled 1 × JC-1 staining buffer solution twice, and 1 ml 1 × JC-1 staining buffer solution was added to resuspend RSC96, followed by analyzing the condition of MMP with a flow cytometer (Beckman Coulter, Inc., United States).

Real-Time Quantitative Polymerase Chain Reaction

RSC96 was washed with cold PBS after treatment. RNAiso Plus was applied to extract total RNA and the detective values of OD260/280 were used to quantify total RNA. Evo M-MLV RT Kit with gDNA Clean for qPCR was used to reverse transcription according to the manufacturer's protocol. Amplification was performed in the CFX Connect Real-Time PCR Detection System (BIO-RAD, Hercules, CA, United States) following the protocol of SYBR® Green Premix Pro Taq HS qPCR Kit. The reaction procedure was as follows: one cycle at 95°C for 30 s for predenaturation and 40 cycles at 95°C for 5 s and at 60°C for 30 s for reaction. The primer GAPDH (B661204) was purchased from Sangon Biotech. Co., Ltd. (Shanghai, China) and the primers of TNF-α IL-6 and IL-1β were also designed by them which were listed in **Table 1**. The 2−ΔΔCT method was used to analyze expression levels of TNF-α IL-6 and IL-1β. Each sample was measured three times and averaged.

Animal

Forty-eight specific pathogen-free (SPF) grade adult male Sprague Dawley (SD) rats were provided by Beijing Huafukang Biotechnology Co., Ltd. (Beijing, China, certificate number SCXK (Jing) 2019-0008). The rats were kept in a 12 h light/dark cycle environment with a temperature of 20–25°C and a humidity of 50–70%. Animal test procedures and general handling comply with the ethical guidelines and standards for the care and use of laboratory animals established by the Animal Test Ethics Committee of Jinan University. All efforts were made to minimize animal suffering.

CCI Surgery

The rats were randomly divided into sham-operated group, CCI model group, and low/medium/high concentration of Hig and gabapentin (GBP) treatment group with eight rats in each group. The specific surgical procedures have been introduced in our previous study (Zhang et al., 2020).

Pharmacological Treatment

The rats accepted medical treatment with oral administration after surgery. Rats in low/medium/high concentration of Hig and GBP group were treated with 25/50/100 $mg{\cdot}kg^{-1}{\cdot}d^{-1}$ Hig and 50 $mg{\cdot}kg^{-1}{\cdot}d^{-1}$ GBP, respectively. Those rats in the sham-operated and CCI groups were not treated with drugs but 6 $ml{\cdot}kg^{-1}{\cdot}d^{-1}$ 0.9% saline.

Behavioral Tests

von Frey filaments (Ugo Basile Biological Research Apparatus, Varese, Italy) were applied to evaluate mechanical allodynia in CCI surgical rats while a hot-plate test was used to assess heat hyperalgesia. The von Frey test and hot-plate test were detailly described in our previous research (Zhang et al., 2020) and they were performed the day before the surgery and days 3, 5, 7, 10, 14, and 21 after surgery.

Enzyme-Linked Immunosorbent Assay

Ipsilateral L4/5 dorsal root ganglion (DRG) was collected to detect the expression level of ROS while serum was collected

TABLE 1 | Primer sequences for RT-qPCR.

Gene	Forward (5′-3′)	Reverse (5′-3′)
TNF-α	CGTCGTAGCAAACCACCAAG	CACAGAGCAATGACTCCAAAG
IL-6	ACTTCCAGCCAGTTGCCTTCTTG	TGGTCTGTTGTGGGTGGTATCCTC
IL-1β	CTCACAGCAGCATCTCGACAAGAG	TCCACGGGCAAGACATAGGTAGC

for inflammatory factors (TNF-α, IL-6, and IL-1β). DRG was weighted and PBS was added to adjust its concentration to 0.1 g/ml. It was homogenized thoroughly and centrifuged at 4°C and 3000 rpm for 20 min. The supernatant was carefully aspirated for testing. And serum was diluted for detection. The experimental operation was performed according to the ELISA kits' instructions and the absorbance was measured at 450 nm with a microplate reader (BioTek, United States).

Measurement of GSH in DRGs

The fresh DRGs are washed twice with PBS and then 0.1 g of the tissue is weighted and homogenized. The remaining steps were carried out according to the kit manufacturer's instructions.

Histopathology

The right sciatic nerve tissues were fixed and washed with water, dehydrated, transparent, and embedded in paraffin. After the slices were processed in 5 μm thick sections, rehydrated, stained with hematoxylin-eosin (HE), washed with ethanol, dehydrated, and made transparent with xylene, they were observed and photographed under the microscope (Olympus, Japan).

Western Blotting Analysis

The obtained RSC96 and ipsilateral L4/5 DRG tissue were used to perform the WB analysis. Cell and tissues were lysed with RIPA lysis buffer (Solarbio Science & Technology Co., Ltd, Beijing, China) and the protein concentration was quantified using BCA Protein Assay Kit (Solarbio Science & Technology Co., Ltd., Beijing, China). 10% SDS-PAGE was carried out to separate obtained protein samples and the proteins were transferred to polyvinylidene fluoride (PVDF) membrane (Millipore, MA, United States). 5% nonfat milk was used to block the membranes for 2 h at room temperature. Primary antibodies, including Bcl-2, Bax, caspase-3, cleaved caspase-3, cytochrome-c, p38 MAPK, phospho-p38 MAPK, phospho-NF-κB p65, GAPDH, TRPA1 (Novus Biologicals, United States), TRPV1 (Novus Biologicals, United States), and anti-NOX2/gp91phox (Abcam Corporation, England), were diluted in 1:1,000. Then, the membranes were put into primary antibodies above at 4°C for incubating overnight. After washing with TBST three times, the diluted secondary primary antibody was applied to incubate the membranes at 4°C for 2 h. TBST was used to wash the obtained protein bands and they were exposed using FGSuper Sensitive ECL Luminescence Reagent.

Molecular Docking

The molecular structure of Hig was downloaded from PubChem database and the three-dimensional structure of Nox2, TRPA1, and TRPV1 protein from the RCSB Protein Data Bank. The AutodockTools 1.5.6 software was used to deal with these structures and determine the coordinates and box size of the Vina molecule docking. In order to increase the accuracy of the calculation, the parameter exhaustiveness was set to 20. Then Autodock Vina 1.1.2 software was performed to do semiflexible docking of molecules and proteins for selecting the best conformation of affinity. The docking binding mode was used to analyze the conformation with the lowest docking score and finally plot it in the Pymol software. Besides, the three-dimensional structures of Nox2 and TRPV1, Nox2, and TRPA1 protein were processed in pymol and protein docking was performed in ZDOCK 3.0.2. As a result, the top ten complexes were selected and scored and the best scores were chosen for mapping.

Statistical Analysis

GraphPad Prism 8 and SPSS 22.0 were used for statistical analyses. All data were expressed as mean ± SEM. All experiments in this study were performed in triplicate. One-way ANOVA was used for comparison between groups, followed by Turkey tests. The behavioral data were analyzed using multivariate analysis of variance in the general linear model to compare data among the groups at each time point, followed by the Student–Newman–Keuls tests. p value less than 0.05 was considered to be statistically significant.

RESULTS

Hig Showed a Protective Effect Against T-BHP-Induced Cell Cytotoxicity

CCK-8 was used to evaluate cell viability with different concentration of Hig (50, 100, 150, 200, 250, 300, 400, and 500 μM). As shown in **Figure 1A**, Hig treated RSC96 at six concentrations for 12 h with no significant difference compared to the control group but 400 and 500 μM concentrations significantly enhanced cell viability. T-BHP decreased obviously the viability of RSC96 at 2 h with 50, 100, 150, 200, 250, 300, and 400 μM, which meant that different concentration even the lowest concentration (50 μM) would increase the risk of cell death (**Figure 1B**). Then, we assessed the underlying protective effect of Hig against t-BHP-induced cell cytotoxicity. The pretreated RSC96 at 50, 100, 150, 200, 250, 300, 400, and 500 μM concentration was exposed to t-BHP at the concentration of 100 and 150 μM for 2 h. Compared with the model group (t-BHP treatment), a dose-dependent manner of cell viability which significantly increased was observed in pretreated Hig at different concentration (**Figures 1C,D**). The final dosing concentration of t-BHP and Hig was determined to be 150 μM and 100/200/400 μM, respectively.

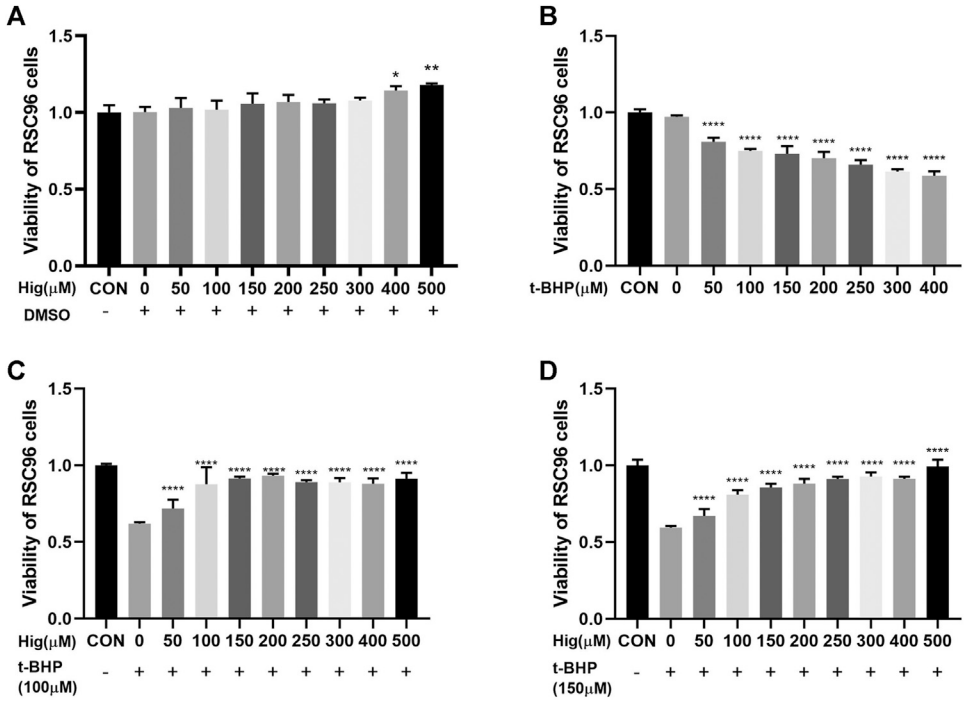

FIGURE 1 | Cell viability of Hig and t-BHP treatment. **(A)** CCK-8 detected the cell viability of RSC96 treated with 50, 100, 150, 200, 250, 300, 400, and 500 μM Hig for 12 h. A DMSO control group was set up to exclude the potential cell cytotoxicity of DMSO. **(B)** CCK-8 detected the cell viability of RSC96 treated with 50, 100, 150, 200, 250, 300, and 400 μM t-BHP for 2 h. **(C)** RSC96 was pretreated with 50, 100, 150, 200, 250, 300, 400, and 500 μM Hig for 12 h and then, respectively, exposed to 100 μM t-BHP for 2 h. **(D)** RSC96 was pretreated with 50, 100, 150, 200, 250, 300, 400, and 500 μM Hig for 12 h and then, respectively, exposed to 150 μM t-BHP for 2 h. CCK-8 was used to assess cell viability. The results are presented as mean ± SEM, $n = 3$. $^{*}p < 0.05$, $^{**}p < 0.01$, and $^{****}p < 0.0001$ vs. the control group.

Hig Attenuated Oxidative Stress Injury *In Vivo* and *In Vitro*

To explore the antioxidant properties of Hig, we adopted the model of t-BHP-induced RSC96 oxidative stress *in vitro* and CCI-induced DRG neuron damage *in vivo*. From the results shown in **Figures 2A–F**, t-BHP treated alone for 2 h significantly increased intercellular levels of ROS and MDA but reduced SOD and GSH levels, which indicated that t-BHP imbalanced the redox system and caused the dysfunction of RSC96. However, pretreatment with Hig reversed these changes compared to the model group. Also, ROS and GSH were mainly evaluation indexes in DRG neuron. In **Figures 2G,H**, the level of ROS in DRG was upregulated by CCI surgery and the content of GSH was reduced. After 21 days of treatment with Hig, the upregulated ROS was significantly decreased by medium and high concentration (50/100 mg/kg) of Hig, and the downregulated GSH was obviously increased by a high concentration of Hig.

Hig Decreased T-BHP-Induced RSC96 Apoptosis

Morphologically, RSC96 in the control group appeared healthy with rich synapse. Apparent cell shrinkage was observed in RSC96 after 2 h treatment with t-BHP but those cells pretreated with Hig remained in relatively healthy appearance compared to the model group (**Figure 3A**). Hoechst 33258/PI staining and flow cytometry assay were applied to detect the apoptosis condition of RSC96 exposed to t-BHP. According to **Figure 3B**, most of the cell nuclei were densely stained with strong blue fluorescence and partly with red fluorescence, indicating that t-BHP could induce the apoptosis and necrosis rate of RSC96. Flow cytometry was usually used to detect the apoptosis ratio by using Annexin V-FITC/PI assay kit. In **Figure 3C**, the sum of quadrants Q2-UR and Q2-LR was representing the percentage of apoptotic cells, and the value of quadrant Q2-UL was representing the percentage of necrotic cells. Therefore, the same as the result of Hoechst 33258/PI staining, t-BHP treatment increased the apoptotic and necrotic rate of RSC96.

Hig Inhibited the Expression Level of Inflammation-Related Mediators

It is known that overproduction of ROS during oxidative stress results in chronic inflammation (Willcox et al., 2004). We had checked whether Hig decreased the expression level of TNF-α, IL-6, and IL-1β after t-BHP treatment and CCI surgery. The results were shown in **Figures 4A–E**. Indeed, t-BHP treatment and CCI surgery upregulated the expression level of TNF-α, IL-6, and IL-1β (the expression level of IL-1β in cells was not shown in **Figure 4**). Pretreatment with Hig decreased the high expressive level of TNF-α and IL-6 but did not show the significant difference of reducing

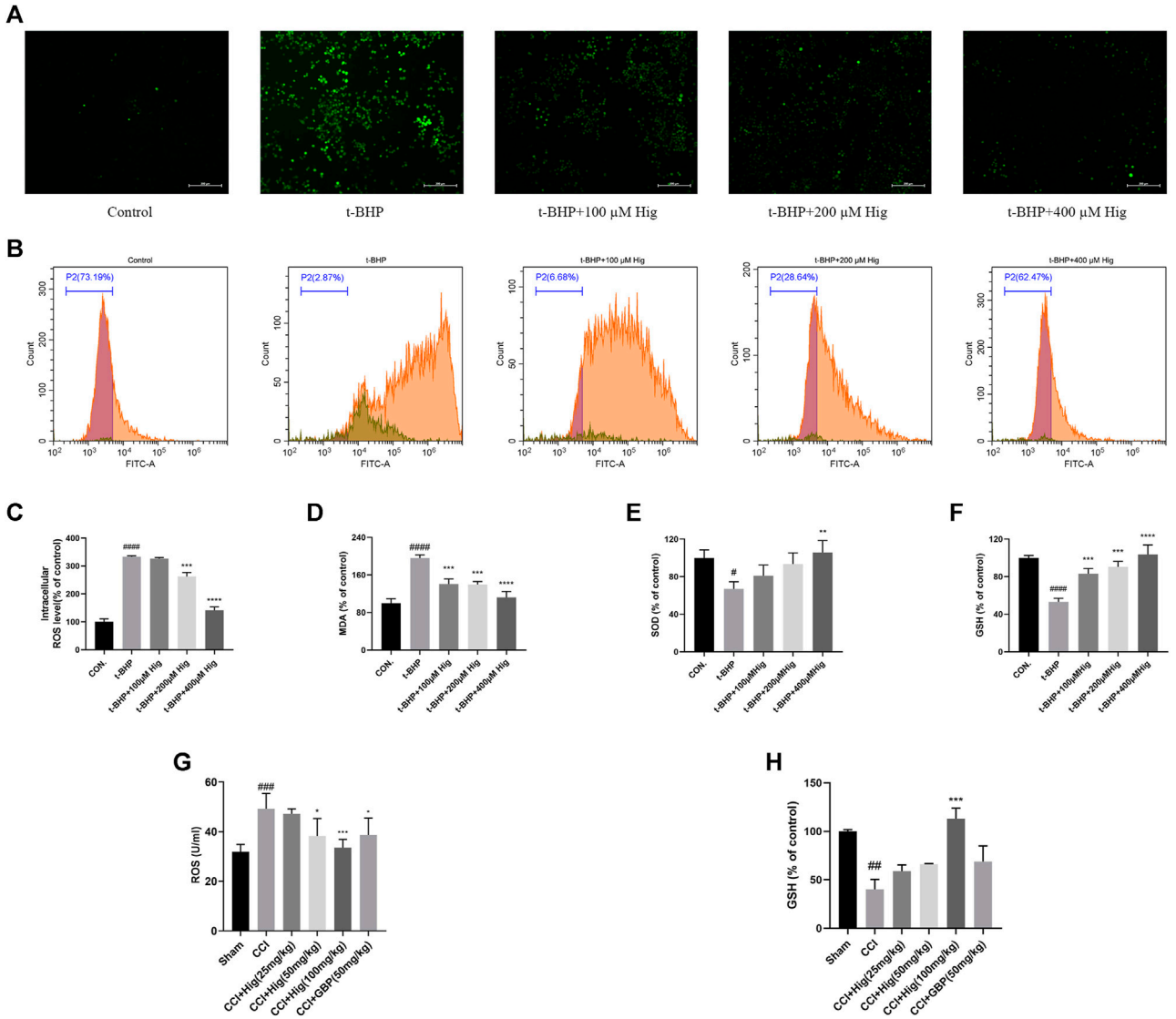

FIGURE 2 | Hig prevented RSC96 and DRG neuron from oxidative stress damage. **(A)** RSC96 intercellular level of ROS stained by DCFH-DA dye was observed under the microscope. Scar bar = 200 μm. **(B)** RSC96 intercellular level of ROS stained by DCFH-DA dye was observed by flow cytometer. **(C)** The ratios of RSC96 intercellular ROS level compared with the control group were calculated. **(D)** Quantification of RSC96 intercellular MDA level in different groups. **(E)** Quantification of RSC96 intercellular SOD level in different groups. **(F)** Quantification of RSC96 intercellular GSH level in different groups. **(G)** The ROS level in rats' DRG tissue was detected by ELISA kit. **(H)** Comparison of GSH level in rat DRG tissues among different groups. The results are presented as mean ± SEM, $n = 3$. #$p < 0.05$, ##$p < 0.01$, ###$p < 0.001$, and ####$p < 0.0001$ vs. the control group. *$p < 0.05$, **$p < 0.01$, ***$p < 0.001$, and ****$p < 0.0001$ vs. the model group.

IL-1β expression level compared with the control group. The results proved that TNF-α and IL-6 were the potential inflammatory targets attenuated by Hig.

Hig Alleviated Mechanical Allodynia and Heat Hyperalgesia in CCI Rats

CCI surgery led to obvious mechanical allodynia and heat hyperalgesia and they were detected by von Frey test and hot-plate test, respectively. As shown in **Figures 5A,B**, mechanical withdrawal threshold (MWT) and thermal withdrawal latency (TWI) both decreased significantly at day 3 after CCI surgery and reached the lowest value on day 7 after the operation. On day 7, obviously, a difference was observed between the high-concentration Hig and CCI groups. After 21 days of treatment, all groups but the low-concentration Hig group showed markedly pain relief effect by reducing mechanical allodynia and heat hyperalgesia in CCI rats.

Hig Protected the Injured Sciatic Nerve in CCI Rats

As shown in **Figure 6**, the sham-operated group had no obvious pathological changes. The sciatic nerve tissue in the CCI group

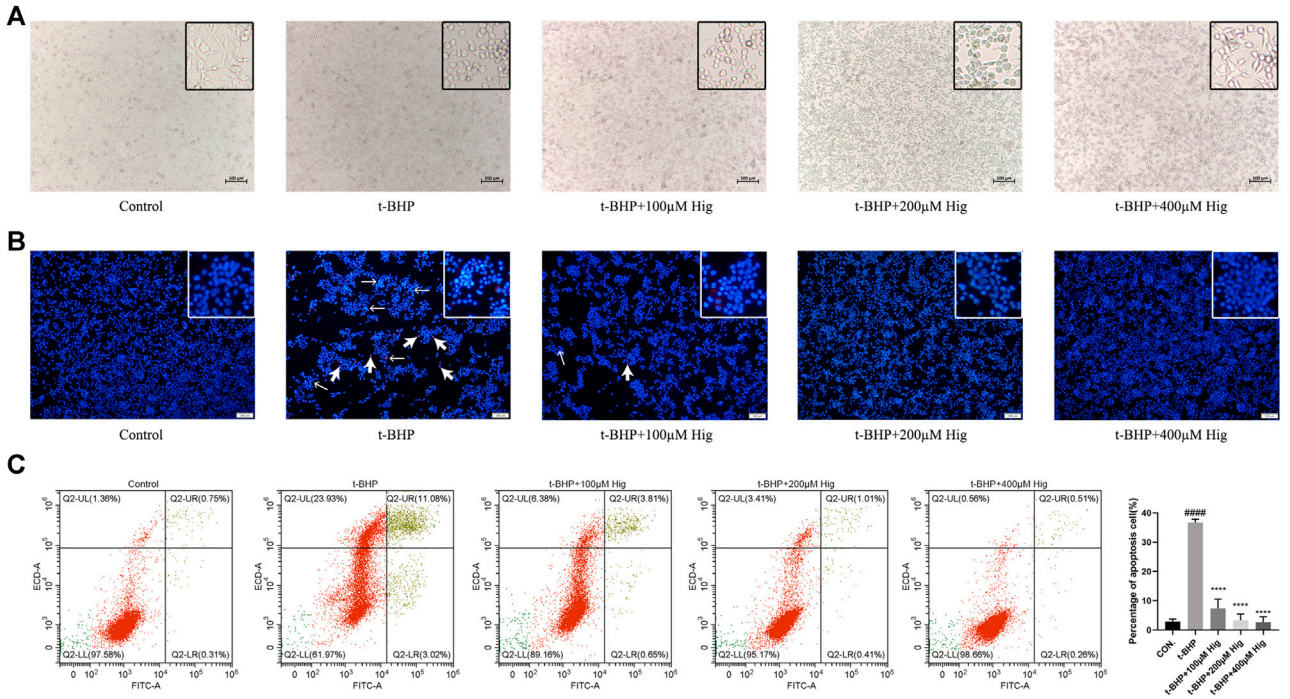

FIGURE 3 | Hig protected RSC96 against t-BHP-induced cell apoptosis. **(A)** The typical morphological images in different groups. **(B)** The stained RSC96 by Hoechst 33258/PI dye was observed under the microscope. The nucleus of RSC96 marked with strong blue (the thin black arrows) and red (the thick black arrows) fluorescence represented cell apoptosis and necrosis, respectively. Scar bar = 100 μm. **(C)** Annexin V-FITC/PI apoptosis kit analyzed the cell apoptosis *via* flow cytometer and the percentage of RSC96 apoptosis was calculated from the addition of Q2-UL, Q2-UR, and Q2-LR. The results are presented as mean ± SEM, n = 3. ####p < 0.0001 vs. the control group. ****p < 0.0001 vs. the t-BHP group.

had shown the nerve fiber structural disorder accompanied by neuron loss, degeneration, and nuclear pyknosis. Myelin vacuolation, proliferation of SC, and inflammatory cell infiltration were also observed by a microscope. After Hig treatment, the above pathological changes were improved in a dose-dependent manner and the occurrence of neuron loss, degeneration, and nuclear pyknosis was inhibited. However, the GBP group, as the positive drug control group, only showed a few improvement effects on the above condition.

Hig Showed the Protective Function in RSC96 and DRG Neuron by Regulating the Mitochondrial Apoptosis Pathway

In vitro JC-1 probe was used to detect MMP (△Ψm), which was generally applied to assess early cell apoptosis. As shown in **Figure 7A**, compared with the control group, △Ψm depolarized after t-BHP stimulation and pretreatment with Hig reversed the depolarization of △Ψm and inhibited early cell apoptosis. WB analysis was performed to analyze the expression level of Bcl-2, Bax, and cytochrome-c (cyt-c) proteins in RSC96 and DRG tissues (**Figures 7B**, **8**). The results showed that both t-BHP treatment and CCI operation reduced the expression level of the antiapoptotic protein Bcl-2 in RSC96 and DRG neurons and increased the proapoptotic proteins Bax and cyt-c. Pretreatment with Hig increased the ratio of bcl-2/bax and downregulated the expression level of cyt-c, indicating further neuroprotection of Hig on RSC96 and DRG neurons. In addition, Hig also decreased the expression level of cleaved caspase 3/caspase 3 in DRG neurons.

Hig Regulated Nox2/ROS/TRP/P38 MAPK/NF-κB Signaling Pathway for Its Therapeutic Effect on Pain Relief, Antioxidation, Anti-Inflammatory

To explore the underlying molecular mechanism of Hig on treating t-BHP-exposed RSC96 and CCI model rats, we detected the expression level of Nox2, TRPA1, TRPV1, p38 MAPK, p-p38 MAPK, and p-NF-κB using WB analysis. The results were shown in **Figures 9A,B**. After t-BHP treatment alone, an obviously upregulating level of Nox2, TRPA1, TRPV1, p-p38 MAPK, and p-NF-κB was observed from the protein bands. Pretreated Hig inhibited the rising trend of the above proteins. The same consequence was also observed *in vivo*. The expression levels of Nox2, TRPA1, TRPV1, p-p38 MAPK, and p-NF-κB proteins were increased in CCI rats while there was a declining tendency of these proteins after 21 days of treatment with Hig. The results showed that Hig played an important role in suppressing the protein expression level of Nox2, TRPA1, TRPV1, p-p38 MAPK, and p-NF-κB.

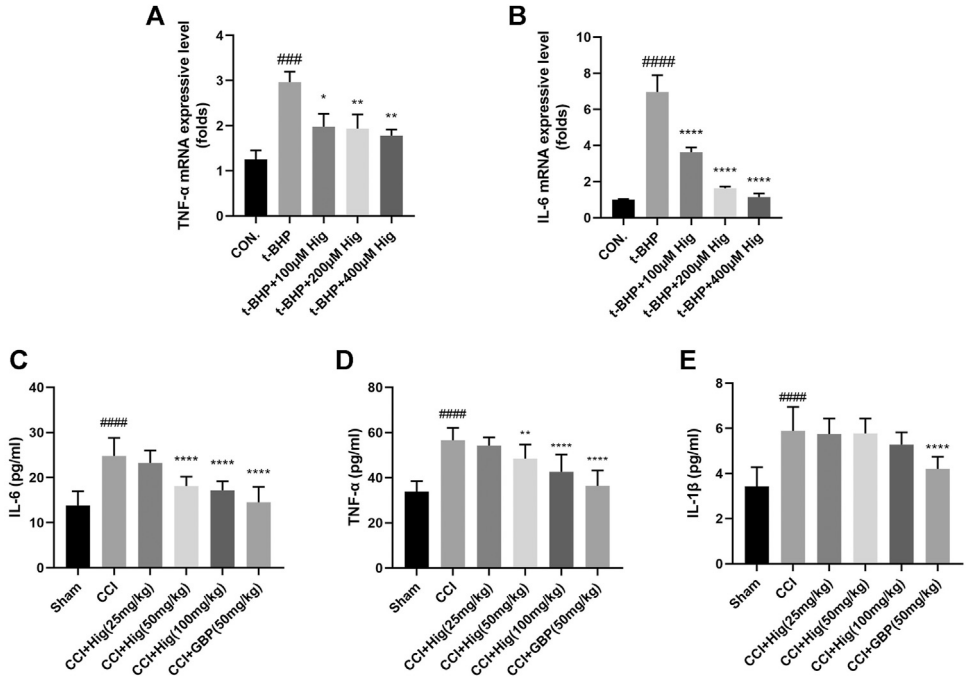

FIGURE 4 | The anti-inflammatory function of Hig was evaluated by its effect on the expression of inflammatory factors. **(A, B)** The RSC96 intercellular mRNA expression levels of TNF-α and IL-6 were measured by RT-qPCR. **(C–E)** The expression levels of TNF-α, IL-6, and IL-1β in rats serum were detected by specific ELISA kits. The results are presented as mean ± SEM, $n = 6$. ###$p < 0.001$ and ####$p < 0.0001$ vs. the control group. *$p < 0.05$, **$p < 0.01$, ***$p < 0.001$, and ****$p < 0.0001$ vs. the model group.

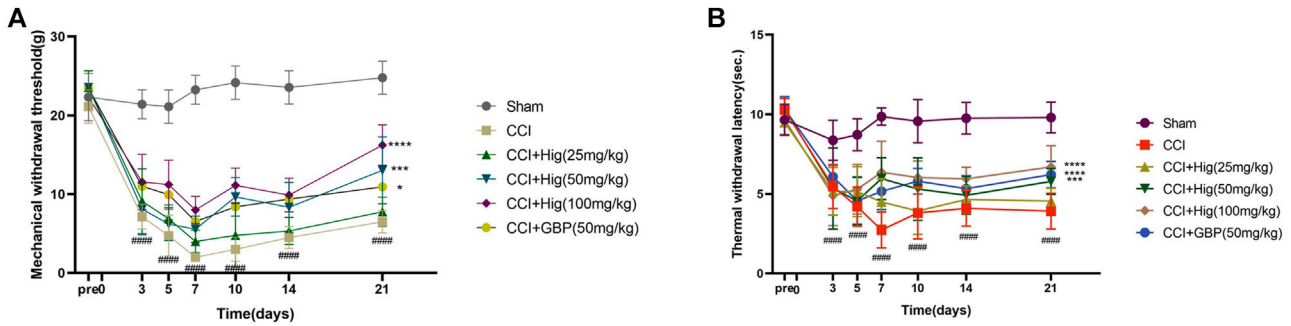

FIGURE 5 | Hig relieved mechanical allodynia and heat hyperalgesia in CCI rats by raising the thresholds of MWT and TWI. **(A)** The value of MWT in each group was detected by the von Frey test on the day before the surgery and days 3, 5, 7, 10, 14, and 21 after surgery. **(B)** The value of TWI in each group was detected by the hot-plate test. The results are presented as mean ± SEM, $n = 8$. ####$p < 0.0001$ vs. the control group. *$p < 0.05$, ***$p < 0.001$, and ****$p < 0.0001$ vs. the CCI group.

According to the results of this work and literature reported (Puntambekar et al., 2005; Marone et al., 2018), we assumed that some connection would exist between Nox2 and TRPV1, Nox2, and TRPA1. The molecular docking was used for preliminary verification and model creation to provide further proof for subsequent experiments. The molecular docking maps were shown in **Figure 10** and the binding sites of Nox2, TRPV1, and TRPA1 protein were listed in **Tables 2**, **3**. The scores for the Hig-Nox2, Hig-TRPV1, and Hig-TRPA1 molecule-protein docking were −6.0 kcal mol^{-1}, −8.0 kcal mol^{-1}, and −8.8 kcal mol^{-1}, suggesting that Hig was tightly bound to Nox2, TRPV1, and TRPA1. Hig formed a hydrogen bond with a bond length of 2.1, 2.2, and 3.1 Å in Nox2 protein amino acids SER163, LEU152, and GLU184, respectively (**Figure 10A**), a hydrogen bond with a bond length of 2.3 and 2.4 Å in TRPA1 protein amino acids HIS983 and ARG852, respectively (**Figure 10B**), and a hydrogen bond with a bond length of 2.6 and 2.7 Å in TRPV1 protein amino acids TYR555 and GLU513, respectively (**Figure 10C**). The protein-protein docking was performed to detect the probably connective binding sites between Nox2 and TRPV1, Nox2 and TRPA1. The amino acids

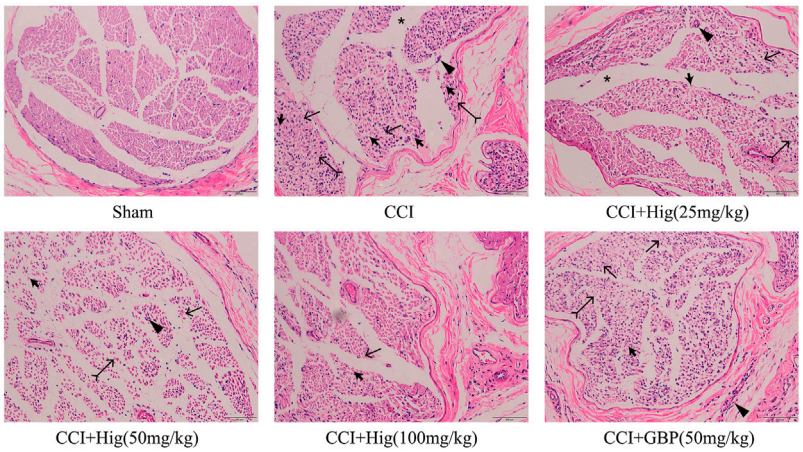

FIGURE 6 | The typical pathological images of DRG tissue in CCI rats. Thick arrow, thin arrow, bifid arrow, triangle arrow, and star symbols illustrate Schwann cell (SC) nuclei, myelin vacuolation, changes of axoplasm, inflammatory cell infiltration, and wide separation between the nerve fibers, respectively. Scar bar = 200 μm.

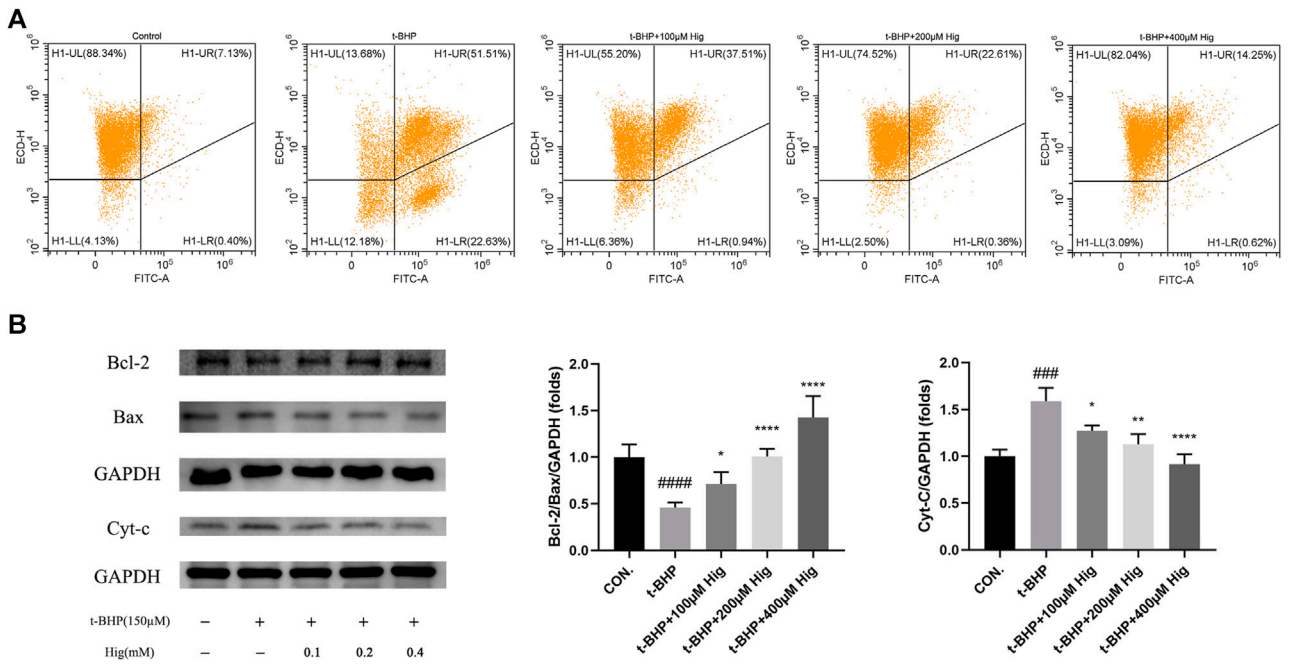

FIGURE 7 | Hig protected RSC96 against oxidative stress-induced apoptosis by regulating mitochondrial pathway. **(A)** △Ψm was detected by JC-1 probe using flow cytometer. The sum of quadrants H1-LL and H1-LR represented the depolarization extent of △Ψm. **(B)** Protein bands were detected by WB analysis. The ratios of Bcl-2/Bax protein level and the expression level of cyt-c protein were quantified. GAPDH served as an internal control. The results are presented as mean ± SEM, $n = 3$. ###$p < 0.001$ and ####$p < 0.0001$ vs. the control group. *$p < 0.05$, **$p < 0.01$, and ****$p < 0.0001$ vs. the t-BHP group.

TYR246, TYR198, and ARG242 in TRPV1 were combined with amino acids TYR127, THR64, THR64, and GLU68 in Nox2 to form stable hydrogen bonds (**Figure 10D**). The optimal score in the complex was 1617.495. As for Nox2-TRPA1, the amino acids VAL1005, ILE1004, GLN1000, ASP999, VAL998, and LEU995 in TRPA1 were combined with amino acids GLN68, GLY-5, and PRO6 in Nox2 to form stable hydrogen bonds (**Figure 10E**). The optimal score in the complex was 2055.496.

DISCUSSION

NP seriously affects the quality of life of patients. It is found that the incidence of NP rises to 3–17% in the recent statistical analysis of epidemiology (van Hecke et al., 2014). Most of the therapies have little benefit to patients and are always accompanied by side effects. Therefore, finding an effective drug for treating NP is the key breakthrough point. However, the pathogenesis of NP is very

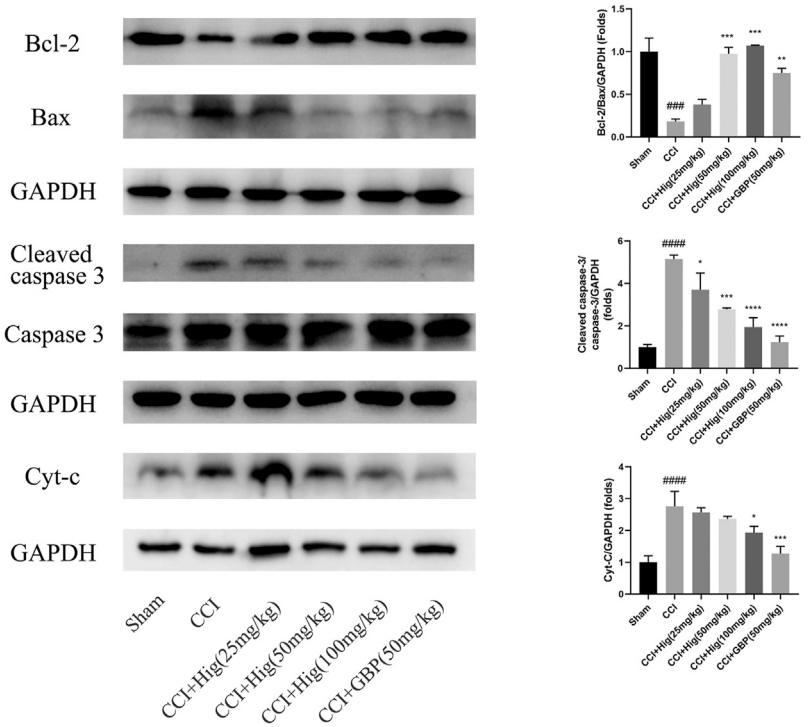

FIGURE 8 | Hig protected DRG neuron against CCI-induced oxidative stress and apoptosis by regulating mitochondrial pathway. WB analysis was used to quantify the ratio of Bcl-2/Bax and cleaved caspase 3/caspase 3 protein level and the expression level of cyt-c protein. GAPDH was considered as an internal control. The results are presented as mean ± SEM, $n = 3$. ###$p < 0.001$ and ####$p < 0.0001$ vs. the control group. *$p < 0.05$, **$p < 0.01$, ***$p < 0.001$, and ****$p < 0.0001$ vs. the t-BHP group.

complicated and there is still no exact statement to reveal the specific mechanism. The development and maintenance of NP not only are related to central and peripheral sensitization but also involve the accumulated products of oxidative stress and inflammatory response, as well as the highly interweaving signaling pathway among neurons, Schwann cells (SC), and immune cells. More and more studies support the view that oxidizing substances (including superoxide and hydrogen peroxide) drive the generation of NP and it is believed that inhibiting the production of oxidizing substances is a potential treatment to alleviate NP (Grace et al., 2016). Many studies have verified that Hig possesses a strong antioxidant effect through *in vivo* and *in vitro* experiments (Guan et al., 2019; Wang et al., 2019; Wen et al., 2019; Guler et al., 2020). In the current study, Hig protected RSC96 against t-BHP-induced oxidative stress and showed the antinociceptive and neuroprotective activities in the rat with CCI.

SC, the most abundant peripheral glial cells, respond to peripheral nerve injury by the way of changing phenotype and releasing of inflammatory mediators (TNF-α, IL-6, and IL-1β), which leads to the exacerbation of NP (Shamash et al., 2002; Kobayashi et al., 2008). Targeted SC also is regarded as a positive therapy for alleviating NP. Thus, RSC96 was chosen to carry on *in vitro* experiments to evaluate drug efficacy. In the study, we found that the exogenous ROS donor (t-BHP) imbalanced the redox system, which is manifested in the excessive release of ROS and MDA, the reduction of SOD and GSH, even the decrease of MMP, and the increase of cell apoptosis and necrosis. However, these changes were reversed after Hig medication.

CCI, the typical model-induced NP, was adopted to further evaluate the antioxidant, analgesic, and neuroprotective properties of Hig. CCI caused inflammation and hyperalgesia in rats, which was consistent with our previous research results (Zhang et al., 2020). In addition, a high level of ROS and low expression of GSH in DRG neurons were observed, indicating that CCI surgery triggered oxidative stress injury in local tissue. Histopathological evaluation of the H & E staining of sciatic nerve sections was applied to illustrate the neuroprotective effect of Hig. The results showed that Hig improved the pathological changes of the sciatic nerve in CCI rats, alleviated thermal hyperalgesia and mechanical allodynia caused by CCI, and attenuated inflammation and oxidative stress in rats.

Mammalian nerves are more vulnerable at an oxidative stress condition for the abundant phospholipids and mitochondria-rich axoplasm (Areti et al., 2014). ROS is a product of the normal metabolism of oxygen in human body. ROS acts as a functional messenger molecule to maintain the normal operation of cell activities (Kallenborn-Gerhardt et al., 2013). Under pathological conditions, a large amount of ROS will destroy cell signal transduction pathways, oxidize proteins and lipid cells, fragment DNA, cause tissue damage, and induce irreversible effects. Nicotinamide adenine dinucleotide phosphate oxidase

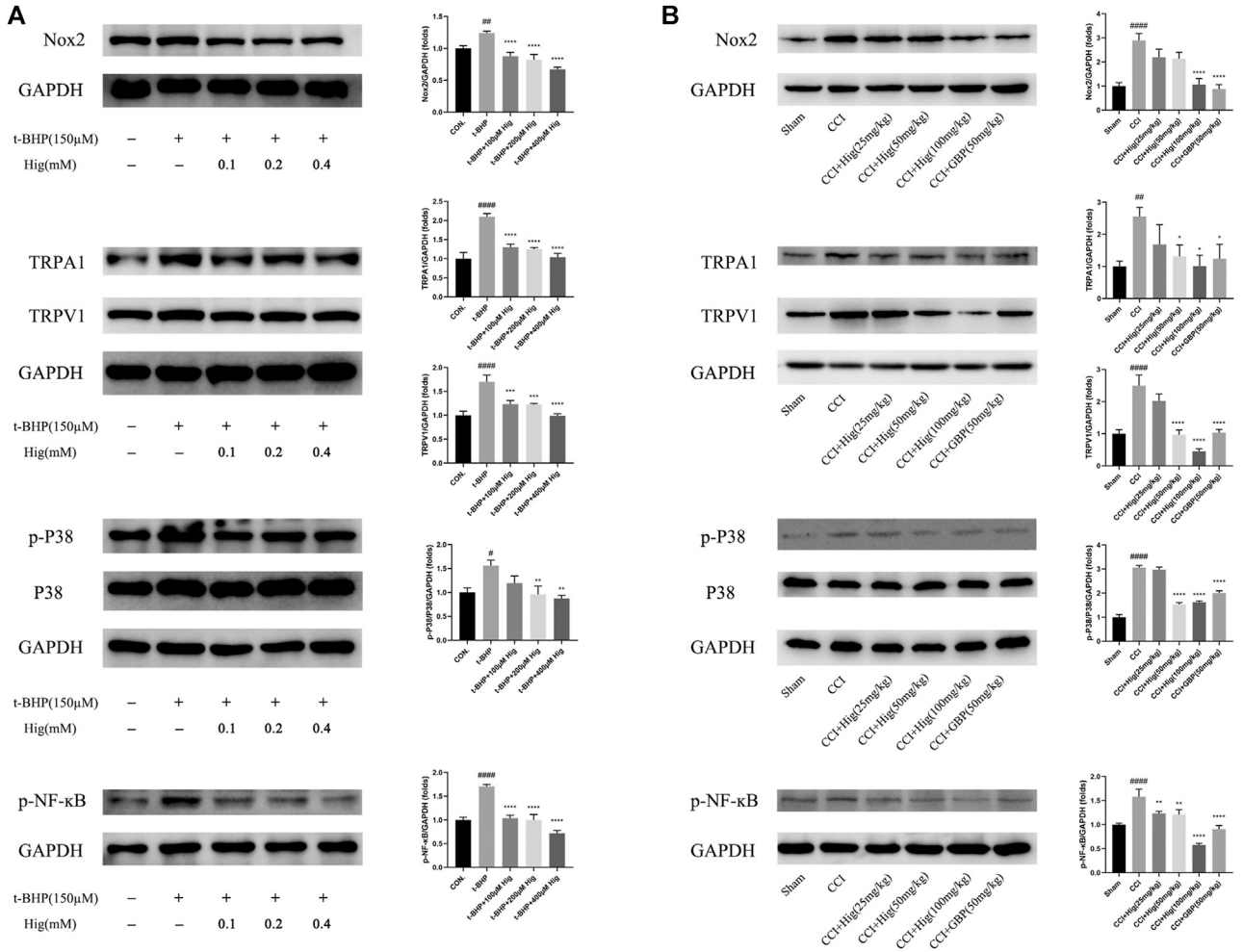

FIGURE 9 | Hig regulated the proteins expressed in Nox2/ROS/TRP/P38 MAPK/NF-κB signaling pathway. **(A)** The control and t-BHP-exposed RSC96 were collected and analyzed by WB for expression level of Nox2, TRPA1, TRPV1, p38 MAPK, p-p38 MAPK, and p-NF-κB. **(B)** The DRG tissues from sham-operated and CCI surgery were collected and analyzed by WB for expression level of Nox2, TRPA1, TRPV1, p38 MAPK, p-p38 MAPK, and p-NF-κB. GAPGH served as internal control. The results are presented as mean ± SEM, $n = 3$. #$p < 0.05$, ##$p < 0.01$, and ####$p < 0.0001$ vs. the control group. *$p < 0.05$, **$p < 0.01$, ***$p < 0.001$, and ****$p < 0.0001$ vs. the model group.

(Nox) is the place that produces ROS and the generation of ROS seems to be its main function. Nox2 is one of the main phenotypes of the enzyme. It is found that NOX2-ROS could cause excessive excitement of DRG neurons in the SNI animal model and promote the plasma membrane translocation of PKCε to induced NP. The use of the specific NOX2 inhibitor gp91-tat could alleviate the above performance (Xu et al., 2021). To well understand the possible potential antioxidant mechanism of Hig in oxidative damage, the experiment also evaluated the protein expression level of Nox2 and discovered that the expression of Nox2 was upregulated in the t-BHP-stimulated RSC96 model. The same result also appeared in DRG neurons. Hig reversed the situation and reduced the generation of ROS, which may be related to its inhibition of Nox2 activity.

Mitochondria are the order place that generates free radicals. Endogenous ROS accumulates in normal respiration or certain dysfunctions. The high potential of $\triangle\Psi m$ triggers the opening of mitochondrial pores to discharge ROS for preventing excessive accumulation of ROS in mitochondria (Zorov et al., 2014). However, the emission of ROS in mitochondria is irreversible in certain pathological processes. At this time, mitochondria will lead to a great quantity of release of ROS, reducing cell apoptosis or autophagy. Once the apoptosis program is initiated, cytochrome-c will translocate from mitochondria to cytoplasm, driving the features of subsequent apoptosis, for instance, the activation of caspase 3 and the overexpression level of proapoptotic protein. Our study results suggested Hig reduced the apoptosis rate of RSC96 and DRG neurons by acting on the mitochondrial apoptosis pathway. It meant that Hig blocked the release of cyt-c and improved the expression of antiapoptotic protein Bcl-2. There was a research that reported that cell necrosis will be induced by significantly increasing levels of intracellular ROS levels (Yeh et al., 2020). Interestingly, a significant increase in the necrosis rate of RSC96 was observed after t-BHP treatment

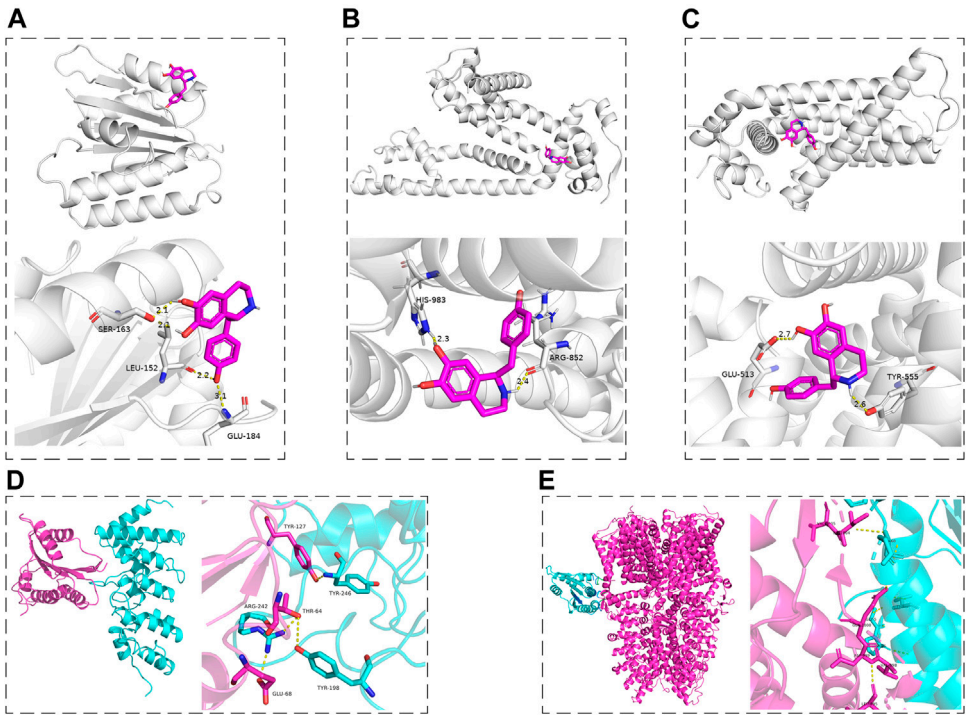

FIGURE 10 | The molecular docking maps. **(A–C)** The three-dimensional structure of Hig combined with Nox2, TRPA1, and TRPV1, respectively. **(D, E)** The schematic diagram of the optimal complex in Nox2-TRPV1 and Nox2-TRPA1 protein docking. The dashed line indicated the hydrogen bond formed between Hig and amino acid residues and the length of the hydrogen bond.

TABLE 2 | The binding sites of Nox2 and TRPV1 protein.

TRPV1	Nox2
TYR246	TYR127
TYR198	THR64
ARG242	THR64 and GLU68

TABLE 3 | The binding sites of Nox2 and TRPA1 protein.

TRPA1	Nox2
VAL1005 and ILE1004	GLN68
GLN1000	GLY-5
ASP999, VAL998, and LEU995	PRO6

for 2 h and pretreatment of Hig protected RSC96 against cell necrosis. Maybe the protective effect is related to its excellent antinecrotic activity but further exploration in subsequent studies should be needed.

The transient receptor potential (TRP) ion channel is one of the abundant ion channels in DRGs. Because of its strong selectivity and wide participation in the process of pain production, it has become a popular target for NP drug screening in recent years. The TRP family represented by TRPV1 and TRPA1 is a nonselective cation channel that could be modulated by harmful stimuli such as ROS (Nishio et al., 2013). TRPV1 is the first TRP ion channel to be discovered. It is widely expressed in tissues and organs (bladder, lungs, blood vessels, and so on) and considered to be closely related to the generation of inflammatory hyperalgesia and thermal hyperalgesia (Sanchez et al., 2001). After peripheral nerve injury, the release of inflammatory substances lowers the thermal and mechanical thresholds of sensory neurons, which will sensitize the exposed neurons (Julius, 2013). TRPA1 is another TRP family member playing an important role in mediating mechanical hyperalgesia and cold hyperalgesia (Obata et al., 2005). In DRG neurons, TRPA1 was observed upon coexpression with TRPV1, both of which induced the activation of sensory nerves and evoked pain and neuroinflammation (Fernandes et al., 2012). All these could result in the persistent pain. TRPA1 and TRPV1 are activated by Nox-dependent ROS release (Ibi et al., 2008; De Logu et al., 2017). Our previous work also revealed an upregulated tendency of TRPA1 and TRPV1 after the stimulus of H_2O_2 (another ROS donor) (Zhang et al., 2021). In the study, we mainly detected the expression of TRPA1 and TRPV1 in DRG and RSC96. The results showed a high expression level of TRPA1 and TRPV1 in the cells and animal model group. Hig pretreatment reversed these changes, which may be related to its targeting of these ion channels.

The chronic overproduction of ROS is an important substance in the progression of inflammatory diseases (Mittal et al., 2014). It

causes the production and secretion of inflammatory mediators (TNF-α; interleukins), which are activating the proinflammatory signal transduction pathway (NF-κB signaling pathway) and promoting the expression of other proinflammatory genes (Lawrence, 2009). p38 MAPK also is the potential downstream target of ROS (Kallenborn-Gerhardt et al., 2013). Many growth factors produced by inflammation are transported to the nociceptors in DRG through the intracellular signaling pathway p38 MAPK to increase the expression of TRP ion channels and then they are transported to peripheral nerves resulting in peripheral sensitization (Patapoutian et al., 2009). Our experimental results indicated that excessive ROS production could lead to inflammatory response accompanied by an increased tendency of phosphorylation of P38 MAPK and NF-κB in RSC96 and DRG neurons. Hig restrained the phosphorylation level of NF-κB and inhibited the release of inflammatory mediators to show its anti-inflammatory activity. However, Hig only showed an inhibitory effect on the two inflammatory factors, TNF-a and IL-6, but no statistical significance in the inhibition of IL-1β.

Hig could be extracted from a variety of botanicals, such as AsariRadix Et Rhizoma, Linderae Radix, and *Aconitum carmichaeli* Debx. As a tetrahydroisoquinolinic (TIQ) derivative, it is provided with neuroprotective property for its unique structure (Peana et al., 2019). Previous studies reported that TIQ derivatives are the ligands of Nox2, TRPV1, and TRPA1 (O'Dell et al., 2007; Cifuentes-Pagano et al., 2013; Kistner et al., 2016). In particular, the core pharmacophore of the first TRPV1 antagonist, capsazepine 3, is the tetrahydroisoquinoline moiety (O'Dell et al., 2007). Our study demonstrated that Hig had good inhibitory effects on the above proteins. It is reported that endogenous ligands and TRPV1 antagonists act on the vanilloid-pocket of TRPV1 (transmembrane domain structure formed by Ser505–Thr550) (Szolcsányi and Sándor, 2012) and the molecules bound to these pocket areas appeared to inhibit the activity of TRPV1 for reducing pain condition (Zheng et al., 2021). The binding pocket near amino acid residues Trp711, Ile858, Val861, Val967, Met978, and Leu982 could be linked with the TRPA1 antagonist (Terrett et al., 2021), which means that targeting the pocket also showed a pain relief effect (Melo et al., 2017; Lee et al., 2020). However, there is little discussion about the active pocket of Nox2 protein at present, so we predicted the possible binding sites of Nox2 by using the DeepSite of PlayMolecule website. The molecular docking was used to verify the hypothesis that Hig may act as a blocker of Nox2, TRPV1, and TRPA1 proteins. The results showed that Hig interacted with the protein through the formation of bond ranges and binding energy in these specific structural regions, indicating that it had the potential to become the antagonist of Nox2, TRPA1, and TRPV1, but further experimental verification is needed. Although Hig formed strong hydrogen bonds with these proteins, further experimental verification is needed. Based on our existing research results, Hig inhibited the activity of Nox2 while the content of TRPA1 and TRPV1 were also been decreased. We assume that there may be some interaction between Nox2 -TRPA1 and/or Nox2-TRPV1. Recent studies reported that Nox2 and TRPA1 were tightly located in the cell bodies of trigeminal ganglion neurons by using proximity ligation assay and speculated that their interaction could be the underlying cause for the effective release of ROS (Marone et al., 2018). The molecular docking was carried out to analyze Nox2-TRPA1 and Nox2-TRPV1. Both of them form stable complexes, which provides novel ideas for our subsequent research on Nox2-TRP. Besides, we used GBP, the first-line treatment for NP, as the positive control group in CCI rats. GBP functions as pain relief by targeting the α2δ-1 subunit of voltage-dependent calcium channels as well as TRPs, inflammatory cytokines, and N-methyl-D-aspartic acid (NMDA) receptors (Kukkar et al., 2013; Alles and Smith, 2018). The fact is the therapeutic effect of Hig showed similar efficacy profiles as GBP in reducing the expression level of TRPA1/TRPV1/TNF-α/IL-6. But other possible mechanisms of Hig on NP deserve our attention, for example, the potential NMDA receptors antagonist or/and α2δ-1 ligand.

In conclusion, it was the first time to verify the neuroprotective effect of Hig *via in vivo* and *in vitro* experiments. Hig acts as a potential candidate drug for NP treatment and probably reacted its function by inhibiting Nox2/ROS/TRP/p38 MAPK/NF-κB signaling pathway. However, further experiments are required to expound the complete molecular mechanism.

DATA AVAILABILITY STATEMENT

The original contributions presented in the study are included in the article/supplementary material; further inquiries can be directed to the corresponding author.

ETHICS STATEMENT

The animal study was reviewed and approved by the Animal Test Ethics Committee of Jinan University.

AUTHOR CONTRIBUTIONS

BY and SM designed the studies, analyzed the data, performed the experiments and BY wrote this manuscript. CZ, JS, DZ, SC, and YL performed some of the experiments. GZ supervised this project, generated resources, and reviewed and approved the manuscript.

FUNDING

The study was supported by the National Science Foundation of China (81874404).

REFERENCES

Alles, S. R. A., and Smith, P. A. (2018). Etiology and Pharmacology of Neuropathic Pain. *Pharmacol. Rev.* 70 (2), 315–347. doi:10.1124/pr.117.014399

Areti, A., Yerra, V. G., Naidu, V., and Kumar, A. (2014). Oxidative Stress and Nerve Damage: Role in Chemotherapy Induced Peripheral Neuropathy. *Redox Biol.* 2, 289–295. doi:10.1016/j.redox.2014.01.006

Baron, R., Binder, A., and Wasner, G. (2010). Neuropathic Pain: Diagnosis, Pathophysiological Mechanisms, and Treatment. *Lancet Neurol.* 9 (8), 807–819. doi:10.1016/S1474-4422(10)70143-5

Campbell, J. N., and Meyer, R. A. (2006). Mechanisms of Neuropathic Pain. *Neuron* 52 (1), 77–92. doi:10.1016/j.neuron.2006.09.021

Cifuentes-Pagano, E., Saha, J., Csányi, G., Ghouleh, I. A., Sahoo, S., Rodríguez, A., et al. (2013). Bridged Tetrahydroisoquinolines as Selective NADPH Oxidase 2 (Nox2) Inhibitors. *Medchemcomm* 4 (7), 1085–1092. doi:10.1039/c3md00061c

Colloca, L., Ludman, T., Bouhassira, D., Baron, R., Dickenson, A. H., Yarnitsky, D., et al. (2017). Neuropathic Pain. *Nat. Rev. Dis. Primers* 3, 17002. doi:10.1038/nrdp.2017.2

Costigan, M., Scholz, J., and Woolf, C. J. (2009). Neuropathic Pain: A Maladaptive Response of the Nervous System to Damage. *Annu. Rev. Neurosci.* 32, 1–32. doi:10.1146/annurev.neuro.051508.135531

De Logu, F., Nassini, R., Materazzi, S., Carvalho Gonçalves, M., Nosi, D., Rossi Degl'Innocenti, D., et al. (2017). Schwann Cell TRPA1 Mediates Neuroinflammation that Sustains Macrophage-Dependent Neuropathic Pain in Mice. *Nat. Commun.* 8 (1), 1887. doi:10.1038/s41467-017-01739-2

Fernandes, E. S., Fernandes, M. A., and Keeble, J. E. (2012). The Functions of TRPA1 and TRPV1: Moving Away from Sensory Nerves. *Br. J. Pharmacol.* 166 (2), 510–521. doi:10.1111/j.1476-5381.2012.01851.x

Finnerup, N. B., Kuner, R., and Jensen, T. S. (2021). Neuropathic Pain: From Mechanisms to Treatment. *Physiol. Rev.* 101 (1), 259–301. doi:10.1152/physrev.00045.2019

Grace, P. M., Gaudet, A. D., Staikopoulos, V., Maier, S. F., Hutchinson, M. R., Salvemini, D., et al. (2016). Nitroxidative Signaling Mechanisms in Pathological Pain. *Trends Neurosci.* 39 (12), 862–879. doi:10.1016/j.tins.2016.10.003

Guan, J., Lin, H., Xie, M., Huang, M., Zhang, D., Ma, S., et al. (2019). Higenamine Exerts an Antispasmodic Effect on Cold-Induced Vasoconstriction by Regulating the PI3K/Akt, ROS/α2C-AR and PTK9 Pathways Independently of the AMPK/eNOS/NO axis. *Exp. Ther. Med.* 18 (2), 1299–1308. doi:10.3892/etm.2019.7656

Güler, M. C., Tanyeli̇, A., Eraslan, E., Ekĭncĭ Akdemĭr, F. N., Nacar, T., and Topdağı, Ö. (2020). Higenamin Ratlarda İskemi Reperfüzyonunun Neden Olduğu Oksidatif Böbrek Hasarını Azaltır. *Kafkas Univ. Vet. Fak Derg* 26 (3), 365–370. doi:10.9775/kvfd.2019.23250

Ibi, M., Matsuno, K., Shiba, D., Katsuyama, M., Iwata, K., Kakehi, T., et al. (2008). Reactive Oxygen Species Derived from NOX1/NADPH Oxidase Enhance Inflammatory Pain. *J. Neurosci.* 28 (38), 9486–9494. doi:10.1523/jneurosci.1857-08.2008

Julius, D. (2013). TRP Channels and Pain. *Annu. Rev. Cel Dev Biol* 29, 355–384. doi:10.1146/annurev-cellbio-101011-155833

Kallenborn-Gerhardt, W., Schröder, K., Geisslinger, G., and Schmidtko, A. (2013). NOXious Signaling in Pain Processing. *Pharmacol. Ther.* 137 (3), 309–317. doi:10.1016/j.pharmthera.2012.11.001

Kistner, K., Siklosi, N., Babes, A., Khalil, M., Selescu, T., Zimmermann, K., et al. (2016). Systemic Desensitization through TRPA1 Channels by Capsazepine and Mustard Oil - a Novel Strategy against Inflammation and Pain. *Sci. Rep.* 6 (1), 28621. doi:10.1038/srep28621

Kobayashi, H., Chattopadhyay, S., Kato, K., Dolkas, J., Kikuchi, S., Myers, R. R., et al. (2008). MMPs Initiate Schwann Cell-Mediated MBP Degradation and Mechanical Nociception after Nerve Damage. *Mol. Cel Neurosci* 39 (4), 619–627. doi:10.1016/j.mcn.2008.08.008

Kukkar, A., Bali, A., Singh, N., and Jaggi, A. S. (2013). Implications and Mechanism of Action of Gabapentin in Neuropathic Pain. *Arch. Pharm. Res.* 36 (3), 237–251. doi:10.1007/s12272-013-0057-y

Lawrence, T. (2009). The Nuclear Factor NF-KappaB Pathway in Inflammation. *Cold Spring Harb Perspect. Biol.* 1 (6), a001651. doi:10.1101/cshperspect.a001651

Lee, G., Choi, J., Nam, Y. J., Song, M. J., Kim, J. K., Kim, W. J., et al. (2020). Identification and Characterization of Saikosaponins as Antagonists of Transient Receptor Potential A1 Channel. *Phytother Res.* 34 (4), 788–795. doi:10.1002/ptr.6559

Marone, I. M., De Logu, F., Nassini, R., De Carvalho Goncalves, M., Benemei, S., Ferreira, J., et al. (2018). TRPA1/NOX in the Soma of Trigeminal Ganglion Neurons Mediates Migraine-Related Pain of Glyceryl Trinitrate in Mice. *Brain* 141 (8), 2312–2328. doi:10.1093/brain/awy177

Melo, L. T., Duailibe, M. A., Pessoa, L. M., da Costa, F. N., Vieira-Neto, A. E., de Vasconcellos Abdon, A. P., et al. (2017). (-)-α-Bisabolol Reduces Orofacial Nociceptive Behavior in Rodents. *Naunyn Schmiedebergs Arch. Pharmacol.* 390 (2), 187–195. doi:10.1007/s00210-016-1319-2

Mittal, M., Siddiqui, M. R., Tran, K., Reddy, S. P., and Malik, A. B. (2014). Reactive Oxygen Species in Inflammation and Tissue Injury. *Antioxid. Redox Signal.* 20 (7), 1126–1167. doi:10.1089/ars.2012.5149

Nishio, N., Taniguchi, W., Sugimura, Y. K., Takiguchi, N., Yamanaka, M., Kiyoyuki, Y., et al. (2013). Reactive Oxygen Species Enhance Excitatory Synaptic Transmission in Rat Spinal Dorsal Horn Neurons by Activating TRPA1 and TRPV1 Channels. *Neuroscience* 247, 201–212. doi:10.1016/j.neuroscience.2013.05.023

O'Dell, D. K., Rimmerman, N., Pickens, S. R., and Walker, J. M. (2007). Fatty Acyl Amides of Endogenous Tetrahydroisoquinolines Are Active at the Recombinant Human TRPV1 Receptor. *Bioorg. Med. Chem.* 15 (18), 6164–6169. doi:10.1016/j.bmc.2007.06.032

Obata, K., Katsura, H., Mizushima, T., Yamanaka, H., Kobayashi, K., Dai, Y., et al. (2005). TRPA1 Induced in Sensory Neurons Contributes to Cold Hyperalgesia after Inflammation and Nerve Injury. *J. Clin. Invest.* 115 (9), 2393–2401. doi:10.1172/jci25437

Patapoutian, A., Tate, S., and Woolf, C. J. (2009). Transient Receptor Potential Channels: Targeting Pain at the Source. *Nat. Rev. Drug Discov.* 8 (1), 55–68. doi:10.1038/nrd2757

Peana, A. T., Bassareo, V., and Acquas, E. (2019). Not Just from Ethanol. Tetrahydroisoquinolinic (TIQ) Derivatives: From Neurotoxicity to Neuroprotection. *Neurotox Res.* 36 (4), 653–668. doi:10.1007/s12640-019-00051-9

Puntambekar, P., Mukherjea, D., Jajoo, S., and Ramkumar, V. (2005). Essential Role of Rac1/NADPH Oxidase in Nerve Growth Factor Induction of TRPV1 Expression. *J. Neurochem.* 95 (6), 1689–1703. doi:10.1111/j.1471-4159.2005.03518.x

Romeo, I., Parise, A., Galano, A., Russo, N., Alvarez-Idaboy, J. R., and Marino, T. (2020). The Antioxidant Capability of Higenamine: Insights from Theory. *Antioxidants (Basel)* 9 (5), 10. doi:10.3390/antiox9050358

Sanchez, J. F., Krause, J. E., and Cortright, D. N. (2001). The Distribution and Regulation of Vanilloid Receptor VR1 and VR1 5' Splice Variant RNA Expression in Rat. *Neuroscience* 107 (3), 373–381. doi:10.1016/S0306-4522(01)00373-6

Shamash, S., Reichert, F., and Rotshenker, S. (2002). The Cytokine Network of Wallerian Degeneration: Tumor Necrosis Factor-Alpha, Interleukin-1alpha, and Interleukin-1beta. *J. Neurosci.* 22 (8), 3052–3060. doi:10.1523/JNEUROSCI.22-08-03052.200220026249

Szolcsányi, J., and Sándor, Z. (2012). Multisteric TRPV1 Nocisensor: A Target for Analgesics. *Trends Pharmacol. Sci.* 33 (12), 646–655. doi:10.1016/j.tips.2012.09.002

Terrett, J. A., Chen, H., Shore, D. G., Villemure, E., Larouche-Gauthier, R., Déry, M., et al. (2021). Tetrahydrofuran-Based Transient Receptor Potential Ankyrin 1 (TRPA1) Antagonists: Ligand-Based Discovery, Activity in a Rodent Asthma Model, and Mechanism-Of-Action *via* Cryogenic Electron Microscopy. *J. Med. Chem.* 64 (7), 3843–3869. doi:10.1021/acs.jmedchem.0c02023

van Hecke, O., Austin, S. K., Khan, R. A., Smith, B. H., and Torrance, N. (2014). Neuropathic Pain in the General Population: A Systematic Review of Epidemiological Studies. *PAIN* 155 (4), 654–662. doi:10.1016/j.pain.2013.11.013

Wang, X., Li, X., Jingfen, W., Fei, D., and Mei, P. (2019). Higenamine Alleviates Cerebral Ischemia-Reperfusion Injury in Rats. *Front. Biosci. (Landmark Ed)* 24, 859–869. doi:10.2741/4756

Wen, J., Wang, J., Li, P., Wang, R., Wang, J., Zhou, X., et al. (2019). Corrigendum to "Protective Effects of Higenamine Combined with [6]-Gingerol against Doxorubicin-Induced Mitochondrial Dysfunction and Toxicity in H9c2 Cells and Potential Mechanisms". *Biomed. Pharmacother.* 115, 108881. doi:10.1016/j.biopha.2019.108881

Willcox, J. K., Ash, S. L., and Catignani, G. L. (2004). Antioxidants and Prevention of Chronic Disease. *Crit. Rev. Food Sci. Nutr.* 44 (4), 275–295. doi:10.1080/10408690490468489

Xu, J., Wu, S., Wang, J., Wang, J., Yan, Y., Zhu, M., et al. (2021). Oxidative Stress Induced by NOX2 Contributes to Neuropathic Pain *via* Plasma Membrane Translocation of PKCε in Rat Dorsal Root Ganglion Neurons. *J. Neuroinflammation* 18 (1), 106. doi:10.1186/s12974-021-02155-6

Yang, S., Chu, S., Ai, Q., Zhang, Z., Gao, Y., Lin, M., et al. (2020a). Anti-Inflammatory Effects of Higenamine (Hig) on LPS-Activated Mouse Microglia (BV2) through NF-Kb and Nrf2/HO-1 Signaling Pathways. *Int. Immunopharmacol* 85, 106629. doi:10.1016/j.intimp.2020.106629

Yang, X., Du, W., Zhang, Y., Wang, H., and He, M. (2020b). Neuroprotective Effects of Higenamine against the Alzheimer's Disease *via* Amelioration of Cognitive Impairment, AβBurden, Apoptosis and Regulation of Akt/GSK3β Signaling Pathway. *Dose-Response* 18 (4), 155932582097220. doi:10.1177/1559325820972205

Yeh, Y. C., Liu, T. J., and Lai, H. C. (2020). Pathobiological Mechanisms of Endothelial Dysfunction Induced by Tert-Butyl Hydroperoxide *via* Apoptosis, Necrosis and Senescence in a Rat Model. *Int. J. Med. Sci.* 17 (3), 368–382. doi:10.7150/ijms.40255

Zhang, D., Sun, J., Yang, B., Ma, S., Zhang, C., and Zhao, G. (2020). Therapeutic Effect of Tetrapanax Papyriferus and Hederagenin on Chronic Neuropathic Pain of Chronic Constriction Injury of Sciatic Nerve Rats Based on KEGG Pathway Prediction and Experimental Verification. *Evid. Based Complement. Alternat Med.* 2020, 2545806. doi:10.1155/2020/2545806

Zhang, D., Yang, B., Chang, S.-Q., Ma, S.-S., Sun, J.-X., Yi, L., et al. (2021). Protective Effect of Paeoniflorin on H2O2 Induced Schwann Cells Injury Based on Network Pharmacology and Experimental Validation. *Chin. J. Nat. Medicines* 19 (2), 90–99. doi:10.1016/S1875-5364(21)60010-9

Zhang, Y., Zhang, J., Wu, C., Guo, S., Su, J., Zhao, W., et al. (2019). Higenamine Protects Neuronal Cells from Oxygen-Glucose Deprivation/reoxygenation-Induced Injury. *J. Cel Biochem* 120 (3), 3757–3764. doi:10.1002/jcb.27656

Zhang, Z. J., Jiang, B. C., and Gao, Y. J. (2017). Chemokines in Neuron-Glial Cell Interaction and Pathogenesis of Neuropathic Pain. *Cell Mol Life Sci* 74 (18), 3275–3291. doi:10.1007/s00018-017-2513-1

Zhao, W., Feng, H., Sun, W., Liu, K., Lu, J. J., and Chen, X. (2017). Tert-Butyl Hydroperoxide (T-BHP) Induced Apoptosis and Necroptosis in Endothelial Cells: Roles of NOX4 and Mitochondrion. *Redox Biol.* 11, 524–534. doi:10.1016/j.redox.2016.12.036

Zheng, G., Gan, L., Jia, L. Y., Zhou, D. C., Bi, S., Meng, Z. Q., et al. (2021). Screen of Anti-Migraine Active Compounds from Duijinsan by Spectrum-Effect Relationship Analysis and Molecular Docking. *J. Ethnopharmacol* 279, 114352. doi:10.1016/j.jep.2021.114352

Zorov, D. B., Juhaszova, M., and Sollott, S. J. (2014). Mitochondrial Reactive Oxygen Species (ROS) and ROS-Induced ROS Release. *Physiol. Rev.* 94 (3), 909–950. doi:10.1152/physrev.00026.2013

Conflict of Interest: The authors declare that the research was conducted in the absence of any commercial or financial relationships that could be construed as a potential conflict of interest.

Publisher's Note: All claims expressed in this article are solely those of the authors and do not necessarily represent those of their affiliated organizations or those of the publisher, the editors, and the reviewers. Any product that may be evaluated in this article or claim that may be made by its manufacturer is not guaranteed or endorsed by the publisher.

frontiers in Pharmacology

ORIGINAL RESEARCH
published: 19 January 2022
doi: 10.3389/fphar.2021.773925

Multifactoriality of Parkinson's Disease as Explored Through Human Neural Stem Cells and Their Transplantation in Middle-Aged Parkinsonian Mice

Anna Nelke[1,2*†], *Silvia García-López*[1,2], *Alberto Martínez-Serrano*[1,2] *and Marta P. Pereira*[1,2*]

[1]*Tissue and Organ Homeostasis Program, Centro de Biología Molecular Severo Ochoa UAM-CSIC, Madrid, Spain,* [2]*Department of Molecular Biology, Faculty of Science, Universidad Autónoma de Madrid, Madrid, Spain*

Parkinson's disease (PD) is an age-associated neurodegenerative disorder for which there is currently no cure. Cell replacement therapy is a potential treatment for PD; however, this therapy has more clinically beneficial outcomes in younger patients with less advanced PD. In this study, hVM1 clone 32 cells, a line of human neural stem cells, were characterized and subsequently transplanted in middle-aged Parkinsonian mice in order to examine cell replacement therapy as a treatment for PD. *In vitro* analyses revealed that these cells express standard dopamine-centered markers as well as others associated with mitochondrial and peroxisome function, as well as glucose and lipid metabolism. Four months after the transplantation of the hVM1 clone 32 cells, striatal expression of tyrosine hydroxylase was minimally reduced in all Parkinsonian mice but that of dopamine transporter was decreased to a greater extent in buffer compared to cell-treated mice. Behavioral tests showed marked differences between experimental groups, and cell transplant improved hyperactivity and gait alterations, while in the striatum, astroglial populations were increased in all groups due to age and a higher amount of microglia were found in Parkinsonian mice. In the motor cortex, nonphosphorylated neurofilament heavy was increased in all Parkinsonian mice. Overall, these findings demonstrate that hVM1 clone 32 cell transplant prevented motor and non-motor impairments and that PD is a complex disorder with many influencing factors, thus reinforcing the idea of novel targets for PD treatment that tend to be focused on dopamine and nigrostriatal damage.

Keywords: aging, behavior, cell replacement therapy, neural stem cell, neuroinflammation, next-generation sequencing, parkinson's disease, proteomics

OPEN ACCESS

Edited by:
Marianthi Papakosta, Takeda, United States

Reviewed by:
Iria Gonzalez Dopeso-Reyes, UMR5535 Institut de Génétique Moléculaire de Montpellier (IGMM), France
Jannette Rodriguez-Pallares, University of Santiago de Compostela, Spain

***Correspondence:**
Anna Nelke
anna.nelke@dpag.ox.ac.uk
Marta P. Pereira
pereiram@cbm.csic.es

***Present address:**
Anna Nelke, Oxford Parkinson's Disease Centre, Department of Physiology, Anatomy and Genetics, University of Oxford, Oxford, United Kingdom

Specialty section:
This article was submitted to Neuropharmacology, a section of the journal Frontiers in Pharmacology

Received: *10 September 2021*
Accepted: *23 December 2021*
Published: *19 January 2022*

Citation:
Nelke A, García-López S, Martínez-Serrano A and Pereira MP (2022) Multifactoriality of Parkinson's Disease as Explored Through Human Neural Stem Cells and Their Transplantation in Middle-Aged Parkinsonian Mice. Front. Pharmacol. 12:773925. doi: 10.3389/fphar.2021.773925

INTRODUCTION

Parkinson's disease is the second most common neurodegenerative disease in the world and the most common movement disorder for which there is presently no cure. It is characterized by the death or impairment of dopaminergic neurons (DAn) in the substantia nigra pars compacta (SNpc) and the depletion of dopamine (DA) in the striatum (Str). It is this pathology that generates the motor symptoms, such as tremors, rigidity, bradykinesia, and postural instability, that are observed in PD patients (Lesage and Brice, 2009; Wirdefeldt et al., 2011; Kalia and Lang, 2015; De Virgilio et al., 2016).

Cell replacement therapy (CRT) is a promising approach to treating PD and is one of the few potential treatments that seek to replace or repair the DAn lost or damaged, respectively, in PD. Various cell sources such as human induced pluripotent stem cells, human mesenchymal stem cells and human neural stem cells (hNSCs), have been and are being used in clinical trials and in experimental PD models with varying degrees of success. Some of the beneficial effects of CRT observed are motor improvement many years post-transplant and surviving tyrosine hydroxylase (TH)+ grafted cells in the PD patients' brain post-mortem (Hallett et al., 2014; Li et al., 2016; Stoker and Barker, 2016; Yasuhara et al., 2017; Stoker et al., 2018; U.S. National Library of Medicine, 2021).

One hNSC line that has thus far only been used in experimental PD models is the hVM1 clone 32 cell line. Upon differentiation *in vitro*, these fetal-derived hNSCs generate approximately 10% TH+ cells and around 12.5% β-III tubulin (TUBB3)+ cells. In addition, improvement of behavioral symptoms is observed in Parkinsonian rats when transplanted with hVM1 clone 32 cells (Ramos-Moreno et al., 2012b). When transplanted in 1-methyl-4-phenyl-1,2,3,6-tetrahydropyridine (MPTP)-intoxicated adult mice, hVM1 clone 32 cell transplant rescued striatal terminals and nigral neurons, reduced hyperactivity in mice, triggered mast cell migration to the superficial cervical lymph nodes, and restored neurogenesis and decreased microglial inflammation in the hippocampus (unpublished data).

Parkinson's disease is an age-associated disorder, as age is the biggest risk factor for the development of the disease. Very few people are diagnosed with PD before the age of 40 and it is usually diagnosed after the age of 60 (Lesage and Brice, 2009; Wirdefeldt et al., 2011; Kalia and Lang, 2015; De Virgilio et al., 2016). Cell replacement therapy is more successful in younger patients with less advanced PD (Stoker and Barker, 2016; Yasuhara et al., 2017). Moreover, most *in vivo* PD transplantation studies using rodents and non-human primates use adult animals, omit age specifications, and/or do not correctly categorize the animals' age group (Chaturvedi et al., 2006; Redmond et al., 2007; Gu et al., 2009; Kriks et al., 2011; Gonzalez et al., 2015; Jackson et al., 2017). By definition, an adult mouse or rat is between two and 3 months old. Considering the average lifespan of a mouse is 2 years and that of a rat is 3 years, the rodents used in many CRT studies extrapolate to a fairly young age in humans, much younger than 60 years old (Sengupta, 2013; Dutta and Sengupta, 2016). Therefore, although there is no doubt that progress has been made and that CRT has shown potential as a treatment for PD, it is important to have more *in vivo* studies done in older rodents in order to study what mechanisms are different from those in younger animals which lead to unsuccessful CRT results in older PD patients. Mice aged 10–15 months old are considered middle-aged and aged mice must be at least 18 months old (Jin et al., 2003; Luo et al., 2006; Dutta and Sengupta, 2016; Apple et al., 2017).

The aim of this study was to further characterize hVM1 clone 32 cells by means of gene and protein expression analyses, and to increase knowledge of CRT for PD in older rodents. To do so, hVM1 clone 32 cells were transplanted in middle-aged Parkinsonian mice, and 4 months later, the nigrostriatal pathway and behavior were analyzed to see if hNSC grafting would lead to an amelioration of these two important aspects in PD pathology.

MATERIALS AND METHODS

Cell Culture

Use of hNSCs was approved by and adhered to the guidelines of the Research Ethics Committees of the Universidad Autónoma de Madrid and the Comunidad de Madrid (PROEX149/15). Details about the hVM1 clone 32 cells used in this study, including their human fetal origin as well as consent and donors, can be found in previous articles describing these cells (Villa et al., 2009; Ramos-Moreno et al., 2012b). Briefly, it is a clone isolated based on increased TH (DAn marker) generation from the stable, *v-myc*-immortalized hVM1 cell line. The hVM1 cells were generated from dissociated tissue of the ventral mesencephalon of a 10 week-old aborted human fetus. The hVM1 clone 32 cell line is a unique biological material developed by the Martínez-Serrano laboratory in 2009 and was authenticated by short tandem repeat profiling.

Cells were routinely cultured on plastic plates treated with 10 μg/ml polylysine (Sigma-Aldrich P1274) in proliferation medium. The proliferation medium composition was as follows: The base was Dulbecco's modified Eagle's medium/F-12, GlutaMAX supplement medium (Gibco 31331028), 1% AlbuMAX (Gibco 11020021), 50 mM HEPES (Gibco 15630106), and 0.6% D-glucose (Merck 104074). To this, 1X N2 supplement (Gibco 17502048), 1X homemade non-essential amino acids (composed of L-alanine, L-asparagine, L-aspartic acid, L-glutamic acid, and L-proline), 100 U/ml penicillin, 0.1 mg/ml streptomycin, 20 ng/ml human recombinant fibroblast growth factor 2 (R&D systems 233-FB), and 20 ng/ml human recombinant epidermal growth factor (R&D systems 236-EG), were added. Cells were grown at 37°C, in a 95% humidity, 5% CO_2, and 5% O_2 atmosphere. For differentiation experiments, multiwell plates were treated with 30 μg/ml polylysine overnight, and then incubated with laminin at 5 μg/ml (Sigma-Aldrich L2020) for 5 h, before seeding cells into wells. Cells were seeded at 20,000 cells/cm^2, in proliferation medium. Twenty-four hours later, this medium was replaced with differentiation medium, which is the same one used for proliferation experiments, but the growth factors are replaced with 2 ng/ml human recombinant glial cell-derived neurotrophic factor (GDNF) (Peprotech 450-10) and 1 mM dibutyryl cAMP (Sigma-Aldrich D0627) (Lotharius et al., 2002). One day later, the differentiation medium was fully changed, and after this, two thirds of the differentiation medium were changed every 2 days. Differentiated cell samples were collected after 7 days of differentiation. Equivalent multiwell plates with proliferation medium were seeded in parallel and these samples were collected at 3 days post-seeding.

Next-Generation Sequencing

An exploratory NGS study was performed using proliferating and differentiated hVM1 clone 32 cells in order to analyze their

differential expression in both of these conditions. Cell culture media was removed and cells were rinsed with 1X PBS. In order to isolate RNA from the samples, TRIzol Reagent (Invitrogen 15596026) was added to the cells and RNA extraction was done using the Direct-zol RNA Miniprep Plus kit (Zymo Research R2071). Whole-transcriptome analysis was done on RNA samples with Illumina total RNA-Seq technology using the ScriptSeq Complete kit (Illumina RS-122-2201), which entailed rRNA removal, cDNA synthesis, 3′ terminal tagging, and PCR purification, followed by sequencing using the NextSeq 550 Sequencing kit and system (Illumina). Reads were generated from raw total RNA-Seq data and mapped to the human genome, and the htseq-count tool was used to count the number of reads mapping each gene. Differential expression analysis was then performed on raw total RNA-Seq data using the DESeq2 package, with differences in gene expression between dividing and differentiated cells being expressed as fold change. Negative fold change indicates that the gene is more highly expressed in proliferating cells, and positive fold change indicates that the gene is more highly expressed in differentiated cells. All NGS datasets can be found online at https://doi.org/10.21950/4IXBTX.

Proteomic Analysis

A proteomic study was employed in order to analyze the differential protein expression of the hVM1 clone 32 cells in proliferation and differentiation conditions. Cells were washed with 1X PBS and dissociated with accutase (Merck SCR005). The 2002 base medium without 1% AlbuMAX was then added to the plates and the cells were centrifuged at 2,500 rpm at RT for 10 min. The supernatant was removed, and pellets were collected and stored at −80°C. Pellets were lysed using lysis buffer containing 7 M urea, 2 M thiourea, 100 mM triethylammonium bicarbonate, 5% sodium dodecyl sulfate, and a nuclease. Total protein concentration was quantified using the Pierce 660 nm protein assay (ThermoFisher Scientific). Reduction of disulfide bonds and subsequent alkylation was then carried out using 50 mM tris(2-carboxyethyl)phosphine and 200 mM methyl methanethiosulfonate, respectively. After this, protein digestion was performed using S-Trap columns (Protifi) according to the manufacturer's instructions. In brief, 20 µg of each sample was digested overnight at 37°C with trypsin at a 20:1 protein to enzyme ratio. The digested samples were then dried in a SpeedVac vacuum concentrator (ThermoFisher), and peptide concentration was quantified using a fluorometer (QuBit). Next, high resolution label free quantitation liquid chromatography-electrospray ionization-tandem mass spectrometry, with the liquid chromatography system and mass spectrometer connected, was performed. To do so, 1 µg of each sample underwent liquid chromatography using a C18 reversed phase column in order to separate the peptides by their polarity, then the eluted peptides were separated using a TripleTOF mass spectrometer (Sciex). Mass spectrometry data was analyzed employing four different database searches, namely Mascot Server version 2.5 (Matrix Science), OMSSA version 2.1.9 (NCBI), X! TANDEM version win-13-02-01-1 (The GPM), and Myrimatch version 2.1 (Vanderbilt University), against the Uniprot *Homo sapiens* database (78,120 proteins when last updated on 2021/03/07). False discovery rate for peptides was < 1% ($q < 0.01$) and < 5% ($q < 0.05$) for proteins. Peptide mass tolerance was set to 0.05 Da and allowed missed cleavages was 2. L-cysteine methyl disulfide was a fixed peptide modification, and the variable modifications were methionine oxidation, pyrogluatmic acid from glutamine, pyroglutamic acid from glutamic acid, and acetylation of protein B-terminus, the latter of which was a post-translational modification. Differential expression of proliferating and differentiated hVM1 clone 32 cells was expressed as fold change. Negative fold change indicates that the gene is more highly expressed in proliferating cells, and positive fold change indicates that the gene is more highly expressed in differentiated cells. The Qiagen Ingenuity Pathway Analysis was then used for functional analysis including canonical pathways, diseases and disorders, biological functions, networks, and top upstream regulators. Because of the large amount of proteins with $q < 0.05$, log2 (Fold change) threshold was set to 0.58 ($q < 0.01$) for these functional analyses in order to increase rigor and only include proteins with the biggest fold change. For canonical pathways and top upstream regulators, z-score threshold was set to ≥1. Inflammatory response was considered a biological function, and not a disease or disorder. Chemicals were omitted and only proteins were reported as top upstream regulators. All proteomic datasets, including all information used to identify peptides and proteins, can be found online at https://doi.org/10.21950/06EW6H.

Immunocytochemistry

For immunocytochemistry studies, cells were seeded on cover glasses in multiwall plates. Cells were fixed with cold 4% paraformaldehyde for 15 min and stored in cryoprotectant solution (30% glycerol and 30% ethylene glycol in 1X PBS). Samples were washed in 1X TBS, blocked in 10% serum in 1X TBS/0.5% TritonX-100, and incubated overnight at 4°C with primary antibodies in 2% serum in 1X TBS/0.5% TritonX-100. The following primary antibodies were used: TH (1:250; Sigma-Aldrich T1299), TUBB3 (1:250; Sigma-Aldrich T2200), Ki-67 (1:200; ThermoFisher Scientific RM-9106-S1), vimentin (VIM) (1:500; Santa Cruz sc-6260), microtubule-associated protein 2 (MAP2) (1:250; Sigma-Aldrich M4403), synapsin I (SYN1) (1:250; Merck AB1543), glial fibrillary acidic protein (GFAP) (1:500; DAKO Z0334), and γ-aminobutyric acid (GABA) (1:1,000; Sigma-Aldrich A2052). The samples were then washed and incubated with appropriate secondary antibodies in 2% serum in 1X TBS/0.5% TritonX-100, at RT for 2 h. The following secondary antibodies were used: Biotinylated Horse Anti-Mouse IgG Antibody, rat adsorbed (1:500; Vector Laboratories BA-2001), Goat anti-Rabbit IgG (H + L) Highly Cross-Adsorbed Secondary Antibody, Alexa Fluor 647 (1:500; Invitrogen A-21245), Goat anti-Rabbit IgG (H + L) Highly Cross-Adsorbed Secondary Antibody, Alexa Fluor 546 (1:500; Invitrogen A-11035), and Goat anti-Mouse IgG (H + L) Highly Cross-Adsorbed Secondary Antibody, Alexa Fluor 546 (1:500; Invitrogen A-11030). For TH and MAP2 immunostainings,

samples were subsequently washed and incubated with streptavidin (Invitrogen SA1010) in 1X TBS/0.5% TritonX-100 at RT for 45 min. Nuclei were stained with 4′,6-Diamidino-2-phenylindole dihydrochloride (DAPI; 1:1,000; Santa Cruz sc-3598). All samples were then washed with 1X TBS, air-dried, and mounted with homemade Mowiol mounting medium, composed of 10% MOWIOL 4-88 Reagent (Merck 475904).

Animal Procedures

All animal work was approved by and adhered to the guidelines of the Research Ethics Committees of the Universidad Autónoma de Madrid and the Comunidad de Madrid (PROEX149/15). Animal procedures were performed at the Animal Facility of the Centro de Biología Molecular Severo Ochoa. All animal experiments complied with the ARRIVE guidelines and were carried out in accordance with the EU Directive 2010/63/EU guidelines. All efforts were made to minimize animal suffering and to reduce the number of animals used.

Male C57BL/6JRccHsd mice (Envigo, Netherlands) were used in this study. Animals were 12 months old with an average weight of 40.5 g at the beginning of the experiment, and were housed in a temperature- and humidity-controlled room on a 12-h light/dark cycle, and fed *ad libitium* with standard food and water. Animals were randomly separated into one of three experimental groups: Control, MPTP + buffer, and MPTP + cell. Control mice were injected i.p., with 0.9% saline once every 2 hours, with a total of three injections, at 10 µl/g. Using the same injection protocol, PD was induced in other mice by injecting MPTP (Sigma-Aldrich M0896) i.p., at 15 mg/kg. The dose of 15 mg/kg was chosen in order to have intermediary nigrostriatal damage before the transplant since it has been shown that when MPTP is administered at 18 mg/kg or 20 mg/kg once every 2 hours, with a total of four injections, there is a major loss of TH+ fibers and cells in the Str and SNpc, respectively (Jackson-Lewis and Przedborski, 2007). During pilot studies, a very high percentage of mice died after the fourth injection and therefore, it was decided that only three injections would be made. Mortality rate was 23% following MPTP injections. One month later, mice injected with MPTP underwent stereotaxic surgery to receive an intracerebral injection in the left Str (Coordinates from Bregma: Anteroposterior 0.25 mm, Mediolateral 2.75 mm, Dorsoventral 3 mm) of either 1.5 µl transplantation medium (MPTP + buffer group) or 100,000 mycoplasm-free, undifferentiated hVM1 clone 32 cells in passage 26 in 1.5 µl transplantation medium (MPTP + cell group). The timepoint of 1 month was used to create a more translational model, transplantation not immediately after the start of PD pathology and later than 1 week post-MPTP injections because the loss of DAn in the SNpc is stable by this time (Jackson-Lewis and Przedborski, 2007). The transplantation medium was composed of the following: 49% Leibovitz's L-15 Medium (ThermoFisher Scientific 11415064), 49% filtered 0.6% Glucose (Merck 104074) in 1X PBS, and 2% B-27 Serum-Free Supplement (Gibco 17504044). The transplantation medium is different than the proliferation medium and contains Leibovitz's L-15 Medium so that the hVM1 clone 32 cells are nourished while transitioning from *in vitro* to *in vivo* in an unstable environment in terms of temperature as well as O_2 and CO_2 levels, and to make sure that these hNSCs are not dividing which could cause tumor growth upon transplantation into the mouse brain.

For surgery, animals were anesthetized with a mixture of ketamine at 80 mg/kg (Merial) and xylazine at 10 mg/kg (Calier) injected i.p., When animals were confirmed to be asleep *via* toe pinching, surgery began. After positioning the animal's head in the frame of the stereotaxic apparatus, the animal's skull was revealed and a 23-gauge needle with 0.635 mm outer diameter was used to make a hole in the skull. Through this hole, a 22-gauge needle (Hamilton Company; 22 gauge, Small Hub RN NDL, length 0.75 in, point style 4 cut at an angle of 10–12°) held in the attached syringe (Hamilton Company; 10 µl, Model 701 RN, 26s gauge, 51 mm, point style 2), was lowered into the brain to inject either the transplantation medium or hNSCs in the left Str. The speed of injection was 1 µl/min, and the needle was left in for 2 min after injecting cells before its slow removal. The antibiotic oxytetracycline (0.2 mg/ml; Terramycin®, Zoetis) was delivered *ad libitium* in drinking water of MPTP-treated animals starting the day of surgery for a total period of 1 week as a preventative measure. In order to avoid graft rejection, 2 days before the transplants and for the first week post-transplant, all animals were given an i.p. injection of cyclosporine A (CSA; Novartis) at 10 mg/kg once daily. For the remainder of the experiment, all animals were treated with daily weekday i.p., injections of CSA at 10 mg/kg, and twice a week, CSA was included in the drinking water, prepared with the following components: 0.25 g/L CSA and sweetener. The immunosuppression protocol was based on previous studies (Courtois et al., 2010; Ramos-Moreno et al., 2012a; Ramos-Moreno et al., 2012b). For the twice weekly inclusion of CSA in drinking water, oral administration has been shown to be effective in combination with injections (Jensen et al., 2012). Preparation of oral CSA was based on the average daily water intake by C57BL mice which is 4 ml (Tordoff et al., 2007) and body weight (approximately 40 g), which amounted to 0.25 g/L CSA in water. Four months post-transplant, all animals were sacrificed.

Behavioral Tests

In order to detect neurological and motor alterations, animals were subjected to the open field test (OFT) and paw print test (PPT) (Prut and Belzung, 2003; Formentini et al., 2014). Animals received three training sessions prior to taking basal measurements for all behavioral tests. All OFTs were performed in the same room, with the same lighting, and at the same time.

Open Field Test

Animals were placed in a 40 cm × 40 cm × 30 cm (L × W × H) four-walled cubic box and their movements were filmed for 10 min. Time spent in the center (20 cm × 20 cm central area), distance traveled, time spent grooming (mouse licks or scratches itself while stationary), time spent rearing (mouse stands on hind legs), urination (number of puddles or streaks of urine), and defecation (number of fecal boli), were measured using the ANY-maze behavioral tracking software.

Paw Print Test

The animals' paws were painted (forelimbs in green and hindlimbs in orange) and the mice then walked on a 40 cm × 12 cm white piece of paper. Contralateral (CL) and ipsilateral (IL) stride length (the distance between two same-sided forelimbs or two same-sided hindlimbs), and CL-IL and IL-CL stride width (the distance between two opposite-sided forelimbs or two opposite-sided hindlimbs), were measured.

Immunohistochemistry

Transcardial perfusion fixation was carried out using cold 4% paraformaldehyde. After 12-h post-fixing with 4% paraformaldehyde, the tissue was dehydrated in 30% sucrose until the tissue sank. Free-floating 15 µm-thick coronal sections of the brain were sliced using a freezing microtome and then stored in cryoprotectant solution at −20°C.

Brain sections were washed and then blocked in 3–5% serum in 1X PBS/0.3% TritonX-100 and incubated overnight with primary antibody in 1% serum in 1X PBS/0.3% TritonX-100 at 4°C. The following primary antibodies were used: STEM121 (1:500; Takara Bio Y40410), GFAP (1:1,000; DAKO Z0334), TH (1:400; Pel-Freez P40101-150), dopamine transporter (DAT) (1:400; Chemicon MAB369), Iba1 (1:1,500; Wako 019-19741), and nonphosphorylated neurofilament heavy (NFH) (1:500; Biolegend 801701).

For the TH immunostaining, sections were incubated with a mix of 1% of 30% hydrogen peroxide, 3% methanol, and 6% 1X PBS for 15 min, prior to blocking. After primary antibody incubation, TH-stained sections were incubated with biotinylated secondary antibody (Biotinylated Goat Anti-Rabbit IgG Antibody; 1:500; Vector Laboratories BA-1000) in 1% serum in 1X PBS/0.3% TritonX-100, washed, incubated in ABC solution (VECTASTAIN Elite ABC HRP Kit, Vector Laboratories PK-6100), washed, and developed with the Vector VIP Peroxidase (HRP) Substrate kit (Vector Laboratories SK-4600). Samples were mounted onto glass slides (Menzel-Gläser), air-dried, dehydrated with xylene, and coverslipped with distyrene, plasticiser, and xylene mounting medium.

For fluorescent immunohistochemistry samples, after primary antibody incubation, sections were washed and incubated with adequate secondary antibodies in 1% serum in 1X PBS/0.3% TritonX-100 at RT for 2 h. The following secondary antibodies were used: Goat anti-Mouse IgG (H + L) Highly Cross-Adsorbed Secondary Antibody, Alexa Fluor 546 (1:1,000; Invitrogen A-11030), Goat anti-Rabbit IgG (H + L) Highly Cross-Adsorbed Secondary Antibody, Alexa Fluor 647 (1:1,000; Invitrogen A-21245), Goat anti-Rat IgG (H + L) Cross-Adsorbed Secondary Antibody, Alexa Fluor 555 (1:500; Invitrogen A-21434), Goat anti-Rabbit IgG (H + L) Highly Cross-Adsorbed Secondary Antibody, Alexa Fluor 488 (1:1,000; Invitrogen A-11034), and Biotinylated Horse Anti-Mouse IgG Antibody, rat adsorbed (1:500; Vector Laboratories BA-2001). Nonphosphorylated NFH sections were subsequently washed and incubated with streptavidin (Invitrogen SA1010) in 1X PBS/0.3% TritonX-100 at RT for 1 h. All fluorescent samples' nuclei were stained with DAPI (1:1,000; Santa Cruz sc-3598). Sections were washed, mounted onto glass slides (Menzel-Gläser), air-dried, and coverslipped with homemade Mowiol mounting medium, composed of 10% MOWIOL 4-88 Reagent (Merck 475904).

Histological Quantifications

Microscope images were obtained for all immunostainings. Anteroposterior coordinate ranges from Bregma for the quantified brain sections were 0.98–0.38 mm for the Str and motor cortex, and −2.80 to −3.64 mm for the SNpc (Paxinos and Franklin, 2001). For TH, DAT, GFAP, and NFH, immunostainings, region of interest was drawn by selecting anatomical borders, threshold was set to be the same for all animals for each immunohistochemistry, and area fraction was measured using a custom macro to analyze the images semi-automatically. The TH area fraction in the Str was made up of fibers and that of the SNpc was made up of cells and their prolongations. ImageJ was used to do all quantifications.

Statistical Analysis

For NGS, three proliferation and three differentiation individual samples were obtained from three independent experiments, however one sample from each group had to be excluded upon analysis because they were identified as outliers likely due to distinct DNA extraction method. Five samples of each experimental condition from at least three individual experiments were analyzed in the proteomic study. The animal experiments and immunostainings were done once, with a total of 30 animals used. A minimum of three animals were used per experimental group. Exact n used for each experiment is indicated in the figure legends. All figures were made and all statistical analyses were done using GraphPad Prism 7. The MA plots in **Figure 1** show the log2 fold changes between two conditions over the mean of normalized counts for all samples. **Figure 1A**, right is a pie chart with slices representing differentially expressed genes in proliferation (blue), differentiation (red), and those that were not statistically significant (black). The volcano plots in **Figures 2A,B** illustrate the fold change on the *x*-axis and the q value on the *y*-axis. **Figure 2C** is a heat map showing proteins with the largest fold changes in proliferation (blue) and differentiation (red) conditions, **Figure 2D** is a bar graph with bars indicating the z-score for each canonical pathway, and **Figure 2E** is an image produced by the QIAGEN Ingenuity Pathway Analysis of one of the top networks. In **Figure 2G**, bars indicate the q value of each top upstream regulator, which are in black, except for those that are activated in dividing and differentiated hNSCs, which are blue and red, respectively. In **Figures 4–6**, graph columns represent mean values and error bars indicate standard error of the mean. For comparisons between more than two groups, the Brown-Forsythe test was used to test the homogeneity of variances. Standard deviations were significantly different only in the case of nonphosphorylated NFH expression in the motor cortex, but the result was not affected as changes between groups were not significant in all cases. Furthermore, the Shapiro-Wilk normality test was used to test the normality of populations. When this normality test was passed or when this normality test was not passed but the Kolmogorov-Smirnov normality test was passed, a one-way analysis of variance (ANOVA) followed by Tukey's multiple

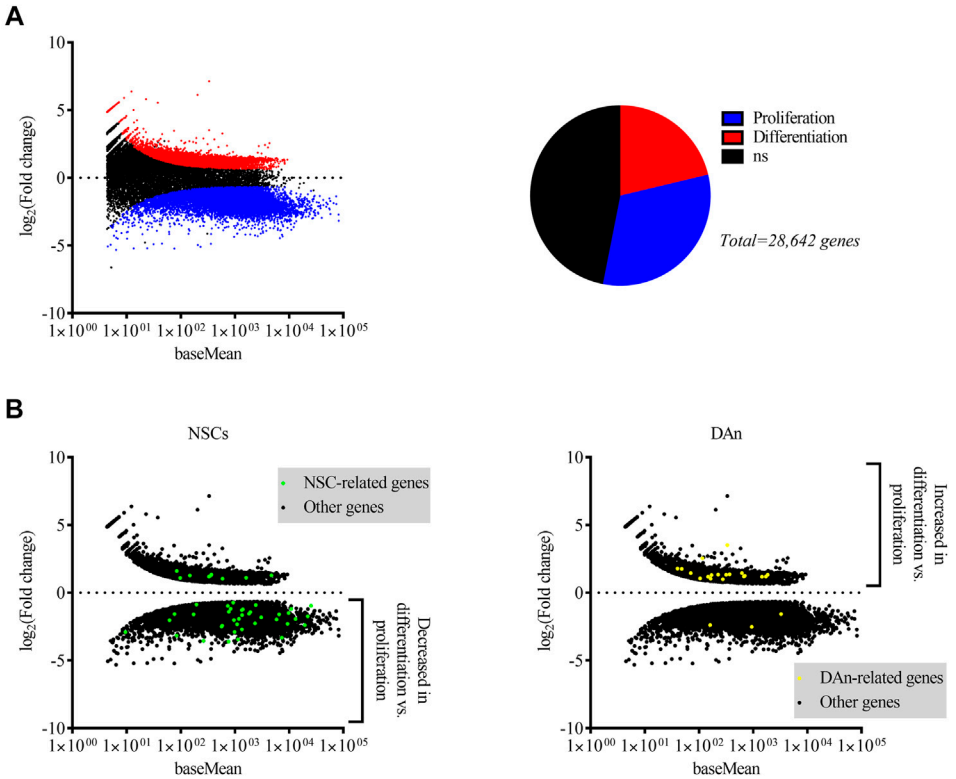

FIGURE 1 | Differential expression of genes by dividing and differentiated hVM1 clone 32 cells indicated upregulation of NSC-associated genes in proliferation and of DAn-associated genes when differentiated. **(A)** MA plot **(left)** and pie chart **(right)** showing genes differentially expressed by hVM1 clone 32 cells in proliferation (blue dots and slice) and differentiation (red dots and slice) conditions. Black dots and slice indicate genes that had a non-significant q value ($0.05 < q < 1$). **(B)** MA plots representing NSC- (**left**; green dots) and DAn-related (**right**; yellow dots) differential gene expression. Black dots indicate differentially expressed genes not associated with either NSCs or DAn. NSC-related genes were increased in proliferation, while those related with DAn were increased in differentiation. All MA plots show the mean of normalized counts on the *x*-axis and log2 fold changes on the *y*-axis. All significantly differentially expressed genes had $q < 0.05$. Proliferation $n = 2$, Differentiation $n = 2$. Data were obtained from two independent experiments.

comparisons post-hoc test were performed in order to compare the mean of each column with the mean of every other column. When neither normality test was passed, the Kruskal-Wallis test followed by Dunn's multiple comparisons post-hoc test were performed in order to compare the mean of each column with the mean of every other column. For NGS and proteomic experiments, a q value of less than 0.05 was considered statistically significant, except for proteomic functional analyses where a q value of less than 0.01 was considered significant. For immunohistochemistry and behavior experiments, a p value of less than 0.05 was considered statistically significant.

RESULTS

Dividing hVM1 Clone 32 Cells Expressed Neural Stem Cell-Associated Genes and When Differentiated, These Cells Expressed Genes Essential for Dopaminergic Neurons

A NGS study was performed on RNA extracted from the hVM1 clone 32 cells in order to do a differential gene expression analysis between proliferating and differentiated hNSCs, allowing us to identify what genes were expressed in both groups and if there was an increase or decrease in the expression of genes found in both groups. Around 34,000 genes were matched to the human genome in proliferating cells and more than 37,000 genes in differentiated cells were mapped to this genome. A total of 28,642 differentially expressed genes with a q value <1 were identified, of which 15,212 were statistically significant. Among these, 6,090 genes had a positive fold change, thus being more highly expressed in differentiated cells, and 9,122 gene had a negative fold change, indicating that they were more highly expressed in dividing cells (**Figure 1A**). The genes of higher interest were those related to NSCs and DAn. The majority of NSC-associated genes were upregulated in dividing cells and downregulated in differentiated cells, while the majority of DAn-associated genes were upregulated in differentiated cells and downregulated in proliferating cells (**Figure 1B**).

Hallmark NSC markers nestin (*NES*) and *VIM* were upregulated in proliferation conditions compared to differentiation, while surprisingly SRY-box transcription factor 2 (*SOX2*) was not detected in the whole-transcriptome analysis. Other NSC-associated genes with higher expression levels in proliferation compared to differentiation, were brain lipid-binding protein

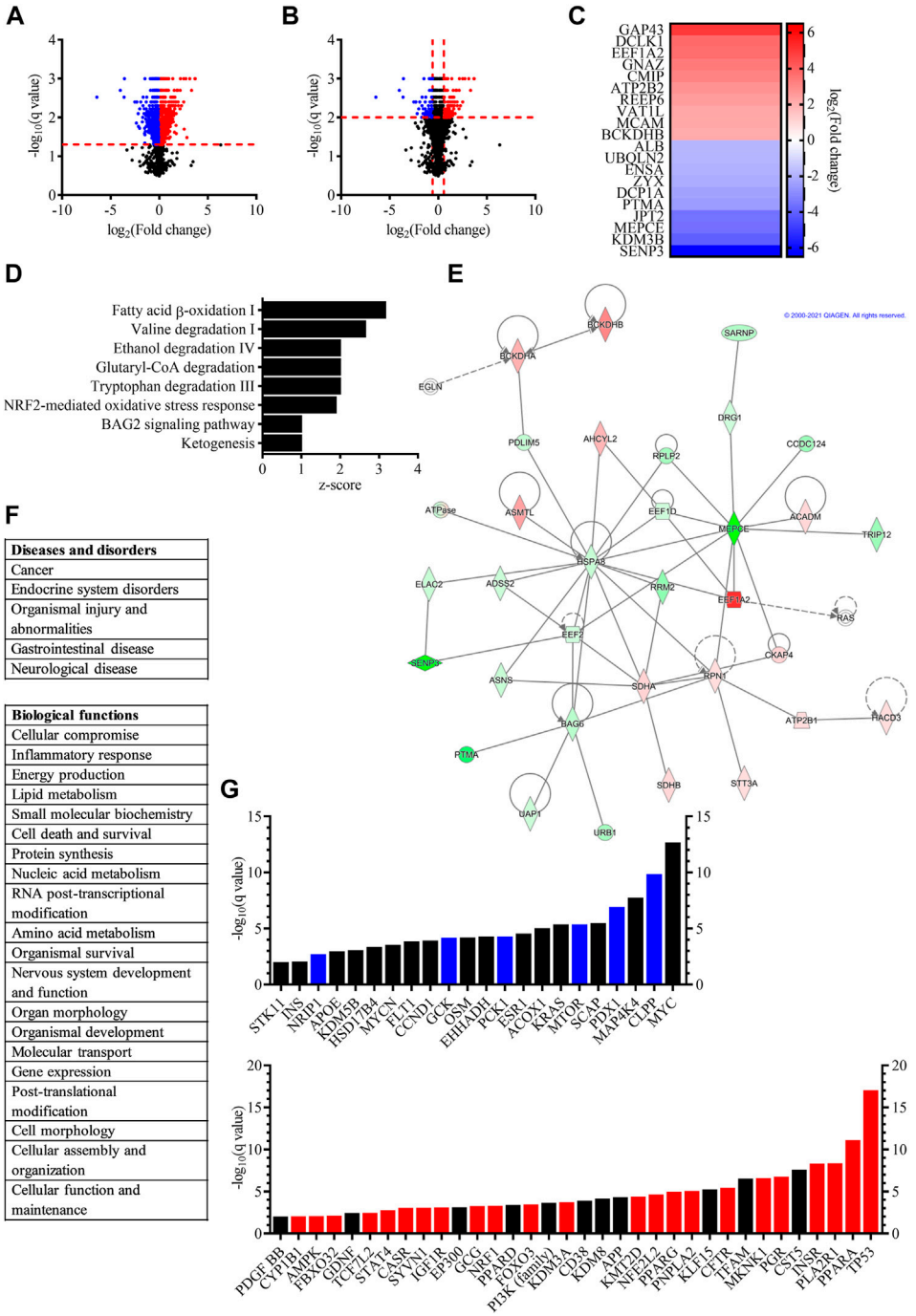

FIGURE 2 | Proteomic study revealed that proliferating and differentiated hVM1 clone 32 cells are influenced by a wide variety of proteins and pathways. **(A)** Volcano plot, with fold change on the *x*-axis and the q value on the *y*-axis, showing differentially expressed proteins in dividing (blue dots) and differentiated (red dots) hNSCs with $q < 0.05$. Black dots indicate proteins that had a non-significant *q* value. **(B)** Volcano plot, with fold change on the *x*-axis and the *q* value on the *y*-axis, demonstrating differentially expressed proteins in proliferating (blue dots) and differentiated (red dots) hNSCs with $q < 0.01$. Black dots indicate proteins that had $q > 0.01$. **(C)** Heat map illustrating the proteins with the biggest fold change increased in dividing (blue) and differentiated (red) hVM1 clone 32 cells. **(D)** Bar graph showing the top canonical pathways of proliferating and differentiated hNSCs, with bars indicating the z-score of each pathway. **(E)** One of the top networks relevant to hVM1 clone 32 cells. Image from QIAGEN Ingenuity Pathway Analysis. **(F)** List of top diseases and disorders **(top)**, and list of top biological functions **(bottom)** of hVM1 clone 32 cells. **(G)** Bar graph illustrating the top upstream regulators of dividing **(top)** and differentiated **(bottom)** hNSCs, with bars indicating the q value. Blue and red bars indicate proteins that were activated in proliferating and differentiated cells, respectively. Black bars represent proteins that were top upstream regulators, but not activated. For panels **(D–G)**, the *q* value was set to 0.01. Proliferation $n = 5$, Differentiation $n = 5$. All data were obtained from at least three independent experiments.

(*BLBP*), hes family bHLH transcription factor 1 (*HES1*), marker of proliferation Ki-67 (*MKI67*), notch receptor 1 (*NOTCH1*), noggin (*NOG*), and NUMB endocytic adaptor protein (*NUMB*). Immature neuron marker stathmin 1 (*STMN1*) had higher expression in division while neuroblast marker doublecortin (*DCX*) had higher expression in differentiation. Many genes important in the maintenance of mature neurons were upregulated in differentiated cells, most notably calbindin 2 (*CALB2*), neural cell adhesion molecule 2 (*NCAM2*), RNA binding protein fox-1 homolog 3 (*NEUN*), neuregulins, neurexins, synapsins including *SYN1* and synapsin II (*SYN2*), synaptotagmins, synaptopodins, synaptoporins, and microtubule associated protein Tau (*MAPT*) (**Supplementary Tables S1, S2**).

As for genes involved in DAn generation and maintenance, *DAT*, potassium inwardly rectifying channel subfamily J member 6 (*GIRK2*), LIM homeobox transcription factor 1 alpha and 1 beta (*LMX1A* and *LMX1B*), paired like homeodomain 3 (*PITX3*), and *TH*, among others, were highly expressed by hVM1 clone 32 cells after 7 days of differentiation. Three genes expressed by DAn, engrailed homeobox 1 and 2 (*EN1* and *EN2*), and orthodenticle homeobox 2 (*OTX2*), had increased expression in dividing hNSCs. Signaling by Wnt family member 2 and 3a (*WNT2* and *WNT3A*), as well as bone morphogenetic protein 2 and 5 (*BMP2* and *BMP5*), have been shown to be important in DAn differentiation (Sousa et al., 2010; Andersson et al., 2013; Liu et al., 2013; Jovanovic et al., 2018), and all of these genes were also positively differentially expressed by the differentiated hNSCs (**Supplementary Table S1**). Furthermore, expression of fibroblast growth factor 1, 2, 8, 9, and 20 (*FGF-1*, *FGF-2*, *FGF-8*, *FGF-9*, and *FGF-20*), all of which play a role in the survival, differentiation, and protection of DAn (Xia et al., 2016; Tome et al., 2017), were present in the differentiated hNSCs' transcriptome (data not shown). Several neurotrophic factor (NTF) receptors involved in DAn survival were upregulated in differentiated cultures, namely genes coding for GDNF, artemin, and neurturin receptors GDNF family receptor alpha 1 and 2 (*GFRA1* and *GFRA2*), as well as neurotrophic receptor tyrosine kinase 1 (*NTRK1*) which binds nerve growth factor and neurotrophin 3, neurotrophic receptor tyrosine kinase 2 (*NTRK2*) which binds brain-derived neurotrophic factor (BDNF), in addition to neurotrophin 3 and 4, and neurotrophic receptor tyrosine kinase 3 (*NTRK3*), which binds neurotrophin 3 (Allen et al., 2013; Tome et al., 2017). Several vascular endothelial growth factor (VEGF) family members, which have been shown to be neuroprotective for DAn both *in vitro* and *in vivo* (Yasuhara et al., 2004; Falk et al., 2010; Piltonen et al., 2011), and their receptors were expressed in both proliferating and differentiated hVM1 clone 32 cells, including VEGF A, B, and C (*VEGFA*, *VEGFB*, and *VEGFC*), VEGF receptor 1 and 2 (*VEGFR1* and *VEGFR2*), and neuropilin 1 and 2 (*NRP1* and *NRP2*). Additionally, astrocyte-secreted NTFs mesencephalic astrocyte-derived neurotrophic factor (*MANF*) and ciliary neurotrophic factor (*CNTF*) were more highly expressed in proliferating cultures. Both of these NTFs promote DAn survival (Sullivan and Toulouse, 2011; Tome et al., 2017) (**Supplementary Table S1**).

Genes involved in central nervous system (CNS) immunity were also differentially expressed in proliferating and differentiated hVM1 clone 32 cells. The monocyte chemoattractant protein 1 (*MCP1*) and stem cell factor (*SCF*) genes were upregulated in proliferating cells, while their receptors, C-C motif chemokine receptor 2 (*CCR2*) and KIT proto-oncogene, receptor tyrosine kinase (*KIT*), respectively, were expressed higher under differentiation conditions. In a PD animal model, *SCF* was shown to have a protective effect on DAn (Yasuhara et al., 2006). Furthermore, genes encoding pro-inflammatory cytokines interleukin 1 beta and 6 (*IL1B* and *IL6*), as well as prostaglandin-endoperoxide synthase 2 (*PTGS2*) were upregulated in differentiated cells (**Supplementary Table S1**).

The hVM1 clone 32 cells also expressed astrocyte-related genes. These included *HES1*, S100 calcium binding protein B (*S100B*), and solute carrier family 1 member 3 (*SLC1A3*), which were more upregulated in dividing hNSCs, as well as aldehyde dehydrogenase 1 family member L1 (*ALDH1L1*) and *GFAP*, which were more highly expressed in the differentiated state. Moreover, oligodendrocyte-associated genes myelin basic protein (*MBP*), myelin-associated oligodendrocyte basic protein (*MOBP*), and oligodendrocytic myelin paranodal and inner loop protein (*OPALIN*), were expressed higher under differentiation conditions compared to proliferation conditions. Serotonergic neuron-related genes solute carrier family 6 member 4 (*SLC6A4*) and tryptophan hydroxylase 2 (*TPH2*), GABAergic neuron-related genes GABA type B receptor subunit 1 and 2 (*GABBR1* and *GABBR2*), and solute carrier family 6 member 1 (*SLC6A1*), glutamatergic neuron-associated genes glutamate ionotropic receptor NMDA type subunit 2B (*GRIN2B*) and solute carrier family 17 member 6 (*SLC17A6*), and cholinergic neuron-associated gene choline O-acetyltransferase (*CHAT*), all had increased expression in differentiated compared to dividing hNSC cultures (**Supplementary Table S1**). Other genes of interest found to be expressed higher in differentiated versus proliferating cultures were synuclein alpha (*SNCA*) and leucine rich repeat kinase 2 (*LRRK2*), two genes mutated in familial PD (Lesage and Brice, 2009; Chai and Lim, 2013) (**Supplementary Table S2**). More genes differentially expressed in proliferating and differentiated hVM1 clone 32 cells can be found in **Supplementary Table S2**.

Proteomic Analyses of hVM1 Clone 32 Cells Demonstrated That Dopaminergic Neurons and Parkinson's Disease are Multifaceted

A differential protein expression analysis between proliferating and differentiated hVM1 clone 32 cells, was performed in order to identify what proteins are expressed in both groups and if there was an increase or decrease in proteins identified in both groups. A total of 3,948 proteins were identified, of which 2,258 proteins were significantly differentially expressed between the two groups, with 1,151 proteins with increased and 1,107 proteins with decreased expression (**Figure 2A**). Among them, proteins

related to NSCs whose expression was significantly decreased in differentiation included Ki-67, NES, SOX2, and VIM, and proteins significantly increased in differentiation were GFAP, MANF, and mature neuronal marker MAP2, as well as aldehyde dehydrogenase, which metabolizes DA aldehyde metabolites in the brain thus preventing neurodegeneration and is involved in DAn differentiation and survival (Villa et al., 2009; Chiu et al., 2015; Grünblatt and Riederer, 2016). Furthermore, although TH was not identified in all differentiation samples, two enzymes involved in the synthesis of the TH cofactor tetrahydrobiopterin which is required for DA production, dihydropteridine reductase and sepiapterin reductase (Meiser et al., 2013), were increased in the differentiated cell group. Early neuronal marker TUBB3 was non-significantly increased ($q > 0.05$). The protein encoded by all other genes identified in the NGS analysis were either not found or not significantly differentially expressed in the proteomic study. For functional analysis, the q value was set to < 0.01 in order to increase rigor. Within this range, 1,012 genes were differentially expressed, 496 of them with increased expression and 516 genes with decreased expression (**Figure 2B**).

The proteins with the biggest fold change in differentiated cells were neuromodulin (GAP43), a protein involved in neuronal and axonal growth and regeneration which is upregulated by BDNF and whose expression has been found to be decreased in PD patient brains (Saal et al., 2017; Chung et al., 2020), doublecortin-like kinase 1 (DCLK1), a protein kinase part of the doublecortin family that participates in neuronal migration and neurogenesis (Shu et al., 2006; Nawabi et al., 2015; Patel et al., 2016), and eukaryotic elongation factor 1 alpha 2 (EEF1A2), a protein implicated in protein translation elongation and autophagy that inhibits apoptotic cell death and may be important for DAn survival (Khwanraj et al., 2016; Prommahom and Dharmasaroja, 2021). These three proteins, along with vesicle amine transport 1 like (VAT1L), were also the only proteins among those with the largest fold change in differentiated cells whose genes also exhibited a significant fold change in the NGS study (data not shown). The proteins with the biggest fold change increase in dividing cells were sentrin-specific protease 3 (SENP3), lysine-specific demethylase 3B (KDM3B), and 7SK snRNA methylphosphate capping enzyme (MEPCE) (**Figure 2C**). All genes encoding the top 10 proteins with the largest fold change were identified in the NGS with significant fold changes and higher expression in dividing hVM1 clone 32 cells, except for ALB, which was more highly expressed in differentiated hNSCs (data not shown).

The top canonical pathways included fatty acid beta-oxidation I, valine degradation I, ethanol degradation IV, glutaryl-coenzyme A (CoA) degradation, tryptophan degradation III, and ketogenesis, all pathways involving energy metabolism and occurring mostly or entirely in the mitochondria and peroxisomes (MetaCyc, 2021). Mitochondria and peroxisomes are known to be dysfunctional in PD (Exner et al., 2012; Jo et al., 2020), thus emphasizing the importance of their functionality in DAn health. Moreover, fatty acids are neuroprotective (Parga et al., 2018), and aldehyde dehydrogenase, which is involved in DA metabolism and associated with DAn generation, is a key enzyme in the ethanol degradation IV pathway (Villa et al., 2009; Grünblatt and Riederer, 2016; MetaCyc, 2021). Ethanol is known to have an effect on DAn (Melis et al., 2009; Ma and Zhu, 2014). As well, the nuclear factor erythroid 2-related factor 2 (NFE2L2/NRF2)-mediated oxidative stress response and BAG family molecular chaperone regulator 2 (BAG2) signaling pathways have both been implicated in PD (Jazwa et al., 2011; Che et al., 2013; Qin et al., 2016; Todorovic et al., 2016) (**Figure 2D**).

One of the top networks of the functional analysis involved five of the proteins with the biggest fold change, namely branched-chain alpha-keto acid dehydrogenase E1 component beta (BCKDHB), EEF1A2, MEPCE, prothymosin alpha (PTMA), and SENP3, and the diseases and disorders of cancer, organismal injury and abnormalities, and gastrointestinal disease (**Figure 2E**). The top diseases and disorders were cancer, endocrine system disorders, organismal injury and abnormalities, gastrointestinal disease, and neurological disease, the last three of which coincide with PD itself and the non-motor symptoms of the disorder affecting the gut (Chaudhuri and Schapira, 2009; Kalia and Lang, 2015) (**Figure 2F**, top). Cancer and diabetes mellitus, one of the most common endocrine system disorders, have been shown to have pathogenic overlaps with PD, thus the involvement of the same proteins in PD and these two prevalent diseases (Khwanraj et al., 2016; Sergi et al., 2019). Notably, the proteins which had the biggest fold change in differentiated hVM1 clone 32 cells, GAP43, DCLK1, and EEF1A2, are implicated in several cancers (Patel et al., 2016; Giudici et al., 2019; Zheng et al., 2019).

Among the top 20 biological functions were cellular compromise, energy production, cell death and survival, nervous system development and function, cell morphology, and cellular function and maintenance, all important functions in the maintenance and survival of DAn (**Figure 2F**, bottom).

The top upstream regulators identified in proliferating and differentiated cells were involved in all of the aforementioned diseases, canonical pathways, and functions, such as cancer, diabetes mellitus, energy metabolism, glucose metabolism, lipid metabolism, and cell survival. In proliferating cells specifically, top upstream regulators also included oncogenes, hormones, as well as insulin and proteins associated with insulin regulation. Of particular interest were Myc proto-oncogene (MYC), involved in the cell cycle and apoptosis (Fults et al., 2002; Hoffman and Liebermann, 2008), as the hVM1 clone 32 cells are immortalized with MYC. Furthermore, mitogen-activated protein kinase kinase kinase kinase 4 (MAP4K4), one of the members of the MAP kinase kinase kinase kinase family, which is involved in the immune response and inflammation (Chuang et al., 2016), and mammalian target of rapamycin (MTOR), which was inhibited, controls cell growth, protein synthesis, and survival (Lan et al., 2017). In differentiated cells specifically, top upstream regulators included tumor suppressors, as well as proteins involved in calcium signaling, cell growth and division, neurite growth, and apoptosis. Several demethylases were also among the top upstream regulators indicating epigenetic regulation. Of particular interest were GDNF, a NTF involved in DAn survival and PD pathology (Allen et al., 2013), platelet-derived growth factor subunit BB (PDGF BB), a PDGF subunit which is implicated in neurogenesis (Mohapel et al., 2005; Yang et al.,

2013), as well as amyloid-beta precursor protein (APP), a protein important for neuronal growth and migration, neurogenesis, and synaptogenesis (Coronel et al., 2019). Another top upstream regulator in differentiated cells was NFE2L2/NRF2. This protein, which was activated, has been described as a key protein in the antioxidant response and plays an important role in PD as well as other neurodegenerative diseases (Todorovic et al., 2016). The phosphoinositide 3-kinase (PI3K) family include kinases that are essential to the PI3K/Akt pathway, which has been shown to regulate autophagy, neuronal survival, proliferation, and differentiation, neurogenesis, and synaptic plasticity (Long et al., 2021). Moreover, several peroxisome proliferator-activated receptor (PPAR) proteins, namely PPAR A, D, and G (PPARA, PPARD, and PPARG), were among the top upstream regulators, and PPARA and PPARG were activated. The PPARs are receptors involved in many biological functions such as cell differentiation, DA signaling, energy metabolism, glucose metabolism, lipid metabolism, mitochondrial function, neuroinflammation, and oxidative stress. By providing neuroprotection through these various functions, PPAR agonists are a potential therapeutic target in PD (Chaturvedi and Beal, 2008; Wójtowicz et al., 2020) (**Figure 2G**).

The proteomic study broadened the scope of factors involved in DAn differentiation and survival as well as PD. Therefore, we decided to reanalyze the NGS data looking for genes involved in the aforementioned functions and pathways, including cancer, glucose, energy, and lipid metabolism, calcium signaling, and other genes of interest, focusing only on genes with a positive fold change in differentiated cells. A list of these genes can be found in **Supplementary Table S3**.

Visualization of hVM1 Clone 32 Cell Markers *In Vitro* and *In Vivo*

In order to look at morphology and verify major NSC and DAn protein markers, immunocytochemistry was performed on hVM1 clone 32 cells after 7 days of differentiation *in vitro*. In concordance with Ramos-Moreno et al. (2012b), which originally described the hVM1 clone 32 cells, the cells expressed DAn marker TH and immature neuronal marker TUBB3. At this stage of differentiation, the hNSCs still expressed NSC markers Ki-67 and VIM, and began to express mature neuronal markers like MAP2 and SYN1. Although the differentiated hVM1 clone 32 cells tend to generate DAn because of their tissue of origin, the ventral mesencephalon, in addition to their purposeful direction of differentiation toward DAn based on the factors in the differentiation media, namely GDNF and dibutyryl cAMP, the culture was not entirely homogeneous; markers for astrocytes (GFAP) and GABAergic neurons (GABA), were found in the culture after 7 days of differentiation, reflecting NGS and proteomic data (**Figure 3A**).

The hVM1 clone 32 cells were subsequently transplanted in the Str of middle-aged Parkinsonian mice. Four months post-transplant, there was little to no surviving hVM1 clone 32 cells found in the Str of transplanted mice. No hNSCs were found in other CNS regions such as the SNpc or Hip either (**Figure 3B**).

Striatal and Nigral Tyrosine Hydroxylase Expression was Decreased in all Parkinsonian Mice

Four months post-transplant, mouse brains were analyzed for TH immunoreactivity in the Str and SNpc, the two main regions affected in PD. In the Str, the means of the groups in terms of TH expression were statistically different ($p < 0.01$). Although not statistically significant, all MPTP-lesioned mice had approximately 25% less TH+ fiber density in the Str compared to control animals (**Figure 4A**). In the SNpc, there was a 46% decrease in TH+ area in buffer-treated mice compared to controls ($p < 0.05$). By contrast, hNSC-treated animals tended to have a 27% decrease in nigral TH+ area compared to control mice and a 26% increase in TH expression in the SNpc compared to buffer-transplanted mice (**Figure 4B**). Expression of TH was markedly decreased in both the Str and SNpc and this diminution of TH+ immunostaining was not alleviated by hVM1 clone 32 cell transplant.

Activity and Gait Changes Were Improved in hVM1 Clone 32-Transplanted Mice

Several mouse behaviors were measured to examine the effects of hVM1 clone 32 transplant 4 months post-transplant. In the OFT, there were no significant differences among the three experimental groups in terms of time spent grooming, time spent rearing, urination, and defecation (data not shown). As for time spent in the center of the OFT box, buffer-treated mice tended to spend around 71% more time in the center compared to controls, indicating hyperactivity. This increased time spent in the center was decreased by 85% in hNSC-transplanted animals ($p < 0.05$). There were no differences among the three experimental groups in terms of distance traveled, suggesting a lack of bradykinesia in the MPTP-lesioned mice (**Figure 5A**). The PPT was performed to analyze changes in gait between the three groups of animals. All stride lengths were decreased by an average of 24% in buffer-treated mice compared to controls ($p < 0.01$) and were then increased by 17% in cell-transplanted mice compared to those that received buffer ($p < 0.05$) (**Figure 5B**). Forelimb stride width was reduced by approximately 19% in buffer-treated animals compared to controls ($p < 0.05$), while with hNSC transplant it tended to increase by 13% compared to those that received buffer, but only reached statistical significance ($p < 0.05$) on one side. By contrast, CL-IL hindlimb stride width was similar in all three experimental groups while IL-CL hindlimb stride width was decreased in buffer-treated mice by 17% ($p < 0.01$) and in cell-transplanted animals by 10% ($p < 0.05$), compared to controls (**Figure 5C**).

Dopamine Functionality, Neuroinflammation, and Motor Cortex Changes Influenced Transplant Outcome

Because of the surprising discrepancy between TH expression in the Str and behavioral symptoms upon administration of MPTP and hVM1 clone 32 transplant, it was important to explain this

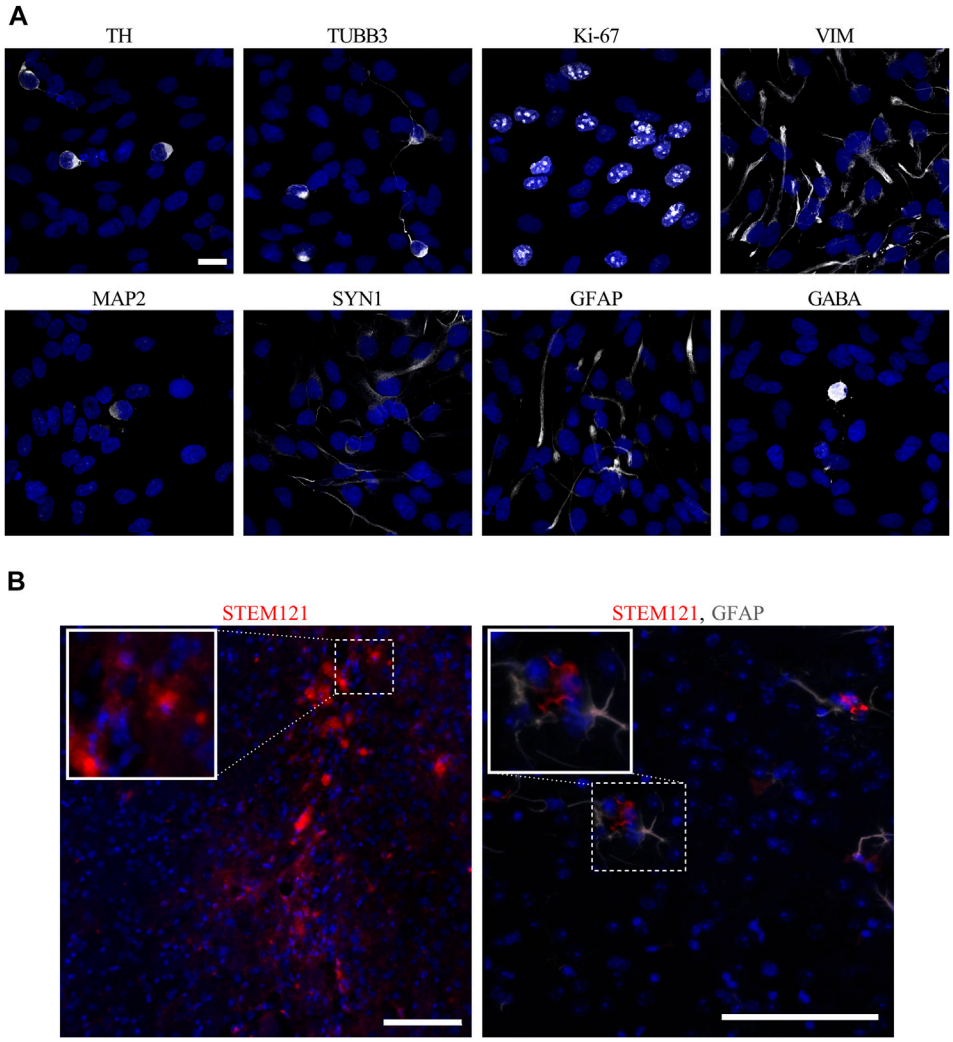

FIGURE 3 | *In vitro* and *in vivo* images of hVM1 clone 32 cell markers. **(A)** After 7 days of differentiation *in vitro*, hVM1 clone 32 cells express a range of proteins including TH, TUBB3, Ki-67, VIM, MAP2, SYN1, GFAP, and GABA (all in white). Nuclei were stained with DAPI (blue). Scale bar = 20 µm. **(B)** Surviving transplanted hNSCs in the Str 4 months post-transplant as marked by STEM121 in red which stains human-specific cytoplasm **(left)**, and astrocytes as marked by GFAP in grey near the transplanted cells **(right)**. Nuclei were stained with DAPI (blue). Scale bars = 100 µm.

occurrence by analyzing several potential contributors to this effect. The functionality of the striatal TH+ fibers, neuroinflammation, and motor cortex changes, were explored. First, another marker for dopaminergic terminals, namely DAT, was tested. Striatal expression of DAT was significantly decreased in buffer-treated animals by around 57% compared to controls ($p < 0.01$). Moreover, DAT+ area tended to be reduced by approximately 32% in the Str of cell-transplanted mice compared to control animals; however, DAT expression tended to be 36% greater in hNSC-treated animals compared to buffer-treated mice (**Figure 6A**).

Second, neuroinflammation, and more specifically GFAP and Iba1 expression in the Str, was examined in order to see a potential role for astrocytes and activated microglia. Astroglial immunoreactivity in the Str tended to increase in buffer-treated mice compared to controls, although this was only statistically significant on the IL side ($p < 0.05$). Microglial populations were increased in animals that received buffer and on the IL side of hNSC-transplanted mice compared to control animals ($p < 0.05$). Furthermore, striatal GFAP expression decreased on the CL side of cell-transplanted mice compared to the IL side of those treated with buffer ($p < 0.05$). Interestingly, when comparing animals from each of the three experimental groups, which were approximately 16 months old at experiment endpoint, to adult (nine month-old) control mice submitted to the same protocol, there was a significant increase in striatal GFAP ($p < 0.05$), and not Iba1, expression (**Figures 6B,C**).

Lastly, nonphosphorylated neurofilament populations were analyzed in the motor cortex, which is connected to the Str, in order to study axonal transport and function. Although not statistically significant, there tended to be higher expression of nonphosphorylated NFH in the motor cortex of MPTP-treated

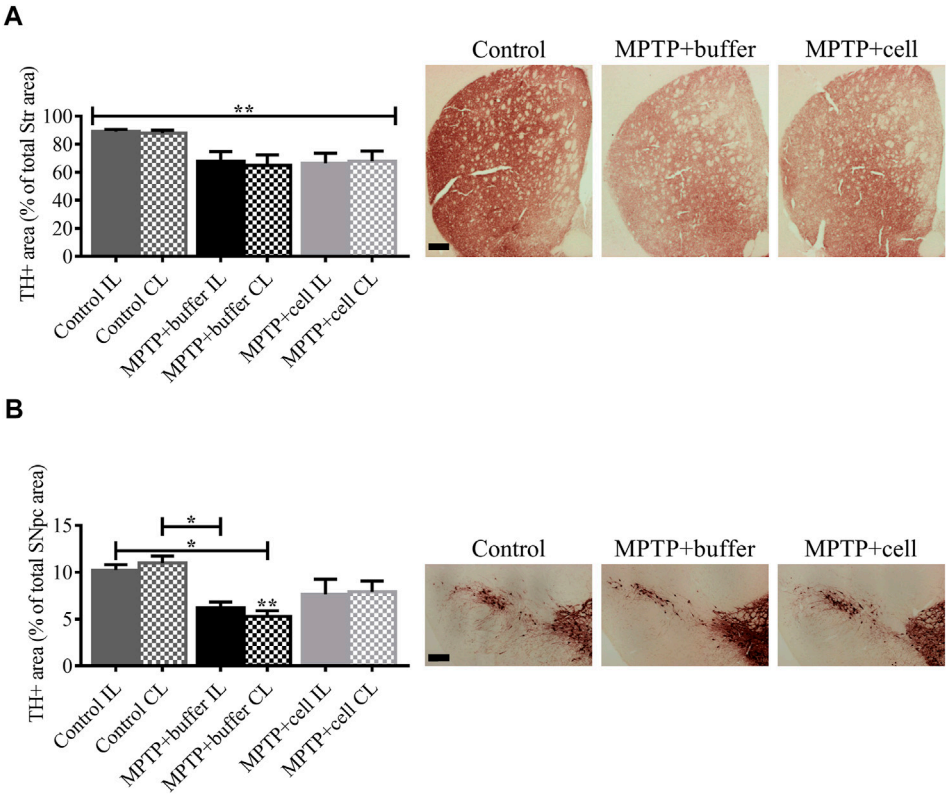

FIGURE 4 | Diminution of striatal and nigral TH expression in Parkinsonian mice. **(A)** In the Str, all MPTP-lesioned mice tended to have around 25% less TH+ fiber density compared to controls. Control $n = 5$, MPTP + buffer $n = 4$, MPTP + cell $n = 5$. Kruskal-Wallis test followed by Dunn´s post-hoc test. **(B)** Nigral TH+ area decreased by 46% in buffer-treated mice ($p < 0.05$) and by 27% in hNSC-transplanted mice, compared to control animals. Control $n = 5$, MPTP + buffer $n = 4$, MPTP + cell $n = 5$. One-way ANOVA followed by Tukey´s post-hoc test. **(A,B)**: * = $p < 0.05$, ** = $p < 0.01$. * = compared to same brain hemisphere of control. Data are expressed as mean ± standard error of the mean. Scale bars = 200 μm.

mice compared to controls, with an increase of 50% in buffer-treated and 69% in hNSC-transplanted animals (**Figure 6D**).

Therefore, further characterization of hVM1 clone 32 cells through gene and protein expression analyses revealed that these are true hNSCs that have the capability of generating DAn. These *in vitro* findings also supported the notion that multiple factors affect PD and DAn, with this study emphasizing the role of mitochondrial and peroxisome function, as well as glucose and lipid metabolism. Although hVM1 clone 32 cells did not survive when transplanted in middle-aged mice, most behavioral symptoms were alleviated by hNSC transplant, which was reinforced by a tendency for striatal DAT expression to be higher in cell-treated animals compared to those that received buffer. Additionally, nigrostriatal TH expression was notably decreased and cortical nonphosphorylated NFH expression was increased in all Parkinsonian mice.

DISCUSSION

Our data show that hVM1 clone 32 cells are hNSCs that have DAn features upon differentiation *in vitro*, and when these cells are transplanted in middle-aged Parkinsonian mice, there is an improvement in both motor and non-motor functioning, which is supported by a tendency of restored functional dopaminergic striatal terminals. Moreover, MPTP administration in these mice leads to notable, although minimal, striatal TH degeneration and motor cortical axonal transport alterations, and CRT was not able to be fully effective in middle-aged MPTP-intoxicated mice because of increased neuroinflammation.

Both NGS and proteomic analyses of differentiated hNSCs allowed us to deviate from classic, DA-centered markers and pathways involved in DAn survival and PD pathology, and emphasize the importance of less-studied factors influencing DAn such as calcium signaling, mitochondrial and peroxisome function, glucose and lipid metabolism, and oxidative stress, thus confirming that PD is multifactorial.

With all of the evidence presented that hVM1 clone 32 cells can generate DAn, it is important to note that 7 days of differentiation is still an early stage of differentiation so it is not out of the ordinary that NSC markers were still expressed. The differentiated hNSC culture was also heterogeneous, with the hVM1 clone 32 cells expressing both genes and proteins associated with other CNS populations such as astrocytes, oligodendrocytes, serotonergic neurons, GABAergic neurons, glutamatergic neurons, and cholinergic neurons. In the future,

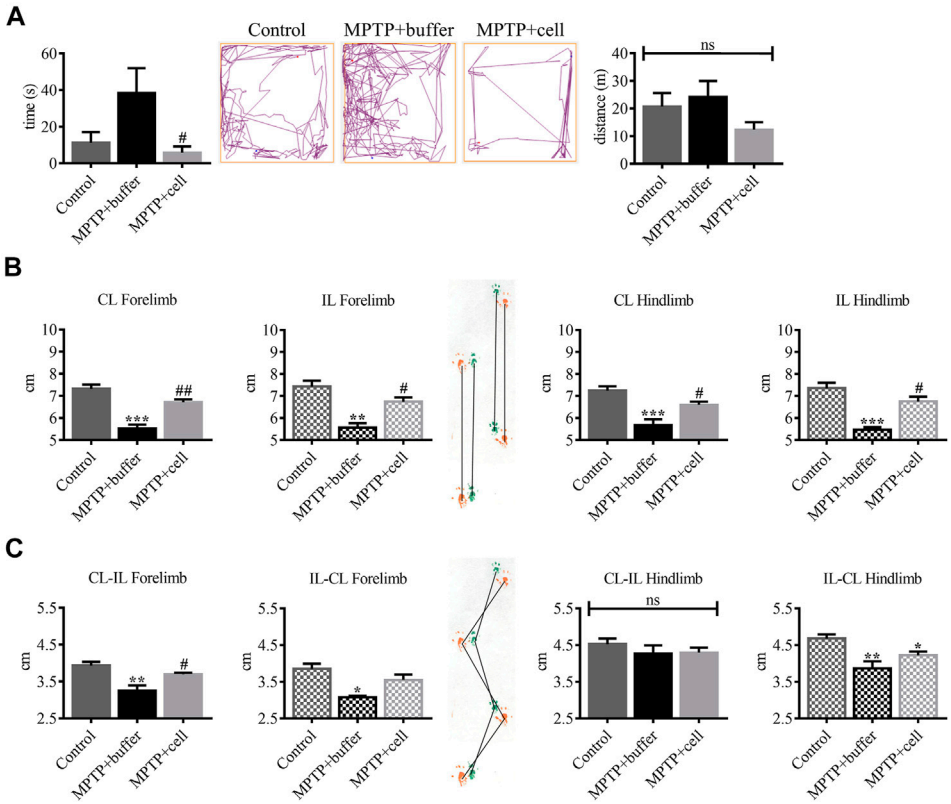

FIGURE 5 | Behavioral improvement was observed in hNSC-transplanted mice. **(A, left)** Buffer-treated animals had a tendency to spend 71% more time in the center of the box compared to controls, while NSC-transplanted mice spent 85% less time in the center compared to those that received buffer ($p < 0.05$). Control $n = 5$, MPTP + buffer $n = 4$, MPTP + cell $n = 5$. One-way ANOVA followed by Tukey's post-hoc test. **(A, right)** All experimental groups had the same distance traveled. Control $n = 5$, MPTP + buffer $n = 4$, MPTP + cell $n = 5$. Kruskal-Wallis test. **(B)** Forelimb and hindlimb stride lengths decreased by approximately 24% in buffer-treated animals compared to controls ($p < 0.01$), and hNSC transplant led to a 17% increase in all stride lengths measured compared to the vehicle group ($p < 0.05$). **(C)** Forelimb stride width was around 19% shorter in buffer-treated mice compared to control animals ($p < 0.05$) and NSC transplant tended to increase forelimb stride width by 13% compared to mice that received buffer, although only attaining significance ($p < 0.05$) on one side measured. CL-IL hindlimb stride width was unchanged among the three experimental groups and when compared to the control group, IL-CL hindlimb stride width was reduced in all MPTP-lesioned mice, although to a greater extent in buffer-treated (17%; $p < 0.01$) than cell-transplanted animals (10%; $p < 0.05$). **(B,C)**: Control $n = 7$, MPTP + buffer $n = 3$, MPTP + cell $n = 5$. One-way ANOVA followed by Tukey's post-hoc test. **(A–C)**: *, $^{\#} = p < 0.05$, **, $^{\#\#} = p < 0.01$, $^{***} = p < 0.001$, ns, not significant. * = compared to control, $^{\#}$ = compared to MPTP + buffer. Data are expressed as mean ± standard error of the mean.

it would be interesting to see the effects of a longer hNSC differentiation.

The amount of surviving transplanted cells in the brain of hNSC-transplanted mice was minimal, yet behavioral improvement was observed, which is in line with other stem cell therapy studies (Fu et al., 2015). Cell survival is a constant problem in CRT, with approximately 95% of transplanted cells dying shortly after grafting in experimental PD animals and PD patients (Emgard et al., 2003; Rafuse et al., 2005; Stoker and Barker, 2016). The CSA protocol was not the cause of transplanted cell death in this study as the equivalent protocol was used in Parkinsonian rats where the hVM1 clone 32 cells survived 2 months post-transplant (Ramos-Moreno et al., 2012b). Furthermore, cell survival has been demonstrated to be negligible in CNS transplants in mice when compared to rats (Roberton et al., 2013). Although the hVM1 clone 32 cells did not survive transplantation in this study, we were still able to explore their effects in middle-aged Parkinsonian mice.

The diminution of TH expression in the Str observed, although notable, was surprising as most studies find that middle-aged and aged Parkinsonian mice exhibit a more substantial decrease in TH expression in the Str and SNpc as well as striatal DA content, and demonstrate more severe behavioral deficits (Date et al., 1990; Ohashi et al., 2006; Guan et al., 2016). However, most of these studies used a larger dose of MPTP. As well, none of the studies used the exact same acute MPTP protocol in C57BL/6 mice of the same vendor, and it has been shown that different MPTP protocols lead to varied nigrostriatal damage, and that mice of the same strain from different providers show diverse susceptibility to MPTP (Jackson-Lewis and Przedborski, 2007). Genetics perhaps plays a role because older mice have higher lethality when given MPTP so the ones that do survive may have a stronger resistance to MPTP and therefore there is less damage to their nigrostriatal pathway.

Spontaneous dopaminergic sprouting has been shown to occur in the Str between 10 days and 5 months post-MPTP

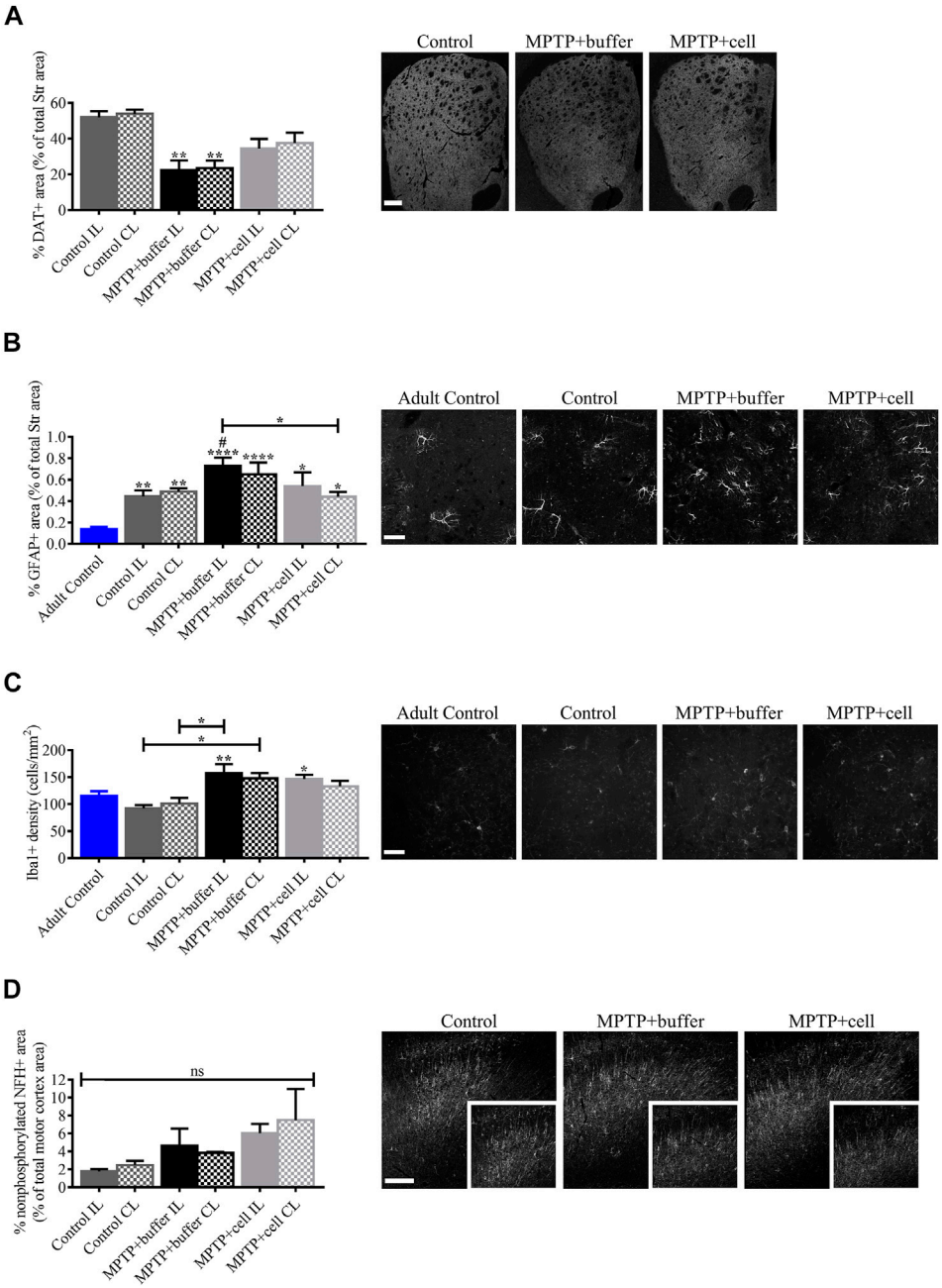

FIGURE 6 | Evaluation of factors that potentially influenced hNSC transplant including DA transport, inflammation, and motor cortex alterations. **(A)** Compared to controls, DAT immunostaining decreased by approximately 57% in buffer-treated mice ($p < 0.01$) and non-significantly by around 32% in cell-transplanted animals, although DAT+ area tended to be increased by 36% in hNSC-treated mice compared to those that received buffer. Control $n = 3$, MPTP + buffer $n = 4$, MPTP + cell $n = 4$. **(B)** Striatal expression of GFAP tended to be higher in buffer-treated animals, reaching statistical significance on the IL side ($p < 0.05$), and was decreased on the CL side of hNSC-transplanted mice compared to the IL side of buffer-treated animals ($p < 0.05$). When compared to adult control mice, all middle-aged mice had increased GFAP expression in the Str ($p < 0.05$). Adult Control $n = 3$, Control n = 5, MPTP + buffer $n = 4$, MPTP + cell $n = 3$. One-way ANOVA followed by Tukey's post-hoc test. *, # = $p < 0.05$, ** = $p < 0.01$, **** = $p < 0.0001$. * = compared to adult control, # = compared to same brain hemisphere of middle-aged control. Data are expressed as mean ± standard error of the mean. Scale bar = 50 µm. **(C)** Iba1+ microglial populations were increased in the Str of all Parkinsonian mice ($p < 0.05$), and age did not affect microglial density. Adult Control $n = 5$, Control $n = 4$, MPTP + buffer $n = 5$, MPTP + cell $n = 5$. One-way ANOVA followed by Tukey´s post-hoc test. * = $p < 0.05$, ** = $p < 0.01$. * = compared to same brain hemisphere of middle-aged control. Data are expressed as mean ± standard error of the mean. Scale bar = 50 µm. **(D)** In the motor cortex, nonphosphorylated NFH+ area tended to be increased in animals intoxicated with MPTP by 50–69% compared to control mice. Control $n = 3$, MPTP+buffer $n = 3$, MPTP + cell $n = 3$. **(A,D)**: One-way ANOVA followed by Tukey's post-hoc test. ** = $p < 0.01$, ns, not significant. * = compared to same brain hemisphere of control. Data are expressed as mean ± standard error of the mean. Scale bars = 200 µm.

administration in mice between the ages of 8 and 10 weeks. However, dopaminergic recovery has not observed in the Str of older (eight month-old) mice, nor in the SNpc of both younger and older MPTP-treated mice (Ho and Blum, 1998; Mitsumoto et al., 1998; Bezard et al., 2000; Jakowec et al., 2004).

In the present study, behavioral deficits were observed in buffer-treated mice in terms of increased hyperactivity and changes in gait; these behavioral aspects tended to be improved by hNSC transplant. Furthermore, parameters measuring anxiety and locomotion were not affected by MPTP treatment or hNSC transplant. Depletion of DA in the prefrontal cortex has been shown to increase hyperactivity and decrease anxiety, and this hyperactivity is due to disinhibition and attention deficit (Rousselet et al., 2003). Attention deficit and impulsivity occur in some PD patients (Nieoullon, 2002; Kehagia et al., 2014; Nombela et al., 2014). Striatal TH fiber abundance did not mimic the behavioral deficits in buffer-treated animals, but the decrease of DAT expression in the Str did follow this trend. This reveals that immunostaining of TH to analyze dopaminergic fiber degeneration is not a functional assessment, and in this case, striatal expression of DAT, stride length, stride width, and time spent in the center, were able to detect differences between buffer-treated and control animals, all of which striatal TH expression studies were not able to do. Also, only behavioral studies, and not immunostaining, were able to uncover statistically significant differences between buffer- and cell-treated groups. Furthermore, in mouse models of PD, behavior does not always reflect disease pathology in the brain (Zhang et al., 2017; Hunn et al., 2019). In this study, improvement of behavioral deficits in cell-transplanted mice with no significant increase in either TH or DAT expression, compared to animals injected with buffer, could be due to a hyperdopaminergic state, where enhanced dopaminergic neurotransmission leads to behavioral improvement while PD pathology remains (Hunn et al., 2019).

Both TH and DAT are used to mark DAn; however, TH marks all catecholaminergic neurons, one of them being DAn, while DAT specifically marks DAn. Tyrosine hydroxylase is the rate-limiting enzyme of DA synthesis, while DAT reuptakes DA at the synapse, thus controlling the availability of DA. In addition, the two proteins differ in expression levels in the Str and SNpc (Miller et al., 1999; Seifert and Wiener, 2013; Vaughan and Foster, 2013; Salvatore et al., 2016). Although TH works in DA synthesis, it does not reveal the activity of DA, which DAT does, as changes in DAT expression levels indicate variations in the transport and release of DA, and can explain the function of these dopaminergic striatal terminals. In addition, it has been hypothesized that abnormal transport of DA can lead to the development of diseases such as PD (Vaughan and Foster, 2013). Both TH and DAT are decreased in the Str of PD patients. However, there is evidence of a compensatory mechanism as a response to striatal DA depletion in PD patients and animals involving augmented synthesis, release and turnover of DA and TH, and increased TH expression and decreased DAT expression in the Str (Miller et al., 1999; Blesa et al., 2017). Interestingly, the visualization of DAT in the Str using positron emission tomography and single photon emission computed tomography imaging such as DATscan is used to help in the diagnosis of PD, thus emphasizing the importance of DAT expression and function, rather than TH expression in PD pathology (Seifert and Wiener, 2013). Most PD and CRT studies quantify nigrostriatal population changes via TH immunostaining (Ang, 2006; Kriks et al., 2011; Stoker and Barker, 2016), but it is clear from this study that TH and DAT expression do not always follow the same pattern. The function of DAT has been associated with the regulation of locomotor activity, which would support the connection between behavioral impairment and expression of DAT, rather than TH (Chotibut et al., 2012). Ultimately, it is important to expand the tests done in experimental PD and CRT as TH, although a good indicator, may not always be the best marker for nigrostriatal degeneration and/or improvement.

Inflammation is known to play an essential role in PD (Sarkar et al., 2016). In this study, buffer-treated animals tended to have higher amounts of striatal astrocytes, while all middle-aged mice had significantly increased striatal inflammation compared to younger controls. This emphasizes just how important the age of the transplant recipient is as CRT is more successful in younger patients (Stoker and Barker, 2016; Yasuhara et al., 2017) perhaps in part due to the fact that higher inflammation levels hamper its effectiveness. Moreover, while microglia were more abundant in the Str of all Parkinsonian mice, the transplant had no effect on microglial activation.

To further support a functionality problem, nonphosphorylated NFH expression in the motor cortex was increased in all MPTP-treated animals compared to control mice. It has been described that PD patients show neuronal loss in the motor cortex (MacDonald and Halliday, 2002). As well, there are structural and functional changes in the motor cortex of PD patients; for example, monoamine deficiencies and both hyperactivity and hypoactivity have been observed (Blesa et al., 2017; Burciu and Vaillancourt, 2018). Furthermore, it has recently been proposed that PD comprises a top-down mechanism meaning that pathological changes in the cortex eventually lead to nigrostriatal neurodegeneration (Foffani and Obeso, 2018). Neurofilament heavy is one of the three subunits of neurofilaments that are present in neurons. Phosphorylation of NFH is key for axonal transport, axonal caliber, axonal diameter, axonal plasticity, and neuronal morphology, and accumulation of neurofilaments as well as variations in modifications to neurofilaments like phosphorylation are present in neurodegenerative diseases such as PD (Nixon and Sihag, 1991; Pant and Veeranna, 1995; Kashiwagi et al., 2003; Liu et al., 2011; Kirkcaldie and Dwyer, 2017). Therefore, an increase in nonphosphorylated NFH suggests a change in axonal function in all MPTP-treated mice in a region of the brain connected to the Str and responsible for movement, although with opposite effects on gait in buffer- and cell-treated animals.

For all immunostaining and behavioral data, the IL and CL sides were affected equally in all three experimental groups, with one exception. Hindlimb stride width was significantly shorter on the IL-CL side in MPTP-treated mice, while no significant

changes were seen among the control and MPTP-administered mice on the CL-IL side.

Many experimental CRT for PD studies are done in adult animals, using rodents from 2 to 4 months old (Courtois et al., 2010; Ramos-Moreno et al., 2012a; Ramos-Moreno et al., 2012b; Zuo et al., 2015; Zuo et al., 2017). However, this translates poorly into clinical situations as PD is a pathology that affects the elderly and age-focused studies need to be more thoroughly explored. Hence, this experimental CRT study was done in middle-aged Parkinsonian mice using the hNSC line hVM1 clone 32. Although there is a lack of data on potential treatments in middle-aged or aged Parkinsonian animals, a few studies have demonstrated some success. The injection of GDNF in the SNpc of 18- and 24-month old Parkinsonian rats led to a significant recovery of TH+ cells in the SNpc, and striatal DA and 3,4-dihydroxyphenylacetic acid levels (Fox et al., 2001). As well, Ourednik et al. (2002), treated 20-month old mice with MPTP and transplanted them with murine NSCs above the SN/ventral tegmental area 1 week or 4 weeks later. There were no changes in behavior in any of the groups throughout the experiment, and 3 weeks post-transplant, TH expression was recovered in the Str and SNpc of hNSC-transplanted mice and expression of DAT was restored to almost control-like levels in these two brain regions (Ourednik et al., 2002).

Our results indicate that differentiated hVM1 clone 32 cells have the profile of DAn required for successful transplant. Although these hNSCs could never be used in clinical trials due to their fetal origin, *v-myc* immortalization, and need for recipient immunosuppression, their characterization helps in understanding and developing NSCs for clinical CRT to treat PD as well as exploring their capability as a source of NTFs in the form of conditioned media (Fričová et al., 2020). When transplanted in their undifferentiated state, although nigrostriatal pathway degeneration was not significantly improved, motor and non-motor impairments were prevented by hNSC transplant in middle-aged Parkinsonian mice, which when translating to human PD cases, is perhaps the most important. Further research is warranted, but these data confirm the efficacy of hNSC transplantation in the treatment of PD and stress the importance of performing experimental CRT studies in aged Parkinsonian mice.

As PD is principally described as a loss of DAn and DA, therapeutic strategies have mostly focused on the preservation or restoration of the nigrostriatal pathway. Our findings, both *in vitro* and *in vivo*, demonstrate that the clinical outcome of PD in humans is far more complex than just nigrostriatal degeneration and motor symptoms, and is indeed multifactorial and includes growth factors and NTFs, mitochondrial and peroxisome function, glucose and lipid metabolism, non-motor neurological aspects, DA functionality, neuroinflammation, and motor cortex changes, all of which could lead to new targets and routes for the treatment of PD.

DATA AVAILABILITY STATEMENT

The NGS and proteomic datasets presented in this study can be found online at https://doi.org/10.21950/4IXBTX and https://doi.org/10.21950/06EW6H, respectively. The remaining raw data supporting the conclusions of this article will be made available by the authors upon reasonable request. **Supplementary Material** includes lists of categorized genes differentially expressed in proliferative and differentiated hNSCs.

ETHICS STATEMENT

The animal study was reviewed and approved by the Research Ethics Committees of the Universidad Autónoma de Madrid and the Comunidad de Madrid (PROEX149/15).

AUTHOR CONTRIBUTIONS

AN, AM-S, and MPP conceived and designed the study. AN, SG-L, and MPP acquired the data. AN and MPP analyzed and interpreted the data. AN drafted the manuscript. AN and MPP substantively revised and edited the manuscript. AM-S and MPP supervised all aspects of the study. AM-S and MPP obtained study funding. All authors read and approved the final manuscript.

FUNDING

This work was funded by the Spanish Ministry of Economy and Competitiveness (SAF 2014-56101-R to AM-S), the Spanish Cell Therapy Network-Instituto de Salud Carlos III (TerCel ISCIII) (RETICS RD16/0011/0032 to AM-S), and the Spanish Ministry of Science and Innovation (PID2020-118189RB-I00 to MPP).

ACKNOWLEDGMENTS

The authors thank the Animal Facility, Confocal Microscopy Service, and Ramón Peiró Pastor of the Genomics & Massive Sequencing Service at the Centro de Biología Molecular Severo Ochoa, as well as Sergio Ciordia and Alberto Paradela of the Proteomics Facility at the Centro Nacional de Biotecnología.

SUPPLEMENTARY MATERIAL

The Supplementary Material for this article can be found online at: https://www.frontiersin.org/articles/10.3389/fphar.2021.773925/full#supplementary-material

REFERENCES

Allen, S. J., Watson, J. J., Shoemark, D. K., Barua, N. U., and Patel, N. K. (2013). GDNF, NGF and BDNF as Therapeutic Options for Neurodegeneration. *Pharmacol. Ther.* 138, 155–175. doi:10.1016/j.pharmthera.2013.01.004

Andersson, E. R., Saltó, C., Villaescusa, J. C., Cajanek, L., Yang, S., Bryjova, L., et al. (2013). Wnt5a Cooperates with Canonical Wnts to Generate Midbrain Dopaminergic Neurons *In Vivo* and in Stem Cells. *Proc. Natl. Acad. Sci. U. S. A.* 110, E602–E610. doi:10.1073/pnas.1208524110

Ang, S. L. (2006). Transcriptional Control of Midbrain Dopaminergic Neuron Development. *Development* 133, 3499–3506. doi:10.1242/dev.02501

Apple, D. M., Solano-Fonseca, R., and Kokovay, E. (2017). Neurogenesis in the Aging Brain. *Biochem. Pharmacol.* 141, 77–85. doi:10.1016/j.bcp.2017.06.116

Bezard, E., Dovero, S., Imbert, C., Boraud, T., and Gross, C. E. (2000). Spontaneous Long-Term Compensatory Dopaminergic Sprouting in MPTP-Treated Mice. *Synapse* 38, 363–368. doi:10.1002/1098-2396(20001201)38:3<363::AID-SYN16>3.0.CO;2-A

Blesa, J., Trigo-Damas, I., Dileone, M., Del Rey, N. L., Hernandez, L. F., and Obeso, J. A. (2017). Compensatory Mechanisms in Parkinson's Disease: Circuits Adaptations and Role in Disease Modification. *Exp. Neurol.* 298, 148–161. doi:10.1016/j.expneurol.2017.10.002

Burciu, R. G., and Vaillancourt, D. E. (2018). Imaging of Motor Cortex Physiology in Parkinson's Disease. *Mov. Disord.* 33, 1688–1699. doi:10.1002/mds.102

Chai, C., and Lim, K. L. (2013). Genetic Insights into Sporadic Parkinson's Disease Pathogenesis. *Curr. Genomics* 14, 486–501. doi:10.2174/13892029146613210195808

Chaturvedi, R. K., and Beal, M. F. (2008). PPAR: a Therapeutic Target in Parkinson's Disease. *J. Neurochem.* 106, 506–518. doi:10.1111/j.1471-4159.2008.05388.x

Chaturvedi, R. K., Shukla, S., Seth, K., and Agrawal, A. K. (2006). Nerve Growth Factor Increases Survival of Dopaminergic Graft, rescue Nigral Dopaminergic Neurons and Restores Functional Deficits in Rat Model of Parkinson's Disease. *Neurosci. Lett.* 398, 44–49. doi:10.1016/j.neulet.2005.12.042

Chaudhuri, K. R., and Schapira, A. H. (2009). Non-motor Symptoms of Parkinson's Disease: Dopaminergic Pathophysiology and Treatment. *Lancet Neurol.* 8, 464–474. doi:10.1016/S1474-4422(09)70068-7

Che, X., Tang, B., Wang, X., Chen, D., Yan, X., Jiang, H., et al. (2013). The BAG2 Protein Stabilises PINK1 by Decreasing its Ubiquitination. *Biochem. Biophys. Res. Commun.* 441, 488–492. doi:10.1016/j.bbrc.2013.10.086

Chiu, C. C., Yeh, T. H., Lai, S. C., Wu-Chou, Y. H., Chen, C. H., Mochly-Rosen, D., et al. (2015). Neuroprotective Effects of Aldehyde Dehydrogenase 2 Activation in Rotenone-Induced Cellular and Animal Models of Parkinsonism. *Exp. Neurol.* 263, 244–253. doi:10.1016/j.expneurol.2014.09.016

Chotibut, T., Apple, D. M., Jefferis, R., and Salvatore, M. F. (2012). Dopamine Transporter Loss in 6-OHDA Parkinson's Model Is Unmet by Parallel Reduction in Dopamine Uptake. *PLoS One* 7, e52322. doi:10.1371/journal.pone.0052322

Chuang, H. C., Wang, X., and Tan, T. H. (2016). MAP4K Family Kinases in Immunity and Inflammation. *Adv. Immunol.* 129, 277–314. doi:10.1016/bs.ai.2015.09.006

Chung, D., Shum, A., and Caraveo, G. (2020). GAP-43 and BASP1 in Axon Regeneration: Implications for the Treatment of Neurodegenerative Diseases. *Front. Cel. Dev. Biol.* 8, 567537. doi:10.3389/fcell.2020.567537

Coronel, R., Lachgar, M., Bernabeu-Zornoza, A., Palmer, C., Domínguez-Alvaro, M., Revilla, A., et al. (2019). Neuronal and Glial Differentiation of Human Neural Stem Cells Is Regulated by Amyloid Precursor Protein (APP) Levels. *Mol. Neurobiol.* 56, 1248–1261. doi:10.1007/s12035-018-1167-9

Courtois, E. T., Castillo, C. G., Seiz, E. G., Ramos, M., Bueno, C., Liste, I., et al. (2010). *In Vitro* and *In Vivo* Enhanced Generation of Human A9 Dopamine Neurons from Neural Stem Cells by Bcl-XL. *J. Biol. Chem.* 285, 9881–9897. doi:10.1074/jbc.M109.054312

Date, I., Felten, D. L., and Felten, S. Y. (1990). Long-term Effect of MPTP in the Mouse Brain in Relation to Aging: Neurochemical and Immunocytochemical Analysis. *Brain Res.* 519, 266–276. doi:10.1016/0006-8993(90)90088-s

De Virgilio, A., Greco, A., Fabbrini, G., Inghilleri, M., Rizzo, M. I., Gallo, A., et al. (2016). Parkinson's Disease: Autoimmunity and Neuroinflammation. *Autoimmun. Rev.* 15, 1005–1011. doi:10.1016/j.autrev.2016.07.022

Dutta, S., and Sengupta, P. (2016). Men and Mice: Relating Their Ages. *Life Sci.* 152, 244–248. doi:10.1016/j.lfs.2015.10.025

Emgård, M., Hallin, U., Karlsson, J., Bahr, B. A., Brundin, P., and Blomgren, K. (2003). Both apoptosis and Necrosis Occur Early after Intracerebral Grafting of Ventral Mesencephalic Tissue: a Role for Protease Activation. *J. Neurochem.* 86, 1223–1232. doi:10.1046/j.1471-4159.2003.01931.x

Exner, N., Lutz, A. K., Haass, C., and Winklhofer, K. F. (2012). Mitochondrial Dysfunction in Parkinson's Disease: Molecular Mechanisms and Pathophysiological Consequences. *EMBO J.* 31, 3038–3062. doi:10.1038/emboj.2012.170

Falk, T., Gonzalez, R. T., and Sherman, S. J. (2010). The Yin and Yang of VEGF and PEDF: Multifaceted Neurotrophic Factors and Their Potential in the Treatment of Parkinson's Disease. *Int. J. Mol. Sci.* 11, 2875–2900. doi:10.3390/ijms11082875

Foffani, G., and Obeso, J. A. (2018). A Cortical Pathogenic Theory of Parkinson's Disease. *Neuron* 99, 1116–1128. doi:10.1016/j.neuron.2018.07.028

Formentini, L., Pereira, M. P., Sánchez-Cenizo, L., Santacatterina, F., Lucas, J. J., Navarro, C., et al. (2014). *In Vivo* inhibition of the Mitochondrial H+-ATP Synthase in Neurons Promotes Metabolic Preconditioning. *EMBO J.* 33, 762–778. doi:10.1002/embj.201386392

Fox, C. M., Gash, D. M., Smoot, M. K., and Cass, W. A. (2001). Neuroprotective Effects of GDNF against 6-OHDA in Young and Aged Rats. *Brain Res.* 896, 56–63. doi:10.1016/s0006-8993(00)03270-4

Fričová, D., Korchak, J. A., and Zubair, A. C. (2020). Challenges and Translational Considerations of Mesenchymal Stem/stromal Cell Therapy for Parkinson's Disease. *NPJ Regen. Med.* 5, 20. doi:10.1038/s41536-020-00106-y

Fu, M. H., Li, C. L., Lin, H. L., Chen, P. C., Calkins, M. J., Chang, Y. F., et al. (2015). Stem Cell Transplantation Therapy in Parkinson's Disease. *Springerplus* 4, 597. doi:10.1186/s40064-015-1400-1

Fults, D., Pedone, C., Dai, C., and Holland, E. C. (2002). MYC Expression Promotes the Proliferation of Neural Progenitor Cells in Culture and *In Vivo*. *Neoplasia* 4, 32–39. doi:10.1038/sj.neo.7900200

Giudici, F., Petracci, E., Nanni, O., Bottin, C., Pinamonti, M., Zanconati, F., et al. (2019). Elevated Levels of eEF1A2 Protein Expression in Triple Negative Breast Cancer Relate with Poor Prognosis. *PLoS One* 14, e0218030. doi:10.1371/journal.pone.0218030

Gonzalez, R., Garitaonandia, I., Crain, A., Poustovoitov, M., Abramihina, T., Noskov, A., et al. (2015). Proof of Concept Studies Exploring the Safety and Functional Activity of Human Parthenogenetic-Derived Neural Stem Cells for the Treatment of Parkinson's Disease. *Cel Transpl.* 24, 681–690. doi:10.3727/096368915X687769

Grünblatt, E., and Riederer, P. (2016). Aldehyde Dehydrogenase (ALDH) in Alzheimer's and Parkinson's Disease. *J. Neural. Transm.* 123, 83–90. doi:10.1007/s00702-014-1320-1

Gu, S., Huang, H., Bi, J., Yao, Y., and Wen, T. (2009). Combined Treatment of Neurotrophin-3 Gene and Neural Stem Cells Is Ameliorative to Behavior Recovery of Parkinson's Disease Rat Model. *Brain Res.* 1257, 1–9. doi:10.1016/j.brainres.2008.12.016

Guan, Q., Wang, M., Chen, H., Yang, L., Yan, Z., and Wang, X. (2016). Aging-related 1-Methyl-4-Phenyl-1,2,3,6-Tetrahydropyridine-Induced Neurochemial and Behavioral Deficits and Redox Dysfunction: Improvement by AK-7. *Exp. Gerontol.* 82, 19–29. doi:10.1016/j.exger.2016.05.011

Hallett, P. J., Cooper, O., Sadi, D., Robertson, H., Mendez, I., and Isacson, O. (2014). Long-term Health of Dopaminergic Neuron Transplants in Parkinson's Disease Patients. *Cell. Rep.* 7, 1755–1761. doi:10.1016/j.celrep.2014.05.027

Ho, A., and Blum, M. (1998). Induction of Interleukin-1 Associated with Compensatory Dopaminergic Sprouting in the Denervated Striatum of Young Mice: Model of Aging and Neurodegenerative Disease. *J. Neurosci.* 18, 56142211–56142229. doi:10.1523/jneurosci.18-15-05614.1998

Hoffman, B., and Liebermann, D. A. (2008). Apoptotic Signaling by C-MYC. *Oncogene* 27, 6462–6472. doi:10.1038/onc.2008.312

Hunn, B. H. M., Vingill, S., Threlfell, S., Alegre-Abarrategui, J., Magdelyns, M., Deltheil, T., et al. (2019). Impairment of Macroautophagy in Dopamine Neurons Has Opposing Effects on Parkinsonian Pathology and Behavior. *Cel. Rep.* 29, 920. doi:10.1016/j.celrep.2019.09.029

Jackson, S. J., Andrews, N., Ball, D., Bellantuono, I., Gray, J., Hachoumi, L., et al. (2017). Does Age Matter? the Impact of Rodent Age on Study Outcomes. *Lab. Anim.* 51, 160–169. doi:10.1177/0023677216653984

Jackson-Lewis, V., and Przedborski, S. (2007). Protocol for the MPTP Mouse Model of Parkinson's Disease. *Nat. Protoc.* 2, 141–151. doi:10.1038/nprot.2006.342

Jakowec, M. W., Nixon, K., Hogg, E., McNeill, T., and Petzinger, G. M. (2004). Tyrosine Hydroxylase and Dopamine Transporter Expression Following 1-Methyl-4-Phenyl-1,2,3,6-Tetrahydropyridine-Induced Neurodegeneration of the Mouse Nigrostriatal Pathway. *J. Neurosci. Res.* 76, 539–550. doi:10.1002/jnr.20114

Jazwa, A., Rojo, A. I., Innamorato, N. G., Hesse, M., Fernández-Ruiz, J., and Cuadrado, A. (2011). Pharmacological Targeting of the Transcription Factor Nrf2 at the Basal Ganglia Provides Disease Modifying Therapy for Experimental Parkinsonism. *Antioxid. Redox Signal.* 14, 2347–2360. doi:10.1089/ars.2010.3731

Jensen, M. B., Krishnaney-Davison, R., Cohen, L. K., and Zhang, S. C. (2012). Injected versus Oral Cyclosporine for Human Neural Progenitor Grafting in Rats. *J. Stem Cel Res. Ther.* Suppl 10, 003. doi:10.4172/2157-7633.S10-003

Jin, K., Sun, Y., Xie, L., Batteur, S., Mao, X. O., Smelick, C., et al. (2003). Neurogenesis and Aging: FGF-2 and HB-EGF Restore Neurogenesis in hippocampus and Subventricular Zone of Aged Mice. *Aging Cell* 2, 175–183. doi:10.1046/j.1474-9728.2003.00046.x

Jo, D. S., Park, N. Y., and Cho, D. H. (2020). Peroxisome Quality Control and Dysregulated Lipid Metabolism in Neurodegenerative Diseases. *Exp. Mol. Med.* 52, 1486–1495. doi:10.1038/s12276-020-00503-9

Jovanovic, V. M., Salti, A., Tilleman, H., Zega, K., Jukic, M. M., Zou, H., et al. (2018). BMP/SMAD Pathway Promotes Neurogenesis of Midbrain Dopaminergic Neurons *In Vivo* and in Human Induced Pluripotent and Neural Stem Cells. *J. Neurosci.* 38, 1662–1676. doi:10.1523/JNEUROSCI.1540-17.2018

Kalia, L. V., and Lang, A. E. (2015). Parkinson's Disease. *Lancet* 386, 896–912. doi:10.1016/S0140-6736(14)61393-3

Kashiwagi, K., Ou, B., Nakamura, S., Tanaka, Y., Suzuki, M., and Tsukahara, S. (2003). Increase in Dephosphorylation of the Heavy Neurofilament Subunit in the Monkey Chronic Glaucoma Model. *Invest. Ophthalmol. Vis. Sci.* 44, 154–159. doi:10.1167/iovs.02-0398

Kehagia, A. A., Housden, C. R., Regenthal, R., Barker, R. A., Müller, U., Rowe, J., et al. (2014). Targeting Impulsivity in Parkinson's Disease Using Atomoxetine. *Brain* 137, 1986–1997. doi:10.1093/brain/awu117

Khwanraj, K., Madlah, S., Grataitong, K., and Dharmasaroja, P. (2016). Comparative mRNA Expression of eEF1A Isoforms and a PI3K/Akt/mTOR Pathway in a Cellular Model of Parkinson's Disease. *Parkinsons Dis.* 2016, 8716016. doi:10.1155/2016/8716016

Kirkcaldie, M. T. K., and Dwyer, S. T. (2017). The Third Wave: Intermediate Filaments in the Maturing Nervous System. *Mol. Cel. Neurosci.* 84, 68–76. doi:10.1016/j.mcn.2017.05.010

Kriks, S., Shim, J. W., Piao, J., Ganat, Y. M., Wakeman, D. R., Xie, Z., et al. (2011). Dopamine Neurons Derived from Human ES Cells Efficiently Engraft in Animal Models of Parkinson's Disease. *Nature* 480, 547–551. doi:10.1038/nature10648

Lan, A. P., Chen, J., Zhao, Y., Chai, Z., and Hu, Y. (2017). mTOR Signaling in Parkinson's Disease. *Neuromol. Med.* 19, 1–10. doi:10.1007/s12017-016-8417-7

Lesage, S., and Brice, A. (2009). Parkinson's Disease: from Monogenic Forms to Genetic Susceptibility Factors. *Hum. Mol. Genet.* 18, R48–R59. doi:10.1093/hmg/ddp012

Li, W., Englund, E., Widner, H., Mattsson, B., van Westen, D., Lätt, J., et al. (2016). Extensive Graft-Derived Dopaminergic Innervation Is Maintained 24 Years after Transplantation in the Degenerating Parkinsonian Brain. *Proc. Natl. Acad. Sci. U. S. A.* 113, 6544–6549. doi:10.1073/pnas.1605245113

Liu, Q., Xie, F., Alvarado-Diaz, A., Smith, M. A., Moreira, P. I., Zhu, X., et al. (2011). Neurofilamentopathy in Neurodegenerative Diseases. *Open Neurol. J.* 5, 58–62. doi:10.2174/1874205X01105010058

Liu, Q., Pedersen, O. Z., Peng, J., Couture, L. A., Rao, M. S., and Zeng, X. (2013). Optimizing Dopaminergic Differentiation of Pluripotent Stem Cells for the Manufacture of Dopaminergic Neurons for Transplantation. *Cytotherapy* 15, 999–1010. doi:10.1016/j.jcyt.2013.03.006

Long, H. Z., Cheng, Y., Zhou, Z. W., Luo, H. Y., Wen, D. D., and Gao, L. C. (2021). PI3K/AKT Signal Pathway: A Target of Natural Products in the Prevention and Treatment of Alzheimer's Disease and Parkinson's Disease. *Front. Pharmacol.* 12, 648636. doi:10.3389/fphar.2021.648636

Lotharius, J., Barg, S., Wiekop, P., Lundberg, C., Raymon, H. K., and Brundin, P. (2002). Effect of Mutant Alpha-Synuclein on Dopamine Homeostasis in a New Human Mesencephalic Cell Line. *J. Biol. Chem.* 277, 38884–38894. doi:10.1074/jbc.M205518200

Luo, J., Daniels, S. B., Lennington, J. B., Notti, R. Q., and Conover, J. C. (2006). The Aging Neurogenic Subventricular Zone. *Aging Cell* 5, 139–152. doi:10.1111/j.1474-9726.2006.00197.x

Ma, H., and Zhu, G. (2014). The Dopamine System and Alcohol Dependence. *Shanghai Arch. Psychiatry* 26, 61–68. doi:10.3969/j.issn.1002-0829.2014.02.002

MacDonald, V., and Halliday, G. M. (2002). Selective Loss of Pyramidal Neurons in the Pre-supplementary Motor Cortex in Parkinson's Disease. *Mov. Disord.* 17, 1166–1173. doi:10.1002/mds.10258

Meiser, J., Weindl, D., and Hiller, K. (2013). Complexity of Dopamine Metabolism. *Cell. Commun. Signal.* 11, 34. doi:10.1186/1478-811X-11-34

Melis, M., Diana, M., Enrico, P., Marinelli, M., and Brodie, M. S. (2009). Ethanol and Acetaldehyde Action on central Dopamine Systems: Mechanisms, Modulation, and Relationship to Stress. *Alcohol* 43, 531–539. doi:10.1016/j.alcohol.2009.05.004

MetaCyc (2021). MetaCyc Database: Metabolic Pathways from All Domains of Life. Available at: https://metacyc.org (Accessed August 3, 2021).

Miller, G. W., Gainetdinov, R. R., Levey, A. I., and Caron, M. G. (1999). Dopamine Transporters and Neuronal Injury. *Trends Pharmacol. Sci.* 20, 424–429. doi:10.1016/s0165-6147(99)01379-6

Mitsumoto, Y., Watanabe, A., Mori, A., and Koga, N. (1998). Spontaneous Regeneration of Nigrostriatal Dopaminergic Neurons in MPTP-Treated C57BL/6 Mice. *Biochem. Biophys. Res. Commun.* 248, 660–663. doi:10.1006/bbrc.1998.8986

Mohapel, P., Frielingsdorf, H., Häggblad, J., Zachrisson, O., and Brundin, P. (2005). Platelet-derived Growth Factor (PDGF-BB) and Brain-Derived Neurotrophic Factor (BDNF) Induce Striatal Neurogenesis in Adult Rats with 6-hydroxydopamine Lesions. *Neuroscience* 132, 767–776. doi:10.1016/j.neuroscience.2004.11.056

Nawabi, H., Belin, S., Cartoni, R., Williams, P. R., Wang, C., Latremolière, A., et al. (2015). Doublecortin-Like Kinases Promote Neuronal Survival and Induce Growth Cone Reformation via Distinct Mechanisms. *Neuron* 88, 704–719. doi:10.1016/j.neuron.2015.10.005

Nieoullon, A. (2002). Dopamine and the Regulation of Cognition and Attention. *Prog. Neurobiol.* 67, 53–83. doi:10.1016/s0301-0082(02)00011-4

Nixon, R. A., and Sihag, R. K. (1991). Neurofilament Phosphorylation: a New Look at Regulation and Function. *Trends Neurosci.* 14, 501–506. doi:10.1016/0166-2236(91)90062-y

Nombela, C., Rittman, T., Robbins, T. W., and Rowe, J. B. (2014). Multiple Modes of Impulsivity in Parkinson's Disease. *PLoS One* 9, e85747. doi:10.1371/journal.pone.0085747

Ohashi, S., Mori, A., Kurihara, N., Mitsumoto, Y., and Nakai, M. (2006). Age-related Severity of Dopaminergic Neurodegeneration to MPTP Neurotoxicity Causes Motor Dysfunction in C57BL/6 Mice. *Neurosci. Lett.* 401, 183–187. doi:10.1016/j.neulet.2006.03.017

Ourednik, J., Ourednik, V., Lynch, W. P., Schachner, M., and Snyder, E. Y. (2002). Neural Stem Cells Display an Inherent Mechanism for Rescuing Dysfunctional Neurons. *Nat. Biotechnol.* 20, 1103–1110. doi:10.1038/nbt750

Pant, H. C., and Veeranna (1995). Neurofilament Phosphorylation. *Biochem. Cel Biol.* 73, 575–592. doi:10.1139/o95-063

Parga, J. A., García-Garrote, M., Martínez, S., Raya, Á., Labandeira-García, J. L., and Rodríguez-Pallares, J. (2018). Prostaglandin EP2 Receptors Mediate Mesenchymal Stromal Cell-Neuroprotective Effects on Dopaminergic Neurons. *Mol. Neurobiol.* 55, 4763–4776. doi:10.1007/s12035-017-0681-5

Patel, O., Dai, W., Mentzel, M., Griffin, M. D., Serindoux, J., Gay, Y., et al. (2016). Biochemical and Structural Insights into Doublecortin-like Kinase Domain 1. *Structure* 24, 1550–1561. doi:10.1016/j.str.2016.07.008

Paxinos, G., and Franklin, K. B. J. (2001). *The Mouse Brain in Stereotaxic Coordinates*. 2nd ed.. San Diego: Academic Press.

Piltonen, M., Planken, A., Leskelä, O., Myöhänen, T. T., Hänninen, A. L., Auvinen, P., et al. (2011). Vascular Endothelial Growth Factor C Acts as a Neurotrophic Factor for Dopamine Neurons *In Vitro* and *In Vivo*. *Neuroscience* 192, 550–563. doi:10.1016/j.neuroscience.2011.06.084

Prommahom, A., and Dharmasaroja, P. (2021). Effects of eEF1A2 Knockdown on Autophagy in an MPP+-Induced Cellular Model of Parkinson's Disease. *Neurosci. Res.* 164, 55–69. doi:10.1016/j.neures.2020.03.013

Prut, L., and Belzung, C. (2003). The Open Field as a Paradigm to Measure the Effects of Drugs on Anxiety-like Behaviors: a Review. *Eur. J. Pharmacol.* 463, 3–33. doi:10.1016/s0014-2999(03)01272-x

Qin, L., Guo, J., Zheng, Q., and Zhang, H. (2016). BAG2 Structure, Function and Involvement in Disease. *Cell. Mol. Biol. Lett.* 21, 18. doi:10.1186/s11658-016-0020-2

Rafuse, V. F., Soundararajan, P., Leopold, C., and Robertson, H. A. (2005). Neuroprotective Properties of Cultured Neural Progenitor Cells Are Associated with the Production of Sonic Hedgehog. *Neuroscience* 131, 899–916. doi:10.1016/j.neuroscience.2004.11.048

Ramos-Moreno, T., Castillo, C. G., and Martínez-Serrano, A. (2012a). Long Term Behavioral Effects of Functional Dopaminergic Neurons Generated from Human Neural Stem Cells in the Rat 6-OH-DA Parkinson's Disease Model. Effects of the Forced Expression of BCL-X(l). *Behav. Brain Res.* 232, 225–232. doi:10.1016/j.bbr.2012.04.020

Ramos-Moreno, T., Lendínez, J. G., Pino-Barrio, M. J., Del Arco, A., and Martínez-Serrano, A. (2012b). Clonal Human Fetal Ventral Mesencephalic Dopaminergic Neuron Precursors for Cell Therapy Research. *PLoS One* 7, e52714. doi:10.1371/journal.pone.0052714

Redmond, D. E., Jr, Bjugstad, K. B., Teng, Y. D., Ourednik, V., Ourednik, J., Wakeman, D. R., et al. (2007). Behavioral Improvement in a Primate Parkinson's Model Is Associated with Multiple Homeostatic Effects of Human Neural Stem Cells. *Proc. Natl. Acad. Sci. U. S. A.* 104, 12175–12180. doi:10.1073/pnas.0704091104

Roberton, V. H., Evans, A. E., Harrison, D. J., Precious, S. V., Dunnett, S. B., Kelly, C. M., et al. (2013). Is the Adult Mouse Striatum a Hostile Host for Neural Transplant Survival? *Neuroreport* 24, 1010–1015. doi:10.1097/WNR.0000000000000066

Rousselet, E., Joubert, C., Callebert, J., Parain, K., Tremblay, L., Orieux, G., et al. (2003). Behavioral Changes Are Not Directly Related to Striatal Monoamine Levels, Number of Nigral Neurons, or Dose of Parkinsonian Toxin MPTP in Mice. *Neurobiol. Dis.* 14, 218–228. doi:10.1016/s0969-9961(03)00108-6

Saal, K. A., Galter, D., Roeber, S., Bähr, M., Tönges, L., and Lingor, P. (2017). Altered Expression of Growth Associated Protein-43 and Rho Kinase in Human Patients with Parkinson's Disease. *Brain Pathol.* 27, 13–25. doi:10.1111/bpa.12346

Salvatore, M. F., Calipari, E. S., and Jones, S. R. (2016). Regulation of Tyrosine Hydroxylase Expression and Phosphorylation in Dopamine Transporter-Deficient Mice. *ACS Chem. Neurosci.* 7, 941–951. doi:10.1021/acschemneuro.6b00064

Sarkar, S., Raymick, J., and Imam, S. (2016). Neuroprotective and Therapeutic Strategies against Parkinson's Disease: Recent Perspectives. *Int. J. Mol. Sci.* 17, 904. doi:10.3390/ijms17060904

Seifert, K. D., and Wiener, J. I. (2013). The Impact of DaTscan on the Diagnosis and Management of Movement Disorders: A Retrospective Study. *Am. J. Neurodegener Dis.* 2, 29–34.

Sengupta, P. (2013). The Laboratory Rat: Relating its Age with Human's. *Int. J. Prev. Med.* 4, 624–630.

Sergi, D., Renaud, J., Simola, N., and Martinoli, M. G. (2019). Diabetes, a Contemporary Risk for Parkinson's Disease: Epidemiological and Cellular Evidences. *Front. Aging Neurosci.* 11, 302. doi:10.3389/fnagi.2019.00302

Shu, T., Tseng, H. C., Sapir, T., Stern, P., Zhou, Y., Sanada, K., et al. (2006). Doublecortin-like Kinase Controls Neurogenesis by Regulating Mitotic Spindles and M Phase Progression. *Neuron* 49, 25–39. doi:10.1016/j.neuron.2005.10.039

Sousa, K. M., Villaescusa, J. C., Cajanek, L., Ondr, J. K., Castelo-Branco, G., Hofstra, W., et al. (2010). Wnt2 Regulates Progenitor Proliferation in the Developing Ventral Midbrain. *J. Biol. Chem.* 285, 7246–7253. doi:10.1074/jbc.M109.079822

Stoker, T. B., and Barker, R. A. (2016). Cell Therapies for Parkinson's Disease: How Far Have We Come? *Regen. Med.* 11, 777–786. doi:10.2217/rme-2016-0102

Stoker, T. B., Torsney, K. M., and Barker, R. A. (2018). Emerging Treatment Approaches for Parkinson's Disease. *Front. Neurosci.* 12, 693. doi:10.3389/fnins.2018.00693

Sullivan, A. M., and Toulouse, A. (2011). Neurotrophic Factors for the Treatment of Parkinson's Disease. *Cytokine Growth Factor. Rev.* 22, 157–165. doi:10.1016/j.cytogfr.2011.05.001

Todorovic, M., Wood, S. A., and Mellick, G. D. (2016). Nrf2: a Modulator of Parkinson's Disease? *J. Neural. Transm.* 123, 611–619. doi:10.1007/s00702-016-1563-0

Tome, D., Fonseca, C. P., Campos, F. L., and Baltazar, G. (2017). Role of Neurotrophic Factors in Parkinson's Disease. *Curr. Pharm. Des.* 23, 809–838. doi:10.2174/1381612822666161208120422

Tordoff, M. G., Bachmanov, A. A., and Reed, D. R. (2007). Forty Mouse Strain Survey of Water and Sodium Intake. *Physiol. Behav.* 91, 620–631. doi:10.1016/j.physbeh.2007.03.025

U.S. National Library of Medicine (2021). Available at: ClinicalTrials.gov (Accessed August 20, 2021).

Vaughan, R. A., and Foster, J. D. (2013). Mechanisms of Dopamine Transporter Regulation in normal and Disease States. *Trends Pharmacol. Sci.* 34, 489–496. doi:10.1016/j.tips.2013.07.005

Villa, A., Liste, I., Courtois, E. T., Seiz, E. G., Ramos, M., Meyer, M., et al. (2009). Generation and Properties of a New Human Ventral Mesencephalic Neural Stem Cell Line. *Exp. Cel Res.* 315, 1860–1874. doi:10.1016/j.yexcr.2009.03.011

Wirdefeldt, K., Adami, H. O., Cole, P., Trichopoulos, D., and Mandel, J. (2011). Epidemiology and Etiology of Parkinson's Disease: a Review of the Evidence. *Eur. J. Epidemiol.* 26 (Suppl. 1), S1–S58. doi:10.1007/s10654-011-9581-6

Wójtowicz, S., Strosznajder, A. K., Jeżyna, M., and Strosznajder, J. B. (2020). The Novel Role of PPAR Alpha in the Brain: Promising Target in Therapy of Alzheimer's Disease and Other Neurodegenerative Disorders. *Neurochem. Res.* 45, 972–988. doi:10.1007/s11064-020-02993-5

Xia, N., Zhang, P., Fang, F., Wang, Z., Rothstein, M., Angulo, B., et al. (2016). Transcriptional Comparison of Human Induced and Primary Midbrain Dopaminergic Neurons. *Sci. Rep.* 6, 20270. doi:10.1038/srep20270

Yang, L., Chao, J., Kook, Y. H., Gao, Y., Yao, H., and Buch, S. J. (2013). Involvement of miR-9/MCPIP1 axis in PDGF-BB-Mediated Neurogenesis in Neuronal Progenitor Cells. *Cell. Death Dis.* 4, e960. doi:10.1038/cddis.2013.486

Yasuhara, T., Shingo, T., Kobayashi, K., Takeuchi, A., Yano, A., Muraoka, K., et al. (2004). Neuroprotective Effects of Vascular Endothelial Growth Factor (VEGF) upon Dopaminergic Neurons in a Rat Model of Parkinson's Disease. *Eur. J. Neurosci.* 19, 1494–1504. doi:10.1111/j.1460-9568.2004.03254.x

Yasuhara, T., Matsukawa, N., Hara, K., Yu, G., Xu, L., Maki, M., et al. (2006). Transplantation of Human Neural Stem Cells Exerts Neuroprotection in a Rat Model of Parkinson's Disease. *J. Neurosci.* 26, 12497–12511. doi:10.1523/JNEUROSCI.3719-06.2006

Yasuhara, T., Kameda, M., Sasaki, T., Tajiri, N., and Date, I. (2017). Cell Therapy for Parkinson's Disease. *Cel Transpl.* 26, 1551–1559. doi:10.1177/0963689717735411

Zhang, Q. S., Heng, Y., Mou, Z., Huang, J. Y., Yuan, Y. H., and Chen, N. H. (2017). Reassessment of Subacute MPTP-Treated Mice as Animal Model of Parkinson's Disease. *Acta Pharmacol. Sin.* 38, 1317–1328. doi:10.1038/aps.2017.49

Zheng, C., Quan, R. D., Wu, C. Y., Hu, J., Lin, B. Y., Dong, X. B., et al. (2019). Growth-associated Protein 43 Promotes Thyroid Cancer Cell Lines Progression via Epithelial-Mesenchymal Transition. *J. Cel. Mol. Med.* 23, 7974–7984. doi:10.1111/jcmm.14460

Zuo, F. X., Bao, X. J., Sun, X. C., Wu, J., Bai, Q. R., Chen, G., et al. (2015). Transplantation of Human Neural Stem Cells in a Parkinsonian Model Exerts Neuroprotection via Regulation of the Host Microenvironment. *Int. J. Mol. Sci.* 16, 26473–26492. doi:10.3390/ijms161125966

Zuo, F., Xiong, F., Wang, X., Li, X., Wang, R., Ge, W., et al. (2017). Intrastriatal Transplantation of Human Neural Stem Cells Restores the Impaired Subventricular Zone in Parkinsonian Mice. *Stem Cells* 35, 1519–1531. doi:10.1002/stem.2616

Conflict of Interest: The authors declare that the research was conducted in the absence of any commercial or financial relationships that could be construed as a potential conflict of interest.

Publisher's Note: All claims expressed in this article are solely those of the authors and do not necessarily represent those of their affiliated organizations, or those of the publisher, the editors, and the reviewers. Any product that may be evaluated in this article, or claim that may be made by its manufacturer, is not guaranteed or endorsed by the publisher.

frontiers in Pharmacology

MINI REVIEW
published: 31 January 2022
doi: 10.3389/fphar.2022.824907

Neuroinflammation and Neutrophils: Modulation by Ouabain

Jacqueline Alves Leite[1†], *Luiz Henrique Agra Cavalcante-Silva*[2†], *Martina Raissa Ribeiro*[3], *Geovanni de Morais Lima*[3], *Cristoforo Scavone*[3*] and *Sandra Rodrigues-Mascarenhas*[2]

[1]*Department of Pharmacology, Institute of Biomedical Science, Federal University of Goiás, Goiânia, Brazil,* [2]*Immunobiotechnology Laboratory, Biotechnology Center, Federal University of Paraíba, João Pessoa, Brazil,* [3]*Laboratory of Molecular Neuropharmacology, Department of Pharmacology, Institute of Biomedical Science, University of São Paulo, São Paulo, Brazil*

Cardiotonic steroids are natural compounds that present many physiological and pharmacological functions. They bind Na^+/K^+-ATPase (NKA) modifying cellular ion concentration and trigger cell signaling mechanisms without altering ion balance. These steroids are known to modulate some immune responses, including cytokine production, neutrophil migration, and inflammation (peripherally and in the nervous system). Inflammation can occur in response to homeostasis perturbations and is related to the development of many diseases, including immune-mediated diseases and neurodegenerative disorders. Considering the neutrophils role in the general neuroinflammatory response and that these cells can be modulated by cardiac steroids, this work aims to review the possible regulation of neutrophilic neuroinflammation by the cardiac steroid ouabain.

Keywords: innate immunity, inflammation, ouabain, neuroimmune interactions, neuropharmacology

OPEN ACCESS

Edited by:
Borja Garcia-Bueno, Universidad Complutense de Madrid, Spain

Reviewed by:
Cristiane Damas Gil, Federal University of São Paulo, Brazil
Violeta Duran Laforet, University of Massachusetts Medical School, United States

***Correspondence:**
Cristoforo Scavone
criscavone@usp.br

†These authors have contributed equally to this work and share first authorship

Specialty section:
This article was submitted to Inflammation Pharmacology, a section of the journal Frontiers in Pharmacology

Received: *29 November 2021*
Accepted: *10 January 2022*
Published: *31 January 2022*

Citation:
Leite JA, Cavalcante-Silva LHA, Ribeiro MR, de Morais Lima G, Scavone C and Rodrigues-Mascarenhas S (2022) Neuroinflammation and Neutrophils: Modulation by Ouabain. Front. Pharmacol. 13:824907. doi: 10.3389/fphar.2022.824907

OUABAIN AND NA^+/K^+-ATPASE

Ouabain is a cardiotonic steroid identified by Hamlyn et al. (1991) in mammalian plasma. Studies have shown that ouabain can be produced by the adrenal gland, hypothalamus, and pituitary, being considered a hormone (Pamnani et al., 1981; Hamlyn et al., 1991; Ferrandi et al., 1997). In relation to the adrenal, ouabain synthesis appears to occur in the glomerulosa of the cortex (Laredo et al., 1995), and its release can be stimulated by two different hormones, angiotensin II, or adrenocorticotropic hormone (Laredo et al., 1994). The physiological levels of circulating ouabain in humans are approximately 0.2 nM and, in rodents, this value can reach 0.5 nM (Blaustein and Hamlyn, 2020).

Its receptor is the NKA, being the only established receptor for cardiotonic steroids such as ouabain, which interacts with amino acids located in the extracellular loops of the α subunit of the enzyme (Dvela et al., 2007). NKA is a membrane protein responsible for establishing and maintaining high K^+ and low Na^+ concentrations in the intracellular environment, in addition to maintaining cellular osmotic balance, the resting potential of most body tissues and the properties of excitable muscle and neural cells (Blanco and Mercer, 1998). The enzyme is composed of the α subunit, responsible for the catalytic activity and ion transport function, and the β subunit, which is necessary for the enzyme activity, regulating the fixation of the α subunit, and modulating the affinity for Na^+ and K^+ ions. There are four α isoforms, with α1 being ubiquitously expressed, while the α2–α4 isoforms present a more restricted cellular distribution (Markov et al., 2020). The modulating actions of this receptor affect both the cellular ionic balance, changing different cellular functions, such as cell migration (Ward and Becker, 1970), but also as an important signal transducer (Liu and

Xie, 2010; Fan et al., 2017). At low concentrations (usually at nanomolar range), ouabain can promote conformational changes in NKA, without inhibiting the transport of sodium and potassium (Liu et al., 2000; Xie, 2003). This process leads to the activation/inhibition of many cell signaling proteins, including Src, MAPKs, and NF-κB (Cui and Xie, 2017).

Therapeutically, cardiotonic steroids are usually recommended for congestive heart failure, but only digoxin remains in use (Alpert, 2021). Despite this, ouabain presents many physiological and pharmacological effects that are more studied in the cardiovascular system, in the renal and brain tissues (reviewed in Blaustein and Hamlyn, 2020 and Bagrov et al., 2009). Other authors also suggest a repurposing of cardiac glycosides, including ouabain, for cancer therapeutics (Schneider et al., 2017; Matozzo et al., 2020; Du et al., 2021). Cardiac glycosides also modulate inflammation and autoimmune diseases (Škubník et al., 2021). Digoxin can inhibit transcriptional factor RORγt, thus inhibiting Th17 cells, a cell type involved in autoimmunity (Huh et al., 2011). Another cardiac glycoside, bufalin, inhibits the allergic inflammation by suppression of nuclear factor-kappa B activity (Zhakeer et al., 2017).

Regarding ouabain, many immune system cells can be modulated (Olej et al., 1994; Rodrigues-Mascarenhas et al., 2009). In thymocytes, precursor cells of T lymphocytes, ouabain inhibits cell proliferation (Szamel et al., 1981), induces the expression of CD69 (Rodrigues Mascarenhas et al., 2003) and the increase of free radicals (Smolyaninova et al., 2013). Also, in thymocytes, ouabain also reduces the activation of the mitogen-activated protein kinase (MAPK) p38 and the levels of the nuclear activating factor of T cells c1 (NFAT1c) (Rodrigues-Mascarenhas et al., 2008). Ouabain also inhibits lymphocyte mitosis. Furthermore, it was also evidenced that ouabain negatively modulates the number of B lymphocytes in the bone marrow, spleen, and peripheral blood (de Paiva et al., 2011), without, however, changing the levels of immunoglobulin G (IgG) and M (IgM). On the other hand, ouabain induces an increase in the number of B lymphocytes in the mesenteric lymph nodes, probably due to the reduction in the expression of the adhesion molecule CD62L and the chemokine receptor CXCR5 (da Silva et al., 2016).

Other immune system cells can also be modulated by ouabain. Nascimento et al. (2014) demonstrated that ouabain regulates the maturation of dendritic cells. In human monocytes, ouabain negatively regulates the expression of mCD14, a cell surface molecule involved in the response against Gram-negative bacteria, through the activation of the epidermal growth factor receptor (EGRF) and MAPK p38 (Valente et al., 2009). In addition, monocytes treated with ouabain have high levels of CD69, HLA DR, CD86, and CD80, molecules related to cell activation, in addition to increasing the phagocytic capacity of these cells (Teixeira and Rumjanek, 2014). Ouabain also inhibits, *in vitro*, the development of an inflammatory monocyte subtype ($mCD14^{+}CD16^{+}$) (Valente et al., 2009) and stimulates the production of cytokines such as IL-1α, IL-1β, TNF-α, IL- 6 and IL-10 (Foey et al., 1997; Matsumori et al., 1997; Teixeira and Rumjanek, 2014).

Moreover, ouabain can modulate inflammation and inflammatory cells (reviewed in Cavalcante-Silva et al., 2017). Dysregulated migration or activation of inflammatory cells, such as neutrophils are involved in the immunopathogenesis of many diseases (Leliefeld et al., 2016; Hellebrekers et al., 2018; Cavalcante-Silva et al., 2021b; Bautista-Becerril et al., 2021; Parackova et al., 2021). Thus, modulating these cells can be a therapeutic approach for inflammatory diseases. The ouabain effect on neutrophil during peripheral and neuro inflammation will be discussed below.

NEUROINFLAMMATION AND NEUTROPHILS

For a long time, the central nervous system (CNS) was recognized as a "privileged immune" organ due to the presence of the blood-brain barrier (BBB), which was previously considered to be almost impenetrable. Nevertheless, several studies have pointed out the flexibility in the BBB in response to inflammatory stimuli, which can generate a process known as neuroinflammation (Kanashiro et al., 2020). Neuroinflammation is related to the emergence of neurodegenerative diseases, such as Parkinson's disease, Alzheimer's disease (AD) and cerebral ischemia as well as its association with neuropsychiatric disorders. Thus, neuroinflammation has been studied as an important therapeutic target for the treatment of neurodegenerative and neuropsychiatric diseases (Akira et al., 2006).

Inflammation in the CNS is orchestrated by resident immune cells such as astrocytes and microglia (Doty et al., 2015), as well as by the migration of monocytes and lymphocytes through the BBB. (Hawkes and McLaurin, 2009; Lampron et al., 2013). Several studies have pointed out the relevance of neutrophils in chronic neuroinflammatory diseases such as AD, but their role still needs to be better elucidated. Neutrophil recruitment can cause neuronal damage and cognitive decline in AD; however, some granular proteins, such as CAP37, neutrophil elastase and cathepsin G can promote Aβ cleavage, facilitating Aβ clearance, preventing the formation of pathogenic aggregates (reviewed in Stock et al., 2018).

CNS cells, such as astrocytes, release several chemokines dependent on the IL-17 pathway, such as CXCL5, CXCL2, and CXCL1, which promote neutrophil migration to the CNS. Furthermore, $IL\text{-}17^{-/-}$ mice have a lower number of neutrophils infiltrating the CNS, but the same was not observed in the spinal cord, as neutrophil migration to the spinal cord appears to be regulated by IFN-γ (Christy et al., 2013; Simmons et al., 2014; Pierson et al., 2018). On the other hand, in chronic neurodegenerative diseases such as AD, neutrophil migration appears to be orchestrated by the chemokines CXCL12 and CCL2 as well as by the LFA-1 integrin (Zenaro et al., 2015). Interestingly, studies in mice have shown that blocking the LFA-1 integrin resulted in the inhibition of neutrophil migration, as well as the activation of microglia, resulting in reduced cognitive deficit in AD (Zenaro et al., 2015).

Neutrophil infiltration in post-ischemic inflammation has been associated with exacerbation of brain injury and neuronal damage due to release of pro-inflammatory cytokines, production of reactive oxygen species and reactive nitrogen species, and (neutrophil extracellular traps) NETs release. Furthermore, these neutrophils have a hypersegmented characteristic and their migration is dependent on the CXCR2 neutrophil-specific chemokine receptor (Herz et al., 2015; Neumann et al., 2015). Additionally, it was observed that blocking through a neutralizing antiserum or selective pharmacological inhibitor for CXCR2 prevented the recruitment of neutrophils to the brain of hyperlipidemic mice ApoE$^{-/-}$ mice (Herz et al., 2015). Furthermore, it was observed that polymorphonuclear cells develop direct neurotoxicity through the secretion of TNF-alpha, matrix metalloproteinase 9, as well as through heterocellular contact, which may thus contribute to secondary damage after brain injury, such as cognitive impairment (Dinkel et al., 2004; Nguyen et al., 2007). Another important point observed in spinal cord injury models is the participation of NF-κB signaling in neutrophil activation and infiltration, since IκB kinase (IKK)-β conditional knockout mice showed lower secretion of CXCL1 and the consequent neutrophil infiltration resulted in less neuronal damage, neuroinflammation and improvement in motor function (Kang et al., 2011). Furthermore, Zenaro et al. showed that neutrophil infiltration plays an important role in microglia activation, accumulation of abnormal Aβ and tau, synaptic dysfunction, and memory decline in the neuroinflammation observed in AD (Zenaro et al., 2015).

On the other hand, the neuroprotective role for neutrophils in post-ischemic inflammation has been observed by different works. In an *in vitro* study conducted by Hou et al. (2019) it was observed that while N1 neutrophils decreased neuronal viability, N2 polarization promoted an improvement in neuronal viability against oxygen glucosedeprivation/re-oxygenation-induced injury, in cultured cortical neurons (Hou et al., 2019). In addition, using an *in vivo* model of injury induced by transient occlusion of the middle cerebral artery, Hou et al. (2019) showed that rats spontaneously regenerate over time, and that there is a negative correlation between the proportion of N2 neutrophils and the number of degenerating neurons, in the ipsilateral brain parenchyma (Hou et al., 2019). Furthermore, a study conducted in mice demonstrated that rosiglitazone, a peroxisome proliferator-activated receptor-γ (PPARγ) agonist, increased the infiltration of N2-type neutrophils, culminating in a neuroprotective effect after stroke. Interestingly, the neuroprotective effect of the PPARγ agonist was reversed after neutrophil depletion, demonstrating their importance in neuroprotection (Cuartero et al., 2013). In another study, García-Culebras et al. (2019) demonstrated that mice deficient in TLR4 have a greater polarization for the N2 profile, resulting in a smaller infarct volume and neuroprotection, elucidating a role of TLR4 signaling for neutrophil polarization during the cerebral ischemia (García-Culebras et al., 2019). In addition, Sas et al. showed a CD14^{+} Ly6G^{low} granulocyte with features of an immature neutrophil with neuroregenerative and neuroprotective properties in models of optic nerve and spinal cord injury, resulting from the secretion of NGF and IGF-1 growth factors by CD14^{+} Ly6G^{low} cells (Sas et al., 2020).

The different findings indicate that neutrophils are highly responsive to CNS lesions and may influence the process of neuroinflammation and neurodegeneration, as well as neuroprotection, affecting the development of neurodegenerative processes. Considering the development of neuroinflammation, ouabain emerge as a possible player in the regulation of this process (**Figure 1A**), as several studies have demonstrated the importance of digitalis and NKA in neuroinflammatory regulation (reviewed in Orellana et al., 2016).

Studies have demonstrated an *in vivo* and *in vitro* neuroprotective activity of ouabain. Kinoshita et al. (2014) have observed *in vivo* that ouabain has a protective effect against LPS-induced neuroinflammation in the rat hippocampus, through a reduction in the activation and consequent translocation of nuclear factor kappa B (NF-κB), leading to reduction in the expression of iNOS and IL-1β. Furthermore, it was observed that the administration of ouabain reduced the activation of astrocytes, in the dentate gyrus, through a reduction in the expression of glial fibrillary acidic protein (GFAP) (Kinoshita et al., 2014). In addition, *in vitro* studies of LPS-stimulated astrocytes found that treatment with ouabain reduced the release of IL-1β (Forshammar et al., 2011). On the other hand, an *in vitro* study using LPS-stimulated rat microglial cell culture, it was shown that treatment with Ouabain did not alter the release of TNF-α and IL-1β, thus suggesting a lack of modulating effect of ouabain on this cell type (Forshammar et al., 2013). Additionally, in a recently published study, Mázala-de-Oliveira et al. (2021) have shown that nanomolar concentrations of ouabain reduced the expression of inflammatory receptors, such as TNFR1, TLR4 and CD14 of rat retinal ganglion cells culture after optic nerve axotomy, in all tested periods. It was also observed that ouabain produced an increased survival of retinal ganglion cells after 48h, and the mechanism was dependent on autophagy, since the use of 3-methyladenine, an autophagy inhibitor, lead to a complete inhibition of the neuroprotective role of ouabain (Mázala-de-Oliveira et al., 2021).

On the other hand, it was shown that α2-NKA knockdown in superoxide dismutase 1 (SOD1) mutant astrocytes protected motor neurons from degeneration (Gallardo et al., 2014). Furthermore, it was observed that the silencing of α2-NKA in primary culture of glial cells from mice promoted a lower responsiveness to the stimulus with LPS, by reducing the production of TNF-α, as well as the activation of ERK and NF-kB, suggesting the participation of α2-NKA in the modulation of LPS-induced neuroinflammation (Kinoshita et al., 2017). Ouabain, *in vitro*, protected motor neurons from degeneration induced by mutant SOD1 astrocytes (Gallardo et al., 2014). Heterozygous KI mice, carrying the G301R disease mutation ($\alpha2^{+/G301R}$ mice), exhibited familial hemiplegic migraine type 2 (FHM2)-related phenotypes, including mood depression and obsessive-compulsive disorder (OCD)-like symptoms (Isaksen and Lykke-Hartmann, 2016). Surprisingly, when subjected to spinal cord injury, $\alpha2^{+/G301R}$ mice show better

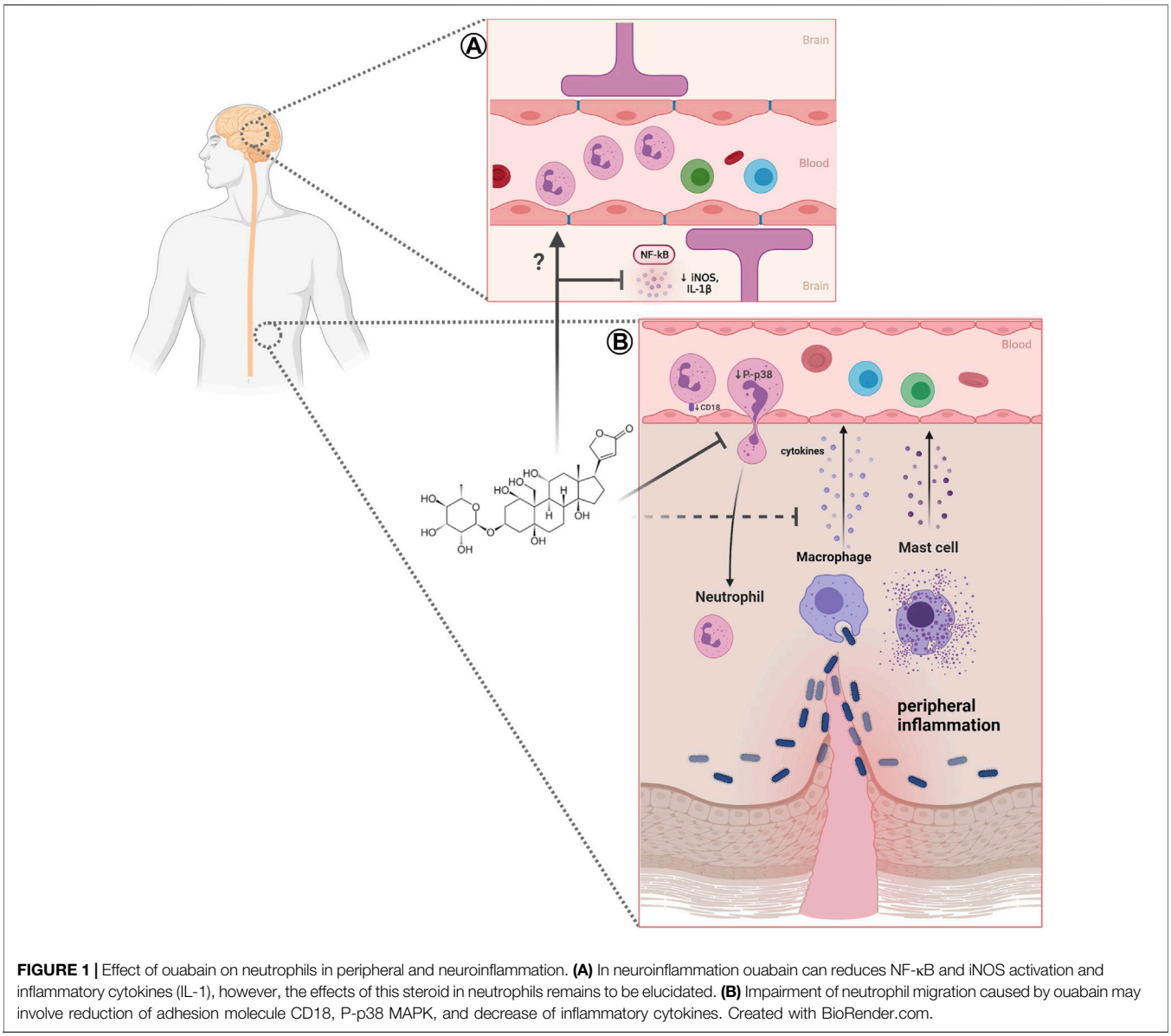

FIGURE 1 | Effect of ouabain on neutrophils in peripheral and neuroinflammation. **(A)** In neuroinflammation ouabain can reduces NF-κB and iNOS activation and inflammatory cytokines (IL-1), however, the effects of this steroid in neutrophils remains to be elucidated. **(B)** Impairment of neutrophil migration caused by ouabain may involve reduction of adhesion molecule CD18, P-p38 MAPK, and decrease of inflammatory cytokines. Created with BioRender.com.

functional recovery and decreased lesion volume compared to littered controls ($\alpha2^{+/+}$). These phenotypes were associated with alterations in pro and anti-inflammatory cytokines levels, such as IL-6, TNF, and IL-10 (Ellman et al., 2017). Furthermore, it was observed that $\alpha2^{+/G301R}$ mice showed a reduction in the systemic levels of the proinflammatory cytokines TNF-α, IL-6 and IL-1β after LPS administration, as well as a reduction in the hypothermic and neuroinflammatory response in the hippocampus and hypothalamus (Leite et al., 2020).

Additionally, peripheral inflammation can also be modulated by ouabain. This steroid can alter vascular permeability induced by different inflammatory agents. In the sheep skin and pleural cavity, ouabain reduces vascular permeability caused by turpentine, an irritant agent (Lancaster and Vegad, 1967). Additionally, in mice peritoneal cavity this steroid decreases vascular permeability induced by zymosan, a fungal wall component (Leite et al., 2015). Also in mice, ouabain can inhibits paw edema, a cardinal signal resulting of increased vascular permeability, induced by carrageenan, compound 48/80, zymosan, prostaglandin E2, and bradykinin (de Vasconcelos et al., 2011). This effect of ouabain in vascular parameters could be related to its effects on histamine (Okazaki et al., 1976) and/or cytokines release (Leite et al., 2015). Indeed, it has been reported that ouabain decreases levels of cytokines TNF-α, IL-1β (Leite et al., 2015), and IFN-γ (Jacob et al., 2013) in peritoneal inflammation.

It is noteworthy that many studies related that ouabain possesses a proinflammatory effect and facilitates immune cell migration (Kennedy et al., 2013; Gonçalves-de-Albuquerque et al., 2014; Chen et al., 2017). The possible dual effect of

ouabain on inflammation may be due to different animal species studied (i.e., BALB/c, Swiss, or C57BL/6 mice; rats; humans) since it could impact NKA sensitivity to ouabain. Moreover, administration route used, presence of a previous inflammatory stimulus, or even different concentrations of this steroid leads to different outcomes. In fact, high levels of ouabain could cause an immune system activation and promote a pathological inflammatory response (Blaustein and Hamlyn, 2020).

NEUTROPHILS: MODULATION BY OUABAIN

During inflammation, endothelial cell activation by cytokines induces vascular permeability and enables migration of immune cells into tissues. Usually, neutrophils are the first immune cell to reach inflamed tissue (Liew and Kubes, 2019). Neutrophils are polymorphonuclear segmented cells with antimicrobial properties (Burn et al., 2021). However, these cells present many other immune functions and participate in the stimulation of adaptive immune responses (Minns et al., 2019), in the resolution of inflammation (Jones et al., 2016) and healing (Phillipson and Kubes, 2019), and have anti or pro-tumor activity (Mishalian et al., 2017; Ocana et al., 2017; Burn et al., 2021). Outside of neutrophils' essential role in immune system homeostasis, they are also involved in autoimmune and inflammatory diseases, such as arthritis (O'Neil and Kaplan, 2019) and COVID-19 (Cavalcante-Silva et al., 2021b). In these pathological conditions, neutrophils may have a dysregulated migration or activation (Hidalgo et al., 2019).

Neutrophil migration requires the interaction between adhesion molecules present on neutrophils and vascular endothelium (Nourshargh and Alon, 2014). Classic neutrophil recruitment involves different steps such as capture, rolling, adhesion, crawling, and subsequent transmigration towards inflammatory signals (Kolaczkowska and Kubes, 2013). Several works have demonstrated the usually low concentrations of ouabain impairs mice neutrophil migration into different tissues. Leite et al. (2015) showed that ouabain reduces neutrophil migration into the peritoneal cavity induced zymosan. Similar findings were obtained using *L. amazonensis* as an inflammatory stimulus (Jacob et al., 2013). Other works provide evidence that ouabain also inhibits neutrophil transmigration into lung tissue in mice models of inflammatory allergy (Galvão et al., 2017) and acute pulmonary injury (Wang et al., 2018). *In vitro* studies also presented the inhibitory effect of ouabain on rabbit (Ward and Becker, 1970), human (Ray and Samanta, 1997), and mice neutrophil chemotaxis (Cavalcante-Silva et al., 2021a). The cardiotonic steroid marinobufagenin also reduces neutrophil migration during inflammation, corroborating the ouabain effect (Carvalho et al., 2019) (**Figure 1B**).

The exact mechanism of action of ouabain in impairment neutrophil migration remains to be fully elucidated, however, some evidence is emerging. Chemoattractant gradients trigger neutrophils intracellular signaling that guides these cells towards inflammatory tissues. The MAPK signaling mediates neutrophils chemotaxis (Liew and Kubes, 2019). It was observed that ouabain reduces p38 phosphorylation, but not ERK activation in mice neutrophils (Cavalcante-Silva L. H. A. et al., 2021). Neutrophil's receptors, including adhesion molecules, can be regulated by p38 MAPK-dependent signaling (Kim and Haynes, 2013). Indeed, ouabain can reduce α (Ninsontia and Chanvorachote, 2014) and β (Cavalcante-Silva et al., 2020) integrins in different types of cells, nevertheless the real impact of this effects in neutrophil migration should still be addressed. On the other hand, ouabain does not reduce the chemokine receptor CXCR2 expression in mice neutrophils or modulates the levels of its ligands CXCL1 (Cavalcante-Silva et al., 2020). However, in human neutrophils, ouabain interferes with chemokine receptor (CXCR1/2) recycling, which in turns decreases neutrophil migration (Ray and Samanta, 1997).

Additionally, in models of peritoneal (Leite et al., 2015) and pulmonary (Wang et al., 2018) inflammation, ouabain also inhibits NF-κB pathway. The activation of this transcription factor is associated with release of proinflammatory cytokines, which in turn stimulates endothelial and immune cells (Netea et al., 2017). In fact, ouabain reduces TNF-α and IL-β release (Leite et al., 2015), therefore this may be associated with impaired migration of neutrophils. Moreover, in A549 cells, this steroid decreases the TNF-α-induced expression of ICAM-1, an adhesion molecule that binds integrin (Takada et al., 2009).

The mechanisms used by neutrophils during an immune response include phagocytosis, NETs, formation of reactive oxygen species and release of microbicidal molecules contained in cytoplasmic granules (i.e., myeloperoxidase, neutrophilic elastase, and others) (Yang et al., 2017). Neutrophils also produce different cytokines (eg, IL-1Ra, IL-12, IL-23, TNF-α, G-CSF, among others) and chemokines (eg, CXCL-1, CCL-20, CCL-2, among others) that modulate the immune response (Mantovani et al., 2011; Yang et al., 2017; Burn et al., 2021). In human neutrophils, it has been shown that ouabain at 100 nM induces DNA release, without promote necrosis, suggesting NETs release (Silva et al., 2021). Additionally, in rat neutrophils, ouabain reduces generation of free radical induced by NO donors, this effect could be related to membrane depolarization (Patel et al., 2009).

Although studies have shown that ouabain interferes with neutrophil infiltration induced by different stimuli in the periphery, such as concanavalin A (de Vasconcelos et al., 2011), Zimosan (Leite et al., 2015), ovalbumin (Galvão et al., 2017) and *Leishmania amazonensis* (Jacob et al., 2013), as well as the activation of these cells, since ouabain modulate the generation of free radicals induced by nitric oxide donors (Patel et al., 2009) and the release of NETs (Silva et al., al, 2021), studies lack data about ouabain modulation on neutrophils in the neuroinflammation; however, a study observed the presence of neutrophils in a model of ouabain-induced injury in zebrafish. Mitchell et al. (2018)

observed that the retinal lesion resulting from the administration of ouabain was accompanied by an early leukocyte infiltration, followed by a period in which there was proliferation of immune cells, possibly from the resident microglia and macrophages derived from extra-retinal regions. Furthermore, the presence of neutrophils was observed in the vitreous leukocyte population, identified by the expression of myeloid-specific peroxidase (mpx) +, supporting that retinal injury induced by ouabain is accompanied by an early migration of leukocytes from the bloodstream. After 24, 48 and 72 h of ouabain administration, very few mpx + neutrophils were identified, suggesting that there was no significant increase in the number of neutrophils at these times (Mitchell et al., 2018).

Despite there is no compelling data on the effects of ouabain and its receptor, NKA, on neutrophil dynamics in neuroinflammatory diseases, robust studies point to the importance of ouabain-NKA signaling in neuroinflammation (reviewed in Orellana et al., 2016; Leite et al., 2020). In addition, the immunomodulatory role of ouabain in neutrophil dynamics has been observed in classical models of peripheral inflammation (Leite et al., 2015; Cavalcante-Silva et al., 2020). These data together suggest that ouabain-NKA signaling may be an important marker to be investigated in neutrophil dynamics in neuroinflammatory diseases, thus favoring a better understanding of the pathophysiology involved in the progression of these diseases, as well as aiding in the discovery of new strategies for neurodegenerative diseases.

AUTHOR CONTRIBUTIONS

Elaborated the figure and wrote the manuscript: JL, LC-S, MR, and GdM. Reviewed topics and concepts: CS and SR-M. Conceived, reviewed and discussed concepts in the manuscript: CS and SR-M. All authors contributed to the article and approved the submitted version.

FUNDING

This publication was made possible by grants from São Paulo Research Foundation (FAPESP) (2016/07427-8); National Council for Scientific and Technological Development (CNPq 405089/2018-0); and Coordenação de Aperfeiçoamento de Pessoal de Nível SuperiorCAPES (CAPES—STINT program 88887.125409/2016-00–Joint Brazilian-Swedish Research Collaboration) and USP Neuroscience Research Support Centres (NAPNA) to CS. JL was a research fellow from FAPESP, and MR, and GdM are Ph.D. fellowship from CNPq; CS and SR-M are research fellows of CNPq.

ACKNOWLEDGMENTS

We thank Elsevier Author Service for English Editing, and Larissa de Sá Lima for technical support. **Figure 1** was created with BioRender.com.

REFERENCES

Akira, S., Uematsu, S., and Takeuchi, O. (2006). Pathogen Recognition and Innate Immunity. *Cell* 124, 783–801. doi:10.1016/J.CELL.2006.02.015

Alpert, J. S. (2021). Is Digitalis Therapy Still Viable? Foxglove Therapy Makes a Comeback. *Am. J. Med.* 134, 1–2. doi:10.1016/J.AMJMED.2020.09.001

Bagrov, A. Y., Shapiro, J. I., and Fedorova, O. V. (2009). Endogenous Cardiotonic Steroids: Physiology, Pharmacology, and Novel Therapeutic Targets. *Pharmacol. Rev.* 61, 9–38. doi:10.1124/pr.108.000711

Bautista-Becerril, B., Campi-Caballero, R., Sevilla-Fuentes, S., Hernández-Regino, L. M., Hanono, A., Flores-Bustamante, A., et al. (2021). Immunothrombosis in Covid-19: Implications of Neutrophil Extracellular Traps. *Biomolecules* 11. 694. doi:10.3390/biom11050694

Blanco, G., and Mercer, R. W. (1998). Isozymes of the Na-K-ATPase: Heterogeneity in Structure, Diversity in Function. *Am. J. Physiol.* 275, F633–F650. doi:10.1152/AJPRENAL.1998.275.5.F633

Blaustein, M. P., and Hamlyn, J. M. (2020). Ouabain, Endogenous Ouabain and Ouabain-like Factors: The Na+ Pump/ouabain Receptor, its Linkage to NCX, and its Myriad Functions. *Cell Calcium* 86, 102159. doi:10.1016/j.ceca.2020.102159

Burn, G. L., Foti, A., Marsman, G., Patel, D. F., and Zychlinsky, A. (2021). The Neutrophil. *Immunity* 54, 1377–1391. doi:10.1016/J.IMMUNI.2021.06.006

Carvalho, D. C. M., Cavalcante-Silva, L. H. A., Lima, É. A., Galvão, J. G. F. M., Alves, A. K. A., Feijó, P. R. O., et al. (2019). Marinobufagenin Inhibits Neutrophil Migration and Proinflammatory Cytokines. *J. Immunol. Res.* 2019, 1–11. doi:10.1155/2019/1094520

Cavalcante-Silva, L. H. A., Carvalho, D. C. M., Lima, É. A., Galvão, J. G. F. M., da Silva, J. S. F., Sales-Neto, J. M., et al. (2021b). Neutrophils and COVID-19: The Road So Far. *Int. Immunopharmacol.* 90, 107233. doi:10.1016/j.intimp.2020.107233

Cavalcante-Silva, L. H. A., Lima, É. A., Carvalho, D. C. M., de Sales-Neto, J. M., Alves, A. K. A., Galvão, J. G. F. M., et al. (2017). Much More Than a Cardiotonic Steroid: Modulation of Inflammation by Ouabain. *Front. Physiol.* 8, 895. doi:10.3389/fphys.2017.00895

Cavalcante-Silva, L. H. A., Lima, É. A., Carvalho, D. C. M., and Rodrigues-Mascarenhas, S. (2020). Ouabain Reduces the Expression of the Adhesion Molecule CD18 in Neutrophils. *Inflammopharmacology* 28, 787–793. doi:10.1007/s10787-019-00602-8

Cavalcante-Silva, L. H. A., Carvalho, D. C. M., de Almeida Lima, É., and Rodrigues-Mascarenhas, S. (2021a). Ouabain Inhibits P38 Activation in Mice Neutrophils. *Inflammopharmacol* 29, 1829–1833. doi:10.1007/S10787-021-00882-Z

Chen, Y., Huang, W., Yang, M., Xin, G., Cui, W., Xie, Z., et al. (2017). Cardiotonic Steroids Stimulate Macrophage Inflammatory Responses through a Pathway Involving CD36, TLR4, and Na/K-ATPase. *Arterioscler. Thromb. Vasc. Biol.* 37, 1462–1469. doi:10.1161/ATVBAHA.117.309444

Christy, A. L., Walker, M. E., Hessner, M. J., and Brown, M. A. (2013). Mast Cell Activation and Neutrophil Recruitment Promotes Early and Robust Inflammation in the Meninges in EAE. *J. Autoimmun.* 42, 50–61. doi:10.1016/J.JAUT.2012.11.003

Cuartero, M. I., Ballesteros, I., Moraga, A., Nombela, F., Vivancos, J., Hamilton, J. A., et al. (2013). N2 Neutrophils, Novel Players in Brain Inflammation after Stroke: Modulation by the PPARγ Agonist Rosiglitazone. *Stroke* 44, 3498–3508. doi:10.1161/STROKEAHA.113.002470

Cui, X., and Xie, Z. (2017). Protein Interaction and Na/K-ATPase-Mediated Signal Transduction. *Molecules* 22. doi:10.3390/molecules22060990

da Silva, J. M., das Neves Azevedo, A., dos Santos Barbosa, R. P., Vianna, T. A., Fittipaldi, J., Teixeira, M. P., et al. (2016). Dynamics of Murine B Lymphocytes Is Modulated by *In Vivo* Treatment with Steroid Ouabain. *Immunobiology* 221, 368–376. doi:10.1016/j.imbio.2015.09.020

de Paiva, L. S., Costa, K. M., Canto, F. B., Cabral, V. R., Fucs, R., Nobrega, A., et al. (2011). Modulation of Mature B Cells in Mice Following Treatment with Ouabain. *Immunobiology* 216, 1038–1043. doi:10.1016/j.imbio.2011.03.002

de Vasconcelos, D. I. B., Leite, J. A., Carneiro, L. T., Piuvezam, M. R., de Lima, M. R. V., de Morais, L. C. L., et al. (2011). Anti-inflammatory and Antinociceptive Activity of Ouabain in Mice. *Mediators Inflamm.* 2011, 1–11. doi:10.1155/2011/912925

Dinkel, K., Dhabhar, F. S., and Sapolsky, R. M. (2004). Neurotoxic Effects of Polymorphonuclear Granulocytes on Hippocampal Primary Cultures. *Proc. Natl. Acad. Sci. U. S. A.* 101, 331–336. doi:10.1073/PNAS.0303510101

Doty, K. R., Guillot-Sestier, M. V., and Town, T. (2015). The Role of the Immune System in Neurodegenerative Disorders: Adaptive or Maladaptive. *Brain Res.* 1617, 155–173. doi:10.1016/J.BRAINRES.2014.09.008

Du, J., Jiang, L., Chen, F., Hu, H., and Zhou, M. (2021). Cardiac Glycoside Ouabain Exerts Anticancer Activity via Downregulation of STAT3. *Front. Oncol.* 11. 1275. doi:10.3389/FONC.2021.684316

Dvela, M., Rosen, H., Feldmann, T., Nesher, M., and Lichtstein, D. (2007). Diverse Biological Responses to Different Cardiotonic Steroids. *Pathophysiology* 14, 159–166. doi:10.1016/J.PATHOPHYS.2007.09.011

Ellman, D. G., Isaksen, T. J., Lund, M. C., Dursun, S., Wirenfeldt, M., Jørgensen, L. H., et al. (2017). The Loss-Of-Function Disease-Mutation G301R in the Na+/K+-ATPase α2 Isoform Decreases Lesion Volume and Improves Functional Outcome after Acute Spinal Cord Injury in Mice. *BMC Neurosci.* 18, 66. doi:10.1186/S12868-017-0385-9

Fan, X., Xie, J., and Tian, J. (2017). Reducing Cardiac Fibrosis: Na/K-ATPase Signaling Complex as a Novel Target. *Cardiovasc. Pharm. Open Access* 6. 204. doi:10.4172/2329-6607.1000204

Ferrandi, M., Manunta, P., Balzan, S., Hamlyn, J. M., Bianchi, G., and Ferrari, P. (1997). Ouabain-like Factor Quantification in Mammalian Tissues and Plasma: Comparison of Two Independent Assays. *Hypertension* 30, 886–896. doi:10.1161/01.HYP.30.4.886

Foey, A. D., Crawford, A., and Hall, N. D. (1997). Modulation of Cytokine Production by Human Mononuclear Cells Following Impairment of Na, K-ATPase Activity. *Biochim. Biophys. Acta* 1355, 43–49. doi:10.1016/S0167-4889(96)00116-4

Forshammar, J., Block, L., Lundborg, C., Biber, B., and Hansson, E. (2011). Naloxone and Ouabain in Ultralow Concentrations Restore Na+/K+-ATPase and Cytoskeleton in Lipopolysaccharide-Treated Astrocytes. *J. Biol. Chem.* 286, 31586–31597. doi:10.1074/JBC.M111.247767

Forshammar, J., Jörneberg, P., Björklund, U., Westerlund, A., Lundborg, C., Biber, B., et al. (2013). Anti-inflammatory Substances Can Influence Some Glial Cell Types but Not Others. *Brain Res.* 1539, 34–40. doi:10.1016/J.BRAINRES.2013.09.052

Gallardo, G., Barowski, J., Ravits, J., Siddique, T., Lingrel, J. B., Robertson, J., et al. (2014). An α2-Na/K ATPase/α-Adducin Complex in Astrocytes Triggers Non-cell Autonomous Neurodegeneration. *Nat. Neurosci.* 17, 1710–1719. doi:10.1038/NN.3853

Galvão, J. G. F. M., Cavalcante-Silva, L. H. A., Carvalho, D. C. M., Ferreira, L. K. D. P., Monteiro, T. M., Alves, A. F., et al. (2017). Ouabain Attenuates Ovalbumin-Induced Airway Inflammation. *Inflamm. Res.* 66, 1117–1130. doi:10.1007/s00011-017-1092-9

García-Culebras, A., Durán-Laforet, V., Peña-Martínez, C., Moraga, A., Ballesteros, I., Cuartero, M. I., et al. (2019). Role of TLR4 (Toll-like Receptor 4) in N1/N2 Neutrophil Programming after Stroke. *Stroke* 50, 2922–2932. doi:10.1161/STROKEAHA.119.025085

Gonçalves-de-Albuquerque, C. F., Burth, P., Silva, A. R., de Moraes, I. M., Oliveira, F. M., Santelli, R. E., et al. (2014). Murine Lung Injury Caused by Leptospira Interrogans Glycolipoprotein, a Specific Na/K-ATPase Inhibitor. *Respir. Res.* 15, 93. doi:10.1186/s12931-014-0093-2

Hamlyn, J. M., Blaustein, M. P., Bova, S., DuCharme, D. W., Harris, D. W., Mandel, F., et al. (1991). Identification and Characterization of a Ouabain-like Compound from Human Plasma. *Proc. Natl. Acad. Sci. U. S. A.* 88, 6259–6263. Available at:http://www.ncbi.nlm.nih.gov/pubmed/1648735 (Accessed December 13, 2018). doi:10.1073/pnas.88.14.6259

Hawkes, C. A., and McLaurin, J. (2009). Selective Targeting of Perivascular Macrophages for Clearance of Beta-Amyloid in Cerebral Amyloid Angiopathy. *Proc. Natl. Acad. Sci. U. S. A.* 106, 1261–1266. doi:10.1073/PNAS.0805453106

Hellebrekers, P., Vrisekoop, N., and Koenderman, L. (2018). Neutrophil Phenotypes in Health and Disease. *Eur. J. Clin. Invest.* 48 Suppl 2, e12943. doi:10.1111/eci.12943

Herz, J., Sabellek, P., Lane, T. E., Gunzer, M., Hermann, D. M., and Doeppner, T. R. (2015). Role of Neutrophils in Exacerbation of Brain Injury after Focal Cerebral Ischemia in Hyperlipidemic Mice. *Stroke* 46, 2916–2925. doi:10.1161/STROKEAHA.115.010620

Hidalgo, A., Chilvers, E. R., Summers, C., and Koenderman, L. (2019). The Neutrophil Life Cycle. *Trends Immunol.* 40, 584–597. doi:10.1016/j.it.2019.04.013

Hou, Y., Yang, D., Xiang, R., Wang, H., Wang, X., Zhang, H., et al. (2019). N2 Neutrophils May Participate in Spontaneous Recovery after Transient Cerebral Ischemia by Inhibiting Ischemic Neuron Injury in Rats. *Int. Immunopharmacol.* 77, 105970. doi:10.1016/J.INTIMP.2019.105970

Huh, J. R., Leung, M. W., Huang, P., Ryan, D. A., Krout, M. R., Malapaka, R. R., et al. (2011). Digoxin and its Derivatives Suppress TH17 Cell Differentiation by Antagonizing RORγt Activity. *Nature* 472, 486–490. doi:10.1038/nature09978

Isaksen, T. J., and Lykke-Hartmann, K. (2016). Insights into the Pathology of the α2-Na(+)/K(+)-ATPase in Neurological Disorders; Lessons from Animal Models. *Front. Physiol.* 7, 161. doi:10.3389/FPHYS.2016.00161

Jacob, P. L., Leite, J. A., Alves, A. K., Rodrigues, Y. K., Amorim, F. M., Néris, P. L., et al. (2013). Immunomodulatory Activity of Ouabain in Leishmania Leishmania Amazonensis-Infected Swiss Mice. *Parasitol. Res.* 112, 1313–1321. doi:10.1007/s00436-012-3146-9

Jones, H. R., Robb, C. T., Perretti, M., and Rossi, A. G. (2016). The Role of Neutrophils in Inflammation Resolution. *Semin. Immunol.* 28, 137–145. doi:10.1016/j.smim.2016.03.007

Kanashiro, A., Hiroki, C. H., da Fonseca, D. M., Birbrair, A., Ferreira, R. G., Bassi, G. S., et al. (2020). The Role of Neutrophils in Neuro-Immune Modulation. *Pharmacol. Res.* 151, 104580. doi:10.1016/J.PHRS.2019.104580

Kang, J., Jiang, M. H., Min, H. J., Jo, E. K., Lee, S., Karin, M., et al. (2011). IKK-β-mediated Myeloid Cell Activation Exacerbates Inflammation and Inhibits Recovery after Spinal Cord Injury. *Eur. J. Immunol.* 41, 1266–1277. doi:10.1002/EJI.201040582

Kennedy, D. J., Chen, Y., Huang, W., Viterna, J., Liu, J., Westfall, K., et al. (20131979). CD36 and Na/K-ATPase-A1 Form a Proinflammatory Signaling Loop in Kidney. *Hypertension* 61, 216–224. doi:10.1161/HYPERTENSIONAHA.112.198770

Kim, D., and Haynes, C. L. (2013). The Role of P38 MAPK in Neutrophil Functions: Single Cell Chemotaxis and Surface Marker Expression. *Analyst* 138, 6826–6833. doi:10.1039/c3an01076g

Kinoshita, P. F., Yshii, L. M., Orellana, A. M. M., Paixão, A. G., Vasconcelos, A. R., Lima, L. S., et al. (2017). Alpha 2 Na+,K+-ATPase Silencing Induces Loss of Inflammatory Response and Ouabain protection in Glial Cells. *Sci. Rep.* 7, 4894. doi:10.1038/s41598-017-05075-9

Kinoshita, P. F., Yshii, L. M., Vasconcelos, A. R., Orellana, A. M., Lima, Lde. S., Davel, A. P., et al. (2014). Signaling Function of Na,K-ATPase Induced by Ouabain against LPS as an Inflammation Model in hippocampus. *J. Neuroinflammation* 11, 218. doi:10.1186/s12974-014-0218-z

Kolaczkowska, E., and Kubes, P. (2013). Neutrophil Recruitment and Function in Health and Inflammation. *Nat. Rev. Immunol.* 13, 159–175. doi:10.1038/nri3399

Lampron, A., Pimentel-Coelho, P. M., and Rivest, S. (2013). Migration of Bone Marrow-Derived Cells into the central Nervous System in Models of Neurodegeneration. *J. Comp. Neurol.* 521, 3863–3876. doi:10.1002/CNE.23363

Lancaster, M. C., and Vegad, J. L. (1967). Suppression of the Early Inflammatory Response in the Sheep by Strophanthin G. *Nature* 213, 840–841. doi:10.1038/213840b0

Laredo, J., Hamilton, B. P., and Hamlyn, J. M. (1994). Ouabain Is Secreted by Bovine Adrenocortical Cells. *Endocrinology* 135, 794–797. doi:10.1210/endo.135.2.8033829

Laredo, J., Hamilton, B. P., and Hamlyn, J. M. (1995). Secretion of Endogenous Ouabain from Bovine Adrenocortical Cells: Role of the Zona Glomerulosa and Zona Fasciculata. *Biochem. Biophys. Res. Commun.* 212, 487–493. doi:10.1006/bbrc.1995.1996

Leite, J. A., Alves, A. K., Galvão, J. G., Teixeira, M. P., Cavalcante-Silva, L. H., Scavone, C., et al. (2015). Ouabain Modulates Zymosan-Induced Peritonitis in Mice. *Mediators Inflamm.* 2015, 1–12. doi:10.1155/2015/265798

Leite, J. A., Isaksen, T. J., Heuck, A., Scavone, C., and Lykke-Hartmann, K. (2020). The α2 Na+/K+-ATPase Isoform Mediates LPS-Induced Neuroinflammation. *Sci. Rep.* 10, 14180. doi:10.1038/S41598-020-71027-5

Leliefeld, P. H., Wessels, C. M., Leenen, L. P., Koenderman, L., and Pillay, J. (2016). The Role of Neutrophils in Immune Dysfunction during Severe Inflammation. *Crit. Care* 20, 73. doi:10.1186/s13054-016-1250-4

Liew, P. X., and Kubes, P. (2019). The Neutrophil's Role during Health and Disease. *Physiol. Rev.* 99, 1223–1248. doi:10.1152/physrev.00012.2018

Liu, J., Tian, J., Haas, M., Shapiro, J. I., Askari, A., and Xie, Z. (2000). Ouabain Interaction with Cardiac Na+/K+-ATPase Initiates Signal Cascades Independent of Changes in Intracellular Na+ and Ca2+ Concentrations. *J. Biol. Chem.* 275, 27838–27844. doi:10.1074/jbc.M002950200

Liu, J., and Xie, Z. J. (2010). The Sodium Pump and Cardiotonic Steroids-Induced Signal Transduction Protein Kinases and Calcium-Signaling Microdomain in Regulation of Transporter Trafficking. *Biochim. Biophys. Acta* 1802, 1237–1245. doi:10.1016/j.bbadis.2010.01.013

Mantovani, A., Cassatella, M. A., Costantini, C., and Jaillon, S. (2011). Neutrophils in the Activation and Regulation of Innate and Adaptive Immunity. *Nat. Rev. Immunol.* 11, 519–531. doi:10.1038/nri3024

Markov, A. G., Fedorova, A. A., Kravtsova, V. V., Bikmurzina, A. E., Okorokova, L. S., Matchkov, V. V., et al. (2020). Circulating Ouabain Modulates Expression of Claudins in Rat Intestine and Cerebral Blood Vessels. *Int. J. Mol. Sci.* 21, 1–16. doi:10.3390/IJMS21145067

Matozzo, F. H., Votto, A. P. S., Rodrigues-Mascarenhas, S., Cavalcante-Silva, L. H. A., Valente, R. C., and Rumjanek, V. M. (2020). Ouabain as an Anti-cancer Agent. *Curr. Top. Biochem. Res.* 21, 25–40. Available at: http://www.researchtrends.net/tia/abstract.asp?in=0&vn=21&tid=40&aid=6579&pub=2020&type=3 (Accessed January 9, 2022).

Matsumori, A., Ono, K., Nishio, R., Igata, H., Shioi, T., Matsui, S., et al. (1997). Modulation of Cytokine Production and protection against Lethal Endotoxemia by the Cardiac Glycoside Ouabain. *Circulation* 96, 1501–1506. doi:10.1161/01.CIR.96.5.1501

Mázala-de-Oliveira, T., de Figueiredo, C. S., de Rezende Corrêa, G., da Silva, M. S., Miranda, R. L., de Azevedo, M. A., et al. (2021). Ouabain-Na+/K+-ATPase Signaling Regulates Retinal Neuroinflammation and ROS Production Preventing Neuronal Death by an Autophagy-dependent Mechanism Following Optic Nerve Axotomy *In Vitro*. *Neurochem. Res.* 2021, 1–16. doi:10.1007/S11064-021-03481-0

Minns, D., Smith, K. J., and Findlay, E. G. (2019). Orchestration of Adaptive T Cell Responses by Neutrophil Granule Contents. *Mediators Inflamm.* 2019, 1–15. doi:10.1155/2019/8968943

Mishalian, I., Granot, Z., and Fridlender, Z. G. (2017). The Diversity of Circulating Neutrophils in Cancer. *Immunobiology* 222, 82–88. doi:10.1016/j.imbio.2016.02.001

Mitchell, D. M., Lovel, A. G., and Stenkamp, D. L. (2018). Dynamic Changes in Microglial and Macrophage Characteristics during Degeneration and Regeneration of the Zebrafish Retina. *J. Neuroinflammation* 15, 163. doi:10.1186/S12974-018-1185-6

Nascimento, C. R., Valente, R. C., Echevarria-Lima, J., Fontes, C. F. L., de Araujo-Martins, L., Araujo, E. G., et al. (2014). The Influence of Ouabain on Human Dendritic Cells Maturation. *Mediators Inflamm.* 2014, 1–15. doi:10.1155/2014/494956

Netea, M. G., Balkwill, F., Chonchol, M., Cominelli, F., Donath, M. Y., Giamarellos-Bourboulis, E. J., et al. (2017). A Guiding Map for Inflammation. *Nat. Immunol.* 18, 826–831. doi:10.1038/NI.3790

Neumann, J., Riek-Burchardt, M., Herz, J., Doeppner, T. R., König, R., Hütten, H., et al. (2015). Very-late-antigen-4 (VLA-4)-Mediated Brain Invasion by Neutrophils Leads to Interactions with Microglia, Increased Ischemic Injury and Impaired Behavior in Experimental Stroke. *Acta Neuropathol.* 129, 259–277. doi:10.1007/S00401-014-1355-2

Nguyen, H. X., O'Barr, T. J., and Anderson, A. J. (2007). Polymorphonuclear Leukocytes Promote Neurotoxicity through Release of Matrix Metalloproteinases, Reactive Oxygen Species, and TNF-Alpha. *J. Neurochem.* 102, 900–912. doi:10.1111/J.1471-4159.2007.04643.X

Ninsontia, C., and Chanvorachote, P. (2014). Ouabain Mediates Integrin Switch in Human Lung Cancer Cells. *Anticancer Res.* 34, 5495–5502. Available at: http://www.ncbi.nlm.nih.gov/pubmed/25275046 (Accessed December 2, 2017).

Nourshargh, S., and Alon, R. (2014). Leukocyte Migration into Inflamed Tissues. *Immunity* 41, 694–707. doi:10.1016/J.IMMUNI.2014.10.008

Ocana, A., Nieto-Jiménez, C., Pandiella, A., and Templeton, A. J. (2017). Neutrophils in Cancer: Prognostic Role and Therapeutic Strategies. *Mol. Cancer* 16, 137. doi:10.1186/s12943-017-0707-7

Okazaki, T., Ilea, V. S., Okazaki, A., Wicher, K., Reisman, R. E., and Arbesman, C. E. (1976). Inhibition of Antigen-Induced Histamine Release by Ouabain. *J. Allergy Clin. Immunol.* 57, 454–462. doi:10.1016/0091-6749(76)90061-0

Olej, B., de La Rocque, L., Castilho, F. P., Mediano, I. F., Campos, M. M., and Rumjanek, V. M. (1994). Effect of Ouabain on Lymphokine-Activated Killer Cells. *Int. J. Immunopharmacol.* 16, 769–774. doi:10.1016/0192-0561(94)90097-3

O'Neil, L. J., and Kaplan, M. J. (2019). Neutrophils in Rheumatoid Arthritis: Breaking Immune Tolerance and Fueling Disease. *Trends Mol. Med.* 25, 215–227. doi:10.1016/J.MOLMED.2018.12.008

Orellana, A. M., Kinoshita, P. F., Leite, J. A., Kawamoto, E. M., and Scavone, C. (2016). Cardiotonic Steroids as Modulators of Neuroinflammation. *Front. Endocrinol. (Lausanne)* 7, 10. doi:10.3389/fendo.2016.00010

Pamnani, M. B., Buggy, J., Huot, S. J., and Haddy, F. J. (1981). Studies on the Role of a Humoral Sodium-Transport Inhibitor and the Anteroventral Third Ventricle (AV3V) in Experimental Low-Renin Hypertension. *Clin. Sci. (Lond)* 61 Suppl 7, 57s–60s. doi:10.1042/CS061057S

Parackova, Z., Bloomfield, M., Klocperk, A., and Sediva, A. (2021). Neutrophils Mediate Th17 Promotion in COVID-19 Patients. *J. Leukoc. Biol.* 109, 73–76. doi:10.1002/JLB.4COVCRA0820-481RRR

Patel, S., Vemula, J., Konikkat, S., Barthwal, M. K., and Dikshit, M. (2009). Ion Channel Modulators Mediated Alterations in NO-Induced Free Radical Generation and Neutrophil Membrane Potential. *Free Radic. Res.* 43, 514–521. doi:10.1080/10715760902887276

Phillipson, M., and Kubes, P. (2019). The Healing Power of Neutrophils. *Trends Immunol.* 40, 635–647. doi:10.1016/j.it.2019.05.001

Pierson, E. R., Wagner, C. A., and Goverman, J. M. (2018). The Contribution of Neutrophils to CNS Autoimmunity. *Clin. Immunol.* 189, 23–28. doi:10.1016/J.CLIM.2016.06.017

Ray, E., and Samanta, A. K. (1997). Receptor-mediated Endocytosis of IL-8: a Fluorescent Microscopic Evidence and Implication of the Process in Ligand-Induced Biological Response in Human Neutrophils. *Cytokine* 9, 587–596. doi:10.1006/cyto.1997.0206

Rodrigues Mascarenhas, S., Echevarria-Lima, J., Fernandes dos Santos, N., and Rumjanek, V. M. (2003). CD69 Expression Induced by Thapsigargin, Phorbol Ester and Ouabain on Thymocytes Is Dependent on External Ca2+ Entry. *Life Sci.* 73, 1037–1051. Available at: http://www.ncbi.nlm.nih.gov/pubmed/12818356 (Accessed November 27, 2017). doi:10.1016/s0024-3205(03)00377-1

Rodrigues-Mascarenhas, S., Bloise, F. F., Moscat, J., and Rumjanek, V. M. (2008). Ouabain Inhibits P38 Activation in Thymocytes. *Cell Biol. Int.* 32, 1323–1328. doi:10.1016/j.cellbi.2008.07.012

Rodrigues-Mascarenhas, S., Da Silva de Oliveira, A., Amoedo, N. D., Affonso-Mitidieri, O. R., Rumjanek, F. D., and Rumjanek, V. M. (2009). Modulation of the Immune System by Ouabain. *Ann. N. Y. Acad. Sci.* 1153, 153–163. doi:10.1111/j.1749-6632.2008.03969.x

Sas, A. R., Carbajal, K. S., Jerome, A. D., Menon, R., Yoon, C., Kalinski, A. L., et al. (2020). A New Neutrophil Subset Promotes CNS Neuron Survival and Axon Regeneration. *Nat. Immunol.* 21, 1496–1505. doi:10.1038/S41590-020-00813-0

Schneider, N. F. Z., Cerella, C., Simões, C. M. O., and Diederich, M. (2017). Anticancer and Immunogenic Properties of Cardiac Glycosides. *Molecules* 22. 1932. doi:10.3390/MOLECULES22111932

Silva, L., Carvalho, D., Lima, E., Nadaes, N., Saraiva, E., and Mascarenhas, S. (2021). Ouabain Triggers Neutrophil Extracellular Traps in Human Neutrophils.6th European Congress of Immunology, 1–4 September 2021, Virtual meeting: European Journal of Immunology: vol 51, No S1, Available at: https://onlinelibrary.wiley.com/toc/15214141/2021/51/S1 (Accessed November 13, 2021).

Simmons, S. B., Liggitt, D., and Goverman, J. M. (2014). Cytokine-regulated Neutrophil Recruitment Is Required for Brain but Not Spinal Cord Inflammation during Experimental Autoimmune Encephalomyelitis. *J. Immunol.* 193, 555–563. doi:10.4049/JIMMUNOL.1400807

Škubník, J., Pavlíčková, V., Rimpelová, S., Atkin-Smith, G., Tixeira, R., and Baxter, A. A. (2021). Cardiac Glycosides as Immune System Modulators. *Biomolecules* 11, 659. doi:10.3390/BIOM11050659

Smolyaninova, L. V., Dergalev, A. A., Kulebyakin, K. Y., Carpenter, D. O., and Boldyrev, A. A. (2013). Carnosine Prevents Necrotic and Apoptotic Death of

Rat Thymocytes via Ouabain-Sensitive Na/K-ATPase. *Cell Biochem. Funct.* 31, 30–35. doi:10.1002/cbf.2856

Stock, A. J., Kasus-Jacobi, A., and Pereira, H. A. (2018). The Role of Neutrophil Granule Proteins in Neuroinflammation and Alzheimer's Disease. *J. Neuroinflammation* 15, 240. doi:10.1186/S12974-018-1284-4

Szamel, M., Schneider, S., and Resch, K. (1981). Functional Interrelationship between (Na+ + K+)-ATPase and Lysolecithin Acyltransferase in Plasma Membranes of Mitogen-Stimulated Rabbit Thymocytes. *J. Biol. Chem.* 256, 9198–9204. Available at: http://www.ncbi.nlm.nih.gov/pubmed/6267065 (Accessed January 16, 2020). doi:10.1016/s0021-9258(19)52528-5

Takada, Y., Matsuo, K., Ogura, H., Bai, L., Toki, A., Wang, L., et al. (2009). Odoroside A and Ouabain Inhibit Na+/K+-ATPase and Prevent NF-kappaB-Inducible Protein Expression by Blocking Na+-dependent Amino Acid Transport. *Biochem. Pharmacol.* 78, 1157–1166. doi:10.1016/j.bcp.2009.06.027

Teixeira, M. P., and Rumjanek, V. M. (2014). Ouabain Affects the Expression of Activation Markers, Cytokine Production, and Endocytosis of Human Monocytes. *Mediators Inflamm.* 2014, 760368. doi:10.1155/2014/760368

Valente, R. C., Nascimento, C. R., Araujo, E. G., and Rumjanek, V. M. (2009). mCD14 Expression in Human Monocytes Is Downregulated by Ouabain via Transactivation of Epithelial Growth Factor Receptor and Activation of P38 Mitogen-Activated Protein Kinase. *Neuroimmunomodulation* 16, 228–236. doi:10.1159/000212383

Wang, C., Meng, Y., Wang, Y., Jiang, Z., Xu, M., Bo, L., et al. (2018). Ouabain Protects Mice against Lipopolysaccharide-Induced Acute Lung Injury. *Med. Sci. Monit.* 24, 4455–4464. doi:10.12659/MSM.908627

Ward, P. A., and Becker, E. L. (1970). Potassium Reversible Inhibition of Leukotaxis by Ouabain. *Life Sci.* 9, 355–360. Available at: http://www.ncbi.nlm.nih.gov/pubmed/4315650 (Accessed December 1, 2017).

Xie, Z. (2003). Molecular Mechanisms of Na/K-ATPase-Mediated Signal Transduction. *Ann. N.Y Acad. Sci.* 986, 497–503. doi:10.1111/j.1749-6632.2003.tb07234.x

Yang, F., Feng, C., Zhang, X., Lu, J., and Zhao, Y. (2017). The Diverse Biological Functions of Neutrophils, beyond the Defense against Infections. *Inflammation* 40, 311–323. doi:10.1007/s10753-016-0458-4

Zenaro, E., Pietronigro, E., Bianca, V. D., Piacentino, G., Marongiu, L., Budui, S., et al. (2015). Neutrophils Promote Alzheimer's Disease-like Pathology and Cognitive Decline via LFA-1 Integrin. *Nat. Med.* 21, 880–886. doi:10.1038/NM.3913

Zhakeer, Z., Hadeer, M., Tuerxun, Z., and Tuerxun, K. (2017). Bufalin Inhibits the Inflammatory Effects in Asthmatic Mice through the Suppression of Nuclear Factor-Kappa B Activity. *Pharmacology* 99, 179–187. doi:10.1159/000450754

Conflict of Interest: The authors declare that the research was conducted in the absence of any commercial or financial relationships that could be construed as a potential conflict of interest.

Publisher's Note: All claims expressed in this article are solely those of the authors and do not necessarily represent those of their affiliated organizations, or those of the publisher, the editors, and the reviewers. Any product that may be evaluated in this article, or claim that may be made by its manufacturer, is not guaranteed or endorsed by the publisher.

frontiers in Pharmacology

OPINION
published: 15 February 2022
doi: 10.3389/fphar.2022.825948

Tracking TRYCAT: A Critical Appraisal of Kynurenine Pathway Quantifications in Blood

Violette Coppens[1,2]*, *Robert Verkerk*[3] *and Manuel Morrens*[1,2]

[1]Faculty of Medicine and Health Sciences, Collaborative Antwerp Psychiatric Research Institute (CAPRI), University of Antwerp, Antwerp, Belgium, [2]Scientific Initiative of Neuropsychiatric and Psychopharmacological Studies (SINAPS), University Psychiatric Centre Duffel, Duffel, Belgium, [3]Laboratory of Medical Biochemistry, University of Antwerp, Antwerp, Belgium

Keywords: psychiatry, kynurenine, tryptophan, depression, mood disorder, schizophrenia

INTRODUCTION

Immune dysregulation contributes extensively to the pathophysiology of multiple psychiatric illnesses (Coppens et al., 2019; Morrens et al., 2020a). Overall, 95% of the essential amino acid tryptophan (TRP) is degraded to kynurenine and either to its neurotoxic or neuroprotective immunogenic metabolites (see **Figure 1** for a schematic illustration of the kynurenine pathway (KP)). A growing body of evidence testifies the neuromodulatory effects these microglia- or astrocyte-derived tryptophan catabolites (TRYCAT) have on the NMDA receptor. Hence, TRYCAT are hypothesized to link (systemic) immune responses to clinical symptomatology in psychotic and mood disorders.

A series of recent meta-analyses (Morrens et al., 2020b; Hebbrecht et al., 2021; Marx et al., 2021) confirm kynurenine pathway (KP) metabolite aberrances in these psychiatric illnesses in over 100 clinical studies. Unfortunately, the KP research field knows substantial though rarely contemplated pitfalls that warrant caution in the interpretation of findings. The current opinion piece will therefore zoom in on the conceptual validity of peripheral kynurenine metabolite quantification in psychiatric biomarker research. Furthermore, we will discuss the impact of sample heterogeneity, methodological reliability, and validity on study results. To conclude, the authors will put forward conceptual and methodological guidelines for future research into the kynurenine pathway and propositions for relevant future research avenues.

The *Bloody* Brain Barrier

The bulk of literature on TRYCAT in psychiatry concerns quantifying metabolite levels in peripheral blood as a proxy measure for central inflammatory processes. However, as summarized in a recent systematic review by Skorobogatov et al. (2021), only TRP and KYN and to some extent 3-HK fluently travel over the blood–brain barrier (BBB). It remains undefined whether peripheral production of non-crossing metabolites such as kynurenic acid (KA) and quinolinic acid (QUIN) could indirectly reflect central inflammatory processes, for instance, through induction by BBB-crossing macrophages or macrophage-secreted cytokines. Nonetheless, for the metabolites traveling to the periphery over the BBB, extrapolation of the significance of KYN metabolization remains cumbersome. Illustratively, Skorobogatov et al. (2021) describe a strong correlation between peripheral and central KYN concentrations in two studies (Yuwiler et al., 1977; Haroon et al., 2020), while such interrelations remain absent for TRP itself. According to Yuwiler et al. (Yuwiler et al., 1977) and Curzon et al. (Curzon 1979), the observed CNS-periphery discrepancies in a mixed population of Huntington disease patients and healthy controls might be (partially) explained by the fact that most TRYCAT are known to bind circulating albumin (even with high affinity in case of TRP and

OPEN ACCESS

Edited by:
Marta P. Pereira, Spanish National Research Council (CSIC), Spain

Reviewed by:
Pablo Gimenez Gomez, University of Massachusetts Medical School, United States

***Correspondence:**
Violette Coppens
violette.coppens@uantwerpen.be

Specialty section:
This article was submitted to Neuropharmacology, a section of the journal Frontiers in Pharmacology

Received: *30 November 2021*
Accepted: *19 January 2022*
Published: *15 February 2022*

Citation:
Coppens V, Verkerk R and Morrens M (2022) Tracking TRYCAT: A Critical Appraisal of Kynurenine Pathway Quantifications in Blood. Front. Pharmacol. 13:825948. doi: 10.3389/fphar.2022.825948

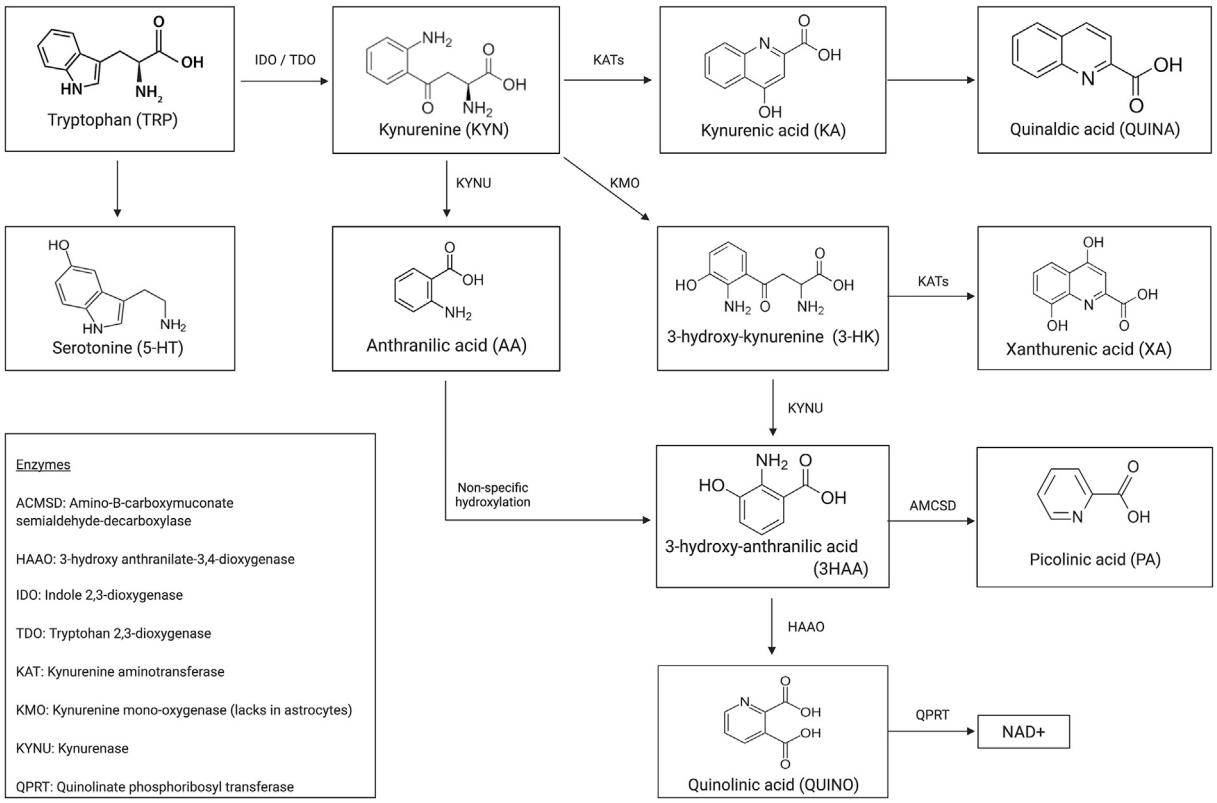

FIGURE 1 | Schematic representation of the kynurenine pathway.

KYN) and that only unbound (free) metabolites can enter the brain (Cangiano et al., 1999). This protein binding is advantageous as it provides a compound reserve in case of a temporal lack of supply. However, factors influencing the rate of albumin binding may intervene in a truthful peripheral representation of the central TRP metabolism. For instance, many drugs such as ibuprofen and valproate, pathology-induced non-esterified fatty acids (NEFAs), and other competing amino acids (tyrosine, phenylalanine, leucine, and valine) (Walker et al., 2019) can displace TRP from its binding site and in so doing directly affect central TRYCAT levels (Yang et al., 2014). Undoubtedly, this contributes substantially to TRYCAT aberrations found in medicated vs. unmedicated patients. Moreover, structural modifiers like glycation (Anguizola et al., 2016) or pH (Walser and Hill 1993) may cause conformational changes to the protein and thereby modify affinities. For detailed discussion, we refer to an excellent review by Feng Yang (Yang et al., 2014).

While their value as peripheral biomarkers for central neuroinflammatory processes remains questionable due to fickle BBB crossing and volatile albumin binding, peripheral TRYCAT levels may "retroactively" influence activity in the brain. *In exemplum*, decreased intracerebral KYN uptake following leucine competition for the active L-type amino acid transporter 1 (LAT1) inhibits depression-like behavior in mice (Walker et al., 2019). Additionally, the essential amino acid TRP inevitably needs to relocate from the periphery to the brain. Again, albumin binding plays a role as only unbound TRP and KYN can bind LAT1 to actively cross the BBB. Whether free or total TRP concentration is the major determinant for *in cerebro* bioavailability remains unelucidated. While centrally, KA is generated in brain astrocytes, skeletal muscle is its major peripheral source of production (Agudelo et al., 2014). As this metabolite is unable to cross the blood–brain barrier and the level of similarity/synchronicity between peripheral and central inflammatory processes is currently undetermined, its suggested anti-inflammatory neuroactive effects may not be directly extrapolatable from its peripheral concentration. At best, somatic metabolization of KYN to KA by kynurenine aminotransferases (KATs) results in lower levels of peripheral KYN available for import in the brain and subsequent central conversion to neurotoxic QUIN. This is indirectly evidenced by experiments with PGC-1a1 overexpression transgenic mice, which specifically upregulate KATs in skeletal muscle and subsequently show elevated blood concentrations of KA, lower (circulating KYN), and stress resistance (Agudelo et al., 2014). This may contribute to the decrease of symptoms observed in depressed patients following physical exercise training. In

reverse, lower baseline KA levels in MDD and SZ patients could originate from decreased muscular production in poorly active patients. Higher levels of non-KA-conversed peripheral KYN increase *in cerebro* bioavailability and could as such induce depression-like behavior, as demonstrated in rodents (O'Connor et al., 2009).

Living the TRYCAT Lifestyle

As illustrated above, muscle movement plays a major role in KA production. A sedentary lifestyle will therefore unquestionably affect kynurenine metabolization (Alme et al., 2021). Previous work showing that most KYN metabolites correlate with BMI (Zahed et al., 2021) indicates that lifestyle influences tryptophan metabolism also at the level of food intake. The amount and type of alimentation strongly define both the essential amino acid's bioavailability and its metabolization. Vitamins B2 and B6 are KP cofactors; consequently, vitamin deficiency impacts kynurenine metabolite levels (Yeh and Brown 1977). TDO and IDO are iron porphyrin metalloproteins; hence, their enzymatic activity is dependent on iron supply. Moreover, prolonged inadequate food intake may result in low levels of serum albumin and as such interfere with free/bound metabolite fractions and consequent peripheral quantification (cfr. supra). As psychiatric patients are renowned for their poor eating habits, it is not inconceivable that varying peripheral TRYCAT levels largely reflect dietary insufficiencies. In support, Fellendorf et al. (Fellendorf et al., 2021) recently found TRP-to-KYN conversion in bipolar disorder to be facilitated by overweight and not by psychiatric symptomatology. This in turn raises the question as to whether TRYCAT aberrations in psychiatry are driven by syndrome-specific phenomena vs. being a by-product of other pan-pathological states like chronic stress-induced glucocorticoid resistance or sickness behavior hallmarking major depression and other psychiatric disorders (Zunszain et al., 2011).

According to Zahed et al. (Zahed et al., 2021), most TRYCAT remain relatively unaffected by smoking, which only appears to decrease QUIN, AA, and 3-HAA (Zahed et al., 2021). This may however be consequent to unassessed gender bias as Naz et al. (2019) demonstrate KYN and KA (but not TRP) levels to be lower in male smokers vs. non-smokers but remain unaffected in female smokers. Last, recreational drugs also interfere with homeostatic KP metabolite levels. Alcoholic beverages contain metabolically significant concentrations of KA, which is easily resorbed *via* the digestive tract and is quantifiable in peripheral blood. Hence, drinking beer and wine will artificially increase plasma [KA] (Turska et al., 2019). Cocaine use, on the other hand, will lower the amount of KA in blood (Araos et al., 2019). As comorbid substance use disorders are highly prevalent (~30% (Toftdahl et al., 2016)) in mental health disorders, at least part of the variation in KP metabolite concentrations in psychiatry may be attributable to the (mis)use of varying types of recreational drugs.

Consult Gostner et al. (2020) for further elaboration on the interplay between lifestyle factors and TRP metabolization (Gostner et al., 2020).

The Enzyme Enigma

Aberrations in KP metabolite levels have been largely attributed to deviant enzyme activity. However, the processing rate of these enzymes has rarely been directly assessed in psychiatric disorders. Instead, enzyme concentrations have mostly been approximated by gene expression analysis (Favennec et al., 2015) or by ratios of metabolite concentrations. Illustratively, the KYN/TRP ratio is suggested to reflect the TRP-to-KYN metabolizer IDO, and KAT activity is deemed deductible from [KA/KYN]. While peripheral metabolite ratios may reflect enzyme activities in closed systems such as cell cultures, assuming those correlations in blood, let alone in the brain, may stretch things too far. In support, non-correspondence of the KYN/TRP ratio with IDO activity was evidenced in patients with hemodialysis (Kato et al., 2010) and in children (Yarbrough et al., 2018). Again, albumin binding proves problematic as bound fractions do not reflect current production rates. Furthermore, several isoforms exist for most pathway enzymes. Does [KYN/TRP] reflect IDO1, IDO2, or TDO? Which of the two main KAT isozymes is represented by [KA/KYN]? Moreover, aberrations in renal clearance or in functionality of downstream enzymes may lead to upstream metabolite accumulation and will as such influence ratios independently of target enzyme activity. An elaborate critical appraisal of the KYN/TRP ratio as proxy for IDO activity can be found in the review by Abdulla et al. (Badawy and Guillemin 2019). Last, a recent review describes several alternative routes of KA synthesis *via* non-KATs and even enzyme-free mechanisms (Blanco Ayala et al., 2015; Ramos-Chávez et al., 2018). It is conceivable that similar alternative means of production also exist for other TRYCAT, which strongly dilutes the relevance of using metabolite ratios as a proxy for single (and mostly rather nonspecific) enzymes. As discrepancies between IDO1 mRNA and protein levels have been reported (Théate et al., 2015), this too proves to unreliably reflect KP enzyme activities and underscores the need for alternative quantification strategies.

Tryptophan Catabolization: Not the Model Pathway!

Research on organs/diseases that are not or only hardly accessible/mimicable in humans often relies on animal studies to expand the pathophysiological knowledge. Nonetheless, caution is recommended when interpreting animal experimentation on TRYCAT in psychiatry. Not only are mood and psychotic disorders hard to model in animals, but the KP shows marked discrepancies in humans *versus* animals (Yeh and Brown 1977). Illustratively, TDO expression in humans is 5 to 10 fold lower than in rodents, and IDO activity suppresses human but not mouse lymphocyte proliferation (Torres Crigna et al., 2020). The latter reveals that these interspecies differences also functionally affect KP immunomodulation. Moreover, the fact that QUIN transport over the BBB occurs in gerbils but not in rats indicates that it even diverges between different species families of the same order (Heyes et al., 1997).

Methodological Mayhem

KP research in the field of psychiatry is typically hallmarked by low sample sizes in heterogeneous study populations. Moreover, patient populations also differ from healthy controls regarding multiple demographic variables (BMI, smoking habits, *etc.*), which may in themselves impact TRYCAT levels. Specifically, all KYN metabolites increase with BMI and with age (except xanthurenic acid (XA) and 3-hydroxyanthranilic acid (3HAA)), and most are higher in males (Pertovaara et al., 2006; Zahed et al., 2021).

Alternate discrepancies in the literature may arise from the use of distinct analytical technologies. TRYCAT are almost exclusively measured using chromatographic methods such as high-pressure liquid chromatography (HPLC). These quantify total concentrations, while unbound concentrations may be more relevant (cfr. supra). Liquid chromatography–mass spectrometry (LCMS) and HPLC are performed with similar frequencies and show disagreement in concentration ranges, with some publications differing up to a staggering 1,000 times (Hartai et al., 2007; De Picker et al., 2019; Ulvik et al., 2020). Moreover, the concentration of several relevant kynurenine metabolites flirts with or even falls below the technological lower limit of detection of these methodologies (LC-MS quantification of QA, AA; unpublished data), implying caution concerning the scientific conclusiveness on their pathophysiological involvement. Last, sample collection is easily overlooked, though it is a crucial source of variance in TRYCAT quantification literature. Demonstrably, TRP is 15% higher in serum than in plasma (Yu et al., 2011) [with higher reproducibility in plasma, presumably due to coagulation-induced variance in serum (Bi et al., 2020)] and strongly increased in hemolytic samples (Kamlage et al., 2014). Heparin, an anticoagulant routinely used for plasma collection, is to be strictly avoided as it introduces severe chemical noise in LC-MS analyses (Yin et al., 2013) and interferes in albumin-TRP binding (Badawy 2010).

DISCUSSION

What Path(way) to Take Next?

Tryptophan degradation through the kynurenine pathway has been widely implicated in the pathophysiology of a multitude of psychiatric disorders. KP derangement could even be involved causatively as mutations in SLC7A5, the gene coding for LAT1, have been linked to autism spectrum disorders (Tărlungeanu et al., 2016). Nonetheless, the research field is hallmarked by several pitfalls which might at least partially be circumvented by the hereby proposed guidelines.

→When quantifying peripheral metabolites to evaluate *in cerebro* bioavailability, unbound fractions in addition to total or bound levels need to be described. Thereby, one should take heed in optimizing their study design to account for modulators influencing freely circulating compound concentrations such as meal intake and type of collection tube (preferably collect fasting blood samples in EDTA-coated plasma tubes) (Badawy 2010). Alternatively, interference of albumin binding should be checked statistically by introducing [serum/plasma albumin] as a model covariate (van den Ameele et al., 2018; De Picker et al., 2019).

→When resorting to animal experimentation for fundamental exploration of kynurenine metabolization, larger mammalian species should be opted over rodent strains as KP characteristics in those animals show a higher degree of overlap with humans (Wang et al., 2018). Preferably, however, an in-depth scrutiny of the KP should be done *in situ* in human populations, for instance, *via* live imaging techniques (PET tracing of microglia activity) (De Picker et al., 2019), widespread characterization of KP metabolites in a multitude of bodily compartments (blood cells, urine, saliva, *etc.*), or clinical trials with compounds known to mediate the KP in animal research or other human pathologies such as IDO or KMO inhibitors (O'Connor et al., 2009; Prendergast et al., 2018; Réus et al., 2018).

→Metabolite ratios should be avoided to infer KP enzyme activity. Instead, enzyme concentrations or activities should be directly quantified in the fluidic compartments and/or judicious selections of blood. Successful assaying of KATs (in serum and erythrocytes), kynureninase (in lymphocytes), and IDO enzymes (in peripheral blood mononuclear cells) has been published elsewhere (Carlin et al., 1989; Ubbink et al., 1991; Hartai et al., 2007). Of note, immunogenic stimulation by for instance IFN-γ, is advised as basal enzyme activities may fall below detection limits in homeostatic circumstances (Edelstein et al., 1989). When direct measurement proves unattainable, enzyme activity can be inferred through detection of surrogate markers produced by high-specificity enzymes that respond to the same stimuli. Illustratively, neopterin, a pro-inflammatory marker of immune cell activation, proxies as a marker for IDO activity as IFN-γ also activates the key enzyme of neopterin synthesis (Werner-Felmayer et al., 1990). In parallel, enzyme activity can be deduced from direct measurement of protein levels. In support, *in vitro* IDO1 activity shows high correlation with protein expression (Wolf et al., 2009).

→In recent years, other pathway metabolites have gained interest as potentially having functional relevance in the pathophysiology of psychiatric disorders. Picolinic and xanthurenic acid, for instance, may act as trait markers for i.a. schizophrenia and therefore deserve to be more elaborately scrutinized in future endeavors (Fazio et al., 2015; Ryan et al., 2020).

→The recent emergence of sensitive commercial ELISA kits allows to demonopolize valuable TRYCAT metabolite and enzyme quantifications away from dedicated fully equipped, time-consuming, and expensive HPLC/LC-MS service labs toward broad-scale implementation to any research group with a basic laboratory infrastructure. As such, high-throughput quantifications on large sample sizes are now within reach.

AUTHOR CONTRIBUTIONS

VC wrote the paper. VC, RV and MM provided conceptual content and revised the text.

FUNDING

This work was fully funded by personal funds of the University of Antwerp and the University Psychiatric Centre Duffel.

REFERENCES

Agudelo, L. Z., Femenía, T., Orhan, F., Porsmyr-Palmertz, M., Goiny, M., Martinez-Redondo, V., et al. (2014). Skeletal Muscle PGC-1α1 Modulates Kynurenine Metabolism and Mediates Resilience to Stress-Induced Depression. *Cell* 159, 33–45. doi:10.1016/j.cell.2014.07.051

Alme, K. N., Askim, T., Assmus, J., Mollnes, T. E., Naik, M., Næss, H., et al. (2021). Investigating Novel Biomarkers of Immune Activation and Modulation in the Context of Sedentary Behaviour: a Multicentre Prospective Ischemic Stroke Cohort Study. *BMC Neurol.* 21, 318. doi:10.1186/s12883-021-02343-0

Anguizola, J., Debolt, E., Suresh, D., and Hage, D. S. (2016). Chromatographic Analysis of the Effects of Fatty Acids and Glycation on Binding by Probes for Sudlow Sites I and II to Human Serum Albumin. *J. Chromatogr. B Analyt. Technol. Biomed. Life Sci.* 1021, 175–181. doi:10.1016/j.jchromb.2015.09.041

Araos, P., Vidal, R., O'Shea, E., Pedraz, M., García-Marchena, N., Serrano, A., et al. (2019). Serotonin Is the Main Tryptophan Metabolite Associated with Psychiatric Comorbidity in Abstinent Cocaine-Addicted Patients. *Sci. Rep.* 9, 16842. doi:10.1038/s41598-019-53312-0

Badawy, A. A., and Guillemin, G. (2019). The Plasma [Kynurenine]/[Tryptophan] Ratio and Indoleamine 2,3-Dioxygenase: Time for Appraisal. *Int. J. Tryptophan Res.* 12, 1178646919868978. doi:10.1177/1178646919868978

Badawy, A. A. (2010). Plasma Free Tryptophan Revisited: what You Need to Know and Do before Measuring it. *J. Psychopharmacol.* 24, 809–815. doi:10.1177/0269881108098965

Bi, H., Guo, Z., Jia, X., Liu, H., Ma, L., and Xue, L. (2020). The Key Points in the Pre-analytical Procedures of Blood and Urine Samples in Metabolomics Studies. *Metabolomics* 16, 68. doi:10.1007/s11306-020-01666-2

Blanco Ayala, T., Lugo Huitrón, R., Carmona Aparicio, L., Ramírez Ortega, D., González Esquivel, D., Pedraza Chaverrí, J., et al. (2015). Alternative Kynurenic Acid Synthesis Routes Studied in the Rat Cerebellum. *Front. Cell. Neurosci.* 9, 178. doi:10.3389/fncel.2015.00178

Cangiano, C., Cardelli, P., Peverini, P., Giglio, R. M., Laviano, A., Fava, A., et al. (1999). Effect of Kynurenine on Tryptophan-Albumin Binding in Human Plasma. *Adv. Exp. Med. Biol.* 467, 279–282. doi:10.1007/978-1-4615-4709-9_35

Carlin, J. M., Borden, E. C., Sondel, P. M., and Byrne, G. I. (1989). Interferon-induced Indoleamine 2,3-dioxygenase Activity in Human Mononuclear Phagocytes. *J. Leukoc. Biol.* 45, 29–34. doi:10.1002/jlb.45.1.29

Coppens, V., Morrens, M., Destoop, M., and Dom, G. (2019). The Interplay of Inflammatory Processes and Cognition in Alcohol Use Disorders-A Systematic Review. *Front. Psychiatry* 10, 632. doi:10.3389/fpsyt.2019.00632

Curzon, G. (1979). Relationships between Plasma, CSF and Brain Tryptophan. *J. Neural Transm. Suppl.* 15, 81–92. doi:10.1007/978-3-7091-2243-3_7

De Picker, L., Fransen, E., Coppens, V., Timmers, M., de Boer, P., Oberacher, H., et al. (2019). Immune and Neuroendocrine Trait and State Markers in Psychotic Illness: Decreased Kynurenines Marking Psychotic Exacerbations. *Front. Immunol.* 10, 2971. doi:10.3389/fimmu.2019.02971

Edelstein, M. P., Ozaki, Y., and Duch, D. S. (1989). Synergistic Effects of Phorbol Ester and INF-Gamma on the Induction of Indoleamine 2,3-dioxygenase in THP-1 Monocytic Leukemia Cells. *J. Immunol.* 143, 2969–2973.

Favennec, M., Hennart, B., Caiazzo, R., Leloire, A., Yengo, L., Verbanck, M., et al. (2015). The Kynurenine Pathway Is Activated in Human Obesity and Shifted toward Kynurenine Monooxygenase Activation. *Obesity (Silver Spring)* 23, 2066–2074. doi:10.1002/oby.21199

Fazio, F., Lionetto, L., Curto, M., Iacovelli, L., Cavallari, M., Zappulla, C., et al. (2015). Xanthurenic Acid Activates mGlu2/3 Metabotropic Glutamate Receptors and Is a Potential Trait Marker for Schizophrenia. *Sci. Rep.* 5, 17799. doi:10.1038/srep17799

Fellendorf, F. T., Gostner, J. M., Lenger, M., Platzer, M., Birner, A., Maget, A., et al. (2021). Tryptophan Metabolism in Bipolar Disorder in a Longitudinal Setting. *Antioxidants (Basel)* 10, 1795. doi:10.3390/antiox10111795

Gostner, J. M., Geisler, S., Stonig, M., Mair, L., Sperner-Unterweger, B., and Fuchs, D. (2020). Tryptophan Metabolism and Related Pathways in Psychoneuroimmunology: The Impact of Nutrition and Lifestyle. *Neuropsychobiology* 79, 89–99. doi:10.1159/000496293

Haroon, E., Welle, J. R., Woolwine, B. J., Goldsmith, D. R., Baer, W., Patel, T., et al. (2020). Associations Among Peripheral and central Kynurenine Pathway Metabolites and Inflammation in Depression. *Neuropsychopharmacology* 45, 998–1007. doi:10.1038/s41386-020-0607-1

Hartai, Z., Juhász, A., Rimanóczy, A., Janáky, T., Donkó, T., Dux, L., et al. (2007). Decreased Serum and Red Blood Cell Kynurenic Acid Levels in Alzheimer's Disease. *Neurochem. Int.* 50, 308–313. doi:10.1016/j.neuint.2006.08.012

Hebbrecht, K., Skorobogatov, K., Giltay, E. J., Coppens, V., De Picker, L., and Morrens, M. (2021). Tryptophan Catabolites in Bipolar Disorder: A Meta-Analysis. *Front. Immunol.* 12, 667179. doi:10.3389/fimmu.2021.667179

Heyes, M. P., Saito, K., Chen, C. Y., Proescholdt, M. G., Nowak, T. S., Li, J., et al. (1997). Species Heterogeneity between Gerbils and Rats: Quinolinate Production by Microglia and Astrocytes and Accumulations in Response to Ischemic Brain Injury and Systemic Immune Activation. *J. Neurochem.* 69, 1519–1529. doi:10.1046/j.1471-4159.1997.69041519.x

Kamlage, B., Maldonado, S. G., Bethan, B., Peter, E., Schmitz, O., Liebenberg, V., et al. (2014). Quality Markers Addressing Preanalytical Variations of Blood and Plasma Processing Identified by Broad and Targeted Metabolite Profiling. *Clin. Chem.* 60, 399–412. doi:10.1373/clinchem.2013.211979

Kato, A., Suzuki, Y., Suda, T., Suzuki, M., Fujie, M., Takita, T., et al. (2010). Relationship between an Increased Serum Kynurenine/tryptophan Ratio and Atherosclerotic Parameters in Hemodialysis Patients. *Hemodial. Int.* 14, 418–424. doi:10.1111/j.1542-4758.2010.00464.x

Marx, W., McGuinness, A. J., Rocks, T., Ruusunen, A., Cleminson, J., Walker, A. J., et al. (2021). The Kynurenine Pathway in Major Depressive Disorder, Bipolar Disorder, and Schizophrenia: a Meta-Analysis of 101 Studies. *Mol. Psychiatry* 26, 4158–4178. doi:10.1038/s41380-020-00951-9

Morrens, M., Coppens, V., and Walther, S. (2020). Do immune Dysregulations and Oxidative Damage Drive Mood and Psychotic Disorders? *Neuropsychobiology* 79, 251–254. doi:10.1159/000496622

Morrens, M., De Picker, L., Kampen, J. K., and Coppens, V. (2020). Blood-based Kynurenine Pathway Alterations in Schizophrenia Spectrum Disorders: A Meta-Analysis. *Schizophr Res.* 223, 43–52. doi:10.1016/j.schres.2020.09.007

Naz, S., Bhat, M., Ståhl, S., Forsslund, H., Sköld, C. M., Wheelock, Å. M., et al. (2019). Dysregulation of the Tryptophan Pathway Evidences Gender Differences in COPD. *Metabolites* 9, 212. doi:10.3390/metabo9100212

O'Connor, J. C., Lawson, M. A., André, C., Moreau, M., Lestage, J., Castanon, N., et al. (2009). Lipopolysaccharide-induced Depressive-like Behavior Is Mediated by Indoleamine 2,3-dioxygenase Activation in Mice. *Mol. Psychiatry* 14, 511–522. doi:10.1038/sj.mp.4002148

Pertovaara, M., Heliövaara, M., Raitala, A., Oja, S. S., Knekt, P., and Hurme, M. (2006). The Activity of the Immunoregulatory Enzyme Indoleamine 2,3-dioxygenase Is Decreased in Smokers. *Clin. Exp. Immunol.* 145, 469–473. doi:10.1111/j.1365-2249.2006.03166.x

Prendergast, G. C., Malachowski, W. J., Mondal, A., Scherle, P., and Muller, A. J. (2018). Indoleamine 2,3-dioxygenase and its Therapeutic Inhibition in Cancer. *Int. Rev. Cel Mol. Biol.* 336, 175–203. doi:10.1016/bs.ircmb.2017.07.004

Ramos-Chávez, L. A., Huitrón, R. L., Esquivel, D. G., Pineda, B., Ríos, C., Silva-Adaya, D., et al. (2018). Relevance of Alternative Routes of Kynurenic Acid Production in the Brain. *Oxid. Med. Cell. Longev.* 2018, 5272741. doi:10.1155/2018/5272741

Réus, G. Z., Becker, I. R. T., Scaini, G., Petronilho, F., Oses, J. P., Kaddurah-Daouk, R., et al. (2018). The Inhibition of the Kynurenine Pathway Prevents Behavioral Disturbances and Oxidative Stress in the Brain of Adult Rats Subjected to an Animal Model of Schizophrenia. *Prog. Neuro-Psychopharmacology Biol. Psychiatry* 81, 55–63. doi:10.1016/j.pnpbp.2017.10.009

Ryan, K. M., Allers, K. A., McLoughlin, D. M., and Harkin, A. (2020). Tryptophan Metabolite Concentrations in Depressed Patients before and after Electroconvulsive Therapy. *Brain Behav. Immun.* 83, 153–162. doi:10.1016/j.bbi.2019.10.005

Skorobogatov, K., De Picker, L., Verkerk, R., Coppens, V., Leboyer, M., Müller, N., et al. (2021). Brain versus Blood: A Systematic Review on the Concordance between Peripheral and Central Kynurenine Pathway Measures in Psychiatric Disorders. *Front. Immunol.* 12, 716980. doi:10.3389/fimmu.2021.716980

Tărlungeanu, D. C., Deliu, E., Dotter, C. P., Kara, M., Janiesch, P. C., Scalise, M., et al. (2016). Impaired Amino Acid Transport at the Blood Brain Barrier Is a Cause of Autism Spectrum Disorder. *Cell* 167, 1481.e18. doi:10.1016/j.cell.2016.11.013

Théate, I., van Baren, N., Pilotte, L., Moulin, P., Larrieu, P., Renauld, J. C., et al. (2015). Extensive Profiling of the Expression of the Indoleamine 2,3-dioxygenase 1 Protein in normal and Tumoral Human Tissues. *Cancer Immunol. Res.* 3, 161–172. doi:10.1158/2326-6066.cir-14-0137

Toftdahl, N. G., Nordentoft, M., and Hjorthøj, C. (2016). Prevalence of Substance Use Disorders in Psychiatric Patients: a Nationwide Danish Population-Based Study. *Soc. Psychiatry Psychiatr. Epidemiol.* 51, 129–140. doi:10.1007/s00127-015-1104-4

Torres Crigna, A., Uhlig, S., Elvers-Hornung, S., Klüter, H., and Bieback, K. (2020). Human Adipose Tissue-Derived Stromal Cells Suppress Human, but Not Murine Lymphocyte Proliferation, via Indoleamine 2,3-Dioxygenase Activity. *Cells* 9. doi:10.3390/cells9112419

Turska, M., Rutyna, R., Paluszkiewicz, M., Terlecka, P., Dobrowolski, A., Pelak, J., et al. (2019). Presence of Kynurenic Acid in Alcoholic Beverages - Is This Good News, or Bad News? *Med. Hypotheses* 122, 200–205. doi:10.1016/j.mehy.2018.11.003

Ubbink, J. B., Hayward Vermaak, W. J., and Bissbort, S. (1991). Rapid High-Performance Liquid Chromatographic Assay for Total Homocysteine Levels in Human Serum. *J. Chromatogr.* 565, 441–446. doi:10.1016/0378-4347(91)80407-4

Ulvik, A., Midttun, Ø., McCann, A., Meyer, K., Tell, G., Nygård, O., et al. (2020). Tryptophan Catabolites as Metabolic Markers of Vitamin B-6 Status Evaluated in Cohorts of Healthy Adults and Cardiovascular Patients. *Am. J. Clin. Nutr.* 111, 178–186. doi:10.1093/ajcn/nqz228

van den Ameele, S., Fuchs, D., Coppens, V., de Boer, P., Timmers, M., Sabbe, B., et al. (2018). Markers of Inflammation and Monoamine Metabolism Indicate Accelerated Aging in Bipolar Disorder. *Front. Psychiatry* 9, 250. doi:10.3389/fpsyt.2018.00250

Walker, A. K., Wing, E. E., Banks, W. A., and Dantzer, R. (2019). Leucine Competes with Kynurenine for Blood-To-Brain Transport and Prevents Lipopolysaccharide-Induced Depression-like Behavior in Mice. *Mol. Psychiatry* 24, 1523–1532. doi:10.1038/s41380-018-0076-7

Walser, M., and Hill, S. B. (1993). Free and Protein-Bound Tryptophan in Serum of Untreated Patients with Chronic Renal Failure. *Kidney Int.* 44, 1366–1371. doi:10.1038/ki.1993.390

Wang, J., Takahashi, R. H., DeMent, K., Gustafson, A., Kenny, J. R., Wong, S. G., et al. (2018). Development of a Mass Spectrometry-Based Tryptophan 2, 3-dioxygenase Assay Using Liver Cytosol from Multiple Species. *Anal. Biochem.* 556, 85–90. doi:10.1016/j.ab.2018.06.025

Werner-Felmayer, G., Werner, E. R., Fuchs, D., Hausen, A., Reibnegger, G., and Wachter, H. (1990). Neopterin Formation and Tryptophan Degradation by a Human Myelomonocytic Cell Line (THP-1) upon Cytokine Treatment. *Cancer Res.* 50, 2863–2867.

Wolf, B., Posnick, D., Fisher, J. L., Lewis, L. D., and Ernstoff, M. S. (2009). Indoleamine-2,3-dioxygenase Enzyme Expression and Activity in Polarized Dendritic Cells. *Cytotherapy* 11, 1084–1089. doi:10.3109/14653240903271230

Yang, F., Zhang, Y., and Liang, H. (2014). Interactive Association of Drugs Binding to Human Serum Albumin. *Int. J. Mol. Sci.* 15, 3580–3595. doi:10.3390/ijms15033580

Yarbrough, M. L., Briden, K. E., Mitsios, J. V., Weindel, A. L., Terrill, C. M., Hunstad, D. A., et al. (2018). Mass Spectrometric Measurement of Urinary Kynurenine-To-Tryptophan Ratio in Children with and without Urinary Tract Infection. *Clin. Biochem.* 56, 83–88. doi:10.1016/j.clinbiochem.2018.04.014

Yeh, J. K., and Brown, R. R. (1977). Effects of Vitamin B-6 Deficiency and Tryptophan Loading on Urinary Excretion of Tryptophan Metabolites in Mammals. *J. Nutr.* 107, 261–271. doi:10.1093/jn/107.2.261

Yin, P., Peter, A., Franken, H., Zhao, X., Neukamm, S. S., Rosenbaum, L., et al. (2013). Preanalytical Aspects and Sample Quality Assessment in Metabolomics Studies of Human Blood. *Clin. Chem.* 59, 833–845. doi:10.1373/clinchem.2012.199257

Yu, Z., Kastenmüller, G., He, Y., Belcredi, P., Möller, G., Prehn, C., et al. (2011). Differences between Human Plasma and Serum Metabolite Profiles. *PLoS One* 6, e21230. doi:10.1371/journal.pone.0021230

Yuwiler, A., Oldendorf, W. H., Geller, E., and Braun, L. (1977). Effect of Albumin Binding and Amino Acid Competition on Tryptophan Uptake into Brain. *J. Neurochem.* 28, 1015–1023. doi:10.1111/j.1471-4159.1977.tb10664.x

Zahed, H., Johansson, M., Ueland, P. M., Midttun, Ø., Milne, R. L., Giles, G. G., et al. (2021). Epidemiology of 40 Blood Biomarkers of One-Carbon Metabolism, Vitamin Status, Inflammation, and Renal and Endothelial Function Among Cancer-free Older Adults. *Sci. Rep.* 11, 13805. doi:10.1038/s41598-021-93214-8

Zunszain, P. A., Anacker, C., Cattaneo, A., Carvalho, L. A., and Pariante, C. M. (2011). Glucocorticoids, Cytokines and Brain Abnormalities in Depression. *Prog. Neuropsychopharmacol. Biol. Psychiatry* 35, 722–729. doi:10.1016/j.pnpbp.2010.04.011

Conflict of Interest: The authors declare that the research was conducted in the absence of any commercial or financial relationships that could be construed as a potential conflict of interest.

Publisher's Note: All claims expressed in this article are solely those of the authors and do not necessarily represent those of their affiliated organizations, or those of the publisher, the editors and the reviewers. Any product that may be evaluated in this article, or claim that may be made by its manufacturer, is not guaranteed or endorsed by the publisher.

frontiers in Pharmacology

ORIGINAL RESEARCH
published: 17 March 2022
doi: 10.3389/fphar.2022.796616

Metformin Inhibits NLR Family Pyrin Domain Containing 3 (NLRP)-Relevant Neuroinflammation *via* an Adenosine-5′-Monophosphate-Activated Protein Kinase (AMPK)-Dependent Pathway to Alleviate Early Brain Injury After Subarachnoid Hemorrhage in Mice

Lei Jin†, Fa Jin†, Shenquan Guo†, Wenchao Liu, Boyang Wei, Haiyan Fan, Guangxu Li, Xin Zhang, Shixing Su, Ran Li, Dazhao Fang, Chuanzhi Duan and Xifeng Li**

Neurosurgery Center, Department of Cerebrovascular Surgery, The National Key Clinical Specialty, The Engineering Technology Research Center of Education Ministry of China on Diagnosis and Treatment of Cerebrovascular Disease, Guangdong Provincial Key Laboratory on Brain Function Repair and Regeneration, The Neurosurgery Institute of Guangdong Province, Zhujiang Hospital, Southern Medical University, Guangzhou, China

Neuroinflammation plays a key role in the pathogenesis of early brain injury (EBI) after subarachnoid hemorrhage (SAH). Previous studies have shown that metformin exerts anti-inflammatory effects and promotes functional recovery in various central nervous system diseases. We designed this study to investigate the effects of metformin on EBI after SAH. Our results indicate that the use of metformin alleviates the brain edema, behavioral disorders, cell apoptosis, and neuronal injury caused by SAH. The SAH-induced NLRP3-associated inflammatory response and the activation of microglia are also suppressed by metformin. However, we found that the blockade of AMPK with compound C weakened the neuroprotective effects of metformin on EBI. Collectively, our findings indicate that metformin exerts its neuroprotective effects by inhibiting neuroinflammation in an AMPK-dependent manner, by modulating the production of NLRP3-associated proinflammatory factors and the activation of microglia.

Keywords: metformin, neuroinflammation, NLRP3 inflammasome, neuron injury, subarachnoid hemorrhage

OPEN ACCESS

Edited by:
Borja Garcia-Bueno, Universidad Complutense de Madrid, Spain

Reviewed by:
Xiangsheng Zhang, Capital Medical University, China
Karina S. MacDowell, Complutense University of Madrid, Spain

****Correspondence:***
Chuanzhi Duan
doctor_duanzj@163.com
Xifeng Li
nflxf@126.com

†These authors have contributed equally to this work and share first authorship

Specialty section:
This article was submitted to Neuropharmacology, a section of the journal Frontiers in Pharmacology

Received: *22 October 2021*
Accepted: *09 February 2022*
Published: *17 March 2022*

Citation:
Jin L, Jin F, Guo S, Liu W, Wei B, Fan H, Li G, Zhang X, Su S, Li R, Fang D, Duan C and Li X (2022) Metformin Inhibits NLR Family Pyrin Domain Containing 3 (NLRP)-Relevant Neuroinflammation via an Adenosine-5′-Monophosphate-Activated Protein Kinase (AMPK)-Dependent Pathway to Alleviate Early Brain Injury After Subarachnoid Hemorrhage in Mice. Front. Pharmacol. 13:796616. doi: 10.3389/fphar.2022.796616

INTRODUCTION

Subarachnoid hemorrhage (SAH) is a life-threatening subtype of stroke, characterized by high rates of mortality and poor prognoses (Laiwalla et al., 2016; Etminan et al., 2019). A previous study attributed the unfavorable prognoses of SAH patients to angiographic vasospasm (Crowley et al., 2008). However, clinical trials have shown that drugs directed against vasospasm failed to improve the poor prognoses of these patients (Macdonald et al., 2011; Macdonald et al., 2012). Recent studies have identified early brain injury (EBI), which occurs within the first 3 days of SAH, as one of the major causes of the unfavorable prognoses of SAH patients (Chen et al., 2014; Li et al., 2018). The EBI phase after SAH includes multiple pathophysiological processes. The overactivation of the inflammatory responses not only directly damages brain tissue but also contributes to the

disruption of the blood–brain barrier and cell apoptosis, which further aggravate the brain injury (Fujii et al., 2013; Liu et al., 2019). A prospective observational study demonstrated that the inflammatory response is an independent predictor of unfavorable outcomes in SAH patients (Badjatia et al., 2015). Therefore, the suppression of neuroinflammation may be an effective strategy to mitigate brain injury after SAH.

The NLR family pyrin domain containing 3 (NLRP3) inflammasome is a multiprotein complex that regulates the innate immune inflammatory response (Zhou et al., 2011). The activation of the NLRP3 inflammasome causes the autocatalytic cleavage of pro-caspase 1, resulting in the processing and secretion of proinflammatory cytokines IL-1β and IL-18, which participate in the inflammatory response in multiple diseases (Mangan et al., 2018; Yang Y. et al., 2019). Recent studies have shown that the NLRP3 inflammasome contributes to the pathogenesis of EBI after SAH, and its suppression protects against brain injury (Dodd et al., 2021; Xu et al., 2021).

Adenosine-monophosphate-activated protein kinase (AMPK) is a sensor of cellular energy and modulates the status of many cellular processes (Meijer and Codogno, 2007). Recent advances in SAH research have demonstrated that the inhibition of NLRP3-inflammasome-associated neuroinflammation by activating AMPK reduces brain injury after SAH (Xu et al., 2019; Peng et al., 2020).

Metformin is widely used to treat patients with type 2 diabetes and metabolic syndrome because it safely and strongly enhances insulin sensitivity (Sanchez-Rangel and Inzucchi, 2017). A randomized controlled trial also reported that the concentrations of blood biomarkers predicting poor outcomes were significantly lower in patients with severe traumatic brain injury (TBI) treated with metformin than in untreated TBI patients (Taheri et al., 2019). Recent studies have shown that metformin exerts anti-inflammatory effects and alleviates ischemia–reperfusion injury by inhibiting the activation of the NLRP3 inflammasome (Jia et al., 2020; Zhang et al., 2020; Xian et al., 2021). In a recent study, we reported that HSP22 relieved SAH-induced EBI by salvaging the mitochondrial function in an AMPK–PGC1α-dependent manner (Fan et al., 2021). Moreover, metformin is be known to be one kind of activator of AMPK (Xie et al., 2011; Grégoire et al., 2018). To our knowledge, there have been no reports of the role of metformin in EBI after SAH. Therefore, in this study, we evaluated the effects of metformin on EBI after SAH and investigated the underlying mechanism.

MATERIALS AND METHODS

Animals

Healthy adult male C57BL/6J mice (weighing 20–25 g) were obtained from the Animal Experiment Center of Southern Medical University (Guangzhou, China). The mice were housed under a 12-h light/dark cycle at a controlled temperature (22 ± 1°C) and humidity (60 ± 5%). The mice had free access to water and food. All experimental procedures involving animals were approved by the Southern Medical University Ethics Committee (Guangzhou, China) and conformed to the Guidelines of the National Institutes of Health on the Care and Use of Animals (China). The Animal Ethics Project Number is LAEC-2020-142.

Experimental Design

This study included four separate experiments, as shown in **Figure 1**.

Experiment 1

Western blotting was used to determine the expression patterns of phosphorylated AMPK (p-AMPK), AMPK, and NLRP3 after SAH. The mice were randomly allocated into the six groups including the sham group and five SAH subgroups (at 6, 12, 24, 48, 72 h after SAH. $n = 6$). The left cerebral cortices from each group were collected for western blotting analysis. Double-labeled immunofluorescence was also used for the cellular localization of p-AMPK and NLRP3 in the SAH group (at 24 h after SAH. $n = 3$).

Experiment 2

To determine the optimal dose of metformin for subsequent experiments, a concentration gradient of metformin was evaluated based on a previous study (Ashabi et al., 2014). Mice were randomly divided into six groups: sham, SAH, SAH + vehicle 1 (normal saline), SAH + metformin (100 mg/kg), SAH + metformin (200 mg/kg), and SAH + metformin (400 mg/kg). Metformin was administered intraperitoneally 30 min after SAH. A neurological test (modified Garcia score) ($n = 8$) was performed and the brain water content of the mice ($n = 8$) was analyzed at 24 h after SAH. After the neurological score was determined, the mice were killed and brain samples collected to assay the brain water content. The effects of different doses of metformin on NLRP3 expression in the SAH (24 h) group were evaluated with western blotting ($n = 6$). The SAH + vehicle 1 group was given the same volume of normal saline intraperitoneally at the same time points as the metformin-treated mice after the induction of SAH. The SAH group was only treated surgically, with no other treatment. The sham group underwent the same surgical procedure without perforation of the blood vessel, with no other treatment.

Experiment 3

The optimal dose of metformin (200 mg/kg) determined in the experiment described above was used in subsequent experiments. Nissl staining ($n = 5$), terminal deoxynucleotidyl transferase dUTP nick end labeling (TUNEL) staining ($n = 5$), immunohistochemical staining ($n = 5$), and western blotting ($n = 6$) were used to evaluate the effects of metformin on brain injury and the expression of proinflammatory factors at 24 h after SAH. The mice were randomly divided into four groups: sham, SAH, SAH + vehicle 1, and SAH + metformin (200 mg/kg).

Experiment 4

To further investigate the mechanism by which metformin inhibits neuroinflammation after SAH, compound C (6-[4-(2-piperidin-1-ylethoxy) phenyl]-3-pyridin-4-ylpyrazolo [1,5-a]

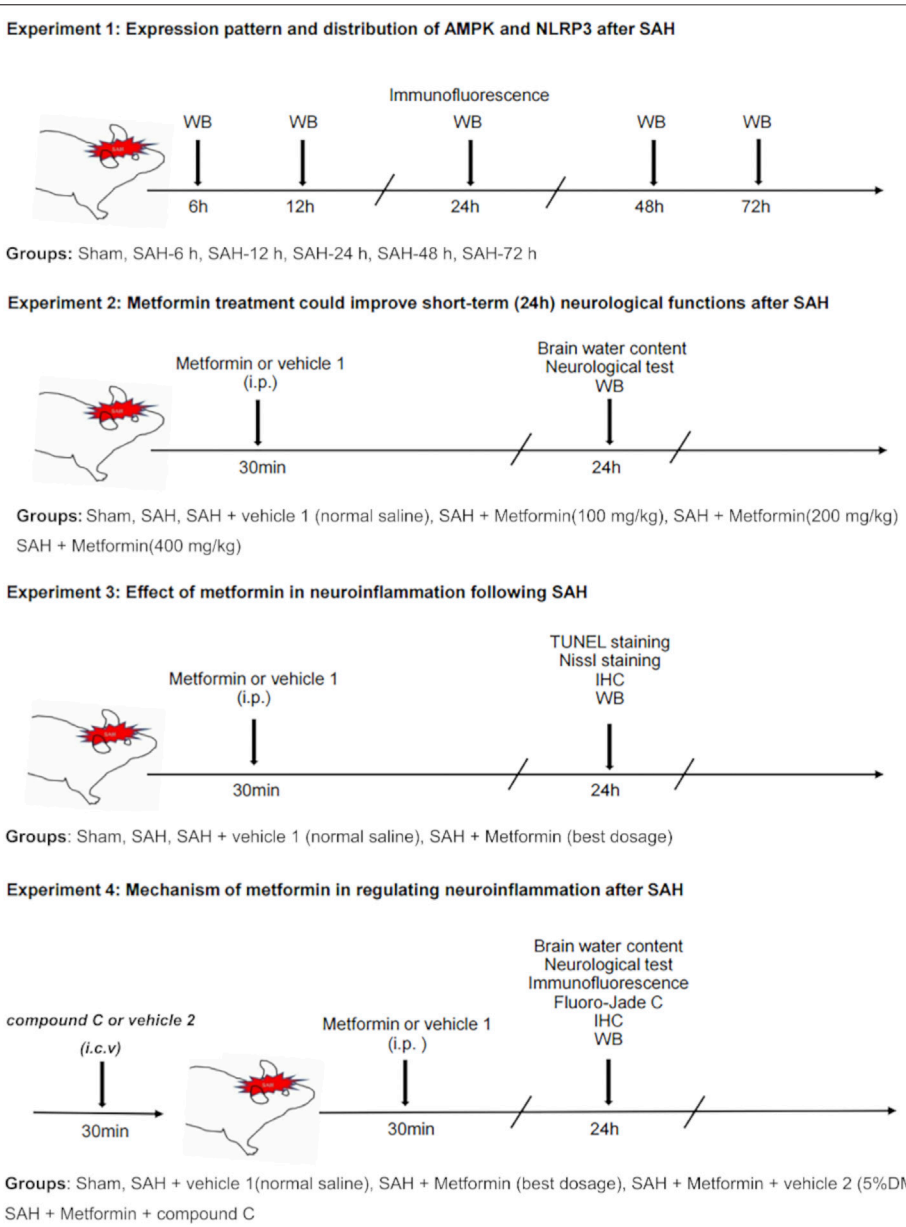

FIGURE 1 | Experimental design and animal groups. Abbreviation: AMPK, adenosine 5′monophosphate-activated protein kinase; NLRP3, nucleotide-binding domain, leucine-rich containing family, pyrin domain-containing-3; SAH, subarachnoid hemorrhage; WB, western blot; IHC, immunohistochemistry; TUNEL, terminal deoxynucleotidyl transferase dUTP nick end labeling; i. p., intraperitoneal injection, i. c. v, intracerebroventricular injection.

pyrimidine]), a selective inhibitor of AMPK signaling, was administered *via* the intracerebroventricular route 30 min before SAH, according to a previous study (Peng et al., 2020). The mice were divided into the sham, SAH + vehicle 1, SAH + metformin, SAH + metformin + vehicle 2 (5% dimethyl sulfoxide [DMSO]), and SAH + metformin + compound C groups. The brain water content (n = 8) and modified Garcia score (n = 8) were determined and western blotting (n = 6), immunofluorescent staining (n = 5), immunohistochemical staining (n = 5), and Fluoro-Jade C staining (n = 5) were performed at 24 h after SAH. The SAH + metformin + vehicle 2 and SAH + metformin + compound C groups were given the same volume of vehicle 2 and compound C intracerebroventricularly, respectively, at the same time points before SAH was induced.

Subarachnoid Hemorrhage Mouse Model

A mouse model of SAH was generated with endovascular perforation, as described previously (Peng et al., 2020). Briefly, C57BL/6 J mice were anesthetized with 2% isoflurane in oxygen for 3 min and anesthesia was maintained with 1.0–1.5% isoflurane in 70% N_2O and 30% O_2 in a small-animal

anesthesia system (Vet Equip, Pleasanton, CA, United States). A sharpened nylon suture was then inserted through the left external carotid artery to the common carotid artery and the internal carotid artery (ICA), ultimately perforating the intracranial bifurcation of the ICA. The sham-operated mice underwent the same procedures but the suture was withdrawn without puncture. During the operation, the body temperatures of the experimental animals were maintained at 37 ± 0.5°C with a heating pad.

Drug Administration

Metformin (Sigma, PHR1084) was dissolved in normal saline and given by intraperitoneal injection 30 min after SAH ictus. The time points and method of drug delivery were based on previous reports (Ashabi et al., 2014; Peng et al., 2020). In accordance with a previous report (Peng et al., 2020), the selective AMPK inhibitor compound C (Apexbio, B3252) was dissolved in 5% DMSO, and a working solution (5 μg in 5 μL) was injected into the intracerebroventricular cavity 30 min before the induction of SAH.

Intracerebroventricular Injection

Intracerebroventricular injections were conducted as previously described (Peng et al., 2020). Briefly, a 10 μL microsyringe (Shanghai High Pigeon Industry & Trade Co., Ltd., Shanghai, China) was inserted into the left lateral ventricle through a small cranial burr hole, which was drilled 0.3 mm posterior, 1.0 mm lateral, and 2.5 mm deep relative to the bregma. Compound C or vehicle 2 were administered slowly into the left lateral ventricle 30 min before surgery. The microsyringe was left *in situ* for an additional 10 min after the administration of the compound C or vehicle 2, and then withdrawn slowly. The burr hole was sealed with bone wax.

Determination of Neurological Scores and Subarachnoid Hemorrhage Grades

The neurological scores (neurobiological deficits) were determined by an independent investigator blinded to the procedural information, using the modified Garcia test (Garcia et al., 1995). The Garcia score consists of six sensorimotor tests: spontaneous activity, spontaneous movement of all limbs, forelimb outstretching, climbing, touching the trunk, and vibrissal touch. Each test was scored from 0 to 3, and the total scores ranged from 0 to 18. A higher score indicated a milder neurological deficit.

The severity of SAH was evaluated blindly at 24 h after SAH, with a previously reported SAH grading system (Sugawara et al., 2008). Briefly, the brain basal cistern was divided into six parts, and each part was scored from 0 to 3 based on the amount of blood clotting present. The total score for the six parts represented the SAH grade. SAH mice with SAH grade ≤7 were excluded from this study.

Brain Water Content

At 24 h after SAH, the mice were killed and their brains quickly removed, and divided into the left hemisphere, right hemisphere, cerebellum, and brain stem. Each segment was weighed immediately to determine their wet weight (WW), and the samples were then dried at 105°C for 72 h to determine their dry weight (DW). The brain water content was calculated as [(WW − DW)/WW] × 100%.

Nissl Staining

Nissl staining was used to evaluate neuronal damage in the ipsilateral cortex, as described previously (Deng et al., 2021). Briefly, at 24 h after SAH, the mice were deeply anesthetized and transcardially perfused with 50 ml of phosphate-buffered saline (PBS; 0.1 M) followed by 50 ml of 4% paraformaldehyde (PFA; pH 7.4). The brain samples were removed quickly and postfixed in 4% PFA for 24 h at 4°C. After the brains were embedded in paraffin, they were cut into serial coronal sections (10 μm thick). The brain slices were deparaffinized and rehydrated. The slices were immersed in methyl violet solution (Nissl Stain Solution, G1432, Solarbio, Beijing). The slices were then dehydrated in 100% alcohol and washed with xylene. Images were obtained and analyzed under a light microscope (Leica-DM2500, Wetzlar, Germany) by a blinded investigator.

Immunofluorescent Staining

Brain coronal slices (4 μm thick) were prepared as described previously (Liu et al., 2019), and deparaffinized in xylene, rehydrated in a graded series of alcohol, and washed with PBS (0.01 M, pH 7.4). After antigen retrieval, the brain slices were blocked with 5% donkey serum for 1 h at room temperature. The sections were incubated overnight at 4°C with the following primary antibodies: rabbit anti-p-AMPK (diluted 1:200; AF3423, Affinity); rabbit anti-NLRP3 (diluted 1:200; NBP1-77080SS, Novus); mouse anti-NEUN (diluted 1:500; ab104224, Abcam); mouse anti-IBA1 (diluted 1:200; GB12105, Servicebio); mouse anti-GFAP (diluted 1:200; GB12096, Servicebio), and mouse anti-GFAP (diluted 1:200; GA5, Cell Signaling Technology). The next day, the sections were washed with PBS and incubated for 1 h at room temperature with secondary antibodies: Alexa-Fluor-555-conjugated donkey anti-rabbit IgG (diluted 1:500; A31572, Invitrogen) and Alexa-Fluor-488-conjugated donkey anti-mouse IgG (diluted 1:500; A21202, Invitrogen). The sections were washed three times with PBS and stained with 4′,6-diamidino-2-phenylindole (DAPI) for 10 min at room temperature. The sections were observed and images captured under a fluorescence microscope (Nikon, TI2-E, Japan). To evaluate the numbers of IBA1-positive cells, three random fields in the ipsilateral cortex from three sections per brain were examined. Data are expressed as the average numbers of IBA1-positive cells per field in cells/mm^2.

Immunohistochemical Staining (IHC)

IHC was used to verify NLRP3 and IBA1 (a microglial marker in the brain) expression in the ipsilateral cortex. The deparaffinized and rehydrated coronal brain slices (4 μm thick) were prepared as described above. The slices were incubated with 3% H_2O_2 for 10 min at room temperature to quench any endogenous peroxidase activity, and then blocked with 5% goat serum for

20 min at room temperature. The slices were then incubated overnight at 4°C with the following primary antibodies: rabbit anti-NLRP3 (diluted 1:50; NBP1-77080SS, Novus) and mouse anti-IBA1 (diluted 1:100; GB12105, Servicebio). The next day, the brain slices were washed with PBS and incubated for 20 min at room temperature with biotinylated goat anti-rabbit IgG (diluted 1:100; ZSGB-Bio, Beijing, China) or goat anti-mouse IgG (diluted 1:100; ZSGB-Bio). The brain slices were then incubated with horseradish peroxidase (HRP)–streptavidin reagent for 10 min and stained with 3,3′-diaminobenzidine peroxidase substrate. Images were obtained with a light microscope (Leica-DM2500, Wetzlar).

Fluoro-Jade C Staining

Fluoro-Jade C (FJC) staining was used to identify degenerate neurons, as previously described (Xu et al., 2021), but with modification. Briefly, the brain slices were immersed in an alcohol solution (1% sodium hydroxide in 80% ethanol) and then in 70% ethanol, and then immersed in 0.06% potassium permanganate solution for 10 min. The slices were then incubated in a 0.0001% working solution of FJC (Millipore, Darmstadt, Germany) for 30 min. Images were obtained under a fluorescence microscope and analyzed by a blinded observer. FJC-positive cells were counted in three different fields of the ipsilateral cortex in three sections per mouse. Data are expressed as the ratio of FJC-positive cells to DAPI-positive cells.

TUNEL Staining

Cell apoptosis was detected with a TUNEL kit (Beyotime, China) at 24 h after SAH in strict accordance with the manufacturer's instructions. Briefly, the deparaffinized and rehydrated coronal brain slices were prepared as described above. After the brain slices were washed with PBS, they were incubated with TUNEL mixture for 1 h at room temperature, and then stained with DAPI. The results of TUNEL staining were observed and analyzed in the same way as FJC staining. The data are expressed as the ratio of TUNEL-positive cells to DAPI-positive cells.

Western Blotting

Western blotting was performed as previously described (Luo et al., 2020). Samples of the left cerebral cortices of the mice were collected after SAH. The tissues were lysed with RIPA lysis buffer (Cwbio, Guangzhou, China) to extract the proteins from the brain samples. Equal amounts of protein from different samples were loaded and separated on a 10% SDS-PAGE gel (Cwbio), and then transferred to a polyvinylidene difluoride filter membrane (Millipore, United States). The membranes were blocked with 5% nonfat milk for 3 h at room temperature and incubated overnight at 4°C with the following primary antibodies: anti-p-AMPK (diluted 1:1000; 40H9, Cell Signaling Technology), anti-AMPK antibody (diluted 1:1000; D5A2, Cell Signaling Technology), anti-NLRP3 (diluted 1:1000; 19771-1-AP, Proteintech), anti-cleaved caspase 1 (diluted 1:1000; E2G2I, Cell Signaling Technology), anti-IL-18 (diluted 1:1000; BS6823, Bioworld Technology), anti-IL-1β (diluted 1:1000; BS3506, Bioworld Technology), and anti-β-actin (diluted 1:1000; AP0060, Bioworld Technology). The membranes were washed three times for 10 min each in Tris-buffered saline containing 0.1% Tween 20, and then with HRP-conjugated goat anti-rabbit IgG (1:10000; Cwbio) at room temperature for 1 h. After the blots were washed, the proteins were visualized with an ECL Western blotting detection system (WBKLS0100, Millipore, United States) and analyzed with the ImageJ software (ImageJ 1.5, National Institutes of Health, Bethesda, MD, United States). β-Actin was used as the internal control.

Statistical Analysis

All data are presented as means ± standard deviations (SD) and all statistical analyses were performed with the SPSS 19.0 software (SPSS, IBM, Armonk, NY, United States). Student's t test was used to determine the statistical significance of differences between two groups and one-way analysis of variance (ANOVA) followed by Tukey's post hoc test was used for comparisons of multiple groups. Statistical significance was accepted at $p < 0.05$. Investigators were blinded to the identity of the groups during the whole experiment.

RESULTS

Subarachnoid Hemorrhage Model and Mortality

The total number of mice used in this study was 304, including those that died or were excluded for each group. The overall mortality rates in the sham-operated and SAH mice were 0 and 19.7%, respectively (**Supplementary Figure S1B**). Typical images of the brains from mice in the sham and SAH groups are shown in **Figures 2A,B**. Previous studies indicated that the inferior basal temporal lobe was always stained with blood and shows the most significant molecular biological changes relative to the control animal. Therefore, we mainly evaluated the basal temporal lobe of the left hemisphere adjacent to the clotted blood (Park et al., 2004; Zhang et al., 2021) (**Figure 2B**). It is noteworthy that the mice treated with metformin (400 mg/kg) after SAH showed an obvious increase in death risk relative to that in the mice treated with other doses of metformin (**Supplementary Figures S2A,B**). Therefore, 400 mg/kg metformin was not included in subsequent experiments.

Temporal Pattern of NLRP3 and p-AMPK After Subarachnoid Hemorrhage Induction

The western blotting results indicated that the protein levels of p-AMPK and AMPK increased after SAH, peaked at 24 h, and then gradually decreased until 72 h relative to those in the sham group (**Figures 2C,D**). Simultaneously, the expression of NLRP3 was similar to that of p-AMPK and AMPK (**Figures 2C,E**). Double immunostaining for p-AMPK and NEUN, IBA1, or GFAP demonstrated that p-AMPK was expressed in neurons and microglia cells at 24 h after SAH. However, astrocytes did not immunostain for p-AMPK (**Figure 3A**). NLRP3 was also observed in neurons and microglial cells at

24 h after SAH. Astrocytes did not immunostain for NLRP3 (**Figure 3B**).

Metformin Administration Improved Short-Term Neurological Functions and Attenuated Brain Edema at 24 h After Subarachnoid Hemorrhage

Besides the sham group, no significant differences were detected in the SAH grade scores among the SAH groups (**Figure 4A**). The mice in the SAH group and SAH + vehicle group showed severe neurological impairment and higher brain water contents than the mice in the sham group at 24 h after SAH. The administration of both 100 mg/kg and 200 mg/kg metformin improved the neurological performance relative to that in the SAH + vehicle group. The modified Garcia test indicated that the SAH-affected mice that received metformin showed a smaller neurological deficit than the mice in the untreated SAH group, but no significant differences were observed in mice treated with different doses of metformin (**Figure 4B**). The brain water content results indicated that 200 mg/kg metformin significantly mitigated brain edema relative to that in the SAH + vehicle group, whereas 100 mg/kg metformin did not (**Figure 4C**). The western blotting results showed that metformin treatment significantly downregulated the SAH-enhanced level of NLRP3 protein 24 h after SAH, and that 200 mg/kg metformin was superior to 100 mg/kg metformin in this regard (**Figures 4D,E**). No significant differences in blood glucose were observed between the mice treated with various doses of metformin and the SAH groups (**Supplementary Figure S3**). Therefore, based on all these results, 200 mg/kg metformin was selected for the subsequent experiments.

Metformin Alleviated Cell Apoptosis and Ameliorated Neuronal Injury at 24 h After Subarachnoid Hemorrhage

According to the TUNEL staining results, the sham group showed negligible TUNEL-positive cells. By contrast, the SAH group and SAH + vehicle group showed markedly increased TUNEL-positive cells. Metformin treatment reduced the proportion of apoptotic cells after SAH (**Figures 5A,C**). Nissl staining was used to further assess the effects of metformin on neuronal injury after SAH. The sham group showed negligible neuronal death. The proportion of surviving neurons was significantly reduced in the SAH and SAH + vehicle groups. However, metformin treatment markedly reduced the neuronal death caused by SAH (**Figures 5B,D**).

Metformin Administration Repressed the Activation of the NLRP3 Inflammasome and the Expression of the Relevant Inflammatory Cytokines at 24 h After Subarachnoid Hemorrhage

Immunohistochemical staining revealed that the expression of NLRP3 was elevated at 24 h after SAH, but this increase was inhibited by metformin (**Figure 6A**). The western blotting results showed that the expressions of p-AMPK, NLRP3, cleaved caspase 1, cleaved IL-1β, and cleaved IL-18 were clearly increased in the SAH and SAH + vehicle groups relative to that in the sham group. Metformin treatment further enhanced the level of p-AMPK, but reduced the levels of NLRP3, cleaved caspase 1, cleaved IL-1β, and cleaved IL-18 relative to those in the SAH mice not treated with metformin (**Figures 6B–G**).

Inhibition of Adenosine-Monophosphate-Activated Protein Kinase Weakened the Protective Effects and Anti-inflammatory Effects of Metformin at 24 h After Subarachnoid Hemorrhage

To determine whether AMPK is required for the protection against EBI offered by metformin after SAH, compound C was administered by intracerebroventricular injection. The metformin-associated alleviation of neurobehavioral deficits and the reduction in the brain water content were abolished by compound C (**Figures 7A,B**). FJC staining was used to further clarify the role of AMPK in metformin-ameliorated neuronal death after SAH. The inhibition of AMPK by compound C reversed the protective role of metformin against neuronal injury compared with that in the SAH + metformin group (**Figures 7C,D**). The western blotting results also indicated that the effects of metformin in increasing AMPK activation and reducing the expression of NLRP3, cleaved caspase 1, cleaved IL-1β, and cleaved IL-18 were suppressed by compound C (**Figures 7E–J**).

The Inhibition of Adenosine-Monophosphate-Activated Protein Kinase Blocked the Inhibitory Effect of Metformin on Microglial Activation at 24 h After Subarachnoid Hemorrhage

Immunofluorescent staining showed that microglia were markedly increased in number and activated (presenting as larger cell bodies with shorter processes) in the SAH + groups compared with those in the sham group, and that the administration of metformin significantly reduced the number of IBA1-positive cells and mitigated the overactivation of microglia. However, compound C blocked these effects of metformin on the regulation of microglia, which was confirmed with immunohistochemical staining (**Figures 8A–C**).

DISCUSSION

In this study, we have demonstrated the beneficial effects of metformin on EBI and neuroinflammation after SAH. The important findings of our experiments are as follows. 1) The levels of p-AMPK and NLRP3 increased markedly and peaked at 24 h after SAH. Both proteins colocalized with neurons and microglia, but no fluorescent signal was detected in astrocytes.

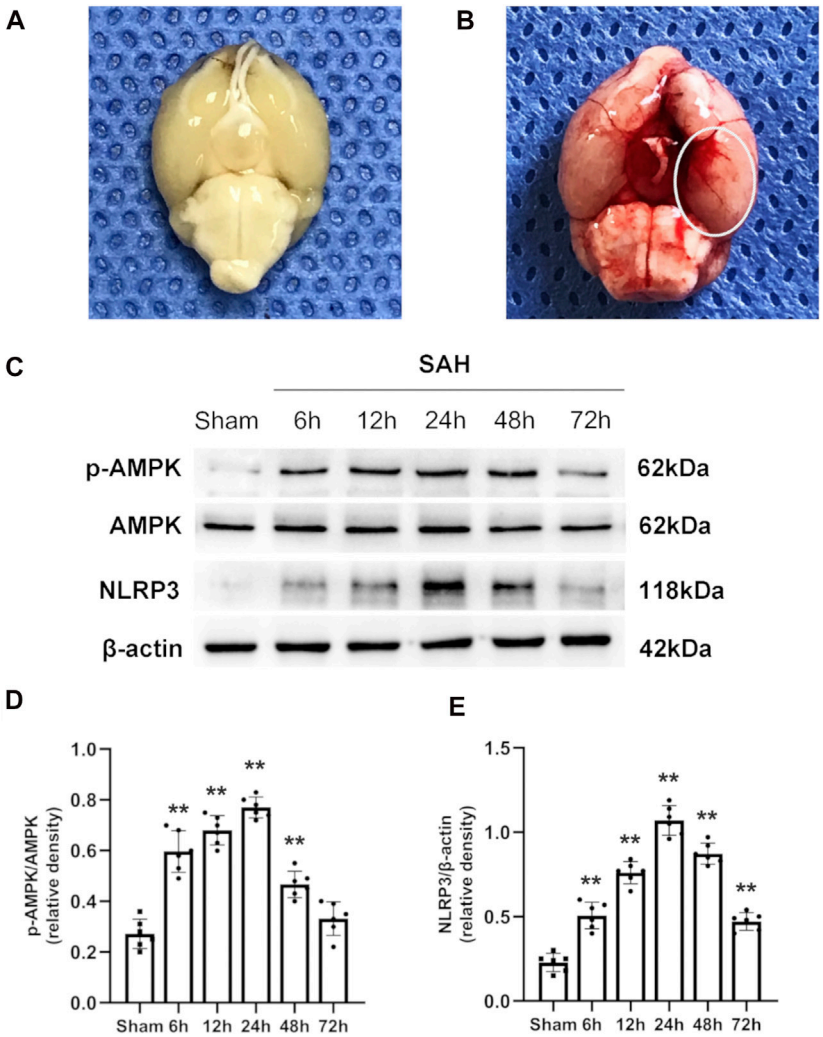

FIGURE 2 | Typical images of SAH model and expression alterations of p-AMPK/AMPK and NLRP3 in the ipsilateral hemisphere after SAH. **(A,B)** Representative photographs of the bottom of mice brains from sham and 24 h after SAH. The area within the white oval was specifically used to observe for immunostaining. **(C)** Representative western blot images. **(D,E)** Quantitative analysis of western blot. Data are expressed as the mean ± SD using one-way ANOVA followed by Tukey's post hoc test (**p < 0.01 vs Sham group, n = 6 per group).

2) The administration of metformin significantly alleviated the neurological deficit and reduced brain edema after SAH. 3) The use of metformin after SAH enhanced AMPK activation and suppressed the expression of NLRP3-relevant inflammatory mediators, thereby mitigating cell apoptosis and neuronal injury. 4) The inhibition of AMPK activation with compound C reversed the favorable effects of metformin on EBI and the inflammatory response. 5) Metformin treatment clearly suppressed microglial activation after SAH, but compound C abolished this effect. Taken together, our findings demonstrate that metformin exerts protective effects against SAH-induced EBI partly by upregulating AMPK activation, thus downregulating the NLRP3 inflammasome-associated inflammatory reaction and inhibits microglial overactivation (**Figure 8D**).

An increasing number of studies support the notion that the inflammatory response is one of the key causes of EBI and is associated with severe complications after SAH (Fujii et al., 2013; Lucke-Wold et al., 2016; Wang et al., 2021). Recent studies have shown that the inhibition of NLRP3 activation significantly ameliorates SAH-induced brain injury and delays cerebral vasospasm, indicating that NLRP3-inflammasome-associated inflammatory factors play a key role in EBI after SAH (Li et al., 2017; Dodd et al., 2021; Zhang et al., 2021). Consistent with a previous study (Zhang et al., 2017; Hu et al., 2021), our data show that the expression of NLRP3 is elevated and peaks at 24 h after SAH, and that NLRP3 is expressed in microglia.

Metformin has recently been reported to exert its protective effects through an anti-inflammatory mechanism by inhibiting the NLRP3 inflammasome in multiple diseases (Bullón et al., 2016; Yang F. et al., 2019). In the present study, we found that the administration of metformin after SAH ameliorated

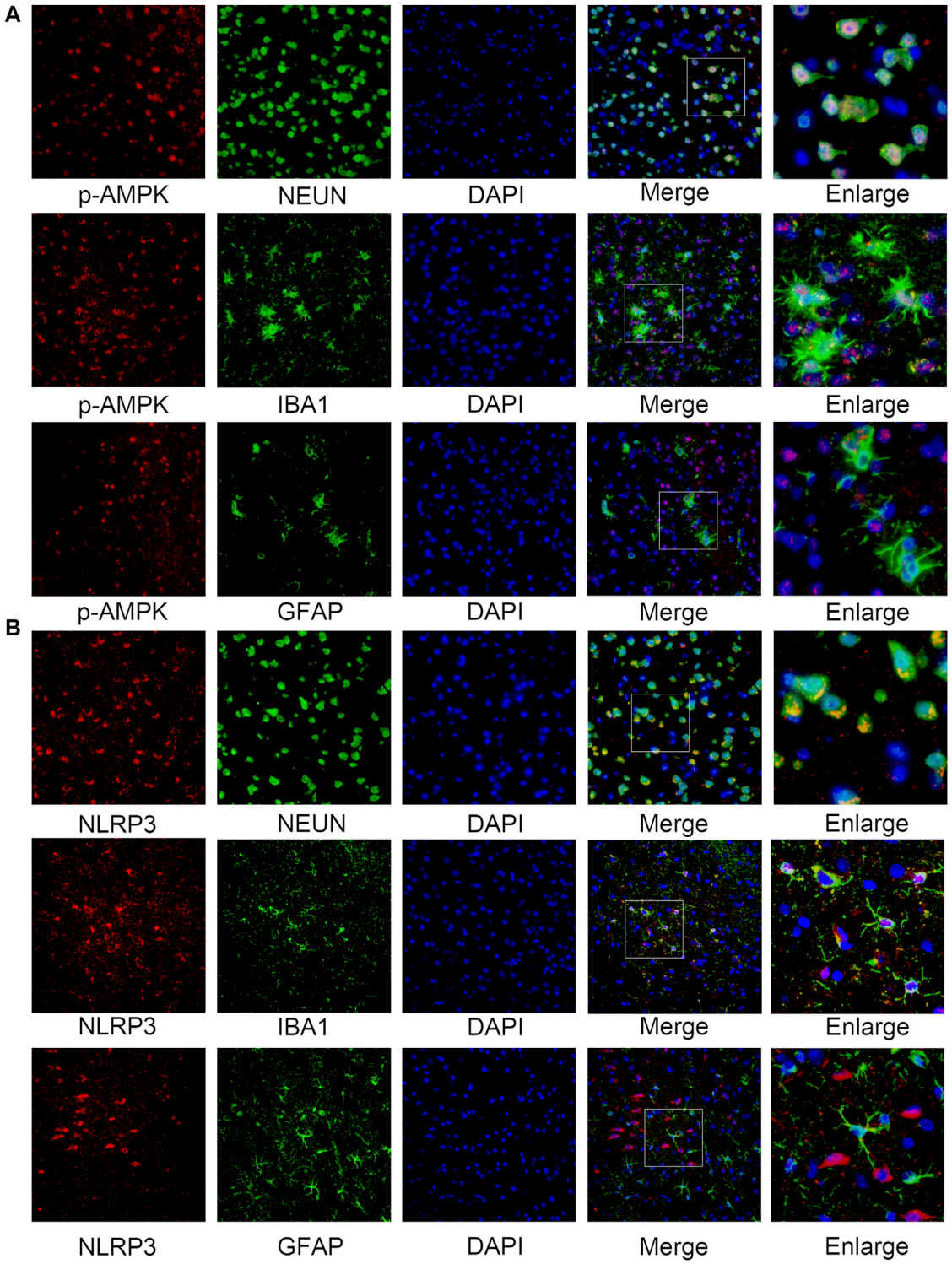

FIGURE 3 | Cellular localization of p-AMPK and NLRP3 in the ipsilateral hemisphere 24 h after SAH. **(A)** Representative images of co-immunofluorescence staining of p-AMPK (red) with neurons (NEUN, green), astrocytes (GFAP, green), and microglia (IBA1, green) in the ipsilateral cortex at 24 h after SAH. Nuclei are stained with DAPI (blue) (Magnification = ×400, scale bar = 50 um, $n = 3$ per group). **(B)** Representative images of co-immunofluorescence staining of NLRP3 (red) with the same aforesaid conditions. Enlarged images come from the areas of a white rectangle within merge images.

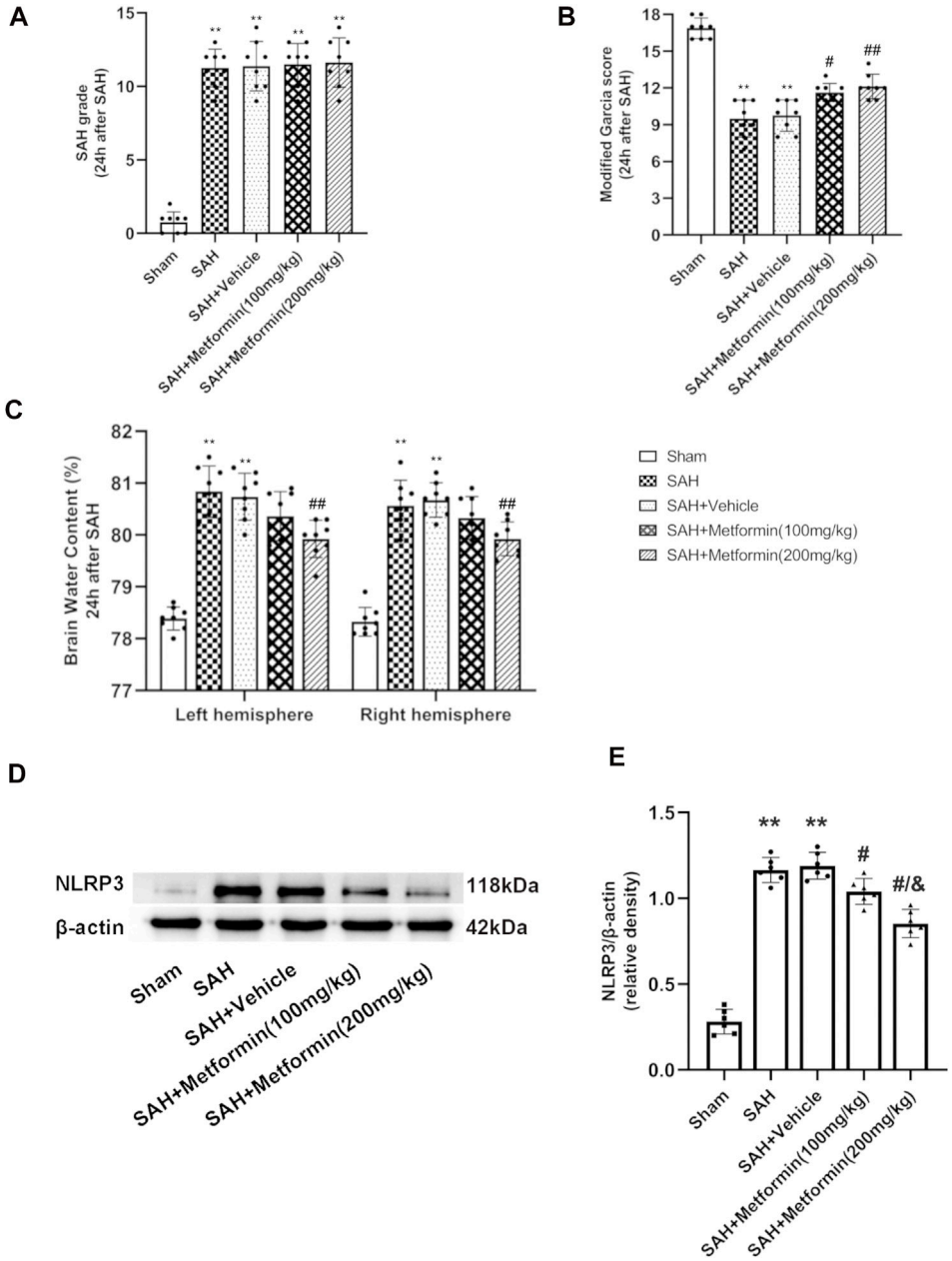

FIGURE 4 | Metformin attenuates short-term neurological deficit and brain edema at 24 h after SAH. **(A)** The SAH grades for each group. **(B)** Modified Garcia scores for each group. **(C)** Quantification of brain water content 24 h after SAH. **(D)** Representative Western blot images. **(E)** Quantitative analyses of NLRP3. N = 6 for each group. Bars represent mean ± SD. $^{**}p < 0.01$ vs. sham group. $^{\#}p < 0.05$, $^{\#\#}p < 0.01$ vs. SAH + Vehicle (normal saline) group. $^{\&}p < 0.05$ vs. SAH + Metformin (100 mg/kg).

neurobehavioral deficits, brain edema, cell apoptosis, and neuronal injury, and reduced the expression of NLRP3, cleaved caspase 1, IL-1β, and IL-18.

AMPK acts as an endocellular energy sensor. Metformin is well-recognized as an activator of AMPK (Hawley et al., 2010; Hardie et al., 2012; Jin et al., 2014). In our earlier study, we demonstrated that the activation of AMPK consistently reduces brain injury by ameliorating mitochondrial dysfunction after SAH (Fan et al., 2021). Therefore, we speculated that metformin may improve brain injury after SAH by activating AMPK. In our experiments, NLRP3 and p-AMPK both localized in neurons and microglial cells, and peaked at 24 h after SAH, consistent with the results of other studies (Xu et al., 2020; Fan et al., 2021). The similar expression trends and cellular localization of p-AMPK and NLRP3 suggested that they interact with each other. It has been reported that AMPK inhibits NLRP3 expression by activating autophagy (Yang F. et al., 2019; Youssef et al., 2021). Previous studies

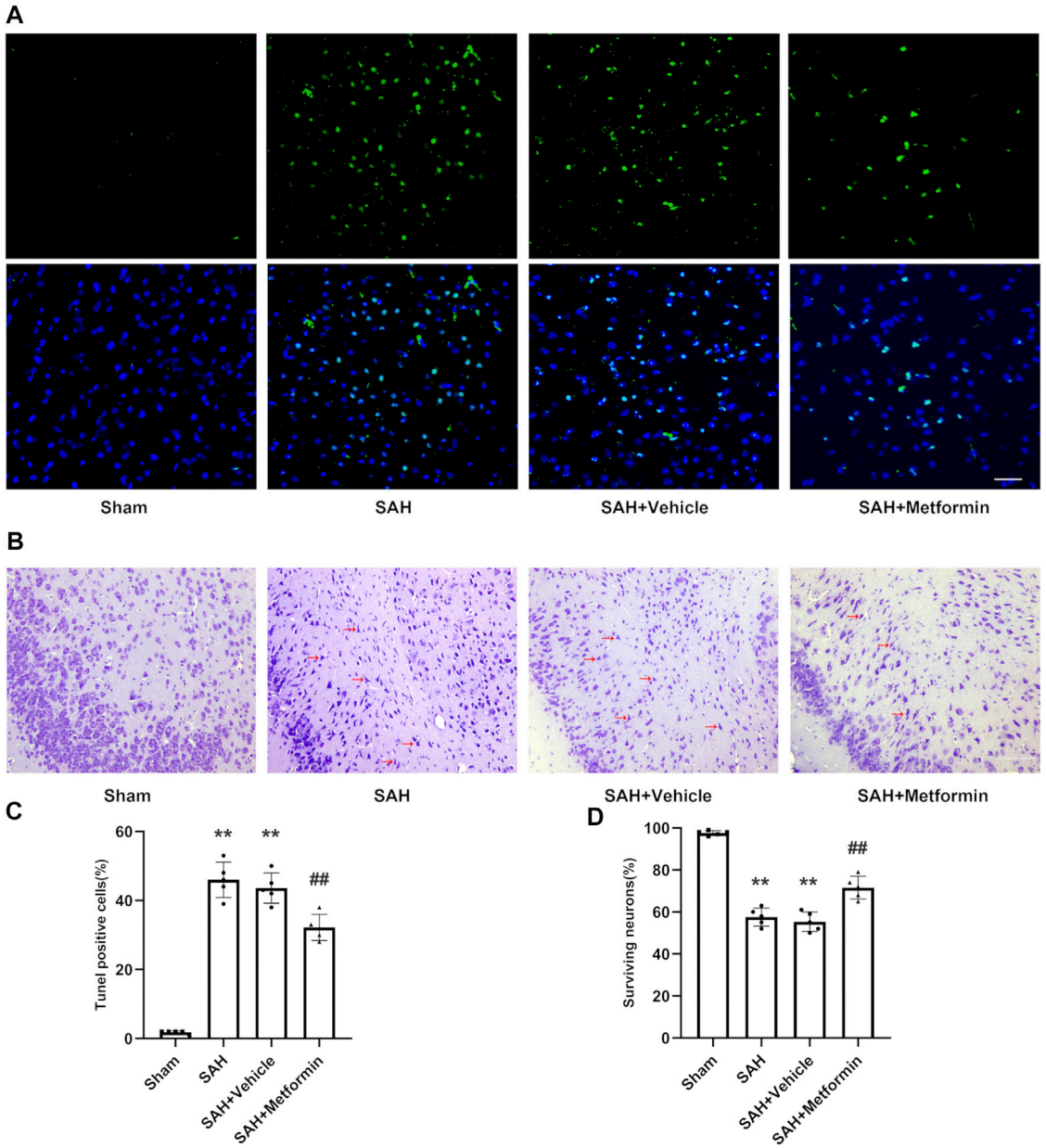

FIGURE 5 | Metformin inhibits cell apoptosis and promotes neuron survival in the cortex after SAH. Abbreviation: Met = metformin. **(A)** Typical photomicrographs of TUNEL staining (Magnification = ×400, scale bar = 50 um, $n = 5$ per group). **(C)** Quantitative analysis of TUNEL staining. **(B)** Representative photomicrographs of Nissl staining. Compared to normal neurons, impaired neurons show shrunken cell body and staining darker nuclei. The representative form of the impaired neurons was marked with a red arrow (Magnification = ×200, scale bar = 100 um, $n = 5$ per group). **(D)** The quantitative analysis of Nissl staining. Data are shown as mean ± SD. $^{**}p < 0.01$ vs. sham group. $^{\#\#}p < 0.01$ vs. SAH + Vehicle (normal saline) group.

demonstrated that AMPK activation alleviates brain injury by suppressing the activation of the endoplasmic-reticulum-stress-associated TXNIP/NLRP3 inflammasome (Li et al., 2015; Xu et al., 2019). Our results indicated that the administration of metformin enhanced the activation of AMPK, which was blocked by compound C. The protective action of metformin treatment against neurological deficit, brain edema, neuronal injury, and NLRP3-relevant inflammatory reactions after SAH were also reversed by compound C. This is consistent with recent studies that have reported that the inhibition of AMPK activation reduces the brain injury after SAH (Xu et al., 2019; Peng et al., 2020).

Microglia, the resident immunocompetent and phagocytic cells of the central nervous system, produce inflammatory mediators and contribute to the neuroinflammation that occurs after SAH (Gris et al., 2019; Zheng et al., 2020). Therefore, the suppression of microglial activation limits the harmful inflammatory response and attenuates inflammation-induced

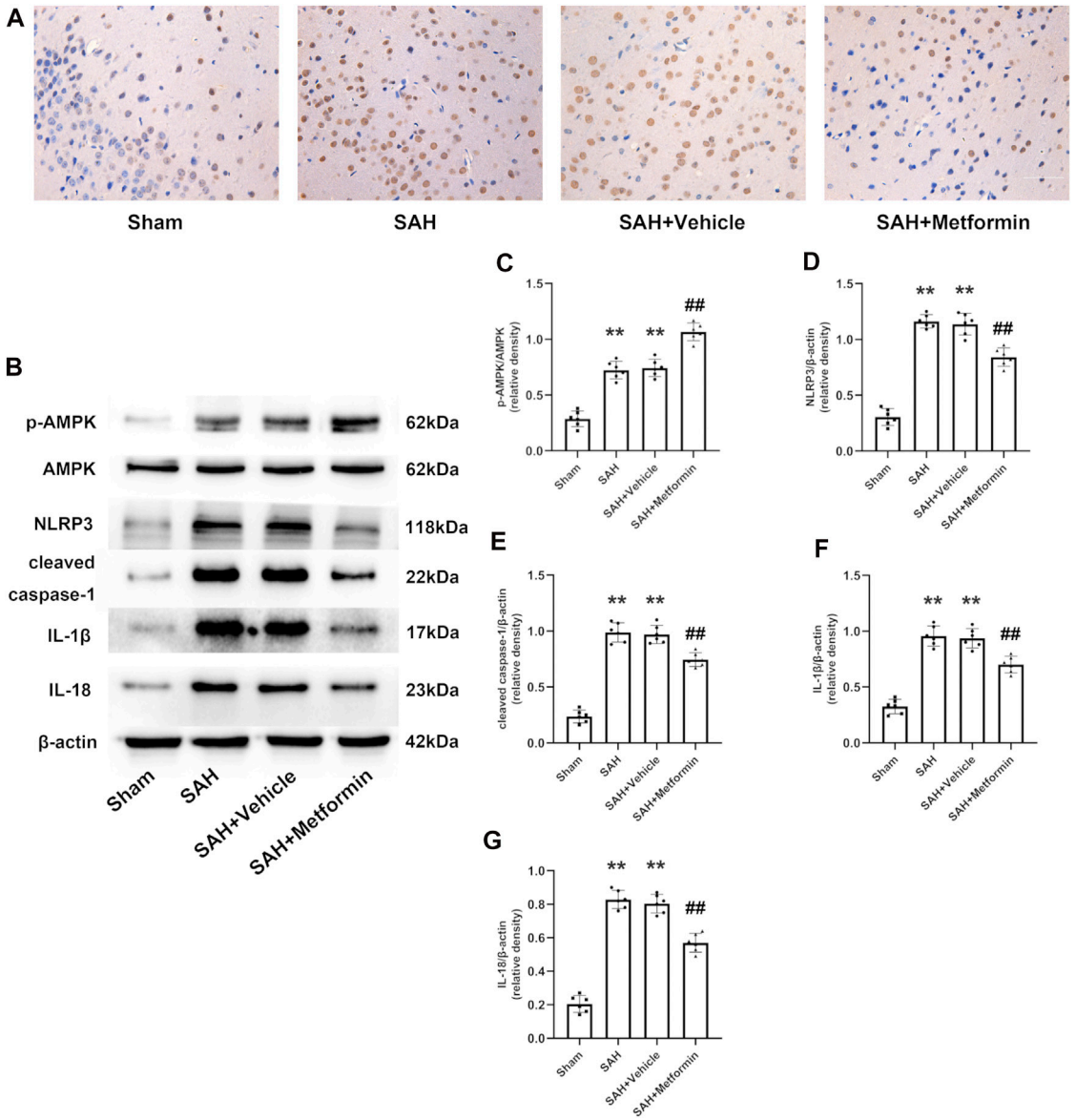

FIGURE 6 | Metformin suppresses NLRP3-associated inflammatory response. **(A)** Representative images of immunohistochemical staining (Magnification = ×400, scale bar = 50 um, $n = 5$ per group). **(B)** Representative western blot images. **(C–G)** Quantitative analysis of western blot. $N = 6$ for each group. Data are shown as mean ± SD. $^{**}p < 0.01$ vs. sham group. $^{\#\#}p < 0.01$ vs. SAH + Vehicle (normal saline) group.

EBI (Xie et al., 2017; Peng et al., 2019; Liu et al., 2020). Recent studies have provided evidence supporting the suppression of microglial activation by metformin through the activation of AMPK, both *in vivo* and *in vitro* (Pan et al., 2016; Inyang et al., 2019). Consistent with previous studies, our results indicate that metformin markedly reduces the number of IBA1-positive cells, whereas compound C abolishes this effect.

Although this study demonstrates the value of metformin in attenuating EBI in a mouse model of SAH, several limitations should be noted. First, we only evaluated the anti-inflammatory characteristics of metformin, and did not examine its possible capacity to affect other regulatory mechanisms in our mouse model of SAH. Second, previous study has shown that the prolonged use of metformin after brain injury promotes angiogenesis and long-term functional recovery (Dadwal et al., 2015). Here, only the effects of a single post-SAH intraperitoneal injection of metformin were investigated, so the long-term outcomes of multiple systemic metformin treatments over different time courses should be examined in future studies.

The recent literature has hinted that metformin plays a beneficial role in improving the poor prognoses of patients with brain injury. A multicenter retrospective analysis indicated that stroke patients with

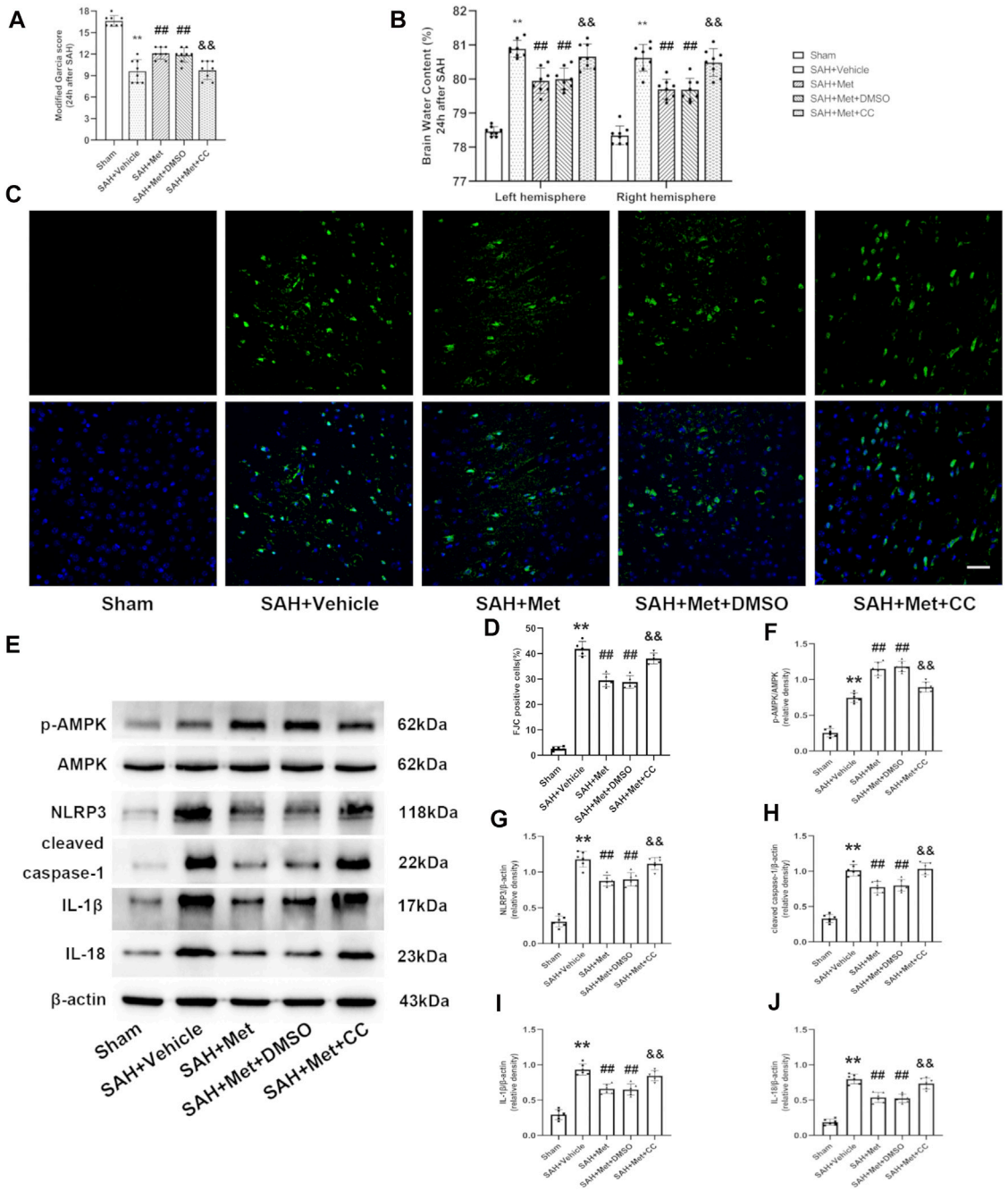

FIGURE 7 | Inhibition of AMPK abolishes the protective effects of metformin after SAH. Abbreviation: Met, metformin, CC, compound C. **(A)** Modified Garcia scores for each group. **(B)**The quantification of brain water content 24 h after SAH. *N* = 8 for each group. **(C)** Representative images of FJC staining (Magnification = ×400, scale bar = 50 um, *n* = 5 per group). **(D)** Quantitative analysis of FJC. **(E)** Representative western blot images. **(F–J)** Quantitative analysis of western blot. N = 6 for each group. Data are shown as mean ± SD. $^{**}p < 0.01$ vs. sham group. $^{\#\#}p < 0.01$ vs. SAH + Vehicle (normal saline) group. $^{\&\&}p < 0.01$ vs. SAH + Metformin + DMSO group.

diabetes who were treated with metformin showed less-severe stroke on admission and better functional outcomes at 3 months than stroke patients with diabetes who were not treated with metformin (Westphal et al., 2020). Therefore, whether metformin can improve the long-term outcomes of SAH and whether it exerts beneficial clinical effects on SAH patients must also be considered in future studies.

In conclusion, our findings support the notion that metformin exerts a neuroprotective effect by inhibiting the NLRP3-associated neuroinflammatory response and suppressing microglial activation in an AMPK-dependent manner. Therefore, metformin may provide a potential therapeutic intervention for improving EBI after SAH.

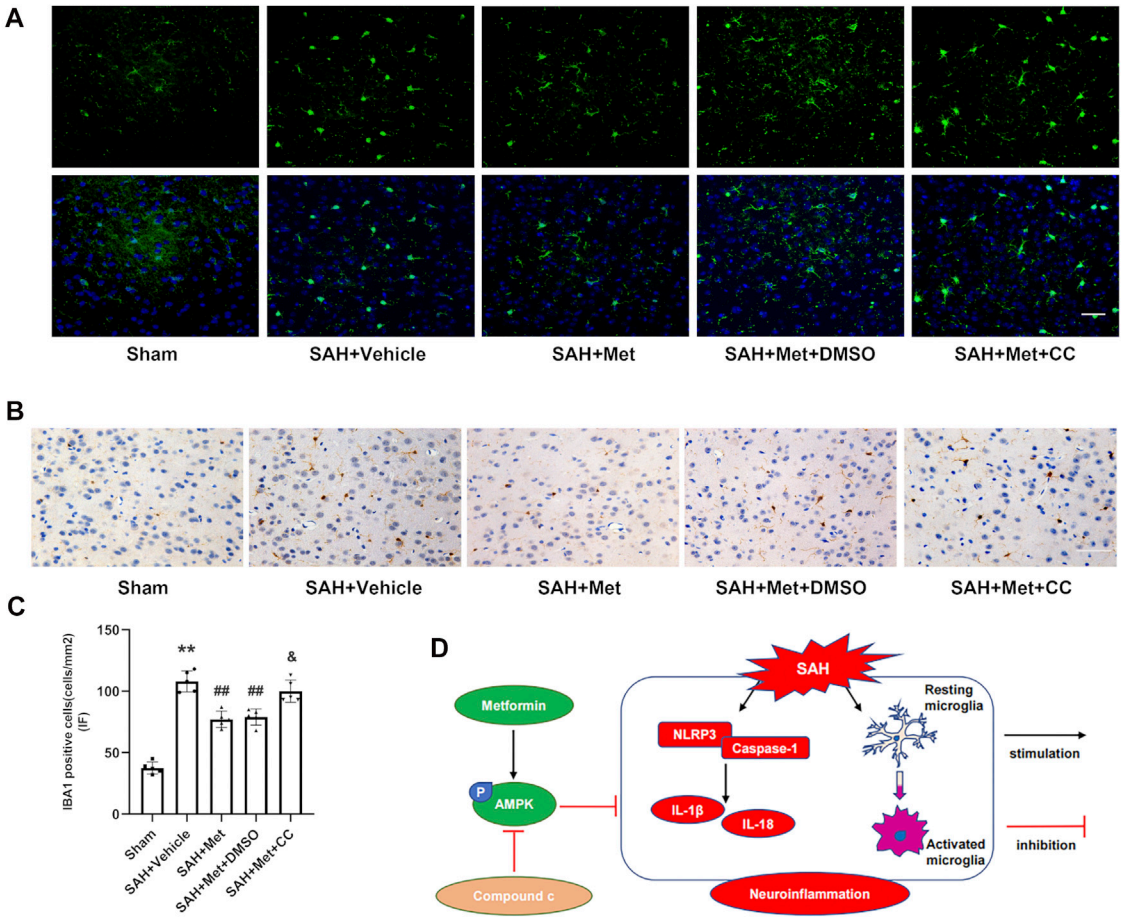

FIGURE 8 | Suppression of AMPK reverses the inhibitory effects of metformin on microglial activation after SAH. **(A,C)** Representative images of immunofluorescence staining and quantification of IBA1 activation. **(B)** Representative images of immunohistochemical staining of IBA1 activation (Magnification = ×400, scale bar = 50 um, $n = 5$ per group). Data are shown as mean ± SD. $^{**}p < 0.01$ vs. sham group. $^{\#\#}p < 0.01$ vs. SAH + Vehicle (normal saline) group. $^{\&}p < 0.05$ vs. SAH + Metformin + DMSO group. **(D)** Graphical abstract of how metformin regulates SAH-induced neuroinflammation *via* AMPK-dependent pathway.

DATA AVAILABILITY STATEMENT

The original contributions presented in the study are included in the article/**Supplementary Material**, further inquiries can be directed to the corresponding author.

ETHICS STATEMENT

The animal study was reviewed and approved by the Southern Medical University Ethics Committee (Guangzhou, China).

AUTHOR CONTRIBUTIONS

This study was designed by LJ and FJ. The experiments were completed by LJ, FJ, SG, and WL. BW, HF, and GL performed the statistical analysis. LJ and FJ, SG finished writing the manuscript. CD and XL revised the manuscript. WL, XZ, SS, RL, and DF participated in discussion development and provided expert guidance.

FUNDING

This work was supported by the National Natural Science Foundation Project (Grant Number: 81974178), the National Natural Science Foundation Project (Grant Number: 81974177), and the National Natural Science Foundation Project (Grant Number: 82001300).

SUPPLEMENTARY MATERIAL

The Supplementary Material for this article can be found online at: https://www.frontiersin.org/articles/10.3389/fphar.2022.796616/full#supplementary-material

REFERENCES

Ashabi, G., Khodagholi, F., Khalaj, L., Goudarzvand, M., and Nasiri, M. (2014). Activation of AMP-Activated Protein Kinase by Metformin Protects against Global Cerebral Ischemia in Male Rats: Interference of AMPK/PGC-1α Pathway. *Metab. Brain Dis.* 29 (1), 47–58. doi:10.1007/s11011-013-9475-2

Badjatia, N., Monahan, A., Carpenter, A., Zimmerman, J., Schmidt, J. M., Claassen, J., et al. (2015). Inflammation, Negative Nitrogen Balance, and Outcome after Aneurysmal Subarachnoid Hemorrhage. *Neurology* 84 (7), 680–687. doi:10.1212/WNL.0000000000001259

Bullón, P., Alcocer-Gómez, E., Carrión, A. M., Marín-Aguilar, F., Garrido-Maraver, J., Román-Malo, L., et al. (2016). AMPK Phosphorylation Modulates Pain by Activation of NLRP3 Inflammasome. *Antioxid. Redox Signal.* 24 (3), 157–170. doi:10.1089/ars.2014.6120

Chen, S., Feng, H., Sherchan, P., Klebe, D., Zhao, G., Sun, X., et al. (2014). Controversies and Evolving New Mechanisms in Subarachnoid Hemorrhage. *Prog. Neurobiol.* 115, 64–91. doi:10.1016/j.pneurobio.2013.09.002

Crowley, R. W., Medel, R., Kassell, N. F., and Dumont, A. S. (2008). New Insights into the Causes and Therapy of Cerebral Vasospasm Following Subarachnoid Hemorrhage. *Drug Discov. Today* 13 (5-6), 254–260. doi:10.1016/j.drudis.2007.11.010

Dadwal, P., Mahmud, N., Sinai, L., Azimi, A., Fatt, M., Wondisford, F. E., et al. (2015). Activating Endogenous Neural Precursor Cells Using Metformin Leads to Neural Repair and Functional Recovery in a Model of Childhood Brain Injury. *Stem Cel Rep.* 5 (2), 166–173. doi:10.1016/j.stemcr.2015.06.011

Deng, H. J., Deji, Q., Zhaba, W., Liu, J. Q., Gao, S. Q., Han, Y. L., et al. (2021). A20 Establishes Negative Feedback with TRAF6/NF-κB and Attenuates Early Brain Injury after Experimental Subarachnoid Hemorrhage. *Front. Immunol.* 12, 623256. doi:10.3389/fimmu.2021.623256

Dodd, W. S., Noda, I., Martinez, M., Hosaka, K., and Hoh, B. L. (2021). NLRP3 Inhibition Attenuates Early Brain Injury and Delayed Cerebral Vasospasm after Subarachnoid Hemorrhage. *J. Neuroinflammation* 18 (1), 163. doi:10.1186/s12974-021-02207-x

Etminan, N., Chang, H. S., Hackenberg, K., de Rooij, N. K., Vergouwen, M. D. I., Rinkel, G. J. E., et al. (2019). Worldwide Incidence of Aneurysmal Subarachnoid Hemorrhage According to Region, Time Period, Blood Pressure, and Smoking Prevalence in the Population: A Systematic Review and Meta-Analysis. *JAMA Neurol.* 76 (5), 588–597. doi:10.1001/jamaneurol.2019.0006

Fan, H., Ding, R., Liu, W., Zhang, X., Li, R., Wei, B., et al. (2021). Heat Shock Protein 22 Modulates NRF1/TFAM-dependent Mitochondrial Biogenesis and DRP1-Sparked Mitochondrial Apoptosis through AMPK-PGC1α Signaling Pathway to Alleviate the Early Brain Injury of Subarachnoid Hemorrhage in Rats. *Redox Biol.* 40, 101856. doi:10.1016/j.redox.2021.101856

Fujii, M., Yan, J., Rolland, W. B., Soejima, Y., Caner, B., and Zhang, J. H. (2013). Early Brain Injury, an Evolving Frontier in Subarachnoid Hemorrhage Research. *Transl. Stroke Res.* 4 (4), 432–446. doi:10.1007/s12975-013-0257-2

Garcia, J. H., Wagner, S., Liu, K. F., and Hu, X. J. (1995). Neurological Deficit and Extent of Neuronal Necrosis Attributable to Middle Cerebral Artery Occlusion in Rats. Statistical Validation. *Stroke* 26 (4), 627–635. doi:10.1161/01.str.26.4.627

Grégoire, M., Uhel, F., Lesouhaitier, M., Gacouin, A., Guirriec, M., Mourcin, F., et al. (2018). Impaired Efferocytosis and Neutrophil Extracellular Trap Clearance by Macrophages in ARDS. *Eur. Respir. J.* 52 (2), 1702590. doi:10.1183/13993003.02590-2017

Gris, T., Laplante, P., Thebault, P., Cayrol, R., Najjar, A., Joannette-Pilon, B., et al. (2019). Innate Immunity Activation in the Early Brain Injury Period Following Subarachnoid Hemorrhage. *J. Neuroinflammation* 16 (1), 253. doi:10.1186/s12974-019-1629-7

Hardie, D. G., Ross, F. A., and Hawley, S. A. (2012). AMPK: a Nutrient and Energy Sensor that Maintains Energy Homeostasis. *Nat. Rev. Mol. Cel Biol.* 13 (4), 251–262. doi:10.1038/nrm3311

Hawley, S. A., Ross, F. A., Chevtzoff, C., Green, K. A., Evans, A., Fogarty, S., et al. (2010). Use of Cells Expressing Gamma Subunit Variants to Identify Diverse Mechanisms of AMPK Activation. *Cell Metab.* 11 (6), 554–565. doi:10.1016/j.cmet.2010.04.001

Hu, X., Yan, J., Huang, L., Araujo, C., Peng, J., Gao, L., et al. (2021). INT-777 Attenuates NLRP3-ASC Inflammasome-Mediated Neuroinflammation *via* TGR5/cAMP/PKA Signaling Pathway after Subarachnoid Hemorrhage in Rats. *Brain Behav. Immun.* 91, 587–600. doi:10.1016/j.bbi.2020.09.016

Inyang, K. E., Szabo-Pardi, T., Wentworth, E., Mcdougal, T. A., Dussor, G., Burton, M. D., et al. (2019). The Antidiabetic Drug Metformin Prevents and Reverses Neuropathic Pain and Spinal Cord Microglial Activation in Male but Not Female Mice. *Pharmacol. Res.* 139, 1–16. doi:10.1016/j.phrs.2018.10.027

Jia, Y., Cui, R., Wang, C., Feng, Y., Li, Z., Tong, Y., et al. (2020). Metformin Protects against Intestinal Ischemia-Reperfusion Injury and Cell Pyroptosis *via* TXNIP-NLRP3-GSDMD Pathway. *Redox Biol.* 32, 101534. doi:10.1016/j.redox.2020.101534

Jin, Q., Cheng, J., Liu, Y., Wu, J., Wang, X., Wei, S., et al. (2014). Improvement of Functional Recovery by Chronic Metformin Treatment Is Associated with Enhanced Alternative Activation of Microglia/macrophages and Increased Angiogenesis and Neurogenesis Following Experimental Stroke. *Brain Behav. Immun.* 40, 131–142. doi:10.1016/j.bbi.2014.03.003

Laiwalla, A. N., Ooi, Y. C., Liou, R., and Gonzalez, N. R. (2016). Matched Cohort Analysis of the Effects of Limb Remote Ischemic Conditioning in Patients with Aneurysmal Subarachnoid Hemorrhage. *Transl. Stroke Res.* 7 (1), 42–48. doi:10.1007/s12975-015-0437-3

Li, Y., Li, J., Li, S., Li, Y., Wang, X., Liu, B., et al. (2015). Curcumin Attenuates Glutamate Neurotoxicity in the hippocampus by Suppression of ER Stress-Associated TXNIP/NLRP3 Inflammasome Activation in a Manner Dependent on AMPK. *Toxicol. Appl. Pharmacol.* 286 (1), 53–63. doi:10.1016/j.taap.2015.03.010

Li, J. R., Xu, H. Z., Nie, S., Peng, Y. C., Fan, L. F., Wang, Z. J., et al. (2017). Fluoxetine-enhanced Autophagy Ameliorates Early Brain Injury *via* Inhibition of NLRP3 Inflammasome Activation Following Subrachnoid Hemorrhage in Rats. *J. Neuroinflammation* 14 (1), 186. doi:10.1186/s12974-017-0959-6

Li, R., Liu, W., Yin, J., Chen, Y., Guo, S., Fan, H., et al. (2018). TSG-6 Attenuates Inflammation-Induced Brain Injury *via* Modulation of Microglial Polarization in SAH Rats through the SOCS3/STAT3 Pathway. *J. Neuroinflammation* 15 (1), 231. doi:10.1186/s12974-018-1279-1

Liu, W., Li, R., Yin, J., Guo, S., Chen, Y., Fan, H., et al. (2019). Mesenchymal Stem Cells Alleviate the Early Brain Injury of Subarachnoid Hemorrhage Partly by Suppression of Notch1-dependent Neuroinflammation: Involvement of Botch. *J. Neuroinflammation* 16 (1), 8. doi:10.1186/s12974-019-1396-5

Liu, G. J., Tao, T., Wang, H., Zhou, Y., Gao, X., Gao, Y. Y., et al. (2020). Functions of Resolvin D1-ALX/FPR2 Receptor Interaction in the Hemoglobin-Induced Microglial Inflammatory Response and Neuronal Injury. *J. Neuroinflammation* 17 (1), 239. doi:10.1186/s12974-020-01918-x

Lucke-Wold, B. P., Logsdon, A. F., Manoranjan, B., Turner, R. C., Mcconnell, E., Vates, G. E., et al. (2016). Aneurysmal Subarachnoid Hemorrhage and Neuroinflammation: A Comprehensive Review. *Int. J. Mol. Sci.* 17 (4), 497. doi:10.3390/ijms17040497

Luo, X., Li, L., Xu, W., Cheng, Y., and Xie, Z. (2020). HLY78 Attenuates Neuronal Apoptosis *via* the LRP6/GSK3β/β-Catenin Signaling Pathway after Subarachnoid Hemorrhage in Rats. *Neurosci. Bull.* 36 (10), 1171–1181. doi:10.1007/s12264-020-00532-4

Macdonald, R. L., Higashida, R. T., Keller, E., Mayer, S. A., Molyneux, A., Raabe, A., et al. (2011). Clazosentan, an Endothelin Receptor Antagonist, in Patients with Aneurysmal Subarachnoid Haemorrhage Undergoing Surgical Clipping: a Randomised, Double-Blind, Placebo-Controlled Phase 3 Trial (CONSCIOUS-2). *Lancet Neurol.* 10 (7), 618–625. doi:10.1016/S1474-4422(11)70108-9

Macdonald, R. L., Higashida, R. T., Keller, E., Mayer, S. A., Molyneux, A., Raabe, A., et al. (2012). Randomized Trial of Clazosentan in Patients with Aneurysmal Subarachnoid Hemorrhage Undergoing Endovascular Coiling. *Stroke* 43 (6), 1463–1469. doi:10.1161/STROKEAHA.111.648980

Mangan, M. S. J., Olhava, E. J., Roush, W. R., Seidel, H. M., Glick, G. D., and Latz, E. (2018). Targeting the NLRP3 Inflammasome in Inflammatory Diseases. *Nat. Rev. Drug Discov.* 17 (8), 688–606. doi:10.1038/nrd.2018.9710.1038/nrd.2018.149

Meijer, A. J., and Codogno, P. (2007). AMP-activated Protein Kinase and Autophagy. *Autophagy* 3 (3), 238–240. doi:10.4161/auto.3710

Pan, Y., Sun, X., Jiang, L., Hu, L., Kong, H., Han, Y., et al. (2016). Metformin Reduces Morphine Tolerance by Inhibiting Microglial-Mediated Neuroinflammation. *J. Neuroinflammation* 13 (1), 294. doi:10.1186/s12974-016-0754-9

Park, S., Yamaguchi, M., Zhou, C., Calvert, J. W., Tang, J., and Zhang, J. H. (2004). Neurovascular protection Reduces Early Brain Injury after Subarachnoid Hemorrhage. *Stroke* 35 (10), 2412–2417. doi:10.1161/01.STR.0000141162.29864.e9

Peng, J., Pang, J., Huang, L., Enkhjargal, B., Zhang, T., Mo, J., et al. (2019). LRP1 Activation Attenuates white Matter Injury by Modulating Microglial Polarization through Shc1/PI3K/Akt Pathway after Subarachnoid Hemorrhage in Rats. *Redox Biol.* 21, 101121. doi:10.1016/j.redox.2019.101121

Peng, Y., Zhuang, J., Ying, G., Zeng, H., Zhou, H., Cao, Y., et al. (2020). Stimulator of IFN Genes Mediates Neuroinflammatory Injury by Suppressing AMPK Signal in Experimental Subarachnoid Hemorrhage. *J. Neuroinflammation* 17 (1), 165. doi:10.1186/s12974-020-01830-4

Sanchez-Rangel, E., and Inzucchi, S. E. (2017). Metformin: Clinical Use in Type 2 Diabetes. *Diabetologia* 60 (9), 1586–1593. doi:10.1007/s00125-017-4336-x

Sugawara, T., Ayer, R., Jadhav, V., and Zhang, J. H. (2008). A New Grading System Evaluating Bleeding Scale in Filament Perforation Subarachnoid Hemorrhage Rat Model. *J. Neurosci. Methods* 167 (2), 327–334. doi:10.1016/j.jneumeth.2007.08.004

Taheri, A., Emami, M., Asadipour, E., Kasirzadeh, S., Rouini, M. R., Najafi, A., et al. (2019). A Randomized Controlled Trial on the Efficacy, Safety, and Pharmacokinetics of Metformin in Severe Traumatic Brain Injury. *J. Neurol.* 266 (8), 1988–1997. doi:10.1007/s00415-019-09366-1

Wang, J., Liang, J., Deng, J., Liang, X., Wang, K., Wang, H., et al. (2021). Emerging Role of Microglia-Mediated Neuroinflammation in Epilepsy after Subarachnoid Hemorrhage. *Mol. Neurobiol.* 58 (6), 2780–2791. doi:10.1007/s12035-021-02288-y

Westphal, L. P., Widmer, R., Held, U., Steigmiller, K., Hametner, C., Ringleb, P., et al. (2020). Association of Prestroke Metformin Use, Stroke Severity, and Thrombolysis Outcome. *Neurology* 95 (4), e362–e373. doi:10.1212/WNL.0000000000009951

Xian, H., Liu, Y., Rundberg Nilsson, A., Gatchalian, R., Crother, T. R., Tourtellotte, W. G., et al. (2021). Metformin Inhibition of Mitochondrial ATP and DNA Synthesis Abrogates NLRP3 Inflammasome Activation and Pulmonary Inflammation. *Immunity* 54 (7), 1463. doi:10.1016/j.immuni.2021.05.004

Xie, Z., He, C., and Zou, M. H. (2011). AMP-activated Protein Kinase Modulates Cardiac Autophagy in Diabetic Cardiomyopathy. *Autophagy* 7 (10), 1254–1255. doi:10.4161/auto.7.10.16740

Xie, Y., Guo, H., Wang, L., Xu, L., Zhang, X., Yu, L., et al. (2017). Human Albumin Attenuates Excessive Innate Immunity *via* Inhibition of Microglial Mincle/Syk Signaling in Subarachnoid Hemorrhage. *Brain Behav. Immun.* 60, 346–360. doi:10.1016/j.bbi.2016.11.004

Xu, W., Li, T., Gao, L., Zheng, J., Yan, J., Zhang, J., et al. (2019). Apelin-13/APJ System Attenuates Early Brain Injury *via* Suppression of Endoplasmic Reticulum Stress-Associated TXNIP/NLRP3 Inflammasome Activation and Oxidative Stress in a AMPK-dependent Manner after Subarachnoid Hemorrhage in Rats. *J. Neuroinflammation* 16 (1), 247. doi:10.1186/s12974-019-1620-3

Xu, W., Mo, J., Ocak, U., Travis, Z. D., Enkhjargal, B., Zhang, T., et al. (2020). Activation of Melanocortin 1 Receptor Attenuates Early Brain Injury in a Rat Model of Subarachnoid Hemorrhage Viathe Suppression of Neuroinflammation through AMPK/TBK1/NF-κB Pathway in Rats. *Neurotherapeutics* 17 (1), 294–308. doi:10.1007/s13311-019-00772-x

Xu, P., Hong, Y., Xie, Y., Yuan, K., Li, J., Sun, R., et al. (2021). TREM-1 Exacerbates Neuroinflammatory Injury *via* NLRP3 Inflammasome-Mediated Pyroptosis in Experimental Subarachnoid Hemorrhage. *Transl. Stroke Res.* 12 (4), 643–659. doi:10.1007/s12975-020-00840-x

Yang, F., Qin, Y., Wang, Y., Meng, S., Xian, H., Che, H., et al. (2019). Metformin Inhibits the NLRP3 Inflammasome *via* AMPK/mTOR-dependent Effects in Diabetic Cardiomyopathy. *Int. J. Biol. Sci.* 15 (5), 1010–1019. doi:10.7150/ijbs.29680

Yang, Y., Wang, H., Kouadir, M., Song, H., and Shi, F. (2019). Recent Advances in the Mechanisms of NLRP3 Inflammasome Activation and its Inhibitors. *Cell Death Dis.* 10 (2), 128. doi:10.1038/s41419-019-1413-8

Youssef, M. E., Abd El-Fattah, E. E., Abdelhamid, A. M., Eissa, H., El-Ahwany, E., Amin, N. A., et al. (2021). Interference with the AMPKα/mTOR/NLRP3 Signaling and the IL-23/IL-17 Axis Effectively Protects against the Dextran Sulfate Sodium Intoxication in Rats: A New Paradigm in Empagliflozin and Metformin Reprofiling for the Management of Ulcerative Colitis. *Front. Pharmacol.* 12, 719984. doi:10.3389/fphar.2021.719984

Zhang, X., Wu, Q., Zhang, Q., Lu, Y., Liu, J., Li, W., et al. (2017). Resveratrol Attenuates Early Brain Injury after Experimental Subarachnoid Hemorrhage *via* Inhibition of NLRP3 Inflammasome Activation. *Front. Neurosci.* 11, 611. doi:10.3389/fnins.2017.00611

Zhang, J., Huang, L., Shi, X., Yang, L., Hua, F., Ma, J., et al. (2020). Metformin Protects against Myocardial Ischemia-Reperfusion Injury and Cell Pyroptosis *via* AMPK/NLRP3 Inflammasome Pathway. *Aging (Albany NY)* 12 (23), 24270–24287. doi:10.18632/aging.202143

Zhang, X. S., Lu, Y., Li, W., Tao, T., Wang, W. H., Gao, S., et al. (2021). Cerebroprotection by Dioscin after Experimental Subarachnoid Haemorrhage *via* Inhibiting NLRP3 Inflammasome through SIRT1-dependent Pathway. *Br. J. Pharmacol.* 178 (18), 3648–3666. doi:10.1111/bph.15507

Zheng, Z. V., Lyu, H., Lam, S. Y. E., Lam, P. K., Poon, W. S., and Wong, G. K. C. (2020). The Dynamics of Microglial Polarization Reveal the Resident Neuroinflammatory Responses after Subarachnoid Hemorrhage. *Transl. Stroke Res.* 11 (3), 433–449. doi:10.1007/s12975-019-00728-5

Zhou, R., Yazdi, A. S., Menu, P., and Tschopp, J. (2011). A Role for Mitochondria in NLRP3 Inflammasome Activation. *Nature* 469 (7329), 221–225. doi:10.1038/nature09663

Conflict of Interest: The authors declare that the research was conducted in the absence of any commercial or financial relationships that could be construed as a potential conflict of interest.

Publisher's Note: All claims expressed in this article are solely those of the authors and do not necessarily represent those of their affiliated organizations, or those of the publisher, the editors and the reviewers. Any product that may be evaluated in this article, or claim that may be made by its manufacturer, is not guaranteed or endorsed by the publisher.

frontiers | Frontiers in Pharmacology

BRIEF RESEARCH REPORT
published: 19 April 2022
doi: 10.3389/fphar.2022.846172

Dysfunction of Inflammatory Pathways and Their Relationship With Psychological Factors in Adult Female Patients With Eating Disorders

Javier R. Caso[1,2]*, *Karina S. MacDowell*[1,2], *Marta Soto*[3,4], *Francisco Ruiz-Guerrero*[5], *Álvaro Carrasco-Díaz*[6], *Juan C. Leza*[1,2], *José L. Carrasco*[2,3,4] *and Marina Díaz-Marsá*[2,3,4]

[1]*Departamento de Farmacología y Toxicología, Facultad de Medicina, Instituto de Investigación Sanitaria Hospital 12 de Octubre (Imas12), Instituto Universitario de Investigación en Neuroquímica UCM, Universidad Complutense de Madrid, Madrid, Spain,* [2]*Centro de Investigación Biomédica en Red de Salud Mental (CIBERSAM), Madrid, Spain,* [3]*Departamento de Medicina Legal, Psiquiatría y Patología, Facultad de Medicina, Universidad Complutense de Madrid, Madrid, Spain,* [4]*Instituto de Investigación Sanitaria, Hospital Clínico San Carlos, Madrid, Spain,* [5]*Hospital Universitario Marqués de Valdecilla, Santander, Spain,* [6]*Facultad de Educación y Psicología, Universidad Francisco de Vitoria, Madrid, Spain*

OPEN ACCESS

Edited by:
Annalisa Bruno,
University of Studies G. d'Annunzio Chieti and Pescara, Italy

Reviewed by:
Marco Di Nicola,
Agostino Gemelli University Polyclinic (IRCCS), Italy
Chafia Touil-Boukoffa,
University of Science and Technology Houari Boumediene, Algeria

***Correspondence:**
Javier R. Caso
jrcaso@med.ucm.es

Specialty section:
This article was submitted to Inflammation Pharmacology, a section of the journal Frontiers in Pharmacology

Received: *30 December 2021*
Accepted: *04 April 2022*
Published: *19 April 2022*

Citation:
Caso JR, MacDowell KS, Soto M, Ruiz-Guerrero F, Carrasco-Díaz Á, Leza JC, Carrasco JL and Díaz-Marsá M (2022) Dysfunction of Inflammatory Pathways and Their Relationship With Psychological Factors in Adult Female Patients With Eating Disorders. Front. Pharmacol. 13:846172. doi: 10.3389/fphar.2022.846172

The attempts to clarify the origin of eating disorders (ED) have not been completely successful and their etiopathogenesis remains unknown. Current research shows an activation of the immune response in neuropsychiatric diseases, including ED. We aimed to investigate immune response parameters in patients with ED and to identify psychological factors influencing the inflammatory response. The relationship between inflammation markers and impulsivity and affective symptomatology was explored as well. Thirty-four adult female patients with current diagnosis of ED, none of them under psychopharmacological treatment (excluding benzodiazepines), were included in this study. Patients were compared with a healthy control group of fifteen adult females. The levels of inflammatory markers and indicators of oxidative/nitrosative stress were evaluated in plasma and/or in peripheral blood mononuclear cells (PBMCs). Subjects were assessed by means of different ED evaluation tools. Additionally, the Barratt Impulsiveness Scale, the Montgomery-Asberg Depression Rating Scale and the Hamilton Anxiety Rating Scale were also employed. Patients with ED shown increased plasma levels of the pro-inflammatory nuclear factor *kappa* B (NFκB) and the cytokine tumor necrosis factor-*alpha* (TNF-α), among other factors and an increment in the oxidative/nitrosative stress as well as increased glucocorticoid receptor (GR) expression levels in their PBMCs. Moreover, the inflammatory prostaglandin E_2 (PGE_2) correlated with impulsiveness and the anti-inflammatory prostaglandin J_2 (15d-PGJ_2) correlated with depressive symptomatology. Our results point towards a relationship between the immune response and impulsiveness and between the immune response and depressive symptomatology in female adult patients with ED.

Keywords: eating disorders, affective disorders, impulsivity, depressive symptomatology, cytokines

INTRODUCTION

Eating disorders (ED) are a group of mental conditions including, among others, Anorexia Nervosa (AN), Bulimia Nervosa (BN), and Unspecified Feeding or Eating Disorder (American Psychiatric Association, 2013). These conditions represent a public health matter not only because of life prevalence of AN (Lindvall Dahlgren et al., 2017) but also for the terrific suffering that they cause in patients and their consequences, in some cases, even death.

Efforts to clarify the origin of ED have not been completely successful to the date. Some psychological factors, sociocultural influences, intergenerational effects, and biological and genetic predispositions have been proposed as risk factors for these disorders (Culbert et al., 2015) but their etiopathogenesis remains unknown.

Among possible biological causes, changes in several neurotransmitters (Grzelak et al., 2017) or genetic components (Scherag et al., 2010; Bulik et al., 2016) have been proposed. Similarly, immuno-endocrine factors have been related with ED (Brambilla et al., 2001). Relationships between hyper-reactivity to stress and raises in cortisol levels have been observed (Monteleone et al., 2014) as well as a linkage between stress response and inflammation (Paszynska et al., 2016). Hypercortisolemia steers to the production and gathering of cytotoxic proinflammatory parameters in the peripheral nervous system (PNS) and in the central nervous system (CNS) (Sorrells et al., 2009).

Attempts on the recognition of potential biomarkers suggest variations in the proinflammatory cytokines expression in patients with ED (Corcos et al., 2003; Dalton et al., 2018). Previous studies have also reported increased levels of pro-inflammatory cytokines such as tumor necrosis factor-*alpha* (TNF-α), interleukin (IL)-1*beta* (IL-1β) and IL-6 in patients with ED (Nova et al., 2002; Kahl et al., 2004; Ahren-Moonga et al., 2011; Macdowell et al., 2013).

Inflammation is controlled by inter- and intracellular processes. Analyses have indicated a stimulation of a number of elements of the immune response [i.e., the nuclear factor *kappa* B (NFκB), the inducible isoform of the nitric oxide synthase (iNOS) and the inducible cyclooxygenase-2 (COX-2)] in rodent models and/or in samples from patients with psychiatric conditions (Dantzer et al., 2008; Garcia-Bueno et al., 2008; Leonard and Maes, 2012). Interestingly, COX-2 and the final markers of lipid peroxidation of the cell membranes have been observed to be augmented in plasma from adult ED patients (Macdowell et al., 2013).

COX-2 also participates in the compensatory anti-inflammatory response. Amongst the most significant anti-inflammatory processes are the cyclopentenone prostaglandins produced from the COX-2 activation by different pathophysiological elements, and the activities of the *gamma* isoform of the peroxisome proliferator-activated receptor (PPARγ) (Kapadia et al., 2008; Popa-Wagner et al., 2013).

Several stress-related neuropsychiatric diseases, including ED, have been related to the dysfunction of both pro- and anti-inflammatory pathways and to an increase in inflammation (Garcia-Bueno et al., 2008; Dunjic-Kostic et al., 2013). Even more, inflammation has been identified as a differential factor in ED subtypes (Anderson et al., 2018).

Some clinical aspects of psychiatric disorders like impulsiveness are related to an impairment in the inflammatory mechanisms (Sutin et al., 2012) and the relationship between impulsivity and ED has been corroborated (Waxman, 2009), including in BN (Merlotti et al., 2013) and in AN (Lavender et al., 2017).

Affective symptoms are comorbid with ED (Hudson et al., 2007) and higher levels of depression and general anxiety correlate with higher ED symptomatology (Smith et al., 2018); therefore, these aspects can determine the evolution of ED, as well as their prognosis and treatment (Vall and Wade, 2015).

The aim of this study was to examine pro/anti-inflammatory parameters and related risk pathways in patients with ED. Usually, studies focus on adolescent patients. We wanted to study a group of patients that we do believe is underrepresented in the usual studies: adult females and with a long history fighting with the disease. That was the reason for choosing a specific age range and gender. Thus, a group of adult female patients with ED (none of them under psychopharmacological treatment, excluding benzodiazepines) and a healthy control group were compared.

Consequently, several immune parameters implicated in the regulation of inflammation and in the pro/anti-inflammatory balance, including the resulting oxidative/nitrosative factors, were studied in plasma and/or peripheral blood mononuclear cells (PBMCs). The choice of PBMCs is founded in their actions providing selective responses to the immune system and in being major cells in the human body immunity as well as their plausible role as a source of inflammatory biomarkers.

Finally, the relationship between inflammation markers and impulsivity and affective symptomatology was explored as well, aiming to identify psychological factors that might potentially influence the inflammatory response in ED.

MATERIAL AND METHODS

Sample and Clinical/Psychological Tests

The criteria of DSM-IV-TR were used for diagnosis (American Psychiatric Association, 2000). Thirty-four female patients with present diagnosis of ED were included in this study: 11 of them were diagnosed with anorexia nervosa (AN), from which 8 had a diagnosis of AN restricting type -ANr- and three had a diagnosis of AN purging type -ANp-, nine had a diagnosis of bulimia nervosa (BN) and 14 had a diagnosis of Not Otherwise Specified (EDNOS). Patients were recruited at the Eating Disorders Unit of a general hospital (*Hospital Clínico San Carlos*, Madrid, Spain) and were evaluated by a senior psychiatrist who was responsible for the process of diagnosis. All subjects were outpatients and none of them was under psychopharmacological treatment (excluding benzodiazepines). To depict the psychopathology of the condition, patients were assessed by means of different ED evaluation tools comprising the Eating Disorders Inventory (EDI) (Garner et al., 1983), the Body Shape Questionnaire (BSQ) (Cooper et al., 1987), and the Bulimic Investigatory Test

Edinburgh (BITE) (Henderson and Freeman, 1987). In addition, the Barratt Impulsiveness Scale (Patton et al., 1995) was employed to assess impulsiveness. Patients also completed the Montgomery-Asberg Depression Rating Scale (MADRS) (Montgomery and Asberg, 1979) and the Hamilton Anxiety Rating Scale (Hamilton, 1960).

Inclusion criteria for patients were: 1) aged 18–45 years; 2) Diagnose of Eating Disorder according to DSM-IV-TR criteria and evaluated by an expert psychiatrist. Exclusion criteria were: 1) severe physical conditions, such as organic brain syndrome or neurological disease that could affect neuropsychological performance; 2) Intelligence Quotient IQ < 85; 3) Major Depression Disorder (MDD) or substance misuse within the last 6 months; and 4) DSM-IV-TR criteria for schizophrenia, severe psychotic disorder or bipolar disorder.

The control group included 15 females which did not present any other current psychiatric medical disorder that could potentially affect inflammatory parameters. Controls were assessed by a psychologist and, in addition to present axis I disorders such as major depression, dysthymia or substance dependence disorders, lifetime history of schizophreniform or bipolar disorder were also counted as exclusion criteria for the research. Inclusion criteria for controls were: 1) aged 18–45 years old; and 2) matched in age, sex, and educational level with patients. Exclusion criteria for controls were the same that for patient, in addition to do not meet full or subthreshold criteria for ED, either restrictive or bulimic types.

No participants had fever or any allergies, ongoing infections, or other serious physical conditions at the time of assessment, and they had not received immunosuppressive drugs or vaccines for at least 6 months or anti-inflammatory drugs for at least 2 days before blood sampling. Ethical approval was obtained from the *Hospital Clínico San Carlos* Ethics Committee. All participants signed written informed consent after receiving a complete description of the study.

Specimen Collection and Preparation

If not acknowledged, the chemicals and reagents utilized were provided by Sigma-Aldrich (Spain).

Venous blood samples (10 ml) were collected between 8:00 and 10:00 h after overnight fasting. Samples were kept at 4°C until preparation after approximately 1 h. Blood tubes were centrifuged (641 g × 10 min, 4°C). The resultant plasma samples were collected and stored at −80°C. The rest of the sample was 1:2 diluted in culture medium (RPMI 1640, LifeTech) and a gradient with Ficoll-Paque (GE Healthcare) was used to isolate mononuclear cells by centrifugation (800 g × 40 min, room temperature–RT-). The PBMC layer was aspired, re-suspended in RPMI and centrifuged (1,116 g, 10 min, room temperature). The supernatant was removed, and the mononuclear cell-enriched pellet was stored at −80°C.

Determinations in Plasma

Cytokine Levels

Enzyme immunoassays (EIA) kits (Cayman Europe, Estonia) adhering to the manufacturer's instructions were employed to measure the TNF-α and IL-1β plasma levels.

Prostaglandin Levels

Commercially available EIA kits (Enzo, Switzerland) were used to measure the prostaglandin (PG) E_2 and 15-deoxy-$\Delta^{12,14}$- PGJ_2 (15d-PGJ_2) plasma levels.

Lipid Peroxidation

It was assessed by Thiobarbituric Acid Reactive Substances (TBARS) assay (Cayman Europe, Estonia) following the manufacturer's instructions.

Measurements in PBMCs

Preparation of Nuclear and Cytosolic Extracts From PBMCs

PBMC samples were first fractionated in nuclear and cytosolic extracts using a procedure extensively utilized which delivers a high purity nuclear extract, almost without cytosolic residue (Garcia-Bueno et al., 2014; Caso et al., 2020).

Western Blot Analysis

The protein levels of the nuclear and cytosolic extracts were adjusted and then mixed with Laemmli sample buffer combined with β-mercaptoethanol (Bio-Rad, Hercules, CA). Then, samples were protein-size split in 10% SDS-polyacrylamide gel electrophoresis (90 V). Proteins from the gels were blotted onto a nitrocellulose membrane with a semi-dry transfer system (Bio-Rad). After the gel electrophoresis the membranes were blocked in 30 ml Tris-buffered saline containing 0.1% Tween 20 and 5% skim milk/BSA and were incubated with specific antibodies. The proteins to analyze were chosen based in a previous study, as well as the antibodies and their dilutions (Caso et al., 2020): 1) iNOS (Santa Cruz Biotechnology Cat# sc-650, RRID:AB_631831, diluted 1:750); 2) COX-2 (Santa Cruz Biotechnology Cat# sc-1747, RRID:AB_2084976, diluted 1:1,000); 3) PPARγ (Santa Cruz Biotechnology Cat# sc-7196, RRID:AB_654710, diluted 1:1,000); 4) phospho-p38 (Santa Cruz Biotechnology Cat# sc-17852-R, RRID:AB_2139810, diluted 1:750); 5) p38 (Santa Cruz Biotechnology Cat# sc-7972, RRID:AB_628079, diluted 1:750); 6) phospho-ERK (Cell Signaling Technology Cat# 8544, RRID:AB_11127856, diluted 1:1,000); 7) ERK (Cell Signaling Technology Cat# 4695, RRID:AB_390779, diluted 1:2,000); 8) NFκB p65 (Santa Cruz Biotechnology Cat# sc-372, RRID:AB_632037, diluted 1:1,000); 9) GR (Santa Cruz Biotechnology Cat# sc-1004, RRID:AB_2155786, diluted 1:1,000); 10) β-actin (Sigma-Aldrich Cat# A5441, RRID:AB_476744, diluted 1:10,000); 11) GAPDH (Sigma-Aldrich Cat# G8795, RRID:AB_1078991, diluted 1:5,000).

After washing with a TBS-Tween solution, the membranes were incubated with the respective horseradish peroxidase-conjugated secondary antibodies for 90 min at room temperature and revealed by ECL™-kit (Amersham Ibérica, Spain).

Blots were imaged utilizing an Odyssey® Fc System (Li-COR Biosciences) and quantified by densitometry (NIH ImageJ® software, RRID:SCR_003070). All measures are stated in arbitrary units of optical density (O.D.). Various exposition times were analyzed to guarantee the linearity in the intensity of the bands. The β-actin and the GAPDH were used as loading

TABLE 1 | Mean tests scores for ED and for anxiety, impulsiveness, and depressive symptomatology.

		Patients with ED Mean (SD)	Control Mean (SD)
BMI		21.15 (7.27)	21.79 (3.81)
BIS-11	*Global Score*	45.72 (16.5)	43.64 (14.47)
	Attentional impulsiveness	14.91 (7.34)	12.55 (4.7)
	Motor impulsiveness	16.25 (8.49)	13.86 (4.8)
	Non planning impulsiveness	15.50 (7.86)	12.55 (4.9)
BITE	*Global Score*	29.23 (16.18)***	3.33 (3.22)
	Symptoms	17.08 (8.85)***	2.50 (2.84)
	Severity of illness	11.54 (8.23)***	0.67 (0.88)
EDI	*Global Score*	74.29 (45.59)***	9.36 (8.59)
	Drive of thinness	12.50 (6.34)**	6.92 (7.24)
	Bulimic symptomatology	6.92 (7.20)***	0.33 (0.88)
	Body dissatisfaction	17.67 (8.53)***	2.42 (3.55)
	Ineffectiveness and low self-esteem	14.08 (8.66)***	0.75 (1.42)
	Perfectionism	6.50 (4.40)***	2.33 (2.57)
	Interpersonal distrust	6.17 (4.84)***	1.25 (1.13)
	Interoceptive awareness	13.00 (7.82)***	1.50 (2.19)
	Maturity Fears	10.67 (6.89)***	1.25 (1.28)
BSQ	*Global Score*	140.79 (46.76)***	56.17 (32.59)
	Body dissatisfaction	77.00 (26.53)***	30.17 (18.11)
	Weight concern	63.79 (20.61)***	31.00 (18.82)
HARS	*Global Score*	27.64 (12.91)***	3.50 (4.8)
MADRS	*Global Score*	23.73 (12.49)***	3.36 (5.44)

Different psychological evaluation tools employed: the Barratt Impulsiveness Scale (BIS), the Bulimic Investigatory Test Edinburgh (BITE), the Eating Disorders Inventory (EDI), the Body Shape Questionnaire (BSQ), the Hamilton Anxiety Rating Scale (HARS) and the Montgomery-Asberg Depression Rating Scale (MADRS). Data are shown as Mean (Standard Deviation–SD-). Data were analyzed using the D'Agostino and Pearson normality test to assess Gaussian distribution, followed by an unpaired two-tailed t *test. When data did not follow a Gaussian distribution, a Mann-Whitney test was performed. When the* F*-test indicated that variances were significantly different, an unpaired two-samples* t*-test with Welch's correction was performed.*

A $p < 0.05$ *was considered statistically significant;* $^{**}p < 0.01$, $^{***}p < 0.001$ *vs. Control.*

controls for the cytosolic fraction and the nuclear fraction, respectively.

Protein Levels

Protein levels were determined employing the method of Bradford, founded on the principle of protein-dye binding.

Statistical Studies

Data are expressed as mean ± SEM. Biochemical data were analyzed using the D'Agostino and Pearson normality test to assess Gaussian distribution, followed by an unpaired two-tailed *t* test. When data did not follow a Gaussian distribution, a Mann-Whitney test was performed. The Grubb's test/extreme studentized deviate method (ESD) was performed with a significance level set at 0.05 for the detection of outliers. For the study of the clinical characteristics data were analyzed using the D'Agostino and Pearson normality test to assess Gaussian distribution, followed by an unpaired two-tailed *t* test. When data did not follow a Gaussian distribution, a Mann-Whitney test was performed. When the *F*-test indicated that variances were significantly different, an unpaired two-samples *t*-test with Welch's correction was performed. Data were analyzed with the GraphPad Prism (v 7.00) software. As previously described (Caso et al., 2020) the association among inflammation biomarkers and clinical variables, measured by the psychometric tests, was evaluated by means of the Pearson correlation coefficient for all the variables except factors of ED: drive for thinness, Bulimic Symptomatology, Body dissatisfaction, Ineffectiveness and low self-esteem, perfectionism, interpersonal distrust, interoceptive awareness and maturity fears. This evaluation was made with SPSS (v.21). In all cases, a p value <0.05 was considered statistically significant.

RESULTS

Clinical Characteristics of Patients and Controls

In patients, the mean duration of the illness was 12.23 (±9.8) years. The sample mean age was 28.56 (±8.5) years old. Mean scores for ED and for impulsiveness are displayed in **Table 1**. The mean value of the body Mass Index (BMI) was 21.15 ± 7.27 kg/m^2.

The control group mean age was 22.53 (±2.5) years. Members of this group did not present any other current psychiatric medical disorder that could potentially affect inflammatory parameters. Mean BMI was 21.79 (±3.81) kg/m^2.

The clinical characteristics and the comparisons between controls and patients can be seen in **Table 1**.

ED Affect Plasma Levels of Pro-Inflammatory Cytokines and Oxidative/Nitrosative Components

Plasma levels of TNF-α (**Figure 1A**) were higher in the group of patients with ED compared with control. The IL-1β levels were not modified in these patients (**Figure 1B**).

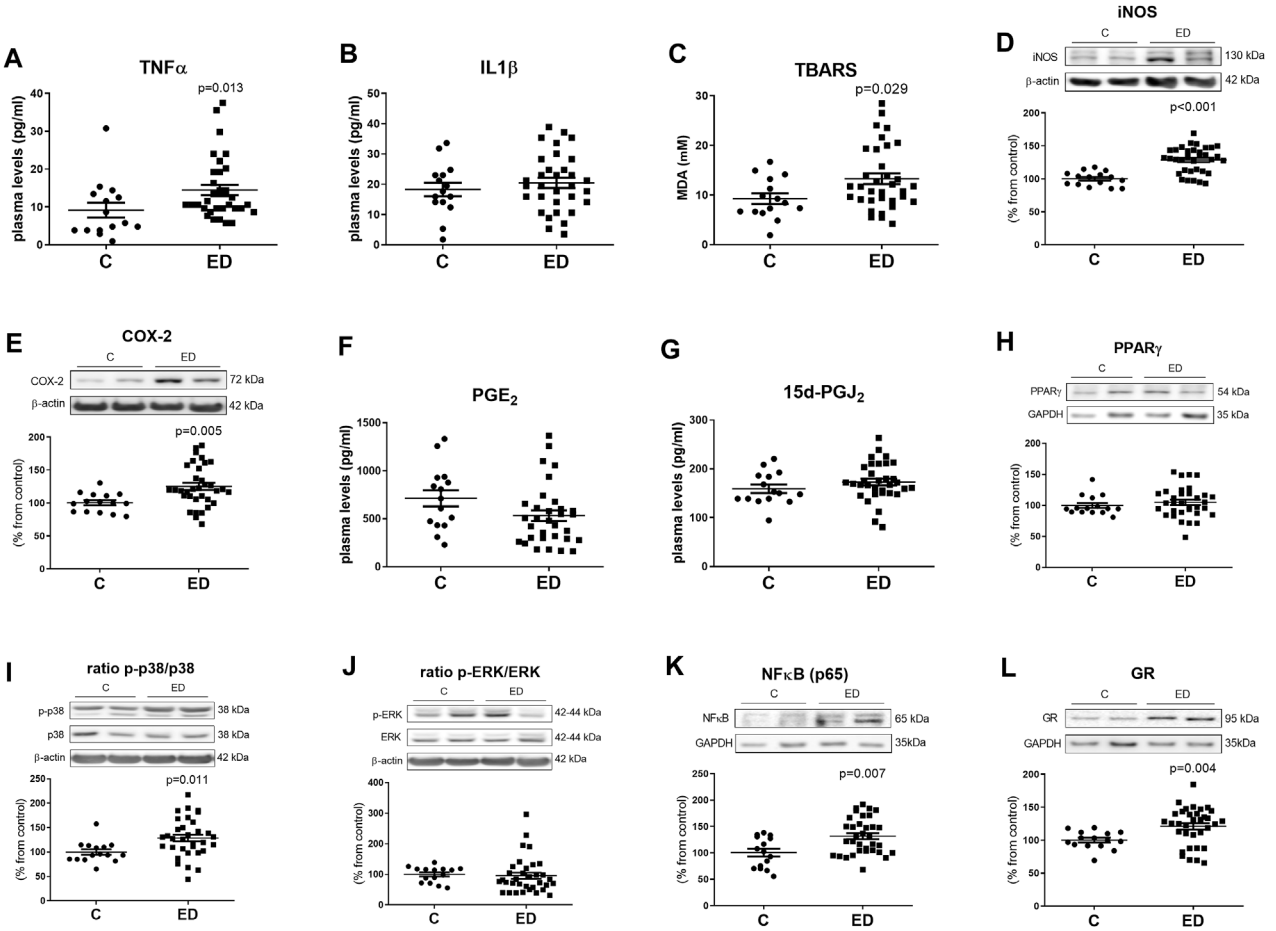

FIGURE 1 | Plasma levels of inflammatory cytokines and oxidative/nitrosative markers **(A–C)**, protein expression levels of inflammatory and oxidative/nitrosative enzymes in the cytosolic fraction of PBMCs **(D,E)**, plasma levels of prostaglandins **(F,G)**, protein expression levels of inflammatory MAPKs in the cytosolic fraction of PBMCs **(I,J)** and protein expression levels of transcription factors **(H,K)** involved in inflammation or receptors involved in the stress response **(L)** in the nuclear fraction of PBMCs. Data are expressed as mean ± SEM on TNFα **(A)**, IL1β **(B)**, TBARS **(C)**, iNOS **(D)**, COX-2 **(E)**, PGE_2 **(F)**, 15d-PGJ_2 **(G)**, PPARγ **(H)**, p-p38/p38 **(I)** and p-ERK/ERK ratio **(J)**, NFκBp65 **(K)** and GR **(L)** between eating disorders (ED) and control **(C)** groups (ED $n = 34$, C $n = 15$). In the Western blots the densitometric data of the respective band of interest were normalized by β-actin in the cytosolic extract or by GAPDH in the nuclear extract (lower bands). Data were analyzed using the D'Agostino and Pearson normality test to assess Gaussian distribution, followed by an unpaired two-tailed *t* test. When data did not follow a Gaussian distribution, a Mann-Whitney test was performed; a $p < 0.05$ was considered statistically significant.

Furthermore, patients with ED shown increased levels of thiobarbituric acid reactive substances (TBARS; a lipid peroxidation marker) (**Figure 1C**) in the plasma and higher levels of the oxidative/nitrosative enzyme iNOS (**Figure 1D**) in PBMCs, when compared with control.

ED Appears to Affect the Protein Expression of COX-2 Without Affecting its Downstream Products

Patients with ED shown higher levels of COX-2 in PBMCs (**Figure 1E**) compared with controls.

Plasma levels of the PGE_2 (proinflammatory) and the 15d-PGJ_2 (anti-inflammatory) did not change in these patients (**Figures 1F,G**). The nuclear expression of the anti-inflammatory factor, and receptor of 15d-PGJ_2, the peroxisome proliferator-activated receptor *gamma* (PPARγ) was not altered in PBMCs from patients either (**Figure 1H**).

ED Alter the MAPK p38, the NFκB p65 and the GR Protein Expression Levels

The ratio between the activated (phosphorylated) MAPK p38 and its total form augmented in PBMCs from patients with ED (**Figure 1I**). However, the ratio between the phosphorylated extracellular signal-regulated kinases (ERK) and its total form did not change when controls and patients were compared (**Figure 1J**).

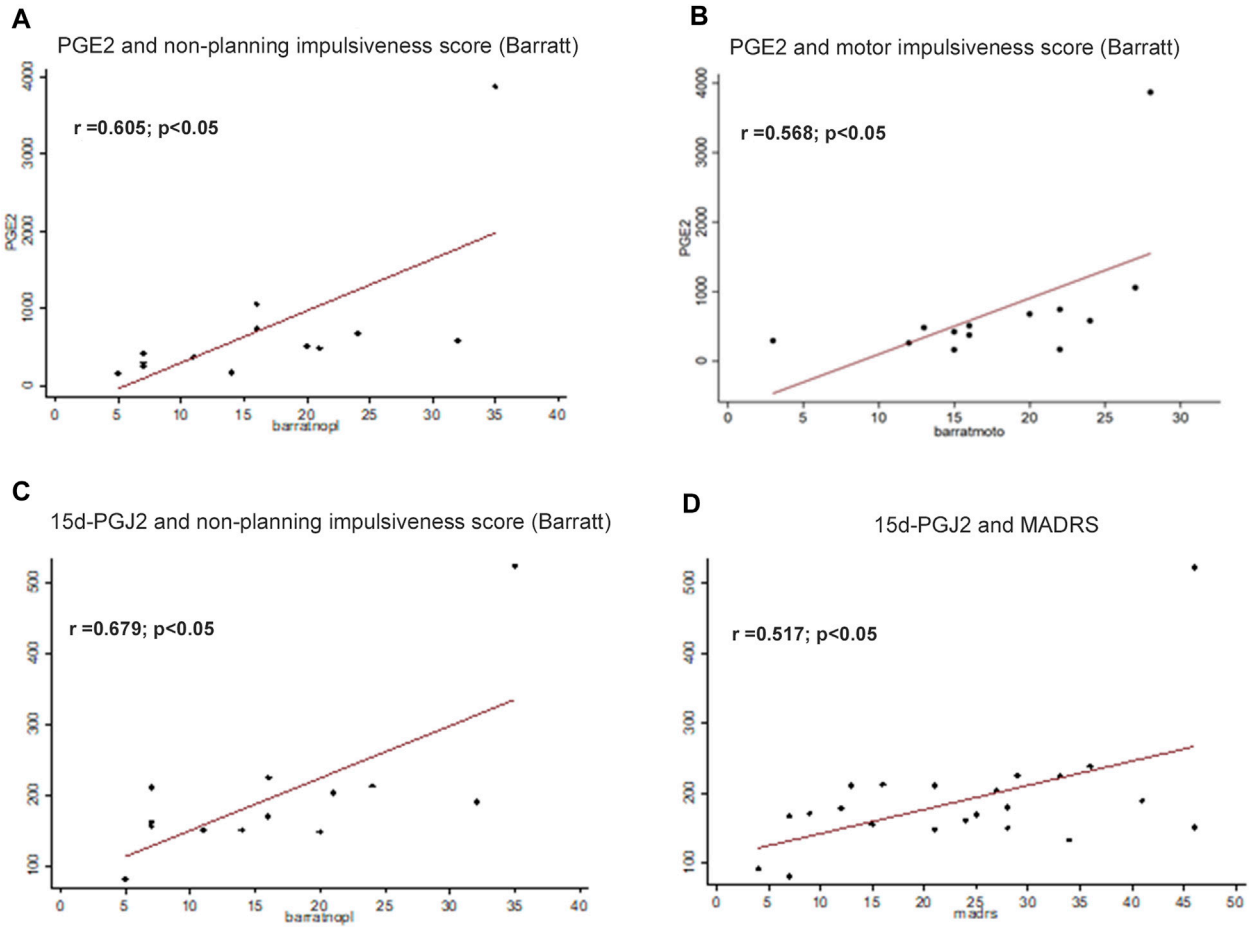

FIGURE 2 | Assessment of correlations among biological parameters and psychological tests. Plasma levels of the inflammatory prostaglandin PGE_2 were correlated with non-planning impulsiveness score **(A)**, and with motor impulsiveness score ($r = 0.568$; $p < 0.05$) **(B)**. Levels of the anti-inflammatory 15d-PGJ_2 correlated with Barratt questionnaire non-planning impulsiveness score **(C)** and Montgomery-Asberg Depression Rating Scale (MADRS) score ($r = 0.517$; $p < 0.05$) **(D)**. Correlations were assessed by using Pearson correlation coefficient. The significance was considered $p < 0.05$.

The pro-inflammatory NFκB p65 subunit (**Figure 1K**) as well as the glucocorticoid receptor (GR) (**Figure 1L**) levels were augmented in PBMCs from patients with ED compared to controls.

Evaluation of Correlations Among Biological Parameters and Psychological Tests

The possible correlations between all the biochemical parameters analyzed in the study and the clinical/psychological test were investigated. Thus, in patients with ED, significant correlations were observed between PGE_2 as well as 15d-PGJ_2 and some clinical parameters.

Attending to the Barratt Impulsiveness Scale scores, plasma levels of the inflammatory prostaglandin PGE_2 correlated with non-planning impulsiveness score ($r = 0.605$; $p < 0.05$) (**Figure 2A**), and with motor impulsiveness score ($r = 0.568$; $p < 0.05$) (**Figure 2B**).

Levels of the anti-inflammatory 15d-PGJ_2 correlated with Barratt questionnaire non-planning impulsiveness score ($r = 0.679$ $p < 0.05$) (**Figure 2C**) and Montgomery-Asberg Depression Rating Scale (MADRS) score ($r = 0.517$; $p < 0.05$) (**Figure 2D**).

DISCUSSION

Our results indicate a relationship between the immune response and impulsiveness and between the immune response and depressive symptomatology in female adult patients with ED. To our knowledge, it is the first time that a relationship between impulsiveness and inflammation in ED has been showed.

The present research shows a dysfunction of the inflammatory/oxidative intra- and intercellular paths in PBMCs and its relationship with impulsivity and affective symptoms in patients with ED. Importantly, none of the

patients was under psychopharmacological treatment (excluding benzodiazepines) when the study was conducted.

Patients with ED shown increased levels in the PBMCs of NFκB (a pro-inflammatory nuclear factor) and in the plasma levels of the cytokine TNF-α, an increase in the iNOS expression in PBMCs and a subsequent increment in the oxidative/nitrosative stress indicated by an augmented lipid peroxidation (TBARS assay in plasma). Patients also presented a rise in the COX-2 levels and an increment of the mainly pro-inflammatory MAPK p38 as well as increased expression levels of the glucocorticoid receptor (GR) in their PBMCs.

All the biochemical parameters analyzed were examined for possible correlations with the clinical parameters. The statistical studies indicated that there were significant correlations between some immune response elements and some clinical parameters. In particular, the inflammatory PGE_2 correlated with motor impulsiveness and with non-planning impulsiveness and the anti-inflammatory 15d-PGJ_2 correlated with depressive symptomatology as well as non-planning impulsiveness.

In a previous study carried out in a similar sample, it was found an activated immune response in patients with ED (Macdowell et al., 2013). Our current data confirms an increase in the expression of the pro-inflammatory factor NFκB and in the plasma levels of the pro-inflammatory cytokine TNF-α in these patients as well as an oxidative/nitrosative stress. Agreeing with the previous study, patients with ED present an increased COX-2 expression, without changes in prostaglandins levels.

The potential role of pro-inflammatory cytokines in ED has been previously suggested as data from several studies indicate that they have direct and indirect effects on the CNS involved in eating behavior (Corcos et al., 2003). Actually, TNF-α affects the hypothalamic neurons involved in the control of appetite and eating behavior (Konsman and Dantzer, 2001), modifies the firing rate of glucose-sensitive neurons in the lateral hypothalamus (Plata-Salaman, 1998) and it has an impact on neuropeptide-neurotransmitter interfaces (Brambilla et al., 2001).

It is well established that stress is related with mental disorders, including ED. Therefore, it is plausible to formulate a model based on the biological and clinical correlation between stress, anxiety, and ED (Holden and Pakula, 1999) in which the induction of an immune response, resulting in the release of pro-inflammatory cytokines, could be caused by stress: the biological response common to each of these disorders.

Cytokines can induce a NFκB pathway stimulation that it could be also responsible of the increased COX-2 and iNOS protein expression levels, as these enzymes are induced by this nuclear factor (Perkins, 2000). Furthermore, the increased expression of iNOS would explain, at least in part, the oxidative/nitrosative stress present in patients with ED.

The number of articles reporting increased expression levels of COX-2 in PBMCs from patients with ED is extremely limited (Macdowell et al., 2013). This increase, together with the results already mentioned indicates, once again, an inflammatory and oxidative/nitrosative status in this clinical setting. Our data is also showing no differences between patients and healthy controls in the plasma levels of the PGE_2 and 15d-PGJ_2 (products of COX-2). A potential explanation could be the moment and the immune scenario at the time of the blood extraction. Another possibility, as it has been described in a previous study employing similar samples, could be the compensatory effect of the cholinergic anti-inflammatory pathway that is being activated in these patients (Macdowell et al., 2013). In any case, more studies are warranted to fully characterize the role of COX-2 in ED.

Regarding the glucocorticoid receptor (GR) our results show an increased expression in PBMCs from patients with ED. Glucocorticoids participate in the modulation of inflammatory processes and an elevation of their levels could translate into a dysregulation of the immune response (Sorrells et al., 2009). Moreover, preceding studies show an anomalous cortisol suppression to dexamethasone test in patients with ED (Diaz-Marsa et al., 2008). Consequently, and although more studies are necessary, it appears like there is an alteration of the hypothalamic-pituitary-adrenal (HPA) axis and a dysfunction in stress management in these patients.

Our work also focused on the psychopathology of ED employing different evaluation tools. In this sense, impulsivity was found to differentiate patients with ED from controls and it has been shown to consistently predict negative outcomes for these patients (Waxman, 2009).

Our data revealed a relationship between impulsiveness and inflammation, as shown by the correlation between the Barratt Scores (motor impulsiveness and non-planning impulsiveness) and the PGE_2 plasma levels, as well as between the 15d-PGJ_2 levels and the non-planning impulsiveness Barratt scores.

Stress dysregulation and impulsive personality disorders are intimately associated, and patients frequently exhibit neurobiological stress response dysfunctions and aroused plasma levels of glucocorticoids (Grossman et al., 2003; Diaz-Marsa et al., 2008). Hence, it could be possible to contemplate GR as a sign of an endophenotype with aggressive/impulsive features (Yehuda and Seckl, 2011). This assumption would increase the potential impact of our results involving the GR in patients with ED, although further research is necessary to characterize the possible role of GR as a marker in this clinical setting.

Besides impulsiveness, affective symptomatology has been related to ED; severe depressive symptoms have been associated to further development of ED and to worse ED symptomatology (Evans et al., 2017; Smith et al., 2018).

In our study, a correlation between depressive symptomatology and levels of 15d-PGJ_2 was found, indicating that there is a relationship between depressive symptoms and the anti-inflammatory pathways. However, no correlation between general anxiety and inflammation was established. Inflammation can be related with depression and anxiety, which often show comorbidity with ED (Hughes et al., 2013). According to our results, depressive symptoms could be mediating between the ED pathology and a dysfunction of inflammatory pathways; this line of research should be pursued in the future to fully comprehend the nature of this correlation.

Our findings need to be weighed in the context of the strengths and limitations of our study. We do believe that a great strength of this work is that none of the patients were taking medication at the time of assessment (for ethics concerns, in emergency cases some of the patients were allowed to take benzodiazepines); this kind of patients, showing great severity of illness and medication-free is quite difficult to recruit. Regarding limitations, this was a study with important ethical issues, as to extract a larger volume of blood from these patients was troublesome. Thus, we were able to study only a limited number of parameters involved in the inflammatory response as the amount of sample was scarce. Another limitation affects the gender of the patients. ED affect people from both genders. However, this is a preliminary observational study, and patients with ED in our population are predominantly females. Thus, we were unable to recruit enough male patients to obtain a sample size with sufficient statistical power and consequently, we decided to focus on female patients. Finally, we lack more information about additional sociodemographic and clinical characteristics of the sample as well as comorbidities with other pathologies, except for the ones included in the exclusion criteria.

In summary, patients with ED without psychopharmacological treatment (excluding benzodiazepines) show an immune activation, displaying increased pro-inflammatory and oxidative/nitrosative stress parameters. From a psychopathological standpoint, plasma levels of the inflammatory prostaglandin PGE_2 are correlated with motor impulsiveness and with non-planning impulsiveness scores. Additionally, the depressive symptomatology and the non-planning impulsiveness scores are correlated with the levels in plasma of the anti-inflammatory 15d-PGJ_2.

Thus, inflammatory factors could be considered as potential therapeutic targets in ED, at least as factors to consider in a co-adjuvant treatment of these disorders. Supporting this idea, impulsiveness and depressive symptomatology seem to be linked to an inflammatory dysfunction in patients with ED. Additional studies in this same line of research are required as they could clarify the mechanisms underlying the observed processes offering additional therapeutic strategies.

DATA AVAILABILITY STATEMENT

The raw data supporting the conclusion of this article will be made available by the authors, without undue reservation.

ETHICS STATEMENT

The studies involving human participants were reviewed and approved by Hospital Universitario Clinico San Carlos Ethics Committee. The patients/participants provided their written informed consent to participate in this study.

AUTHOR CONTRIBUTIONS

JRC conceived the experiments, interpreted the data, and wrote the manuscript; KM performed the preparation of samples and the biochemical determinations; MS, FR-G, AC-D, and MD-M recruited the patients and performed the clinical tests; JLC, JCL, and MD-M conceived the experiments and reviewed the manuscript. All authors contributed to manuscript revision, read, and approved the submitted version.

FUNDING

This work was funded by the CIBERSAM (CB/07/09/0026 to JCL), Instituto de Salud Carlos III (FIS PI13/00781 to MDM), Fondo Europeo de Desarrollo Regional (FEDER) and the Spain's Ministry of Science and Innovation (MICINN, PID2020-113103RB-I00 to JRC). JRC was a Ramón y Cajal Researcher (Spain's Ministry of Science and Innovation, and FEDER).

REFERENCES

Ahrén-Moonga, J., Lekander, M., Von Blixen, N., Rönnelid, J., Holmgren, S., and Af Klinteberg, B. (2011). Levels of Tumour Necrosis Factor-Alpha and Interleukin-6 in Severely Ill Patients with Eating Disorders. *Neuropsychobiology* 63, 8–14. doi:10.1159/000321832

American Psychiatric Association (2000). *Diagnostic and Statistical Manual of Mental Disorders*. Washington, DC: Elsevier-Masson.

American Psychiatric Association (2013). *Diagnostic and Statistical Manual of Mental Disorders*. Washington, DC: Médica Panamericana.

Anderson, L. K., Claudat, K., Cusack, A., Brown, T. A., Trim, J., Rockwell, R., et al. (2018). Differences in Emotion Regulation Difficulties Among Adults and Adolescents across Eating Disorder Diagnoses. *J. Clin. Psychol.* 74, 1867–1873. doi:10.1002/jclp.22638

Brambilla, F., Bellodi, L., Arancio, C., Ronchi, P., and Limonta, D. (2001). Central Dopaminergic Function in Anorexia and Bulimia Nervosa: a Psychoneuroendocrine Approach. *Psychoneuroendocrinology* 26, 393–409. doi:10.1016/s0306-4530(00)00062-7

Bulik, C. M., Kleiman, S. C., and Yilmaz, Z. (2016). Genetic Epidemiology of Eating Disorders. *Curr. Opin. Psychiatry* 29, 383–388. doi:10.1097/YCO.0000000000000275

Caso, J. R., Graell, M., Navalón, A., MacDowell, K. S., Gutiérrez, S., Soto, M., et al. (2020). Dysfunction of Inflammatory Pathways in Adolescent Female Patients with Anorexia Nervosa. *Prog. Neuropsychopharmacol. Biol. Psychiatry* 96, 109727. doi:10.1016/j.pnpbp.2019.109727

Cooper, P. J., Taylor, M. J., Cooper, Z., and Fairbum, C. G. (1987). The Development and Validation of the Body Shape Questionnaire. *Int. J. Eat. Disord.* 6, 485–494. doi:10.1002/1098-108x(198707)6:4<485::aid-eat2260060405>3.0.co;2-o

Corcos, M., Guilbaud, O., Paterniti, S., Moussa, M., Chambry, J., Chaouat, G., et al. (2003). Involvement of Cytokines in Eating Disorders: a Critical Review of the Human Literature. *Psychoneuroendocrinology* 28, 229–249. doi:10.1016/s0306-4530(02)00021-5

Culbert, K. M., Racine, S. E., and Klump, K. L. (2015). Research Review: What We Have Learned about the Causes of Eating Disorders - a Synthesis of Sociocultural, Psychological, and Biological Research. *J. Child. Psychol. Psychiatry* 56, 1141–1164. doi:10.1111/jcpp.12441

Dalton, B., Bartholdy, S., Robinson, L., Solmi, M., Ibrahim, M. A. A., Breen, G., et al. (2018). A Meta-Analysis of Cytokine Concentrations in Eating Disorders. *J. Psychiatr. Res.* 103, 252–264. doi:10.1016/j.jpsychires.2018.06.002

Dantzer, R., O'connor, J. C., Freund, G. G., Johnson, R. W., and Kelley, K. W. (2008). From Inflammation to Sickness and Depression: when the Immune System Subjugates the Brain. *Nat. Rev. Neurosci.* 9, 46–56. doi:10.1038/nrn2297

Díaz-Marsá, M., Carrasco, J. L., Basurte, E., Sáiz, J., López-Ibor, J. J., and Hollander, E. (2008). Enhanced Cortisol Suppression in Eating Disorders with Impulsive Personality Features. *Psychiatry Res.* 158, 93–97. doi:10.1016/j.psychres.2007.06.020

Dunjic-Kostic, B., Ivkovic, M., Radonjic, N. V., Petronijevic, N. D., Pantovic, M., Damjanovic, A., et al. (2013). Melancholic and Atypical Major Depression-Cconnection between Cytokines, Psychopathology and Treatment. *Prog. Neuropsychopharmacol. Biol. Psychiatry* 43, 1–6. doi:10.1016/j.pnpbp.2012.11.009

Evans, E. H., Adamson, A. J., Basterfield, L., Le Couteur, A., Reilly, J. K., Reilly, J. J., et al. (2017). Risk Factors for Eating Disorder Symptoms at 12 Years of Age: A 6-year Longitudinal Cohort Study. *Appetite* 108, 12–20. doi:10.1016/j.appet.2016.09.005

García-Bueno, B., Bioque, M., Mac-Dowell, K. S., Barcones, M. F., Martínez-Cengotitabengoa, M., Pina-Camacho, L., et al. (2014). Pro-/anti-inflammatory Dysregulation in Patients with First Episode of Psychosis: toward an Integrative Inflammatory Hypothesis of Schizophrenia. *Schizophr Bull.* 40, 376–387. doi:10.1093/schbul/sbt001

García-Bueno, B., Caso, J. R., and Leza, J. C. (2008). Stress as a Neuroinflammatory Condition in Brain: Damaging and Protective Mechanisms. *Neurosci. Biobehav Rev.* 32, 1136–1151. doi:10.1016/j.neubiorev.2008.04.001

Garner, D. M., Olmstead, M. P., and Polivy, J. (1983). Development and Validation of a Multidimensional Eating Disorder Inventory for Anorexia Nervosa and Bulimia. *Int. J. Eat. Disord.* 2, 15–34. doi:10.1002/1098-108x(198321)2:2<15::aid-eat2260020203>3.0.co;2-6

Grossman, R., Yehuda, R., New, A., Schmeidler, J., Silverman, J., Mitropoulou, V., et al. (2003). Dexamethasone Suppression Test Findings in Subjects with Personality Disorders: Associations with Posttraumatic Stress Disorder and Major Depression. *Am. J. Psychiatry* 160, 1291–1298. doi:10.1176/appi.ajp.160.7.1291

Grzelak, T., Dutkiewicz, A., Paszynska, E., Dmitrzak-Weglarz, M., Slopien, A., and Tyszkiewicz-Nwafor, M. (2017). Neurobiochemical and Psychological Factors Influencing the Eating Behaviors and Attitudes in Anorexia Nervosa. *J. Physiol. Biochem.* 73, 297–305. doi:10.1007/s13105-016-0540-2

Hamilton, M. (1960). A Rating Scale for Depression. *J. Neurol. Neurosurg. Psychiatry* 23, 56–62. doi:10.1136/jnnp.23.1.56

Henderson, M., and Freeman, C. P. (1987). A Self-Rating Scale for Bulimia. The 'BITE'. *Br. J. Psychiatry* 150, 18–24. doi:10.1192/bjp.150.1.18

Holden, R. J., and Pakula, I. S. (1999). Tumor Necrosis Factor-Alpha: Is There a Continuum of Liability between Stress, Anxiety States and Anorexia Nervosa? *Med. Hypotheses* 52, 155–162. doi:10.1054/mehy.1997.0641

Hudson, J. I., Hiripi, E., Pope, H. G., Jr., and Kessler, R. C. (2007). The Prevalence and Correlates of Eating Disorders in the National Comorbidity Survey Replication. *Biol. Psychiatry* 61, 348–358. doi:10.1016/j.biopsych.2006.03.040

Hughes, E. K., Goldschmidt, A. B., Labuschagne, Z., Loeb, K. L., Sawyer, S. M., and Le Grange, D. (2013). Eating Disorders with and without Comorbid Depression and Anxiety: Similarities and Differences in a Clinical Sample of Children and Adolescents. *Eur. Eat. Disord. Rev.* 21, 386–394. doi:10.1002/erv.2234

Kahl, K. G., Kruse, N., Rieckmann, P., and Schmidt, M. H. (2004). Cytokine mRNA Expression Patterns in the Disease Course of Female Adolescents with Anorexia Nervosa. *Psychoneuroendocrinology* 29, 13–20. doi:10.1016/s0306-4530(02)00131-2

Kapadia, R., Yi, J. H., and Vemuganti, R. (2008). Mechanisms of Anti-inflammatory and Neuroprotective Actions of PPAR-Gamma Agonists. *Front. Biosci.* 13, 1813–1826. doi:10.2741/2802

Konsman, J. P., and Dantzer, R. (2001). How the Immune and Nervous Systems Interact during Disease-Associated Anorexia. *Nutrition* 17, 664–668. doi:10.1016/s0899-9007(01)00602-5

Lavender, J. M., Goodman, E. L., Culbert, K. M., Wonderlich, S. A., Crosby, R. D., Engel, S. G., et al. (2017). Facets of Impulsivity and Compulsivity in Women with Anorexia Nervosa. *Eur. Eat. Disord. Rev.* 25, 309–313. doi:10.1002/erv.2516

Leonard, B., and Maes, M. (2012). Mechanistic Explanations How Cell-Mediated Immune Activation, Inflammation and Oxidative and Nitrosative Stress Pathways and Their Sequels and Concomitants Play a Role in the Pathophysiology of Unipolar Depression. *Neurosci. Biobehav Rev.* 36, 764–785. doi:10.1016/j.neubiorev.2011.12.005

Lindvall Dahlgren, C., Wisting, L., and Rø, Ø. (2017). Feeding and Eating Disorders in the DSM-5 Era: a Systematic Review of Prevalence Rates in Non-clinical Male and Female Samples. *J. Eat. Disord.* 5, 56. doi:10.1186/s40337-017-0186-7

Macdowell, K. S., Díaz-Marsá, M., Güemes, I., Rodríguez, A., Leza, J. C., and Carrasco, J. L. (2013). Inflammatory Activation and Cholinergic Anti-inflammatory System in Eating Disorders. *Brain Behav. Immun.* 32, 33–39. doi:10.1016/j.bbi.2013.04.006

Merlotti, E., Mucci, A., Volpe, U., Montefusco, V., Monteleone, P., Bucci, P., et al. (2013). Impulsiveness in Patients with Bulimia Nervosa: Electrophysiological Evidence of Reduced Inhibitory Control. *Neuropsychobiology* 68, 116–123. doi:10.1159/000352016

Monteleone, P., Scognamiglio, P., Monteleone, A. M., Perillo, D., and Maj, M. (2014). Cortisol Awakening Response in Patients with Anorexia Nervosa or Bulimia Nervosa: Relationships to Sensitivity to Reward and Sensitivity to Punishment. *Psychol. Med.* 44, 2653–2660. doi:10.1017/S0033291714000270

Montgomery, S. A., and Asberg, M. (1979). A New Depression Scale Designed to Be Sensitive to Change. *Br. J. Psychiatry* 134, 382–389. doi:10.1192/bjp.134.4.382

Nova, E., Gómez-Martínez, S., Morandé, G., and Marcos, A. (2002). Cytokine Production by Blood Mononuclear Cells from In-Patients with Anorexia Nervosa. *Br. J. Nutr.* 88, 183–188. doi:10.1079/BJNBJN2002608

Paszynska, E., Dmitrzak-Weglarz, M., Tyszkiewicz-Nwafor, M., and Slopien, A. (2016). Salivary Alpha-Amylase, Secretory IgA and Free Cortisol as Neurobiological Components of the Stress Response in the Acute Phase of Anorexia Nervosa. *World J. Biol. Psychiatry* 17, 266–273. doi:10.3109/15622975.2016.1163419

Patton, J. H., Stanford, M. S., and Barratt, E. S. (1995). Factor Structure of the Barratt Impulsiveness Scale. *J. Clin. Psychol.* 51, 768–774. doi:10.1002/1097-4679(199511)51:6<768::aid-jclp2270510607>3.0.co;2-1

Perkins, N. D. (2000). The Rel/NF-Kappa B Family: Friend and Foe. *Trends Biochem. Sci.* 25, 434–440. doi:10.1016/s0968-0004(00)01617-0

Plata-Salamán, C. R. (1998). Cytokines and Anorexia: a Brief Overview. *Semin. Oncol.* 25, 64–72.

Popa-Wagner, A., Mitran, S., Sivanesan, S., Chang, E., and Buga, A. M. (2013). ROS and Brain Diseases: the Good, the Bad, and the Ugly. *Oxid Med. Cel Longev* 2013, 963520. doi:10.1155/2013/963520

Scherag, S., Hebebrand, J., and Hinney, A. (2010). Eating Disorders: the Current Status of Molecular Genetic Research. *Eur. Child. Adolesc. Psychiatry* 19, 211–226. doi:10.1007/s00787-009-0085-9

Smith, K. E., Mason, T. B., Leonard, R. C., Wetterneck, C. T., Smith, B. E. R., Farrell, N. R., et al. (2018). Affective Predictors of the Severity and Change in Eating Psychopathology in Residential Eating Disorder Treatment: The Role of Social Anxiety. *Eat. Disord.* 26, 66–78. doi:10.1080/10640266.2018.1418314

Sorrells, S. F., Caso, J. R., Munhoz, C. D., and Sapolsky, R. M. (2009). The Stressed CNS: when Glucocorticoids Aggravate Inflammation. *Neuron* 64, 33–39. doi:10.1016/j.neuron.2009.09.032

Sutin, A. R., Milaneschi, Y., Cannas, A., Ferrucci, L., Uda, M., Schlessinger, D., et al. (2012). Impulsivity-related Traits Are Associated with Higher white Blood Cell Counts. *J. Behav. Med.* 35, 616–623. doi:10.1007/s10865-011-9390-0

Vall, E., and Wade, T. D. (2015). Predictors of Treatment Outcome in Individuals with Eating Disorders: A Systematic Review and Meta-Analysis. *Int. J. Eat. Disord.* 48, 946–971. doi:10.1002/eat.22411

Waxman, S. E. (2009). A Systematic Review of Impulsivity in Eating Disorders. *Eur. Eat. Disord. Rev.* 17, 408–425. doi:10.1002/erv.952

Yehuda, R., and Seckl, J. (2011). Minireview: Stress-Related Psychiatric Disorders with Low Cortisol Levels: a Metabolic Hypothesis. *Endocrinology* 152, 4496–4503. doi:10.1210/en.2011-1218

Conflict of Interest: The authors declare that the research was conducted in the absence of any commercial or financial relationships that could be construed as a potential conflict of interest.

frontiers | Frontiers in Pharmacology

ORIGINAL RESEARCH
published: 19 May 2022
doi: 10.3389/fphar.2022.848939

The Pyroptosis-Related Signature Predicts Diagnosis and Indicates Immune Characteristic in Major Depressive Disorder

Zhifang Deng[1], *Jue Liu*[1], *Shen He*[2]* *and Wenqi Gao*[3]*

[1]Department of Pharmacy, The Central Hospital of Wuhan, Tongji Medical College, Huazhong University of Science and Technology, Wuhan, China, [2]Division of Mood Disorders, Shanghai Mental Health Center, Shanghai Jiao Tong University School of Medicine, Shanghai, China, [3]Institute of Maternal and Child Health, Wuhan Children's Hospital (Wuhan Maternal and Child Healthcare Hospital), Tongji Medical College, Huazhong University and Technology, Wuhan, China

Pyroptosis is recently identified as an inflammatory form of programmed cell death. However, the roles of pyroptosis-related genes (PS genes) in major depressive disorder (MDD) remain unclear. This study developed a novel diagnostic model for MDD based on PS genes and explored the pathological mechanisms associated with pyroptosis. First, we obtained 23 PS genes that were differentially expressed between healthy controls and MDD cases from GSE98793 dataset. There were obvious variation in immune cell infiltration profiles and immune-related pathway enrichment between healthy controls and MDD cases. Then, a novel diagnostic model consisting of eight PS genes (*GPER1*, *GZMA*, *HMGB1*, *IL1RN*, *NLRC4*, *NLRP3*, *UTS2*, and *CAPN1*) for MDD was constructed by random forest (RF) and least absolute shrinkage and selection operator (LASSO) analyses. ROC analysis revealed that our model has good diagnostic performance, AUC = 0.795 (95% CI 0.721–0.868). Subsequently, the consensus clustering method based on 23 differentially expressed PS genes was constructed to divide all MDD cases into two distinct pyroptosis subtypes (cluster A and B) with different immune and biological characteristics. Principal component analysis (PCA) algorithm was performed to calculate the pyroptosis scores ("PS-scores") for each sample to quantify the pyroptosis regulation subtypes. The MDD patients in cluster B had higher "PS-scores" than those in cluster A. Furthermore, we also found that MDD patients in cluster B showed lower expression levels of 11 interferon (IFN)-α isoforms. In conclusion, pyroptosis may play an important role in MDD and can provide new insights into the diagnosis and underlying mechanisms of MDD.

Keywords: pyroptosis, diagnostic, MDD, immune, gene cluster analysis

OPEN ACCESS

Edited by:
Javier R. Caso,
Universidad Complutense de Madrid, Spain

Reviewed by:
Li Tian,
University of Tartu, Estonia
Silvia Alboni,
University of Modena and Reggio Emilia, Italy

***Correspondence:**
Shen He
shenhe0204@126.com
Wenqi Gao
gwq1103@ctgu.edu.cn

Specialty section:
This article was submitted to Neuropharmacology, a section of the journal Frontiers in Pharmacology

Received: *05 January 2022*
Accepted: *28 April 2022*
Published: *19 May 2022*

Citation:
Deng Z, Liu J, He S and Gao W (2022) The Pyroptosis-Related Signature Predicts Diagnosis and Indicates Immune Characteristic in Major Depressive Disorder. Front. Pharmacol. 13:848939. doi: 10.3389/fphar.2022.848939

INTRODUCTION

Pyroptosis, a programmed cell death mode closely related to the inflammatory response, plays an important role in a variety of physiological processes and disease progression (Broz et al., 2020). The characteristics of pyroptosis include activation of caspase-1, 4, 5, and 11; formation of cell membrane pores mediated by gasdermin protein; cell swelling and rapid rupture; and release of intracellular inflammatory factors (Shi et al., 2017). Therefore, inflammatory vesicles, gasdermin protein, and

pro-inflammatory cytokines are key factors involved in pyroptosis. The expressions and functions of these core regulatory components influence pyroptosis progression. Further study of these regulatory components may help to clarify the role of pyroptosis in disease pathogenesis (Ahechu et al., 2018).

Major depressive disorder (MDD) is a serious neuropsychiatric disorder and a leading cause of suicide (Lépine and Briley, 2011). The incidence of depression is increasing annually to rank third among global disease burdens (Malhi and Mann, 2018). The pathogenesis of depression is complex, and inflammation is one of the main pathogenic factors (Troubat et al., 2021). Inflammation results from abnormal immune system activation. The imbalance of immune cells in the body can lead to illness, including mental illness such as MDD. Patients with depression show dysregulation of the innate and adaptive immune systems; for example, monocyte activation, decreased T-cell number and/or activity, and increased production of pro-inflammatory cytokines (Beurel et al., 2020). Excessive inflammation caused by pyroptosis and the release of various inflammatory factors after cell rupture may aggravate the disease development by forming an inflammatory immune microenvironment (Xia et al., 2019).

Comprehensive analysis of pyroptosis characteristics alteration in depression may be a key strategy for diagnosis and physiopathologic mechanism exploration of depression. Due to technical limitations, previous studies were limited to one or two key factors of pyroptosis. However, disease occurrence and progression involve a series of factors that form a highly synergistic network. Nowadays, the developments of high-throughput genomics technology and bioinformatics analysis have helped researchers to study genes expression profiles at the genomic level, generated new ideas for the interpretation of genomic results, and provided an ideal resource for the comprehensive analysis of pyroptosis and immune regulation in MDD (Gururajan et al., 2016; Ferrúa et al., 2019; Takahashi et al., 2019). In this study, we first established a novel diagnostic model by eight pyroptosis-related genes (PS genes) for MDD based on the GSE98793 dataset from the Gene Expression Omnibus (GEO) database. We found that MDD patients could obtain a good clinical benefit based on this model. Secondly, we explored the role of pyroptosis in physiopathologic mechanism of MDD. According to PS genes, data from patients with depression were clustered and two MDD subtypes were identified. We observed different immune properties and biological functions of these two subtypes. In all, our present study indicated that pyroptosis plays an important role in depression occurrence and progression, which may guide depression diagnosis, treatment and intervention plans.

MATERIALS AND METHODS

Data Acquisition and Processing

GSE98793 dataset, the expression profile of whole blood samples, was downloaded from the Gene Expression Omnibus (GEO) database. This dataset totally included 128 MDD cases (64 with anxiety symptoms and 64 without) and 64 healthy controls. 64 MDD cases without anxiety symptoms and 64 healthy controls were included in our analysis. All the participants of GSE98793 were from the GlaxoSmithKline–High-Throughput Disease-specific target Identification Program (GSK-HiTDiP) study. The MDD patients were evaluated by the semi-structured Schedule for Clinical Assessment in Neuropsychiatry (SCAN) (Wing et al., 1990), which was administered by trained staff. Furthermore, patients had a diagnosis of recurrent MDD (at least two episodes of depression satisfying DSM-IV or ICD10 criteria) were included as well. The exclusion criteria were as follows: if they had experienced mood incongruent psychotic symptoms, a lifetime history of intravenous drug use or diagnosis of drug dependency, depression secondary to alcohol or substance abuse or depression as clear consequence of medical illnesses or use of medications. Patients with co-morbid anxiety disorders, with the exception of obsessive compulsive and post traumatic stress disorders, were included. Patients with diagnosis of schizophrenia, schizoaffective disorders and other axis I disorders were excluded from the study (Leday et al., 2018). The detail information of participants included in the present study was showed in **Table 1**. GPL570 (Affymetrix Human Genome U133 Plus 2.0 Array) was detection platforms for GSE98793. Gene symbols were used to annotate the downloaded gene probes, eliminate probes without matching, and retain any gene probes with multiple matching.

TABLE 1 | Clinical and demographic characteristics of participants (GSE98793) included in the present study.

	All participants	MDD	Healthy controls
	128	64	64
Gender			
Male	32	16	16
Female	96	48	48
Comorbidities			
Anxiety	0	0	0
Without anxiety	128	64	64
Age (years)	52.06 ± 11.49	52.03 ± 11.41	52.09 ± 11.66

Screening for Pyroptosis-Related Differentially Expressed Genes

"Limma" package (R Foundation for Statistical Computing) was used for gene differential expression analysis with the processed gene expression matrix (Diboun et al., 2006). Before the bioinformatic analysis, all the samples were tested in two batches, and batch information could be extracted from phenotypic data. Thus, removeBatchEffect from the limma package was used to remove the batch effect (Ritchie et al., 2015). We conducted the gene differential expression analysis with set threshold: $|\log_2(FC)|>0.1$ and Benjamini–Hochberg-adjusted $p < 0.05$. Finally, we identified 2,216 DEGs in GSE98793. A total of 184 PS genes were obtained by inputting

TABLE 2 | Clinical and demographic characteristics of participants (GSE76826).

Dataset		Participants	Age (years)	Source
GSE76826	Healthy	18	48.44 ± 10.82	PBMCs
	Male	10	47.30 ± 11.47	
	Female	8	49.88 ± 10.52	
	MDD	16	56.5 ± 9.96	
	Male	10	46.30 ± 10.18	
	Female	6	46.83 ± 10.53	

the keyword "pyroptosis" in the GeneCards database. The overlap of 2,216 DEGs in GSE98793 dataset and 184 PS genes were defined as pyroptosis-related DEGs, totally 23 pyroptosis-related DEGs acquired.

Screening MDD-Specific Genes and Constructing Diagnostic Model for MDD

We applied random forest (RF) and least absolute shrinkage and selection operator (LASSO) to establish a diagnostic model for MDD. First, we used RF to screen candidate MDD-specific genes from pyroptosis-related DEGs. RF is a general technique for the training and prediction of samples based on the classification tree. The number of decision trees (ntree) and the value of MTRY in this study were 300 and 4, respectively. The RF was performed by R package "randomforest" (Kursa, 2014). Subsequently, to reduce the number of genes in the model and to solve the multicollinearity problem in regression analysis, we used LASSO logistic regression to screen feature genes and then construct a diagnostic model for MDD. The "glmnet" package was applied for LASSO algorithm (Friedman et al., 2010). Finally, a receiver operating characteristic (ROC) curve was created to investigate whether the built model could effectively predict MDD.

Internal and External Validation for Diagnostic Model

10-fold cross-validation as internal validation method was performed to confirm the predictive performance of our diagnostic model for MDD (Martinez et al., 2011). We chosed 10-fold cross-validation because 10-fold cross-validation techniques could test all data in the dataset and produce stable predictive accuracy. Therefore, the 10-fold cross-validation method with 2000 iterations of resampling was used for internal validatIon.

GSE76826 was used as an external validation dataset to examine the universality and reliability of the diagnostic model. GSE76826 dataset (expression profiling by array) included 20 MDD patients and 12 healthy controls (Miyata et al., 2016).

In addition to this, we examined the effectiveness of this diagnostic model in other mental illness as well. The GSE38484 dataset was used to analyze the diagnostic model. This dataset, based on the microarray platform of the Illumina HumanHT-12 V3.0 expression beadchip (GPL6947), included 96 healthy controls and 106 schizophrenia patients (Van Eijk et al., 2015).

TABLE 3 | Clinical and demographic characteristics of participants (GSE38484) included in the present study.

Dataset		Participants	Age (years)	Source
GSE38484	Healthy	96	39.46 ± 12.47	Whole blood
	Male	42	39.52 ± 14.41	
	Female	54	39.15 ± 14.15	
	SCZ	106	39.58 ± 10.74	
	Male	76	39.47 ± 10.50	
	Female	30	39.87 ± 11.49	

TABLE 4 | Clinical and demographic characteristics of participants (GSE53987) included in the present study.

Dataset		Participants	Age (years)	Source
GSE53987	Healthy	12	62.50 ± 9.39	Striatum
	Male	5	58.00 ± 6.44	
	Female	7	65.71 ± 10.24	
	MDD	20	71.45 ± 11.71	
	Male	9	68.56 ± 14.45	
	Female	11	73.82 ± 8.93	

The same model and the same coefficient were conducted for GSE76826 and GSE38484. The characteristic information of participants in GSE76826 and GSE38484 datasets were exhibited in **Tables 2**, **3**.

Diagnostic Markers Verified by Postmortem Brain Tissue Samples

GSE53987 was based on the platform of the Affymetrix Human Genome U133 Plus 2.0 Array (Lanz et al., 2019). There were 17 subjects with MDD and 18 healthy controls in this dataset, and three brain regions (hippocampus, prefrontal cortex, and striatum) were included. We used the GSE53987 dataset to verify the diagnostic model. The characteristic information of participants in GSE53987 dataset were showed in **Table 4**.

Consensus Clustering of 23 PS Genes by Partitioning Around Medoids

Consensus clustering is an algorithm used to identify subgroup members and verify subgroups based on resampling. We performed consensus clustering with PAM mehod (Wilkerson and Hayes, 2010) to identify distinct pyroptosis regulation clusters according to the expression profiles of 23 PS genes. PCA was then used to further validate different regulation clusters.

Immune Cell Infiltration Estimation by ssGSEA

Single-sample gene set enrichment analysis (ssGSEA) was used to quantify the relative abundance of 28 immune cell types related to immune response. In ssGSEA, the relative abundance of each immune cell was expressed as an enrichment score that was

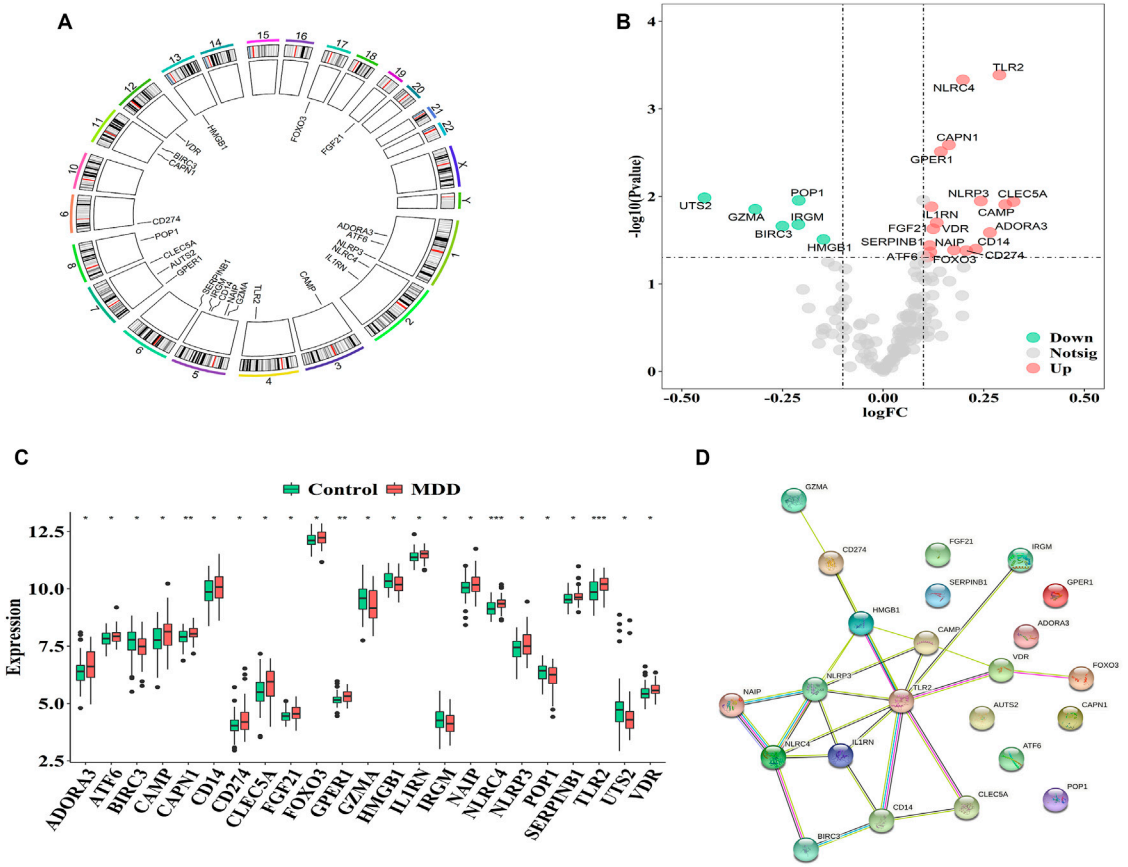

FIGURE 1 | Characterization of pyroptosis-related genes in MDD **(A)**. The location of pyroptosis-related genes on chromosomes by GSE98793 **(B–C)**. The Volcano and heat map of 23 differentially expressed pyrotopsis-related genes **(D)**. Box plot of differential expression of 23 differentially expressed pyrotopsis-related genes in control and depression samples. Adjusted *p*-values were showed as: ns, not significant; **p* < 0.05; ***p* < 0.01; ****p* < 0.001.

normalized to a uniform distribution of 0–1. A deconvolution approach CIBERSORT (http://cibersort.stanford.edu/) was used to evaluate the relative abundances of 22 distinct leukocyte subsets with gene expression profiles in the blood samples.

Gene Set Variation Analysis and Gene Ontology Annotation

We utilized GSVA analysis by "GSVA" package (Hänzelmann et al., 2013) to explore the differentiation in biological processes between different pyroptosis regulation clusters. The well-defined biological signatures were derived from the Hallmark geneset (MSigDB database v7.1) (Denny et al., 2018). The GO annotation for different clusters was performed using the R package "clusterProfiler" (Kursa, 2014) with a false discovery rate (FDR) cutoff of <0.01.

Identification of DEGs in Distinct Pyroptosis Regulation Subtypes

The consensus clustering algorithm classified MDD patients into two distinct pyroptosis regulation subtypes. We next identified DEGs between two different clusters using the "limma" package. Specifically, gene expression data were normalized using "voom" function and then inputted to the "lmFit" and "eBayes" functions to calculate the differential expressed statistics. The selection criteria were an adjusted P of <0.01 and |FC| of >1.0.

Construction of the Pyroptosis Score

To quantitatively analyze the pyroptosis subtypes, PCA was used to quantify the pyroptosis level of individual patients. First, PCA was used to distinguish pyroptosis subtypes. Then, the formula was performed to measure the pyroptosis scores (PS) as following: PS score = $PC1_i$, where PC1 represents principal component 1 and i represents DEG expression.

RESULTS

Study Design

The framework and workflow are described as following. First, the characteristic information and gene expression profiles of MDD cases and healthy controls in GSE98793, GSE76826, and GSE53987 were obtained from the GEO database (https://www.st-va.ncbi.nlm.

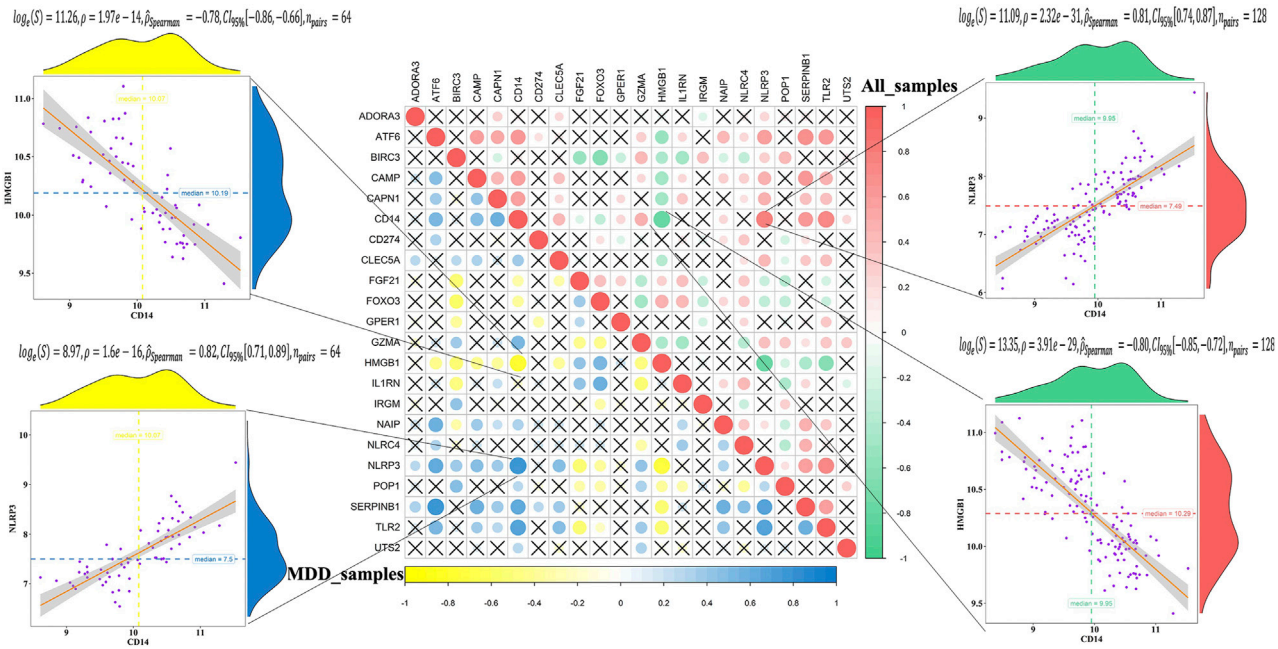

FIGURE 2 | Correlation analysis of 23 differentially expressed pyroptosis-related genes in all samples and MDD samples.

nih.gov/gds/?term=). Using GSE98793 dataset, we developed a novel diagnostic model for MDD based on PS genes by machine learning methods (RF and LASSO). GSE76826 and GSE53987 datasets were used as external validation and postmortem brain tissue samples valiadtion. Furthermore, GSE38484 dataset (96 healthy controls and 106 schizophrenia patients) was used to examine whether this diagnostic model was unique for MDD. Then, immune cell infiltration profiles and immune-related pathway enrichment were compared between healthy controls and MDD cases as well.

To discover the connections between PS genes and MDD subtypes, MDD cases were divided into two subtypes (A and B clusters) by consensus clustering analysis according to the PS genes expression profiles. The particular immune and biological characteristics of these two clusters were observed.

We developed a pyroptosis-related signature score, the "PS-score," to quantify the pyroptosis phenotype subtype.

Identification of DEGs Between Healthy Controls and MDD Cases

The GSE98793 dataset and Genecard database included 2,216 DEGs and 184 PS genes, respectively, among which 23 PS genes with significant expression differences were distributed on chromosomes as shown in **Figure 1A**. The upregulated genes included C-type lectin member 5 A (*CLEC5A*); cathelicidin antimicrobial peptide (*CAMP*); Toll-like receptor 2 (*TLR2*); adenosine A3 receptor (*ADORA3*); NOD-, LRR-, and pyrin domain-containing protein 3 (*NLRP3*); cluster of differentiation 14 (*CD14*); *CD274*; NLR family CARD domain containing 4 (*NLRC4*), NLR family apoptosis inhibitory protein (*NAIP*); calpain 1 (CAPN1), G-protein coupled estrogen receptor 1 (*GPER1*); Vitamin D receptor (*VDR*); fibroblast growth factor 21 (*FGF21*); interleukin-1 receptor antagonist (*IL1RN*); forkhead box O3 (FOXO3); serpin family B member 1 (*SERPINB1*); and activating transcription factor 6 (*ATF6*). The downregulated genes included high mobility group box 1 (*HMGB1*), processing of precursor 1 (*POP1*), immunity-related GTPase family (*IRGM*), baculoviral IAP repeat-containing protein3 (*BIRC3*), granzyme A (*GZMA*), and urotensin-II (*UTS2*) (**Figures 1B,C**).

Interactions among the 23 pyroptosis-related DEGs were observed, and each gene was mapped to the STRING database to show their interaction relationships (interaction minimum>0.9, highest confidence) and visualize in Cytoscape.

There were totally 54 interaction relationships among 23 pyroptosis-related DEGs. **Figure 1D** indicated the protein-protein interaction (PPI) network diagram.

The correlation analysis showed that CD14 was significantly positively correlated with NLRP3, while CD14 was significantly negatively correlated with HMGB1 in all healthy controls and MDD samples (**Figure 2**). These results indicated that expression imbalances of PS genes played important roles in the occurrence and development of MDD.

A Diagnostic Model for MDD Constituting of PS Genes

Firstly, the RF was used to screen MDD-specific genes that optimally differentiated MDD cases from healthy controls. When the number of decision trees reached 300, the error changes of the three kinds gradually decrease (**Figure 3A**). The 23 PS genes identified by MeanDecreaseAccuracy and MeanDecreaseGini were showed in **Figure 3B**. The top 10 of

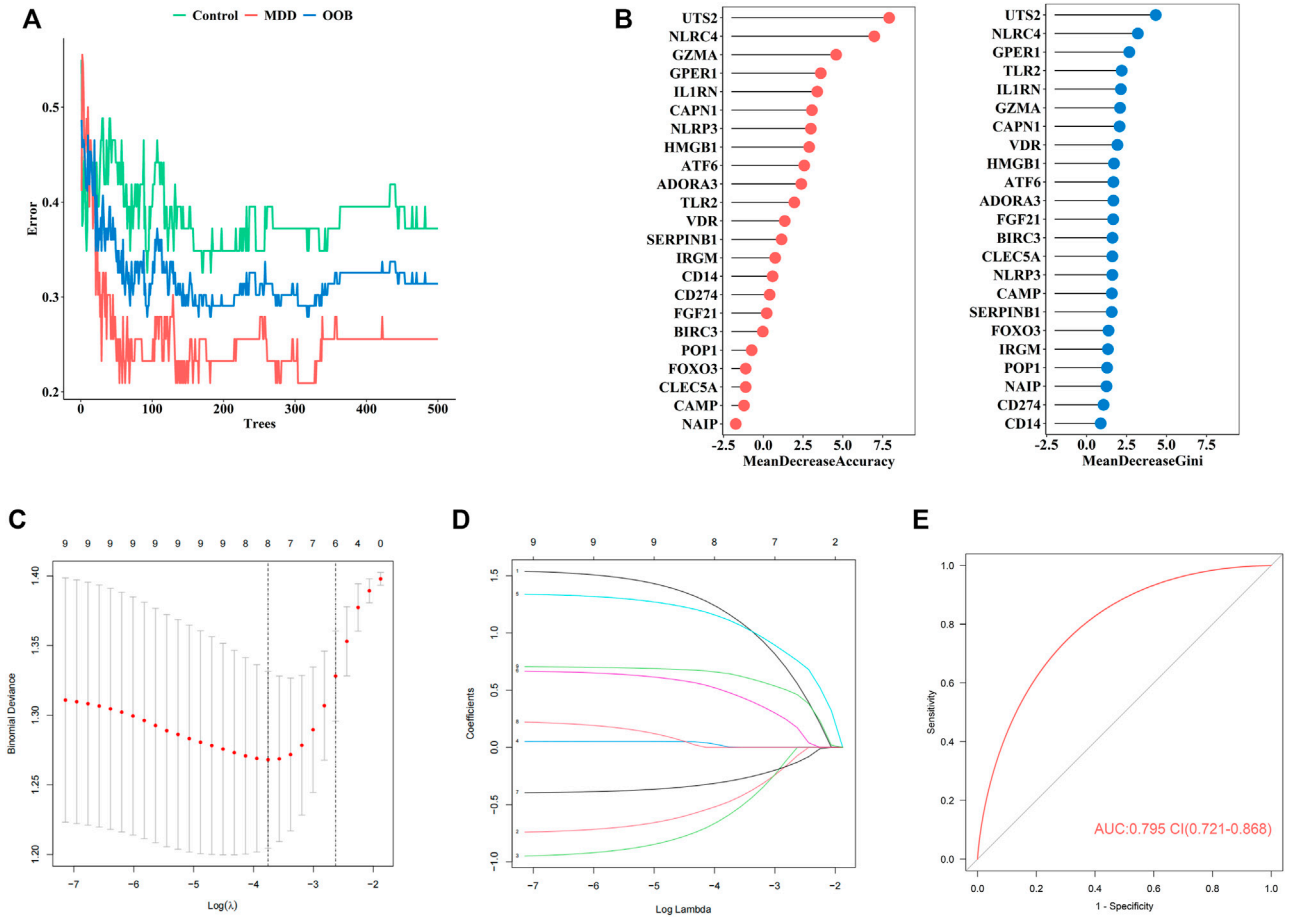

FIGURE 3 | The construction of our diagnostic model for MDD **(A)**. Error between the number of decision trees and different groups **(B)**. The MeanDecreaseAccuracy and MeanDecreaseGini of 23 pyroptosis-related genes **(C)**. Screening of the optimal parameter (using lambda.1se as the best lambda) at which the vertical lines were drawn **(D)**. LASSO coefficient profiles of the 23 differentially expressed PS genes plus age and sex **(E)**. The ROC value of our diagnostic model in GSE98793 dataset.

TABLE 5 | The coefficient of eight genes.

Gene	Coefficient
GPER1	1.162
GZMA	−0.474
HMGB1	−0.588
IL1RN	0.003
NLRC4	1.112
NLRP3	0.479
UTS2	−0.294
CAPN1	0.644

these—*UTS2, NLRC4, GZMA, GPER1, IL1RN, CAPN1, NLRP3, HMGB1, ATF6*, and *ADORA3*—were candidate genes.

Secondly, to establish an MDD-specific diagnostic model, LASSO regression was conducted based on the above 10 genes and basic phenotype information (age and sex), we contained eight genes (*GPER1, GZMA, HMGB1, IL1RN, NLRC4, NLRP3, UTS2, CAPN1*) according to lambda.1se (**Figures 3C,D**).

Furthermore, to improve the diagnostic efficiency of biomarkers, a novel diagnostic risk score was constructed by multiplying the gene expression. The total risk score was imputed as follows: (1.163 × *GPER1* expression level) + (−0.474 × *GZMA* expression level) + (−0.588 × *HMGB1* expression level) + (0.003 × *IL1RN* expression level) + (1.111 × *NLRC4* expression level) + (0.479 × *NLRP3* expression level) + (−0.294 × *UTS2* expression level) + (0.644 × *CAPN1* expression level). Receiver operating characteristic (ROC) analysis was used to evaluate the diagnostic ability of eight genes, which showed a favorable diagnostic value, with an AUC of 0.795 (95% CI 0.721–0.868) (**Figure 3E**). The coefficient of eight genes were showed in **Table 5**.

Internal and External Validation of Diagnostic Model Performance

The internal validation of our diagnostic model was performed by 10-fold cross-validation ($n = 2000$). The model demonstrated good discrimination (bias-corrected AUC = 0.774, 95% CI =

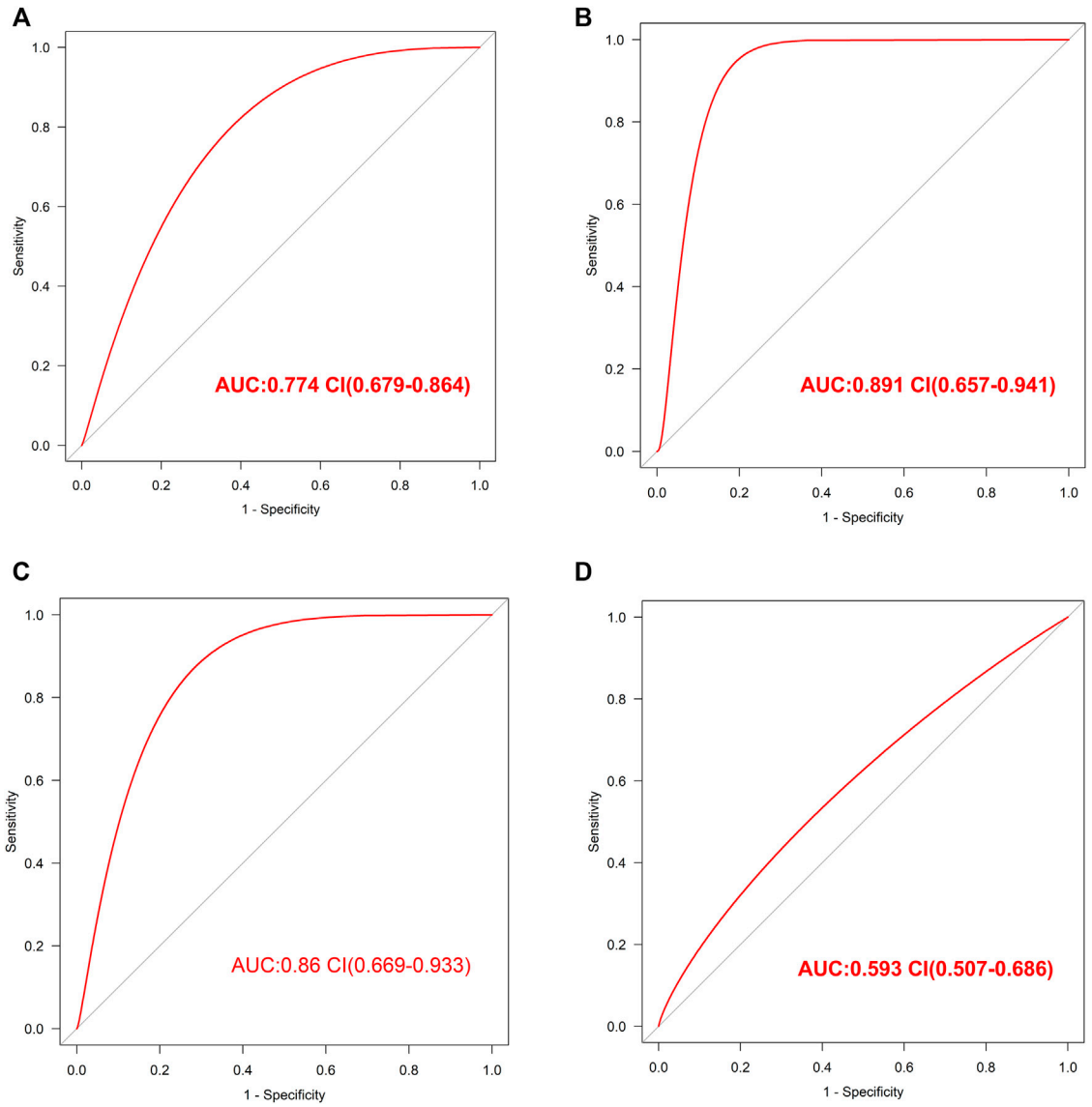

FIGURE 4 | The validation of this diagnostic model **(A)**. The ROC value in internal validation of this diagnostic model **(B)**. The ROC value in external validation of this diagnostic model by GSE76826 dataset **(C)**. The ROC value in validation of this diagnostic model by GSE53987 dataset **(D)**. The ROC value in validation of this diagnostic model by GSE38484 dataset.

0.679–0.864) (**Figure 4A**). The external analysis using independent dataset GSE76826 revealed a good performance of our diagnostic model for stratifying MDD patients (AUC = 0.891, 95% CI = 0.657–0.941) (**Figure 4B**).

Furthermore, the accuracy of our diagnostic model was validated using brain tissue GSE53987 dataset. The AUC was 0.86 (95% CI = 0.669–0.933), which also indicated good performance (**Figure 4C**).

In order to observe the effectiveness of this diagnostic model in other mental illness, the analysis of schizophrenia GSE38484 dataset was performed. The AUC of GSE38484 dataset was 0.593 (95% CI = 0.507–0.686) (**Figure 4D**), suggesting that this diagnostic model was not effective and accurate for schizophrenia. We speculated that our diagnostic model constituting of eight PS genes was more appropriate for MDD.

Immune Cell Infiltration Profile and Immune-Related Pathway Enrichment Between Healthy Controls and MDD Cases

Many studies have indicated that MDD is accompanied by immune dysregulation, pyroptosis is closely related to immune response as well, thus we want to further explore the relationship between pyroptosis and immune response in MDD. The differences in immune cell infiltration profile and immune-

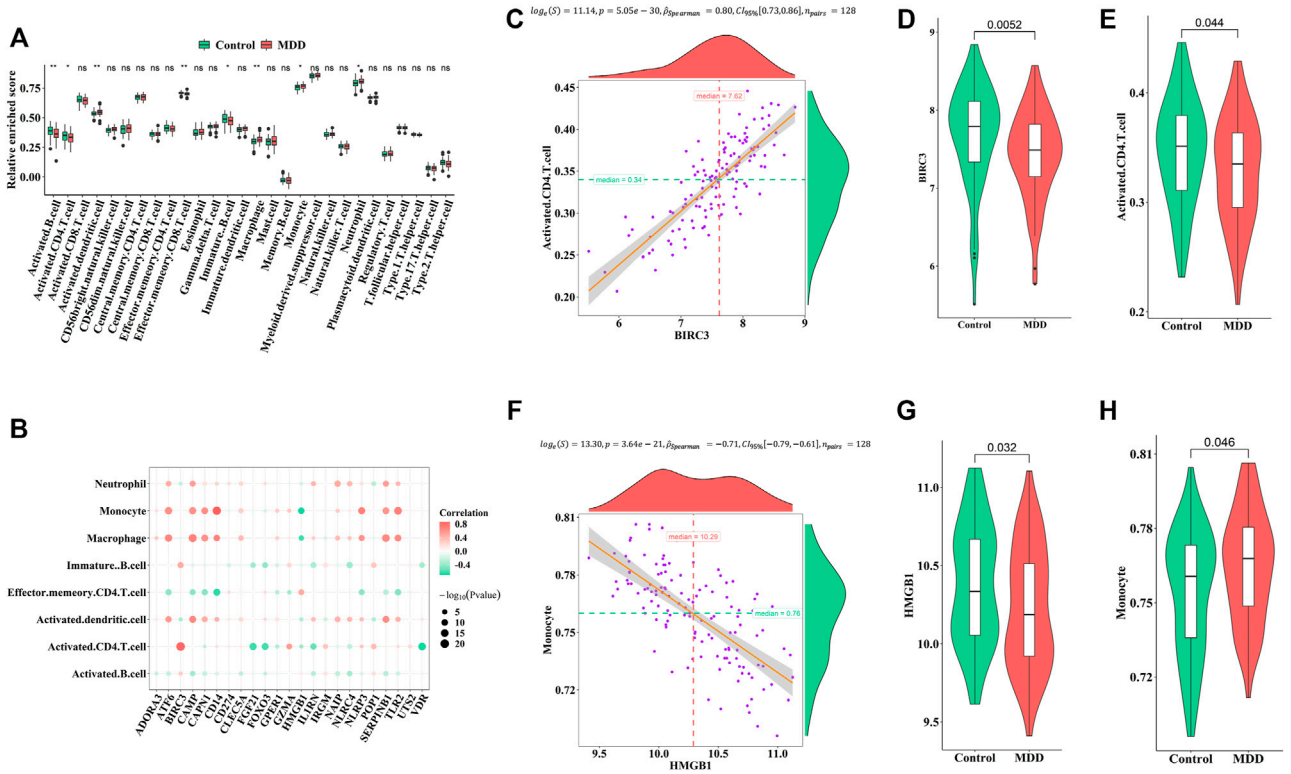

FIGURE 5 | Correlation between pyroptosis-related genes and immune infiltrating cells **(A)**. Differences in the abundance of immune infiltrating cells between healthy control and MDD samples **(B)**. Correlation between pyroptosis-related genes and immune infiltrating cells **(C–E)**. The most positive correlation between immune infiltrating and pyroptosis-related genes **(F–H)**. The most negative correlation between immune infiltrating and pyroptosis-related genes. Adjusted *p*-values were showed as: ns, not significant; **p* < 0.05; ***p* < 0.01.

related pathway enrichment between healthy controls and MDD cases were quantified.

Firstly, ssGSEA was used to calculate the relative abundance of immune cells in each sample. Eight of the immune cell types discovered significant changes in depression samples, with activated dendritic cells, immature dendritic cells, monocytes, and neutrophils showing upregulation and activated B cells, activated CD4 T-cells, effector memory CD8 T-cells, and immature B cells showing downregulation (**Figure 5A**). These results suggested significantly altered immune cell profiles in MDD cases comparing with healthy controls (**Figure 5B**). BIRC3 exhibited the most obvious positive correlation with activated CD4 cells, with low scores in MDD (**Figures 5C–E**). Meanwhile, HMGB1 showed a significant negative correlation with monocyte. The score for HMGB1 was lower in MDD, while monocytes showed the opposite phenomenon (**Figures 5F–H**).

Similarly, the enrichment fractions of immune-related pathways were also calculated by ssGSEA (**Figure 6A**). We observed differences in the antimicrobial pathway, B cell receptor (BCR) signaling pathway, chemokines, cytokines, TCR signaling pathway, and transforming growth factor (TGF)-β family member receptors between healthy controls and MDD cases (**Figure 6B**). CAPN1 was positively correlated with antimicrobials (**Figures 6C–E**), while FOXO3 was negatively correlated with the TCR signaling pathway (**Figures 6F–H**). We speculated that these changes immune cells and immune-related pathways played important roles in occurrence and development of MDD.

Identification of MDD Subtypes Based on 23 PS Genes

To explore the connections between the expression profiles of 23 PS genes (*CLEC5A, CAMP, TLR2, ADORA3, NLRP3, CD14, CD274, NLRC4, NAIP, CAPN1, GPER1, VDR, FGF21, IL1RN, FOX O 3, SERPINB1, ATF6, HMGB1, POP1, IRGM, BIRC3, GZMA,* and *UTS2*) and MDD subtypes, we performed unsupervised clustering using data from 64 MDD cases. By increasing the clustering variable (k) from 2 to 10, we observed the highest intra-group correlation and lowest inter-group correlation for k = 2, suggesting that the 64 MDD cases could be divided into two clusters according to these genes. Cluster A included 30 samples and cluster B contained 34 samples (**Figures 7A–C**).

PCA analysis indicated these two clusters differentiated significantly (**Figure 7D**). The heatmap and boxplot showed the expression differences of 23 PS genes between two clusters,

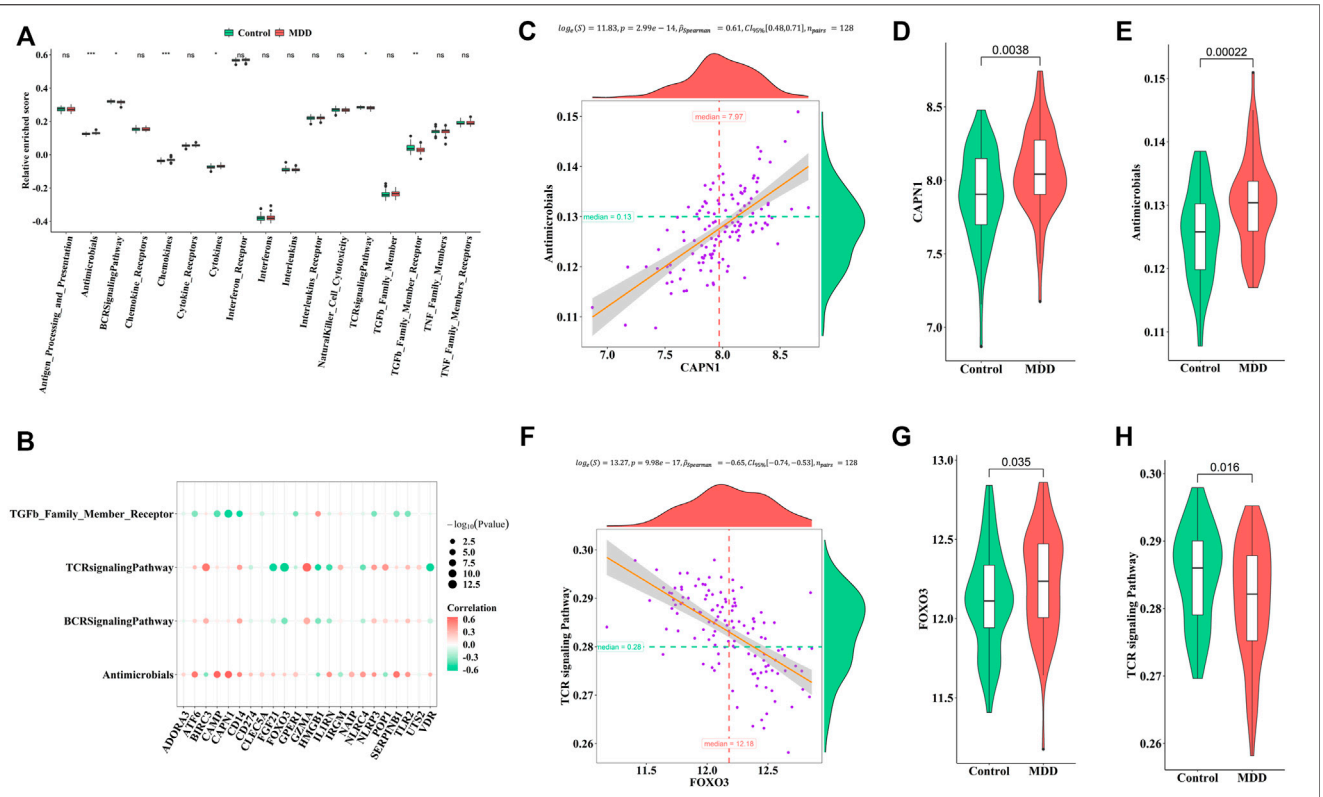

FIGURE 6 | Correlation between pyroptosis-related genes and immune response geneset **(A)**. Differences in the abundance of immune response geneset between healthy control and MDD samples **(B)**. Correlation between pyroptosis-related genes and immune response geneset **(C–E)**. The most positive correlation between immune response geneset and pyroptosis-related genes **(F–H)**. The most negative correlation between immune response geneset and pyroptosis-related genes Adjusted *p*-values were showed as: ns, not significant; **p* < 0.05; ***p* < 0.01; ****p* < 0.001.

in which the expressions of *ATF6, BIRC3, CAMP, CAPN1, CD14, CLEC5A, GZMA, NLRP3, POP1, SEPRINB1*, and *TLR2* were significantly increased in cluster B, while the expressions of *FGF21, FOX O 3, HMGB1, IL1RN*, and *VDR* were significantly decreased. *ADORA3, CD274, GPER1, IRGM, NAIP, NARC4*, and *UTS2* did not differ significantly (**Figures 7E,F**).

Distinct Immune and Biological Characteristics Between Two Clusters

To explore the immune characteristics between these two clusters, we measured the immune cells enrichment fractions, immune pathway activity, and human leukocyte antigen (HLA) gene expression profiles. The two clusters revealed completely different immune characteristics: for example, memory B cells and cytokines were mainly enriched in cluster A, while HLA genes mostly concentrated in cluster B (**Figures 8A–C**).

In addition to immune characteristics, we further explored the biological functions. We analyzed the enrichment scores of the Hallmark pathways and Kyoto Encyclopedia of Genes and Genomes (KEGG) pathways in the two clusters by GSVA, which revealed enrichment of pathways in cluster A, including fatty acid metabolism and neuroactive receptor interaction (**Figures 8D,E**).

Generation of "PS-Scores" and Functional Annotation

To further explore the pathological mechanisms of MDD related to pyroptosis, we developed a pyroptosis-related signature score, the "PS-score," including the phenotype-related genes to quantify the pyroptosis regulation pattern of each MDD sample. The "PS-scores" for two distinct subtypes were calculated. The "PS-scores" of cluster B was significantly higher than that of cluster A (**Figure 9A**). **Figure 9B** exhibited that the relationships between gender, pyroptosis clusters, and "PS-scores".

IFN-α is currently suggested to be an important link in the pathogenesis of MDD. Clinical studies have shown significantly higher serum IFN levels in depression patients than those of normal people. After 12 weeks of antidepressant treatment, IFN levels were significantly lower than those before treatment (Shelton et al., 2011). Thus, we explored the relationship between two subtypes and expression profiles of IFN-α isoforms. **Figure 9C** indicated that the expression profiles of IFN-α1, IFN-α2, IFN-α4, IFN-α5, IFN-α7, IFN-α8, IFN-α10, IFN-α14, IFN-α16, IFN-α17, and IFN-α21 were all lower in cluster B, although the difference was not significant for IFN-α17.

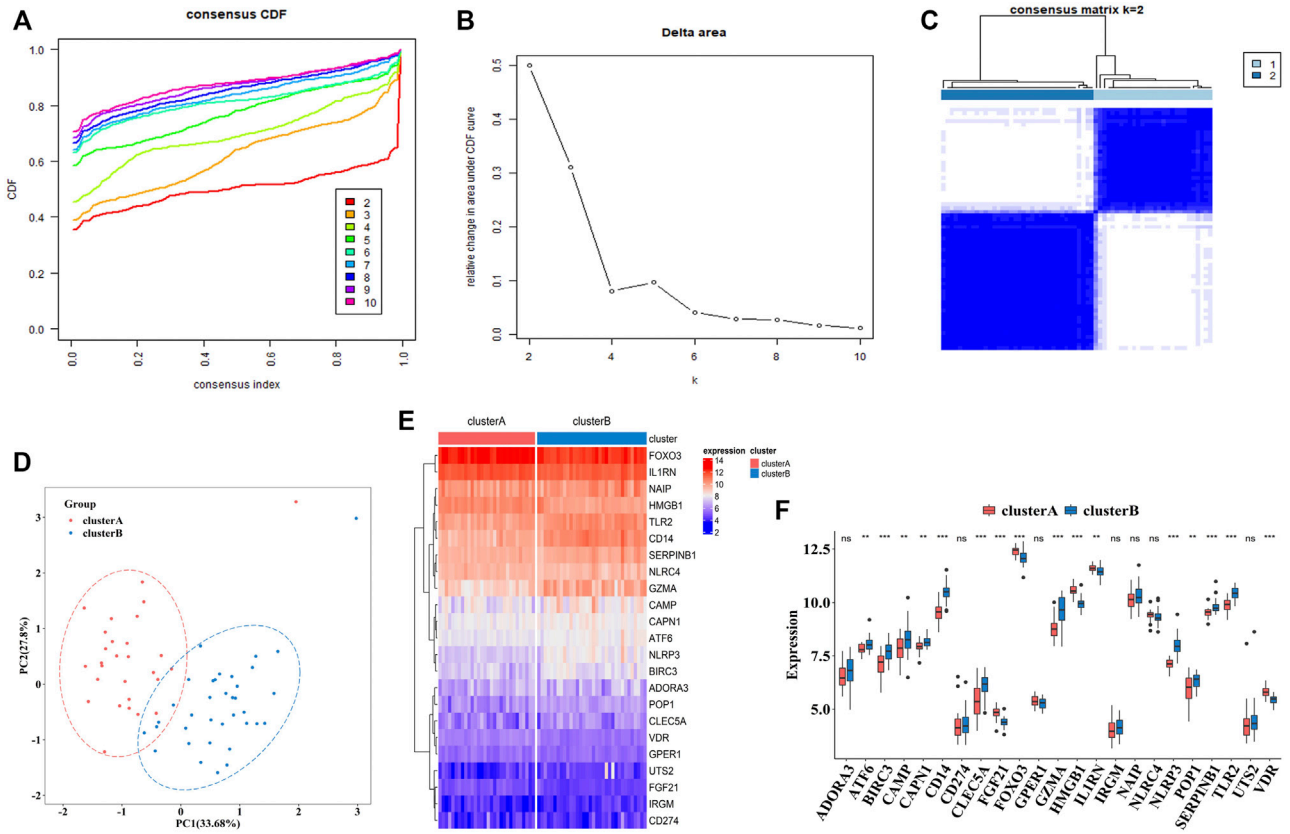

FIGURE 7 | The construction of pyroptosis-related MDD subtypes **(A)**. The empirical cumulative distribution function (CDF) plots revealed the consensus distributions for each k (k = 2–10) **(B)**. Area change under CDF curve when K = 2–10. **(C)**. Two pyroptosis-related MDD clusters were generated *via* unsupervised consensus cluster **(D)**. PCA for the expression profiles of the 23 pyroptosis-related genes **(E,F)**. Expression heat map and boxplot map of the 23 pyroptosis-related genes in cluster A and cluster B. Adjusted *p*-values were showed as: ns, not significant; $^{**}p < 0.01$; $^{***}p < 0.001$.

DISCUSSION

Major depression is a debilitating mental illness and a leading cause of suicide (Ting et al., 2020). Pyroptosis is originally identified as a key mechanism in fighting infection, and a growing number of research suggests its role in the development of several diseases. However, the role of pyroptosis in MDD remains unclear. Our present study first constructed a diagnosis model for depression based on PS genes and then explored the role of pyroptosis in depression.

Currently, there is no clear boundary between normal and depressive behavioral manifestations (Wakefield et al., 2007); thus, the diagnosis of depression is subjective and difficult to implement (Pan et al., 2018). Previous studies have reported several diagnostic biomarkers for depression. Leday, the original author of the GSE98793 dataset, reported an AUC of 0.71 for 165 gene combinations (Leday et al., 2018). In addition, in two independent sample sets of patients with depression, Papakostas et al. (2013) reported high diagnostic performance and sensitivity and specificity >80% for nine biomarkers (alpha1 antitrypsin, apolipoprotein CIII, brain-derived neurotrophic factor, cortisol, epidermal growth factor, myeloperoxidase, prolactin, resistin, and soluble tumor necrosis factor-alpha receptor type II). We previously constructed a diagnostic model with the signature of four autophagy-related genes used GSE98793 dataset and autophagy gene set as well. The AUC of autophagy-related diagnostic model was 0.779 (He et al., 2021). In the present study, we explored a molecular diagnostic model for MDD based on PS genes and observed whether this model had higher efficiency. We firstly identified 23 differentially expressed PS genes between MDD cases and healthy controls. Further analysis using RF in machine learning identified *UTS2, NLRC4, GZMA, GPER1, IL1RN, CAPN1, NLRP3, HMGB1, ATF6*, and *ADORA3* as key PS genes affecting MDD classification. Then, the LASSO logistic regression finally screened feature genes and develop a diagnostic model based on eight genes (*GPER1, GZMA, HMGB1, IL1RN, NLRC4, NLRP3, UTS2, CAPN1*). Our present diagnostic model showed the AUC was 0.795 (95% CI: 0.721–0.868) for this model, indicating the high performance for differentiating MDD cases from healthy controls.

Of these eight genes (*GPER1, GZMA, HMGB1, IL1RN, NLRC4, NLRP3, UTS2, CAPN1*), *GPER1, IL1RN, NLRP3*, and *HMGB1* are reported associated with MDD previously. Pattern recognition receptors (PRRs) may play an important role in the interaction between inflammatory response and behavior. Several damage-associated molecular patterns (DAMPs) are associated

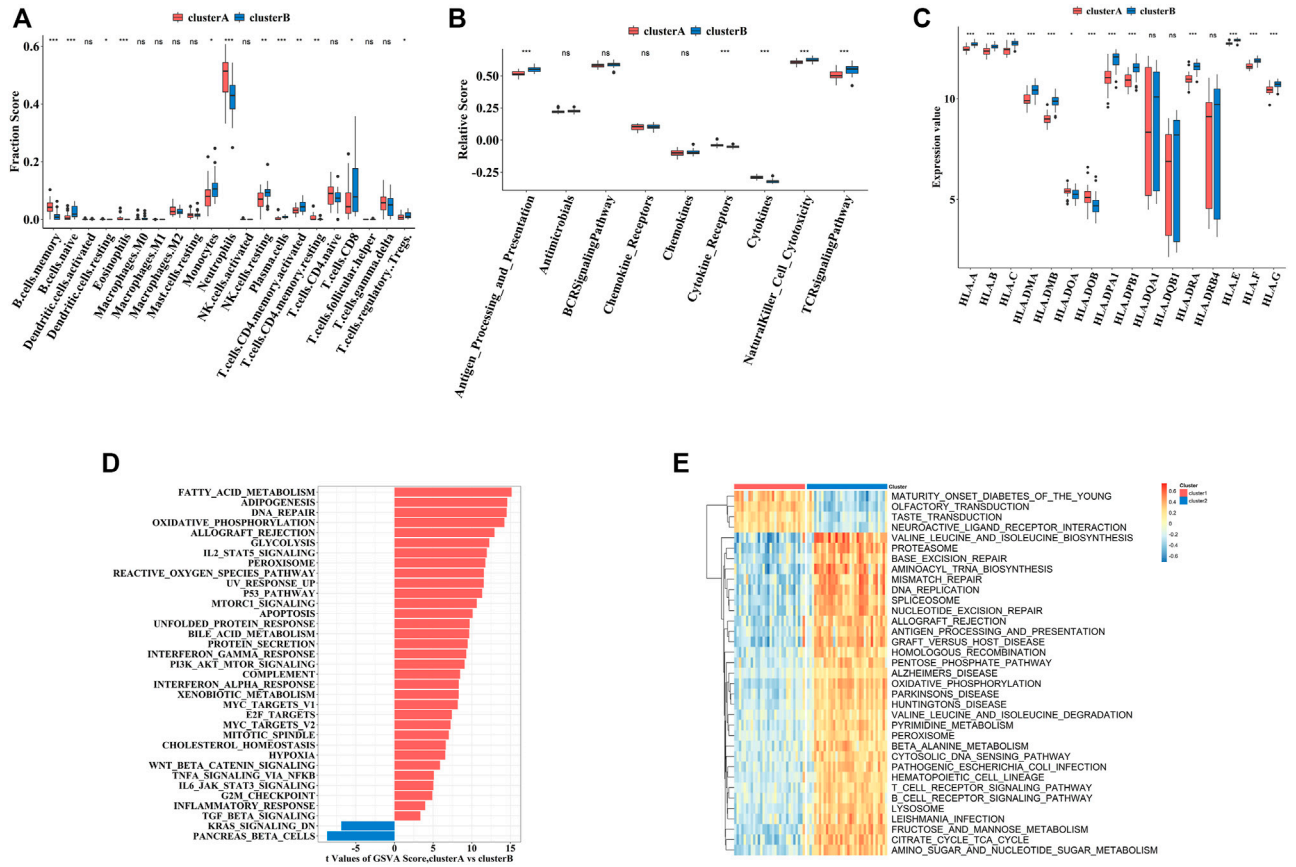

FIGURE 8 | The immune and biological landscapes of two pyroptosis-related clusters **(A–C)**. The results of immune infiltrating cells **(A)**, immune response gene set **(B)**, and HLA gene set **(C)**: boxplot map of the enrichment scores among cluster A and cluster B **(D,E)**. The results of Hallmark pathways **(D)** and Kyoto Encyclopedia of Genes and Genomes (KEGG) pathways **(E)**: heat map of the enrichment scores among cluster A and cluster B Adjusted *p*-values were showed as: ns, not significant; $^{*}p < 0.05$; $^{**}p < 0.01$; $^{***}p < 0.001$.

with stress and depression, especially NLRP3 and HMGB1. The NLRP3 inflammasome is activated and GSDMD cleavage, subsequent IL-1β and IL-18 release, finally pytoptosis occurs. HMGB1 can induce NLRP3 activation, play an important role in pyroptosis as well.

The activation level of NLRP3 inflammasome was increased in multi-pathway induced depressed mouse models. Furthermore, the specific inflammasome inhibitor VX-765 blocked NLRP3 activation in the hippocampus and improved depression-like behavior in chronically unpredictable stressed mice. Clinical investigation reported increased NLRP3 mRNA and protein levels in peripheral blood mononuclear cells of MDD patients compared with healthy controls (Kaufmann et al., 2017). HMGB1 can be highly expressed in the cerebral cortex (Lian et al., 2017) and hippocampus (Liu et al., 2019) of CUMS mice. It is reported that stress can induce depression-like behaviours through the HMGB1/TLR4/NF-κB signalling pathway in the hippocampus (Liu et al., 2019) and PFC (Xu et al., 2020). G protein-coupled receptor 30 (*GPR30*), also known as G protein-coupled estrogen receptor 1 (*GPER1*), levels in MDD patients were significantly higher than that in the healthy controls (Findikli et al., 2017). GPER stimulates IL-1β secretion *via* JNK and p38 MAPK signaling pathways, and then induce pyroptosis (Deng et al., 2020). *IL1RN* (the gene encoding IL-1RA) encodes a classical signal peptide that secretes cytokines through the endoplasmic reticulum and Golgi apparatus (Lennard, 2017). The NLRP3 and caspase-1 affect the release of IL-1RA, which has a broad effect on the inflammatory response and pyroptosis in bladder epithelial cells (Lindblad et al., 2019). A meta-analysis reported significantly higher levels of cytokine receptor antagonists (IL-1RA) in MDD patients compared to those in normal controls (Goldsmith et al., 2016). However, no associations between the other six candidate genes and depression have been reported. We believe that our present results will provide a direction for future research on early diagnosis of depression based on pyroptosis.

A growing number of studies have reported the associations between pro-inflammatory cytokines and emotional, cognitive and behavioral changes, many of which are associated with depression. For example, higher levels of pro-inflammatory cytokines such as interleukin-6 and C-reactive protein have been discovered in MDD patients (Howren et al., 2009). Poor response to antidepressant treatment is obviously associated with elevated levels of proinflammatory cytokines (Hiles et al., 2012). Traditional antidepressants, such as fluoxetine and imipramine, had no

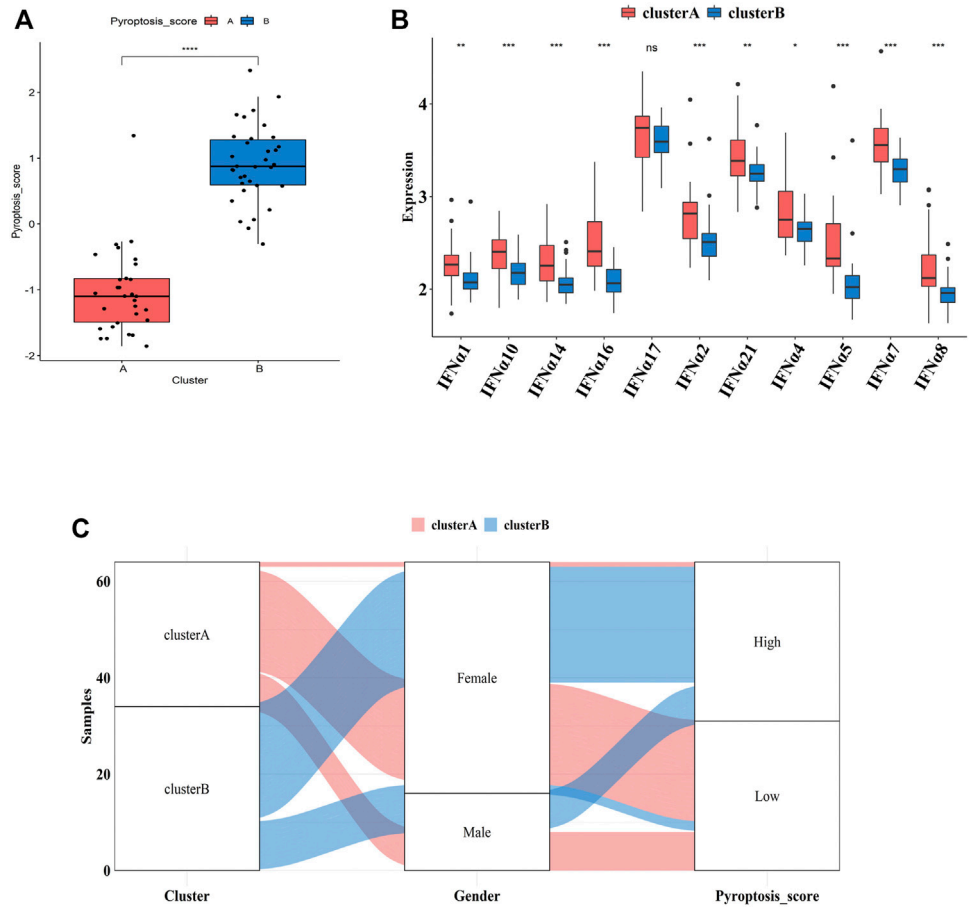

FIGURE 9 | Differences in PS-scores and IFN-α isoforms between two pyroptosis-related clusters **(A)**. Differences in PS-scores between cluster A and cluster B **(B)**. The relationships between clusters, gender, and "PS-scores" **(C)**. Differential expression levels of IFN-α isoforms between cluster A and cluster B. Adjusted *p*-values were showed as: ns, not significant; **p* < 0.05; ***p* < 0.01; ****p* < 0.001.

obvious effects on more than 40% of MDD patients. Surprisingly, the use of anti-inflammatory drugs in conjunction with antipsychotics can relieve a range of psychotic symptoms (Berk et al., 2020). Therefore, we next observed the immune status of MDD patients and healthy controls in GSE98793 dataset. We found that activated dendritic cells, immature dendritic cells, monocytes, and neutrophils were higher, and activated B cells, activated CD4 T-cells, effector memory CD8 T-cells, and immature B cells were lower in MDD patients compared with healthy controls, with similar to Pfau' (Pfau et al., 2018) and Kronfol's studies (Kronfol, 2002). The up-regulation profiles of dendritic cells, monocytes, and neutrophils illustrate infection and inflammation occur and progress. Our results indicated MDD patients might present immune imbalance and inflammatory status.

Pyroptosis is a type of programmed cell death that is closely related to the inflammatory response. In the process of pyroptosis, cells form various vesicles, with pores 10–20 nm in diameter appearing on the cell membrane after gasdermin shear. It is reported that the release of many inflammatory factors leads to cascade amplification of cellular inflammatory responses (Frank and Vince, 2019), and pyroptosis is closely related to the immune response. We also discovered PS genes were closely associated with the changes of immune cells and immune-related pathway in GSE98793 dataset. Furthermore, our molecular diagnostic model based on pyroptosis showed a good performance. It was attractive for us to explore the immune-related mechanisms and search effective therapy based on pyroptosis can target a specific group of depression patients. So, we divided the MDD patients in GSE98793 into two subtypes according to pyroptosis, and found the immune characteristics and "PS scores" of subtypes were different. The "PS score" of cluster B was significantly higher than that of cluster A, and patients in cluster B presented lower profiles of B cells memory, dendritic cells, eosinophil, cytokines receptor pathway, and IFN-α family, which suggesting higher "PS score" might indicate lower levels of inflammatory condition. In addition, HLA genes play an important role in immune response and immune therapy. Attractively, most HLA genes were up-regulated in cluster B, indicating that patients in cluster B might be more sensitive to immune therapy. Previous studies identified different pyroptosis-related subtypes for gastric cancer and melanoma, providing a new method for the prognosis and survival of tumor patients and promoting the development of personalized therapy (Liu et al.,

2021). According to our results, deep exploration of immune regulation in depression could help us understand and develop accurate and effective anti-inflammatory therapy for MDD patients. However, unfortunately, the clinical information of MDD patients is very limited, so we only conducted a partial study to observe the phenomenon, and further study is needed.

Few studies have assessed the role of pyroptosis in depression. This preliminary study explored the diagnostic values of PS genes in depression, and systematically analyzed the relationships between PS genes and the immune response in depression, providing theoretical support for future research. However, our study has some limitations. First, the total sample size was relatively small (MDD: n = 64; Normal: n = 64). Secondly, this study was based on bioinformatics analysis; thus many of the results were theoretical. However, as experiments are the only standard for verifying the results, their accuracy requires verification without experimental methods. Third, due to the lack of abundant clinical data, we cannot determine the specific role of these PS genes in depression, which warrants further study.

In summary, our study provided a molecular model for MDD diagnosis. We additionally revealed the pyroptosis was closely related with immune imbalance in MDD. Comprehensive analysis of the pyroptosis pattern of MDD will improve our understanding of the internal mechanism of the MDD immune regulatory network and inform the development of more effective treatment methods.

DATA AVAILABILITY STATEMENT

The datasets presented in this study can be found in online repositories. The names of the repository/repositories and accession number(s) can be found in the article

AUTHOR CONTRIBUTIONS

WG and SH designed the study. ZD analyzed the data and drafted the manuscript. JL analyzed the data.

FUNDING

National Natural Science Foundation of China (81903592, 81901371). Wuhan Yellow Crane Talent-Outstanding Young Talent Project. Shanghai Municipal Public Health Excellent Young Talents Training Program (GWV-10.2-YQ45).

ACKNOWLEDGMENTS

We sincerely thank the original researchers of GSE98793, GSE76826, GSE53987, and GSE38484 for their work.

REFERENCES

Ahechu, P., Zozaya, G., Martí, P., Hernández-Lizoáin, J. L., Baixauli, J., Unamuno, X., et al. (2018). NLRP3 Inflammasome: A Possible Link between Obesity-Associated Low-Grade Chronic Inflammation and Colorectal Cancer Development. *Front. Immunol.* 9, 2918. doi:10.3389/fimmu.2018.02918

Berk, M., Woods, R. L., Nelson, M. R., Shah, R. C., Reid, C. M., Storey, E., et al. (2020). Effect of Aspirin vs Placebo on the Prevention of Depression in Older People: A Randomized Clinical Trial. *JAMA psychiatry* 77 (10), 1012–1020. doi:10.1001/jamapsychiatry.2020.1214

Beurel, E., Toups, M., and Nemeroff, C. B. (2020). The Bidirectional Relationship of Depression and Inflammation: Double Trouble. *Neuron* 107 (2), 234–256. doi:10.1016/j.neuron.2020.06.002

Broz, P., Pelegrín, P., and Shao, F. (2020). The Gasdermins, a Protein Family Executing Cell Death and Inflammation. *Nat. Rev. Immunol.* 20 (3), 143–157. doi:10.1038/s41577-019-0228-2

Deng, Y., Miki, Y., and Nakanishi, A. (2020). Estradiol/GPER Affects the Integrity of Mammary Duct-like Structures *In Vitro*. *Sci. Rep.* 10 (1), 1386. doi:10.1038/s41598-020-57819-9

Denny, P., Feuermann, M., Hill, D. P., Lovering, R. C., Plun-Favreau, H., and Roncaglia, P. (2018). Exploring Autophagy with Gene Ontology. *Autophagy* 14 (3), 419–436. doi:10.1080/15548627.2017.1415189

Diboun, I., Wernisch, L., Orengo, C. A., and Koltzenburg, M. (2006). Microarray Analysis after RNA Amplification Can Detect Pronounced Differences in Gene Expression Using Limma. *BMC genomics* 7 (1), 252. doi:10.1186/1471-2164-7-252

Ferrúa, C. P., Giorgi, R., da Rosa, L. C., do Amaral, C. C., Ghisleni, G. C., Pinheiro, R. T., et al. (2019). MicroRNAs Expressed in Depression and Their Associated Pathways: A Systematic Review and a Bioinformatics Analysis. *J. Chem. Neuroanat.* 100, 101650. doi:10.1016/j.jchemneu.2019.101650

Findikli, E., Kurutas, E. B., Camkurt, M. A., Karaaslan, M. F., Izci, F., Fındıklı, H. A., et al. (2017). Increased Serum G Protein-Coupled Estrogen Receptor 1 Levels and its Diagnostic Value in Drug Naïve Patients with Major Depressive Disorder. *Clin. Psychopharmacol. Neurosci.* 15 (4), 337–342. doi:10.9758/cpn.2017.15.4.337

Frank, D., and Vince, J. E. (2019). Pyroptosis versus Necroptosis: Similarities, Differences, and Crosstalk. *Cell Death Differ.* 26 (1), 99–114. doi:10.1038/s41418-018-0212-6

Friedman, J., Hastie, T., and Tibshirani, R. (2010). Regularization Paths for Generalized Linear Models via Coordinate Descent. *J. Stat. Softw.* 33 (1), 1–22. doi:10.18637/jss.v033.i01

Goldsmith, D. R., Rapaport, M. H., and Miller, B. J. (2016). A Meta-Analysis of Blood Cytokine Network Alterations in Psychiatric Patients: Comparisons between Schizophrenia, Bipolar Disorder and Depression. *Mol. Psychiatry* 21 (12), 1696–1709. doi:10.1038/mp.2016.3

Gururajan, A., Clarke, G., Dinan, T. G., and Cryan, J. F. (2016). Molecular Biomarkers of Depression. *Neurosci. Biobehav Rev.* 64, 101–133. doi:10.1016/j.neubiorev.2016.02.011

Hänzelmann, S., Castelo, R., and Guinney, J. (2013). GSVA: Gene Set Variation Analysis for Microarray and RNA-Seq Data. *BMC Bioinforma.* 14 (1), 7–15. doi:10.1186/1471-2105-14-7

He, S., Deng, Z., Li, Z., Gao, W., Zeng, D., Shi, Y., et al. (2021). Signatures of 4 Autophagy-Related Genes as Diagnostic Markers of MDD and Their Correlation with Immune Infiltration. *J. Affect Disord.* 295, 11–20. doi:10.1016/j.jad.2021.08.005

Hiles, S. A., Baker, A. L., de Malmanche, T., and Attia, J. (2012). Interleukin-6, C-Reactive Protein and Interleukin-10 after Antidepressant Treatment in People with Depression: a Meta-Analysis. *Psychol. Med.* 42 (10), 2015–2026. doi:10.1017/S0033291712000128

Howren, M. B., Lamkin, D. M., and Suls, J. (2009). Associations of Depression with C-Reactive Protein, IL-1, and IL-6: a Meta-Analysis. *Psychosom. Med.* 71 (2), 171–186. doi:10.1097/PSY.0b013e3181907c1b

Kaufmann, F. N., Costa, A. P., Ghisleni, G., Diaz, A. P., Rodrigues, A. L. S., Peluffo, H., et al. (2017). NLRP3 Inflammasome-Driven Pathways in Depression: Clinical and Preclinical Findings. *Brain Behav. Immun.* 64, 367–383. doi:10.1016/j.bbi.2017.03.002

Kronfol, Z. (2002). Immune Dysregulation in Major Depression: a Critical Review of Existing Evidence. *Int. J. Neuropsychopharmacol.* 5 (4), 333–343. doi:10.1017/S1461145702003024

Kursa, M. B. (2014). Robustness of Random Forest-based Gene Selection Methods. *BMC Bioinforma.* 15 (1), 8. doi:10.1186/1471-2105-15-8

Lanz, T. A., Reinhart, V., Sheehan, M. J., Rizzo, S. J. S., Bove, S. E., James, L. C., et al. (2019). Postmortem Transcriptional Profiling Reveals Widespread Increase in Inflammation in Schizophrenia: a Comparison of Prefrontal Cortex, Striatum, and hippocampus Among Matched Tetrads of Controls with Subjects Diagnosed with Schizophrenia, Bipolar or Major Depressive Disorder. *Transl. Psychiatry* 9 (1), 151. doi:10.1038/s41398-019-0492-8

Leday, G. G. R., Vértes, P. E., Richardson, S., Greene, J. R., Regan, T., Khan, S., et al. (2018). Replicable and Coupled Changes in Innate and Adaptive Immune Gene Expression in Two Case-Control Studies of Blood Microarrays in Major Depressive Disorder. *Biol. Psychiatry* 83 (1), 70–80. doi:10.1016/j.biopsych.2017.01.021

Lennard, A. C. (2017). lnterleukin-1 Receptor Antagonist. *Crit. Rev. Immunol.* 37 (2-6), 531–559. doi:10.1615/CritRevImmunol.v37.i2-6.160

Lépine, J. P., and Briley, M. (2011). The Increasing Burden of Depression. *Neuropsychiatr. Dis. Treat.* 7 (Suppl. 1), 3–7. doi:10.2147/NDT.S19617

Lian, Y. J., Gong, H., Wu, T. Y., Su, W. J., Zhang, Y., Yang, Y. Y., et al. (2017). Ds-HMGB1 and Fr-HMGB Induce Depressive Behavior through Neuroinflammation in Contrast to Nonoxid-HMGB1. *Brain Behav. Immun.* 59, 322–332. doi:10.1016/j.bbi.2016.09.017

Lindblad, A., Persson, K., and Demirel, I. (2019). IL-1RA Is Part of the Inflammasome-Regulated Immune Response in Bladder Epithelial Cells and Influences Colonization of Uropathogenic E. coli. *Cytokine* 123, 154772. doi:10.1016/j.cyto.2019.154772

Liu, L., Dong, Y., Shan, X., Li, L., Xia, B., and Wang, H. (2019). Anti-depressive Effectiveness of Baicalin *In Vitro* and *In Vivo*. *Molecules* 24 (2), 326. doi:10.3390/molecules24020326

Liu, L. P., Lu, L., Zhao, Q. Q., Kou, Q. J., Jiang, Z. Z., Gui, R., et al. (2021). Identification and Validation of the Pyroptosis-Related Molecular Subtypes of Lung Adenocarcinoma by Bioinformatics and Machine Learning. *Front. Cell Dev. Biol.* 9, 756340. doi:10.3389/fcell.2021.756340

Malhi, G. S., and Mann, J. J. (2018). Depression. *Lancet* 392 (10161), 2299–2312. doi:10.1016/S0140-6736(18)31948-2

Martinez, J. G., Carroll, R. J., Müller, S., Sampson, J. N., and Chatterjee, N. (2011). Empirical Performance of Cross-Validation with Oracle Methods in a Genomics Context. *Am. Stat.* 65 (4), 223–228. doi:10.1198/tas.2011.11052

Miyata, S., Kurachi, M., Okano, Y., Sakurai, N., Kobayashi, A., Harada, K., et al. (2016). Blood Transcriptomic Markers in Patients with Late-Onset Major Depressive Disorder. *PLoS One* 11 (2), e0150262. doi:10.1371/journal.pone.0150262

Pan, J. X., Xia, J. J., Deng, F. L., Liang, W. W., Wu, J., Yin, B. M., et al. (2018). Diagnosis of Major Depressive Disorder Based on Changes in Multiple Plasma Neurotransmitters: a Targeted Metabolomics Study. *Transl. Psychiatry* 8 (1), 130. doi:10.1038/s41398-018-0183-x

Papakostas, G. I., Shelton, R. C., Kinrys, G., Henry, M. E., Bakow, B. R., Lipkin, S. H., et al. (2013). Assessment of a Multi-Assay, Serum-Based Biological Diagnostic Test for Major Depressive Disorder: a Pilot and Replication Study. *Mol. Psychiatry* 18 (3), 332–339. doi:10.1038/mp.2011.166

Pfau, M. L., Ménard, C., and Russo, S. J. (2018). Inflammatory Mediators in Mood Disorders: Therapeutic Opportunities. *Annu. Rev. Pharmacol. Toxicol.* 58, 411–428. doi:10.1146/annurev-pharmtox-010617-052823

Ritchie, M. E., Phipson, B., Wu, D., Hu, Y., Law, C. W., Shi, W., et al. (2015). Limma Powers Differential Expression Analyses for RNA-Sequencing and Microarray Studies. *Nucleic Acids Res.* 43 (7), e47. doi:10.1093/nar/gkv007

Shelton, R. C., Claiborne, J., Sidoryk-Wegrzynowicz, M., Reddy, R., Aschner, M., Lewis, D. A., et al. (2011). Altered Expression of Genes Involved in Inflammation and Apoptosis in Frontal Cortex in Major Depression. *Mol. Psychiatry* 16 (7), 751–762. doi:10.1038/mp.2010.52

Shi, J., Gao, W., and Shao, F. (2017). Pyroptosis: Gasdermin-Mediated Programmed Necrotic Cell Death. *Trends Biochem. Sci.* 42 (4), 245–254. doi:10.1016/j.tibs.2016.10.004

Takahashi, M., Lim, P. J., Tsubosaka, M., Kim, H. K., Miyashita, M., Suzuki, K., et al. (2019). Effects of Increased Daily Physical Activity on Mental Health and Depression Biomarkers in Postmenopausal Women. *J. Phys. Ther. Sci.* 31 (4), 408–413. doi:10.1589/jpts.31.408

Ting, E. Y., Yang, A. C., and Tsai, S. J. (2020). Role of Interleukin-6 in Depressive Disorder. *Int. J. Mol. Sci.* 21 (6), 2194. doi:10.3390/ijms21062194

Troubat, R., Barone, P., Leman, S., Desmidt, T., Cressant, A., Atanasova, B., et al. (2021). Neuroinflammation and Depression: A Review. *Eur. J. Neurosci.* 53 (1), 151–171. doi:10.1111/ejn.14720

Van Eijk, K. R., De Jong, S., Strengman, E., Buizer-Voskamp, J. E., Kahn, R. S., Boks, M. P., et al. (2015). Identification of Schizophrenia-Associated Loci by Combining DNA Methylation and Gene Expression Data from Whole Blood. *Eur. J. Hum. Genet.* 23 (8), 1106–1110. doi:10.1038/ejhg.2014.245

Wakefield, J. C., Schmitz, M. F., First, M. B., and Horwitz, A. V. (2007). Extending the Bereavement Exclusion for Major Depression to Other Losses: Evidence from the National Comorbidity Survey. *Arch. Gen. Psychiatry* 64 (4), 433–440. doi:10.1001/archpsyc.64.4.433

Wilkerson, M. D., and Hayes, D. N. (2010). ConsensusClusterPlus: a Class Discovery Tool with Confidence Assessments and Item Tracking. *Bioinformatics* 26 (12), 1572–1573. doi:10.1093/bioinformatics/btq170

Wing, J. K., Babor, T., Brugha, T., Burke, J., Cooper, J. E., Giel, R., et al. (1990). SCAN. Schedules for Clinical Assessment in Neuropsychiatry. *Arch. Gen. Psychiatry* 47 (6), 589–593. doi:10.1001/archpsyc.1990.01810180089012

Xia, X., Wang, X., Cheng, Z., Qin, W., Lei, L., Jiang, J., et al. (2019). The Role of Pyroptosis in Cancer: Pro-cancer or Pro-"host"? *Cell Death Dis.* 10 (9), 650. doi:10.1038/s41419-019-1883-8

Xu, X., Zeng, X. Y., Cui, Y. X., Li, Y. B., Cheng, J. H., Zhao, X. D., et al. (2020). Antidepressive Effect of Arctiin by Attenuating Neuroinflammation via HMGB1/TLR4- and TNF-A/tnfr1-Mediated NF-Kb Activation. *ACS Chem. Neurosci.* 11 (15), 2214–2230. doi:10.1021/acschemneuro.0c00120

Conflict of Interest: The authors declare that the research was conducted in the absence of any commercial or financial relationships that could be construed as a potential conflict of interest.

Publisher's Note: All claims expressed in this article are solely those of the authors and do not necessarily represent those of their affiliated organizations, or those of the publisher, the editors and the reviewers. Any product that may be evaluated in this article, or claim that may be made by its manufacturer, is not guaranteed or endorsed by the publisher.

frontiers | Frontiers in Pharmacology

TYPE Original Research
PUBLISHED 26 July 2022
DOI 10.3389/fphar.2022.886514

OPEN ACCESS

EDITED BY
Marta P Pereira,
Centre for Molecular Biology Severo Ochoa (CSIC), Spain

REVIEWED BY
Shawn Fletcher Sorrells,
University of Pittsburgh, United States
Gilda Angela Neves,
Federal University of Rio de Janeiro, Brazil

*CORRESPONDENCE
Esther Berrocoso,
esther.berrocoso@uca.es

†These authors have contributed equally to this work and share first authorship

SPECIALTY SECTION
This article was submitted to Neuropharmacology, a section of the journal Frontiers in Pharmacology

RECEIVED 28 February 2022
ACCEPTED 30 June 2022
PUBLISHED 26 July 2022

CITATION
Garcia-Partida JA, Torres-Sanchez S, MacDowell K, Fernández-Ponce MT, Casas L, Mantell C, Soto-Montenegro MDL, Romero-Miguel D, Lamanna-Rama N, Leza JC, Desco M and Berrocoso E (2022), The effects of mango leaf extract during adolescence and adulthood in a rat model of schizophrenia. *Front. Pharmacol.* 13:886514. doi: 10.3389/fphar.2022.886514

The effects of mango leaf extract during adolescence and adulthood in a rat model of schizophrenia

Jose Antonio Garcia-Partida[1,2†], Sonia Torres-Sanchez[2,3,4†], Karina MacDowell[4,5], Maria Teresa Fernández-Ponce[6], Lourdes Casas[6], Casimiro Mantell[6], María Luisa Soto-Montenegro[4,7,8], Diego Romero-Miguel[7,9], Nicolás Lamanna-Rama[7,9], Juan Carlos Leza[4,5], Manuel Desco[4,7,9,10] and Esther Berrocoso[2,3,4*]

[1]Neuropsychopharmacology and Psychobiology Research Group, Department of Neuroscience, University of Cádiz, Cádiz, Spain, [2]Instituto de Investigación e Innovación en Ciencias Biomédicas de Cádiz, INiBICA, Hospital Universitario Puerta del Mar, Cádiz, Spain, [3]Neuropsychopharmacology and Psychobiology Research Group, Psychobiology Area, Department of Psychology, University of Cádiz, Cádiz, Spain, [4]Ciber of Mental Health (CIBERSAM), ISCIII, Madrid, Spain, [5]Department of Pharmacology and Toxicology, Faculty of Medicine, Universidad Complutense de Madrid (UCM), Health Research Institute Hospital 12 de Octubre (imas12), Institute of Research in Neurochemistry IUIN-UCM, Madrid, Spain, [6]Department of Chemical Engineering and Food Technology, Science Faculty, University of Cádiz, Cádiz, Spain, [7]Instituto de Investigación Sanitaria Gregorio Marañón, Madrid, Spain, [8]High Performance Research Group in Physiopathology and Pharmacology of the Digestive System (NeuGut), Universidad Rey Juan Carlos, Madrid, Spain, [9]Departamento de Bioingeniería e Ingeniería Aeroespacial, Universidad Carlos III de Madrid, Madrid, Spain, [10]Centro Nacional de Investigaciones Cardiovasculares (CNIC), Madrid, Spain

There is evidence that in schizophrenia, imbalances in inflammatory and oxidative processes occur during pregnancy and in the early postnatal period, generating interest in the potential therapeutic efficacy of anti-inflammatory and antioxidant compounds. Mangiferin is a polyphenolic compound abundant in the leaves of *Mangifera indica L.* that has robust antioxidant and anti-inflammatory properties, making it a potential candidate for preventive or co-adjuvant therapy in schizophrenia. Hence, this study set-out to evaluate the effect of mango leaf extract (MLE) in a model of schizophrenia based on maternal immune activation, in which Poly I:C (4 mg/kg) is administered intravenously to pregnant rats. Young adult (postnatal day 60–70) or adolescent (postnatal day 35–49) male offspring received MLE (50 mg/kg of mangiferin) daily, and the effects of MLE in adolescence were compared to those of risperidone, assessing behavior, brain magnetic resonance imaging (MRI), and oxidative/inflammatory and antioxidant mediators in the adult offspring. MLE treatment in adulthood reversed the deficit in prepulse inhibition (PPI) but it failed to attenuate the sensitivity to amphetamine and the deficit in novel object recognition (NOR) induced. By contrast, adolescent MLE treatment prevented the sensorimotor gating deficit in the PPI test, producing an effect similar to that of risperidone. This MLE treatment also produced a reduction in grooming behavior, but it had no effect on anxiety or novel object recognition memory. MRI studies revealed that adolescent MLE administration partially counteracted the cortical shrinkage, and cerebellum and ventricle enlargement.

In addition, MLE administration in adolescence reduced iNOS mediated inflammatory activation and it promoted the expression of biomarkers of compensatory antioxidant activity in the prefrontal cortex and hippocampus, as witnessed through the reduction of Keap1 and the accumulation of NRF2 and HO1. Together, these findings suggest that MLE might be an alternative therapeutic or preventive add-on strategy to improve the clinical expression of schizophrenia in adulthood, while also modifying the time course of this disease at earlier stages in populations at high-risk.

KEYWORDS

mangiferin, schizophrenia, Poly I:C, oxidative/nitrosative stress, neuroinflammation, magnetic resonace imaging (MRI)

Introduction

Schizophrenia (SZ) is a severe, chronic psychiatric disorder that affects around 24 million people worldwide (GBD 2019 Diseases and Injuries Collaborators, 2020). It is characterized by a set of heterogeneous symptoms that lead to impaired cognitive, social and occupational performance (rev. in Owen et al., 2016), and it is considered one of the leading causes of disability worldwide (GBD 2019 Mental Disorders Collaborators, 2022). Moreover, in addition to the deterioration in quality of life, patients with SZ experience a reduction in life expectancy of about 15 years (rev. in Hjorthøj et al., 2017). Therefore, even though SZ does not have a high prevalence (<1%), its huge impact on patients, their family and society makes it one of the most burdensome illnesses (Chong et al., 2016; Charlson et al., 2018).

Although the aetiology and biological substrates involved in SZ are still not fully understood, it is currently considered a neurodevelopmental disorder triggered by the interaction of a large number of genetic and/or environmental factors that alter normal brain development (rev. in Owen et al., 2016; McCutcheon et al., 2019). Although one of the most relevant risk factors is exposure to stressful events during the perinatal period (Van Os et al., 2010; Millan et al., 2016; Arango et al., 2021), epidemiological studies indicate that exposure to infections during pregnancy increases the risk of developing SZ in adulthood (rev. in Brown and Derkits, 2010). Accordingly, preclinical studies suggest that maternal immune activation is one of the key components in the post-pubertal emergence of SZ-like behavioral and neurobiological alterations (rev. in Gilmore and Jarskog, 1997; Talukdar et al., 2020). Likewise, pharmacological interventions during peri-adolescence can prevent the emergence of the behavioral and brain structural abnormalities produced by a prenatal insult (Zuckerman et al., 2003; Piontkewitz et al., 2009; Casquero-Veiga et al., 2021), while treatment in adulthood might only alleviate the symptomatology presented.

A large number of preclinical and clinical studies suggest that altered immune responses (e.g., increased brain-blood barrier permeability and glial activation), and changes to inflammatory pathways (cytokine imbalances) and in oxidative stress (redox dysregulation) are key aspects of the pathophysiology of SZ (rev. in Leza et al., 2015; Müller, 2018; Upthegrove and Khandaker, 2020). In addition, antioxidant and anti-inflammatory agents have been proposed as alternative or add-on therapeutic strategies to combat SZ. In fact, several studies showed beneficial effects of compounds with these pharmacological actions, such as N-acetylcysteine (Berk et al., 2008), α-lipoic acid (rev. in Salehi et al., 2019), vitamins C (Dakhale et al., 2005) and E (Soares-Weiser et al., 2018), minocycline (Romero-Miguel et al., 2021) or even omega-3 fatty acids (Casquero-Veiga et al., 2021).

Mangiferin (1,3,6,7-tetrahydroxyxanthone-C2-β-D-glucoside) is a bioactive polyphenolic molecule predominantly found in the leaves, bark, fruit skin and root of the mango tree (*Mangifera indica L.*). This compound has generated growing interest due to its anti-inflammatory and antioxidant properties but also, due to other biological activities that include anti-diabetic, analgesic, anti-microbial, anti-tumour or immunomodulatory effects (rev. in Saha et al., 2016; Du et al., 2018). These pharmacological activities have shown to improve inflammation and oxidative damage induced by stress (Márquez et al., 2012); anxiety- and depressive-like behaviors (Jangra et al., 2014) and cognitive deficit in a model of Alzheimer's disease (Infante-Garcia et al., 2017b), suggesting a neuroprotective role of mangiferin. Furthermore, mangiferin improved the behavioral and oxidative damage produced by a ketamine model of SZ (Rao et al., 2012).

Therefore, in this study the aim was to evaluate the effect of administering a mango leaf extract (MLE) with a high content of mangiferin, in a model of SZ induced by maternal Poly I:C immune activation. This animal model is a well-establish model of SZ based on neurodevelopmental changes that mimics the clinical course of this disorder and the behavioral and neurobiological alterations observed in SZ patients (rev. in Meyer and Feldon, 2012). In this study, both young adult and adolescent rats were administered MLE, the effects of which were assessed through behavioral evaluations, magnetic resonance imaging (MRI) and biochemical measurement of inflammatory and antioxidant markers. As a result, we hoped

to gain support for the testing and use of this extract to manage SZ.

Materials and methods

Animals

Male Wistar rats from the University of Cadiz were used in the experiments, maintained on a 12 h light/dark cycle with *ad libitum* access to food and water. All procedures were carried out in accordance with the European Communities Council Directive 2010/63/UE and they were approved by the Ethics Committee for Animal Experimentation at the School of Medicine of the University of Cadiz.

Prenatal Poly I:C treatment

Prenatal Poly I:C treatment was performed as described previously (Zuckerman et al., 2003; Zuckerman and Weiner, 2003; Casquero-Veiga et al., 2019). On gestational day (GD) 15, pregnant dams were anesthetized with 4%–2% isoflurane and a single intravenous injection of the synthetic Poly I:C analogue of double-stranded RNA (4 mg/kg dissolved in saline; batch#37M4011V, Sigma Aldrich, Spain) was administered to their tail vein. An equivalent volume of saline alone (vehicle, VH) was injected into the control animals. Dams were weighed 0, 8, 24 and 48 h after Poly I:C or saline administration, and the body weight of their offspring was also evaluated on PND 1 (Lins et al., 2018; Supplementary Figure S1). On postnatal day (PND) 21, male pups were weaned and housed in groups of 2-4 per cage.

Mango leaf extract (MLE)

Supercritical fluid extraction of mango leaves was used to obtain extracts with a high phenolic content and potent antioxidant activity. Briefly, mango (*Mangifera indica L.*) leaves were extracted by a high-pressure technique in a pilot-plant scale apparatus (model SF 2000; Thar Technology, PA, United States). Subcritical water was used as the extraction solvent at a pressure of 20 MPa and a temperature of 80°C based on our previous work (Fernández-Ponce et al., 2015). The use of solvents at high temperature and high pressure enhances the extraction performance as compared with conventional processes carried out at room temperature and atmospheric pressure (Fernández-Ponce et al., 2015; Casas-Cardoso et al., 2021). Three extraction procedures were carried out in batch mode for 12 h and subsequently, extracts were collected, sterilized and stored at −20°C in the absence of light until they were analyzed (Fernández-Ponce et al., 2015). The extract was characterized in terms of global extraction yield, antioxidant and anti-inflammatory activity, and the quantity of phenolic compounds. For each extraction procedure, the global extraction yield obtained was calculated as the ratio of the dry extract to the dry raw material and they were expressed as g extract/100 g raw material.

The antioxidant activity of the MLE was determined by means of the 2,2-diphenyl-1-picrylhydrazyl (DPPH) assay (Brand-Williams et al., 1995) and expressed as the antioxidant activity index (AAI): poor antioxidant activity when the AAI<0.5; moderate antioxidant activity when the AAI is 0.5–1.0; strong antioxidant activity when the AAI is 1.0–2.0; and very strong at an AAI >2.0 (Scherer and Godoy, 2009). Only a MLE obtained with a very strong antioxidant activity was used in this study. To determine the anti-inflammatory activity of the MLE, the capacity of the agent to prevent the denaturation of egg albumin was measured by spectrophotometry at 660 nm (Rahman et al., 2015), expressed as the concentration of 50% efficiency (IC_{50}). The phenolic compounds in the extract were quantified by Ultra High-Performance Liquid Chromatography (UHPLC), as described previously (Fernández-Ponce et al., 2015) and using a Thermo Scientific Dionex Ultimate 3000 model with a Diode Array detector connected to the Chromeleon TM 7 software application for data analysis.

Experimental design, groups and MLE treatment

To study the effectiveness of MLE in reversing the alterations to Poly I:C offspring, two different treatment approaches were assessed, the therapeutic treatment in young adults and a preventive strategy treating during peri-adolescence.

To assess the effect of MLE in young adults, four experimental groups were evaluated: male offspring derived from dams injected with Poly I:C or VH during pregnancy that were treated in adulthood with MLE (VH-MLE and Poly I:C-MLE groups) or drinking water (VH-H_2O and Poly I:C-H_2O groups). The MLE was orally administered and diluted in the drinking water based on their daily water consumption. Dosage was adjusted to 50 mg/kg of mangiferin per day on the basis of our experience and the previous data available in the literature using this phenolic compound (Márquez et al., 2012; Rao et al., 2012; Infante-Garcia et al., 2017a; Infante-Garcia et al., 2017b). To guarantee minimal phenolic degradation, MLE solutions was prepared freshly every day. In this treatment approach, the MLE was administered to young adults from PND 60 until the end of experiments and behavioral evaluation were carried out between PND 70-80 (Figure 1A).

However, in order to evaluate the effect of MLE during the peri-adolescence period, male offspring derived from dams injected with Poly I:C or VH during pregnancy were treated during adolescence (PND 35-49) with MLE (VH-MLE and Poly I:C-MLE groups) or drinking water (VH-H_2O and Poly I:C-H_2O groups). MLE was also orally administered at the same dose of mangiferin (50 mg/kg) diluted in the drinking water. Preclinical and some clinical studies hint

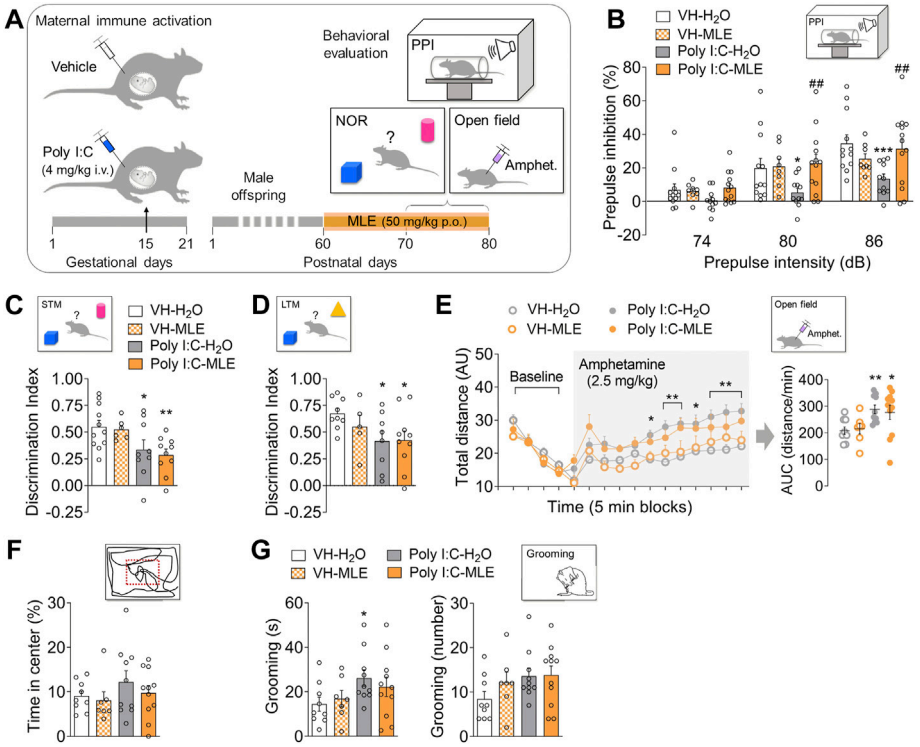

FIGURE 1
The effect of MLE treatment in adulthood on the behavior of the Poly I:C offspring. **(A)** Experimental timeline showing the design to study the effect of MLE treatment in adults. Maternal immune activation was induced in pregnant dams by administering Poly I:C (4 mg/kg i.v., intravenously) or the vehicle alone (controls) on gestational day (GD) 15. Male offspring were treated orally (p.o.) with MLE at a daily dose of 50 mg/kg of mangiferin in young adults since postnatal day (PND) 60. Then, behavioral evaluation was performed (PND 70-80). **(B)** In the prepulse inhibition (PPI) test, the effect of MLE treatment in adulthood is represented as the percentage PPI for 74, 80 and 86 dB prepulse intensity. **(C,D)** The effect of MLE treatment in adulthood on the object discrimination index for the short-term (STM) and long-term memory (LTM) phases of the novel object recognition test (NOR). **(E)** The effect of MLE treatment in adulthood on amphetamine sensitivity in the Poly I:C offspring. The total distance travelled in the open field is represented in 5 min (min) blocks, before and after amphetamine injection (shaded area, 2.5 mg/kg, i.p.). In addition, the area under the curve (AUC) values of amphetamine-induced activity were represented from 5 min after amphetamine injection. **(F)** The effect of MLE treatment in adulthood on anxiety-like behavior. The time spent (%) in the center is represented during the baseline period of free exploration in the open field. **(G)** The effect of MLE treatment in adulthood on grooming behavior. The total time spent grooming and number of grooming events are represented during the last 10 min of the baseline period in the open field. The data are represented as the mean ± SEM of 8–13 animals per group in the PPI test, n = 5-11 animals per group in STM and LTM phases of NOR test, and 9-11 animals per group in amphetamine-induced activity, anxiety-like and grooming behaviors. $^{*}p < 0.05$, $^{**}p < 0.01$, $^{***}p < 0.001$ vs. VH-H_2O; $^{\#\#}p < 0.01$ vs. Poly I:C-H_2O, as assessed by two-way or two-way RM ANOVA followed by the LSD post-hoc test.

that the use of preventive treatments with atypical antipsychotics (e.g., risperidone) in patients at high risk of psychosis during the prodromal period of SZ could prevent the progression of the disease (Piontkewitz et al., 2011b; Marshall and Rathbone, 2011; Subotnik et al., 2015). In this way, the effects of risperidone during adolescence were evaluated. Thus, a set of offspring received a daily intraperitoneal administration (PND 35-49) of 0.3 mg/kg of risperidone (VH-RIS and Poly-RIS groups; Janssen Cork, Belgium). Behavioral evaluation was performed in adulthood (PND 70-80). Then, MRI studies were carried out (PND 115-120 approximately) and subsequently brain tissue was collected to evaluate the oxidative/inflammatory and antioxidant mediators (Figure 2A).

Behavioral studies

Behavioral studies were performed on the adult offspring beginning at PND 70 and they included an assessment of prepulse inhibition of the startle response (PPI), novel object recognition (NOR), amphetamine-induced activity, anxiety-like and grooming behaviors.

Prepulse inhibition (PPI) test

PPI of the acoustic startle response was measured in a sound attenuated chamber using a movement-sensitive piezoelectric measuring platform (Cibertec, Spain). The test session began with a 10 min acclimatization to the startle chamber in the presence of 70 dB background

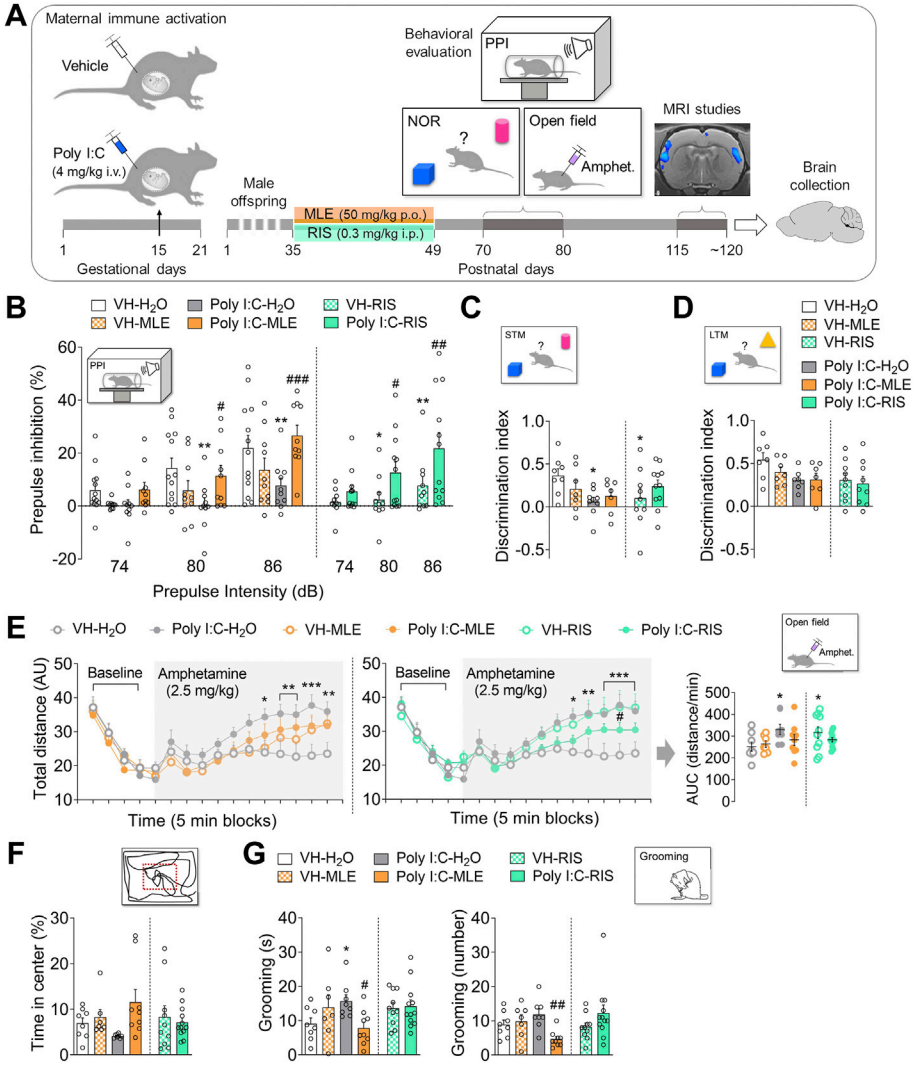

FIGURE 2
The effect of MLE or risperidone (RIS) treatment during adolescence on the behavior of the Poly I:C offspring. **(A)** Experimental timeline showing the design to study the effect of MLE treatment during adolescence. Maternal immune activation was induced in pregnant dams by administering Poly I:C (4 mg/kg i.v., intravenously) or the vehicle alone (controls) on gestational day (GD) 15. Male offspring were treated orally (p.o.) with MLE at a daily dose of 50 mg/kg of mangiferin during adolescence (postnatal day, PND 39-54) or administered intraperitoneally (i.p.) with risperidone (RIS, 0.3 mg/kg) as an adolescence reference treatment. Behavioral evaluation and magnetic resonance imaging (MRI) studies were performed at adulthood (PND 70-80 and PND 115-120, respectively). Finally, brain samples were collected at the end of the experiments. **(B)** The effect of adolescent MLE or RIS treatment on prepulse inhibition (PPI) test. The percentage PPI is represented for a 74, 80 and 86 dB prepulse intensity. **(C,D)** The effect of adolescent MLE or RIS treatment on the short-term (STM) and long-term memory (LTM) discrimination index between objects in the novel object recognition test (NOR). **(E)** The effect of adolescent MLE (left) or RIS (right) treatment on amphetamine sensitivity. The total distance travelled in the open field is represented in 5 min (min) blocks, before and after amphetamine injection (shaded area, 2.5 mg/kg i.p.). In addition, the area under the curve (AUC) values of amphetamine-induced activity were represented from 5 min after amphetamine injection. **(F)** The effect of adolescent MLE or RIS treatment on anxiety-like behavior. The time spent (%) in the center is represented during the baseline period of free exploration in the open field. **(G)** The effect of adolescent MLE or RIS treatment on grooming behavior. The total time spent grooming and the number of grooming events are represented during the last 10 min of the baseline period in the open field. The data are represented as the mean ± SEM of 10–13 animals per group in PPI test, 7-11 animals per group in the STM and LTM phases of the NOR test, and 7-12 animals per group for amphetamine induced activity, anxiety-like and grooming behaviors. $^{*}p < 0.05$, $^{**}p < 0.01$, $^{***}p < 0.001$ vs. VH-H_2O; $^{\#}p < 0.05$, $^{\#\#}p < 0.01$, $^{\#\#\#}p < 0.001$ vs. Poly I:C-H_2O as assessed by two-way or two-way RM ANOVA followed by the LSD post-hoc test.

noise, followed by five trials of startle stimulus (pulse, 120 dB). The rats were then subjected to 10 trials of pseudorandomly presented stimuli: pulse (120 dB); prepulse (74, 80 or 86 dB) + pulse (120 dB); or no stimulus (only background noise). Finally, they were subjected to five pulse trials (120 dB). The pulse and

prepulse lasted 40 ms, the interval between the prepulse and pulse was set at 100 ms, whereas the inter-trial interval ranged from 10 to 20 s. The % PPI for each prepulse intensity was calculated from the pseudorandom presentations as follows: 100-[(startle response to prepulse + pulse)/startle response to pulse) x100)] (Casquero-Veiga et al., 2021).

Novel object recognition (NOR) test

Rats were tested in a plastic, black, square arena (45 × 45 × 35 cm) located in a room with dim lighting. The NOR memory tests were performed as described previously (Llorca-Torralba et al., 2019). Briefly, two identical objects were placed in the arena during the training phase and subsequently, NOR memory was evaluated in two test sessions 2–3 h (short-term memory, STM) and 24 h (long-term memory, LTM) after the training session: one with a familiar object and one with a novel object. Each session lasted 10 min. The objects used were of different shapes, colors and textures, and they were thoroughly cleaned with 70% ethanol between trials to ensure the absence of any olfactory cues. The time spent exploring each object was recorded and the relative exploration of the novel object was expressed as a discrimination index [DI = $(t_{novel} - t_{familiar})/(t_{novel} + t_{familiar})$](Llorca-Torralba et al., 2019). The criteria for exploration were based strictly on active exploration, and circling or sitting on the object were not considered exploratory behaviors.

Open field test

Locomotor activity was also measured in a plastic, black, square arena (45 × 45 × 35 cm) in dim lit boxes. Rats were placed individually in the arena for 20 min of free exploration and in this period, the baseline motor activity was evaluated, as were anxiety-like and grooming behaviors. The animals then received a single, intraperitoneal (i.p.) injection of amphetamine (2.5 mg/kg; Merck, France) and they were returned to the activity chamber for 60 min to evaluate their amphetamine-induced activity (modified from Yee et al., 2005). The sessions were videotaped and the total distance travelled was then analyzed using the SMART (Spontaneous Motor Activity Recording and Tracking) video 3.0 software (Panlab, Spain). Both spontaneous and amphetamine induced-activity were expressed in arbitrary units (AU), in 5 min blocks, and the area under the curve (AUC) values of the total distance travelled was represented from 5 min after amphetamine administration. The time spent in the central area of the arena (%) was measured in this 20 min free exploration phase, considered as anxiety-like behavior. For grooming behavior, the total time spent grooming and the number of grooming events were evaluated over the last 10 min of the free exploration period, when the explorative behavior was reduced.

MRI studies

Anesthetized animals (sevoflurane, inhaled; Romero-Miguel et al., 2021) treated during adolescence were scanned (~ PND 115-120) using a 7-T Biospec 70/20 scanner (Bruker, Germany). A coronal T2-weighted spin-echo sequence was acquired: TE = 33 ms, TR = 3732 ms, averages 2 and slice thickness 0.4 mm. The matrix size was 256 × 256 pixels at a FOV of 3.5 × 3.5 cm^2.

Data processing and analysis. Two types of analysis were performed: a predefined regions of interest (ROI) analysis of primarily subcortical areas; and a voxel-based morphometry (VBM) approach of the entire brain. For the VBM analysis, MRI processing was performed as reported previously (Casquero-Veiga et al., 2019). T2 images were preprocessed, realigned and resliced to a rat brain template space using SPM12 software (Valdés-Hernández et al., 2011; http://www.fil.ion.ucl.ac.uk/spm/software/spm12). These data were used to create a custom brain template (Avants and Gee, 2004) and all the resliced images were registered to the template. The modulated images for the gray matter (GM), white matter (WM) and cerebrospinal fluid (CSF) were then obtained using the probabilistic maps of the brain template (Valdés-Hernández et al., 2011) and the Jacobian determinants from the spatial normalization process. Modulated images were smoothed with a 10 mm FWHM Gaussian filter and then used for statistical analyses with SPM12. A 1500 voxel clustering (spatial extent) threshold was applied to minimize type I error.

To analyze the ROIs, raw T2-images were registered to a common CT reference using the algorithms described in Gasull-Camós et al. (2017). Subsequently, five ROIs were manually segmented onto each MRI image in the whole brain, hippocampus, frontal lobe, all ventricles and fourth ventricle, according to the Paxinos and Watson Rat Brain Atlas (Paxinos and Watson, 2006).

Oxidative/inflammatory and antioxidant evaluations

At the end of the experiments, animals treated during adolescence were anesthetized and their brains were rapidly dissected and frozen at −80°C. For biochemical studies, cytosolic fraction and nuclear extracts from the prefrontal cortex (PFC) and hippocampus tissue samples were prepared according to published protocols (MacDowell et al., 2013).

Western Blot: Inflammatory mediators as the inducible isoforms of nitric oxide synthase (iNOS) and cyclooxygenase (COX2), p38 MAP kinase (p38), lipid peroxidation product 4-hydroxynonenal (4-HNE) and the antioxidant pathway kelch-like ECH-associated protein 1 (Keap1), heme-oxygenase 1 (HO1), NAD(P)H:quinone oxidoreductase 1 (NQO1) were

performed in cytosolic extracts (MacDowell et al., 2016). Protein levels were measured using the Bradford method, loaded onto electrophoresis gel and blotted onto a membrane using a semi-dry transfer system. The membranes were blocked with 5% BSA for 1 h at room temperature and probed overnight at 4°C with: rabbit anti-iNOS (sc-650, 1:750, BSA 2%; SCBT, Germany), goat anti-COX2 (sc-1747, 1:750, BSA 2.5%; SCBT, Germany), rabbit anti-phospho-p38 (sc-17852, 1:750 BSA 1%; SCBT, Germany), mouse anti-p38 (sc-7972, 1:750 BSA 1%; SCBT, Germany), mouse anti-4-HNE (MAB3249, 1:1,000 TBSt; R&D, United Kingdom), mouse anti-Keap1 (MAB3024, 1:1,000, TBSt; R&D, United Kingdom), mouse anti-4-HNE (MAB3249, 1:1,000, TBSt; R&D, United Kingdom), rabbit anti-HO1 (ab68477, 1:1,000, TBSt; abcam, United Kingdom), goat anti-NQO1 (sc16464, 1:750, BSA 1%; SCBT, Germany) and mouse anti-β-actin (A5441, 1:10,000, TBSt; Merck, France). These primary antibodies were detected with horseradish peroxidase-linked secondary antibodies by incubating for 1.5 h at room temperature, the binding of which was detected with an Odyssey Fc System (LICOR®, Germany) and ChemiDoc (Biorad, United States). All measurements were obtained at least three times in separate assays and the results were expressed relative to the controls. Supplementary Figures S2,S3 show uncropped blots and 2 replicates of the bands for each biomarker assessed in the PFC and hippocampus, respectively.

Nuclear Factor erythroid-related 2 (NRF2) activity was measured in nuclear extracts using a commercial ELISA-based kit (600590; Cayman Chemical, United State). For antioxidant status and enzyme activity, tissue samples were sonicated in 400 µl PBS (pH 7) containing a protease inhibitor cocktail (Complete®; Merck, France) and the homogenates were then centrifuged at 10,000 g for 15 min at 4°C. Supernatants were used for determinations of the Superoxide Dismutase (SOD, K028-H1; Arbor Assay, United State), Catalase (CAT, K033-H1; Arbor Assay, United State), Glutathione Peroxidase (GPx, 703102; Cayman Chemical, United State), Glutathione (GSH, K006-H1; Arbor Assay, United State) and Total Antioxidant Capacity (TAOC) was measured with a commercial kit based on the ABTS method (E-BC-K219-M; Elabscience, United State). Nitrites levels were measured by using the Griess method (Green et al., 1982). Briefly, in an acidic solution with 1% sulphanilamide and 0.1% NEDA, nitrites convert into a pink compound that is photometrically calculated at 540 nm in a microplate reader (Synergy 2; BioTek, United State).

Statistical analysis

All the data are represented as the means ± S.E.M and the results were analyzed using STATISTICA 10.0 (StatSoft, United State), applying a Student's t-test (unpaired, two-tailed), or a one-way or two-way analysis of variance (ANOVA), with or without repeated measures (RM), followed by a LSD post-hoc test. The differences were considered significant at $p < 0.05$ except for the VBM analysis where they were considered significant at $p < 0.01$ (uncorrected) (Supplementary Tables S1–S4).

TABLE 1 Mango leaf extract characteristics.

Global extraction yield (g/100 g dried leaves)	37.1 ± 0.6
Antioxidant activity (AAI, µg DPPH/µg dried extract)	4.5 ± 0.4
Anti-inflammatory activity (IC_{50}, µg/mL)	104.5 ± 1.5
Phenolic compounds (g/100 g dried extract)	
mangiferin	11.11 ± 0.02
iriflophenone 3-C-β-d-glucoside	8.95 ± 1.03
iriflophenone 3-C-(2-O-p-hydroxybenzoyl)-β-d-glucoside	5.89 ± 0.50
gallic acid	2.84 ± 0.04
iriflophenone 3-C-(2-O-galloyl)-β-d-glucoside	2.14 ± 0.65
quercetin 3-d-galactoside	1.08 ± 0.08
quercetin 3-β-d-glucoside	0.42 ± 0.57

Results

Prenatal Poly I:C treatment

Maternal immune activation was confirmed by the effect of administering Poly I:C or the vehicle alone (VH), on the body weight of both pregnant dams and their offspring. This indirect measurement was chosen to avoid extra maternal stress by collecting blood samples for inflammatory mediators' evaluation. Thus, intravenous Poly I:C injection significantly reduced the dam's weight relative to the VH dams when assessed 8 h after injection ($p < 0.05$; Supplementary Figure S1A). Furthermore, Poly I:C offspring also weighed less than VH pups on PND 1 ($p < 0.01$; Supplementary Figure S1B).

MLE characterization

This extract was characterized in terms of its global extraction yield, its antioxidant and anti-inflammatory activities, as well as the presence of phenolic compounds (Table 1). Thus, subcritical water extraction at 20 MPa and 80°C gave a high global extraction yield (37.1 ± 0.6 g/100 g of dried leaves), producing an extract with an AAI value of 4.5 ± 0.4 µg DPPH/µg dried extract and an IC_{50} value of 104.5 ± 1.5 µg/ml. Thus, this extract had very strong antioxidant activity and substantial anti-inflammatory activity, in conjunction with a high total polyphenol content, which included major phenolic compounds like mangiferin, iriflophenones and gallic acid (Table 1).

MLE treatment of young adults

In these studies, the effects of administering MLE to young adults that were the offspring of dams that had received Poly I:C or VH during gestation were behaviorally examined (Figure 1A).

Behavioral studies

PPI test

The PPI test we performed to assess whether MLE treatment in young adults would be able to normalize the sensorimotor gating deficit described in the Poly I:C model. Thus, RM ANOVA tests revealed statistically significant differences in this test for the prepulse factor ($p < 0.001$), and a significant interaction between Poly I:C and MLE ($p < 0.05$), as well as between the prepulse, MLE and Poly I:C factors ($p < 0.05$; Supplementary Table S1). Note that the presentation of a prepulse inhibited the acoustic startle response to the pulse in control animals (VH-H_2O) in an intensity-dependent manner (Figure 1B). A post-hoc test showed Poly I:C administration provoked a significant reduction in PPI relative to the controls (VH-H_2O) for the 80 and 86 dB intensities ($p < 0.05$ and $p < 0.001$, respectively; Figure 1B). MLE prevented the reduction in PPI provoked by Poly I:C in the offspring relative to Poly I:C-H_2O group both at 80 and 86 dB ($p < 0.01$; Figure 1B). However, MLE did not significantly modify the PPI values in VH animals (Figure 1B).

NOR test

The effect of MLE treatment in young adults on cognitive function were assessed in the NOR test. During this test, two different concepts were studied: the acquisition of information or learning and the storage of information or memory that were evaluated in the STM and LTM phases of this paradigm, respectively. In this sense, two-way ANOVA revealed Poly I:C produced significant differences in the discrimination index for both the STM ($p < 0.01$) and LTM ($p < 0.05$) phases of the paradigm, with no significant interaction between Poly I:C and MLE treatment ($p > 0.05$; Supplementary Table S1). Thus, there was a significant reduction in the STM discrimination index in Poly I:C animals (Poly I:C-H_2O, $p < 0.05$; Poly I:C-MLE, $p < 0.01$), as well as in the LTM test session (both $p < 0.05$) relative to control animals (VH-H_2O; Figures 1C,D). MLE treatment did not modify the discrimination index in either Poly I:C or VH offspring ($p > 0.05$; Figures 1C,D).

Amphetamine-induced activity

Locomotor activity in response to a systemic administration of amphetamine was measured in our model of SZ after MLE treatment in adulthood. The RM ANOVA highlighted the significant differences in total distance travelled following amphetamine administration (Poly I:C, $p < 0.05$; time, $p < 0.001$; time and Poly I:C interaction, $p < 0.05$; Supplementary Table S1). As such, a post-hoc test showed that amphetamine administration provoked an increase in motor activity over time in all the experimental groups, although this was significantly exacerbated in Poly I:C animals (min 50, $p < 0.05$; min 55–60, $p < 0.01$; min 65, $p < 0.05$; min 70–80, $p < 0.01$; Figure 1E). When the AUC values were analyzed, two-way ANOVA revealed a main effect of Poly I:C ($p < 0.05$; Supplementary Table S1). Thus, a locomotor hyperactivity was observed in Poly I:C offspring measured as a significant increase in the AUC relative to VH offspring (Poly I:C-H_2O, $p < 0.01$; Poly I:C-MLE, $p < 0.05$; Figure 1E). However, MLE administration did not significantly affect the motor activity exhibited by Poly I:C or the VH animals ($p > 0.05$; Figure 1E).

Anxiety-like behavior

To evaluate anxiety-like behavior in this model of SZ and the effect of MLE administration in adulthood on this behavior, the time spent in the central area of the arena (%) was measured during the free exploration phase of the amphetamine-induced activity. However, no significant effects were found on the time spent in the central area of the arena in Poly I:C groups, irrespective of whether they received MLE or not ($p > 0.05$; Supplementary Table S1, Figure 1F).

Grooming behavior

Psychosis-like animal models often exhibit an excessive self-grooming phenotype (Kalueff et al., 2016). In this sense, to explore the effect of MLE treatment in young adults on this behavior, time spent and number of grooming events were measured in the Poly I:C-induced model of SZ. Thus, two-way ANOVA revealed significant differences in the total time spent grooming for Poly I:C factor ($p < 0.05$; Supplementary Table S1). The post-hoc test showed that Poly I:C-H_2O animals spent more time grooming than the controls (VH-H_2O, $p < 0.05$; Figure 1G). Nevertheless, the total grooming time was not modified by MLE administration in the offspring irrespective of whether the dams had received the VH alone or Poly I:C ($p > 0.05$; Figure 1G). Likewise, no significant effects were evident in the number of grooming events in the Poly I:C offspring even after MLE treatment ($p > 0.05$; Supplementary Table S1, Figure 1G).

Adolescent MLE treatment

In these studies, the effects of administering MLE to peri-adolescent rats that were the offspring of dams that had received Poly I:C or VH during gestation were behaviorally examined. Then, MRI studies were conducted and finally, brains were collected to evaluate the oxidative/inflammatory and antioxidant mediators in the PFC and hippocampus (Figure 2A).

Behavioral studies

PPI test

The effect of adolescent MLE treatment on the sensorimotor gating response was assessed in adult Poly I:C offspring. Thus, the RM ANOVA revealed significant differences in the prepulse of the PPI test ($p < 0.001$), a significant interaction between Poly I:C and adolescent treatment ($p < 0.01$) and between the prepulse, treatment and Poly I:C ($p < 0.05$; Supplementary Table S2). The post-hoc test showed that MLE administration prevented the reduction in PPI showed in Poly I:C-H_2O group at 80 and 86 dB ($p < 0.05$, $p < 0.001$, respectively; Figure 2B). Nevertheless, MLE did not modify the PPI values in control animals. As expected, risperidone treatment also significantly influenced PPI, increasing the PPI in Poly I:C offspring (80 dB, $p < 0.05$; 86 dB, $p < 0.01$) relative to Poly I:C-H_2O group (Figure 2B). However, risperidone also significantly decreased PPI in the control (VH) offspring at both 80 ($p < 0.05$) and 86 dB ($p < 0.01$; Figure 2B).

NOR test

The possible preventing effect of MLE treatment in adolescents on NOR deficit induced by this model of SZ was evaluated at adulthood in this test. Two-way ANOVA revealed a significant interaction between Poly I:C and treatment on the discrimination index in the STM ($p < 0.05$) but it was not significant in the LTM phase ($p > 0.05$; Supplementary Table S2). Thus, Poly I:C animals showed a significantly lower discrimination index in the STM than control animals (Poly I:C-H_2O relative to VH-H_2O animals, $p < 0.05$; Figures 2C,D). MLE did not significantly modify the discrimination index in either Poly I:C offspring or in the control (VH) rats ($p > 0.05$; Figures 2C,D). In this paradigm, risperidone treatment did not influence the discrimination index in the STM or LTM phases in Poly I:C animals ($p > 0.05$; Figures 2C,D), although it did significantly reduce the discrimination index over STM in VH offspring (VH-RIS compared to VH-H_2O animals, $p < 0.05$; Figure 2C) without affecting the performance of LTM ($p > 0.05$; Figure 2D).

Amphetamine-induced activity

Locomotor activity after amphetamine administration in adult Poly I:C offspring was evaluated in order to investigate whether adolescent MLE treatment was able to reverse the enhanced sensitivity to these compounds at adulthood. The RM ANOVA showed significant differences in the total distance travelled following amphetamine administration (time, $p < 0.001$; interaction between Poly I:C and treatment, $p < 0.05$ and interaction between time, treatment and Poly I:C, $p < 0.01$; Supplementary Table S2). Amphetamine administration increased the motor activity over time in all the experimental groups, although this effect was significantly stronger in Poly I:C-H_2O rats than in the control animals (VH-H_2O, min 60, $p < 0.05$; min 65–70, $p < 0.01$; min 75, $p < 0.001$; min 80, $p < 0.01$; Figure 2E). Although MLE administration did not affect motor activity in this paradigm ($p > 0.05$; Figure 2E), risperidone treatment significantly increased the total distance travelled in VH offspring (VH-RIS compared to VH-H_2O animals, min 60, $p < 0.05$; min 65, $p < 0.01$; min 70–80, $p < 0.001$; Figure 2E) and it did reduce the hyperactivity induced by Poly I:C (min 75, $p < 0.05$; Figure 2E). Furthermore, AUC ANOVA revealed a significant interaction on the motor activity induced ($p < 0.05$; Supplementary Table S2), with larger AUC values in Poly I:C-H_2O relative to the VH-H_2O rats ($p < 0.05$; Figure 2E). However, MLE administration did not alter the AUC in VH or Poly I:C offspring ($p > 0.05$; Figure 2E). By contrast, control animals treated with risperidone had significantly higher AUC values relative to VH-H_2O animals ($p < 0.05$; Figure 2E), although no significant effect was observed in Poly I:C animals administered risperidone ($p > 0.05$; Figure 2E).

Anxiety-like behavior

Likewise, in order to assess the effect of adolescent MLE treatment on anxiety-like behavior in Poly I:C offspring, we evaluated in adults the time spent in the central area of the arena during the free exploration phase of the amphetamine-induced activity test. However, two-way ANOVA did not reveal a significant effect of Poly I:C or treatment on anxiety-like behavior ($p > 0.05$; Supplementary Table S2; Figure 2F).

Grooming behavior

In addition to test the effect of adolescent MLE treatment in the previous behavioral paradigms, this treatment was also assessed on grooming behavior exhibited by the adult Poly I:C offspring. In this way, the ANOVA revealed a significant interaction regarding both the total time spent grooming and the number of grooming events (both $p < 0.05$; Supplementary Table S2). Thus, the post-hoc test showed that Poly I:C-H_2O animals spent significantly more time grooming than the control animals (VH-H_2O, $p < 0.05$; Figure 2G) and that MLE administration impeded this increase in Poly I:C offspring ($p < 0.05$; Figure 2G) accompanied by a reduction of grooming events ($p < 0.01$; Figure 2G). By contrast, no significant differences in grooming behavior were evident in VH animals and in Poly I:C offspring that were administered risperidone ($p > 0.05$; Figure 2G).

MRI studies

MRI studies using this model of SZ have identified volumetric changes in some brain areas that emerges at adulthood as a consequence of the maternal immune activation (Piontkewitz et al., 2011b; Casquero-Veiga et al., 2019). Therefore, adult offspring were scanned to evaluate whether MLE treatment during the peri-adolescence period

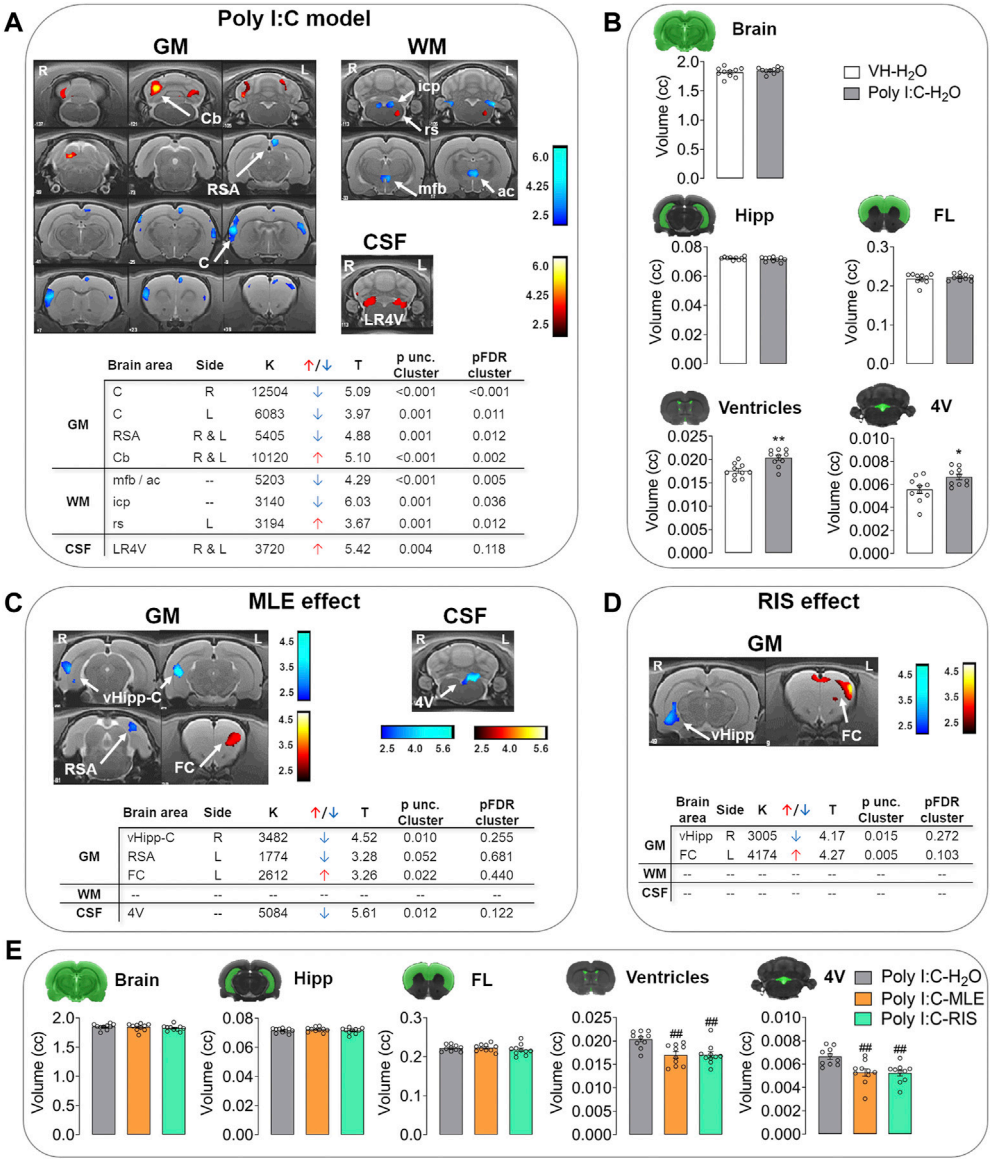

	Brain area	Side	K	↑/↓	T	p unc. Cluster	pFDR cluster
GM	C	R	12504	↓	5.09	<0.001	<0.001
	C	L	6083	↓	3.97	0.001	0.011
	RSA	R & L	5405	↓	4.88	0.001	0.012
	Cb	R & L	10120	↑	5.10	<0.001	0.002
WM	mfb / ac	--	5203	↓	4.29	<0.001	0.005
	icp	--	3140	↓	6.03	0.001	0.036
	rs	L	3194	↑	3.67	0.001	0.012
CSF	LR4V	R & L	3720	↑	5.42	0.004	0.118

	Brain area	Side	K	↑/↓	T	p unc. Cluster	pFDR cluster
GM	vHipp-C	R	3482	↓	4.52	0.010	0.255
	RSA	L	1774	↓	3.28	0.052	0.681
	FC	L	2612	↑	3.26	0.022	0.440
WM	--	--	--	--	--	--	--
CSF	4V	--	5084	↓	5.61	0.012	0.122

	Brain area	Side	K	↑/↓	T	p unc. Cluster	pFDR cluster
GM	vHipp	R	3005	↓	4.17	0.015	0.272
	FC	L	4174	↑	4.27	0.005	0.103
WM	--	--	--	--	--	--	--
CSF	--	--	--	--	--	--	--

FIGURE 3
The effect of MLE or risperidone (RIS) treatment during adolescence on brain volumetric changes measured by MRI. **(A)** Voxel-based morphometry (VBM) and **(B)** regions of interest (ROI) analysis in the Poly I:C model (phenotype). VBM results are represented in T-maps overlaid on a T2-MR template showing the volumetric changes in the gray matter (GM), white matter (WM) and cerebrospinal fluid (CSF) in Poly I:C-H_2O animals relative to the controls (VH-H_2O). The color bars represent the T-values corresponding to volumetric enlargement (warm) and shrinkage (cold). Tables show the phenotype-related effects on brain volumetric changes in the GM, WM and CSF of Poly I:C animals from the VBM analysis. The ROI results are represented in column plots of global and regional volumetric changes in whole brain, hippocampus (Hipp), frontal lobe (FL), all ventricles and the fourth ventricle (4 V) of Poly I:C- H_2O animals relative to the controls (VH-H_2O). **(C)** VBM results after adolescent treatment with MLE or **(D)** RIS. The VBM results are represented in T-maps overlaid on a T2-MR template showing the volumetric changes in the GM, WM and CSF of Poly I:C offspring treated with MLE or RIS relative to Poly I:C-H_2O animals. The color bars represent the T-values corresponding to volumetric enlargement (warm) and shrinkage (cold). The tables show treatment-related effects on the brain volumetric changes in the GM, WM and CSF of Poly I:C animals in the VBM analysis. **(E)** The ROI results after MLE or RIS treatment are represented as column plots of global and regional volumetric changes in whole brain, Hipp, FL, all ventricles and the 4 V compared to Poly I:C-H_2O animals. The VBM tables include: side, right (R) and left (L); T, t value; k, cluster size; volume, increase (↑) or decrease (↓); p unc., *p* value uncorrected; FDR, false discovery rate. The data are represented as the mean ± SEM of 10 animals per group. $^{*}p < 0.05$, $^{**}p < 0.01$ vs. VH-H_2O; $^{\#\#}p < 0.01$ vs. Poly I:C-H_2O as assessed with a Student's t-test (unpaired, two-tailed), or one-way ANOVA followed by the LSD post-hoc test. Abbreviations: AA, amygdaloid area; ac, anterior commissure; C, cortex; Cb, cerebellum; icp, inferior cerebellar peduncle; LR4V, lateral recess of the fourth ventricle; mfb, medial forebrain bundle; rs, rubrospinal tract; RSA, retrosplenial area; vHipp, ventral hippocampus.

was able to prevent brain structural abnormalities induced by this model of SZ.

VBM analysis

VBM analysis revealed that Poly I:C animals showed a reduced GM volume in the frontal cortical areas and the retrosplenial cortex area, in addition to an enlargement of the GM in the cerebellum relative to the control animals (VH-H_2O; Figure 3A). MLE treatment enlarged the GM in the frontal cortex in the Poly I:C animals, while it decreased it in the retrosplenial area and the ventral hippocampus-cortical area relative to Poly I:C-H_2O rats (Figure 3C). In addition, there was a significant enlargement of the GM in the frontal cortex of Poly I:C animals treated with risperidone, coupled to a loss of GM in the ventral hippocampus relative Poly I:C-H_2O animals (Figure 3D). Poly I:C immune activation also provoked a loss of WM volume in the inferior cerebellar peduncle, medial forebrain bundle and anterior commissure, along with WM enlargement in the rubrospinal tract compared to VH-H_2O rats (Figure 3A). No significant changes in WM were found in Poly I:C animals that were then treated with MLE or risperidone (Figures 3C,D).

Poly I:C-H_2O group showed CSF enlargements in the fourth ventricle relative to the control animals (VH-H_2O; Figure 3A). However, MLE but not risperidone treatment significantly reduced this increase in the Poly I:C offspring (Figures 3C,D).

Manual ROI analysis

In evaluating the changes on ROIs analysis induced by Poly I:C animal model, a *t*-test showed significant increase were provoked in ventricular volume ($p < 0.01$), including the fourth ventricle ($p < 0.05$; Supplementary Table S3, Figure 3B). In terms of the effect of MLE and risperidone administration to offspring from dams that received Poly I:C, an ANOVA analysis showed a significant effect in ventricular brain regions (ventricles and fourth ventricle, $p < 0.01$; Supplementary Table S3), and the post-hoc test revealed that both MLE and risperidone prevented an enlargement of the ventricles (ventricles and fourth ventricle, $p < 0.01$; Figure 3E).

Oxidative/inflammatory and antioxidant mediators

Finally, after MRI studies, brains were collected to study the effect of adolescent MLE treatment on modulation of oxidative/inflammatory and antioxidant mediators in both the PFC and hippocampus of the adult Poly I:C offspring. Thus, iNOS and COX2 were assessed as two pro-inflammatory cytokines often overexpressed in this experimental model. In the PFC, ANOVA revealed an interaction ($p < 0.001$; Supplementary Table S4) of iNOS and the post-hoc test showed a significant increase in the iNOS protein levels in the Poly I:C animals ($p < 0.01$; Figure 4A), an effect that was prevented by MLE or risperidone administration ($p < 0.01$ and $p < 0.001$, respectively; Figure 4A). In terms of COX2, no significant differences were found ($p > 0.05$; Supplementary Table S4; Figure 4B). p38 signaling was also evaluated to know if this intracellular pathway contributes to the inflammatory process as well as indicators of oxidative/nitrosative damage (nitrites and 4-HNE, a specific lipid peroxidation marker) due to this damage is often triggered as consequence of that inflammatory response. However, no differences were found in the ratio of the pro-inflammatory mediator MAPK p38, nor in the oxidative/nitrosative damage markers based on nitrite levels or 4-HNE, a derivative of lipid peroxidation ($p > 0.05$; Figures 4C–E). In this context, adolescent treatment with this antioxidant extract could modify compensatory antioxidant mechanisms, so these mechanisms were assessed in terms of Keap1, NRF2, SOD, CAT, GSH/GSSG, GPx, NQO1, HO1 and TAOC. Similarly, no significant changes were observed in the PFC in some of the NRF2-dependent antioxidant compensatory mechanisms (SOD, CAT, GPx and NQO1; Figures 4H,I,M,N). However, ANOVA revealed an interaction with the Keap1 levels and with the antioxidant enzyme HO1 (both $p < 0.05$; Supplementary Table S4). In this sense, the post-hoc test revealed a significant increase in Keap1 levels in Poly I:C animals relative to the control group (VH-H_2O, $p < 0.05$; Figure 4F) and an increased expression of HO1 after MLE administration to Poly I:C animals (Poly I:C-MLE compared to Poly I:C-H_2O animals, $p < 0.05$; Figure 4O). A significant reduction in Keap1 levels was induced by risperidone treatment in Poly I:C animals ($p < 0.05$) whereas it increased these levels in control animals (VH-RIS, $p < 0.05$; Figure 4F). Regarding the nuclear NRF2 activity, a main effect of Poly I:C was found ($p < 0.05$; Supplementary Table S4) and the post-hoc test revealed that Poly I:C offspring treated with risperidone had lower levels of NRF2 than control groups (VH-H_2O, $p < 0.01$; VH-RIS, $p < 0.05$; Figure 4G).

Similarly, the levels of total (GSH_{total}), oxidized (GSSG) and reduced (GSH_{free}) GSH were studied (Figures 4J–L), and a significant effect of treatment on GSSG was evident ($p < 0.05$), the post-hoc test revealing a significant decrease of GSSG in Poly I:C animals treated with MLE relative to the Poly I:C-H_2O and VH-H_2O rats (both $p < 0.05$; Figure 4K). Finally, two-way ANOVA revealed a significant interaction of the total antioxidant capacity of the samples ($p < 0.05$; Supplementary Table S4) and post-hoc test showed that risperidone treatment in Poly I:C rats increased this capacity relative to VH-RIS and Poly I:C-H_2O groups ($p < 0.01$ and $p < 0.05$, respectively; Figure 4P).

In the hippocampus, the ANOVA analysis revealed an interaction for iNOS ($p < 0.05$; Supplementary Table S4), with the post-hoc tests demonstrating a significant decrease in the expression of iNOS in the Poly I:C offspring treated with MLE relative to the untreated animals (Poly I:C-H_2O, $p < 0.05$; Figure 5A). No alterations to other inflammatory mediators were found, like COX2 or the p38 ratio, nor to nitrite or 4-HNE levels ($p > 0.05$; Supplementary Table S4; Figures 5B–E).

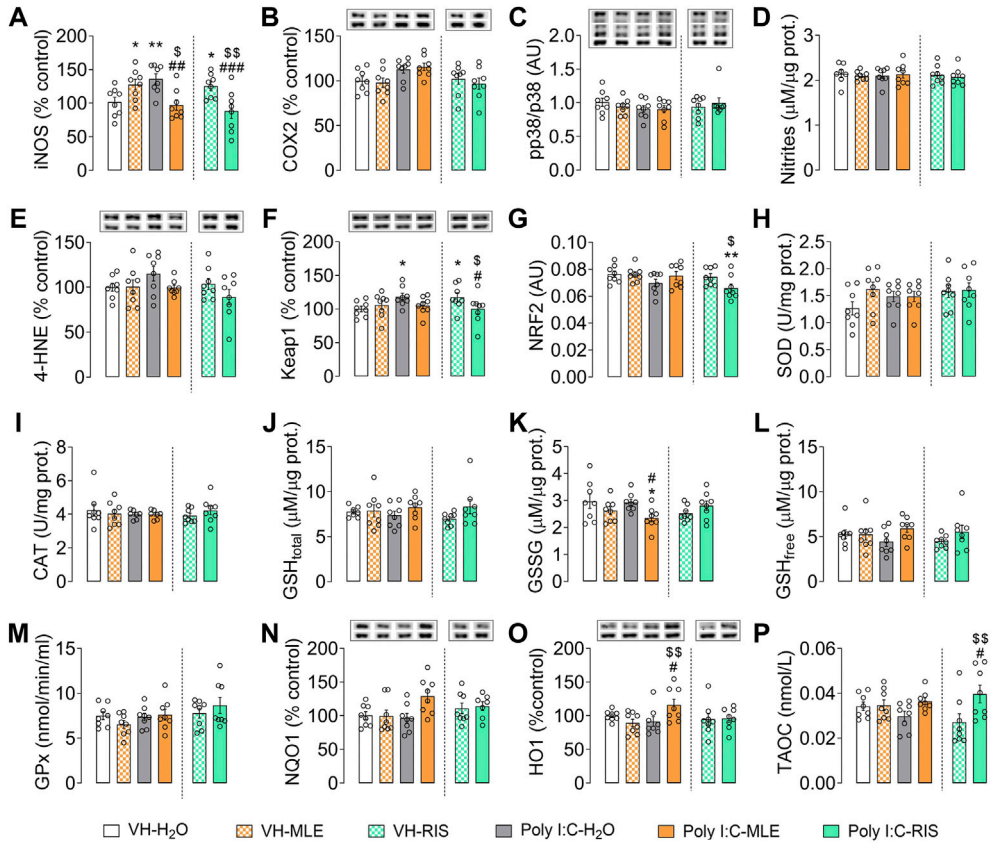

FIGURE 4
The effect of adolescent MLE or risperidone (RIS) treatment on the expression of oxidative/inflammatory mediators in the PFC. **(A–C)** The expression of the inflammatory mediators iNOS, COX2 and p38 relative to the controls, represented as the percentage (%) change, except for p38 which is represented as the ratio of phosphorylated relative to total p38 protein. **(D,E)** The concentrations of the indicators of oxidative/nitrosative damage (nitrites and 4-HNE) are expressed as µM/µg of protein, and as the % of the control expression. **(F–P)** Evaluation of the biomarkers of compensatory antioxidant mechanisms (Keap1, NRF2, SOD, CAT, GSH/GSSG, GPx, NQO1, HO1, TAOC). Keap1, NQO1 and HO1 expression is represented as the % of the controls; NRF2 activity is expressed in arbitrary units (AU); SOD and CAT enzyme activities are expressed as U/mg of protein; the levels of total (GSH_{total}), oxidized (GSSG) and reduced (GSH_{free}) glutathione are expressed as µM/µg of protein; Glutathione Peroxidase (GPx) is expressed as nmol/min/ml; and the Total Antioxidant Capacity (TAOC) is expressed in nmol/L. The data are represented as the mean ± SEM of 7-8 PFC samples per group. Representative bands of iNOS, COX2, 4-HNE, Keap1, NQO1 and HO1 (upper bands), and of the β-actin loading control (lower bands), are shown above their corresponding bars in the graph. For p38 protein expression, phosphorylated and total p38 representative bands are shown relative to β-actin (lower bands). *$p < 0.05$, **$p < 0.01$ vs. $VH\text{-}H_2O$; $^{\$}p < 0.05$, $^{\$\$}$followed by the LSD post-hoc test.

However, ANOVA revealed a main effect for Poly I:C on Keap1 ($p < 0.001$) and a significant interaction ($p < 0.001$; Supplementary Table S4). Indeed, the post-hoc test showed that MLE significantly decreased the Keap1 levels in Poly I:C animals relative to the other groups of animals ($VH\text{-}H_2O$ and VH-MLE, $p < 0.001$; Poly I:C-H_2O, $p < 0.01$; Figure 5F). The same reduction was induced by risperidone in Poly I:C animals ($VH\text{-}H_2O$ and Poly I:C-H_2O, $p < 0.01$; VH-RIS, $p < 0.001$) but in VH offspring it significantly increased Keap1 levels (VH-RIS, $p < 0.05$; Figure 5F). This reduction in Keap1, an NRF2-inhibitory protein, was translated into an increase in nuclear NRF2 activity relative to the VH offspring ($p < 0.05$; Figure 5G), and ANOVA showed a significant effect of Poly I:C for NRF2 ($p < 0.01$). Two-way ANOVA indicated no change in the other antioxidant components (Figures 5H–K,M–P) except for a significant interaction of the free GSH ($p < 0.05$; Supplementary Table S4). The post-hoc test showed that Poly I:C animals treated with risperidone had higher levels of GSH_{free} than Poly I:C-H_2O ($p < 0.05$) and VH-RIS animals ($p < 0.01$; Figure 5L).

Discussion

This study demonstrates that the administration of MLE during adolescence or in adulthood exerts a beneficial effect in the maternal immune activation model of SZ, improving

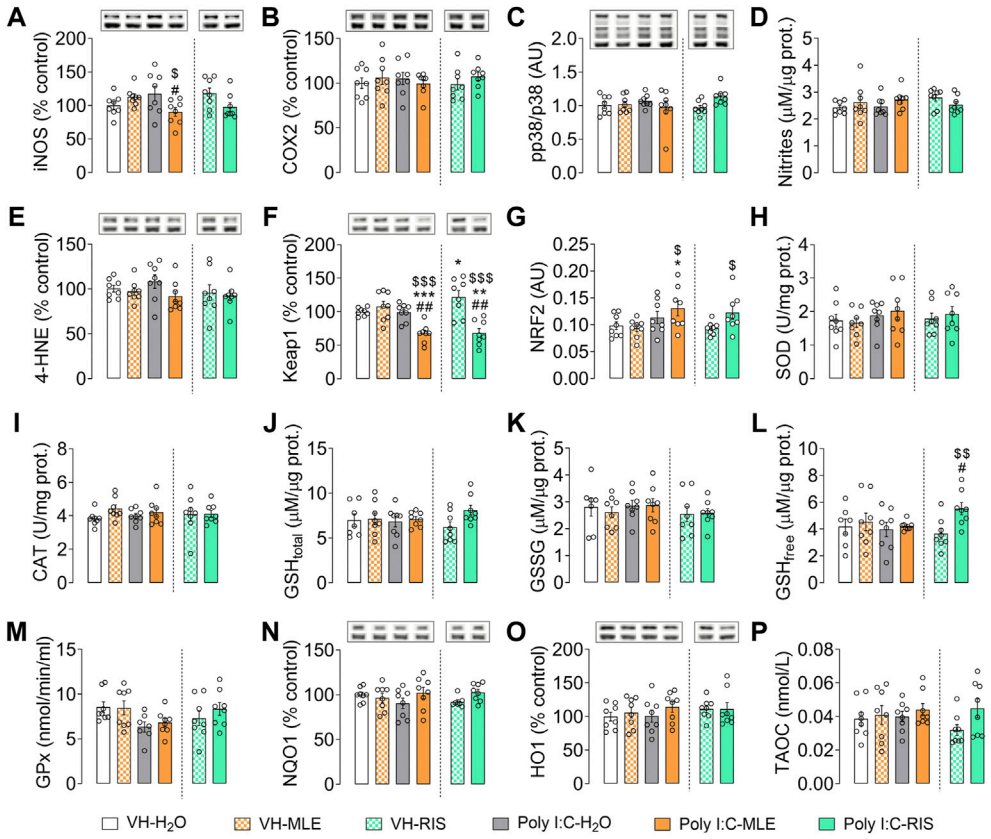

FIGURE 5
The effect of adolescent MLE or risperidone (RIS) treatment on the expression of oxidative/inflammatory mediators in the hippocampus. **(A–C)** The expression of the inflammatory mediators iNOS, COX2 and p38 represented as the percentage (%) of the control expression, with the exception of p38 which is represented as the ratio of phosphorylated relative to total p38 protein. **(D,E)** Indicators of oxidative/nitrosative damage (nitrites and 4-HNE) are expressed as their concentration (µM/µg of protein) and the % of the control expression, respectively. **(F–P)** The evaluation of biomarkers of compensatory antioxidant mechanisms (Keap1, NRF2, SOD, CAT, GSH/GSSG, GPx, NQO1, HO1, TAOC). Keap1, NQO1 and HO1 expression is represented as the % of the control expression; NRF2 activity is expressed in arbitrary units (AU); SOD and CAT enzyme activities are expressed as U/mg of protein; the levels of total (GSH_{total}), oxidized (GSSG) and reduced (GSH_{free}) glutathione are expressed as µM/µg of protein; Glutathione Peroxidase (GPx) is expressed in nmol/min/ml; and the Total Antioxidant Capacity (TAOC) is expressed in nmol/L. The data are represented as the mean ± SEM of 7-8 hippocampal samples per group. Representative bands of iNOS, COX2, 4-HNE, Keap1, NQO1 and HO1 (upper bands) and the β-actin loading control (lower bands) are shown above their corresponding bars in the graph. For p38 protein expression, phosphorylated and total p38 representative bands are shown relative to β-actin (lower bands). $^{*}p < 0.05$, $^{**}p < 0.01$, $^{***}p < 0.01$ vs. VH-H_2O; $^{\$}p < 0.05$, $^{\$\$}p < 0.01$, $^{\$\$\$}p < 0.001$ vs. VH-MLE or VH-RIS; $^{\#}p < 0.05$, $^{\#\#}p < 0.01$ vs. Poly I:C-H_2O as assessed by two-way ANOVA followed by the LSD post-hoc test.

behavioral deficits particularly when administered in adolescence. In addition, MRI images and oxidative/inflammatory and antioxidant biomarkers were evaluated after adolescent treatment, with MLE partially counteracting the morphometric brain alterations detected in the SZ model (cortical shrinkage, and cerebellar and ventricles enlargement), and dampening the inflammatory iNOS pathway while enhancing antioxidative mechanisms. This effect was achieved with a MLE characterized by a strong antioxidant and anti-inflammatory activity, in conjunction with a higher content of mangiferin and other polyphenolic compounds, as seen previously (Liu et al., 2021). Moreover, the extraction method was environmentally friendly as it was based on high pressure extraction techniques that allow us to more efficiently recover more phenolic compounds from mango leaves with stronger antioxidant activity than conventional methods (Guamán-Balcázar et al., 2017).

According to previous studies, adult offspring from Poly I:C immune activated dams exhibit a sensorimotor gating deficit, reduced PPI, representing a core symptom of this animal model of SZ (Hadar et al., 2015; Casquero-Veiga et al., 2021). Cognitive impairment has also been observed in learning and memory phases of the NOR test, along with exacerbated amphetamine-induced activity (Zuckerman et al., 2003; Ozawa et al., 2006).

Enhanced grooming behavior was also seen in Poly I:C offspring as a repetitive behavior related to maternal immune activation models (Amodeo et al., 2019).

To evaluate the effectiveness of MLE in reversing the alterations to Poly I:C offspring, two different treatment approaches were assessed, the therapeutic treatment in young adults and a preventive strategy during peri-adolescence, considering a prodromal and a critical therapeutic window for this neuropsychiatric disorder (rev. in Meyer et al., 2011; Piontkewitz et al., 2011b; Sommer and Arango, 2017). MLE administration to young adults produced a robust effect in the PPI test, reversing the sensorimotor gating deficit characteristic of this model of SZ. This effect of MLE on PPI was similar to that reported after treatment with an antipsychotic drug, e.g., clozapine (Ribeiro et al., 2013). However, MLE did not affect amphetamine-induced activity, recognition memory or grooming behavior. Previous studies suggest that this symptomatology might already be established by the time the animals received this adult MLE treatment (Ribeiro et al., 2013; Mattei et al., 2017; Talukdar et al., 2020). Chronic mangiferin treatment at the same dose as that used here improved the grooming and stereotyped abnormalities produced by an acute model of SZ induced by ketamine administration, as well as restoring IL-6 levels and lipid peroxidation (Rao et al., 2012). On the other hand, peri-adolescent MLE treatment prevented the emergence of the adult sensorimotor gating deficit and interestingly, the magnitude of this effect was similar to that of preventive treatment with risperidone or other antipsychotic drugs, or even that of anti-inflammatory/antioxidant compounds like polyunsaturated fatty acids (Meyer et al., 2010; Piontkewitz et al., 2011a; Casquero-Veiga et al., 2019; Casquero-Veiga et al., 2021; Romero-Miguel et al., 2021). MLE administration during adolescence also reverses the increased grooming behavior exhibited in Poly I:C offspring. Nevertheless, MLE failed to modify the development of sensitivity to amphetamines and the cognitive alterations seen in Poly I:C model. Therefore, although MLE prevent the hallmark PPI deficit in this model of SZ, unfortunately not all behavioral abnormalities could be halted by MLE administration in adulthood or adolescence.

Regarding the morphometric brain changes in the Poly I:C model, significant cortical shrinkage (frontal and retrosplenial) and ventricle enlargement was observed in this study, consistent with the brain alterations described previously in this model and in patients with SZ (Mitelman et al., 2005; Piontkewitz et al., 2009; Haijma et al., 2013; Casquero-Veiga et al., 2019). In addition, an augmentation on cerebellar areas was also seen in the offspring of Poly I:C dams. Morphometric changes in the cerebellum are not consistently reported in the literature, and while most previous studies have described a shrinkage, some reports have shown an enlargement of this brain area in SZ (Shenton et al., 2001; Lee et al., 2007; Moberget et al., 2018). Moreover, a reduction in WM fibers was observed, including a reduced volume of the anterior commissure/medial forebrain bundle and inferior cerebellar peduncle, along with an increased volume of the rubrospinal tract. Most of these WM alterations are consistent with WM deficits described in patients with SZ (Kubicki et al., 2007; Koch et al., 2010). Preventive MLE therapy during adolescence partially counteracts the morphometric changes observed in the offspring of Poly I:C dams. Thus, MLE increased the volume of the frontal cortex, in addition to reducing the ventricular and retrosplenial area volume. Bearing in mind the effect of risperidone detected by MRI previously (Piontkewitz et al., 2011a; Casquero-Veiga et al., 2019), the ROI analysis indicates that risperidone appears to reverse most brain structural alterations described in this model of SZ. A similar effect to the MRI changes to those achieved by this antipsychotic drug was observed after MLE treatment. The reversion of the PPI deficit found with MLE in Poly I:C offspring suggests that the brain structures involved in PPI processing might be preserved by MLE treatment during adolescence as occurred in the frontal cortex. Thus, although the corticostriatal-pallido-pontine circuit is the main neuroanatomic substrate underlying PPI processing, there is evidence that the PFC plays an important role in its modulation (Swerdlow et al., 2001; Tapias-Espinosa et al., 2019). Indeed, alterations to PFC integrity, activity and volume have been related to a PPI deficit (Koch and Bubser, 1994; Japha and Koch, 1999; Schneider and Koch, 2005; Uehara et al., 2007; Tapias-Espinosa et al., 2019) and conversely, the sensorimotor gating deficit observed in neurodevelopmental models of SZ has been related to abnormalities in the PFC (Day-Wilson et al., 2006; Wischhof et al., 2015; Toriumi et al., 2016). Moreover, frontal cortex preservation by adolescent MLE treatment could be involved in reducing grooming behavior that has been associated with alterations in corticostriatal connectivity (Kalueff et al., 2016; Wu et al., 2019). On the other hand, limited action of MLE on NOR test might be related with the inability to produce a beneficial effect on the hippocampus and the perirhinal cortex (Squire et al., 2007).

The offspring of Poly I:C dams showed an inflammatory process mediated by iNOS in the PFC accompanied by an increased in Keap1 levels as oxidative biomarker. The activation of these inflammatory and oxidative pathways has been described previously in this animal model of SZ (Casquero-Veiga et al., 2019; Romero-Miguel et al., 2021). However, no alterations were observed in other oxidative and antioxidant biomarkers in the adult Poly I:C offspring, at least at this point of the clinical course. MLE treatment during adolescence exerted an anti-inflammatory effect through the dampening of the iNOS pathway in both the PFC and hippocampus, similar to the effects of the antipsychotic risperidone, and those of other anti-inflammatory agents like polyunsaturated fatty acids (Casquero-Veiga et al., 2019; Casquero-Veiga et al., 2021). Indeed, the anti-inflammatory effects of mangiferin were previously proposed to be driven by reducing iNOS and COX2 expression (Bhatia et al., 2008;

Márquez et al., 2012). Furthermore, adolescent MLE treatment promoted the expression of biomarkers of compensatory antioxidant mechanisms in the PFC and hippocampus of Poly I:C animals. Thus, a reduction in cytosolic Keap1 and GSSG was seen in Poly I:C offspring treated with MLE, accompanied by enhanced expression of nuclear NRF2 and HO1. These results indicate that the antioxidant effect of MLE was mediated by the NRF2-ARE pathway, contributing to NRF2 translocation to the nucleus, and the ensuing expression of the antioxidant enzyme HO1 (van Muiswinkel and Kuiperij, 2005). It has been widely demonstrated that mangiferin enhances the expression of NRF2 and its nuclear translocation exerts a neuroprotective role against inflammatory and oxidative stress via NRF2-ARE signaling (rev. in Du et al., 2018; Liu et al., 2021). Thus, MLE could improve the inflammatory imbalance evident in this model of SZ and promote antioxidant effects. Risperidone treatment also reduced Keap1 expression in the PFC and hippocampus, albeit with weaker antioxidant activity *via* the NRF2-ARE pathway. However, risperidone also had an effect on the antioxidant capacity enhancing the TAOC in the PFC. Note that the changes in oxidative, inflammatory and antioxidant biomarkers observed in this study may be the final or last mediators of these pathways, suggesting that the inflammatory mechanisms and oxidative damage occurred early in the time course of this model of SZ, and that MLE partially resolved these events.

Although the mechanisms involved in the beneficial effect of MLE must be further elucidated, as has been argued above, the reversal of the PPI deficit could be mainly due to the recovery of frontal cortex volume in conjunction with the inflammatory and antioxidative mechanisms that enhance in this brain area in the Poly I:C offspring. Furthermore, there is evidence of a correlation between the neuroprotective role of mangiferin, and the promotion of anti-inflammatory and antioxidant events, mainly in cortical brain areas (Márquez et al., 2012; Jangra et al., 2014; Infante-Garcia et al., 2017a; rev. in Liu et al., 2021). Therefore, the frontal cortex could represent the target area where the anti-inflammatory and antioxidant effect of MLE might act and produce its benefits.

This study is subject to some limitations including that we have only evaluated the effects of MLE in male offspring. This is mainly due to the fact that the female response to Poly I:C prenatal insult is lower and more variable than those of male animals (Haida et al., 2019). However, further studies with females must be performed to shed light on possible sex differences in the beneficial effect of MLE. Additionally, to avoid extra maternal stress by collecting blood samples for inflammatory mediators' evaluation, the maternal immune activation was evaluated through the reduction in body weight of pregnant mothers after the inflammatory insult, which is an indirect measurement previously associated to Poly I:C-induced immune activation (Piontkewitz et al., 2011b; Howland et al., 2012; Missault et al., 2014; Lins et al., 2018). However, it would also be interesting to evaluate the immune response induced by Poly I:C in dams by measuring cytokines levels. Moreover, the peri-adolescent MLE treatment (PND 35-49) exhibited a limited efficacy. This limitation could come from the MLE per se. Despite the analysis of some aspects of the antioxidant and anti-inflammatory activity of MLE, it is a natural and heterogeneous extract which mixture could not be fully characterized. Nonetheless, better results could be achieved through sustained MLE treatment from adolescence until adulthood in this model of SZ. In this sense, it would be interesting to study if longer treatment could increase MLE efficacy and, considering the results found in NRF2, to discern if adolescent MLE treatment acts during this critical period by increasing anti-inflammatory/antioxidant mechanisms or perhaps by promoting neuronal plasticity and synaptogenesis.

In summary, the results presented here indicate that MLE administration in adulthood could reverse the sensorimotor gating deficit that is a hallmark of SZ, whereas its administration during adolescence completely prevents this deficit, while improving grooming behavior. The behavioral improvement produced by adolescent MLE treatment was accompanied by an improvement to both morphological brain alterations, and to the inflammatory and redox imbalance in this maternal immune activation model. Hence, this study demonstrates the efficacy of MLE therapy, not only in adults but also during adolescence, when it seems to be able to disrupt the pathological progression of the SZ-related phenotype induced by a prenatal Poly I:C insult. Consequently, these results suggest that peri-adolescence represents a critical neurodevelopment window where early pharmacological interventions with anti-inflammatory/antioxidant compounds may be relevant in the course of this psychiatric disease.

Data availability statement

The raw data supporting the conclusion of this article will be made available by the authors, without undue reservation.

Ethics statement

The animal study was reviewed and approved by Ethics Committee for Animal Experimentation at the School of Medicine of the University of Cadiz.

Author contributions

JAG-P: Acquisition and analysis of behavioral studies and writing-original draft; ST-S: Supervision of the study, experimental design, analysis of behavioral studies and oxidative/inflammatory and antioxidant parameters and

writing-original draft; KM: Acquisition and analysis of oxidative/inflammatory and antioxidant parameters; MS-M: Acquisition and analysis of imaging studies; DR-M and NL-R: Analysis of imaging studies; MF-P, LC and CM: mango leaf extraction and characterization; EB: Conception and supervision of the study, experimental design. Authors EB, MD and JL revised and edited the article. All authors provided the conceptual advice, commented on the manuscript, and approved the final version of the manuscript for submission.

Funding

EB, JAG-P and ST-S work was supported by the "Fondo Europeo de Desarrollo Regional" (FEDER)-UE "A way to build Europe" from the "Ministerio de Economía y Competitividad" (RTI2018-099778-B-I00); from the "Plan Nacional sobre Drogas, Ministerio de Sanidad, Consumo y Bienestar Social" (2019I041); from the "Ministerio de Salud-Instituto de Salud Carlos III" (PI18/01691); from the "Programa Operativo de Andalucía FEDER, Iniciativa Territorial Integrada ITI 2014-2020 Consejería Salud y Familias, Junta de Andalucía" (PI-0080-2017, PI-0009-2017), "Consejería de Salud y Familias, Junta de Andalucía" (PI-0134-2018 and PEMP-0008-2020); from the "Consejería de Transformación Económica, Industria, Conocimiento y Universidad, Junta de Andalucía" (P20_00958 and CTS-510); from the CEIMAR (CEIJ-003); from the "Instituto de Investigación e Innovación en Ciencias Biomédicas de Cádiz-INiBICA" (LI19/06IN-CO22; IN-C09); from the "CIBERSAM": CIBER-Consorcio Centro de Investigación Biomédica en Red- (CB07/09/0033), Instituto de Salud Carlos III, Ministerio de Ciencia e Innovación and from the European Union's Horizon 2020 research and innovation programme under the Marie Sklodowska-Curie grant agreement No 955684. CM, LC and MTF-P were supported by the Spanish Ministry of Science and Technology (PID2020-116229RB-I00) and European Regional Development Fund (ERDF). KM and JCL were supported by the "MICINN" (PID2019-109033RB-I00) and the "CIBERSAM": CIBER-Consorcio Centro de Investigación Biomédica en Red- (CB07/09/0026), Instituto de Salud Carlos III, Ministerio de Ciencia e Innovación. MLS-M was supported by the "Ministerio de Ciencia, Innovación, Instituto de Salud Carlos III" (PI17/01766, BA21/00030), co-financed by European Regional Development Fund (ERDF), "A way to make Europe"; from the "CIBERSAM": CIBERConsorcio Centro de Investigación Biomédica en Red- (CB07/09/0031), Instituto de Salud Carlos III, Ministerio de Ciencia e Innovación; from the "Delegación del Gobierno para el Plan Nacional sobre Drogas" (2017/085); from the "Fundación Mapfre" and "Fundación Alicia Koplowitz." MD work was supported by the "Ministerio de Ciencia e In review 18/28 Innovación" (MCIN) and "Instituto de Salud Carlos III" (ISCIII) (PT20/00044); from the "CIBERSAM" CIBER-Consorcio Centro de Investigación Biomédica en Red-(CB07/09/0031). The CNIC is supported by the ISCIII, the MCIN and the Pro CNIC Foundation, and is a Severo Ochoa Center of Excellence (SEV-2015-0505).

Acknowledgments

We are very grateful to Ms Elena Marín Álvarez and Beatriz Moreno for their excellent technical assistance. The Central Services of Scientific and Technological Research, Health Sciences and Animal Research from the University of Cádiz.

Conflict of interest

The authors declare that the research was conducted in the absence of any commercial or financial relationships that could be construed as a potential conflict of interest.

Publisher's note

Supplementary material

The Supplementary Material for this article can be found online at: https://www.frontiersin.org/articles/10.3389/fphar.2022.886514/full#supplementary-material

References

Amodeo, D. A., Lai, C. Y., Hassan, O., Mukamel, E. A., Behrens, M. M., and Powell, S. B. (2019). Maternal immune activation impairs cognitive flexibility and alters transcription in frontal cortex. *Neurobiol. Dis.* 125, 211–218. doi:10.1016/j.nbd.2019.01.025

Arango, C., Dragioti, E., Solmi, M., Cortese, S., Domschke, K., Murray, R. M., et al. (2021). Risk and protective factors for mental disorders beyond genetics: an evidence-based atlas. *World Psychiatry.* 20, 417–436. doi:10.1002/wps.20894

Avants, B., and Gee, J. C. (2004). Geodesic estimation for large deformation anatomical shape averaging and interpolation. *NeuroImage* 23 (Suppl. 1), S139–S150. doi:10.1016/j.neuroimage.2004.07.010

Berk, M., Copolov, D., Dean, O., Lu, K., Jeavons, S., Schapkaitz, I., et al. (2008). N-acetyl cysteine as a glutathione precursor for schizophrenia-A double-blind, randomized, placebo-controlled trial. *Biol. Psychiatry* 64, 361–368. doi:10.1016/j.biopsych.2008.03.004

Bhatia, H. S., Candelario-Jalil, E., de Oliveira, A. C. P., Olajide, O. A., Martínez-Sánchez, G., and Fiebich, B. L. (2008). Mangiferin inhibits cyclooxygenase-2 expression and prostaglandin E2 production in activated rat microglial cells. *Arch. Biochem. Biophys.* 477, 253–258. doi:10.1016/j.abb.2008.06.017

Brand-Williams, W., Cuvelier, M. E., and Berset, C. (1995). Use of a free radical method to evaluate antioxidant activity. *LWT - Food Sci. Technol.* 28, 25–30. doi:10.1016/S0023-6438(95)80008-5

Brown, A. S., and Derkits, E. J. (2010). Prenatal infection and schizophrenia: a review of epidemiologic and translational studies. *Am. J. Psychiatry* 167, 261–280. doi:10.1176/appi.ajp.2009.09030361

Casas-Cardoso, L., Mantell, C., Obregón, S., Cejudo-Bastante, C., Alonso-Moraga, Á., de la Ossa, E. J. M., et al. (2021). Health-promoting properties of borage seed oil fractionated by supercritical carbon dioxide extraction. *Foods* 10, 2471. doi:10.3390/foods10102471

Casquero-Veiga, M., García-García, D., MacDowell, K. S., Pérez-Caballero, L., Torres-Sánchez, S., Fraguas, D., et al. (2019). Risperidone administered during adolescence induced metabolic, anatomical and inflammatory/oxidative changes in adult brain: A PET and MRI study in the maternal immune stimulation animal model. *Eur. Neuropsychopharmacol.* 29, 880–896. doi:10.1016/j.euroneuro.2019.05.002

Casquero-Veiga, M., Romero-Miguel, D., MacDowell, K. S., Torres-Sanchez, S., Garcia-Partida, J. A., Lamanna-Rama, N., et al. (2021). Omega-3 fatty acids during adolescence prevent schizophrenia-related behavioural deficits: Neurophysiological evidences from the prenatal viral infection with PolyI:C. *Eur. Neuropsychopharmacol.* 46, 14–27. doi:10.1016/j.euroneuro.2021.02.001

Charlson, F. J., Ferrari, A. J., Santomauro, D. F., Diminic, S., Stockings, E., Scott, J. G., et al. (2018). Global epidemiology and burden of schizophrenia: findings from the global burden of disease study 2016. *Schizophr. Bull.* 44, 1195–1203. doi:10.1093/schbul/sby058

Chong, H. Y., Teoh, S. L., Wu, D. B. C., Kotirum, S., Chiou, C. F., and Chaiyakunapruk, N. (2016). Global economic burden of schizophrenia: a systematic review. *Neuropsychiatr. Dis. Treat.* 12, 357–373. doi:10.2147/NDT.S96649

Dakhale, G. N., Khanzode, S. D., Khanzode, S. S., and Saoji, A. (2005). Supplementation of vitamin C with atypical antipsychotics reduces oxidative stress and improves the outcome of schizophrenia. *Psychopharmacol. Berl.* 182, 494–498. doi:10.1007/s00213-005-0117-1

Day-Wilson, K. M., Jones, D. N. C., Southam, E., Cilia, J., and Totterdell, S. (2006). Medial prefrontal cortex volume loss in rats with isolation rearing-induced deficits in prepulse inhibition of acoustic startle. *Neuroscience* 141, 1113–1121. doi:10.1016/j.neuroscience.2006.04.048

Du, S., Liu, H., Lei, T., Xie, X., Wang, H., He, X., et al. (2018). Mangiferin: an effective therapeutic agent against several disorders (review). *Mol. Med. Rep.* 18, 4775–4786. doi:10.3892/mmr.2018.9529

Fernández-Ponce, M. T., Casas, L., Mantell, C., and De La Ossa, E. M. (2015). Use of high pressure techniques to produce Mangifera indica L. leaf extracts enriched in potent antioxidant phenolic compounds. *Innov. Food Sci. Emerg. Technol.* 29, 94–106. doi:10.1016/j.ifset.2015.04.006

Gasull-Camós, J., Soto-Montenegro, M. L., Casquero-Veiga, M., Desco, M., Artigas, F., and Castane, A. (2017). Differential patterns of subcortical activity evoked by glial GLT-1 blockade in prelimbic and infralimbic cortex: relationship to antidepressant-like effects in rats. *Int. J. Neuropsychopharmacol.* 20, 988–993. doi:10.1093/ijnp/pyx067

GBD 2019 Diseases and Injuries Collaborators (2020). Global burden of 369 diseases and injuries in 204 countries and territories, 1990-2019: A systematic analysis for the Global Burden of Disease Study 2019. *Lancet* 396 (10528), 1204–1222. doi:10.1016/S0140-6736(20)30925-9

GBD 2019 Mental Disorders Collaborators (2022). Global, regional, and national burden of 12 mental disorders in 204 countries and territories, 1990–2019: a systematic analysis for the global burden of disease study 2019. *Lancet Psychiatry* 9, 137–150. doi:10.1016/s2215-0366(21)00395-3

Gilmore, J. H., and Jarskog, L. F. (1997). Exposure to infection and brain development: Cytokines in the pathogenesis of schizophrenia. *Schizophr. Res.* 24, 365–367. doi:10.1016/s0920-9964(96)00123-5

Green, L. C., Wagner, D. A., Glogowski, J., Skipper, P. L., Wishnok, J. S., and Tannenbaum, S. R. (1982). Analysis of nitrate, nitrite, and [15N]nitrate in biological fluids. *Anal. Biochem.* 126 (1), 131–138. doi:10.1016/0003-2697(82)90118-X

Guamán-Balcázar, M. C., Montes, A., Pereyra, C., and de la Ossa, E. M. (2017). Precipitation of mango leaves antioxidants by supercritical antisolvent process. *J. Supercrit. Fluids* 128, 218–226. doi:10.1016/j.supflu.2017.05.031

Hadar, R., Soto-Montenegro, M. L., Götz, T., Wieske, F., Sohr, R., Desco, M., et al. (2015). Using a maternal immune stimulation model of schizophrenia to study behavioral and neurobiological alterations over the developmental course. *Schizophr. Res.* 166, 238–247. doi:10.1016/j.schres.2015.05.010

Haida, O., Al Sagheer, T., Balbous, A., Francheteau, M., Matas, E., Soria, F., et al. (2019). Sex-dependent behavioral deficits and neuropathology in a maternal immune activation model of autism. *Transl. Psychiatry* 9, 124. doi:10.1038/s41398-019-0457-y

Haijma, S. V., Van Haren, N., Cahn, W., Koolschijn, P. C. M. P., Hulshoff Pol, H. E., and Kahn, R. S. (2013). Brain volumes in schizophrenia: a meta-analysis in over 18 000 subjects. *Schizophr. Bull.* 39, 1129–1138. doi:10.1093/schbul/sbs118

Hjorthøj, C., Stürup, A. E., McGrath, J. J., and Nordentoft, M. (2017). Years of potential life lost and life expectancy in schizophrenia: a systematic review and meta-analysis. *Lancet Psychiatry* 4, 295–301. doi:10.1016/S2215-0366(17)30078-0

Howland, J. G., Cazakoff, B. N., and Zhang, Y. (2012). Altered object-in-place recognition memory, prepulse inhibition, and locomotor activity in the offspring of rats exposed to a viral mimetic during pregnancy. *Neuroscience* 201, 184–198. doi:10.1016/j.neuroscience.2011.11.011

Infante-Garcia, C., Jose Ramos-Rodriguez, J., Marin-Zambrana, Y., Teresa Fernandez-Ponce, M., Casas, L., Mantell, C., et al. (2017a). Mango leaf extract improves central pathology and cognitive impairment in a type 2 diabetes mouse model. *Brain Pathol.* 27, 499–507. doi:10.1111/bpa.12433

Infante-Garcia, C., Ramos-Rodriguez, J. J., Delgado-Olmos, I., Gamero-Carrasco, C., Fernandez-Ponce, M. T., Casas, L., et al. (2017b). Long-term mangiferin extract treatment improves central pathology and cognitive deficits in APP/PS1 mice. *Mol. Neurobiol.* 54, 4696–4704. doi:10.1007/s12035-016-0015-z

Jangra, A., Lukhi, M. M., Sulakhiya, K., Baruah, C. C., and Lahkar, M. (2014). Protective effect of mangiferin against lipopolysaccharide-induced depressive and anxiety-like behaviour in mice. *Eur. J. Pharmacol.* 740, 337–345. doi:10.1016/j.ejphar.2014.07.031

Japha, K., and Koch, M. (1999). Picrotoxin in the medial prefrontal cortex impairs sensorimotor gating in rats: reversal by haloperidol. *Psychopharmacol. Berl.* 144, 347–354. doi:10.1007/s002130051017

Kalueff, A. V., Stewart, A. M., Song, C., Berridge, K. C., Graybiel, A. M., and Fentress, J. C. (2016). Neurobiology of rodent self-grooming and its value for translational neuroscience. *Nat. Rev. Neurosci.* 17, 45–59. doi:10.1038/nrn.2015.8

Koch, K., Wagner, G., Dahnke, R., Schachtzabel, C., Schultz, C., Roebel, M., et al. (2010). Disrupted white matter integrity of corticopontine-cerebellar circuitry in schizophrenia. *Eur. Arch. Psychiatry Clin. Neurosci.* 260, 419–426. doi:10.1007/s00406-009-0087-0

Koch, M., and Bubser, M. (1994). Deficient sensorimotor gating after 6-hydroxydopamine lesion of the rat medial prefrontal cortex is reversed by haloperidol. *Eur. J. Neurosci.* 6, 1837–1845. doi:10.1111/j.1460-9568.1994.tb00576.x

Kubicki, M., McCarley, R., Westin, C. F., Park, H. J., Maier, S., Kikinis, R., et al. (2007). A review of diffusion tensor imaging studies in schizophrenia. *J. Psychiatr. Res.* 41, 15–30. doi:10.1016/j.jpsychires.2005.05.005

Lee, K. H., Farrow, T. F. D., Parks, R. W., Newton, L. D., Mir, N. U., Egleston, P. N., et al. (2007). Increased cerebellar vermis white-matter volume in men with schizophrenia. *J. Psychiatr. Res.* 41, 645–651. doi:10.1016/j.jpsychires.2006.03.001

Leza, J. C., Bueno, B., Bioque, M., Arango, C., Parellada, M., Do, K., et al. (2015). Inflammation in schizophrenia: a question of balance. *Neurosci. Biobehav. Rev.* 55, 612–626. doi:10.1016/j.neubiorev.2015.05.014

Lins, B. R., Hurtubise, J. L., Roebuck, A. J., Marks, W. N., Zabder, N. K., Scott, G. A., et al. (2018). Prospective analysis of the effects of maternal immune activation on rat cytokines during pregnancy and behavior of the male offspring relevant to Schizophrenia. *eNeuro* 5, ENEURO.0249–18.2018. doi:10.1523/ENEURO.0249-18.2018

Liu, T., Song, Y., and Hu, A. (2021). Neuroprotective mechanisms of mangiferin in neurodegenerative diseases. *Drug Dev. Res.* 82, 494–502. doi:10.1002/ddr.21783

Llorca-Torralba, M., Suárez-Pereira, I., Bravo, L., Camarena-Delgado, C., Garcia-Partida, J. A., Mico, J. A., et al. (2019). Chemogenetic silencing of the locus coeruleus–basolateral amygdala pathway abolishes pain-induced anxiety and enhanced aversive learning in rats. *Biol. Psychiatry* 85, 1021–1035. doi:10.1016/j.biopsych.2019.02.018

MacDowell, K. S., Caso, J. R., Martín-Hernández, D., Moreno, B. M., Madrigal, J. L. M., Mico, J. A., et al. (2016). The atypical antipsychotic paliperidone regulates endogenous antioxidant/anti-inflammatory pathways in rat models of acute and chronic restraint stress. *Neurotherapeutics* 13, 833–843. doi:10.1007/s13311-016-0438-2

MacDowell, K. S., García-Bueno, B., Madrigal, J. L. M., Parellada, M., Arango, C., Mico, J. A., et al. (2013). Risperidone normalizes increased inflammatory parameters and restores anti-inflammatory pathways in a model of neuroinflammation. *Int. J. Neuropsychopharmacol.* 16, 121–135. doi:10.1017/S1461145711001775

Márquez, L., García-Bueno, B., Madrigal, J. L. M., and Leza, J. C. (2012). Mangiferin decreases inflammation and oxidative damage in rat brain after stress. *Eur. J. Nutr.* 51, 729–739. doi:10.1007/s00394-011-0252-x

Marshall, M., and Rathbone, J. (2011). Early intervention for psychosis. *Cochrane Database Syst. Rev.* (6), CD004718. doi:10.1002/14651858.CD004718

Mattei, D., Ivanov, A., Ferrai, C., Jordan, P., Guneykaya, D., Buonfiglioli, A., et al. (2017). Maternal immune activation results in complex microglial transcriptome signature in the adult offspring that is reversed by minocycline treatment. *Transl. Psychiatry* 7, e1120. doi:10.1038/tp.2017.80

McCutcheon, R. A., Abi-Dargham, A., and Howes, O. D. (2019). Schizophrenia, dopamine and the striatum: from Biology to symptoms. *Trends Neurosci.* 42, 205–220. doi:10.1016/j.tins.2018.12.004

Meyer, U., and Feldon, J. (2012). To poly(I:C) or not to poly(I:C): Advancing preclinical schizophrenia research through the use of prenatal immune activation models. *Neuropharmacology* 62, 1308–1321. doi:10.1016/j.neuropharm.2011.01.009

Meyer, U., Spoerri, E., Yee, B. K., Schwarz, M. J., and Feldon, J. (2010). Evaluating early preventive antipsychotic and antidepressant drug treatment in an infection-based neurodevelopmental mouse model of schizophrenia. *Schizophr. Bull.* 36, 607–623. doi:10.1093/schbul/sbn131

Meyer, U., Weiner, I., McAlonan, G. M., and Feldon, J. (2011). The neuropathological contribution of prenatal inflammation to schizophrenia. *Expert Rev. Neurother.* 11, 29–32. doi:10.1586/ern.10.169

Millan, M. J., Andrieux, A., Bartzokis, G., Cadenhead, K., Dazzan, P., Fusar-Poli, P., et al. (2016). Altering the course of schizophrenia: Progress and perspectives. *Nat. Rev. Drug Discov.* 15, 485–515. doi:10.1038/nrd.2016.28

Missault, S., Van den Eynde, K., Vanden Berghe, W., Fransen, E., Weeren, A., Timmermans, J. P., et al. (2014). The risk for behavioural deficits is determined by the maternal immune response to prenatal immune challenge in a neurodevelopmental model. *Brain Behav. Immun.* 42, 138–146. doi:10.1016/j.bbi.2014.06.013

Mitelman, S. A., Shihabuddin, L., Brickman, A. M., Hazlett, E. A., and Buchsbaum, M. S. (2005). Volume of the cingulate and outcome in schizophrenia. *Schizophr. Res.* 72, 91–108. doi:10.1016/j.schres.2004.02.011

Moberget, T., Doan, N. T., Alnæs, D., Kaufmann, T., Córdova-Palomera, A., CordovA-PAlomerA, A., et al. (2018). Cerebellar volume and cerebellocerebral structural covariance in schizophrenia: a multisite mega-analysis of 983 patients and 1349 healthy controls. *Mol. Psychiatry* 23, 1512–1520. doi:10.1038/mp.2017.106

Müller, N. (2018). Inflammation in schizophrenia: pathogenetic aspects and therapeutic considerations. *Schizophr. Bull.* 44, 973–982. doi:10.1093/schbul/sby024

Owen, M. J., Sawa, A., and Mortensen, P. B. (2016). Schizophrenia. *Lancet. Author Manuscr.* 388, 86–97. doi:10.1016/S0140-6736(15)01121-6

Ozawa, K., Hashimoto, K., Kishimoto, T., Shimizu, E., Ishikura, H., and Iyo, M. (2006). Immune activation during pregnancy in mice leads to dopaminergic hyperfunction and cognitive impairment in the offspring: A neurodevelopmental animal model of schizophrenia. *Biol. Psychiatry* 59, 546–554. doi:10.1016/j.biopsych.2005.07.031

Paxinos, G., and Watson, C. (2006). *The rat brain in stereotaxic coordinates.* Netherlands: Elsevier. doi:10.1016/c2009-0-63235-9

Piontkewitz, Y., Arad, M., and Weiner, I. (2011a). Abnormal trajectories of neurodevelopment and behavior following *in utero* insult in the rat. *Biol. Psychiatry* 70, 842–851. doi:10.1016/j.biopsych.2011.06.007

Piontkewitz, Y., Arad, M., and Weiner, I. (2011b). Risperidone administered during asymptomatic period of adolescence prevents the emergence of brain structural pathology and behavioral abnormalities in an animal model of schizophrenia. *Schizophr. Bull.* 37, 1257–1269. doi:10.1093/schbul/sbq040

Piontkewitz, Y., Assaf, Y., and Weiner, I. (2009). Clozapine administration in adolescence prevents postpubertal emergence of brain structural pathology in an animal model of schizophrenia. *Biol. Psychiatry* 66, 1038–1046. doi:10.1016/j.biopsych.2009.07.005

Rahman, H., Eswaraiah, M. C., and Dutta, A. M. (2015). *In-vitro* anti-inflammatory and anti-arthritic activity of oryza sativa var. Joha rice (an aromatic indigenous rice of Assam) Anurag pharmacy college, kodad, telengana state, India. *Am. J. Agric. Environ. Sci.* 15, 115–121. doi:10.5829/idosi.aejaes.2015.115.121

Rao, V. S., Carvalho, A. C., Trevisan, M. T. S., Andrade, G. M., Nobre, H. V., Moraes, M. O., et al. (2012). Mangiferin ameliorates 6-hydroxydopamine induced cytotoxicity and oxidative stress in ketamine model of schizophrenia. *Pharmacol. Rep.* 64, 848–856. doi:10.1016/S1734-1140(12)70879-4

Ribeiro, B. M. M., do Carmo, M. R. S., Freire, R. S., Rocha, N. F. M., Borella, V. C. M., de Menezes, A. T., et al. (2013). Evidences for a progressive microglial activation and increase in iNOS expression in rats submitted to a neurodevelopmental model of schizophrenia: reversal by clozapine. *Schizophr. Res.* 151, 12–19. doi:10.1016/j.schres.2013.10.040

Romero-Miguel, D., Casquero-Veiga, M., Macdowell, K. S., Torres-Sanchez, S., Garcia-Partida, J. A., Lamanna-Rama, N., et al. (2021). A characterization of the effects of minocycline treatment during adolescence on structural, metabolic, and oxidative stress parameters in a maternal immune stimulation model of neurodevelopmental brain disorders. *Int. J. Neuropsychopharmacol.* 24, 734–748. doi:10.1093/ijnp/pyab036

Saha, S., Sadhukhan, P., and Sil, P. C. (2016). Mangiferin: a xanthonoid with multipotent anti-inflammatory potential. *BioFactors* 42, 459–474. doi:10.1002/biof.1292

Salehi, B., Berkay Yılmaz, Y., Antika, G., Boyunegmez Tumer, T., Fawzi Mahomoodally, M., Lobine, D., et al. (2019). Insights on the use of α-lipoic acid for therapeutic purposes. *Biomolecules* 9, E356. doi:10.3390/biom9080356

Scherer, R., and Godoy, H. T. (2009). Antioxidant activity index (AAI) by the 2, 2-diphenyl-1-picrylhydrazyl method. *Food Chem.* 112, 654–658. doi:10.1016/j.foodchem.2008.06.026

Schneider, M., and Koch, M. (2005). Behavioral and morphological alterations following neonatal excitotoxic lesions of the medial prefrontal cortex in rats. *Exp. Neurol.* 195, 185–198. doi:10.1016/j.expneurol.2005.04.014

Shenton, M. E., Dickey, C. C., Frumin, M., and McCarley, R. W. (2001). A review of MRI findings in schizophrenia. *Schizophr. Res.* 49, 1–52. doi:10.1016/S0920-9964(01)00163-3

Soares-Weiser, K., Maayan, N., and Bergman, H. (20182018). Vitamin E for antipsychotic-induced tardive dyskinesia. *Cochrane Database Syst. Rev.* 1, CD000209. doi:10.1002/14651858.CD000209.pub3

Sommer, I. E., and Arango, C. (2017). Moving interventions from after to before diagnosis. *World Psychiatry* 16, 275–276. doi:10.1002/wps.20454

Squire, L. R., Wixted, J. T., and Clark, R. E. (2007). Recognition memory and the medial temporal lobe: a new perspective. *Nat. Rev. Neurosci.* 8, 872–883. doi:10.1038/nrn2154

Subotnik, K. L., Casaus, L. R., Ventura, J., Luo, J. S., Hellemann, G. S., Gretchen-Doorly, D., et al. (2015). Long-acting injectable risperidone for relapse prevention and control of breakthrough symptoms after a recent first episode of schizophrenia a randomized clinical trial. *JAMA Psychiatry* 72, 822–829. doi:10.1001/jamapsychiatry.2015.0270

Swerdlow, N. R., Geyer, M. A., and Braff, D. L. (2001). Neural circuit regulation of prepulse inhibition of startle in the rat: Current knowledge and future challenges. *Psychopharmacol. Berl.* 156, 194–215. doi:10.1007/s002130100799

Talukdar, P. M., Abdul, F., Maes, M., Binu, V., Venkatasubramanian, G., Kutty, B. M., et al. (2020). Maternal immune activation causes schizophrenia-like behaviors in the offspring through activation of immune-inflammatory, oxidative and apoptotic pathways, and lowered antioxidant defenses and neuroprotection. *Mol. Neurobiol.* 57, 4345–4361. doi:10.1007/s12035-020-02028-8

Tapias-Espinosa, C., Río-Álamos, C., Sánchez-González, A., Oliveras, I., Sampedro-Viana, D., Castillo-Ruiz, M. D. M., et al. (2019). Schizophrenia-like reduced sensorimotor gating in intact inbred and outbred rats is associated with decreased medial prefrontal cortex activity and volume. *Neuropsychopharmacology* 44, 1975–1984. doi:10.1038/s41386-019-0392-x

Toriumi, K., Oki, M., Muto, E., Tanaka, J., Mouri, A., Mamiya, T., et al. (2016). Prenatal phencyclidine treatment induces behavioral deficits through impairment of GABAergic interneurons in the prefrontal cortex. *Psychopharmacol. Berl.* 233, 2373–2381. doi:10.1007/s00213-016-4288-8

Uehara, T., Sumiyoshi, T., Matsuoka, T., Itoh, H., and Kurachi, M. (2007). Effect of prefrontal cortex inactivation on behavioral and neurochemical abnormalities in rats with excitotoxic lesions of the entorhinal cortex. *Synapse* 61, 391–400. doi:10.1002/syn.20383

Upthegrove, R., and Khandaker, G. M. (2020). Cytokines, oxidative stress and cellular markers of inflammation in schizophrenia. *Curr. Top. Behav. Neurosci.* 44, 49–66. doi:10.1007/7854_2018_88

Valdés-Hernández, P. A., Sumiyoshi, A., Nonaka, H., Haga, R., Aubert-Vásquez, E., Ogawa, T., et al. (2011). An *in vivo* MRI template set for morphometry, tissue segmentation, and fMRI localization in rats. *Front. Neuroinform.* 5, 26. doi:10.3389/fninf.2011.00026

van Muiswinkel, F. L., and Kuiperij, H. B. (2005). The Nrf2-ARE signalling pathway: promising drug target to combat oxidative stress in neurodegenerative disorders. *Curr. Drug Targets. CNS Neurol. Disord.* 4, 267–281. doi:10.2174/1568007054038238

Van Os, J., Kenis, G., and Rutten, B. P. F. (2010). The environment and schizophrenia. *Nature* 468, 203–212. doi:10.1038/nature09563

Wischhof, L., Irrsack, E., Osorio, C., and Koch, M. (2015). Prenatal LPS-exposure - a neurodevelopmental rat model of schizophrenia - differentially affects cognitive functions, myelination and parvalbumin expression in male and female offspring. *Prog. Neuropsychopharmacol. Biol. Psychiatry* 57, 17–30. doi:10.1016/j.pnpbp.2014.10.004

Wu, W. L., Cheng, S. J., Lin, S. H., Chuang, Y. C., Huang, E. Y. K., and Chen, C. C. (2019). The effect of ASIC3 knockout on corticostriatal circuit and mouse self-grooming behavior. *Front. Cell. Neurosci.* 13, 86. doi:10.3389/fncel.2019.00086

Yee, B. K., Keist, R., Von Boehmer, L., Studer, R., Benke, D., HageNbuchN., et al. (2005). A schizophrenia-related sensorimotor deficit links α3-containing GABAA receptors to a dopamine hyperfunction. *Proc. Natl. Acad. Sci. U. S. A.* 102, 17154–17159. doi:10.1073/pnas.0508752102

Zuckerman, L., Rehavi, M., Nachman, R., and Weiner, I. (2003). Immune activation during pregnancy in rats leads to a postpubertal emergence of disrupted latent inhibition, dopaminergic hyperfunction, and altered limbic morphology in the offspring: A novel neurodevelopmental model of schizophrenia. *Neuropsychopharmacology* 28, 1778–1789. doi:10.1038/sj.npp.1300248

Zuckerman, L., and Weiner, I. (2003). Post-pubertal emergence of disrupted latent inhibition following prenatal immune activation. *Psychopharmacol. Berl.* 169, 308–313. doi:10.1007/s00213-003-1461-7

frontiers | Frontiers in Pharmacology

TYPE Original Research
PUBLISHED 26 September 2022
DOI 10.3389/fphar.2022.866574

OPEN ACCESS

EDITED BY
Marta P. Pereira,
Centre for Molecular Biology Severo Ochoa (CSIC), Spain

REVIEWED BY
Colm Cunningham,
Trinity College Dublin, Ireland
Marta Llansola,
Principe Felipe Research Center (CIPF), Spain

*CORRESPONDENCE
Laura Orio,
lorio@psi.ucm.es

SPECIALTY SECTION
This article was submitted to Neuropharmacology, a section of the journal Frontiers in Pharmacology

RECEIVED 31 January 2022
ACCEPTED 29 July 2022
PUBLISHED 26 September 2022

CITATION
Moya M, Escudero B, Gómez-Blázquez E, Rebolledo-Poves AB, López-Gallardo M, Guerrero C, Marco EM and Orio L (2022), Upregulation of TLR4/MyD88 pathway in alcohol-induced Wernicke's encephalopathy: Findings in preclinical models and in a postmortem human case.
Front. Pharmacol. 13:866574.
doi: 10.3389/fphar.2022.866574

Upregulation of TLR4/MyD88 pathway in alcohol-induced Wernicke's encephalopathy: Findings in preclinical models and in a postmortem human case

Marta Moya[1], Berta Escudero[1], Elena Gómez-Blázquez[2], Ana Belen Rebolledo-Poves[2], Meritxell López-Gallardo[3], Carmen Guerrero[2], Eva M. Marco[4] and Laura Orio[1,5]*

[1]Department of Psychobiology and Methods in Behavioral Science, Faculty of Psychology, Complutense University of Madrid, Madrid, Spain, [2]Biobanco of Hospital Universitario Fundación Alcorcón, Alcorcón, Spain, [3]Department of Physiology, Faculty of Medicine, Complutense University of Madrid, Madrid, Spain, [4]Department of Genetics, Physiology and Microbiology, Faculty of Biology, Complutense University of Madrid, Madrid, Spain, [5]Research Network in Primary Care in Addictions (Red de Investigación en Atención Primaria en Adicciones), Riapad, Spain

Wernicke's encephalopathy (WE) is a neurologic disease caused by vitamin B1 or thiamine deficiency (TD), being the alcohol use disorder its main risk factor. WE patients present limiting motor, cognitive, and emotional alterations related to a selective cerebral vulnerability. Neuroinflammation has been proposed to be one of the phenomena that contribute to brain damage. Our previous studies provide evidence for the involvement of the innate immune receptor Toll-like (TLR)4 in the inflammatory response induced in the frontal cortex and cerebellum in TD animal models (animals fed with TD diet [TDD] and receiving pyrithiamine). Nevertheless, the effects of the combination of chronic alcohol consumption and TD on TLR4 and their specific contribution to the pathogenesis of WE are currently unknown. In addition, no studies on TLR4 have been conducted on WE patients since brains from these patients are difficult to achieve. Here, we used rat models of chronic alcohol (CA; 9 months of forced consumption of 20% (w/v) alcohol), TD hit (TDD + daily 0.25 mg/kg i.p. pyrithiamine during 12 days), or combined treatment (CA + TDD) to check the activation of the proinflammatory TLR4/MyD88 pathway and related markers in the frontal cortex and the cerebellum. In addition, we characterized for the first time the TLR4 and its coreceptor MyD88 signature, along with other markers of this proinflammatory signaling such as phospo-NFκB p65 and IκBα, in the postmortem human frontal cortex and cerebellum (gray and white matter) of an alcohol-induced WE patient, comparing it with negative (no disease) and positive (aged brain with Alzheimer's disease) control subjects for neuroinflammation. We found an increase in the cortical TLR4 and its adaptor molecule MyD88, together with an upregulation of the proinflammatory signaling molecules p-NF-κB and IκBα in the CA + TDD animal model. In the patient diagnosed with alcohol-induced

WE, we observed cortical and cerebellar upregulation of the TLR4/MyD88 pathway. Hence, our findings provide evidence, both in the animal model and the human postmortem brain, of the upregulation of the TLR4/MyD88 proinflammatory pathway in alcohol consumption–related WE.

KEYWORDS

Wernicke–Korsakoff syndrome, neuroinflammation, frontal cortex, cerebellum, thiamine deficiency, alcohol use disorder (AUD)

Introduction

Wernicke's encephalopathy (WE) and Korsakoff's syndrome are considered different stages of the same disease because of vitamin B1 or thiamine deficiency (TD), where WE represents the acute and reversible (when treated with thiamine) form of the disease and Korsakoff is an advanced and irreversible state characterized by neuronal death. This neurologic disease, also named the Wernicke–Korsakoff syndrome (WKS), is characterized by ocular abnormalities (nystagmus and/or ophthalmoplegia), mental status changes, and gait disturbances (Kohnke and Meek, 2021). Because of limiting motor, cognitive, and emotional alterations, these patients require heavy dependence to complete daily life activities.

Alcohol use disorder (AUD) is the main risk factor for this disease, although other causes with no history of alcohol dependence may also induce the pathology, such as repetitive vomiting, gastric disorder, or after bariatric surgery (Kopelman, 1995; Deb et al., 2001). The nutritional TD in AUD is associated with malnourishment and decreased absorption of thiamine, due to the direct effects of alcohol on its metabolism, besides reduced storage in the liver because of alcoholic liver disease (Arts et al., 2017).

The bioactive form of thiamine (thiamine diphosphate) is necessary for energy metabolism in all cells. Therefore, the brain is the main site of TD-induced damage because of its immense energy requirement in comparison with the rest of the body (Clarke and Sokoloff, 1999). Brain damage has been extensively described in several brain regions in WE, mainly including diencephalic regions such as the thalamus and mammillary bodies (Manzo et al., 2014). However, some authors pointed out the presence of damage in other structures less studied in this pathology, such as the frontal cortex (Jacobson and Lishman, 1990; Jernigan et al., 1991; Paller et al., 1997; Aupée et al., 2001; Gibson et al., 2016) and the cerebellum (Mulholland, 2006; Manzo et al., 2014). In our previous preclinical studies about WE, we selected these less studied frontal cortex and cerebellum (Moya et al., 2021, 2022) as structures of great interest to be investigated, since both participate in motor function control, cognition, and emotional responses (Baillieux et al., 2008; Molinari et al., 2008; Rudebeck et al., 2008; Leggio et al., 2011; Clausi et al., 2017). Indeed, the frontal cortex is particularly important in executive control tasks and behavioral inhibition, including cognitive processes, social behavior, and inhibition of motor responses. Within the cerebellum, the mapping of associative learning with emotional, motor, and cognitive functions follows a medial-to-lateral cerebellar distribution: the sensorimotor functions are distributed more toward the midline, whereas the cognitive functions are located more laterally in the cerebellar hemispheres. Executive functions, including verbal working memory, are related to both cerebellar hemispheres, whereas affective functions are primarily midline in the so-called "limbic cerebellum." It is of interest that the left cerebellar hemisphere, the region analyzed in the present study, also appears to be involved in visuospatial functions and in linguistic processes (Klein et al., 2016; Amore et al., 2021). Therefore, the cerebellum and the frontal cortex are two brain areas directly involved in the behavioral alterations manifested in the WE, which deserve further investigation.

The exact cause of brain damage in WE is unclear, but neuroinflammation has been proposed as a contributing factor (Neri et al., 2011; Zahr et al., 2014; Toledo Nunes et al., 2019). Proinflammatory cytokines, enzymes, and different constituents of this process have been reported, but how the inflammatory response is activated in the brain tissue remains unknown. At present, our research group reported for the first time the involvement of the innate immune receptor Toll-like (TLR) 4 in the pathogenesis of nonalcoholic WE, showing a selective vulnerability of the frontal cortex and cerebellum, the two brain structures understudied in comparison with diencephalic regions, in this pathology over time (Moya et al., 2021).

The activation of the canonical proinflammatory TLR4 pathway induces, via myeloid differentiation factor 88 (MyD88), the recruitment of downstream signaling molecules that triggers the stimulation of transcriptional factors, such as the nuclear factor κB (NF-κB), which lead to the induction of genes encoding inflammation-associated molecules and cytokines. In addition to cytokines, NF-κB transcriptional activity induces the expression of other proinflammatory markers that lead to oxidative and nitrosative stress, such as the inducible nitric oxide synthase (iNOS) and cyclooxygenase-2 (COX-2) enzymes, and different caspases, generating lipid peroxidation and apoptotic cell death, respectively. Some other molecules can be released in response to injured tissue, such as heat shock proteins and the high mobility group box 1 protein (HMGB1), inducing more neuroinflammation in a vicious cycle [reviewed in (Orio et al., 2019)]. The TLR4-induced neuroinflammatory

pathway has been extensively studied in the context of AUD (Pascual et al., 2011; Crews et al., 2013; Montesinos et al., 2016; Antón et al., 2017), and we recently reported that the TLR4-induced neuroinflammation in the frontal cortex and cerebellum in TD animals could be related to the cognitive and motor deficits, respectively (Moya et al., 2021). However, the specific contribution of TD and chronic alcohol (CA) use to the impact of TLR4 signaling and their contribution to the pathogenesis of WE are currently unknown.

In the present study, we aimed to further characterize the role of the TLR4 in WE by using combined models with TD and CA exposure, the two main known contributing factors of the pathology, and we also explored the TLR4 activation and signaling in the frontal cortex and cerebellum of a postmortem alcohol-induced WE brain. The presence of postmortem brains of WE-diagnosed patients in biobanks is extremely scarce. Here, we reported a deep analysis (in white and gray matter in the frontal cortex and cerebellum) in a single case, using a matched control subject and a positive control in which TLR4-induced neuroinflammation has been extensively reported, as in an aged brain with Alzheimer's disease.

Materials and methods

Rodent studies

Animals and housing

Male Wistar rats (Envigo©, Barcelona, Spain) (n = 50), weighing 100–125 g at arrival were used. Animals were housed in groups of 2–3 per cage and maintained at a constant room temperature (21°C ± 1°C) and humidity (60 ± 10%) in a reversed 12 h dark–light cycle (lights on at 8:00 p.m.). Standard food and tap water were available *ad libitum* during an acclimation period of 12 days prior to experimentation, and then, rats were randomly assigned to the experimental groups.

All procedures followed ARRIVE guidelines and adhered to the guidelines of the Animal Welfare Committee of the Complutense University of Madrid (reference: PROEX 312-19) in compliance with the Spanish Royal Decree 118/2021 and following the European Directive 2010/63/EU on the protection of animals used for research and other scientific purposes.

Experimental groups

The experimental design and all the procedures of this animal study are described in detail and can be viewed in Moya et al. (2022).

In a word, to explore the different conditions that contribute to developing WE, the following experimental groups were used:

CA: animals exposed to forced consumption of 20% (w/v) alcohol for 9 months (n = 9).

TD diet (TDD): TD hit (TDD* + pyrithiamine 0.25 mg/kg dissolved in saline (0.9% NaCl) i.p. daily injections the last 12 days of experimentation; *TDD specific composition is detailed in the Supplementary Material) (n = 9).

Chronic alcohol combined with TDD in the last days of treatment (CA + TDD): both combined treatments (n = 10).

These groups were compared with the corresponding *control group* (*C*), animals drinking water with standard chow (n = 8).

During the last 12 days of TDD protocol, the remaining animals (C and CA) received equivalent daily injections of vehicle (saline, i.p.).

The number of animals in the alcohol and TDD groups was slightly higher than in control groups for the possible loss of experimental subjects.

We consider that the group with the combined CA + TDD treatment is the most relevant in this translational study, since is the animal model that most closely approximates the WE related to alcohol use.

Tissue samples collection

On day 12 of TDD protocol, at least 1 h after treatment administration, all animals were killed via rapid decapitation after anesthesia overdose of sodium pentobarbital (320 mg/kg, i.p., Dolethal®, Vétoquinol, Spain). Brains were immediately isolated from the skull, discarding meninges and blood vessels, and the frontal cortex (area between Bregma +4.7 and +1.2 mm approx.) and the left cerebellar hemisphere were dissected on ice and frozen at −80°C until assayed. The liver was also immediately taken out and kept at −80°C for other assays.

Western blot analysis

Frontal cortex and cerebellar hemisphere samples were processed and analyzed using western blotting following the methodology previously detailed in Moya et al. (2022).

In a word, the tissue samples were homogenized at a ratio of 1:3 (w/v) in ice-cold lysis buffer with protease inhibitors, followed by centrifugation to obtain the supernatants. Protein levels were measured using Bradford's method (Bradford, 1976). The samples were adjusted with the loading buffer to a final concentration of 1 mg/ml, and 15–20 µg of total protein were separated using SDS–polyacrylamide gels and transferred to nitrocellulose membranes. Blots were incubated with specific primary and secondary antibodies, using the housekeeping ß-actin protein as a loading control (see Table 1 for a complete list of antibodies and their details). Bands were visualized using an ECL kit and quantified via densitometry using ImageJ software (NIH, United States).

Liver damage

The status of the liver in the animals was checked by measuring the hepatic nitrites and malondialdehyde (MDA) levels, due to the major role of these processes in the

TABLE 1 Specific antibodies used in western blotting to detect proteins of interest.

Protein	*Primary antibody*[a]		*Secondary antibody*
TLR4	*sc-293072*	1:500 BSA 1%	Mouse (1:2000)
MyD88	*ab2064*	1:750 BSA 5%	Rabbit (1:2000)
phospo-NFκB p65	*(27.Ser 536) sc-136548*	1:400	Mouse (1:2000)
NFκB p65	*sc-372*	1:1000	Rabbit (1:2000)
IκBα	*sc-371*	1:1000 BSA 5%	Rabbit (1:2000)
COX-2	*sc-376861*	1:750 BSA 2%	Mouse (1:2000)
iNOS	*sc-650*	1:500 BSA 2%	Rabbit (1:2000)
HSP70	*sc-1060*	1:1000	Goat (1:4000)
β-actin	*A5441 Sigma*	1:10,000	Mouse (1:10,000)

[a]References (codes) and dilutions. Abbreviations: [TLR4, Toll-like receptor 4; MyD88, myeloid differentiation factor 88; Phosphorylated p65 subunit of NFκB: nuclear factor kappa B; IκBα, I kappa B alpha protein; COX-2, cyclooxygenase-2; iNOS, inducible oxide nitric synthase; HSP70, heat shock protein 70; BSA, Bovine serum albumin; sc, Santa Cruz Biotechnology; ab, Abcam]. Sources of secondary antibodies: Anti-Mouse IgG, HRP-linked whole Ab (from sheep) (GE, Healthcare, ref. NXA931); Anti-Goat IgG (whole molecule)–Peroxidase antibody produced in rabbit (Sigma-Aldrich, ref. A5420); Anti-Rabbit IgG (H + L) Cross-Adsorbed Secondary Antibody, HRP, conjugate (from donkey) (ThermoFisher Scientific, ref. 31,458).

pathogenesis of alcoholic liver disease (ALD) (McKim et al., 2003; Galicia-Moreno and Gutiérrez-Reyes, 2014; Pérez-Hernández et al., 2017; Tan et al., 2020; Yang et al., 2022). For details, see Supplementary Data S1.5.

Postmortem human studies

Cases. Three cases were selected from brains donated to the Biobank of the Hospital Universitario Fundación Alcorcón (HUFA), Madrid, Spain:

Case diagnosed with WE: woman, 62 years old. History of chronic alcohol consumption of at least one bottle of wine per day for 10–15 years. The patient showed classical symptoms of WE: altered mental state such as confusional syndrome, disorientation in space and time, and scarce and incoherent spontaneous language; ocular signs (horizontal nystagmus) and motor disturbances (extrapyramidal symptoms, decreased reflexes). The liver enzyme (transaminase) values and other information are reported in Supplemental Section S1.1. The WE was diagnosed based on the (previous) clinical presentation along with the confirmation via postmortem neuropathological analyses.

Negative control case: woman, 53 years old. Cause of death: a nonneurological disease or psychiatric disorder.

Positive control case: aged brain with Alzheimer's disease (AD): woman, 76 years old. Primary progressive aphasia, logopenic subtype. Frontotemporal lobar degeneration. Neuropathological diagnosis with changes of AD advanced stage. This was the positive control to observe neuroinflammation, since it had a double hit: aged brain with AD. (It has already been demonstrated that TLR4 neuroinflammation is involved in AD pathology (Zhang et al., 2012; Fiebich et al., 2018; Miron et al., 2018; Calvo-Rodriguez et al., 2020), and an aged brain is also susceptible of having more neuroinflammation).

The extended clinical history of each case can be found in Supplementary Section 1.1.

Sample processing

Postmortem proceedings were carried out in the HUFA, Madrid, Spain. All studies were performed complying with national ethical and legal regulations, being approved by the Drug Research Ethics Committee of the HUFA (ref 62-2018).

According to the brain bank protocol, in conventional donation cases, immediately after extraction, the left half of the brain was fixed via immersion in phosphate-buffered 4% formaldehyde for at least 3 weeks. Then, the brain is processed using coronal slices, except for the cerebellum, which is sectioned sagittally. Brain samples from the dorsolateral frontal cortex (Brodmann area 9) and the left cerebellar hemisphere (corresponding to the area from the superior cerebellum to the dentate nucleus) were selected for this study. The tissue was embedded in paraffin, and 4 μm sections were obtained via microtomy for subsequent immunostaining.

Immunohistochemistry

A detailed description of the immunohistochemistry (IHC) protocol is provided in Supplementary Section S1.2. In a word, slides were incubated with specific primary antibodies against TLR4, MyD88, p-NFκB p65, and IκB-α and were developed using diaminobenzidine (DAB) along with Carazzi's hematoxylin as counterstaining.

To evaluate the specificity of the staining, several technical controls were run including, on the one hand, the omission of the primary antibody and, on the other hand, the omission of the secondary antibody. These technical controls resulted in the absence of staining, and they were performed in both the frontal cortex and cerebellar tissue from the control, alcohol-induced WE, and AD cases. In addition, the specificity of the TLR4 and MyD88 antibodies selected for this study was

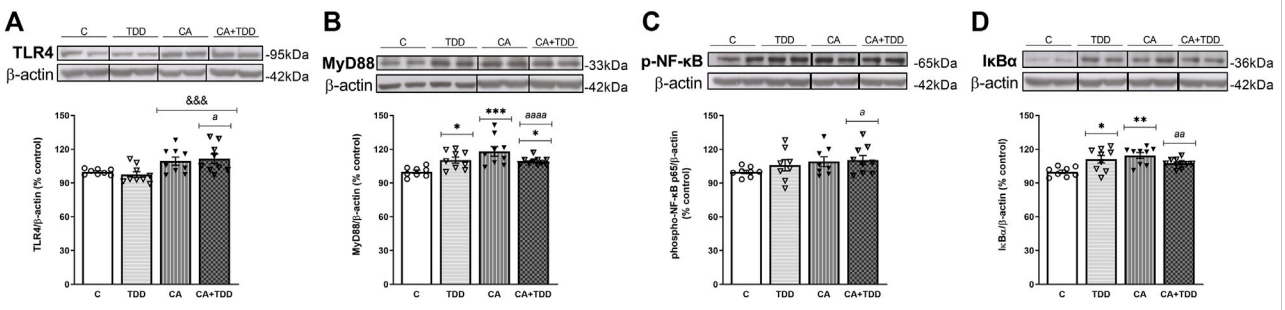

FIGURE 1
Effects in the TLR4 signaling pathway in frontal cortex of thiamine deficiency diet (TDD), chronic alcohol (CA), and CA + TDD-treated rats. Graphs indicate protein levels of **(A)** TLR4, **(B)** MyD88 **(C)** p-NF-κB, and **(D)** IκBα markers via western blotting; data of the respective bands of interest (upper bands) were normalized by β-actin (lower band) and expressed as a percentage of change in comparison with the control group. Some blots were cropped from the original (black lines) for improving the clarity and conciseness of the presentation. Mean ± S.E.M. (n = 8–10). Two-way ANOVA or nonparametric Kruskal–Wallis test. Overall alcohol effect: &&&$p < 0.001$; different from control group: *$p < 0.05$, **$p < 0.01$, ***$p < 0.001$. Since the combined CA + TDD treatment mimics better the human case of alcohol-induced Wernicke's encephalopathy (WE), this group was also compared with the C group using an unpaired Student's t-test or Mann–Whitney (CA + TDD vs. C): a $p < 0.05$, aa $p < 0.01$, aaaa $p < 0.0001$.

previously demonstrated in human brain tissue by using IHC and western blotting (Zurolo et al., 2011; MacDowell et al., 2017; Martín-Hernández et al., 2018).

Imaging and quantification

Slides immunostaining of the frontal cortex and cerebellar hemisphere were observed under light microscopy (Zeiss Axioplan Microscope, Germany). The microscope had a high-resolution camera attached (Zeiss Axioplan 712 color, Germany), which was used for capturing the images that were then processed using Axiovision 40V 4.1 (Carl Zeiss Vision, Germany) and ZEN2 software (Carl Zeiss AG, Oberkochen, Germany). Light, shine, and contrast conditions were kept constant during the capture process. For the study of each tissue section per patient, a total of 16 visual fields, 8 within the gray matter and another 8 within the white matter, were examined. An image of each visual field was taken at 40× magnification for the frontal cortex and at 20× magnification for the cerebellum to capture its three layers.

In addition, manual neuronal counting of each image was performed, in which a total number range for an accurate comparison between the cases was obtained.

Positive signals (in brown color due to DAB) on immunohistochemically stained tissues were semiquantitatively evaluated via visual and automatic scoring, comparing both methods to achieve the most reliable results. Images were always evaluated in a blinded manner without prior knowledge of the clinical information.

Visual/observational analysis: immunopositivity of the images was visually assessed by the investigator using a scoring system adapted to our study. The modified immunoreactivity score (IRS) is a composite score assigned to the distribution and intensity of immunostaining, based on (Wang et al., 2011) and (Meyerholz and Beck, 2018) (see Supplementary Section S2.1 and Figure 1). In a word, the observer must assign subscores for immunoreactive distribution (on a 0–4 scale) and intensity (on a 0–3 scale), multiplying them to calculate the total score for each image (ranging from 0 to 12). The final IRS was obtained by averaging the values in the eight fields for each section.

Automated analysis: a semiquantitative analysis of images was carried out using the *ImageJ Fiji* software, following the color deconvolution protocol previously described by Crowe and Yue (2019). In brief, a threshold value was set to remove the background signal after the deconvolution of images, followed by the quantification of the DAB signal within the image. The average intensity of the DAB signal in IHC images was calculated. Last, the mean value of the eight images was taken to represent the specific immunoreactivity of each target protein.

Since valuable information might be neglected by the above-mentioned scoring systems, we included a brief description of the cell types and tissue components positively marked, as well as the intensity and characteristics of the staining (see Supplementary Section S1.3).

Both visual IRS and automatic *Fiji* methods were employed for the analysis of frontal cortex images. Since both procedures reported comparable and reliable results (see results section), the cerebellar hemisphere was subsequently analyzed only using the *Fiji* method.

Statistical analysis

Data are expressed as mean ± S.E.M. In the animal study, two-way ANOVAs were used to assess the overall effects or interactions between two factors: CA and TDD. In addition, an

unpaired Student's t-test was used to compare the CA + TDD group with the control group. Regarding immunohistochemistry analyses, automated *Fiji* measures were analyzed using one-way ANOVA. For manual IRS data, the nonparametric Kruskal–Wallis test followed by paired comparisons with the Mann–Whitney test was used. A comparison between manual and automated IHC measurements was performed using Pearson's correlation and linear regression analyses. Parametric tests were performed when normality and homoscedasticity were verified (checked by Kolmogorov–Smirnov and Barlett's tests, respectively). Otherwise, data were transformed, or the alternative nonparametric analysis was applied. In the ANOVAs, the Bonferroni *post hoc* test was used when appropriate. Outliers were analyzed using Grubbs' test. A p value of <0.05 was set as the threshold for statistical significance in all statistical analyses. The data were analyzed using GraphPad Prism version 8.0 (GraphPad Software, Inc., La Jolla, CA, United States).

Results

Frontal cortex findings

CA + TDD-treated rats showed an increased expression of TLR4, MyD88, p-NF-κB, and IκBα proteins in the frontal cortex

CA increased TLR4 expression levels (Figure 1A, overall effect $F_{(1, 31)} = 13.7$, $p = 0.0008$). Regarding its coreceptor, rats exposed to TDD showed a significant increase in the MyD88 protein levels compared with controls ($p = 0.0434$), being higher in the CA group ($p = 0.0007$ compared to C). Likewise, the combined CA + TDD treatment induced MyD88 upregulation respect to control animals ($p = 0.0315$) (Figure 1B, differences between groups H = 15.82, $p = 0.0012$).

CA exposure induced an increasing trend in the phosphorylation of NF-κB that did not reach significance using ANOVA (Figure 1C, overall effect $F_{(1, 29)} = 2.995$, $p = 0.0941$). We report the results of the phosphorylated-NFkB protein normalized by the structural protein β-actin, as done with the rest of the markers, in accordance with other authors (Yang et al., 2021), since the increase of the phosphorylation in the p65 subunit is indicative of NF-κB activation to mediate inflammatory gene transcription. The levels of total NFkB were measured, with no changes (see Supplementary Section S2.3 and Figure 5). We analyzed also the IκBα protein as a reporter of NF-κB activity, finding an increase in its levels by the effect of TDD ($p = 0.042$) and CA ($p = 0.0039$) treatments relative to controls (Figure 1D, differences between groups H = 12.75, $p = 0.0052$). The increased expression of the NF-κB inhibitory protein IκBα can be considered an autoregulatory mechanism switched on by NF-κB to block its stimulation.

Moreover, the COX-2 enzyme was studied in the frontal cortex, showing an interaction between CA and TDD factors ($F_{(1, 25)} = 7.407$, $p = 0.0117$). *Post hoc* analysis revealed no statistical differences among groups (Supplementary Section S2.3 and Figure 4A).

In addition, trying to achieve the best approximation between the animal model and the human case, we consider that the combined CA + TDD treatment is an animal model that mimics better the WE related to alcohol use. According to this, we analyzed separately the CA + TDD group via Student's t-test or Mann–Whitney test. The CA + TDD group showed higher protein levels of TLR4 and MyD88 compared with controls (Figures 1A, B, U = 13, $p = 0.0274$; t = 5.208, df = 16, $p < 0.0001$, respectively). In addition, an elevation in p-NF-κB and IκBα protein expression was observed in this group respect to control (Figures 1C,D, t = 2.260, df = 15, $p = 0.0391$; t = 3.862, df = 16, $p = 0.0014$, respectively). No significant changes were observed in COX-2 levels of CA + TDD animals versus control (U = 22, $p > 0.05$, n. s.) and other markers (see Supplementary Section S2.3 and Figure 4).

Postmortem human frontal cortex of alcohol-induced Wernicke's encephalopathy showed an increased expression of TLR4, its coreceptor MyD88, and phospo-NFκB p65

Prior to visual and automatic analysis of the images, the results of the manual counting of the total number of neurons (mainly pyramidal) showed that the three cases studied were within the same range; thus, they were comparable (data not shown).

The findings reported below were obtained using the automatic *ImageJ Fiji* software, which were confirmed via comparison with the manual IRS analyses. Correlations between both measurements were high (Supplementary Section S2.2 and Figure 3; Table 1, for TLR4: r = 0.6375; for MyD88: r = 0.7958; for both $p < 0.0001$) supporting that the *Fiji* protocol here used is a robust automated measure for TLR4 and MyD88 IHC staining in the brain tissue. In addition, *Fiji* data were chosen as representative results since this method is the most objective. Manual IRS results for frontal cortex images can be found in Supplementary Section S2.2 and Figure 2.

In the cortical gray matter of the control case, weak TLR4 immunoreactivity was occasionally detected in a few pyramidal neurons and glial cells (Figure 2A). In the same brain area of the WE patient, we observed a strong TLR4 expression in most pyramidal neurons (with cytoplasmic localization, Figure 2Ba), as well as in glial cells (Figure 2Bb) and slightly in the neuropil. Tissue edema was also evident, with parenchymal distension ("gaps or empty spaces") (Figure 2B). Some endothelial cells in the blood vessels also appeared to be TLR4 positive (Figure 8). Likewise, in the AD case, we found a heavy TLR4 expression in the cytoplasm of the pyramidal neurons and glial cells and in the vicinity of some

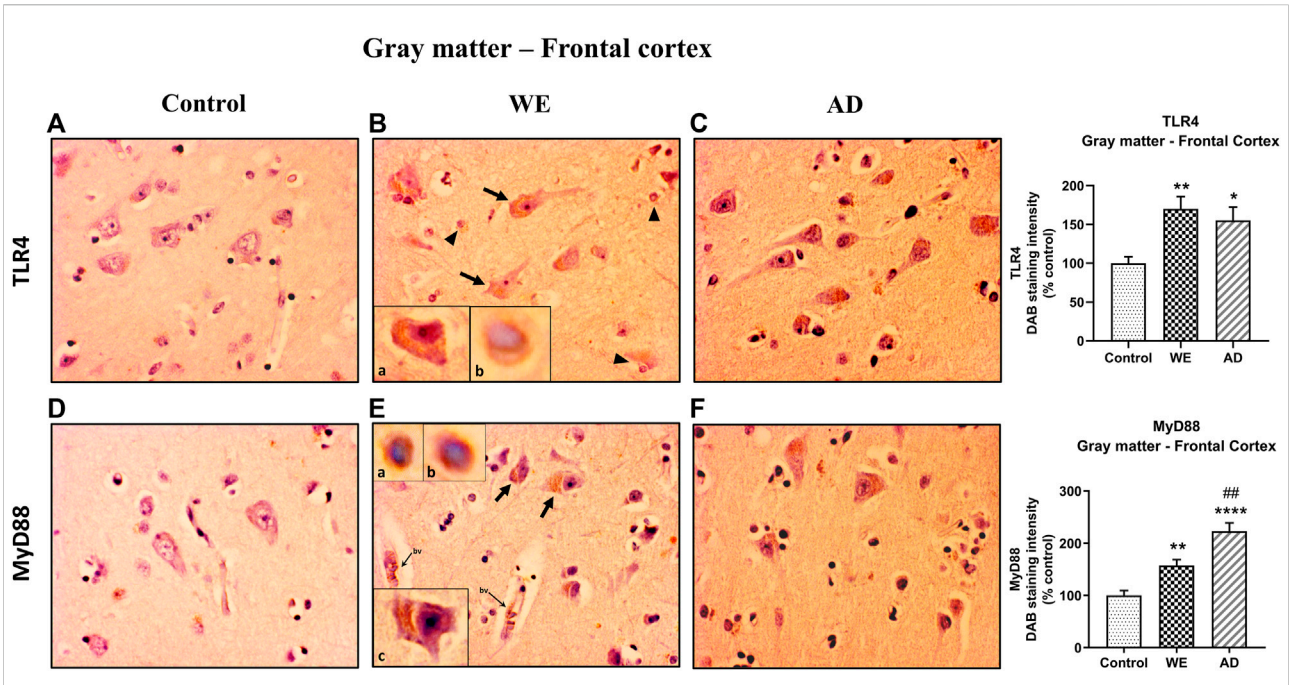

FIGURE 2
Representative images of immunohistochemical detection for TLR4 and MyD88 in the gray matter of the frontal cortex of control, alcohol-related WE, and Alzheimer's disease (AD) cases. Regarding TLR4 and MyD88 results in the WE case **(B)**, pyramidal neurons were strongly stained especially in the cytoplasm (arrows; high magnification in inset **(Ba; Ec)**) and also glial immunoreactivity (arrowheads; high magnification in inset (**Bb; Ea, b**)); this staining pattern was also found in the AD **(C)**. MyD88 also around the endothelial cells in blood vessels (*bv*). Tissue edema (parenchymal distension/"gaps") is prominent **(B,E)**. Images taken with a 40× objective. On the right panel, semiquantitative analysis of DAB images using the *ImageJ Fiji* software is shown. Data represent the mean of eight images/fields per section ±S.E.M and are expressed as a percentage of change in comparison with the control group. Different from control: *$p < 0.05$, **$p < 0.01$, ****$p < 0.0001$; different from WE: ##$p < 0.01$.

blood vessels (Figures 2C, 8). Thus, we found significant differences between the cases ($F_{(2, 21)} = 6.758$, $p = 0.0054$), with an increased TLR4 signal in WE ($p = 0.0066$) and AD ($p = 0.0358$) cortical gray matter compared with the TLR4 positive staining in the control case. In addition, we found higher MyD88 expression in WE ($p = 0.0086$) and AD ($p < 0.0001$) compared with the MyD88 staining in the control case (Figures 2E,F; $F_{(2, 20)} = 24.62$, $p < 0.0001$). MyD88 immunoreactivity was observed in the cytoplasm of pyramidal neurons (Figure 2Ec), in some glial cells (Figure 2Ea,b) and around the endothelial cells in blood vessels in the WE tissue (Figures 2E, 8). A similar pattern of greater intensity was observed in the AD case (Figures 2F, 8, $p = 0.0039$).

Regarding the results found in the cortical white matter, control and WE cases showed faint TLR4 staining (Figures 3A,B), but a higher TLR4 immunoreactivity was detected in the AD patient mostly between the fibers and in glial cells, showing that the AD case has a higher TLR4 expression than the WE case ($p = 0.0028$) (Figure 3C; $F_{(2, 20)} = 7.53$, $p = 0.0036$).

It is worth noting that we found an increase in MyD88 expression in the cortical white matter of both the WE and AD patients when compared with the control case ($p < 0.0001$ and $p = 0.0018$, respectively), and such an increase was particularly prominent in the WE case ($p < 0.0001$, compared with the AD case) (Figures 3D–F; $F_{(2, 21)} = 139.4$, $p < 0.0001$). This pronounced WE positive signal appears to be detected by the surrounding fibers and glial cells (Figure 3E, magnified box).

In addition, we checked the p-NFκB p65 and IκB-α markers in the animals. In the cortical gray matter, we noticed comparatively elevated immunoreactivity of p-NFκB p65 in the WE case than in the control case ($p = 0.0204$), finding mostly a cell nuclear localization of this mediator of inflammation. This can be observed mainly in neurons (especially pyramidal) (Figure 4Ba,b). A very similar staining pattern was also found in the positive control for neuroinflammation, the AD case, being significantly different from the control ($p = 0.0003$) (Figure 4Cc) (Figure 4, p-NFκB p65 U = 16.14, $p = 0.0003$).

Regarding the IκB-α, in the gray matter of the frontal cortex, we found certain differences between the cases (Figure 4, $F_{(2, 21)} = 4.406$, $p = 0.0253$). In the WE patient, a slight staining of the cell cytoplasm was observed in some neurons, although it was not significant compared with the control (Figure 4E, $p > 0.05$, n.s.). Likewise, the AD-positive control showed no differences in IκB-α staining versus the control (Figure 4E, $p > 0.05$, n.s.). However, although lower total levels of immunoreactivity were detected in

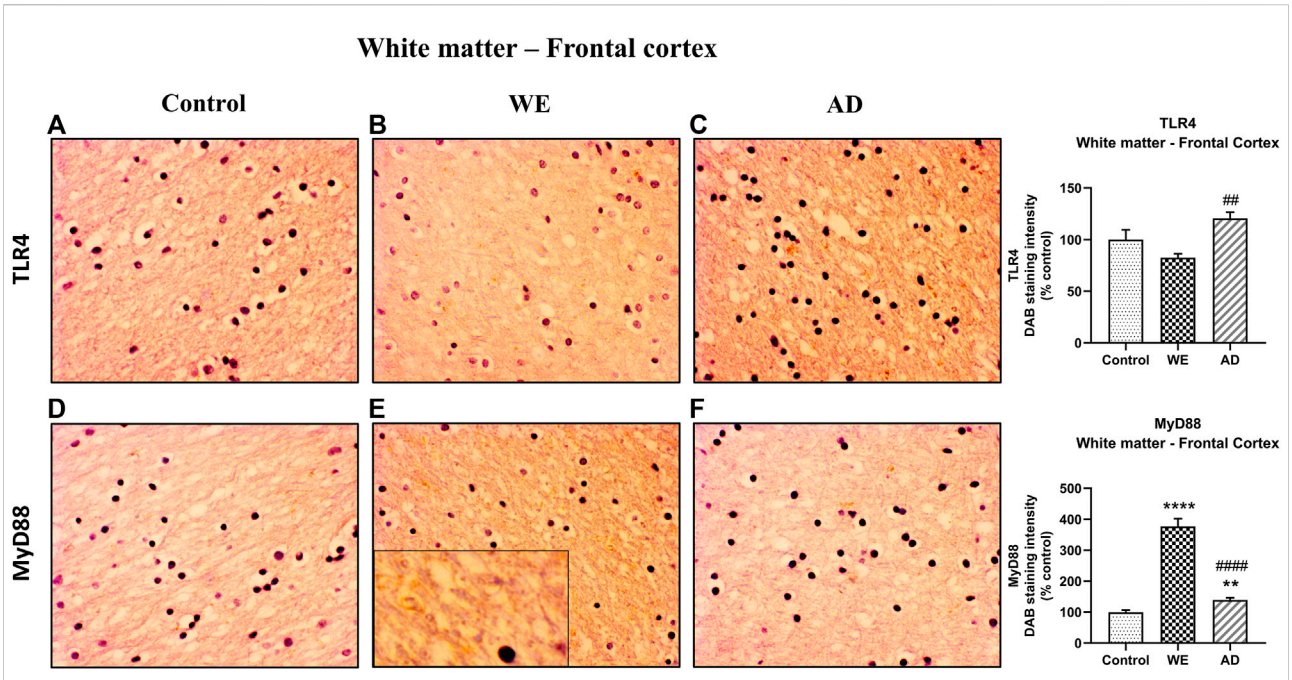

FIGURE 3
Representative images of immunohistochemical detection for TLR4 and MyD88 in the white matter of the frontal cortex of control, alcohol-related WE, and AD cases. WE patient showed the highest elevation in MyD88 expression (E). Images taken with a 40× objective. On the right panel, semiquantitative analysis of DAB images using the *ImageJ Fiji* software is shown. Data represent the mean of eight images/fields per section ± S.E.M and are expressed as a percentage of change versus the control group. Different from control: $^{**}p < 0.01$, $^{****}p < 0.0001$; different from WE: $\#\#p < 0.01$, $\#\#\#\#p < 0.0001$.

the AD subject than in the WE case ($p = 0.0221$), it is noteworthy to highlight that a striking IκB-α labeling was observed in the astrocytes (Figures 4Fe,f), which was also found in the WE case with less intensity, with some astrocytes reacting in the same way to this marker (Figures 4Ed).

In the cortical white matter, we found no significant differences between cases with p-NF-κB and those with IκB-α (Figure 5, $p > 0.05$, n.s.).

Cerebellar findings

Unaffected expression of TLR4 signaling markers in the cerebellar hemisphere of thiamine deficiency diet, chronic alcohol, and CA + TDD-treated rats

None of the experimental conditions induced significant changes in the markers studied (Figures 6A–D; total NF-κB: Supplementary Section S2.3 and Figure 5, $p > 0.05$, n.s.). iNOS enzyme and heat shock protein 70 (HSP70) were also analyzed, showing no alterations in their levels by any of the treatments ($p > 0.05$, n.s., SupplementarySection S2.3 and Figures 4B,C, respectively).

Likewise, no significant differences were found when comparing the CA + TDD group with the control in any of these markers ($p > 0.05$, n.s.).

Postmortem human cerebellar hemisphere of alcohol-induced Wernicke's encephalopathy showed an increased expression of TLR4 and its coreceptor MyD88 and IκB-α immunoreactivity

In the cerebellum sections, the three cellular layers of the cerebellar cortex–the molecular layer, Purkinje cells and the granular layer–were observed and analyzed together as cerebellar gray matter. The control case showed only occasional and low TLR4 immunoreactivity, mainly in some cells in the transition between the molecular and the granular layer (Figure 7A). By contrast, the WE case showed a more intense TLR4 staining, especially in the granular layer, in the cells and between the branching or neuropil; endothelial cells of blood vessels also showed TLR4 staining (Figures 7B, 8). Likewise, TLR4 in the AD patient was found mostly throughout the granular layer and in blood vessels (Figures 7C, 8). Therefore, the semiquantitative analysis demonstrated a significant increase in TLR4 expression in the cerebellar hemisphere gray matter ($F_{(2, 20)} = 13.81$, $p = 0.0002$) of WE ($p = 0.0006$) and AD ($p = 0.0006$) patients compared to the control case.

In the cerebellar cortex, MyD88 staining was predominant in the WE patient, with a main distribution within the granular layer, as well as TLR4 (Figure 7E), whereas a weak MyD88 immunoreactivity was found in both the control case

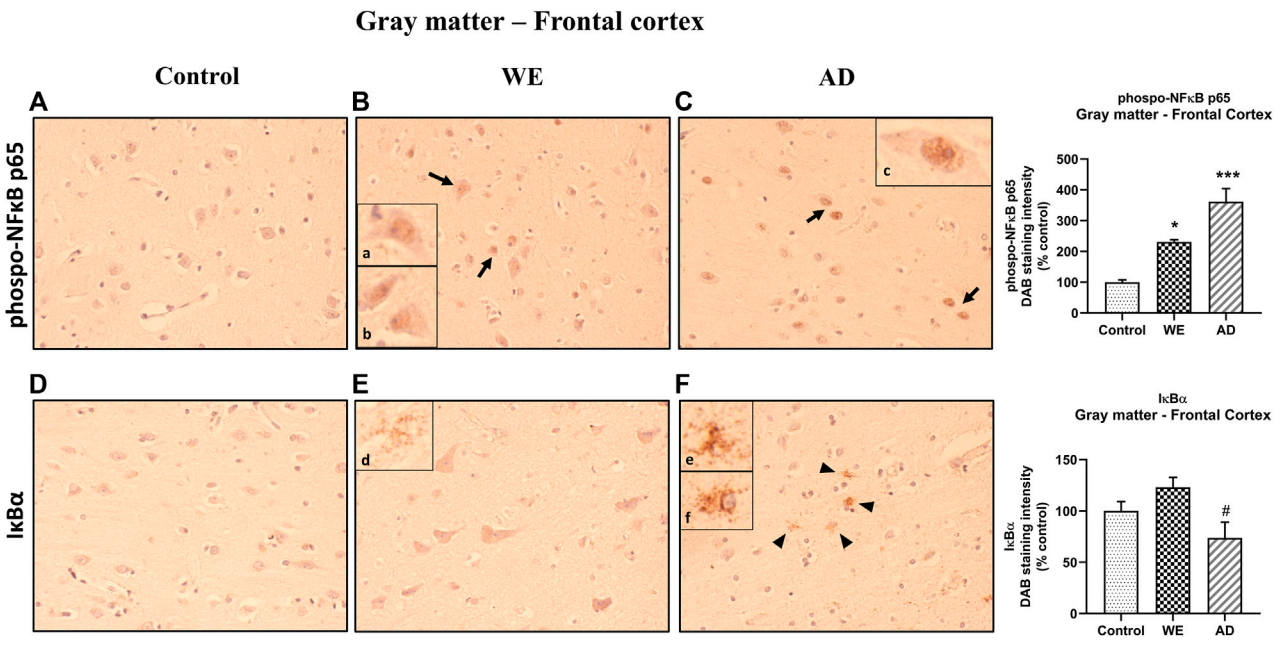

FIGURE 4
Representative images of immunohistochemical detection for p-NFκB p65 and IκB-α in the gray matter of the frontal cortex of control, alcohol-related WE, and AD cases. p-NF-κB exhibited nucleus localization in WE and AD cases (see especially in pyramidal neurons: arrows; high magnification in inset **(Ba, b; Cc)**). IκB-α manifested cytoplasmic localization but highlighting a striking immunoreactivity in the astrocytes, mainly in the AD (arrowheads; high magnification in inset **(Fe, f)**), but also, although to a lesser extent, found in the WE case (high magnification in inset **(Ed)**). Images taken with a 40× objective. On the right panel, semiquantitative analysis of DAB images using the *ImageJ Fiji* software is shown. Data represent the mean of eight images/fields per section ± S.E.M and are expressed as a percentage of change versus the control group. Different from control: *$p < 0.05$, ***$p < 0.001$; different from WE: #$p < 0.05$.

and the AD patient (Figures 7D,F, respectively). MyD88 expression intensity was significantly increased in the cerebellar hemisphere gray matter ($F_{(2, 21)} = 54.03$, $p < 0.0001$), showing the WE patient the highest levels compared to the AD patient ($p < 0.0001$) and control case ($p < 0.0001$).

In contrast, cerebellar hemisphere white matter did not show any differences in either TLR4 or MyD88 immunostaining in the human cases analyzed (Figure 9).

In addition, p-NF-κB and IκB-α immunoreactivity were also analyzed in the cerebellar hemisphere, and the p-NF-κB results in the gray matter showed no differences in the WE compared with the control (Figure 10, $p > 0,05$ n.s.). There was a slight difference between the cases (Figure 10, $F_{(2, 20)} = 12.27$, $p = 0.0003$), with an apparent lower level of labeling in the AD case compared to the control ($p = 0.0002$) and to the WE subject ($p = 0.0369$).

With regard to IκB-α, we observed significant differences between the patients (Figure 10, $F_{(2, 20)} = 5.466$, $p = 0.0128$), finding an increased IκB-α immunoreactivity in the WE case compared with the control ($p = 0.0462$) and with the AD subject ($p = 0.0207$). This IκB-α-labeling appears to be observed mainly through the granular layer, as was the case for TLR4 and MyD88.

In agreement with the results of TLR4 and MyD88 found in the white matter of the cerebellar hemisphere, we observed no significant changes between cases in this area in p-NF-κB and IκB-α markers (Figure 11, $p > 0.05$, n.s.).

Thiamine levels

Plasma thiamine levels were measured in all animals in our study. In brief, after 9 months of alcohol exposure and after TDD treatment, we found a trend toward a decrease in total thiamine levels due to an alcohol effect [for detailed results see (Moya et al., 2022)].

In the case of the WE patient studied here, it was not possible to perform thiamine determinations, since she died very quickly. Nevertheless, neuropathological analyses confirmed the diagnosis of WE without comorbidity with other pathologies such as HE, as we have already explained.

Liver status

We checked the status of the liver in the animals by measuring the hepatic nitrites MDA levels, due to the major role of these processes in the pathogenesis of ALD (McKim et al.,

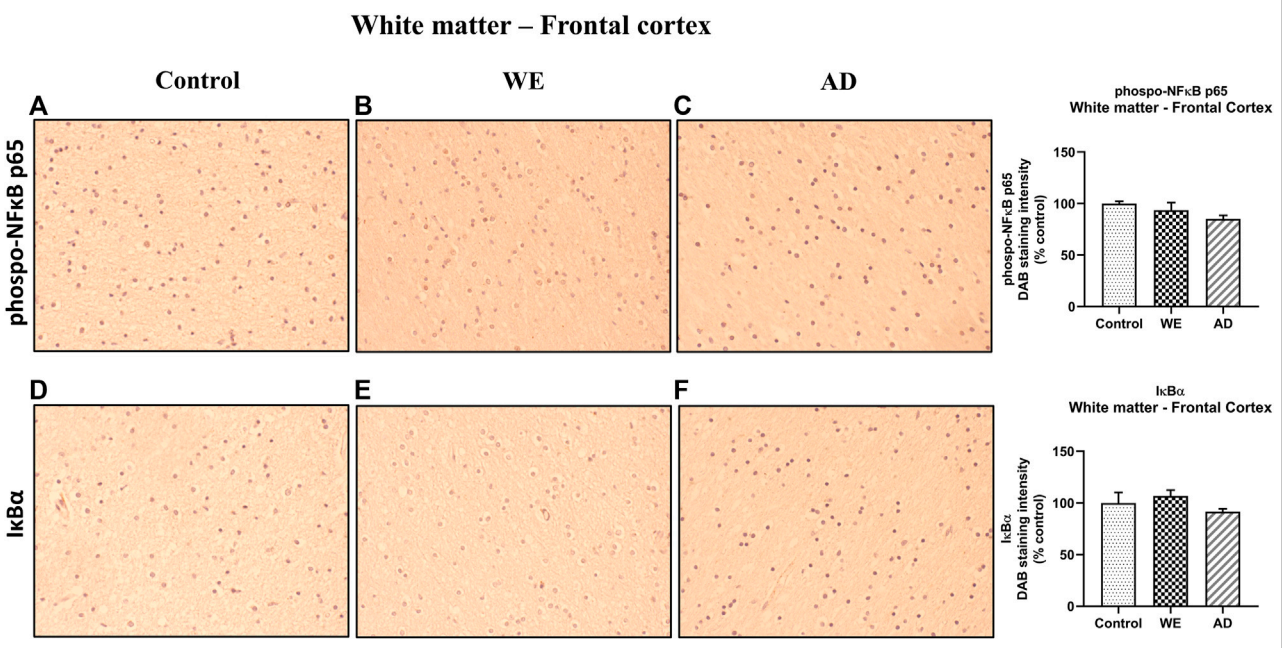

FIGURE 5
Representative images of immunohistochemical detection for p-NFκB p65 and IκB-α in the white matter of the frontal cortex of control, alcohol-related WE, and AD cases. Images taken with a 40× objective. On the right panel, semiquantitative analysis of DAB images using the *ImageJ Fiji* software is shown. Data represent the mean of eight images/fields per section ± S.E.M and are expressed as a percentage of change versus the control group.

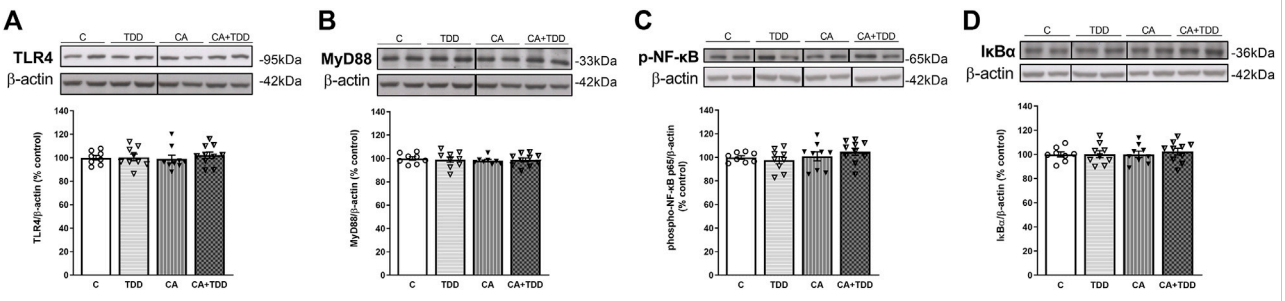

FIGURE 6
Unaffected expression of the TLR4 signaling pathway in the cerebellar hemisphere of TDD, CA, and CA + TDD-treated rats. Graphs indicate protein levels of **(A)** TLR4, **(B)** MyD88, **(C)** p-NF-κB, and **(D)** IκBα markers via western blotting; data of the respective bands of interest (upper bands) were normalized by β-actin (lower band) and expressed as a percentage of change versus the control group. Some blots were cropped from the original (black lines) for improving the clarity and conciseness of the presentation. Mean ± S.E.M. (n = 8–10). Two-way ANOVA. Since the combined CA + TDD treatment mimics better the human case of alcohol-induced WE, this group was also compared with the C group using an unpaired Student's t-test or Mann–Whitney (CA + TDD vs. C).

2003; Galicia-Moreno and Gutiérrez-Reyes, 2014; Pérez-Hernández et al., 2017; Tan et al., 2020; Yang et al., 2022). The levels of hepatic MDA and NO_2^- showed no significant changes by any of the treatments (Supplementary Section S2.4 and Figure 6).

Regarding the human case, the liver enzyme (transaminase) values were in the upper limit but without exceeding reference levels (See Supplementary Section S1.1). The patient exhibited no other symptoms or clinical signs of liver disease, suggesting that she was an alcohol-induced WE patient without ALD.

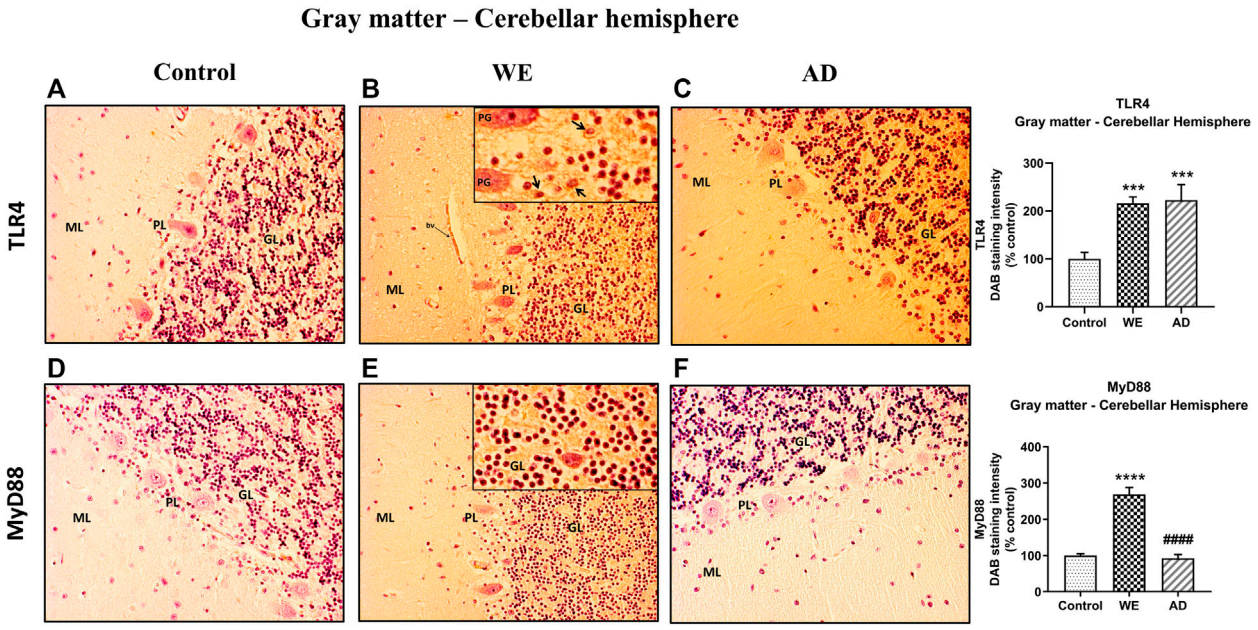

FIGURE 7
Representative images of immunohistochemical detection for TLR4 and MyD88 in the gray matter of the cerebellar hemisphere of control, alcohol-related WE, and AD cases. Gray matter with molecular layer (*ML*), Purkinje cell layer (*PL*), and granular layer (*GL*). In the WE **(B)** and AD cases **(C)**, an increased TLR4 immunoreactivity was detected especially in the granular layer (high magnification in the inset in B; Purkinje cell, PG; arrows pointing to positive cells) and blood vessels (*bv*), compared with the control **(A)**. WE patient also showed the highest elevation in MyD88 expression, mainly by the granular layer (high magnification in the inset in E), compared with AD **(F)** and control **(D)**. Images taken with a 20× objective. On the right panel, semiquantitative analysis of DAB images using the *ImageJ Fiji* software is shown. Data represent the mean of eight images/fields per section ±S.E.M and are expressed as a percentage of change versus the control group. Different from control: ***$p < 0.001$; ****$p < 0.0001$; different from WE: ####$p < 0.0001$.

Discussion

Little is known about the possible role of TLR4 in the WE, since there are no studies in humans, and to our knowledge, only our previous work with TD animal models provides evidence about the contribution of this receptor to this pathology (Moya et al., 2021). In the present study, we further characterized the role of this receptor in WE by studying animal models with combined TD and CA use. Thus, here, we report the importance of the double hit (TD and CA use) in the magnitude of the expression of the proinflammatory TLR4 signaling cascade in the frontal cortex but not in the cerebellum. We also described the presence of an upregulated cortical and cerebellar TLR4 and its adaptor molecule MyD88, along with specific changes in the signaling molecules phospo-NFκB p65 and IκBα, in a single case of alcohol-induced WE, by using postmortem brain tissue.

WE patients show neuropsychological symptoms such as memory alterations, apathy, executive deficit, and disinhibition, which suggest dysfunction of frontal structures. The vulnerability of the frontal lobe to CA consumption with or without TD is widely accepted based on neuropathological and neuroimaging studies [reviewed in (Jung et al., 2012)]. Inflammation, among other processes, may contribute to the WE symptomatology, as it increases cell damage and causes neuronal death. The innate immune receptor TLR4 plays a critical role in determining the pathological outcomes in several neurological and neuropsychiatric disorders, including AUD, AD, depression, schizophrenia, and trauma (Crews et al., 2013; García Bueno et al., 2016). By using WE animal models resulting from TD exposure, we were able to identify TLR4 as a key molecule in the emotional, cognitive, and motor disturbances associated with these models in a previous study (Moya et al., 2021). To our knowledge, there are no previous works that examine TLR4 signaling in the brain in the context of WE, either in animals or in human subjects.

However, since the main documented cause of WE is alcohol consumption, it is needed to explore more complex animal models, in which we can combine TD and CA consumption and explore the specific contribution of each factor to the pathophysiology of the disease. Indeed, in a very recent publication of our group we described the contribution of both factors (TD and alcohol abuse) to the induction of neuronal damage in the frontal cortex and how the combination of both (CA + TDD) correlates with

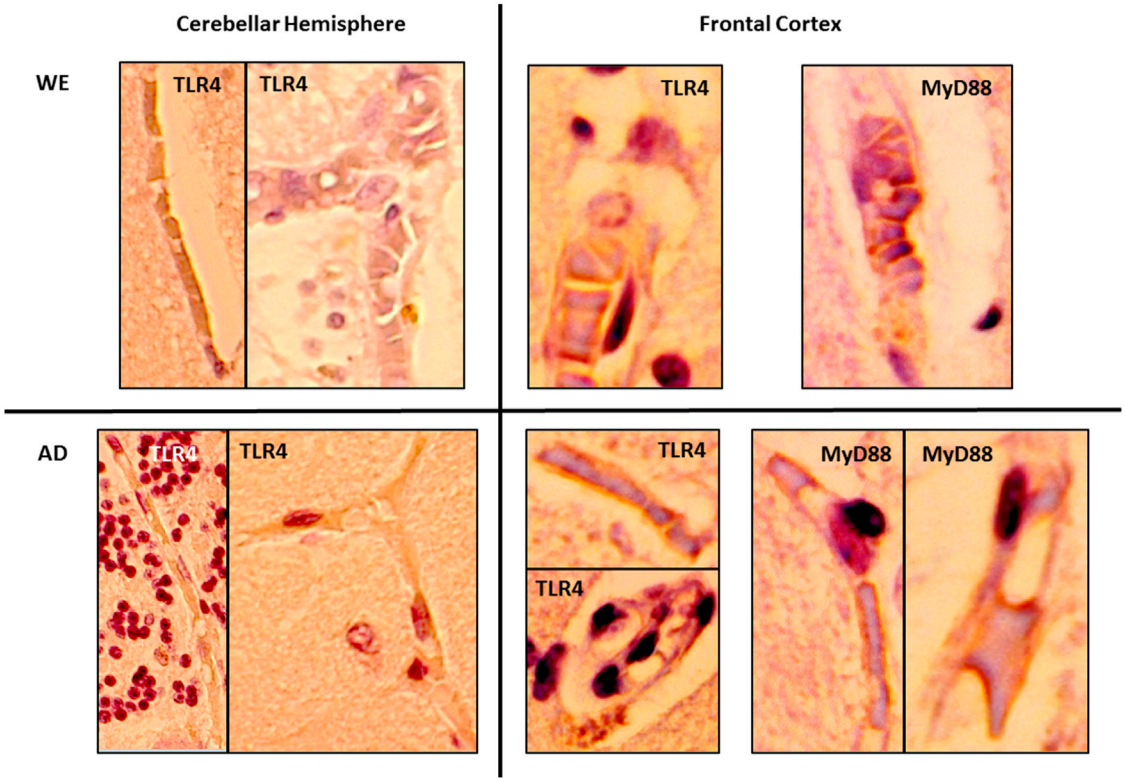

FIGURE 8
Details showing the endothelial cells of blood vessels with immunohistochemical reactivity of TLR4 and MyD88 in the gray matter of the cerebellar hemisphere and frontal cortex of alcohol-related WE and AD cases. High magnification from 20× (cerebellar hemisphere) and 40× (frontal cortex) images.

disinhibition-like behavior in animals (Moya et al., 2022), which is a core symptom of the pathology. Likewise, in the present study, we used the same combined animal models to explore the specific role of TLR4 in the induction of a neuroinflammatory cascade in the frontal cortex and cerebellum and added the description of the TLR4/MyD88 upregulation in the postmortem brain of an alcohol-induced WE case.

Among the animal models investigated here, the CA + TDD model is the one that better represents the pathology, as expected (Moya et al., 2022), and it is also the best approach to be compared with the alcohol-related WE case (postmortem human brain) studied here. In the animal model, we observed a significant upregulation in the protein expression of TLR4, MyD88, p-NF-κB, and IκBα in the frontal cortex (CA + TDD versus the control group). It is to note that neuroinflammation is a very complex response that involves the activation of several factors. The upregulation of phosphorylated NF-κB p65 is indicative of activation of this nuclear factor, since phosphorylation of Ser536 in the cytosolic p65 promotes the nuclear translocation and facilitates p65 binding to specific promoter sequences, activating the inflammatory gene expression (Giridharan and Srinivasan, 2018). In addition, its inhibitor gene IκBα contains NF-κB binding sites in its promoter, so the NF-κB is able to autoregulate the transcription of this own inhibitor, meaning that the "NF-κB-IκBα autoregulatory feedback loop" would be trying to suppress a prolonged activation of NF-κB to limit the inflammatory response (Doremus-Fitzwater et al., 2015; Gano et al., 2016; Toledo Nunes et al., 2019; Moya et al., 2021). Indeed, this autoregulatory mechanism switched on by NF-κB to block its stimulation is widely known in neuroinflammatory studies induced by LPS (Sayd et al., 2015), alcohol (Doremus-Fitzwater et al., 2015; Gano et al., 2016), TD (Moya et al., 2021), or combined TD and alcohol (Toledo Nunes et al., 2019). Hence, the IκBα protein levels are useful reporters of NF-κB activity and increase neuroinflammatory status.

It could be surprising that the TLR4 was not upregulated in the TD model, as opposed to our previous studies (Moya et al., 2021). It is known that neuroinflammation is a complex response where markers peak at different time-points, so the lack of significant effect in TLR4 in the TD animals of this study could be indicative that we did not catch the TLR4 peak at the precise moment of the samples collection. This is probably related to the age difference between the animals in both studies.

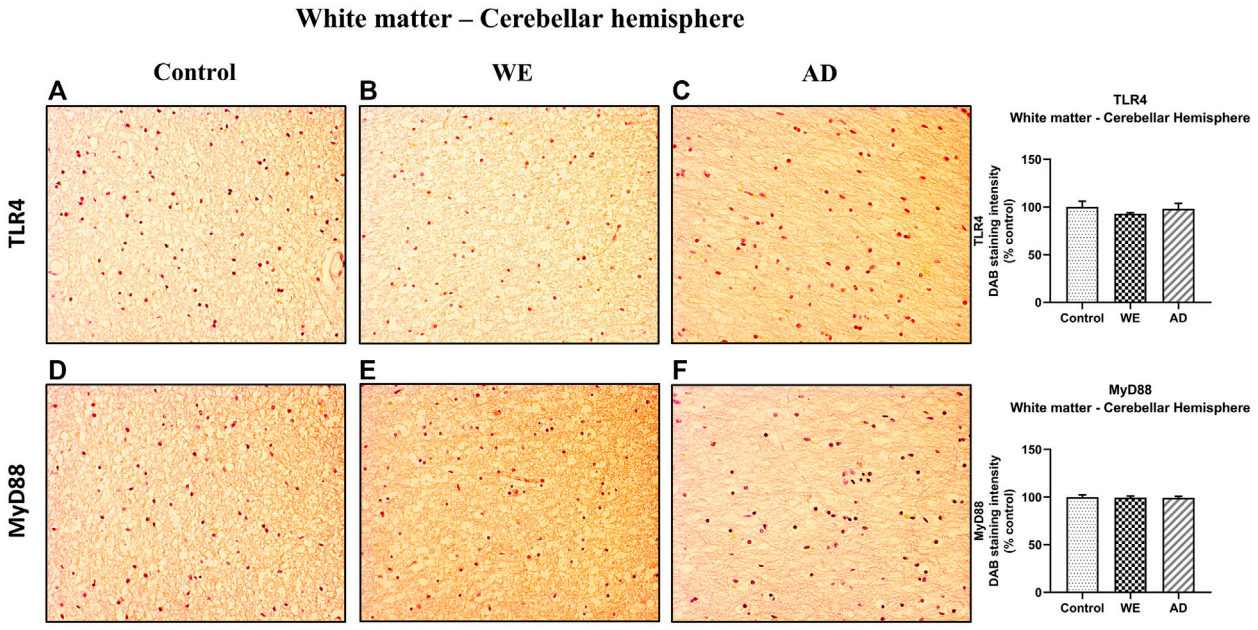

FIGURE 9
Representative images of immunohistochemical detection for TLR4 and MyD88 in the white matter of the cerebellar hemisphere of control, alcohol-related WE, and AD cases. Images taken with a 20× objective. On the right panel, semiquantitative analysis of DAB images using the *ImageJ Fiji* software is shown. Data represent the mean of eight images/fields per section ± S.E.M and are expressed as a percentage of change versus the control group.

Whereas in the previous study the animals were 8–9 weeks old, in the current study, the animals were approximately 10 months old. The younger animals may react differently (they show a particular timing of TLR4 upregulation profile) than the older animals. Nevertheless, there is certain evidence of a TLR4 signaling pathway overactivation in these animals, as some other inflammatory signals were observed (MyD88, IκBα) in the frontal cortex. Indeed, the upregulation of the TLR4 coreceptor MyD88 could be interpreted as a sign of TLR4 signaling overresponse, in absence of significant receptor overexpression. However, TLR4 is upregulated in the combined animal model, CA + TDD, although the increase is moderate compared to controls. In this regard, it is to note that the animals were exposed to a chronic treatment of moderate alcohol intake, so we are facing a process of chronic neuroinflammation, where we cannot expect such pronounced elevations as in a *binge drinking* model, for example, where there is a peak of acute neuroinflammation with a prominent increase in cortical levels of the TLR4 pathway (Antón et al., 2017). In addition, there is an absence of synergic effect by the combination of CA and TDD, since the elevations in the TLR4 pathway proteins were not higher than in the CA and/or TD exposure alone, which is maybe a consequence of the long alcohol exposure (9 months), rendering cells less sensitive to the TDD response.

It is to note that together with the upregulation of the TLR4 neuroinflammatory pathway found in CA + TDD animals in this study, we have already described, to complement the mechanisms, that other processes associated with TLR4 activation such as oxidative and nitrosative stress, lipid peroxidation, apoptosis death, and cell damage are upregulated in the frontal cortex of the same animals and correlate with disinhibition-like behavior (Moya et al., 2022). All these markers are more representative of the latest stages of a neuroinflammatory response, traditionally linked to neurotoxicity (Moya et al., 2022). Thus, altogether, these studies shed light on the relative contributions of each factor (alcohol and TD, either isolated or in interaction) to the potential disease-specific mechanisms involved in the WKS pathophysiology, resulting in brain damage and behavioral problems.

In a complementary way, here, we show, for the first time, a case of WE associated with CA consumption in which there is an upregulation of TLR4 and MyD88 protein expression in the postmortem frontal cortex and cerebellum. Neuroinflammation involves all the cell types present within the central nervous system (Shabab et al., 2017). In this way, microglia and astrocytes, as well as neurons and oligodendrocytes all contribute to innate immune responses in the CNS through the expression of TLR4, among other TLRs. Thus, TLR4 is

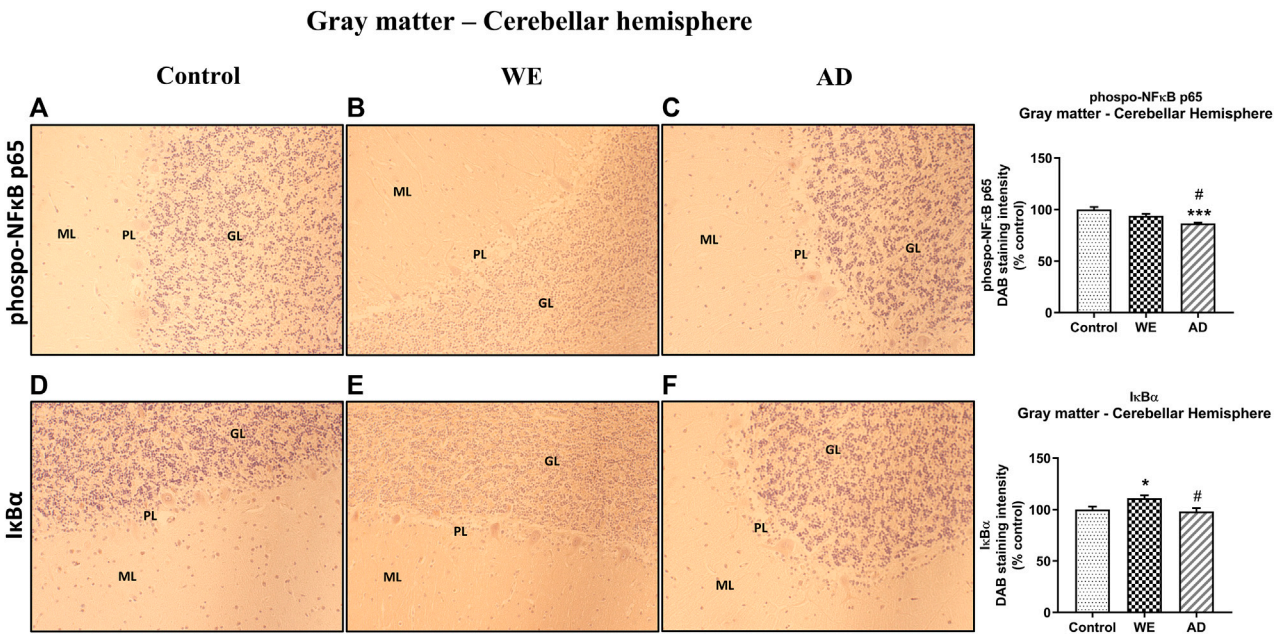

FIGURE 10
Representative images of immunohistochemical detection for p-NFκB p65 and IκB-α in the gray matter of the cerebellar hemisphere of control, alcohol-related WE, and AD cases. Gray matter with molecular layer (*ML*), Purkinje cell layer (*PL*), and granular layer (*GL*). In the WE **(E)**, an increased IκB-α immunoreactivity was detected especially in the granular layer compared with the control **(D)**. Images taken with a 20× objective. On the right panel, the semiquantitative analysis of DAB images using the *ImageJ Fiji* software is shown. Data represent the mean of eight images/fields per section ± S.E.M and are expressed as a percentage of change versus the control group. Different from control: $*p < 0.05$; $***p < 0.001$; different from WE: $\#p < 0.05$.

expressed in human brain cells, including neurons, microglia, astrocytes, and oligodendrocytes (Vaure and Liu, 2014; Stephenson et al., 2018; Frederiksen et al., 2019; Kumar, 2019; Leitner et al., 2019). In the WE cortical gray matter, immunohistochemical analysis showed an increased TLR4 staining in glial cells and pyramidal neurons, mainly in the cytoplasm, since TLR4 can signal both at the plasma membrane and intracellularly (Gangloff, 2012). TLR4 immunoreactivity was also observed in endothelial cells of the blood vessels, in agreement with Nagyoszi and colleagues, who demonstrated the expression of TLR4 on rat and human cerebral endothelial cells induced by inflammatory stimuli or oxidative stress (Nagyoszi et al., 2010). MyD88 expression in the WE patient showed a staining pattern similar to that observed for TLR4: it was mainly detected in pyramidal neurons and glial cells. Such a result may suggest that the upregulation of TLR4 has functional consequences in the associated signaling pathway. Likewise, endothelial cells of blood vessels showed immunoreactivity, which could fit with a study reporting that activation of the MyD88 pathway in endothelial cells of the cerebral microvasculature is involved in the regulation of inflammatory events (Gosselin and Rivest, 2008).

Similar findings have been previously reported in the AD brain, considered as a positive control, showing an activation of TLR4 in both human AD diagnosed patients and AD animal models (Fiebich et al., 2018; Calvo-Rodriguez et al., 2020; Zhou et al., 2020). The increase in TLR4 expression was particularly observed in the frontal cortex of AD subjects when compared with age-matched controls (Miron et al., 2018). Therefore, MyD88 levels were also reported to be elevated in the cortex of patients with AD and in a mouse model of AD (Rangasamy et al., 2018).

Preclinical and human studies have demonstrated that exposure to severe alcohol alone or combined with TD leads to white matter damage in the cortex (Kril et al., 1997; Harper, 2009; de la Monte and Kril, 2014; Chatterton et al., 2020) suggesting that neuroinflammation participates in the myelin and white matter disruptions (Alfonso-Loeches et al., 2012; Toledo Nunes et al., 2019). Here, we found a prominent increase in MyD88 immunoreactivity in the WE cortical white matter, and this excessive signaling could be leading to lower TLR4 levels in this cortical area by a compensatory downregulation mechanism. Indeed, depending on the temporal status in which these parameters were measured, the balance between TLR4 and MyD88 upregulation can be differentially affected.

Thereby, the concurrence of TLR4 and MyD88 immunoreactivity suggests an activation of the TLR4-

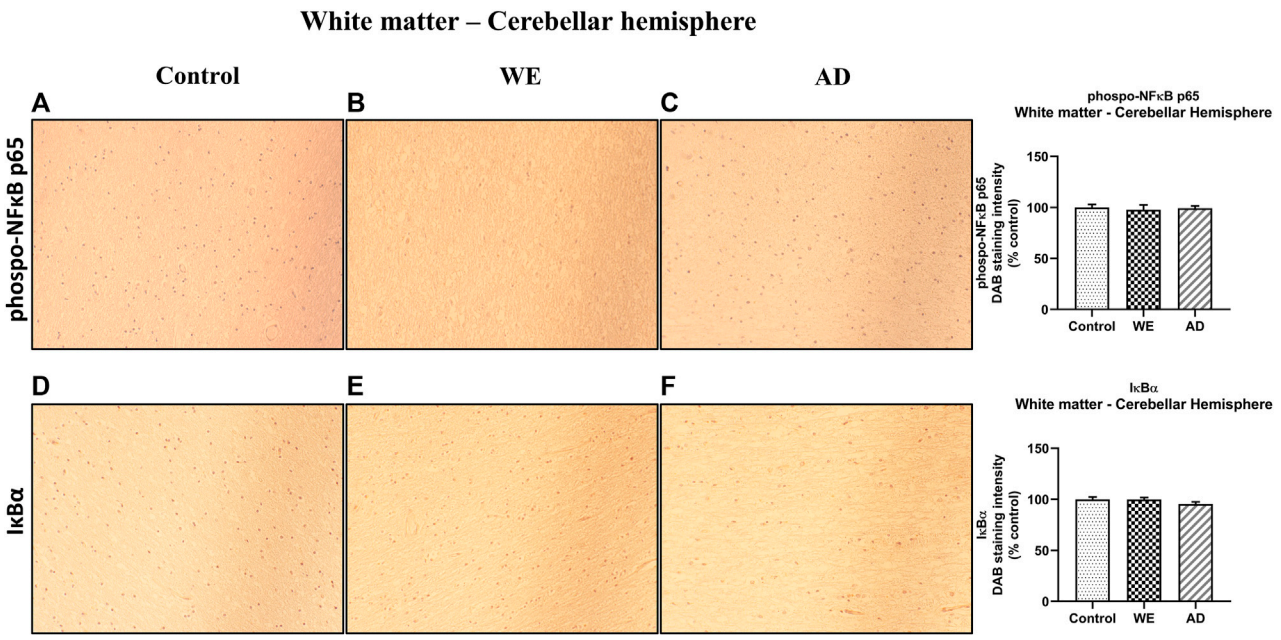

FIGURE 11
Representative images of immunohistochemical detection for p-NFκB p65 and IκB-α in the white matter of the cerebellar hemisphere of control, alcohol-related WE, and AD cases. Images taken with a 20× objective. On the right panel, semiquantitative analysis of DAB images using the *ImageJ Fiji* software is shown. Data represent the mean of eight images/fields per section ± S.E.M and are expressed as a percentage of change versus the control group.

MyD88 signaling pathway, although we cannot exclude other alternative pathways. It is possible that other TLR4 MyD88-independent signal transduction pathways such as the TRIF-dependent pathway could also be activated. Thus, the TLR4 immunoreactivity detected in our study could be indicative of signaling both from the membrane through Myd88 and internally from TRIF, and the MyD88 immunoreactivity could be somehow nonspecific for TLR4 and may include other TLRs (Biswas, 2018). Nevertheless, even if different pathways are activated, all of them converge and activate the NF-κB factor, in which we are particularly interested because it is the foremost important transcriptional manager of inflammation-associated genes (Marongiu et al., 2019; Ciesielska et al., 2021; Lin et al., 2021; Duan et al., 2022).

Indeed, we found an increase of the proinflammatory mediator p-NF-κB in the cortical gray matter of the WE case compared with control, as well as in the positive-AD-control, with a predominant expression or nuclear localization, indicating that this proinflammatory factor is active, which is, presumably, a direct consequence of the activation of the TLR4 signaling in the frontal cortex. Results regarding IκB-α are sometimes difficult to explain as both factors regulate their levels through compensatory mechanisms, as explained above. In this study, we found an interesting striking pattern of IκB-α labeling in glial cells such as astrocytes in the AD case, which was reproduced, to a lesser degree, in the WE patient.

Regarding the cerebellum, a damage induced by alcohol and TD has been previously reported (Mulholland, 2006; Manzo et al., 2014). Moderate shrinkage of the vermis and cerebellar hemispheres was observed in postmortem examination in patients diagnosed with alcohol abuse and with WE (Harper, 1979). It is of interest that our analyses in the postmortem cerebellar hemisphere of the WE patient showed an increase in TLR4 expression compared to the control brain, mainly detected in the granular layer and in endothelial cells of blood vessels. In addition, MyD88 and IκB-α were also upregulated and observed mostly in the granular layer of the WE subject. Therefore, the cerebellum is also considered as a vulnerable region for AD pathology (Hoxha et al., 2018). AD patients showed severe astrocytosis in the cerebellar granular layer (Fukutani et al., 1996), and studies with cerebellar granule cells reported increased secretion of ß-amyloid related to the neurodegeneration of nearby cells (Galli et al., 1998) (reviewed in (Hoxha et al., 2018)). Here, we also found an elevated TLR4 signal in the cerebellar hemisphere of the AD patient compared with the control case, although this increase was not observed for MyD88. As explained above, we cannot exclude the implication of other independent pathways to MyD88; thus, TLR4 could mediate

their effects through different inflammatory mediators in this brain area in AD.

In contrast to the data found in the WE patient, none of the treatments appeared to affect the TLR4 signaling in the cerebellar hemisphere of the rats compared with controls. In our previous study (Moya et al., 2021), the 12 days TD-induced model did not show a neuroinflammation signature in the cerebellum, coincident with an absence of motor impairment. However, we found the neuroinflammatory markers increased in the cerebellum in another model with a deeper degree of TD due to severe TDD treatment of 16 days, where the decline in animals' motor performance positively correlated with an upregulation of p65 NF-κB in this brain region (Moya et al., 2021). In the present study, we observe no evidence of motor dysfunction, such as ataxia, in any of the animal models tested, thus explaining the lack of changes observed in the cerebellum. However, it is to note that the clinic history of the WE patient showed hypotonia, hyporeflexia, oculomotor deficits such as nystagmus and saccadic intrusions, and altered speech, which are presumably signs of cerebellar dysfunction (Bodranghien et al., 2016; Jafar-Nejad et al., 2017) and may explain the changes observed in the cerebellum of the postmortem WE brain. Thus, the TLR4 signature in the cerebellum appears to precisely coincide with the manifestation of cerebellar symptoms, as reported by us previously (Moya et al., 2021).

Last, it is noteworthy to take into account possible hepatic alterations when this pathology is induced by alcohol consumption. It is known that the hepatotoxic properties of alcohol abuse may lead to ALD. However, despite alcohol consumption being the main cause of WE, the prevalence and characteristics of the relationship between ALD and WE remain unclear because of the lack of available data (Chamorro Fernández et al., 2011). ALD is a possible comorbidity in WE patients, which presents specific clinical, analytical, and radiological characteristics and a poorer prognosis compared with alcoholic WE patients without ALD (Novo-Veleiro et al., 2022). Hepatic encephalopathy (HE) induced by CA consumption is an extreme example of brain and liver interaction. Although both HE and WE occurs frequently in the setting of alcoholism, HE is due to liver disease and/or shunting of portal blood around the liver resulting in altered metabolism of nitrogenous substances, whereas WE is due to a deficiency of thiamin (Schenker et al., 1980). Three types of HE are traditionally differentiated (A, B, and C) (Weissenborn, 2019), but, in a term, HE occurs when toxins that are normally cleared from the body by the liver accumulate in the blood, eventually traveling to the brain. Elevated levels of ammonia appear to play a central role in this disorder, primarily by acting as a neurotoxin that generates astrocyte swelling, resulting in cerebral edema and intracranial hypertension. Other factors, such as oxidative stress, neurosteroids, systemic inflammation, increased bile acids, impaired lactate metabolism, and altered blood–brain barrier permeability likely contribute to the process of HE (Liere et al., 2017; Hadjihambi et al., 2018). In patients with underlying liver cirrhosis, distinguishing between HE and WE sometimes becomes a tough problem (Novo-Veleiro et al., 2022). HE is characterized by a wide spectrum of nonspecific neurological, psychiatric, and motor disturbances; hence, most of them may coincide with those in WE, since no mental alteration is unique for both disorders. Notwithstanding, mental alteration is usually the most noticeable symptom of WE (Zhao et al., 2016). The recent ISHEN (International Society for Hepatic Encephalopathy and Nitrogen Metabolism) consensus uses the onset of disorientation or asterixis as the initial sign of overt HE (Ferenci, 2017). In due course, the diagnosis of HE is based on history and physical examination, exclusion of other causes of altered mental status, and the laboratory clinical findings and is sometimes confirmed through a trial of therapy for this disorder. Therefore, when difficulties exist in distinguishing between HE and WE, intravenous vitamin B1 can be considered to be a discriminative method or a preemptive treatment (Zhao et al., 2016).

Nevertheless, although most heavy drinkers develop fatty liver, only a 20–40% subset of patients progresses to alcoholic hepatitis, and approximately 10–15% develop frank cirrhosis (Ghosh Dastidar et al., 2018). The WE case studied here is an alcoholic patient with WE without ALD, since she did not develop a severe liver injury, thus far from being comorbid with HE.

Likewise, regarding our animal model of CA consumption, the existing literature indicates that rodent models exposed to a CA administration equivalent to the one performed in this study developed mild or moderate steatosis but with no inflammation, no fibrosis, and no portal hypertension (Nevzorova et al., 2020). The steatosis or fatty liver is relatively benign and represents the initial stage in the ALD spectrum. To achieve greater damage to the liver, the alcohol drinking model is combined with other stressors to stimulate inflammation, fibrosis, or hepatocellular carcinoma. These second-hit models include additional factor(s) as dietary, chemical, genetic manipulations, or single or multiple alcohol binges to facilitate progression to advanced ALD (Ghosh Dastidar et al., 2018; Lamas-Paz et al., 2018; DeMorrow et al., 2021).

Notwithstanding, we checked the status of the liver in the animals by measuring the hepatic nitrites and MDA levels, because of the major role of these processes in the pathogenesis of ALD (McKim et al., 2003; Galicia-Moreno and Gutiérrez-Reyes, 2014; Pérez-Hernández et al., 2017; Tan et al., 2020; Yang et al., 2022). The results suggest that the protocol of CA consumption used in this study did not produce oxidative damage in the liver in the long term, since both the nitrite and the MDA levels, indicative of nitrosative stress and lipid peroxidation, respectively, showed no significant changes in the CA and CA + TDD

animals versus controls. We cannot discard that CA consumption has produced some mild to moderate alterations in the liver of our animals; however, in that case, it has not apparently progressed to a state of inflammatory/oxidative injury. Thus, these results suggest that the brain inflammatory response found in this study was achieved in absence of deep liver alterations.

Limitations, strengths, and future perspectives

Several limitations of our study should be acknowledged. On the one hand, our three human cases consisted of women and only male rats were used, which does not represent the real population of the disease. Further studies are needed to investigate the potential sex differences in this TLR4 pathway. On the other hand, in the control human case, ischemic anoxia was detected in the postmortem neuropathological diagnosis. However, signs of ischemia or hypoxia were not observed in the samples employed here. Moreover, since there is evidence for an involvement of inflammatory pathways, including TLR4 upregulation, after ischemia or hypoxia (Paschon et al., 2016; Mohsin Alvi et al., 2020), the present results may suggest an even higher increase in the TLR4 inflammation pathway if the data had been compared with another healthy control. Moreover, there is a difference of 9 years of age between the WE patient and the control. Nevertheless, we consider it to be within a comparable valid range, as observed in other studies where the difference between controls and patients also ranges from 8 to 10 years (Dabos et al., 2015; Ishiki et al., 2015; Ivanski et al., 2018). In addition, we are aware that the sample size in the postmortem brain study is very limited, but due to the poor records of WE cases, access to postmortem tissue is very complicated; hence, the obtained results in this study are even more noteworthy. The postmortem study is descriptive, and the results should be considered as a pilot study and nonfirmly conclusive. Furthermore, we are aware that the results in humans and animals have been obtained by different methodological techniques, so in future studies, we will verify these findings both by these and other methods. Nevertheless, obtaining results pointing in the same direction coming from two different techniques is also interesting and noteworthy. This indicates to us that both methodologies complement each other supporting common conclusions.

Despite these limitations, this study is the first to characterize TLR4 in the frontal cortex and cerebellum of a human subject with WE. Moreover, we demonstrated the utility of automatic *Fiji* and the visual IRS methods to analyze particularly DAB-based IHC images, since a strong correlation between both results was observed. Notwithstanding, automated analysis was chosen for the results report because it reduces subjective bias and allows the detection of signals that are not so easily identifiable to the naked eye by the observer.

Future research is required to analyze more markers of this TLR4 signaling pathway in postmortem cerebral tissue from WE patients, including the exploration of other vulnerable brain regions. Moreover, the study of WE cases with other etiology, as nonalcoholic patients, is also needed.

Conclusion

Taken together, our study shed light on the relative contributions of alcohol consumption and TD, either isolated or in interaction, to the activation of the TLR4/MyD88 signaling, which may act as an underlying mechanism to the pathogenesis of WE. The findings provided here using animal models, along with complementary results (Moya et al., 2022), and our previous work (Moya et al., 2021) suggest that the TLR4/MyD88 signaling may be a potential disease-specific mechanism involved in the WE pathophysiology, resulting in brain damage and behavioral problems. We provide also the first preliminary evidence of the TLR4/MyD88 upregulation in the postmortem brain tissue of a human case of WE.

Our results offer valuable information to guide future studies to further investigate these specific inflammatory mechanisms in the context of WE. The knowledge about how the inflammatory response is triggered in the WE brain and its relationship with the course of the disease is critical to understanding this disabling disorder and developing new therapeutic strategies.

Data availability statement

The original contributions presented in the study are included in the article/Supplementary Material, further inquiries can be directed to the corresponding author.

Ethics statement

The studies involving human participants were reviewed and approved by Drug Research Ethics Committee (Comité Ético de Investigación con Medicamentos/Investigación Clínica, CEIm del HUFA, ref. 62-2018). Written informed consent was not obtained from the individual(s) for the publication of any potentially identifiable images or data included in this article. Written informed consent for participation was not required for this study in accordance with the national legislation and the institutional requirements. The animal study was reviewed and approved by Animal

Welfare Committee of the Complutense University of Madrid (reference: PROEX 312-19).

Author contributions

Study design: MM and LO; experiments: MM and BE; imaging: MM, EMM, ML-G, EG-B, ABR-P, and CG; data analysis: MM, EMM, ML-G, and LO; original draft: MM; revision and funding: LO. Final version revision: all authors.

Funding

This study has been supported by grants RTI 2018-099535-B-I00 and PID2021-127256OB-I00 (FEDER (European Union)/Ministerio de Ciencia e Innovación–Agencia Estatal de Investigación (Spain)) to LO; and UCM research groups UCM951579 and UCM962049. MM is recipient of a research contract from Instituto de Salud Carlos III (ISCIII), programa RETICS: Red de Trastornos Adictivos (Ref: RD16/0017/0021) and BE is recipient of a FPU predoctoral research scholarship (FPU18/01575).

Conflict of interest

The authors declare that the research was conducted in the absence of any commercial or financial relationships that could be construed as a potential conflict of interest.

Publisher's note

All claims expressed in this article are solely those of the authors and do not necessarily represent those of their affiliated organizations, or those of the publisher, the editors, and the reviewers. Any product that may be evaluated in this article, or claim that may be made by its manufacturer, is not guaranteed or endorsed by the publisher.

Supplementary material

The Supplementary Material for this article can be found online at: https://www.frontiersin.org/articles/10.3389/fphar.2022.866574/full#supplementary-material

References

Alfonso-Loeches, S., Pascual, M., Gómez-Pinedo, U., Pascual-Lucas, M., Renau-Piqueras, J., and Guerri, C. (2012). Toll-like receptor 4 participates in the myelin disruptions associated with chronic alcohol abuse. *Glia* 60, 948–964. doi:10.1002/glia.22327

Amore, G., Spoto, G., Ieni, A., Vetri, L., Quatrosi, G., Di Rosa, G., et al. (2021). A focus on the cerebellum: From embryogenesis to an age-related clinical perspective. *Front. Syst. Neurosci.* 15, 646052. doi:10.3389/fnsys.2021.646052

Antón, M., Alén, F., Gómez de Heras, R., Serrano, A., Pavón, F. J., Leza, J. C., et al. (2017). Oleoylethanolamide prevents neuroimmune HMGB1/TLR4/NF-kB danger signaling in rat frontal cortex and depressive-like behavior induced by ethanol binge administration: OEA blocks ethanol TLR4 signaling. *Addict. Biol.* 22, 724–741. doi:10.1111/adb.12365

Arts, N. J., Walvoort, S. J., and Kessels, R. P. (2017). Korsakoff's syndrome: A critical review. *Neuropsychiatr. Dis. Treat.* 13, 2875–2890. doi:10.2147/NDT.S130078

Aupée, A. M., Desgranges, B., Eustache, F., Lalevée, C., de la Sayette, V., Viader, F., et al. (2001). Voxel-based mapping of brain hypometabolism in permanent amnesia with PET. *Neuroimage* 13, 1164–1173. doi:10.1006/nimg.2001.0762

Baillieux, H., De Smet, H. J., Paquier, P. F., De Deyn, P. P., and Mariën, P. (2008). Cerebellar neurocognition: Insights into the bottom of the brain. *Clin. Neurol. Neurosurg.* 110, 763–773. doi:10.1016/j.clineuro.2008.05.013

Biswas, C. (2018). "Chapter 18 - inflammation in systemic immune diseases: Role of TLR9 signaling and the resultant oxidative stress in pathology of lupus," in *Immunity and inflammation in health and disease*. Editors S. Chatterjee, W. Jungraithmayr, and D. Bagchi (Academic Press), 223–237. doi:10.1016/B978-0-12-805417-8.00018-4

Bodranghien, F., Bastian, A., Casali, C., Hallett, M., Louis, E. D., Manto, M., et al. (2016). Consensus paper: Revisiting the symptoms and signs of cerebellar syndrome. *Cerebellum* 15, 369–391. doi:10.1007/s12311-015-0687-3

Bradford, M. M. (1976). A rapid and sensitive method for the quantitation of microgram quantities of protein utilizing the principle of protein-dye binding. *Anal. Biochem.* 72, 248–254. doi:10.1006/abio.1976.9999

Calvo-Rodriguez, M., García-Rodríguez, C., Villalobos, C., and Núñez, L. (2020). Role of toll like receptor 4 in Alzheimer's disease. *Front. Immunol.* 11, 1588. doi:10.3389/fimmu.2020.01588

Chamorro Fernández, A. J., Marcos Martín, M., and Laso Guzmán, F. J. (2011). Wernicke encephalopathy in alcoholic patients. *Rev. Clin. Esp.* 211, 458–463. doi:10.1016/j.rce.2011.04.001

Chatterton, B. J., Nunes, P. T., and Savage, L. M. (2020). The effect of chronic ethanol exposure and thiamine deficiency on myelin-related genes in the cortex and the cerebellum. *Alcohol. Clin. Exp. Res.* 44, 2481–2493. doi:10.1111/acer.14484

Ciesielska, A., Matyjek, M., and Kwiatkowska, K. (2021). TLR4 and CD14 trafficking and its influence on LPS-induced pro-inflammatory signaling. *Cell. Mol. Life Sci.* 78, 1233–1261. doi:10.1007/s00018-020-03656-y

Clarke, D. D., and Sokoloff, L. (1999). *Circulation and energy metabolism of the brain. Basic neurochemistry: Molecular, cellular and medical aspects*. 6th edition. Available at: https://www.ncbi.nlm.nih.gov/books/NBK20413/(Accessed January 28, 2022).

Clausi, S., Iacobacci, C., Lupo, M., Olivito, G., Molinari, M., and Leggio, M. (2017). The role of the cerebellum in unconscious and conscious processing of emotions: A review. *Appl. Sci.* 7, 521. doi:10.3390/app7050521

Crews, F. T., Qin, L., Sheedy, D., Vetreno, R. P., and Zou, J. (2013). High mobility group box 1/Toll-like receptor danger signaling increases brain neuroimmune activation in alcohol dependence. *Biol. Psychiatry* 73, 602–612. doi:10.1016/j.biopsych.2012.09.030

Crowe, A. R., and Yue, W. (2019). Semi-quantitative determination of protein expression using immunohistochemistry staining and analysis: An integrated protocol. *Bio. Protoc.* 9, e3465. doi:10.21769/BioProtoc.3465

Dabos, K. J., Parkinson, J. A., Sadler, I. H., Plevris, J. N., and Hayes, P. C. (2015). (1)H nuclear magnetic resonance spectroscopy-based metabonomic study in patients with cirrhosis and hepatic encephalopathy. *World J. Hepatol.* 7, 1701–1707. doi:10.4254/wjh.v7.i12.1701

de la Monte, S. M., and Kril, J. J. (2014). Human alcohol-related neuropathology. *Acta Neuropathol.* 127, 71–90. doi:10.1007/s00401-013-1233-3

Deb, S., Law-Min, R., and Fearnley, D. (2001). Wernicke-Korsakoff syndrome following small bowel obstruction. *Behav. Neurol.* 13, 89–94. doi:10.1155/2002/702526

DeMorrow, S., Cudalbu, C., Davies, N., Jayakumar, A. R., and Rose, C. F. (2021). 2021 ISHEN guidelines on animal models of hepatic encephalopathy. *Liver Int.* 41, 1474–1488. doi:10.1111/liv.14911

Doremus-Fitzwater, T. L., Gano, A., Paniccia, J. E., and Deak, T. (2015). Male adolescent rats display blunted cytokine responses in the CNS after acute ethanol or lipopolysaccharide exposure. *Physiol. Behav.* 148, 131–144. doi:10.1016/j.physbeh.2015.02.032

Duan, T., Du, Y., Xing, C., Wang, H. Y., and Wang, R.-F. (2022). Toll-like receptor signaling and its role in cell-mediated immunity. *Front. Immunol.* 13. Available at: https://www.frontiersin.org/article/10.3389/fimmu.2022.812774 (Accessed April 1, 2022).

Ferenci, P. (2017). Hepatic encephalopathy. *Gastroenterol. Rep.* 5, 138–147. doi:10.1093/gastro/gox013

Fiebich, B. L., Batista, C. R. A., Saliba, S. W., Yousif, N. M., and de Oliveira, A. C. P. (2018). Role of microglia TLRs in neurodegeneration. *Front. Cell. Neurosci.* 12, 329. doi:10.3389/fncel.2018.00329

Frederiksen, H. R., Haukedal, H., and Freude, K. (2019). Cell type specific expression of toll-like receptors in human brains and implications in Alzheimer's disease. *Biomed. Res. Int.* 2019, 7420189. doi:10.1155/2019/7420189

Fukutani, Y., Cairns, N. J., Rossor, M. N., and Lantos, P. L. (1996). Purkinje cell loss and astrocytosis in the cerebellum in familial and sporadic Alzheimer's disease. *Neurosci. Lett.* 214, 33–36. doi:10.1016/0304-3940(96)12875-5

Galicia-Moreno, M., and Gutiérrez-Reyes, G. (2014). The role of oxidative stress in the development of alcoholic liver disease. *Rev. Gastroenterol. Mex.* 79, 135–144. doi:10.1016/j.rgmx.2014.03.001

Galli, C., Piccini, A., Ciotti, M. T., Castellani, L., Calissano, P., Zaccheo, D., et al. (1998). Increased amyloidogenic secretion in cerebellar granule cells undergoing apoptosis. *Proc. Natl. Acad. Sci. U. S. A.* 95, 1247–1252. doi:10.1073/pnas.95.3.1247

Gangloff, M. (2012). Different dimerisation mode for TLR4 upon endosomal acidification? *Trends biochem. Sci.* 37, 92–98. doi:10.1016/j.tibs.2011.11.003

Gano, A., Doremus-Fitzwater, T. L., and Deak, T. (2016). Sustained alterations in neuroimmune gene expression after daily, but not intermittent, alcohol exposure. *Brain Res.* 1646, 62–72. doi:10.1016/j.brainres.2016.05.027

García Bueno, B., Caso, J. R., Madrigal, J. L. M., and Leza, J. C. (2016). Innate immune receptor Toll-like receptor 4 signalling in neuropsychiatric diseases. *Neurosci. Biobehav. Rev.* 64, 134–147. doi:10.1016/j.neubiorev.2016.02.013

Ghosh Dastidar, S., Warner, J. B., Warner, D. R., McClain, C. J., and Kirpich, I. A. (2018). Rodent models of alcoholic liver disease: Role of binge ethanol administration. *Biomolecules* 8, E3. doi:10.3390/biom8010003

Gibson, G. E., Hirsch, J. A., Fonzetti, P., Jordan, B. D., Cirio, R. T., and Elder, J. (2016). Vitamin B1 (thiamine) and dementia: Vitamin B1 (thiamine) and dementia. *Ann. N. Y. Acad. Sci.* 1367, 21–30. doi:10.1111/nyas.13031

Giridharan, S., and Srinivasan, M. (2018). Mechanisms of NF-κB p65 and strategies for therapeutic manipulation. *J. Inflamm. Res.* 11, 407–419. doi:10.2147/JIR.S140188

Gosselin, D., and Rivest, S. (2008). MyD88 signaling in brain endothelial cells is essential for the neuronal activity and glucocorticoid release during systemic inflammation. *Mol. Psychiatry* 13, 480–497. doi:10.1038/sj.mp.4002122

Hadjihambi, A., Arias, N., Sheikh, M., and Jalan, R. (2018). Hepatic encephalopathy: A critical current review. *Hepatol. Int.* 12, 135–147. doi:10.1007/s12072-017-9812-3

Harper, C. (2009). The neuropathology of alcohol-related brain damage. *Alcohol Alcohol* 44, 136–140. doi:10.1093/alcalc/agn102

Harper, C. (1979). Wernicke's encephalopathy: A more common disease than realised. A neuropathological study of 51 cases. *J. Neurol. Neurosurg. Psychiatry* 42, 226–231. doi:10.1136/jnnp.42.3.226

Hoxha, E., Lippiello, P., Zurlo, F., Balbo, I., Santamaria, R., Tempia, F., et al. (2018). The emerging role of altered cerebellar synaptic processing in Alzheimer's disease. *Front. Aging Neurosci.* 10, 396. doi:10.3389/fnagi.2018.00396

Ishiki, A., Okamura, N., Furukawa, K., Furumoto, S., Harada, R., Tomita, N., et al. (2015). Longitudinal assessment of tau pathology in patients with Alzheimer's disease using [18F]THK-5117 positron emission tomography. *PLoS One* 10, e0140311. doi:10.1371/journal.pone.0140311

Ivanski, F., Nascimento, L. D. P., Fermino, B. L., Bonini, J. S., Silva, W. C. F. N. da, Valério, J. M. S., et al. (2018). Nutritional evaluation of geriatric patients with Alzheimer's disease in southern Brazil: Case-control study. *Nutr. Hosp.* 35, 564–569. doi:10.20960/nh.1626

Jacobson, R. R., and Lishman, W. A. (1990). Cortical and diencephalic lesions in korsakoff's syndrome: A clinical and CT scan study. *Psychol. Med.* 20, 63–75. doi:10.1017/s0033291700013234

Jafar-Nejad, P., Maricich, S. M., and Zoghbi, H. Y. (2017). "91 - the cerebellum and the hereditary ataxias," in *Swaiman's pediatric neurology*. Editors K. F. Swaiman, S. Ashwal, D. M. Ferriero, N. F. Schor, R. S. Finkel, A. L. Gropman, et al. Sixth Edition (Elsevier), 689–700. doi:10.1016/B978-0-323-37101-8.00091-6

Jernigan, T. L., Schafer, K., Butters, N., and Cermak, L. S. (1991). Magnetic resonance imaging of alcoholic Korsakoff patients. *Neuropsychopharmacology* 4, 175–186.

Jung, Y.-C., Chanraud, S., and Sullivan, E. V. (2012). Neuroimaging of Wernicke's encephalopathy and Korsakoff's syndrome. *Neuropsychol. Rev.* 22, 170–180. doi:10.1007/s11065-012-9203-4

Klein, A. P., Ulmer, J. L., Quinet, S. A., Mathews, V., and Mark, L. P. (2016). Nonmotor functions of the cerebellum: An introduction. *AJNR. Am. J. Neuroradiol.* 37, 1005–1009. doi:10.3174/ajnr.A4720

Kohnke, S., and Meek, C. L. (2021). Don't seek, don't find: The diagnostic challenge of Wernicke's encephalopathy. *Ann. Clin. Biochem.* 58, 38–46. doi:10.1177/0004563220939604

Kopelman, M. D. (1995). The Korsakoff syndrome. *Br. J. Psychiatry* 166, 154–173. doi:10.1192/bjp.166.2.154

Kril, J. J., Halliday, G. M., Svoboda, M. D., and Cartwright, H. (1997). The cerebral cortex is damaged in chronic alcoholics. *Neuroscience* 79, 983–998. doi:10.1016/s0306-4522(97)00083-3

Kumar, V. (2019). Toll-like receptors in the pathogenesis of neuroinflammation. *J. Neuroimmunol.* 332, 16–30. doi:10.1016/j.jneuroim.2019.03.012

Lamas-Paz, A., Hao, F., Nelson, L. J., Vázquez, M. T., Canals, S., Gómez Del Moral, M., et al. (2018). Alcoholic liver disease: Utility of animal models. *World J. Gastroenterol.* 24, 5063–5075. doi:10.3748/wjg.v24.i45.5063

Leggio, M. G., Chiricozzi, F. R., Clausi, S., Tedesco, A. M., and Molinari, M. (2011). The neuropsychological profile of cerebellar damage: The sequencing hypothesis. *Cortex.* 47, 137–144. doi:10.1016/j.cortex.2009.08.011

Leitner, G. R., Wenzel, T. J., Marshall, N., Gates, E. J., and Klegeris, A. (2019). Targeting toll-like receptor 4 to modulate neuroinflammation in central nervous system disorders. *Expert Opin. Ther. Targets* 23, 865–882. doi:10.1080/14728222.2019.1676416

Liere, V., Sandhu, G., and DeMorrow, S. (2017). Recent advances in hepatic encephalopathy. *F1000Res.* 6, 1637. doi:10.12688/f1000research.11938.1

Lin, C., Wang, H., Zhang, M., Mustafa, S., Wang, Y., Li, H., et al. (2021). TLR4 biased small molecule modulators. *Pharmacol. Ther.* 228, 107918. doi:10.1016/j.pharmthera.2021.107918

MacDowell, K. S., Pinacho, R., Leza, J. C., Costa, J., Ramos, B., and García-Bueno, B. (2017). Differential regulation of the TLR4 signalling pathway in post-mortem prefrontal cortex and cerebellum in chronic schizophrenia: Relationship with SP transcription factors. *Prog. Neuropsychopharmacol. Biol. Psychiatry* 79, 481–492. doi:10.1016/j.pnpbp.2017.08.005

Manzo, G., De Gennaro, A., Cozzolino, A., Serino, A., Fenza, G., and Manto, A. (2014). MR imaging findings in alcoholic and nonalcoholic acute wernicke's encephalopathy: A review. *Biomed. Res. Int.* 2014, 503596, 1–12. doi:10.1155/2014/503596

Marongiu, L., Gornati, L., Artuso, I., Zanoni, I., and Granucci, F. (2019). Below the surface: The inner lives of TLR4 and TLR9. *J. Leukoc. Biol.* 106, 147–160. doi:10.1002/JLB.3MIR1218-483RR

Martín-Hernández, D., Caso, J. R., Javier Meana, J., Callado, L. F., Madrigal, J. L. M., García-Bueno, B., et al. (2018). Intracellular inflammatory and antioxidant pathways in postmortem frontal cortex of subjects with major depression: Effect of antidepressants. *J. Neuroinflammation* 15, 251. doi:10.1186/s12974-018-1294-2

McKim, S. E., Gäbele, E., Isayama, F., Lambert, J. C., Tucker, L. M., Wheeler, M. D., et al. (2003). Inducible nitric oxide synthase is required in alcohol-induced liver injury: Studies with knockout mice. *Gastroenterology* 125, 1834–1844. doi:10.1053/j.gastro.2003.08.030

Meyerholz, D. K., and Beck, A. P. (2018). Principles and approaches for reproducible scoring of tissue stains in research. *Lab. Invest.* 98, 844–855. doi:10.1038/s41374-018-0057-0

Miron, J., Picard, C., Frappier, J., Dea, D., Théroux, L., and Poirier, J. (2018). TLR4 gene expression and pro-inflammatory cytokines in Alzheimer's disease and in response to hippocampal deafferentation in rodents. *J. Alzheimers Dis.* 63, 1547–1556. doi:10.3233/JAD-171160

Mohsin Alvi, A., Tariq Al Kury, L., Umar Ijaz, M., Ali Shah, F., Tariq Khan, M., Sadiq Sheikh, A., et al. (2020). Post-treatment of synthetic polyphenolic 1, 3, 4 oxadiazole compound A3, attenuated ischemic stroke-induced neuroinflammation and neurodegeneration. *Biomolecules* 10, E816. doi:10.3390/biom10060816

Molinari, M., Chiricozzi, F. R., Clausi, S., Tedesco, A. M., De Lisa, M., and Leggio, M. G. (2008). Cerebellum and detection of sequences, from perception to cognition. *Cerebellum* 7, 611–615. doi:10.1007/s12311-008-0060-x

Montesinos, J., Alfonso-Loeches, S., and Guerri, C. (2016). Impact of the innate immune response in the actions of ethanol on the central nervous system. *Alcohol. Clin. Exp. Res.* 40, 2260–2270. doi:10.1111/acer.13208

Moya, M., López-Valencia, L., García-Bueno, B., and Orio, L. (2022). Disinhibition-like behavior correlates with frontal cortex damage in an animal model of chronic alcohol consumption and thiamine deficiency. *Biomedicines* 10, 260. doi:10.3390/biomedicines10020260

Moya, M., San Felipe, D., Ballesta, A., Alén, F., Rodríguez de Fonseca, F., García-Bueno, B., et al. (2021). Cerebellar and cortical TLR4 activation and behavioral impairments in Wernicke-Korsakoff Syndrome: Pharmacological effects of oleoylethanolamide. *Prog. Neuropsychopharmacol. Biol. Psychiatry* 108, 110190. doi:10.1016/j.pnpbp.2020.110190

Mulholland, P. (2006). Susceptibility of the cerebellum to thiamine deficiency. *Cerebellum* 5, 55–63. doi:10.1080/14734220600551707

Nagyoszi, P., Wilhelm, I., Farkas, A. E., Fazakas, C., Dung, N. T. K., Haskó, J., et al. (2010). Expression and regulation of toll-like receptors in cerebral endothelial cells. *Neurochem. Int.* 57, 556–564. doi:10.1016/j.neuint.2010.07.002

Neri, M., Cantatore, S., Pomara, C., Riezzo, I., Bello, S., Turillazzi, E., et al. (2011). *Wernicke's encephalopathy*, 207, 652–658. doi:10.1016/j.prp.2011.07.005Immunohistochemical expression of proinflammatory cytokines IL-1β, IL-6, TNF-α and involvement of COX-2, quantitatively confirmed by Western blot analysis*Pathology - Res. Pract.*

Nevzorova, Y. A., Boyer-Diaz, Z., Cubero, F. J., and Gracia-Sancho, J. (2020). Animal models for liver disease - a practical approach for translational research. *J. Hepatol.* 73, 423–440. doi:10.1016/j.jhep.2020.04.011

Novo-Veleiro, I., Herrera-Flores, J., Rosón-Hernández, B., Medina-García, J.-A., Muga, R., Fernández-Solá, J., et al. (2022). Alcoholic liver disease among patients with Wernicke encephalopathy: A multicenter observational study. *Drug Alcohol Depend.* 230, 109186. doi:10.1016/j.drugalcdep.2021.109186

Orio, L., Alen, F., Pavón, F. J., Serrano, A., and García-Bueno, B. (2019). Oleoylethanolamide, neuroinflammation, and alcohol abuse. *Front. Mol. Neurosci.* 11, 490. doi:10.3389/fnmol.2018.00490

Paller, K. A., Acharya, A., Richardson, B. C., Plaisant, O., Shimamura, A. P., Reed, B. R., et al. (1997). Functional neuroimaging of cortical dysfunction in alcoholic korsakoff's syndrome. *J. Cogn. Neurosci.* 9, 277–293. doi:10.1162/jocn.1997.9.2.277

Paschon, V., Takada, S. H., Ikebara, J. M., Sousa, E., Raeisossadati, R., Ulrich, H., et al. (2016). Interplay between exosomes, microRNAs and toll-like receptors in brain disorders. *Mol. Neurobiol.* 53, 2016–2028. doi:10.1007/s12035-015-9142-1

Pascual, M., Baliño, P., Alfonso-Loeches, S., Aragón, C. M. G., and Guerri, C. (2011). Impact of TLR4 on behavioral and cognitive dysfunctions associated with alcohol-induced neuroinflammatory damage. *Brain Behav. Immun.* 25, S80–S91. doi:10.1016/j.bbi.2011.02.012

Pérez-Hernández, O., González-Reimers, E., Quintero-Platt, G., Abreu-González, P., Vega-Prieto, M. J. D., Sánchez-Pérez, M. J., et al. (2017). Malondialdehyde as a prognostic factor in alcoholic hepatitis. *Alcohol Alcohol* 52, 305–310. doi:10.1093/alcalc/agw094

Rangasamy, S. B., Jana, M., Roy, A., Corbett, G. T., Kundu, M., Chandra, S., et al. (2018). Selective disruption of TLR2-MyD88 interaction inhibits inflammation and attenuates Alzheimer's pathology. *J. Clin. Invest.* 128, 4297–4312. doi:10.1172/JCI96209

Rudebeck, P. H., Bannerman, D. M., and Rushworth, M. F. S. (2008). The contribution of distinct subregions of the ventromedial frontal cortex to emotion, social behavior, and decision making. *Cogn. Affect. Behav. Neurosci.* 8, 485–497. doi:10.3758/CABN.8.4.485

Sayd, A., Anton, M., Alen, F., Caso, J. R., Pavon, J., Leza, J. C., et al. (2015). Systemic administration of oleoylethanolamide protects from neuroinflammation and anhedonia induced by LPS in rats. *Int. J. Neuropsychopharmacol.* 18, pyu111. doi:10.1093/ijnp/pyu111

Schenker, S., Henderson, G. I., Hoyumpa, A. M., and McCandless, D. W. (1980). Hepatic and wernicke's encephalopathies: Current concepts of pathogenesis. *Am. J. Clin. Nutr.* 33, 2719–2726. doi:10.1093/ajcn/33.12.2719

Shabab, T., Khanabdali, R., Moghadamtousi, S. Z., Kadir, H. A., and Mohan, G. (2017). Neuroinflammation pathways: A general review. *Int. J. Neurosci.* 127, 624–633. doi:10.1080/00207454.2016.1212854

Tan, H. K., Yates, E., Lilly, K., and Dhanda, A. D. (2020). Oxidative stress in alcohol-related liver disease. *World J. Hepatol.* 12, 332–349. doi:10.4254/wjh.v12.i7.332

Toledo Nunes, P., Vedder, L. C., Deak, T., and Savage, L. M. (2019). A pivotal role for thiamine deficiency in the expression of neuroinflammation markers in models of alcohol-related brain damage. *Alcohol. Clin. Exp. Res.* 43, 425–438. doi:10.1111/acer.13946

Vaure, C., and Liu, Y. (2014). A comparative review of toll-like receptor 4 expression and functionality in different animal species. *Front. Immunol.* 5, 316. doi:10.3389/fimmu.2014.00316

Wang, Q., Tan, Y., Ren, Y., Dong, L., Xie, Z., Tang, L., et al. (2011). Zinc finger protein ZBTB20 expression is increased in hepatocellular carcinoma and associated with poor prognosis. *BMC Cancer* 11, 271. doi:10.1186/1471-2407-11-271

Weissenborn, K. (2019). Hepatic encephalopathy: Definition, clinical grading and diagnostic principles. *Drugs* 79, 5–9. doi:10.1007/s40265-018-1018-z

Yang, B., Ma, S., Zhang, C., Sun, J., Zhang, D., Chang, S., et al. (2021). Higenamine attenuates neuropathic pain by inhibition of NOX2/ROS/TRP/P38 mitogen-activated protein kinase/NF-κB signaling pathway. *Front. Pharmacol.* 12. Available at: https://www.frontiersin.org/article/10.3389/fphar.2021.716684 (Accessed April 1, 2022).

Yang, Y. M., Cho, Y. E., and Hwang, S. (2022). Crosstalk between oxidative stress and inflammatory liver injury in the pathogenesis of alcoholic liver disease. *Int. J. Mol. Sci.* 23, 774. doi:10.3390/ijms23020774

Zahr, N. M., Alt, C., Mayer, D., Rohlfing, T., Manning-Bog, A., Luong, R., et al. (2014). Associations between *in vivo* neuroimaging and postmortem brain cytokine markers in a rodent model of Wernicke's encephalopathy. *Exp. Neurol.* 261, 109–119. doi:10.1016/j.expneurol.2014.06.015

Zhang, W., Wang, L.-Z., Yu, J.-T., Chi, Z.-F., and Tan, L. (2012). Increased expressions of TLR2 and TLR4 on peripheral blood mononuclear cells from patients with Alzheimer's disease. *J. Neurol. Sci.* 315, 67–71. doi:10.1016/j.jns.2011.11.032

Zhao, P., Zhao, Y., Wei, Z., Chen, J., and Yan, L. (2016). Wernicke encephalopathy in a patient with liver failure: Clinical case report. *Med. Baltim.* 95, e3651. doi:10.1097/MD.0000000000003651

Zhou, Y., Chen, Y., Xu, C., Zhang, H., and Lin, C. (2020). TLR4 targeting as a promising therapeutic strategy for alzheimer disease treatment. *Front. Neurosci.* 14, 602508. doi:10.3389/fnins.2020.602508

Zurolo, E., Iyer, A., Maroso, M., Carbonell, C., Anink, J. J., Ravizza, T., et al. (2011). Activation of Toll-like receptor, RAGE and HMGB1 signalling in malformations of cortical development. *Brain* 134, 1015–1032. doi:10.1093/brain/awr032

Advantages of publishing in Frontiers

OPEN ACCESS
Articles are free to read for greatest visibility and readership

FAST PUBLICATION
Around 90 days from submission to decision

HIGH QUALITY PEER-REVIEW
Rigorous, collaborative, and constructive peer-review

TRANSPARENT PEER-REVIEW
Editors and reviewers acknowledged by name on published articles

Frontiers
Avenue du Tribunal-Fédéral 34
1005 Lausanne | Switzerland

Visit us: www.frontiersin.org
Contact us: frontiersin.org/about/contact

REPRODUCIBILITY OF RESEARCH
Support open data and methods to enhance research reproducibility

DIGITAL PUBLISHING
Articles designed for optimal readership across devices

FOLLOW US
@frontiersin

IMPACT METRICS
Advanced article metrics track visibility across digital media

EXTENSIVE PROMOTION
Marketing and promotion of impactful research

LOOP RESEARCH NETWORK
Our network increases your article's readership